THE UNIVERSITY
of EDINBURGH

Sedimentary response to the tectonic uplift of the Kyrenia Range, northern Cyprus, in its Eastern Mediterranean tectonic setting

Romesh Palamakumbura
M. Earth Sci. (University of Edinburgh)

THE UNIVERSITY
of EDINBURGH

Thesis submitted in fulfilment of the requirements for the degree of
Doctor of Philosophy
University of Edinburgh
2015

Declaration

I declare that this thesis has been composed solely by myself and that it has not been submitted, either in whole or in part, in any previous application for a degree. Except where otherwise acknowledged, the work presented is entirely my own.

Romesh Palamakumbura
May 2015

Abstract

The Kyrenia Range forms part of an approximately east-west lineament extending from northern Cyprus to southern Turkey. During Plio-Pleistocene the northern Cyprus segment of the lineament uplifted to ca. 1000 m above modern sea level. Plio-Pleistocene sediments document the uplift of the Kyrenia Range. A combination of sedimentology and a range of dating techniques including uranium series, optical stimulated luminescence (OSL), strontium isotopes and magnetostratigraphy are used to help understand the geological processes controlling uplift. Shallowing from a deep-marine basin to a shallow-marine, cool-water carbonate ramp represents the earliest uplift of the Kyrenia Range. The base of the carbonate ramp is made up of thick-bedded, benthic foraminiferal-rich grainstones, which are discontinuously overlain by calcareous red algal-rich rudstones. Erosively overlying this sequence is a coral- and mollusc-rich conglomerate, representing a short-lived relative sea-level fall. The upper part of the carbonate ramp sequence is composed of cross-bedded grainstone representing a shoreface environment. Interbedded with the upper grainstone facies are occasional fluvial conglomerates. The shallowing-upward marine environment represents the earliest emergence of the Kyrenia Range. After a major break in deposition, six marine and non-marine terraces (K0 to K5) reflect the sedimentary response to the main phase of tectonic uplift of the Kyrenia Range. The K0 terrace, the oldest and highest terrace, is composed of megabreccia and is interpreted as representing a major phase of rapid tectonic uplift. The K2-K5 terraces form a series marine to non-marine terraces on the northern flank of the range and also non-marine terraces on the southern flank of the range. The terraces on the northern flank each begin with a major marine transgression followed by a regressive sedimentary sequence. Marine environments range from nearshore open-marine below the storm-wave base, to shoreface, foreshore (beachrock), and backshore lagoonal environments. The non-marine environments range from aeolian dune to fluvial drainage systems. The fluvial systems are characterised by channelised debris-flow deposits interbedded with mudstones and palaeosols. The non-marine deposits on the southern flank of the range comprise a series of fluvial drainage systems. The fluvial systems on the southern flank of the range comprise a mixture of planar-bedded and channelised conglomerates, mudstones and aeolianites. Portable luminescence data are used to correlate quantitatively the K4 and K5 terraces on both the northern and southern flanks of the range. Each of the K4 and K5 terraces produce a unique luminescence signal, which is used as the basis for correlating the lower terraces. The unique luminescence signals of the K4 and K5 terraces are likely to be caused by varying sedimentary histories of the quartz and feldspar grains within the two terraces. The shallow-marine environments surrounding the Kyrenia Range prior to major uplift

were dated using strontium isotopes and palaeomagnetism. The results of this dating suggest that marine environments persisted throughout the Early Pleistocene. U-series and OSL dating were used to date the K4 and K5 terraces on the northern flank of the range. The U-series results indicate that the marine deposits of the K4 terrace formed during several Middle Pleistocene interglacial stages. The OSL dating shows that the aeolian dunes of the K5 terrace formed during a Late Pleistocene glacial stage. The formation of the K2-K5 terraces was controlled by the interaction between tectonic uplift, climatic change and global eustatic sea-level change. The basal marine deposit of each terrace formed during an interglacial stage. Major fluvial deposition also occurs during the interglacial period as a result of a wetter climate. The interglacial-glacial transition resulted in major fluvial erosion as a result of falling global sea-level. Aeolian carbonate deposition was dominant during the glacial stage, which represent arid climatic conditions. The only exception to this is the K4 terrace, which represents three glacial stages. The K1-K3 terraces can be correlated with the global sea-level curve suggesting approximate ages for each terrace, and ca. 600 ka for the entire K1-K5 terrace sequence. The Kyrenia Range underwent rapid uplift during the late Early Pleistocene at >1.2 mm/yr, followed by continuous but slower uplift during the Middle to Late Pleistocene. These results indicate that the uplift occurred in tandem with the Troodos Massif in southern Cyprus. The driving mechanism of the uplift of the Kyrenia Range is likely to be related to the collision of the Eratosthenes Seamount with the Cyprus trench to the south of the island. The seamount-trench collision resulted in compressional tectonics around Cyprus within the large-scale tectonic setting resulting from the early stages of convergence of the African and Eurasian plates.

Lay summary

This thesis focuses on the uplift of the Kyrenia mountain range in northern Cyprus during the last 5 million years. Cyprus comprises two mountain ranges, the Kyrenia Range in the north and the Troodos Massif in the south. The uplift of Cyprus resulted in a gradual change from a deep-marine basin to a shallow-marine basin from 5 to 1.5 millions years ago. During the last 1.5 million years the Kyrenia Range underwent rapid uplift and formed a series of terraces on its northern and southern flanks. The terraces of the Kyrenia Range are known as K0 to K5, where the K0 terrace is the oldest and highest above modern sea level and the K5 is the youngest and lowest above modern sea level. The K0 terrace comprises a deposit of angular rock fragments ranging in size from 1 cm to 10 m and represents a phase of rapid uplift at approximately 1.5 million years ago. The K1 to K5 terraces represent both marine and non-marine deposits. The formation of each terrace is a result of the interaction of plate tectonics, climate change and rising and falling global sea level during the last 1.5 million years. The timings of uplift of the Kyrenia Range are shown using a range of dating techniques including strontium isotopes, palaeomagnetism, uranium isotopes and optically stimulated luminescence. The results of the dating show that the Kyrenia Range has uplifted in tandem with the Troodos Massif. It is suggested that the plate tectonic processes that caused the uplift of the Troodos Massif also drove the uplift of the Kyrenia Range.

Acknowledgements

This thesis is dedicated to Éimear Deady who has helped, supported and shown continuous interest throughout the project, for which I will be forever grateful. Of course, many thanks to my family Manel, Tamara and Roshani Palamakumbura for continuous support in everything I do.

I owe many thanks to Alastair Robertson for his discussion, interest and guidance throughout my academic training. I was greatly appreciative and inspired by Dick Kroon's unrelenting enthusiasm for all aspects of geology. Many thanks to Mehmet Necdet for his support while in northern Cyprus. I would also like to thank Tim Kinnaird for his help and patience with the luminescence work.

I would like to thank Jenny Tait (Edinburgh University), Conall Mac Niocaill (Oxford University) and Chuang Xuan (Southampton University) for help with the palaeomagnetism data gathering and analysis. Many thanks to Peter van Calsteren (Open University) for carrying out the U-series analysis. I am much obliged to Mike Hall for creating many thin sections from some very soft "rocks"!

This project was funded by the Natural Environment Research Council (NERC), the DARIUS programme and the John Dixon Memorial Fund. I am immensely gratefully for this financial support, as it was essential for the success of the project.

A special thanks to Darren Wilkinson who has been a truly inspirational friend throughout my time in Edinburgh. Many thanks to Johannes Miocic for his friendship and inspirational passion for all things sandstone.

A final thank you to all my friends who have put up with me over the last few years. I thank Madeleine Berg, Rachel Kilgallon, Matthew Holloway, Rory McKavney, Jack King, Andrew Miles, Kit Carruthers and Adam Cross.

Thesis objectives

The main objective of this thesis is to understand the sedimentary processes related to the tectonic uplift of the Kyrenia Range, northern Cyprus. The Plio-Pleistocene sedimentary cover of northern Cyprus covers an array of depositional environments, including: shallow-marine carbonate systems, fluvial-drainage networks, megabreccias, debris flows and carbonate aeolianites. The interaction and evolution of these depositional environments is related to the tectonic uplift of the Kyrenia Range. This thesis aims to firstly, describe how these depositional environments have developed, secondly, understand how this is related to tectonic uplift and sea-level change, and thirdly, use this information to improve upon the current understanding of the tectonic setting of the Eastern Mediterranean during the Pliocene-Pleistocene.

Thesis outline

Chapter 1

Chapter 1 summarises the geological setting of the Eastern Mediterranean focusing on the geological history of northern Cyprus. This chapter focuses on the sediments related to the Plio-Pleistocene uplift of the Kyrenia Range and the Troodos Massif, of southern Cyprus. The purpose of this chapter is to outline the state of research in the region related to the Pleistocene uplift of the island of Cyprus.

Chapter 2 to 4

These chapters describe the sedimentology related to the Pleistocene uplift of the Kyrenia Range, northern Cyprus.

Chapter 5

This chapter presents new portable luminescence data from the younger terrace deposits in northern Cyprus. The chapter has been accepted for publication in the International Journal of Earth Sciences (Geologische Rundschau). The reference for this publication is DOI 10.1007/s00531-015-1173-3.

Chapter 6

This chapter presents new quantitative dating results from the uplift related deposits of northern Cyprus. The dating techniques used are principally: uranium series, optically stimulated luminescence (OSL), strontium isotope dating and magnetostratigraphy.

Chapter 7 to 8

The final chapters are a synthesis of the entire thesis.

Greek and Turkish names

The island Cyprus is currently divided into a northern territory known as the Turkish Republic of Northern Cyprus and a southern territory known as the Republic of Cyprus. As a result, Turkish language is used in the north of the island, with relevant literature published in English, Greek, Turkish and French. For the purpose of the stratigraphy the original name is given alongside the newer Turkish name. For the purpose of relocating localities the Turkish name is given, followed by the Greek name. The only exception to this is for newly defined formations and members within this study where the Turkish name is given followed by the Greek. The purpose of presenting both names is for an easy comparison of older and newer literature and to enable anyone following up this work in northern Cyprus to find the described localities with ease.

Pliocene-Pleistocene boundary

An integral part of this thesis is the study of deposits of Pliocene and Pleistocene ages. Since 2010 the boundary between the Pliocene and Pleistocene has changed. The Plio-Pleistocene boundary is now defined at 2.58 Ma (Cohen and Gibbard, 2010), whereas it was previously defined at 1.8 Ma. Consequently, studies from 2010 or older define various deposits as Late Pliocene, whereas they would currently be defined as Early Pleistocene. When referring to dates from the literature the defined stages have been changed based upon the current Plio-Pleistocene boundary at 2.58 Ma.

Contents

Chapter 1

Introduction

1.1 Introduction

The Kyrenia Range, northern Cyprus, is an east-west running lineament reaching approximately 1000 m above modern sea-level (AMSL). The geological history of the Kyrenia Range spans the Permian to the Holocene. This study focuses on the most recent Plio-Pleistocene geological history, during which time the Kyrenia Range underwent tectonic uplift from below sea-level to its present height. New evidence to be presented here will document the sediments associated with the Pleistocene uplift to understand the interaction of tectonic processes and global eustatic sea-level change. A wider aim is to use the resulting information to help better understand the tectonic setting of the Eastern Mediterranean region during the early stages of collision of the African and Eurasian plates during the Plio-Pleistocene.

1.2 Rationale

The geological development of Cyprus has been a very active research area for the past half century. Research has focused on the islands Permian to the Recent geological history, including the palaeo-rotation of the Troodos Massif, the Mesozoic depositional environments, and tectonic uplift events of the Troodos Massif and the Kyrenia Range. However, due to political constraints research in northern Cyprus has stalled since the mid 1970s. However, during the last ten years access to northern Cyprus has been eased, making this study possible.

This study therefore focuses on the Plio-Pleistocene geological development of northern Cyprus, with the key aim of understanding how tectonic and eustatic sea-level processes shaped the Kyrenia Range. The project combined sedimentology with a range of quantitative dating techniques to understand the processes that affected the Kyrenia Range during the Plio-Pleistocene. The uplift resulted in a transition from an open marine setting to non-marine aeolian and fluvial setting. The environments have been dynamically controlled by a combination of tectonics, global eustatic sea-level change and climatic change.

Natural resources in the Eastern Mediterranean are of growing economic importance. Academic studies focusing on the geological history of the Eastern Mediterranean provide an integral dataset for both the mineral and hydrocarbon industries. As a consequence of recent earthquakes, numerous projects have been funded to better understand the potential earthquake related hazards on the island. Focused studies in Cyprus are essential to develop an understanding of the geological development of the Eastern Mediterranean and to aid these industries and earthquake hazard studies.

1.3 Hypotheses

Hypothesis I

The interaction between tectonic, eustatic and climatic processes controlled the formation of marine and non-marine terraces on the northern and southern flanks of the Kyrenia Range.

Objectives I

The tectonic, eustatic and climatic signals are likely to be recorded in the Pliocene and Pleistocene sedimentary cover of northern Cyprus. A detailed understanding of the various depositional environments of the Pliocene and Pleistocene and how these various settings have evolved and interacted is needed.

Methods I

Extensive field work was undertaken to document the Pliocene and Pleistocene sediments of northern Cyprus, combined with petrological descriptions to document any variation in composition of the sediments. This new facies data provides an in depth understanding of how the depositional environments in northern Cyprus have evolved during the Pliocene and Pleistocene. Interpretations based upon this facies data can be made as to the likely wider scale controls of deposition, such as tectonic uplift, sea-level change and climate change.

Hypothesis II

Climatic changes related to glacial cycles controlled the depositional environments surrounding the Kyrenia Range during the Plio-Pleistocene.

Objectives II

The Pliocene and Pleistocene represents a period of dynamic glacial cyclicity, which is likely to have strongly controlled the depositional environments around northern Cyprus. Changes in climate during interglacial-glacial cycles are likely to be represented by changes in facies in the sedimentary cover of the Kyrenia Range.

Methods II

To assess climatic controls on deposition, a combination of facies analysis and quantitative dating are used on the Pleistocene terrace deposits on the northern flank of the range. Uranium series and optically stimulated luminescence dating were used to date shallow marine and aeolian dune deposits from the lowest terraces on the northern coast. The new age data is used to correlate various depositional environments with Pleistocene glacial cycles.

Hypothesis III

Tectonically driven Pleistocene uplift of the Kyrenia Range and the Troodos Massif is related to the collision of Eratosthenes Seamount with the Cyprus trench to the south

of the island.

Objectives III

Tectonics are likely to have been a major control on the uplift and formation of the Kyrenia Range in northern Cyprus. The Eratosthenes Seamount collision with the Cyprus trench is a major tectonic event during the Early Pleistocene and is the driving mechanism for the uplift of the Troodos Massif in southern Cyprus. If the Kyrenia Range was also affected by the seamount-trench collision during the Early Pleistocene, then this is likely to have been recorded in the sedimentary cover of northern Cyprus.

Methods III

To assess the tectonic processes driving the uplift of Kyrenia Range a combination of detailed facies analysis and quantitative dating are used. Facies analysis is focused on deposits that are related to the various stages of uplift, including: pre uplift, syn uplift and post uplift. The pre-uplift stage is dated using a combination of palaeomagnetism and strontium isotope dating. The syn- to post-uplift stages are dating using a combination of uranium series and optically stimulated luminescence dating. The new facies data combined with quantitative age data can then be compared with the various tectonic models of the Eastern Mediterranean during the Pliocene to Pleistocene to understand the tectonic controls of uplift of the Kyrenia Range.

1.4 Methodology

To understand the processes controlling deposition in northern Cyprus during the Pliocene and Pleistocene a combination of sedimentology and a range analytical techniques were used. The analytical techniques included optically stimulated luminescence (OSL), uranium series dating, strontium isotope dating, palaeomagnetism and oxygen and carbon isotopes. The following sections detail the justification and methodology of each technique.

1.4.1 Sedimentology

To understand the depositional environments represented by the deposits of Pliocene and Pleistocene age in northern Cyprus a total of 8 months of field work were carried out. This work involved extensive logging of deposits from the northern and southern flanks of the Kyrenia Range, the Mesaoria (Mesarya) Plain and the Karpaz (Karpas) Peninsula. Petrological descriptions and point count data were carried out on a selection of samples from these deposits. This data was used to aid the interpretations of depositional environments and to understand the local sediment provenance history. The sedimentology results are presented in chapters 2 to 4, which include short summaries at the end of each chapter discussing the findings.

Point counting

Point counting was carried out on grainstone samples to help intepret the depositional environments and provenance history of the deposits. 400 grains were counted per sample to reduce statistical error within the data, providing ca. 5% error on the data (Van der Plas and Tobi, 1965). Traditional point-count methods such as the Gazzi-Dickinson point-counting method developed by Gazzi (1966) and Dickinson (1970) and the rock-fragment method developed by Folk (1974) mainly focus on clastic rock provenance studies and, therefore, mainly count variations in the composition of the detrital grains. To determine the depositional processes of the grainstone deposits point counting was used to determine: firstly, the ratio of silicic grains and reworked rock fragments to carbonate material and secondly, the variations in the type of bioclastic material. The following categories were used for collecting the point-count data: monocrystalline quartz, polycrystalline quartz, chert, volcanic clasts (reworked), metamorphic clasts (reworked), sedimentary clasts (reworked), plagioclase, calcareous red algae, benthic foraminifera, echinoderm plates, bivalve fragments, calcareous algal fragments, planktonic foraminifera, bryozoa and ostracods. The bivalve fragments, algal fragments, planktonic foraminifera, bryozoa and ostracods are grouped together under 'other carbonates' for graphical plotting due to their relatively minor concentrations. The reworked volcanic, metamorphic and sedimentary clastic grains are also grouped together under 'reworked clastic grains'.

1.4.2 Analytical techniques

A large range of analytical techniques are employed to understand the depositional processes, the diagenetic history and the timings of deposition related to the uplift of the Kyrenia Range. Dating of the Mesaoria (Mesarya) Group deposits provides a constraint on firstly when the deposits fit into the Pliocene and Pleistocene, secondly how the deposits relate to glacial cycles during the late Cenozoic and thirdly, a constraint on the timings and rates of uplift of the Kyrenia Range. Furthermore, OSL profiling and oxygen and carbon isotope analysis are used to aid the facies interpretations of the various deposits. The following section describes the basic principles of each of the techniques used, the analytical methodology and any relevant previous studies from each of the techniques. The results of the various analytical methods are presented in chapters 5 and 6.

For all the analytical techniques all the sample selection was carried out by myself. The sample preparation and analysis was also carried out by myself for the luminescence field and laboratory profiling and all the palaeomagnetism analysis. Sample preparation for the strontium isotope dating and the oxygen and carbon isotope analysis was carried out by myself, while the analysis for these techniques was carried out by others. Finally, all the sample preparation and analysis for OSL and Uranium series dating was carried out externally. Further details on the specifics of the sample selection, preparation and analysis of each technique is described below.

Optically stimulated luminescence (OSL)

Introduction

OSL is used here to quantitatively correlate terrace deposits along the flanks of range, understand depositional processes within the lower terrace deposits and finally to date deposits of the lowest terrace on the northern flank of the range. Three OSL-based methods were used, including field profiling, laboratory profiling and full OSL dating. The methodology for each of these techniques is described below. Both field and laboratory profiling sampling and analysis were carried out by myself. However, the full OSL dating was carried out by Dr Tim Kinnaird at the OSL laboratories at SUERC, East Kilbride.

OSL is widely used to determine the depositional age of sediments in a diverse range of environments (see Rhodes (2011)). The underlying principle is that naturally occurring minerals can store energy through crystal defects trapping charge in response to ionising radiation from the natural environment. Stimulated luminescence measurements are used to register the extent of trapping and, in combination with known laboratory radiation exposure, to determine the radiation dose received since an earlier zeroing event (caused by surface exposure in the past). A luminescence age (ka) is the quotient of the stored dose (Gy) and the environmental dose rate (mGy a^{-1}). Where sediments are well zeroed, for example by multiple cycles of exposure to daylight prior to final deposition, the method can give highly accurate and precise ages for events ranging from recent time back to several hundred thousand years (Lian and Roberts, 2006).

In luminescence dating it is important to understand that the degree of zeroing or optical bleaching which is dependent on the mineral type/composition, depositional mechanism and environmental setting. The term bleaching refers to the removal of trapped charge populations from a sample (Rhodes, 2011). The term luminescence residual refers to the geological and/or environmental luminescence signals (previous to growth of an *in situ* luminescence signal during a depositional cycle) that remain following a zeroing event. A number of OSL screening methods have been developed to provide insights into the luminescence properties of sediment and to interpret the depositional mechanisms and zeroing process. These range from instrumentation developments, such as the portable OSL equipment developed at the Scottish Universities Environmental Research Centre (SUERC) for field profiling, and methodological developments such as laboratory profiling (Sanderson *et al.*, 2001; Sanderson *et al.*, 2003; Burbidge *et al.*, 2007), "rangefinder" ages (Roberts *et al.*, 2009b) and standardized growth curves (e.g. Roberts and Duller (2004)).

Previous work

Previous luminescence studies in Cyprus have focused on the timing of neotectonic faulting in southern Cyprus (Kinnaird and Robertson, 2013) and the Mesaoria (Mesarya) Basin (Harrison *et al.*, 2004), local uplift rates along the southern coast of Cyprus (Harrison *et al.*, 2012), and determining the age of Holocene aeolianite deposits in northern Cyprus (Erginal *et al.*, 2012). These studies have shown the successful

use of OSL dating in Cyprus. Key observations include: quartz and feldspar within the sediment produce a datable luminescence signal, and Pleistocene deposits generate enough background radiation for luminescence dating. These important observations indicate that the required geological criteria for luminescence dating are met in Cyprus.

Luminescence dating has also been successfully used in a number of studies of Pleistocene terrace uplift along the coasts of Italy (Ferranti *et al.* (2006)), New Zealand (Wilson *et al.*, 2007) and South Korea (Choi *et al.*, 2009). Such studies have correlated deposits with both glacial and interglacial cycles and help understand the timings of surface uplift. Furthermore, such studies show viable dates from carbonate-sand deposits, similar to the carbonate aeolianites used for OSL dating in this study.

OSL field profiling

OSL field profiling is a screening method used to relatively quickly assess the luminescence characteristics of sedimentary deposits in the field (Sanderson and Murphy, 2010). The field luminescence data can be used to aid with sedimentary interpretations and to help chose potential full dating samples (Sanderson and Murphy, 2010).

OSL field profiling was conducted in the field, and subsequently in the laboratory (for bleaching experiments), using the SUERC portable luminescence reader. Full details of the SUERC portable OSL reader are given in Sanderson and Murphy (2010). In brief, the OSL reader consists of a sample chamber, a detector head including an ETL photo detector module with a 25 mm bi-alkali photomultiplier. Stimulation is delivered through either blue LEDs emitting 470 nm (optically stimulated luminescence (OSL)), or infrared LEDs emitting 880 nm (infra-red stimulated luminescence (IRSL)). The blue diodes are outfitted with GG420 long-pass filters; whereas, the IR diode ports are outfitted with RG780 long pass filters. Both signals pass through UG11 filters and detection is attained by a 24-bit photon counter, which is set for continuous wave counting (see Sanderson and Murphy, 2010).

At each selected section, the sediment profile was first cut back by at least 10 cm, to remove superficial material which had been light-exposed and subjected to weathering, or near-surface drying. All of the samples were collected under light-safe conditions using opaque (black) covers. The samples were collected either by driving 20 mm x 50

mm-diameter copper tubes into the cleaned section, or by using a pick to remove the sediment from the section directly into 50 mm-sized petridishes for measurement in the portable reader. The marine and aeolian grainstone deposits, although relatively young, were semi-lithified and, therefore, only required the use of a toothpick to granulate the samples into a petridish in the field. *in situ* field gamma spectrometer (FGS) measurements were taken from a number of representative lithologies in each terrace. FGS measurements were made using a Health Physics Instrument Rainbow Multi-Channel Analyser with a 2 x 2 NaI probe.

This measurement cycle utilised an interleaved sequence of system dark count (background), IRSL and OSL, similar to that described by Sanderson and Murphy (2010). This enabled net IRSL and OSL signal intensities, depletion indices and the IRSL:OSL ratio to be calculated for each sample. The interpretation of the OSL signal intensities, their depletion indices and the IRSL:OSL ratio have been discussed in a number of recent publications (Sanderson and Murphy, 2010; Muñoz-Salinas *et al.*, 2011; Kinnaird *et al.*, 2012; Munyikwa *et al.*, 2012). The IRSL and OSL intensities may act as age proxies in well-bleached sedimentary units, assuming common sensitivities and dose rates. Luminescence sensitivity is a measure of signal intensity per unit of absorbed radiation dose. Whereas OSL intensity is a function of the amount of radiation exposure to the minerals since burial, sensitivity relates to the efficiency with which the absorbed radiation is transmitted as luminescence. Any discontinuities or inversions in the OSL signal intensity profiles may reflect differences in the initial sedimentary characteristics or depositional circumstances. If mineralogical composition, grain size or diagenesis varies throughout a section, then signal intensities will also reflect such changes. The depletion index, which represents the proportion of signal released in the first half of a stimulation cycle relative to the second half, is an indicator of sample transparency, coupled with information about whether a sample contains an inherited or signal cycle signal. Higher depletion indices would indicate better-bleached material. The IRSL:OSL ratio is potentially sensitive to mineralogical input changes, reflecting quartz/feldspar relative contents, and the weathering history of the sediment. These proxies are used here, in conjunction with the sedimentalogical observations, to provide an initial interpretation of the luminescence properties of individual samples, with a view to generating luminescence stratigraphies. The aim is to obtain information on individual sample luminescence characteristics and sample-to-sample variations between, and also within, the terrace deposits. A further objective of the luminescence investigation is to explore the variation in the residual luminescence signals of the near-shore

versus the terrestrial sediments of the two terrace systems, and to interpret the processes of sediment bleaching in contrasting depositional environments with different sediment sources and transport histories.

The sensitivities of the quartz and the polymineral signals to bleaching were also investigated. Samples were selected from terrace deposits at Alagadi beach and from the K5 terrace deposits at Mersinlik. These sections were selected because they represented the full range of lithologies and terraces profiled. Representative samples were exposed to natural daylight for a number of different time durations (between 1 and 90 minutes), prior to recording the net IRSL and OSL signal intensities, as outlined above.

Laboratory profiling

Luminescence profiling is a method for producing quick estimates of the stored doses and sensitivities from a large number of samples, (Sanderson *et al.*, 2001, 2003; Burbidge *et al.*, 2007; Kinnaird *et al.*, 2015). This technique has been used in various studies to understand the luminescence characteristics of sedimentary sections associated with archaeological and sedimentary investigations and to improve dating reliability. Examples of profiling studies include those in Cambodia (Sanderson *et al.*, 2003), Eastern Europe (Burbidge *et al.*, 2007) and Orkney (Kinnaird *et al.*, 2012). The aim of the laboratory profiling of the deposits from northern Cyprus was to firstly assess the hypotheses developed by field profiling, and secondly, to assess the luminescence characteristics of the K4 and K5 terrace deposits.

Two sites were selected for laboratory profiling. The sites both contain K4 and K5 terrace deposits that are preserved within ca. 100 m of each other. Deposits at Alagadi Beach and Mersinlik town (see Chapter 5 for locality details) were selected because they represent a range of facies and include both K4 and K5 terrace deposits. The samples used for the laboratory profiling were from the same positions within the sedimentary sections as those used for field profiling. The following procedure was carried out under safelight conditions in the SUERC luminescence laboratories, based on the method described by Burbidge *et al.* (2007).

1. Wet sieve sample down to a grainsize of 90-250 μm.
2. Treat sample with 1 molar HCL for 10 mins.

3. Wash sample with deionised water, followed by acetone.
4. Separate sample into two parts (A and B).
5. Leave Sample A in oven to dry.
6. Treat Sample B with 40% hydroflouric acid (HF) for 40 minutes.
7. Wash Sample B with deionised water followed by acetone.
8. Leave Sample B in oven to dry.
9. Dispense all samples onto 10 mm wide stainless steel disks.

Each sample is separated into two sub-samples: Sample A- HCL treated polymineral sample, and sample B- HF-etched quartz predominant sample. Sample A was only treated with HCL, which was enough to remove carbonate grains and any carbonate cement coating the grains. In contrast, sample B was treated with HCL followed by HF, which removed carbonate grains, feldspars and etched the surface of the quartz grains. Each sample was dispensed onto three stainless steel disks (aliquots); two were analysed to show any variation in results within the sample, and the third was put in storage. The samples were then analysed using the Risø luminescence reader at the SUERC luminescence laboratory. The following treatment sequence was carried out on both the polymineral and quartz aliquots-

1. Preheat (260^oC for 10 seconds).
2. IRSL (50^oC for 60 seconds) stimulation and measurement.
3. IRSL (225^oC for 60 seconds) stimulation and measurement.
4. OSL (125^oC for 60 seconds) stimulation and measurement.
5. Test dose of 3.97 Gy.
6. Repeat steps 1-4.
7. Test dose of 39.59 Gy.
8. Repeat steps 1-4.
9. Test dose of 3.97 Gy.
10. Repeat steps 1-4.

The only variation in the sequence between the polymineral (PM) and quartz (QTZ) aliquots is that the IRSL step is not run for the quartz aliquot because it is unlikely that there is any feldspar to stimulate within this sample set.

OSL dating

The basis of OSL dating derives from the principle that naturally occurring minerals store energy from background radiation during burial and this stored radiation can be removed by natural daylight; this was first developed as a dating technique by Huntley *et al.* (1985). The basic steps of OSL dating are summarised by Rhodes (2011) as:

1. The removal of trapped charge within mineral grains (such as quartz and feldspar) by natural light during transportation.
2. The accumulation of charge by minerals during burial from background radiation within a deposit.
3. Sampling and measuring of the amount of trapped charge within the laboratory.
4. Comparison of trapped charge with the amount of radiation produced by the deposit over time.

The first step involves the removal of charge during transportation by natural daylight; this is essential because this process zeros (or bleaches) the grains prior to deposition (Godfrey-Smith *et al.*, 1988). The second step involves the deposition of the zeroed (bleached) grains, where they can accumulate charge from background radiation over time (Huntley *et al.*, 1985). The key to the technique is the difference in time over which steps 1 and 2 occur; mineral charge accumulate occurs over 10^1-10^5 years; in contrast minerals are bleached over 10^0-10^2 seconds (Rhodes, 2011). The third step involves sampling under dark conditions at the outcrop; this either involves sampling beneath a tarpaulin or inserting opaque (often copper) tubes into the sediment. Samples were brought back to the laboratory for analysis using a Risø luminescence reader (Botter-Jensen *et al.*, 2000). The Risø luminescence reader uses blue (OSL) (470nm) and infrared (IRSL)(830nm) light to release the trapped charge from the quartz and feldspar grains, respectively. The radiation released as a consequence of the blue and infrared stimulation is measured and used to calculate a stored dose (or equivalent dose (D_e))(Huntley *et al.*, 1985). Before stimulation, the samples undergo a preheat step, this involves heating the samples up to between 200-300^{o}C to remove any unstable charge (Murray and Wintle, 2000). The final step involves a comparison of the equivalent dose to the dose rate; the dose rate is the radiation absorbed each year by the luminescence minerals. To calculate the dose rate requires investigating the amount of radioactive emissions from the sediment surrounding the sample. High-resolution gamma spectrometry can be used for multi-nuclide analysis,

providing activity concentrations of various radioactive isotopes including ^{40}K, ^{238}U and ^{228}Th (Frank *et al.*, 2008). Water contained within the sample during burial can absorb background radiation affecting the amount of radiation received by the sample. Therefore, the water content is measured and the dose rate is corrected based upon this measurement (see Rhodes (2011)). The final step in deducing a burial age is the comparison of the equivalent dose and the dose rate, based upon the follow relationship:

$$\text{Burial age (ka)} = \frac{\text{Equivalent dose } (D_e)(\text{Gy})}{\text{Dose rate}(\text{Gy/ka})}$$

$$(\text{Gy} = \text{Grays} = 1 \text{ J.kg}^{-1})$$

(Huntley *et al.*, 1985)

A range of minerals show luminescence characteristics; however, quartz and feldspar are used in most dating studies for a number reasons: 1) their abundance in a range of deposits; 2) their resistance to weathering; 3) the luminescence signal in both minerals is bleachable by daylight; and 4) the trapped charge in both minerals grows over geological time and can be explained using mathematical functions (Frank *et al.*, 2008). Quartz has generally been the favoured mineral for luminescence dating due to an excellent understanding of the decay components through experimental work (Bailey *et al.*, 1997). However, a major disadvantage of quartz is the relatively low-charge saturation in contrast to feldspar (Frank *et al.*, 2008). The specific luminescence characteristics of feldspar could allow it to be used in dating older deposits than those for which quartz can be used, due to the relatively brighter luminescence signal and higher saturation limits (Frank *et al.*, 2008). Thermoluminescence dating uses thermal energy rather than optical energy to stimulate the trapped charge within grains and is used for dating older deposits (see Wintle and Huntley (1982)); however, this technique was not used here and is therefore not discussed further.

The luminescence signal from feldspars continues to grow to far higher doses than those of quartz; this offers the possibility of dating significantly older material providing sufficiently stable signals can be achieved. The IRSL and TL signals from feldspars are expected to respond to additional radiation of up to the 1 to 5 kGy range. In a low dose rate environment, this means that there is the potential to date sediments well beyond ca. 250 Ka. However, feldspars have been shown to undergo a process called "anomalous fading" (Wintle, 1973), which involves the fading of the luminescence signal from certain, but not all, charge traps over time. The affect of "anomalous fading" on dat-

ing is such that when the mineral is stimulated the signal comes from both stable and unstable charge traps causing a higher stimulated signal relative to natural signal. The incorrect stimulated signal results in an underestimate of the palaeodose and, therefore, an underestimation of the age of the sample. Preheating of the sample prior to measurement removes most of the unstable charge but not all (see Frank *et al.* (2008)). An alternative method called "post-infrared infrared-stimulated luminescence" (post-IR IRSL) is used for measuring the stable component within the feldspar system to reduce the affect of "anomalous fading" (Buylaert *et al.*, 2009; Murray *et al.*, 2009; Thomsen *et al.*, 2011). The increased signal stability from post-IR IRSL is a consequence of the removal of unstable charges in close lattice proximity to each other during the prior infra-red stimulation at 50°C. The subsequent post-IR IRSL signal is interpreted as originating in more stable charges, which can be accessed by re-stimulating the sample at elevated temperatures. Post-IR IRSL involves high-temperature preheating (225°C) followed by a IRSL stimulation after the normal IRSL measurement (Buylaert *et al.*, 2009).

Luminescence-dating laboratory analysis and calculations were carried out by Dr Tim Kinnaird at the SUERC luminescence laboratory, East Kilbride (See appendix for dating report). The dating analysis was done externally due to time limitations, as the analysis took over 8 months to carry out. Only two samples were analysed due to financial constraints and the high costs associated with the technique.

Uranium series (U series) dating

Introduction

U-series dating has been used in numerous Pleistocene terrace studies to constrain the age of tectonically uplifted marine deposits (Poole *et al.*, 1990; Goy *et al.*, 2003; Roberts *et al.*, 2009a; Turner *et al.*, 2010). The dating technique is used here to date well-preserved coral in marine deposits from the lower terraces on the northern flank of the Kyrenia Range.

U-series dating involves the measurement of the uranium parent and daughter isotopes, which include ^{234}U and ^{230}Th (thorium), respectively. ^{234}U has a half-life (λ) of ca. 76 kyr, decaying by alpha particle decay to ^{230}Th. The initial system should contain no ^{230}Th, meaning the radiometric clock starts at zero (reviewed in Van Calsteren and

Thomas (2006)). Age is calculated by the comparison of concentrations the daughter isotope ^{230}Th and the parent isotope ^{234}U as their relationship progresses towards secular equilibrium (Ivanovich, 1982; Schwarcz, 1989).

Previous studies

U-series dating was carried out on preserved *Cladocora* solitary corals from the northern flank of the Kyrenia Range. *Cladocora* coral have been used successfully in numerous coastal uplift studies including southern Cyprus (Poole *et al.*, 1990), the Gulf of Corinth, Greece, (Roberts *et al.*, 2009a; Turner *et al.*, 2010) and along the Mediterranean and Atlantic coastlines of Spain (Goy *et al.*, 2003).

Sample selection

The *Cladocora* coral are chosen for U-series as they are composed of aragonite, which contains a high concentration of uranium and a low concentration of ^{230}Th daughter isotope, and the aragonite acts as a closed radioactive system (Hillaire-Marcel, 2009). However, aragonite is susceptible to low temperature alteration to calcite, causing contamination of the uranium isotope concentrations and making the sample undatable; therefore, only samples with >95% aragonite can be used for reliable U-series dating.

Analytical method

Sample preparation, analysis and calculations were carried out by Dr Peter Van Calsteren at the Open University, Milton Keynes. The method used for preparation and analysis of the samples is described in Dia *et al.* (1997). Analysis was carried out using thermal ionisation mass spectrometry (TIMS); details of this technique are given by Van Calsteren and Schwieters (1995). XRD analysis to assess the amount of calcite alteration of the coral samples were carried out by myself at the School of GeoSciences, University of Edinburgh.

Strontium isotope dating

Introduction

Strontium isotope dating is used to date marine shells of Cambrian to Pleistocene age (Mcarthur *et al.*, 2012). The technique is used here to date the samples from the shallow-marine environment surrounding the Kyrenia Range prior to major uplift.

The basis of strontium (Sr) isotope dating is the evolving $^{87}Sr/^{86}Sr$ isotope ratio of sea-water through geological time, due to varying amounts of strontium derived from continental crust and upper mantle sources (Elderfield, 1986; McArthur, 1994; McArthur *et al.*, 2001). The global marine $^{87}Sr/^{86}Sr$ isotope ratio specifically responds to three main processes: river runoff, hydrothermal input and carbonate dissolution (Brass, 1976; Palmar and Elderfield, 1985). Howarth and McArthur (1997) plotted 1849 $^{87}Sr/^{86}Sr$ isotope data points, from numerous studies, from 0 to 206 Ma, using the LOWESS (LOcally WEighted Scatterplot Smoother) method to produce a best fit curve (Fig. 1.1). The LOWESS marine Sr-isotope curve is used as a reference for $^{87}Sr/^{86}Sr$ isotope ratios through time to derive an age for any carbonate formed within an open marine setting (McArthur *et al.*, 2001).

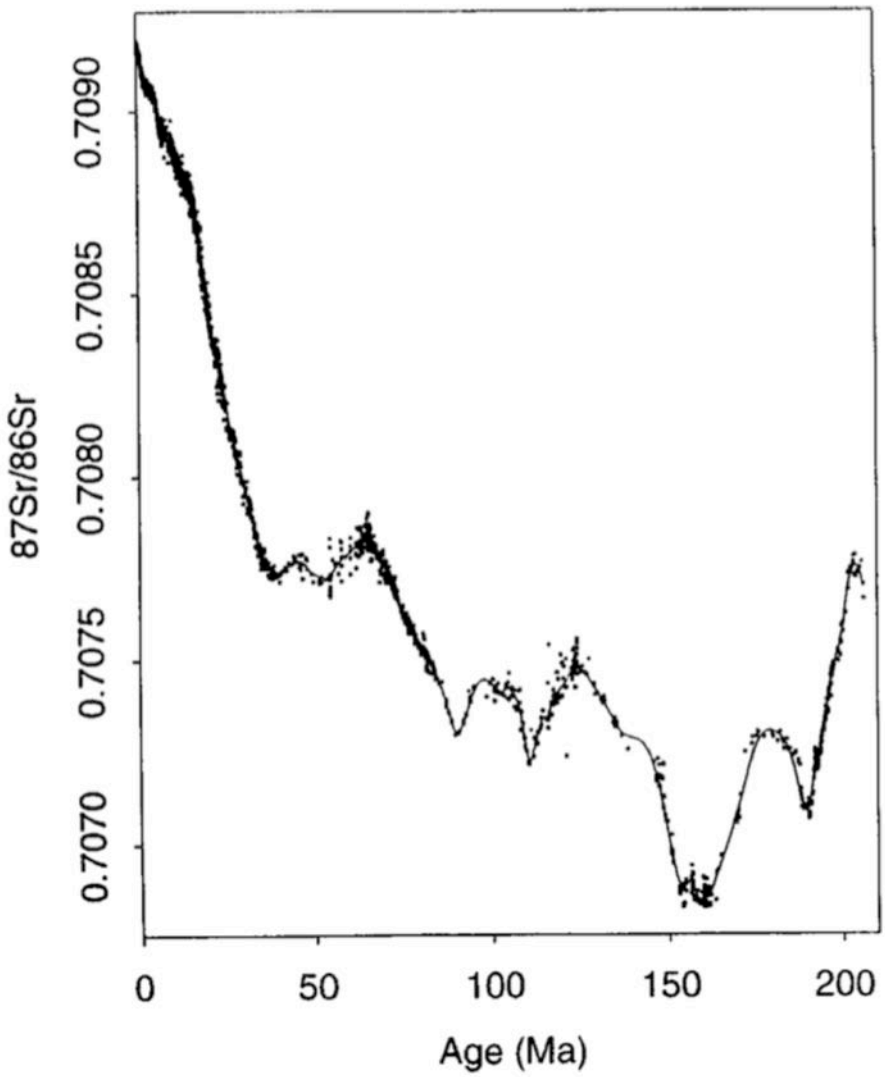

Figure 1.1: Variation in the $^{87}Sr/^{86}Sr$ isotope ratio in global oceans from the Mesozoic to Recent (Howarth and McArthur, 1997).

Previous strontium dating studies

Previous strontium isotope dating in northern Cyprus focused on Eocene to Pliocene sediments (McCay, 2010; McCay *et al.*, 2012). Planktonic foraminifera and calcareous nannofossils were dated from chalk and marl deposits of the Kythrea (Değirmenlik) Group and from the Myrtou (Çamlıbel) Formation. A detailed dated stratigraphy was produced for the various formations of the Kythrea (Değirmenlik) Group. The strontium dating also indicated an early Pliocene age for the pelagic marls of the Myrtou (Çamlıbel) Formation in northern Cyprus. Strontium isotope dating was also used to understand the processes and timings of formation of Middle Pliocene sapropels in northern Cyprus of the Kythrea (Değirmenlik) Group (Taylforth *et al.*, 2014).

Previous studies have shown that the Myrtou (Çamlıbel) Formation is conformably overlain by interbedded chalks and marls of the Nicosia (Lefkoşa) Formation (Henson *et al.*, 1949; Baroz, 1979). The Nicosia (Lefkoşa) Formation is conformably overlain by the Athalassa (Gürpınar) Formation (Henson *et al.*, 1949; McCallum and Robertson, 1995a). The sedimentary relationship suggests a change from open-marine (Myrtou (Çamlıbel) and Nicosia (Lefkoşa) Formations), to shallow marine conditions during the deposition of the Athalassa (Gürpınar) Formation. However, no quantitative dating has been carried out on these deposits and, therefore, the timing of the change from open- to shallow-marine environments is unknown.

Sample preparation

Sample preparation was carried out by myself at the School of GeoSciences, University of Edinburgh and at SUERC, East Kilbride. Two types of sample where used for the dating: bivalve shells and bulk-rock grainstone. Both types of sample were placed in 2.5 molar hydrochloric acid (HCl) to dissolve the carbonate material. The solution was centrifuged for five minutes to remove any undissolved material. The solution was then transferred to teflon beakers and dried on a hot plate. 1 ml of 8 molar nitric acid (HNO_3) was then added to each sample and left to stand for 30 minutes. The Sr isotopes were then extracted using a strontium specific resin. The full method of sample preparation is described in Henderson *et al.* (1994).

Stable isotope analysis method

The samples were analysed at the Scottish Universities Environmental Research Centre (SUERC) in East Kilbride by Anne Kelly. The strontium isotope analysis was carried out on a VG Sector 54-30 mass spectrometer in a Dynamic Multi-collection mode.

Error

Bivalve shells were cleaned with distilled water and then dissolved in acid in order to minimise the detrital strontium input. The well-lithified grainstone was crushed and treated with acid (HCl) to remove secondary carbonate cements and minimise detrital strontium; a similar method is documented by Bailey *et al.* (2000). The acid-treated grainstone was then prepared for strontium analysis using the method described previously.

Two sources of error can be introduced into the data set, from both the analytical technique and the LOWESS marine strontium curve. To help clearly demonstrate the error calculation, sample KYSR-01 (from the final results) will be used as an example.

KYSR-01 has a $^{87}Sr/^{86}Sr$ ratio= 0.708768 with a percentage error= 0.0014%

To accurately present an age for each sample, the analytical and LOWESS curve errors need to be combined. The analytical error can be used to calculate maximum and minimum strontium isotope ratios. For each calculated maximum and minimum isotope ratio, a corresponding age can be deduced from the LOWESS strontium curve.

Max. $^{87}Sr/^{86}Sr$ ratio= 0.708768 + 9.92275 x 10^{-6} = 0.708777923 = 15.08 Ma
Min. $^{87}Sr/^{86}Sr$ ratio= 0.708768 - 9.92275 x 10^{-6} = 0.708758077 = 15.40 Ma

The LOWESS curve gives a maximum and minimum for each deduced age which can be used to give a maximum age range for each data point; this range is shown in Table 6.3.

LOWESS strontium curve age range for 15.08 Ma = 14.96 Ma - 15.23 Ma
LOWESS strontium curve age range for 15.40 Ma = 15.31 Ma - 15.49 Ma
Final calculated age range = 14.96 Ma - 15.49 Ma

Palaeomagnetism

Introduction

The aim of Palaeomagnetism analysis in northern Cyprus is to constrain the age of the marine and non-marine deposits from the Mesaoria (Mesarya) Basin and from the northern flank of the Kyrenia Range immediately before and after major tectonic uplift.

Palaeomagnetism is a geophysical technique that can be used to date sedimentary or volcanic sequences. The basis of the technique is the measurement of the magnetic orientation of the grains or crystals, which are then compared to the Earth's magnetic field over geological time. The technique has been an essential tool in understanding the geological evolution of southern Cyprus, including the the Plio-Pleistocene sedimentary cover of the Troodos Massif (Kinnaird *et al.*, 2011; Weber *et al.*, 2011). The only palaeomagnetic study in northern Cyprus focused upon the Maastrichtian and Palaeocene volcanic rocks, which showed a small amount of palaeorotation of the Karpaz (Karpas) Peninsular during the Neogene, reflecting the arcuate shape of the range (Hodgson *et al.*, 2010).

The palaeomangnetism experiments were carried out at the Univeristy of Edinburgh, the University of Southampton and the University of Oxford. All field sampling, sample preparation and analysis were carried out by myself.

Previous palaeomagnetism studies

Palaeomagnetism work has recently been carried out on the Plio-Pleistocene cover of the Troodos Massif to better understand the timing and processes associated with the uplift of the Troodos Massif. Kinnaird *et al.* (2011) studied the Athalassa (Gürpınar) Formation from the Mesaoria and Pissouri Basins, southern Cyprus. This work identified rapid uplift between 2.14 Ma to 1.95 Ma or immediately before 1.77 Ma. Based upon the most recently redefined Plio-Pleistocene boundary this is during the Early Pleistocene (previously, Late Pliocene, as suggested by Kinnaird *et al.* (2011)). We-

ber *et al.* (2011) focused on the Apalos Formation within the Mesaoria Basin, dating stacked fluvial sequences (Schirmer *et al.*, 2010) related to the earliest uplift of the Troodos Massif. Figure 1.2 shows a comparison of the magnetic reversals during the Pleistocene with the deposits studied and dated by Kinnaird *et al.* (2011) and Weber *et al.* (2011) from the Mesaoria Basin, southern Cyprus. The combination of the work by Kinnaird *et al.* (2011) and by Weber *et al.* (2011) shows, firstly, a marine environment within the Mesaoria Plain during the Early Pleistocene; secondly, fluvial run off from the Troodos Massif into the Mesaoria Plain during the Early Pleistocene; and thirdly, that the F1-F4 marine terraces are <0.781 Ma (Middle to Late Pleistocene).

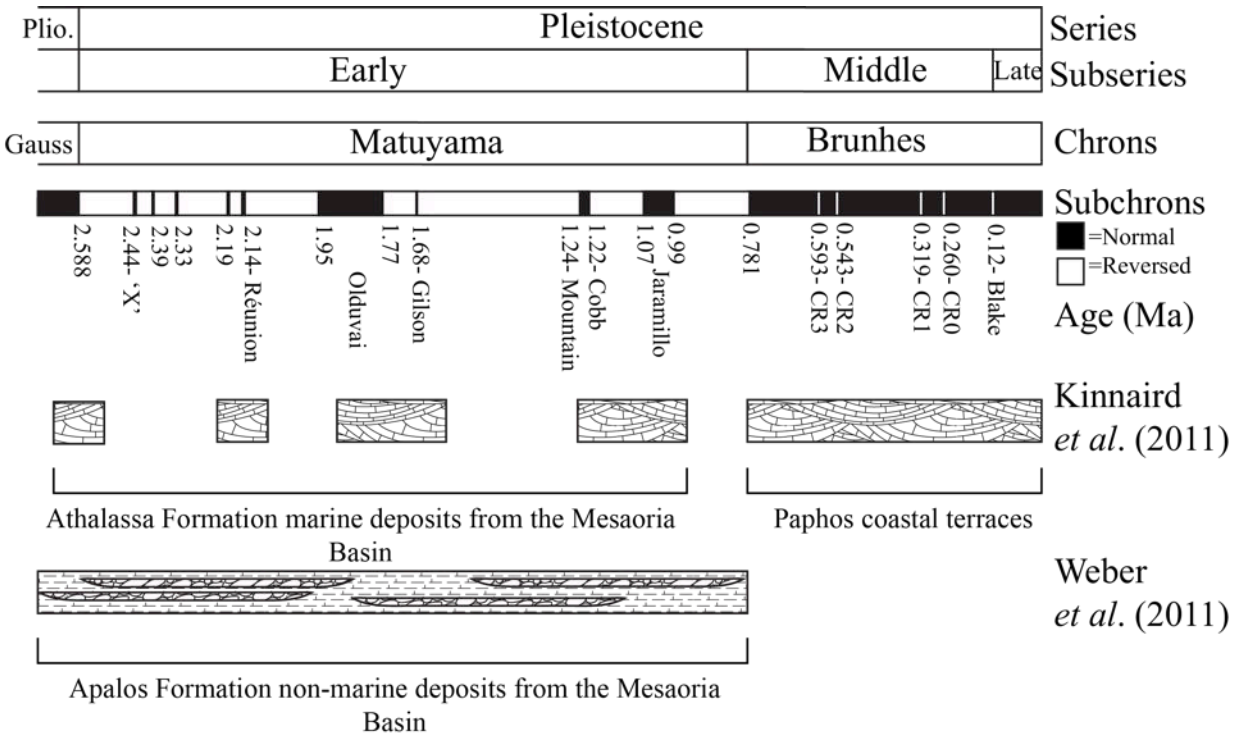

Figure 1.2: Magnetic reversals during the Pleistocene compared with dates from studies of deposits within the Mesaoria Basin, southern Cyprus.

High-temperature magnetic susceptibility experiments

Magnetic susceptibility is a quantitative measurement of how a material is magnetised by an applied magnetic field. The magnetic susceptibility characteristics of a sample are controlled by the Curie temperature of the magnetic grains contained

(Butler, 1992). Measuring the magnetic susceptibility characteristic of a sample during heating can be used to deduce the types of magnetic grains contained within the sample. This information is used to customise the demagnetisation measurements and improve the accuracy of the analysis. High temperature susceptibility experiments were carried out on the AGICO kappabridge apparatus at the School of GeoSciences, Univeristy of Edinburgh.

Demagnetisation experiments

Demagnetisation analyses are used to assess the stability and orientation of the magnetic signal of each sample (Butler, 1992). The technique involves measuring the magnetic orientation of samples at incrementally increased alternating magnetic fields (AF demagnetisation) or temperatures (thermal demagnetisation). Principle component analysis (PCA) can be carried out on the demagnetisation results to measure the stable and unstable magnetic components to finally calculate the inclination and declination of a sample from the stable magnetic component.

AF demagnetisation was carried out at the National Oceanography Centre, University of Southampton, using a 2G Enterprises Superconducting Rock Magnetometer that is set up for measuring discrete samples. AF demagnetisation is a relatively fast technique compared to thermal demagnetisation due to its automated nature, and was therefore used to assess the magnetic signal strength of all the samples. A number of sample sites appear to have no magnetic signal or no stable magnetic orientation. AF-demagnetisation was not able to remove the stable magnetic component from any of these samples; therefore, it was not used for calculating declinations and inclinations. Samples that showed promising magnetic signals were selected for thermal demagnetisation analysis.

Thermal demagnetisation was carried out at the University of Oxford using a 2-G Enterprises DC Squid Cryogenic Magnetometer for measuring magnetic field orientations and MMTD24 thermal demagnetiser for heating the sample to various temperatures. The thermal demagnetisation steps were: 50^{o}C steps from 0-300^{o}C, followed by 30^{o}C steps increasing up 590^{o}C. The increased frequency of steps was to focus analysis around the Curie temperate of magnetite (based upon the results from the susceptibility experiments, previously discussed). The quality of the data was based upon inspection

of the results when plotted on Zeijderled plots and from the intensity decay-curves. Each sample was ranked from A-C based upon the system developed by Richter *et al.* (1998), with 'A' representing samples with a clear stable magnetic direction and 'C' representing samples with either stable direction or no magnetic signal. The A and B quality data were selected from PCA analysis and are discussed in the next section.

Oxygen and carbon isotopes

Introduction

The stable isotopic signature of carbonate cements can be used to help understand the pore fluid and diagenetic history (Hudson, 1977; Allan and Matthews, 1977; Matthews and Allan, 1982). Two stable isotopes ratios are used, oxygen ($^{18}O/^{16}O$), and carbon ($^{13}C/^{12}C$); these are expressed as $\delta^{18}O$ and $\delta^{13}C$, respectively. The stable oxygen isotopic ratio ($\delta^{18}O$) is controlled by the composition, salinity and temperature of the host fluid (Nelson and Smith, 1996). The stable carbon isotopic ratio ($\delta^{13}C$) is controlled by the source of the CO_2 within the precipitating carbonate cement; for example, meteoric or sea-water, amount of shell dissolution or biochemical controls (Nelson and Smith, 1996).

Sample preparation

The carbonate cement between the grains within the grainstone was sampled using a dremel drill by myself. The cement was removed as a powder for isotopic analysis.

Stable isotope analysis method

Isotopic analysis was carried out in the Wolfson Laboratory, of the School of Geo-Sciences, University of Edinburgh. The analysis was carried out using the Thermo Electron Delta+ Mass Spectrometer with a Kiel Preparation Device by Colin Chilcott.

1.5 Eastern Mediterranean geological history

The following review describes the geological evolution of the Eastern Mediterranean, focusing on the aspects related to the geological history of Cyprus.

1.5.1 Pre-Mesozoic history

Prior to the Late Permian, the easternmost Mediterranean region formed the northern part of the Gondwanan continental margin (Garfunkel and Derin, 1984; Robertson and Woodcock, 1986). Rifting of the northern Gondwana margin began by the Middle to Late Permian, resulting in a widespread marine transgression of the area, giving rise to Middle Permian shallow-marine limestones in the Kyrenia Range (Robertson, 1998a)(Fig. 1.3).

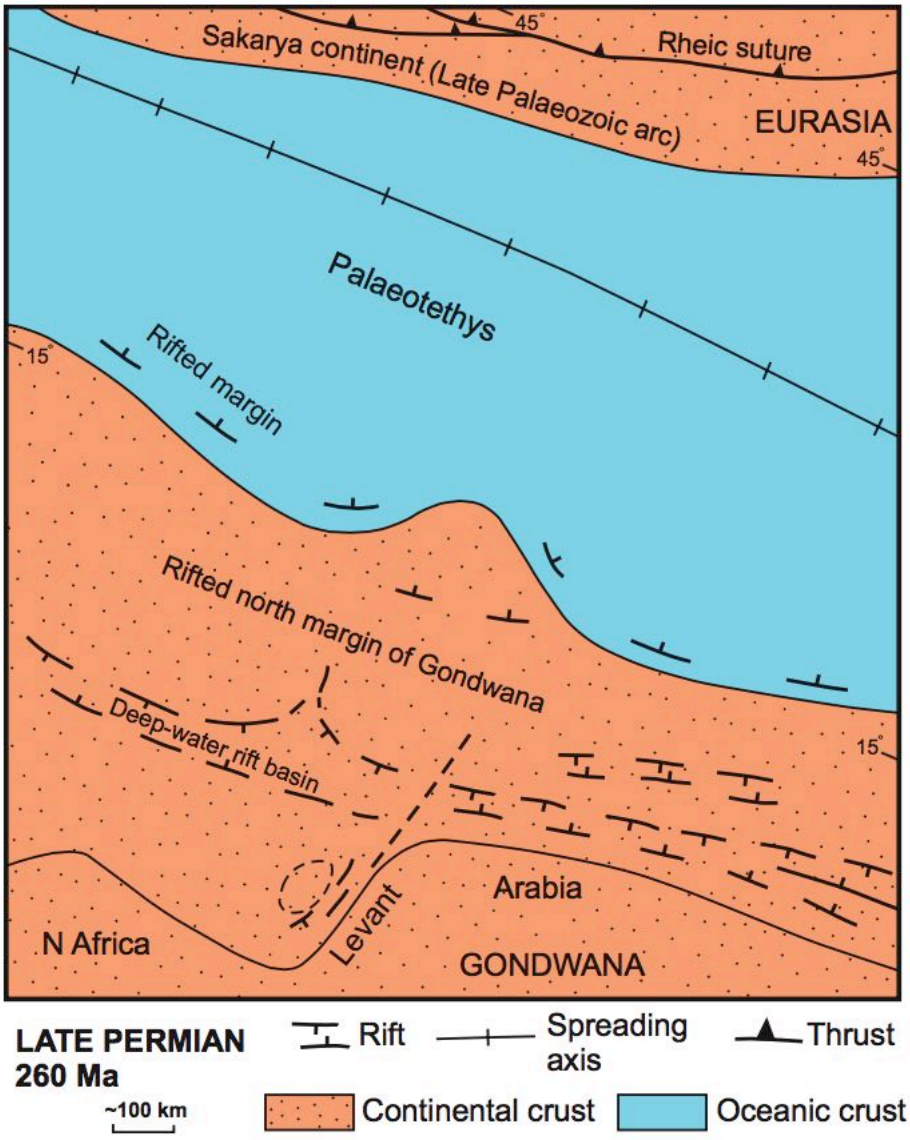

Figure 1.3: Late Permian tectonic setting of the Eastern Mediterranean (Robertson *et al.*, 2012a).

1.5.2 Triassic

Break-up of the Gondwanan margin took place between the Middle to Late Triassic (Robertson, 1998a). Ocean-floor spreading began during the Late Triassic (Carnian to Norian), with the eruption of MORB-type volcanics (Robertson, 1998a). The Eratosthenes Seamount (which plays a significant role in the Plio-Pleistocene evolution of Cyprus) lay to the south of the developing rift, but to the north of the Gondwana passive margin (Robertson, 1998a). During this period, large continental fragments rifted from Gondawa to form a mosaic of continents and basins within the Eastern Mediterranean region (Robertson and Dixon, 1984; Sengor *et al.*, 1984).

1.5.3 Jurassic to Early Cretaceous

The southern margin of the Neotethys experienced passive subsidence during this time. This subsidence is recorded by the development of carbonate platforms and the deposition of deep-water sediments along the Neotethyan passive margins (Robertson, 1998a)(Fig. 1.4).

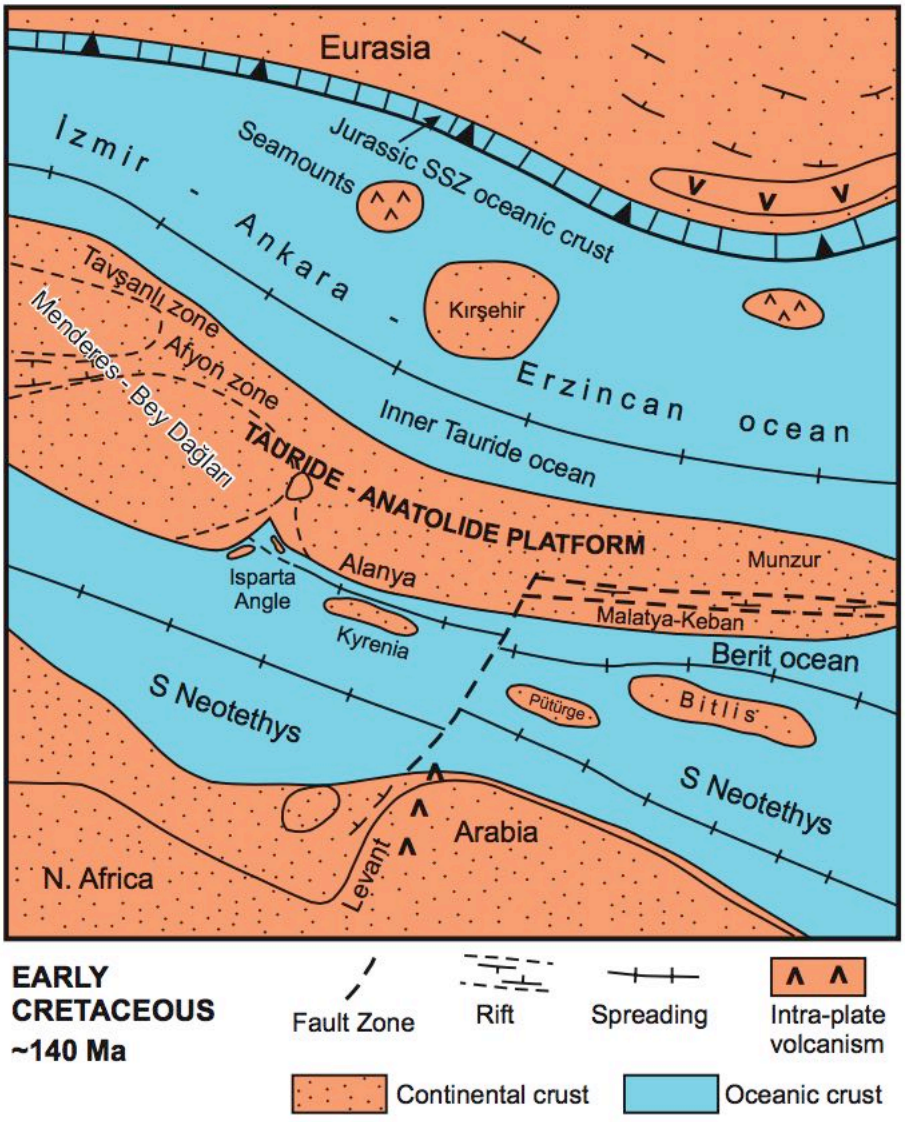

Figure 1.4: Early Cretaceous tectonic setting of the Eastern Mediterranean (SSZ= supra-subduction zone)(Robertson *et al.*, 2012a).

1.5.4 Late Cretaceous: Cenomanian to Turonian

From the early Late Cretaceous, African and Eurasian plates began to converge as the South Atlantic opened (Robertson, 1998a). A consequence of this convergence was the development of northward-dipping subduction zones within the southern Neotethys.

Cold, dense Triassic oceanic crust rolled back creating an extensional setting (ca. 150 km wide). Within this supra-subduction zone ophiolites formed, including the Troodos ophiolite (southern Cyprus) (Pearce and Robinson, 2010; Robertson, 1998a; Robertson, 2002). Carbonate platforms subsided leading to the deposition of pelagic sediments, e.g. on the Levant passive margin and in the Taurides.

1.5.5 Late Cretaceous: Turonian to Maastrichtian

Northward intra-oceanic subduction continued and the trench migrated towards the Arabian passive margin. Eventually, the trench collided with the Arabian passive margin around 70 Ma. The Troodos part of the supra-subduction zone shifted to the south, still remaining within the Neotethys ocean. Subduction was impeded by the collision of the intra-oceanic subduction zone with the Arabian margin; this resulted in ophiolite emplacement from Syria to Oman. The convergence of Africa and Eurasia then resulted in the counter-clockwise rotation of the Troodos microplate by ca. 90^o between the Late Campanian and the Early Eocene (Moores and Vine, 1971; Clube *et al.*, 1985; Morris, 1996; Robertson, 1998a; Inwood *et al.*, 2009).

The convergence of the African and Eurasian plates generated a continental margin-type subduction zone along the northern margin of the Southern Neotethys ocean (Robertson, 1998a). The Upper Cretaceous to Late Miocene development of the active continental margin was the dominant influence on the Kyrenia Range. The active margin extended eastward into the Misis-Andırın lineament of mainland southern Turkey (Robertson and Woodcock, 1986; Robertson, 1998a; Robertson *et al.*, 2012b).

1.5.6 Paleocene to Eocene

During the early Cenozoic (70 Ma to 48 Ma) the convergence of Africa and Eurasia may have paused temparilly (Robertson and Dixon, 1984; Savostin *et al.*, 1986). Dur-

ing the Eocene, convergence resumed and the remaining Neotethyan oceanic crust was subducted. This convergence resulted in the final closure of the seaway between the Arabian plate and Eurasia (Anatolia), which was complete by the Middle Miocene. During this time, ocean basins in the southern Neotethys closed as part of the African-Eurasia convergence with a resulting strong influence on the Kyrenia Range (Robertson *et al.*, 2013). During this time the Troodos Massif remained far enough south to avoid the deformation. Deep-sea carbonates accumulated on the Troodos ophiolite during this time.

1.5.7 Oligocene

Accumulation of siliciclastic turbidity currents derived from southern Anatolia occured in the Kyrenia Range during this time (Robertson, 1998a; McCay and Robertson, 2012a) (see Sec 1.5.8). To the south, pelagic carbonates accumulated on the Troodos Massif.

1.5.8 Miocene

Northwards subduction became active to the south of Cyprus (Robertson, 1998a). From the Early Miocene onwards, the Troodos was located on the over-riding plate of this northward-dipping subduction zone (Fig. 1.5). The Mesaoria (Mesarya) basin that separates the Kyrenia Range from the Troodos Massif and was undergoing extension due to slab roll-back at the Cyprus trench (Kinnaird and Robertson, 2013; McCay and Robertson, 2012b) The Messinian salinity crisis at the end of the Miocene is represented by gypsum deposits in shallow-water basins with halite precipitating in the deeper basins (Necdet and Anl, 2006; McCay and Robertson, 2012a).

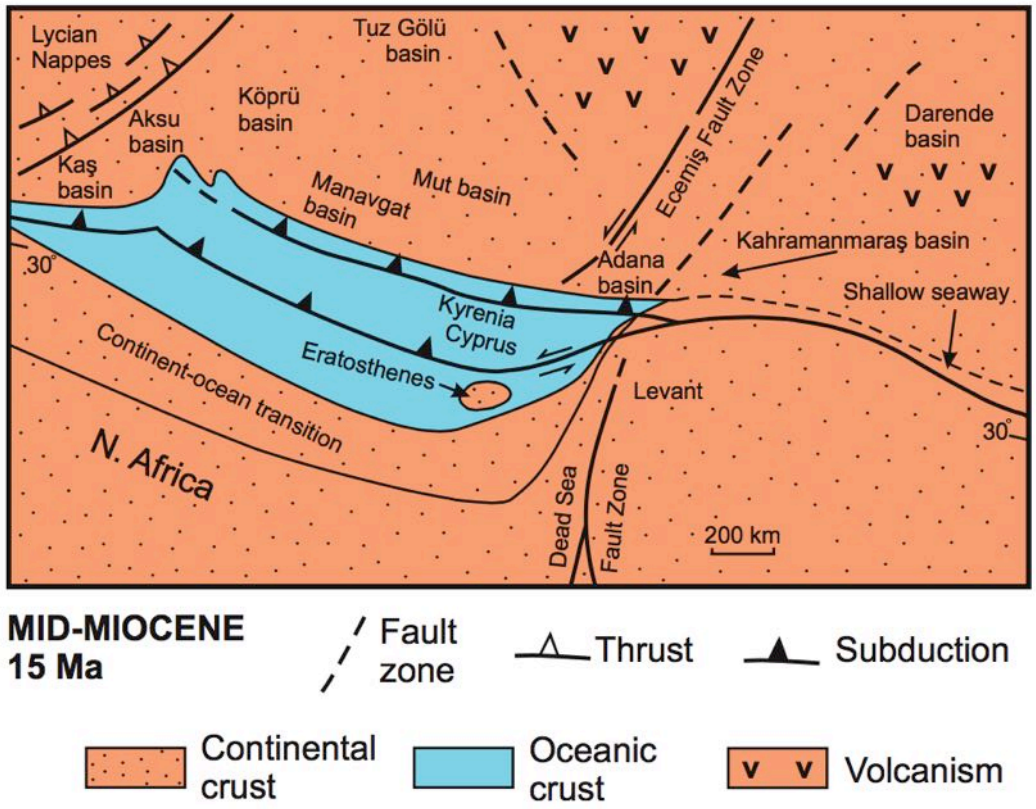

Figure 1.5: Middle Miocene tectonic setting of the Eastern Mediterranean (Robertson *et al.*, 2012a).

1.5.9 Pliocene to Pleistocene

The Pliocene begins with a major marine transgression after the Mediterranean salinity crisis. This resulted in the deposition of interbedded marls and chalks within the basins around Cyprus (Robertson, 1998a). The Late Pliocene to Early Pleistocene is represent by shallowing upwards marine facies within the Mesaoria (Mesarya) basin (McCallum and Robertson (1990, 1995a)). The details of the Plio-Pleistocene facies will be discussed in more detail in Section 1.7.

Northward convergence of Africa with Eurasia continued and finally brought the Erathosthenes Seamount into collision with the Cyprus trench to the south of Cyprus (Robertson, 1998a; Kempler, 1998). Rapid uplift of the Troodos Massif and the Kyrenia Range began during the Early Pleistocene as a result of the collision (Poole *et al.*, 1990; Poole and Robertson, 1991; Robertson and Xenophontos, 1993; Robertson, 1998a; Kin-

naird *et al.*, 2011). Ultramafic rocks within the overriding slab were serpentinzed and rose upwards diapirically, updoming the Troodos ophiolite (Robertson, 1998b).

Figure 1.6 illustrates the current tectonic setting of the Eastern Mediterranean. The Kyrenia Range lineament runs through the Levant Sea and connects with the Misis Mountains in Southern Turkey (Biju-Duval *et al.*, 1974; Biju-Duval and Montadert, 1977; Robertson and Woodcock, 1986; Aksu *et al.*, 1992; Robertson, 1998a; Robertson, 2000). The Plio-Pleistocene tectonics and uplift in the Eastern Mediterranean will be discussed in more detail in Section 1.7.

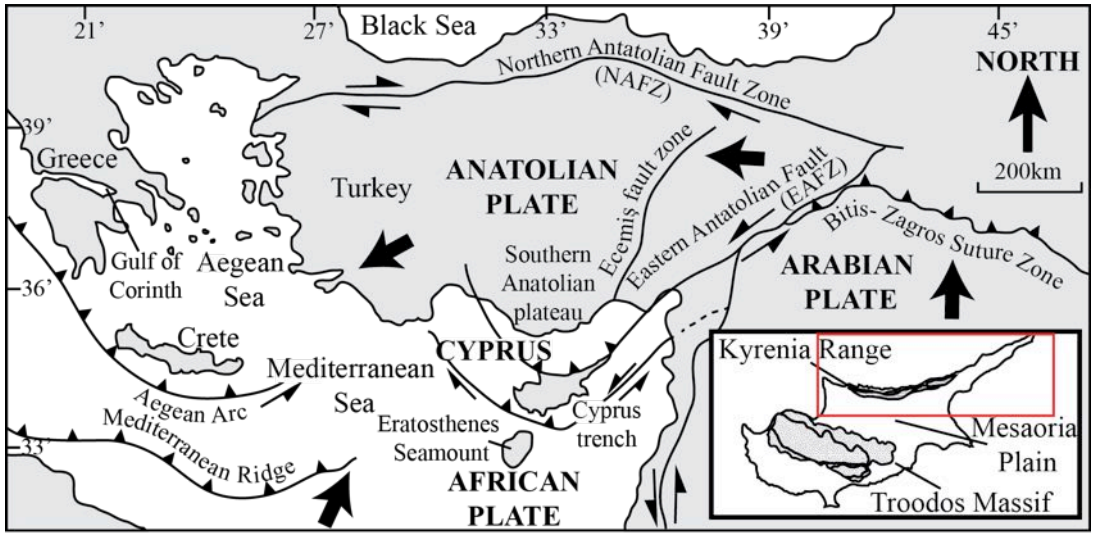

Figure 1.6: Tectonic setting of the eastern Mediterranean during the Plio-Pleistocene, adapted from McCay *et al.* (2012).

1.6 Lithostratigraphic framework of the Kyrenia Range

The geological history of the north of Cyprus is represented by four distinct Groups; the Trypa (Tripa), Lapithos (Lapta), Kythrea (Değirmenlik) and Mesaoria (Mesarya) Groups (Figs. 1.7, 1.8). The following section discusses the stratigraphy of these four group based upon previous authors work.

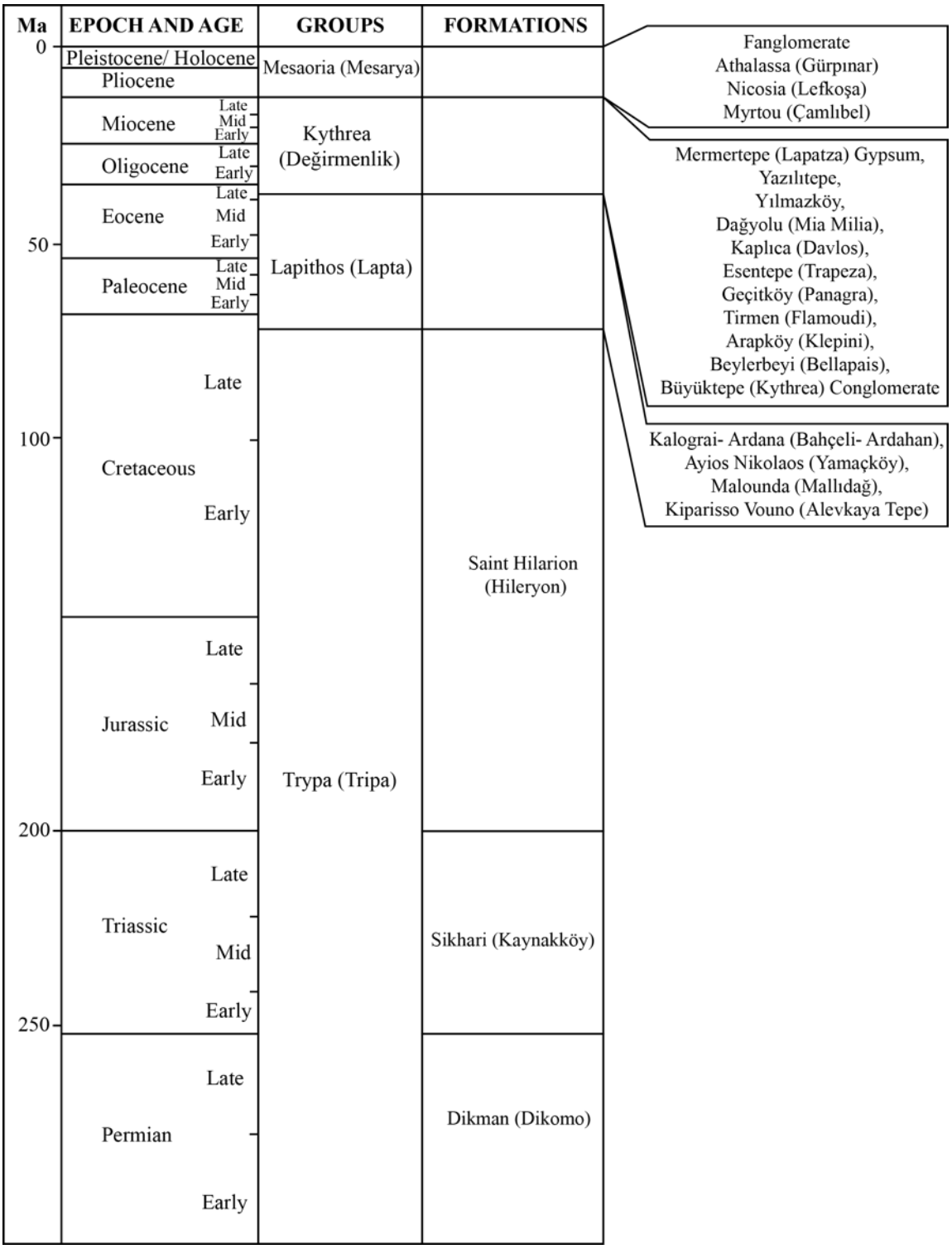

Figure 1.7: Summary diagram of the stratigraphy of northern Cyprus, adapted from Robertson and Woodcock, 1986; Robertson *et al.*, 2012b; and McCay *et al.*, 2012.

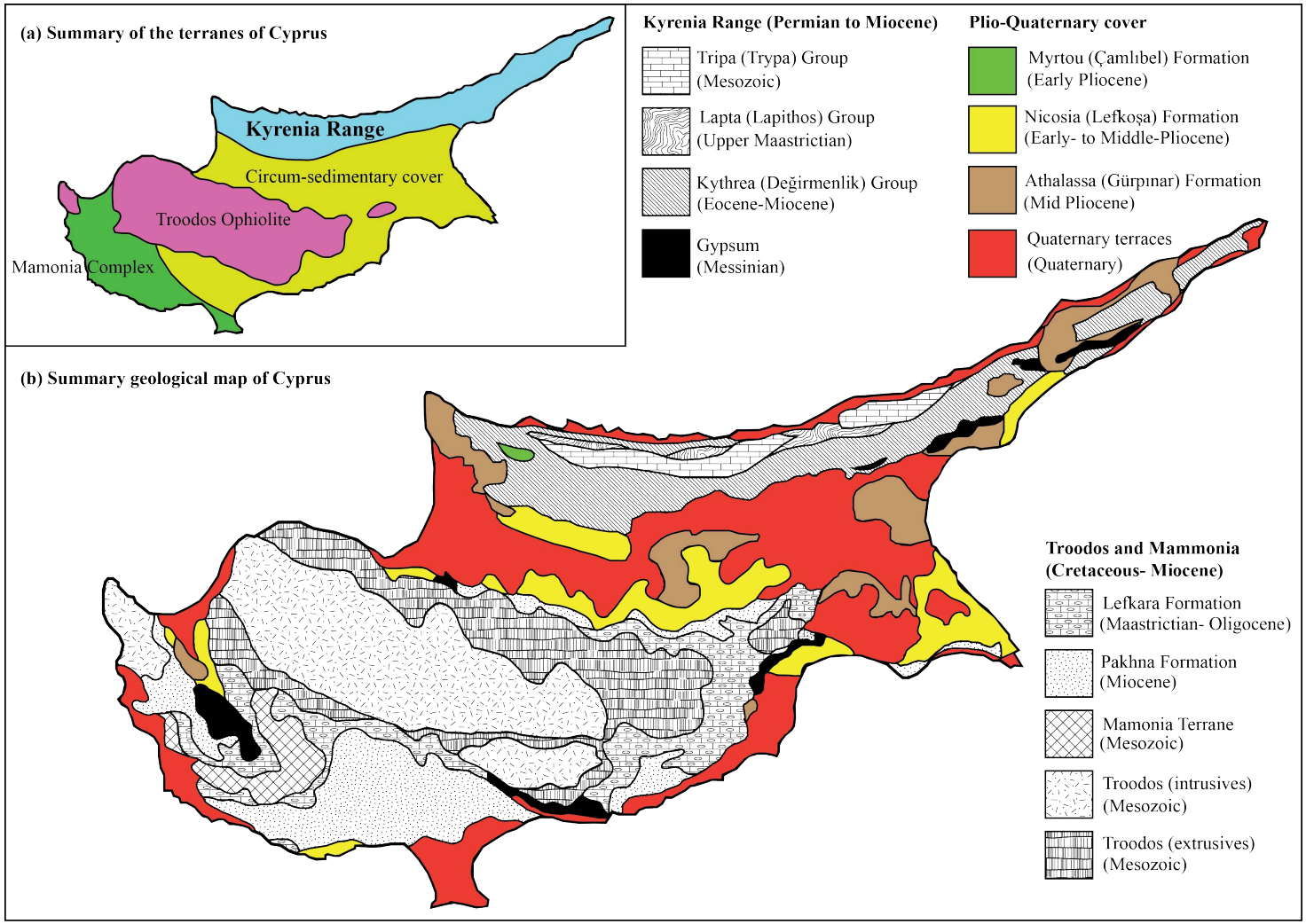

Figure 1.8: Simplified geological map of Cyprus with emphasis on the distribution of Plio-Pleistocene deposits, adapted from McCay *et al.* (2012) and McCay and Robertson (2012b).

1.6.1 Tripa (Trypa) Group (Permian-Cretaceous)

During the Mesozoic, the Kyrenia Range was a shallow-marine environment with extensive carbonate deposition. The carbonate form the Trypa (Tripa) Group, comprising the Dikmen (Dikomo), Sikhari (Kaynakköy) and Hilarion (Hileryon) Formations (Ducloz, 1972; Baroz, 1979; Robertson and Woodcock, 1986; Robertson *et al.*, 2012b). During this period, the range represented a passive margin undergoing subsidence (Ducloz, 1972; Baroz, 1979; Robertson and Woodcock, 1986). The Kyrenia Range underwent greenschist-facies metamorphism prior to Late Maastriction time, due to burial to ca. 5 km to 7 km (Baroz, 1979; Robertson and Woodcock, 1986). Robertson *et al.* (2012b) suggests that the southern edge of the platform was a detached thrust beneath the Tauride Platform, before exhumation due to either buoyancy of the crust or slab roll-back related to a subduction zone further south.

1.6.2 Lapta (Lapithos) Group (Upper Maastrictian)

The Lapithos (Lapta) Group represents the Late Maastrictian to Late Eocene time period. This group comprises intercalated basic and silicic lavas, pelagic carbonates and breccias. The Lapithos Group comprises the Kiparisso Vouno (Alevkaya Tepe member), Melounda (Mallıdağ), Ayios Nikolaos (Yamaçköy) and Kalograi-Ardana (Bahçeli-Ardahan) Formations (Ducloz, 1972; Baroz, 1979; Robertson and Woodcock, 1986; Robertson *et al.*, 2012b).

1.6.3 Kythrea (Değirmenlik) Group (Eocene-Miocene)

The Lapta (Lapithos) Group is unconformably overlain by the Kythrea (Değirmenlik) Group, which represents the Late Eocene to Late Miocene time period. The Kythrea (Değirmenlik) Group is made up of twelve formations including the Büyüktepe (Kythrea), Bellapais (Beylerbeyi), Arapköy (Klepini), Tirmen (Flamoudi), Geçitköy (Panagra), Beşparmak (Trapeza), Kaplıca (Davlos), Dağyolu (Mia Milia), Yılmazköy, Yazılıtepe, Mermertepe (Lapatza) and Çamlıbel Formations (Robertson and Woodcock, 1986; McCay *et al.*, 2012; McCay and Robertson, 2012a; McCay and Robertson, 2012b).

The Büyüktepe (Kythrea) conglomerate and the Bellapais (Beylerbeyi) Formation represent a basal conglomerate and a coarse- to medium-grained sandstone, respectively.

The basal conglomerate is 50-70 m thick and mainly consists of channelised, parallel and cross-bedded, clast-supported conglomerates and coarse sandstones. The Bellapais (Beylerbeyi) Fomation is dominated by coarse- to medium-grained lithic sandstones. The Arapköy (Klepini) Formation is composed of fine-grained sandstones, siltstones and marls. The Tirmen (Flamoudi) Formation is composed of medium- to fine-grained calcareous sandstones and marls. The Geçitköy (Panagra) Formation is made up of red hemipelagic marls. The Esentepe (Trapeza) Formation is composed of grey and white marls. The Kaplıca (Davlos) Formation is a thick-bedded, massive, fine-grained sandstone unit. The Dağyolu (Mia Milia) formation is composed of fine-grained sandstones and marls. The Yılmazköy Formation is composed of brown marls, mudstones and sandstones. The Yazılıtepe Formation is composed of chalky clay, limestone, sandstone and marl. The Mermertepe (Lapatza) Formation is a gypsum deposit (Weiler, 1970; Ducloz, 1972; Hakyemez *et al.*, 2000; McCay *et al.*, 2012; McCay and Robertson, 2012a; McCay and Robertson, 2012b).

The basal conglomerate was sourced from the, by then, uplifted Kyrenia Range and from Anatolia to the north during the Late Eocene in a non-marine to shallow-marine environment. The overlying sandstones and siltstones represent tectonic subsidence and submergence of Kyrenia Range during the Oligocene to Early Micocene (McCay and Robertson, 2012a). Clastic sediment during this period was supplied from southern Turkey. During the Middle to Late Miocene the local E-W Kythrea (Değirmenlik) Fault divided the basin in two sub-basins, with dominant sedimentation occuring in the northern sub-basin (McCay *et al.*, 2012). The Late Eocene to Late Miocene sediments of northern Cyprus accumulated in a relict deep-sea basin that remained during and after the final collision of the Southern Neotethys (McCay and Robertson, 2012a).

1.6.4 Mesaoria (Mesarya) Group (Pliocene-Pleistocene)

The Mesaoria (Mesarya) Group represents the most recent phase in the geological history of Cyprus. The group can be divided into several formations including, the Myrtou (Çamlıbel), Nicosia (Lefkoşa), Athalassa (Gürpınar), Kakkaristra, Apalos and Fanglomerate Formations (Baroz, 1979 and McCallum and Robertson, 1995b). The distribution of the Mesaoria (Mesarya) Group in Cyprus is shown in Figure 1.8.

Myrtou (Çamlıbel) Formation

The Myrtou (Çamlıbel) Formation is composed of a mixture of marls and siltstones, with abundant benthic foraminifera. In local areas, the base of the section contains conglomerates with clasts of gypsum and occasional sandstones and mudstones (Lytras, 1962; Baroz 1979; and Yetis *et al.*, 1995; McCay *et al.*, 2012). The base of the formation unconformably overlies the Kythrea (Değirmenlik) Group. The upper boundary of the formation is a conformable transition to the Nicosia (Lefkoşa) Formation (Baroz, 1979; Hakyemez *et al.*, 2000). The Myrtou (Çamlıbel) Formation is only found in the western part of northern Cyprus (Fig. 1.8). Thickness estimates vary from 50 m to 300 m (Baroz, 1979 and Yetis *et al.*, 1995). The formation is dated using planktic foraminifera, *Globorotalia margaritae* as recognised by Baroz (1979), providing an Early Pliocene age for the formation (Yetis *et al.*, 1995).

Nicosia (Lefkoşa) Formation

Name and type locality

The formation was initially defined by Russell (1882) as the Nicosia Beds and was redefined by Henson *et al.* (1949) as the Nicosia Formation; it was renamed the Lefkoşa Formation by Hakyemez *et al.* (2000). Hakyemez *et al.* (2000) describes the best exposure of this deposit in the north of Cyprus, at Dilekkaya (Agia) village.

Lithology and variations

The Nicosia (Lefkoşa) Formation is composed of bioclastic limestones, sandstones, mudstones, marls, chalks and conglomerates (Saucier and Major, 1963; Baroz, 1979; Yetis *et al.*, 1995). In the north of Cyprus the dominant lithologies are chalks and marls. Both of these units are rich in planktic and benthic foraminifera as well as various macro fossils (Baroz, 1979).

Lower and upper boundaries

The lower boundary of the Nicosia (Lefkoşa) Formation unconformably overlies the Tripa (Trypa), Lapta (Lapithos) and Kythrea (Dęgirmernlik) Groups (McCay and

Robertson, 2012a). The upper boundary of the unit is generally conformable or occasional disconformable with the Athalassa (Gürpınar) Formation (Baroz, 1979; Robertson and Woodcock, 1986; Harrison *et al.*, 2004).

Thickness and regional extent

The Nicosia (Lefkoşa) Formation is up to 20 m thick (Baroz, 1979) and is found on the southeast and southwestern regions of northern Cyprus (Fig. 1.8). In particular, significant Nicosia (Lefkoşa) Formation deposits are preserved within the eastern and western ends of the Mesaoria (Mesarya) Plain.

Dating evidence

The planktic foraminifera, *Globorotalia puncticulata* was found by Baroz (1979) and delineates the formation as within the Piacenzian Stage of the Pliocene.

Athalassa (Gürpınar) Formation

Name and type locality

The unit was first defined by Reed (1935) as the "Upper Pliocene deposit" and was later termed the Athalassa Formation by Henson *et al.* (1949). The formation was then renamed the Gürpınar Formation by Hakyemez *et al.* (2000). The Athalassa (Gürpınar) Formation takes its name from the Athalassa district within Nicosia (Lefkoşa) city.

Lithology and variations

The main lithologies that form the Athalassa (Gürpınar) Formation are calcarenite or calcirudite, depending on the ratio of detrital fragments to carbonate debris (McCallum and Robertson, 1995; Harrison *et al.*, 2004). Three types of calcarenite are documented; first, planar-stratified calcarenites; second, cross-stratified calcarenites; and third, fine-grained, massive calcirudites (McCallum and Robertson,1995a). Other facies occur as minor horizons in the Athalassa (Gürpınar) Formation, include wacke-

stones which contain macro fossil fragments and thin conglomerate horizons.

Lower and upper boundaries

The Athalassa (Gürpınar) Formation overlies older lithologies such as those of the Tripa (Trypa), Lapta (Lapithos) and Kythrea (Dęgirmernlik) Groups on the western and eastern parts of the Kyrenia Range. The lower boundary of the Athalassa (Gürpınar) Formation is a conglomerate consisting of Kyrenia- and Troodos-derived clasts (Baroz 1979; Robertson and Woodcock, 1986; McCallum and Robertson, 1995a). Overlying this, is the main unit of calcarenites and calcirudites (McCallum and Robertson, 1995; Harrison *et al.*, 2004).

Thickness and regional extent

The Athalassa (Gürpınar) Formation can be found on the western and eastern flanks of the Kyrenia Range and the Mesaoria (Mesarya) Basin (Fig. 1.8). The thickness of this deposit is up to ca. 50 m in the Ovgos (Dar Dere) area (Baroz, 1979).

Dating evidence

The planktic foraminifera, *Globorotalia crassaformis* was identified by Baroz (1979) and is used to define the formation as Middle Pliocene onwards.

Fanglomerate Formation

The Fanglomerate Formation in northern and southern Cyprus is discussed in Section 1.7.

1.6.5 Ovgos (Dar Dere) fault zone

The Ovgos (Dar Dere) fault zone divides the Kyrenia (Girne) and Troodos tectonic domains (McCay and Robertson, 2012b). The Ovgos (Dar Dere) fault zone has undergone multiple phases of deformation, including northward extension (or transtension)

during the Oligocene to Mid-Miocene, sinistral strike-slip to transpression during the Late Miocene, and finally left-lateral, strike-slip during the Late Pliocene to Pleistocene (Harrison *et al.*, 2004; McCay and Robertson, 2012b). The most recent deformation along the Ovgos (Dar Dere) fault zone is related to the stress regime caused by the tectonic escape of Anatolia from the Neogene onwards (Fig. 1.6)(Reilinger *et al.*, 2000; McClusky *et al.*, 2000; Harrison *et al.*, 2004; McCay and Robertson, 2012b).

1.7 The Eastern Mediterranean during the Plio-Pleistocene

The ongoing convergence of the African and Eurasian plates in the Eastern Mediterranean has been demonstrated in several studies using extensive GPS data collected over the last three decades (Kahle *et al.*, 1998; Fernandes, 2003; McClusky *et al.*, 2003). The convergence of the African and Eurasian plates results in the northward movement of the African and Arabian plates and the westward "tectonic escape" of the Anatolian plate (Barka and Reilinger, 1997; McClusky *et al.*, 2000; Westaway, 2003)(Fig. 1.9). The "tectonic escape" of the Anatolian plate is likely to be taken up, at least in part, in Cyprus along the Ovgos (Dar Dere) Fault zone, which seperates northern and southern Cyprus (Harrison *et al.*, 2004; McCay and Robertson, 2012b)(Fig. 1.9).

A variety of tectonic processes are observed during the Plio-Pleistocene in the Eastern Mediterranean, including: uplift, subsidence, brittle and ductile deformation, varying rates of plate convergence and divergence, slab detachment, seamount-trench collision and volcanism (summarised by Schattner (2010)). The interplay of several Plio-Pleistocene tectonic processes results in the surface uplift of various regions within the Eastern Mediterranean (Fig. 1.9). A number of studies have focused on uplift in Southern Anatolia (Faccenna *et al.*, 2006; Schildgen *et al.*, 2012), the Ecemiş fault zone (Jaffey and Robertson, 2005), Misis-Andirin Ridge (Kempler and Garfunkel, 1994), the Syrian coastline (Dodonov *et al.*, 2008) and finally, the Troodos Massif in southern Cyprus (Robertson, 1977; McCallum and Robertson, 1990; Poole *et al.*, 1990; Kinnaird *et al.*, 2011). These studies have shown varying timings and rates of uplift in the region, with areas of major uplift (ca. >0.5 mm/yr) and areas of minor uplift (ca. <0.3 mm/yr)(Fig. 1.9). Focused major uplift occurs in southern Cyprus (Poole *et al.*, 1990; Kinnaird *et al.*, 2011) and southern Anatolia (Schildgen *et al.*, 2012) during the Early

Pleistocene. The tectonic mechanisms that drove the uplift include the Eratosthenes crustal edifice collision with the Cyprus Arc (Robertson, 1998b) and slab detachment of the down-going African oceanic crust beneath southern Anatolia (Faccenna *et al.*, 2006; Dilek and Sandvol, 2009).

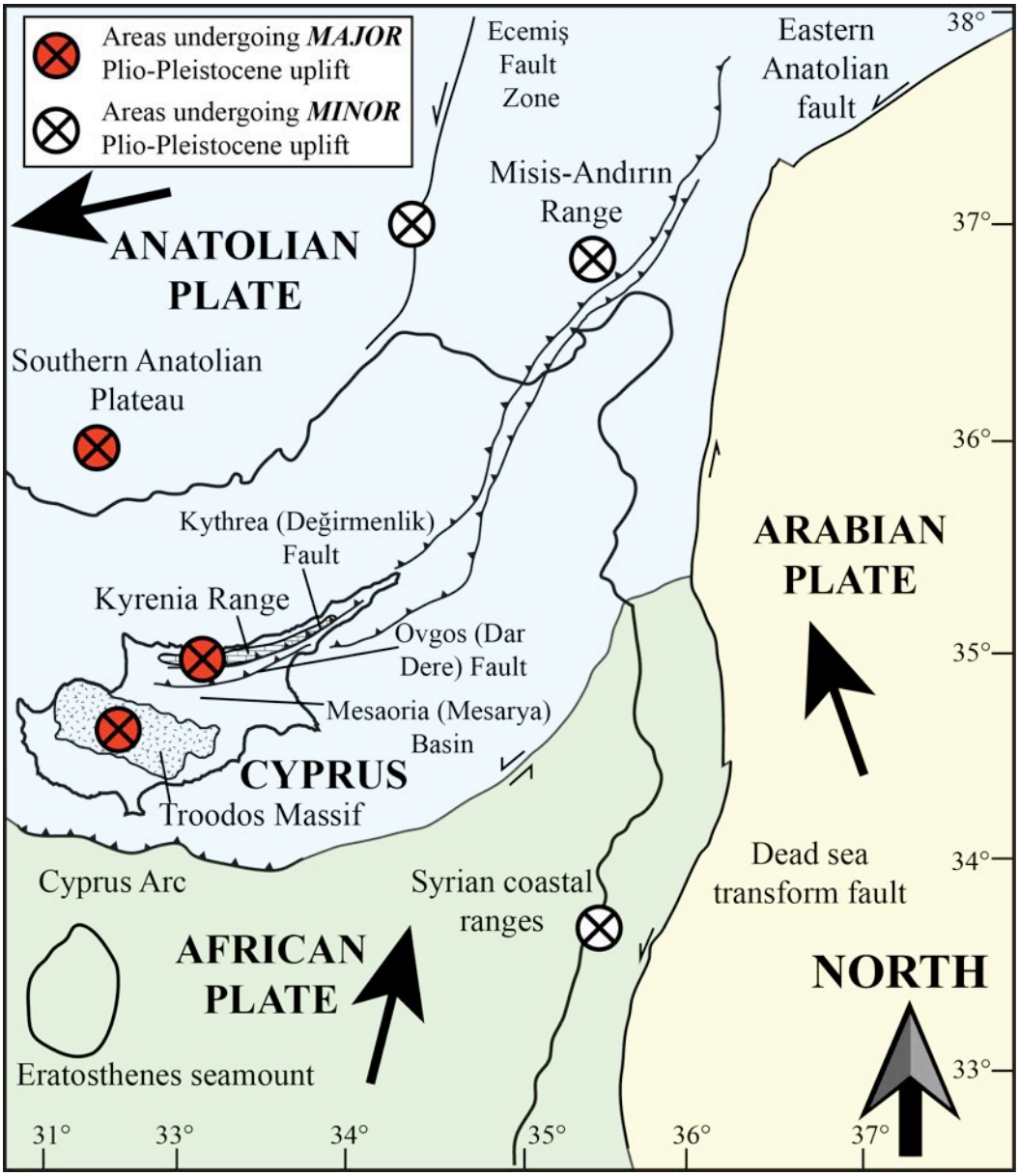

Figure 1.9: Summary diagram of the tectonic setting surrounding Cyprus during the Plio-Pleistocene, adapted from Kempler and Garfunkel (1994) with additional information taken from Barka and Reilinger (1997); Jaffey and Robertson (2004); McClusky *et al.* (2003); Calon *et al.* (2005b); Dilek and Sandvol (2009); Schattner (2010); McCay and Robertson (2012b); Schildgen *et al.* (2012).

1.7.1 Pleistocene uplift of Cyprus

The uplift of Cyprus can be divided into two geographic areas, the Troodos Massif and the Kyrenia Range (Fig. 1.8). During the Pliocene to Pleistocene, the Troodos Mountains and the Kyrenia Range uplifted from roughly sea level to 1,952 m (Mount Olympus in the Troodos Mountains) and 1,024 m (Selvili tepe (Kiparissovouno) in the Kyrenia Range).

The uplift of the Troodos Massif

The Troodos Massif is defined as an uplifted Late Cretaceous-aged ophiolite by a variety of studies, using a combination of field mapping, structural studies, palaeomagnetic analysis, borehole and geochemical evidence (summarised by Robertson and Xenophontos (1993)). During the Plio-Pleistocene the Troodos Massif underwent domal uplift, exposing the basal oceanic crust lithologies at the centre and highest points, progressively moving up through the ophiolite sequence, away from the centre of the mountain range (Robertson, 1977). The uplift was shown to be driven by the collision of Eratosthenes Seamount (crustal edifice) with the Cyprus Trench (Robertson, 1998b), south of the island, which resulted in diapiric protrusion of serpentine in the lower crust causing domal uplift (Shelton, 1993).

The focus of research for understanding the timings and rates of uplift of the Troodos Massif has been on the sedimentary cover and understanding how the depositional environments during the Plio-Pleistocene have responded to tectonic, eustatic and climatic processes. The shallowing of the Mesaoria Basin from a shallow-marine sea-way to non-marine environments during the Early Pleistocene represents the earliest stage of uplift (McCallum and Robertson, 1995a). During this early phase of uplift fan-delta systems develop, draining off the Troodos Massif and into the Mesaoria Plain (McCallum and Robertson, 1995b; Schirmer *et al.*, 2010; Weber *et al.*, 2011). Combined sedimentary facies and structural studies suggested gradual uplift during the Early Pleistocene followed by focused rapid uplift during the Early to Middle Pleistocene (McCallum and Robertson, 1990).

The main Pleistocene uplift resulted in a series of marine and non-marine terraces, which were studied and dated to understand the rates and timings of uplift. The Pleistocene terraces can be divided into either coastal marine and aeolianite terraces (Poole

and Robertson, 2000) or a series of fluvial drainage systems (Poole and Robertson, 1998). Five major terraces are defined in southern Cyprus, F0-F4, at 350 m to 360 m, 110 m to 100 m, 60 m to 50 m, 11 m to 8 m and 2 m to 3 m above modern sea level. The marine terraces all show a similar history, firstly a marine transgression (maximum flooding) and then a gradual regression. The transgression is marked by a basal clastic lag, boring, mollusc death assemblages and red algae, with coral representing sea-level high stands. The regression is marked by heavy reworking, clastic input and a change in depositional environment from shore face to back shore (Poole and Robertson, 2000). The fluvial deposits are mainly composed of interbedded conglomerates and mudstones. The more proximal deposits are matrix supported, poorly sorted, weakly consolidated and immature. The more distal deposits compose of fine-grained clastic sediments with occasional cross-bedding structures (Poole and Robertson, 1991).

Several quantitative dating studies of Pliocene and Pleistocene terraces constrained the timings and rates of uplift of the Troodos Massif. Uranium-series dating of coral from the marine terraces showed that the marine terraces formed during the Middle to Late Pleistocene (Poole *et al.*, 1990). Palaeomagnetic analysis was carried out on the shallow-marine and fan-delta deposits within the Mesaoria Basin and marine and non-marine terraces along the southern coast (Kinnaird *et al.*, 2011). The palaeomagnetism results showed that the shallow marine environment within the Mesaoria Basin continued into the Early Pleistocene, during which time the Troodos Massif was undergoing gradual uplift. In addition, the coastal terraces were shown to be <0.78 Ma, indicating continued uplift during the Middle to Late Pleistocene.

The development of the terraces was principally controlled by tectonic processes, however a number of studies have shown that the Pleistocene terraces were also strongly affected by global sea-level changes and climate. To form the stepped terraces along the Cypriot coast and for each terrace to have a regressive sedimentary sequence requires a combination of both tectonic and eustatic processes (Poole and Robertson, 1991; Poole and Robertson, 2000). The youngest terraces in Cyprus that formed during the Late Pleistocene are likely to have been affected by the interaction of sea-level change and tectonic uplift (Poole and Robertson, 1991).

The Pleistocene fluvial drainage systems are made up of massive bedded to channelised conglomerates interbedded with mudstone deposits, and are draining away from the Troodos Massif and towards the coast (Poole and Robertson, 1998). The drainage

systems represent a series of fluvial terraces (F0-F4) with older terraces being truncated by the younger terraces. Poole and Robertson (1998) suggested that the primary control of terrace morphology and sedimentology was tectonics. More recent studies have shown the nature of the conglomerate facies within the Late Pleistocene deposit is also strongly controlled by climate (Waters *et al.*, 2010). This study suggested increased precipitation during the Late Pleistocene causing higher-energy fluvial drainage during a time of limited tectonic activity.

1.7.2 Uplift of the Kyrenia Range

The Kyrenia Range is suggested to have uplifted contemporaneously with the Troodos Massif during the Plio-Pleistocene (De Vaumas, 1961; Robertson, 1977). Three major issues are apparent when trying understand the uplift of the Kyrenia Range. Firstly, what is the structure of the crust of the Kyrenia Range and the Mesaoria Basin. Secondly, is the Kyrenia Range affected by deeper mantle processes during the Plio-Pleistocene? Thirdly, is the Kyrenia Range uplifted related to the uplift of the Troodos Massif?

Crustal structure

Several models have been have proposed for the crustal structure of the Kyrenia Range and Mesaoria (Mesarya) Basin (Fig 1.10). The evidence for these models is either based on field sedimentology and structural measurements or offshore seismic profiles. The model proposed by McCallum and Robertson (1990) described the Mesaoria Basin as an asymmetric half graben (Fig 1.10(a)). The asymmetric half graben is suggested to have initially formed during an older phase of extension, following this, the older extensional faults were reactivated as compressional faults during the Plio-Pleistocene. The model proposed by Calon *et al.* (2005b) describes a "piggy-back" basin with deep-seated thrust faults driving uplift (Fig 1.10(b)). This model suggests that the older extensional faults were not reactivated, in stead new, deep-rooted, thrusts developed in response to the compressional setting. Harrison *et al.* (2004) focused on the Ovgos (Dar Dere) fault zone in the Mesaoria (Mesarya) Basin describing it as undergoing strike-slip deformation during the Pleistocene. From this work the underlying structure of northern Cyprus was also postulated as a series of thrust faults (Fig 1.10(c)), although this was not based on any new data from the Kyrenia Range. McCay and Robertson (2012b) focused on the Upper Miocene to Pleistocene structures of the Kyrenia Range

and in Mesaoria (Mesarya) Basin. This study showed southward-directed thrusting and sinistral transpression during the Late Miocene to Early Pliocene, resulting in a series of major thrust sheets making up the Kyrenia Range and the Mesaoria (Mesarya) Basin (Fig 1.10(d)). The studies by McCay and Robertson (2012b) and Harrison *et al.* (2004) do not focus on the Pleistocene uplift, but nevertheless, do present more recent onshore data regarding the structure of the Kyrenia Range and the Mesaoria (Mesarya) Basin.

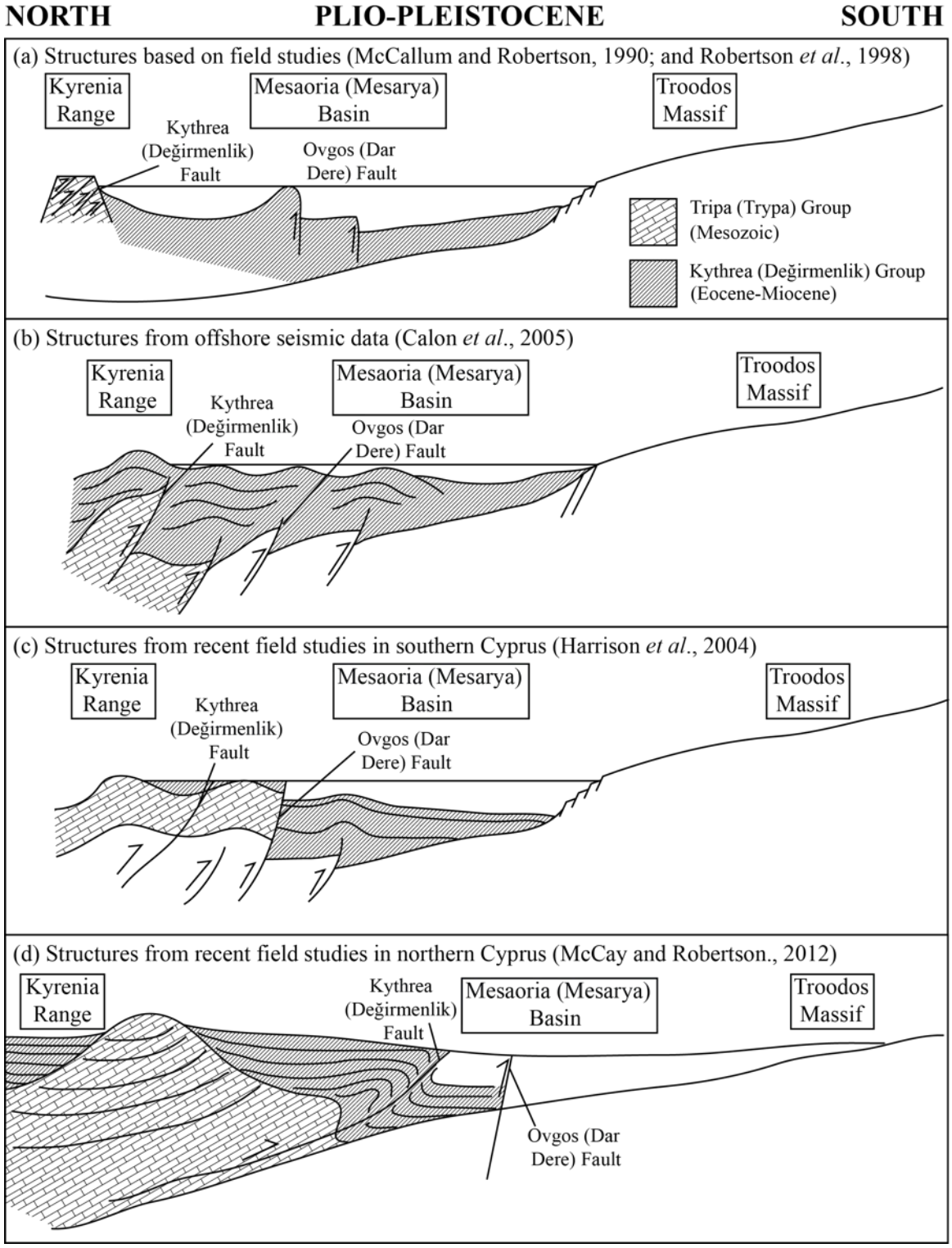

Figure 1.10: Alternative models for the structure of northern Cyprus (McCallum and Robertson, 1990; Robertson, 1998a; Harrison *et al.*, 2004; Calon *et al.*, 2005b; McCay, 2010; McCay and Robertson, 2012b).

Slab detachment

Uplift of the southern margin of the Central Anatolian plateau in Turkey has been an ongoing process during the Late Cenozoic (Schildgen *et al.*, 2012). This uplift has been primarily attributed to the detachment of the down-going African oceanic crust (Faccenna *et al.*, 2006; Schildgen *et al.*, 2012; Delph *et al.*, 2015). Several studies have used p-wave seismic tomography and gravity anomaly data to understand the nature of the disarticulated African oceanic crust, which is subducting northward of the Cyprus trench (Faccenna *et al.*, 2006; Dilek and Altunkaynak, 2009). The process of slab detachment has been suggested to have a major control on the uplift of southern Anatolia and on the Northern Anatolian fault zone (Faccenna *et al.*, 2006; Dilek and Altunkaynak, 2009; Schildgen *et al.*, 2012; Schildgen *et al.*, 2014; Cosentino *et al.*, 2012). The various models suggest that the tearing on the down going slab occurs north of Cyprus hence crustal influences of Anatolia but not Cyprus.

Eratosthenes Seamount

The Eratosthenes Seamount is a crustal fragment that was rifted from the African continental margin during the Triassic. During the convergence of the African and Eurasian margins the Eratosthenes Seamount has progressively moved towards Cyprus (Robertson, 1998b). Collision of the seamount with the Cyprus Trench occurred during the Early Pleistocene and was the primary driving mechanism for the uplift of the Troodos Massif (Robertson, 1977; Kempler, 1998; Robertson, 1998b). It is implied by numerous workers that the impact of the Eratosthenes Seamount collision not only influenced Cyprus but caused wider reaching compression and uplift in the Eastern Mediterranean (Schattner, 2010; Schildgen *et al.*, 2012; Schildgen *et al.*, 2014). Schildgen *et al.* (2012) suggests that increased uplift rates of the Southern Anatolian Plateau from 1.6 Ma (Early Pleistocene) to present are attributed to major regional compression due to the collision of the Eratosthenes Seamount with the Cyprus Trench. Hence, when discussing the uplift of the Kyrenia Range the Eratosthenes Seamount must be taken into account.

1.8 Uplifted terraces of the Kyrenia Range

The uplift of the Kyrenia Range resulted in the formation of a series of marine and non-marine terrace deposits on the northern and southern flanks of the range. Unlike,

that of the Troodos Massif, the Pleistocene cover of the Kyrenia Range has been the focus of only a handful of studies. Previous work has provided a limited stratigraphy of the Pleistocene deposits. No modern sedimentology or quantitative dating studies had been carried out upon these deposits. The following sections describes the stratigraphy and mapping work previously carried out on the Pleistocene terraces in northern Cyprus.

1.8.1 Previous Pleistocene terrace mapping

During the early 1960s, C. Ducloz and P. Knup worked on a United Nations funded project to map and understand the geology of the Kyrenia Range. This work resulted in the first geological map that demonstrated the distribution of the Pleistocene terraces in the central Kyrenia Range. This work differentiated the Pleistocene terraces based upon their geomorphology and relative differences in height above modern sea-level.

Ducloz mapped the area between Çatalcöy (Agios Epikitikos) and Karaagaç (Charkeia), whereas Knup mapped a region further east, between Karaagaç (Charkeia) and Kaplıca (Davlos). Ducloz (1964) defined five terraces on the northern side of the central Kyrenia Range. By comparison, Knup (1965) defined twelve terraces on both the northern and southern flanks of the range.

Ducloz and Knup briefly described the stratigraphy of each of the defined terraces. Generally their descriptions agree, however, there are a few exceptions. The Karka terrace is described by both authors as being composed of fossil talus breccias, lacustrine deposits, marls, chalks and gravels. The upper continental terraces defined by Knup are described as being composed of gravel. The lower terraces are described by both authors as being composed of calcarenite, gravel, marl, sand and a calcitic crust. The only exception to this description of the lower terraces is by Knup, who describes the Kyrenia (Girne) terrace as being made up of calcarenite and gravel whereas, the Koupia terrace is only made up of calcarenite.

1.8.2 Previous Pleistocene terrace stratigraphy

A more detailed stratigraphy of the the Pleistocene terraces was given by Ducloz (1972) and by Baroz (1979). Ducloz (1972) produced a bulletin for the Cyprus Geological Survey describing the stratigraphy of the Pleistocene terrace deposits around Arapköy (Klepini) village in the central Kyrenia Range. This work documented five terraces, namely the Karka, Klepini (Arapkóy), Trapeza (Beşparmak), Agios Epikitikos (Çatalcöy) and Kyrenia (Girne) terraces. Ducloz (1972) compared his terrace stratigraphy to terraces around the Mediterranean and used biostratigraphy to approximate ages for each terrace. F. Baroz completed his Doctor of Science degree on the Geology of northern Cyprus in 1979. Within his thesis, a chapter was dedicated to the Pleistocene geology of northern Cyprus, following on from the work of Ducloz and Knup. Baroz documented a detailed stratigraphy for seven Pleistocene terraces. The following section describes and compares the stratigraphic descriptions of Baroz and Ducloz (Fig. 1.11).

<table>
<tr><th colspan="2" rowspan="2">Relative ages</th><th rowspan="2">C. Ducloz (1964)</th><th colspan="2" rowspan="2">P. Knup (1965)</th><th rowspan="2">F. Baroz (1979)</th></tr>
<tr></tr>
<tr><td rowspan="11">Pleistocene</td><td rowspan="2">Late</td><td rowspan="2">Kyrenia (Girne)</td><td rowspan="11">Marine</td><td>Koupia</td><td rowspan="2">Koupia</td></tr>
<tr><td>Kyrenia (Girne)</td></tr>
<tr><td rowspan="3">Mid</td><td rowspan="3">Ayios Epiktitos (Çatalköy)</td><td>Ayios Epiktitos (Çatalköy)</td><td rowspan="2">Kyrenia (Girne)</td></tr>
<tr><td>Toumba</td></tr>
<tr><td rowspan="6">Early</td><td rowspan="3">Toumba</td><td>Trapeza (Beşparmak)</td><td rowspan="2">Agios Ermolaos (Çirinevlar)</td></tr>
<tr><td>Klepini (Arapköy)</td></tr>
<tr><td rowspan="2">Trapeza (Beşparmak)</td><td>Kharcha II</td><td rowspan="2">Ayios Epiktitos (Çatalköy)</td></tr>
<tr><td>Kharcha I</td></tr>
<tr><td rowspan="3">Klepini (Arapköy)</td><td rowspan="4">Continental</td><td>Agios Lakovos (Altınova)</td><td rowspan="2">Klepini (Arapköy)</td></tr>
<tr><td>Tripimeni (Tirmen)</td></tr>
<tr><td>Kounia</td><td rowspan="2">Tripimeni (Tirmen)</td></tr>
<tr><td>Pliocene</td><td>Late</td><td>Karka</td><td>Karka</td><td>Karka</td></tr>
</table>

Figure 1.11: Comparison of the Pleistocene terraces in northern Cyrus as defined by C. Ducloz (1964), P. Knup (1965) and F. Baroz (1979).

Karka terrace

The Karka terrace deposits are described in terms of two units; first, a lacustrine deposit and second, a talus deposit (Ducloz, 1972). The lacustrine deposits are composed of oolitic and pisolitic limestones intercalated with stratified chalk containing plant remains. The deposits are found at ca. 300 m above modern sea-level and form a sub-horizontal bench surface.

The talus deposit is a breccia made up of angular fragments of marble and dolomitic limestone, cemented by a hard salmon-coloured matrix, with occasional well-preserved *Helicidae*. The thickness of the deposit varies from a few centimetres to 12 m but on average is around 1 m to 2 m thick. The deposits are found at the base of faults within the range. Tilting of the Karka surface is due to younger fault activity (Ducloz, 1972).

Klepini (Arapkóy) terrace

The Klepini (Arapkóy) terrace is described by Baroz (1979) as being made up of a brown calcarenite at the base, passing upwards into a claystone, white calcareous clay with plant debris, and finally into a cream to grey calcareous mudstone with conglomerate lenses. This terrace sits unconformably on the Kythrea (Değirmenlik) Group. The type sections are generally found between the villages of Klepini (Arapkóy) and Trapeza (Beşparmak) on the northern side of the range.

Ducloz (1972) described the Klepini (Arapkóy) terrace deposit at Arapköy (Klepini) village. The base of the section is composed of a coarse breccia with a white chalk matrix, which is conformably overlain by a reddish-brown clay, medium- to coarse-grained fossiliferous calcarenite, and finally a breccia or conglomerate with a chalky matrix.

Tripimeni (Tirmen) terrace

The Tripimeni (Tirmen) terrace is best preserved on the southern side of the range, with two reference sections at Kormakiti and at Agios Ermolaos (Çirinevlar) (in the south east)(Baroz (1979)). These sections comprise marine calcarenites at the base, followed by an ochre-coloured calcarenite, a red algal claystone, brown marls, a limestone, and

finally by dune deposits.

The village of Kormakiti, in the western range, exposes the type section of the Tripimeni (Tirmen) terrace. This terrace is made up of a fine-grained aeolianite at the base, containing crossbedding and roots, and then passes into a palaeosol layer and a calcareous mudstone containing conglomerate lenses, finally overlain by a calcarenite.

Trapeza (Beşparmak) terrace

The Trapeza (Beşparmak) terrace deposits have only been described by Ducloz (1972). The terrace is described as comprising white basal calcarenite, grey marls with interstratified thin beds of calcarenite, white stratified chalky gravels with intercalations of marly sand, and a calcitic crust. The basal calcarenite contains smaller gastropods and foraminifera (*Millolidae*, *Globigerina* and *Rotalidae*).

Toumba terrace

Ducloz (1972) mentions a Toumba terrace however, he did not describe the terrace deposit as it was outside his mapping area. Baroz (1979) has no descriptions of this terrace in his thesis.

Agios Epikitikos (Çatalcöy) terrace

Ducloz (1972) described the Agios Epikitikos (Çatalcöy) terrace at the village of Çatalcöy (Agios Epikitikos), to the east of Kyrenia (Girne) town. The Agios Epikitikos (Çatalcöy) terrace deposit is described as a basal marine calcarenite and an upper continental gravel overlain by a calcitic crust. Inland, southwards, the continental unit increases in thickness (up to 20 m) whereas the marine base gradually tapers out.

Baroz (1979) described the same section at Çatalcöy (Agios Epikitikos) village. This terrace is generally found at 60 m to 70 m above modern sea level. The base of the sequence is a white claystone, passing up into a calcarenite deposit, clay-rich limestone and finally into an ochre-coloured calcarenite.

Kyrenia (Girne) terrace

Ducloz (1972) described the Kyrenia (Girne) terrace as generally consisting of a marine base and an upper, continental unit. The marine base is a conglomerate containing marine molluscs and corals that have been reworked as a beach deposit. The upper continental deposit is a cross-bedded and cross-laminated calcarenite, representing an aeolianite.

Ducloz (1972) suggests that the marine base of the Kyrenia (Girne) terrace is Tyrrhenian aged, based upon the presence of molluscs including *Strombus bubonis* and *Natica lactea*. The marine base is interpreted as having been deposited during the sea-level high of an interglacial to glacial cycle.

Baroz (1979) describes the Kyrenia (Girne) terrace deposit at Ayia Phanourias town to the west of Kyrenia (Girne) town. This section is dominated by calcarenites with cross bedding and roots. Organisms are abundant and include calcareous algae, benthic foraminifera, gastropods and brachiopods. In some localities there are also lithified mammal remains such as pygmy hippopotamus.

Koupia terrace

Finally, the Koupia terrace dominates the northern coastline of the Kyrenia Range and comprises cross-bedded aeolianite deposits (Baroz, 1979). Corals and biological debris (gastropods and bivalves) are also commonly found within this terrace, implying a littoral depositional zone.

1.8.3 Work by William Dreghorn

William Dreghorn produced a guide called the "Landforms in the Girne Range Northern Cyprus" in 1978. This summarised the geology of the Kyrenia Range based on the previous work by Ducloz, Knup and Baroz and his own excellent field observations. This work summarised the Pleistocene terraces but does not attempt to extend the previous work, as Dreghorn states: "so far only a passing mention has been made of the marine terraces which form the coastal plain. They were excluded from detailed examination because such an undertaking would have almost doubled the field work,

and the final publication".

1.8.4 Discussion of the Plio-Pleistocene deposits of northern Cyprus

The review of the work by Ducloz, Knup and Baroz identifies a number of discrepancies in the number of Pleistocene terraces and the stratigraphy of each terrace. The detailed maps produced by Ducloz and Knup differentiate the terraces based upon height above modern sea-level and provide a brief description on the terrace stratigraphy. Baroz followed-up this work by providing a more detailed stratigraphy. A focused study on the Kyrenia Range terraces was necessary to provide a better understanding of how the Pleistocene terraces can be correlated around the range and with the Troodos Massif terraces.

1.9 New Plio-Pleistocene stratigraphy of northern Cyprus

A new stratigraphy for Mesaoria (Mesarya) Group in northern Cyprus is put forward based upon the new data presented within this thesis. The main changes to the older stratigraphy include the separation of the Karka terrace into a terrace deposit and the Taşkent (Vouno) Member, the consolidation the of the various terraces described by numerous authors into six defined terraces, and the incorporation of the Kalkalı (Kapouti) Member to the stratigraphy as part of the upper Athalassa (Gürpınar) Formation. Although this is based upon work presented in the following chapters, a summary is presented here to make the stratigraphy clearer for the reader during the succeeding chapters. Figure 1.12 shows an updated version of the Mesaoria (Mesarya) Group stratigraphy for northern Cyprus.

The Karka terrace is differentiated based on two different depositional environments represented by the Karka talus deposits and the Karka lacustrine deposits, as described by Ducloz (1972). The depositional environment of both deposits will be discussed in more detail in Chapter 3. The addition of the Kalkalı (Kapouti) Member is due to the discovery of deposits of the Athalassa (Gürpınar) Formation that were not described in

southern Cyprus and are unique to the Kyrenia Range. The deposits from the newly defined Kalkalı (Kapouti) Member are described in Chapter 2. Finally, the new terrace nomenclature system presented is based on the stratigraphy from the central Kyrenia Range presented by Ducloz (1972). This work described six major terraces, which are based on new sedimentology rather than variations in height above sea-leve and can be correlated along both flanks of the range.

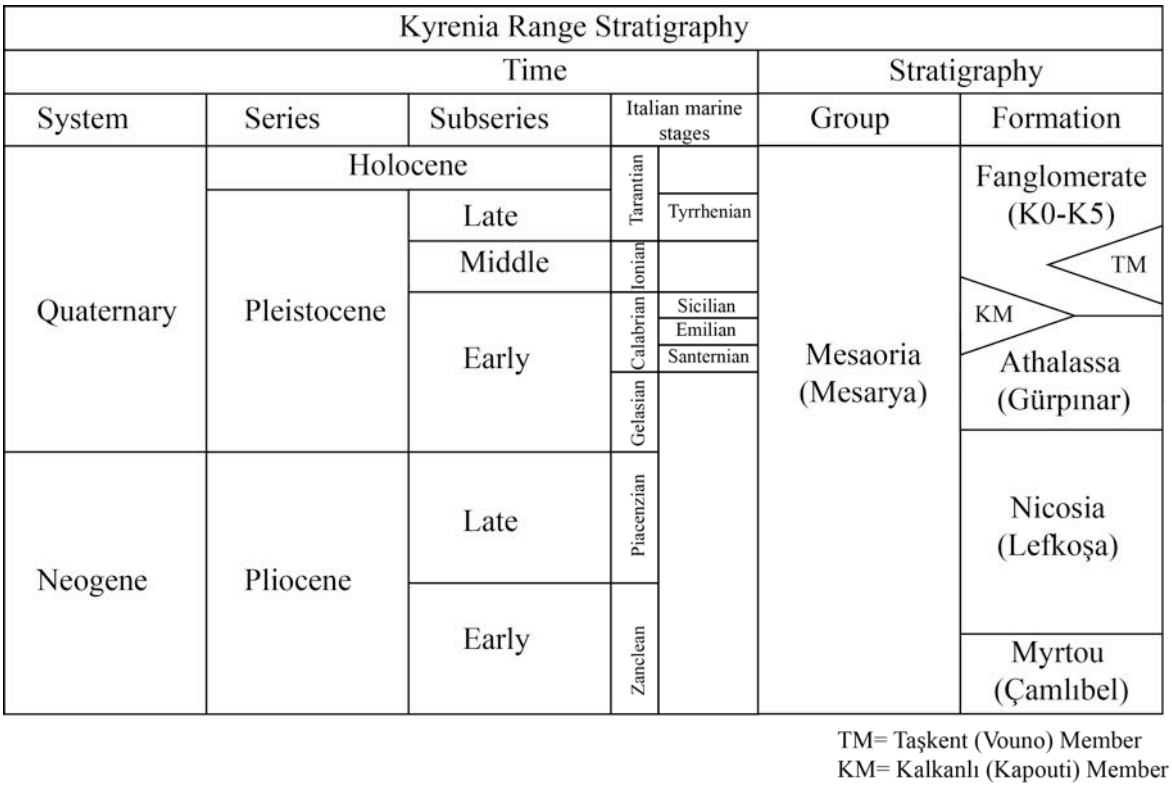

Figure 1.12: New stratigraphy of northern Cyprus from the Pliocene to Holocene (Data adapted from Henson *et al.* (1949); Ducloz (1972); Baroz (1979); Hakyemez *et al.* (2000); McCay *et al.* (2012)).

1.9.1 New terrace nomenclature system

Ducloz (1963), Knup (1964), Ducloz (1972) and Baroz (1979) defined twelve different Pleistocene terraces around the Kyrenia Range. This study examined these terraces and looked in detailed at the sedimentology and the sedimentary relationships between each terraces. Six terraces are presented, which can be correlated along both northern

and southern flanks of the Kyrenia Range.

Table 1.1 compares the terraces defined by C. Ducloz (1972) with the new terrace nomenclature system for the Pleistocene terraces in northern Cyprus. The terraces are numbered 0 to 5 with the oldest terrace being '0', equivalent to the Karka terrace and the youngest terrace labelled '5', equivalent to the Koupia terrace. Each terrace is defined by the letter 'K' to represent a Kyrenia Range terrace, resulting in the sequence K0 to K5 (Table 1.1). Various parts of the terrace system are defined within this nomenclature system, including the terrace surface (S), the marine deposit (M) and the non-marine deposit (C)(Fig. 1.13). The terrace surface is defined as the upper topographic surface of the terrace, this is either overlying the uppermost deposit or the erosional surface if no deposit is preserved (Fig. 1.13).

Terrace	**Terrace number**	**Terrace deposits**		
		Surface	**Marine**	**Non-marine**
Karka	K0	S0	-	C1
Klepini (Arapköy)	K1	S1	M1	C1
Trapeza (Beşparmak)	K2	S2	M2	C2
Ayios Epititikos (Çatalcöy)	K3	S3	M3	C3
Kyrenia (Girne)	K4	S4	M4	C4
Koupia	K5	S5	M5	C5

Table 1.1: Proposed Kyrenia Range terrace stratigraphy

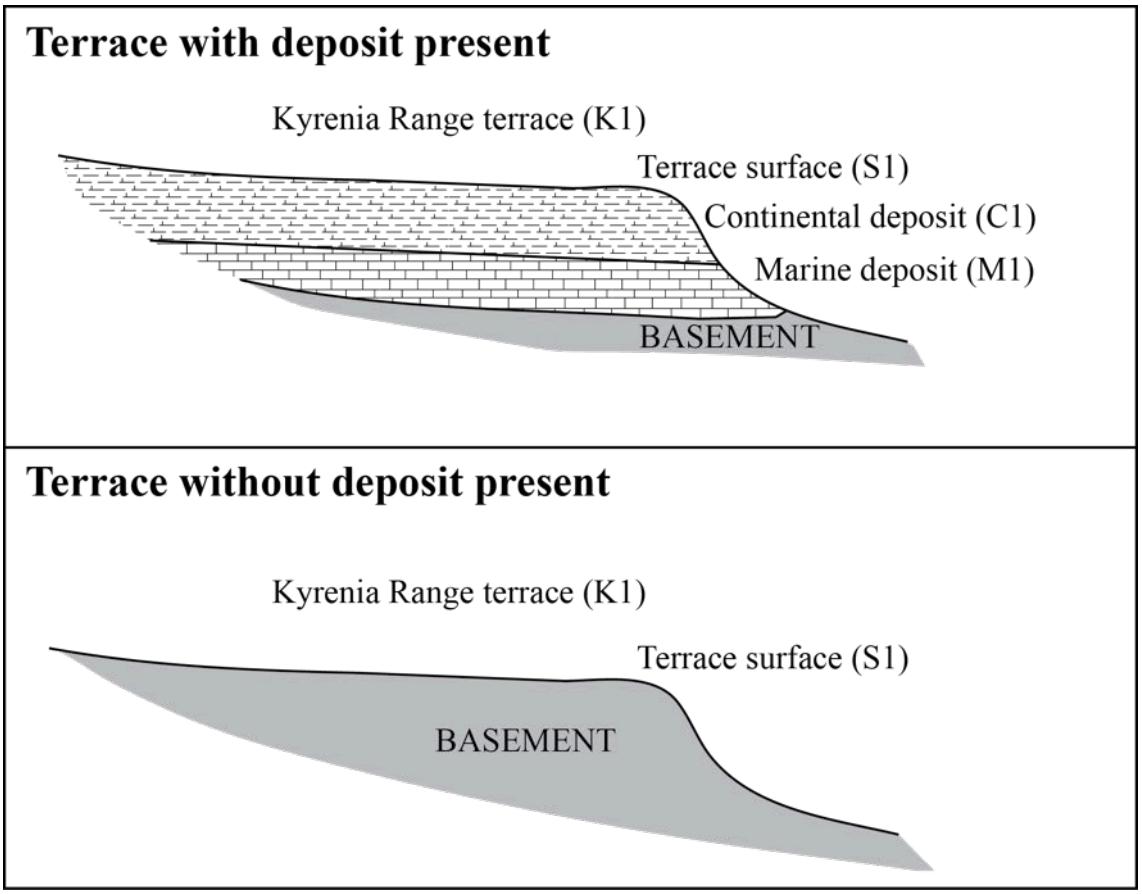

Figure 1.13: Schematic diagram illustrating the new terrace nomenclature system.

Chapter 2

Sedimentology of Upper Pliocene deposits on the flanks of Kyrenia Range in northern Cyprus

2.1 Introduction

The Pliocene deposits of northern Cyprus represent the last major marine environment (Henson *et al.*, 1949; Ducloz, 1972; Baroz, 1979) prior to Pleistocene tectonic uplift. The extensive preservation of Pliocene-aged deposits in northern Cyprus (Ducloz, 1972; Baroz, 1979; McCay, 2010; McCay *et al.*, 2012) provides an excellent opportunity to study the sedimentary processes associated with tectonically driven regression.

Prior to the Quaternary uplift of the Troodos Massif and the Kyrenia Range, the Mesaoria (Mesarya) Plain was a shallow-marine seaway that separated the two mountain ranges (McCallum and Robertson, 1995a)(Fig. 2.1). The stratigraphy of the Mesaoria (Mesarya) Group represents a change from marine to non-marine environments during the Pliocene and Pleistocene times. (Ducloz, 1972; Baroz, 1979; McCallum and Robertson, 1990; Hakyemez *et al.*, 2000; Lord *et al.*, 2000; Harrison *et al.*, 2004). There are no modern comprehensive sedimentological studies of the Pliocene deposits on the northern side of the Mesaoria (Mesarya) Plain. Knowledge of the stratigraphy of the Mesaoria (Mesarya) Group in northern Cyprus comes from Baroz (1979) and Harrison *et al.* (2004) (Fig. 2.2). The Baroz (1979) stratigraphy is based upon deposits in northern Cyprus. In comparison Harrison *et al.* (2004) made a stratigraphy based on

deposits on the southern side of the Mesaoria (Mesarya) Plain, however this work was focused on the Ovgos (Dar Dere) fault zone. For further details on formations and the associated facies of these stratigraphic sequences see chapter 1. A new stratigraphy is presented here for the Mesaoria (Mesarya) Group based on Pliocene deposits within the Mesaoria (Mesarya) Plain and the Karpaz (Karpas) Peninsula (Fig. 2.2).

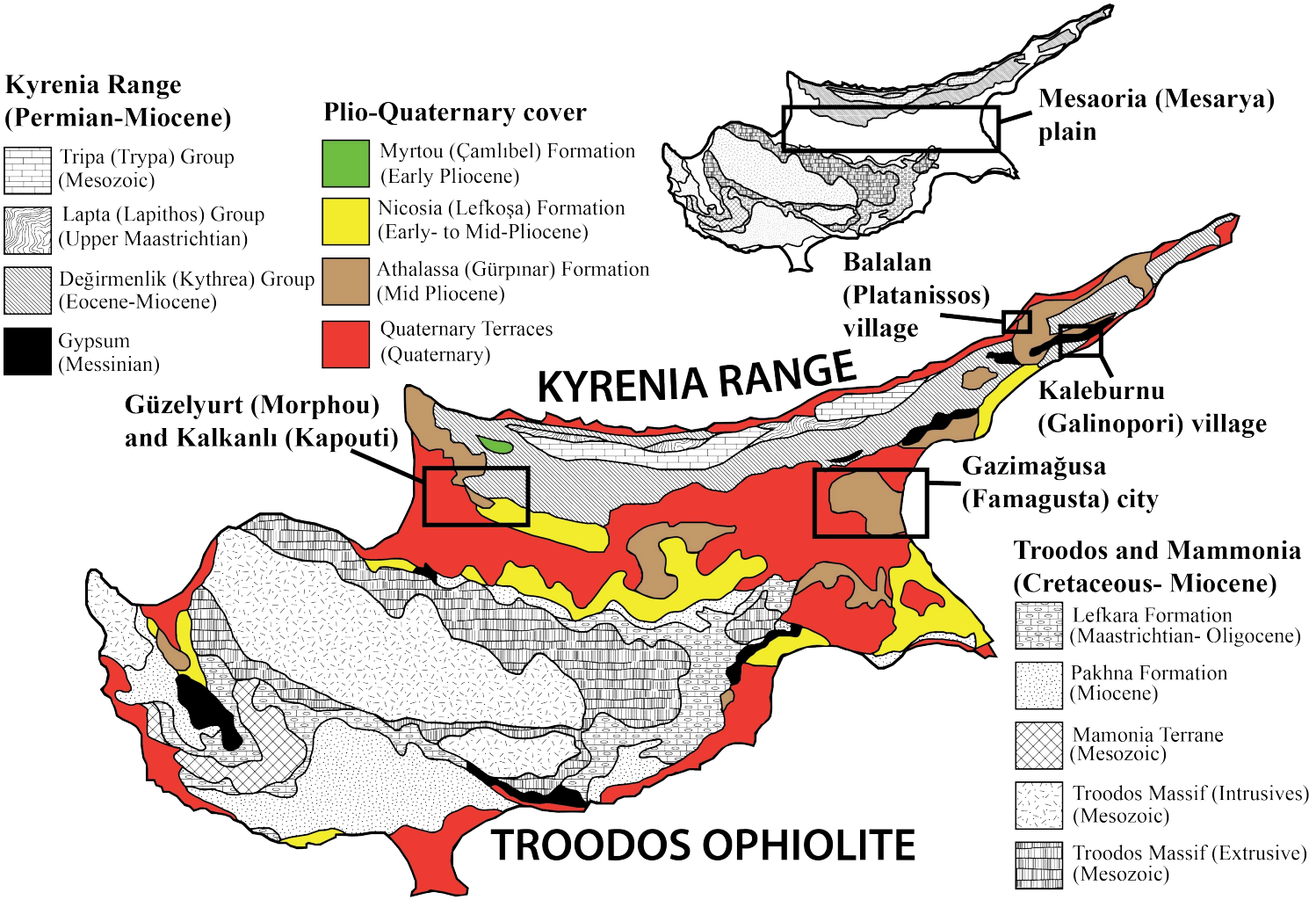

Figure 2.1: Simplified geological map of Cyprus with emphasis on the distribution of Pliocene and Quaternary deposits, adapted from McCay *et al.* (2012) and McCay and Robertson (2012b).

The main differences between the stratigraphic nomenclatures of different authors for Pliocene deposits in northern Cyprus is the age and relationship of the Nicosia (Lefkoşa) Formation relative to the Athalassa (Gürpınar) Formation. Early work by Baroz (1979) in northern Cyprus suggested that the Athalassa (Gürpınar) Formation overlies the Nicosia (Lefkoşa) Formation, comparable with southern Cyprus (Ducloz, 1972; McCallum, 1989). More recently, Harrison *et al.* (2004) suggested that the Athalassa (Gürpınar) Formation bioclastic limestones interfingers with the Nicosia (Lefkoşa) Formation, based upon work on the southern side of the Mesaoria (Mesarya) Plain. The differences in stratigraphy between the various published works has implications for the interpretion of the evolving Pliocene depositional environment. If the Athalassa (Gürpınar) Formation is overlying the Nicosia (Lefkoşa) Formation, this implies a shallowing marine environment. However, if the Nicosia (Lefkoşa) and Athalassa (Gürpınar) Formations are interfingering, shallow and hemipelagic marine environments are contemporaneous.

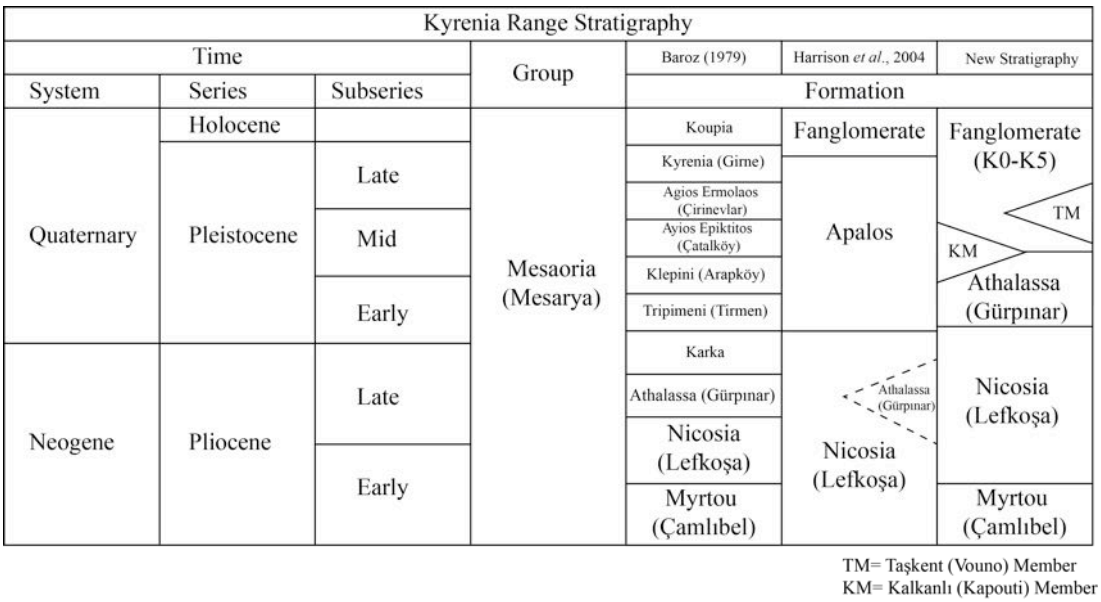

Figure 2.2: Comparison of the stratigraphies developed for the sedimentary cover of the Kyrenia Range (Baroz, 1979; Harrison *et al.*, 2004).

The focus of this chapter is on the transition from a marine to a non-marine environment during the late Pliocene. Fieldwork was aimed at studying the transition from the marine setting represented by the Nicosia (Lefkoşa) Formation to the first non-marine Fanglomerate group deposit. The Myrtou (Çamlıbel) Formation is pre-

dominantly made up of marls and siltstone, with abundant planktic foraminifera. The Nicosia (Lefkoşa) Formation is composed of bioclastic limestones, sandstones and marls and conformably overlies the the Myrtou (Çamlıbel) Formation. Finally, the Athalassa (Gürpınar) Formation conformably overlies the Nicosia (Lefkoşa) Formation and is made up of a bioclastic limestone. For a more detailed facies descriptions of the Mesaoria (Mesarya) Group see Chapter 1.

The only focused sedimentological study of Pliocene sediments was carried out on the southern side of the Mesaoria (Mesarya) Basin (McCallum, 1989; McCallum and Robertson, 1995a; McCallum and Robertson (1995b)). These studies documented the sedimentary processes associated with the evolving depositional environment within the Mesaoria (Mesarya) Basin related to the early-stage uplift of the Kyrenia Range and the Troodos Massif. The work by McCallum as part of her PhD (McCallum, 1989; McCallum and Robertson, 1995a) focused on several aspects of the Pliocene geology of southern Cyprus: firstly, the sedimentology of the Nicosia (Lefkoşa) Formation to better constrain the earliest phase of uplift of the Troodos massif. Secondly, a detailed discussion on the sedimentology of the Athalassa (Gürpınar) Formation on the southern side of Mesaoria (Mesarya) Plain (McCallum and Robertson, 1995a). Thirdly, a preliminary study on the drainage systems, sourced from the Troodos Massif, into the Mesaoria (Mesarya) Plain during the earliest stages of Quaternary uplift of the Troodos Massif (McCallum and Robertson, 1995b).

This work showed that the uplift of the Troodos Massif began during the early Pliocene (McCallum, 1989). During the late Pliocene, the Mesaoria (Mesarya) Plain was a shallow marine environment within which the Athalassa (Gürpınar) Formation clastic limestone accumulated. The Athalassa (Gürpınar) Formation clastic limestone was strongly controlled by major storm events and minor faulting in the southwestern side of the Mesaoria (Mesarya) Plain (McCallum and Robertson, 1995a). McCallum and Robertson, 1995a focused on the Kakkaristra fan-deltaic system draining from the Troodos Massif into the central Mesaoria (Mesarya) Plain. The Kakkaristra fan-deltaic system has been stratigraphical described as representing a late stage deltaic system prior to the deposition of the Fanglomerate Formation during the Quaternary. This work was mainly focused on the southern margin of the Mesaoria (Mesarya) Plain and did not include the equivalent deposits on the flanks of the Kyrenia Range.

The earliest age constraints on the Pliocene deposits were through various studies fo-

cused on the biostratigraphy of the Myrtou (Çamlıbel), Nicosia (Lefkoşa) and Athalassa (Gürpınar) Formations (Baroz, 1979; Lord *et al.*, 2000; Hakyemez *et al.*, 2000; Harrison *et al.*, 2008). The focused biostratigraphy studies showed a range of foraminifera within the Myrtou (Çamlıbel) and Nicosia (Lefkoşa) Formations including: *Globigerina*, *Globigerinoides*, *Globorotalia* and *Orbulina*. The foraminifera identified within the Myrtou (Çamlıbel) and Nicosia (Lefkoşa) Formations indicate firstly a pelagic environment and secondly, a Pliocene to Pleistocene age. This work also describes the same foraminifera within the Athalassa (Gürpınar) Formation ((Baroz, 1979; Hakyemez *et al.*, 2000); however the deposits associated with the Athalassa (Gürpınar) Formation are well documented as representing a shallow marine basin (McCallum and Robertson, 1995a). Therefore, any planktonic foraminifera within the Athalassa (Gürpınar) Formation should be reworked from the older Myrtou (Çamlıbel) and Nicosia (Lefkoşa) Formations.

The only quantitative dating of the Pliocene sediments was by strontium isotope dating, carried out by McCay *et al.* (2012). This study focused on the stratigraphy of the Eocene to early Pliocene sediments in the northern Mesaoria (Mesarya) Basin. A combination of $^{87}Sr/^{86}Sr$ isotopic, nannofossil and planktonic foraminifera dating was used to help understand the biostratigraphy of the sediments within the Kythrea (Değirmenlik) Group (Miocene) and the Myrtou (Çamlıbel) Formation (Early Pliocene). The $^{87}Sr/^{86}Sr$ isotopic dating of planktonic foraminifera from the Myrtou (Çamlıbel) Formation gave an Early Pliocene age.

Pliocene deposits in northern Cyprus are preserved within the Mesaoria (Mesarya) Plain and on the Karpaz (Karpas) Peninsula (Constantinou, 1995). The Mesaoria (Mesarya) Plain includes the Ovgos (Dar Dere) fault zone which is the boundary between the Kyrenia Range to the north and the Troodos Massif to the south, (Cleintuar *et al.*, 1977; Harrison *et al.*, 2004; McCay and Robertson, 2012b)(Fig. 2.3). The Pliocene deposits are preserved on both sides of the Ovgos (Dar Dere) fault zone and, therefore, unconformably overlie both the Troodos Massif (Pakhna Formation) to the Kyrenia Range (Kythrea (Değirmenlik) Group)(Fig. 2.3). The relationship of the Pliocene deposits and the Ovgos (Dar Dere) fault zone is significant because the provenance of clastic material within the Pliocene deposit could vary from north to south, depending upon the geology of the southern areas. Late Pliocene tectonic activity along the Ovgos (Dar Dere) fault zone could have acted as a control on sedimentation within the

Mesaoria (Mesarya) Plain (Harrison *et al.*, 2004; McCay and Robertson, 2012b).

To understand the sedimentary processes associated with the Pliocene uplift of the Kyrenia Range this study focusses on the sedimentology of the Nicosia (Lefkoşa) and Athalassa (Gürpınar) Formations in northern Cyprus. The Kalkanlı (Kapouti) Member is added to the stratigraphy of northern Cyprus, encompassing specific deposits that are proximal to the Kyrenia Range within the upper part of the Athalassa (Gürpınar) Formation. For more details on the stratigraphy of the Pliocene deposits in northern Cyprus see chapter 2. The following section describes the sedimentology of the Pliocene sediments in northern Cyprus; including field descriptions, petrology and strontium dating. The data aim to better constrain the sedimentary processes and timing of the Pliocene regression in northern Cyprus.

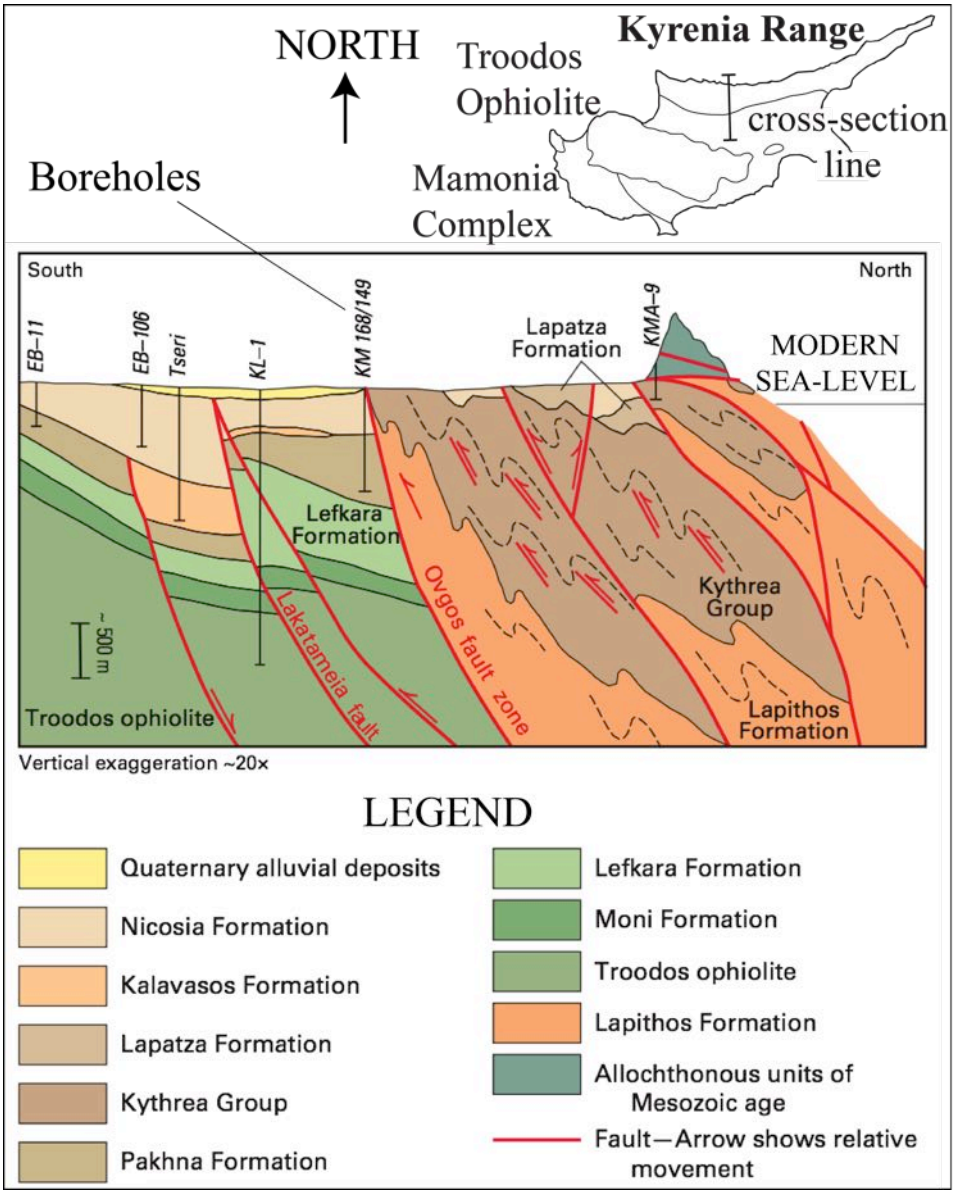

Figure 2.3: Cross section through the Ovgos (Dar Dere) fault zone within the central Mesaoria (Mesarya) Plain taken from Harrison *et al.* (2008).

2.2 Nicosia (Lefkoşa) and Athalassa (Gürpınar) Formations

The Nicosia (Lefkoşa) and Athalassa (Gürpınar) Formations are exposed on the Mesaoria (Mesarya) Plain and the Karpaz (Karpas) Peninsula (Fig. 2.1). The following section focusses on three areas including: Güzelyurt (Morphou) town in the western Mesaoria (Mesarya) Plain, Gazimağusa (Famagusta) city in the Mesaoria (Mesarya) Plain and several localities on the Karpaz (Karpas) Peninsula.

2.2.1 Güzelyurt (Morphou) town

Güzelyurt (Morphou) town is in the western part of northern Cyprus, ca. 30 km west of Lefkoşa (Nicosia) city (Fig. 2.1). Previous workers documented the Nicosia (Lefkoşa) and Athalassa (Gürpınar) Formations as unconformably overlying Late Miocene and older stratigraphic units (Harrison *et al.*, 2004; McCay and Robertson, 2012b)(Fig. 2.4). Previously, the focus of interest in this area has been on the Ovgos (Dar Dere) fault zone owing to its surface expression and the exposure of deformed lithologies (Harrison *et al.*, 2004; McCay and Robertson, 2012b). The focus of this study is on the depositional environment represented by the Pliocene sediments; therefore the following section describes the sedimentology and the distribution of the Nicosia (Lefkoşa) and Athalassa (Gürpınar) Formation deposits.

A key feature within the area is a NW trending chalk ridgeline, which has Pliocene sediments preserved against it on its southwest side (Fig. 2.4; Fig. 2.5). The chalkridge line ranges in height from ca. 280 m AMSL in the northwest, and ca. 170 m AMSL in the southeast. The northeastern side forms a gentle slope, dipping to the northeast; in contrast, the southwestern side forms a relatively steep cliffline. The Athalassa (Gürpınar) Formation deposits are preserved as a series of isolated hills on the southwestern side of the chalk ridge (Fig. 2.5). A series of logged sections are presented from numerous localities within the area that illustrate the depositional environment during the Pliocene and the relationship of the Pliocene deposits to the chalk ridge. The lower part of the Athalassa (Gürpınar) Formation is made up of a series of southwestward dipping beds (Fig. 2.6).

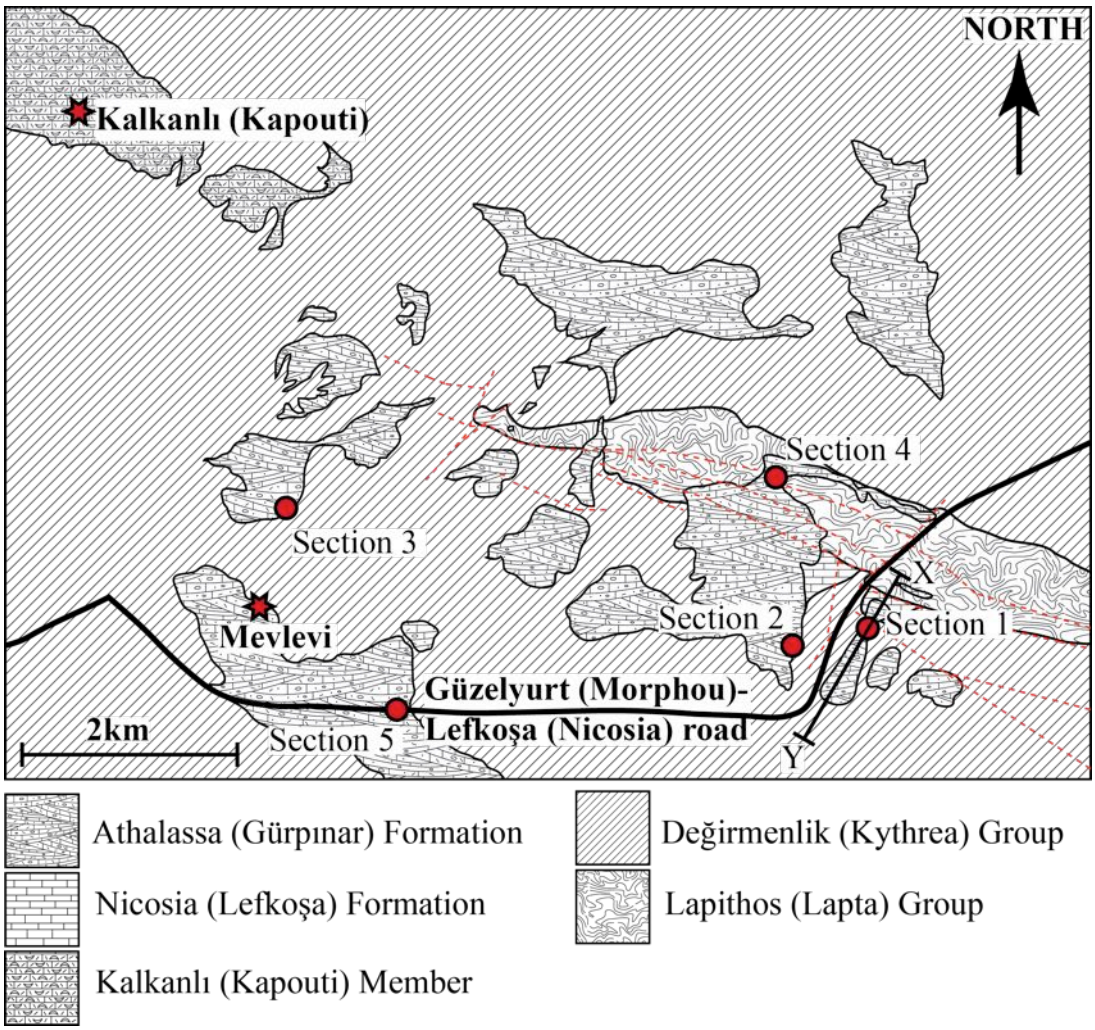

Figure 2.4: Geological map of the area east of Güzelyurt (Morphou) town, the underlying geology and structure is adapted from Harrison *et al.* (2004) and McCay and Robertson (2012b). The distributions of the deposits from the Nicosia (Lefkoşa) and Athalassa (Gúrpınar) Formations is from the new stratigraphy. X-Y section is shown in Figure 2.5.

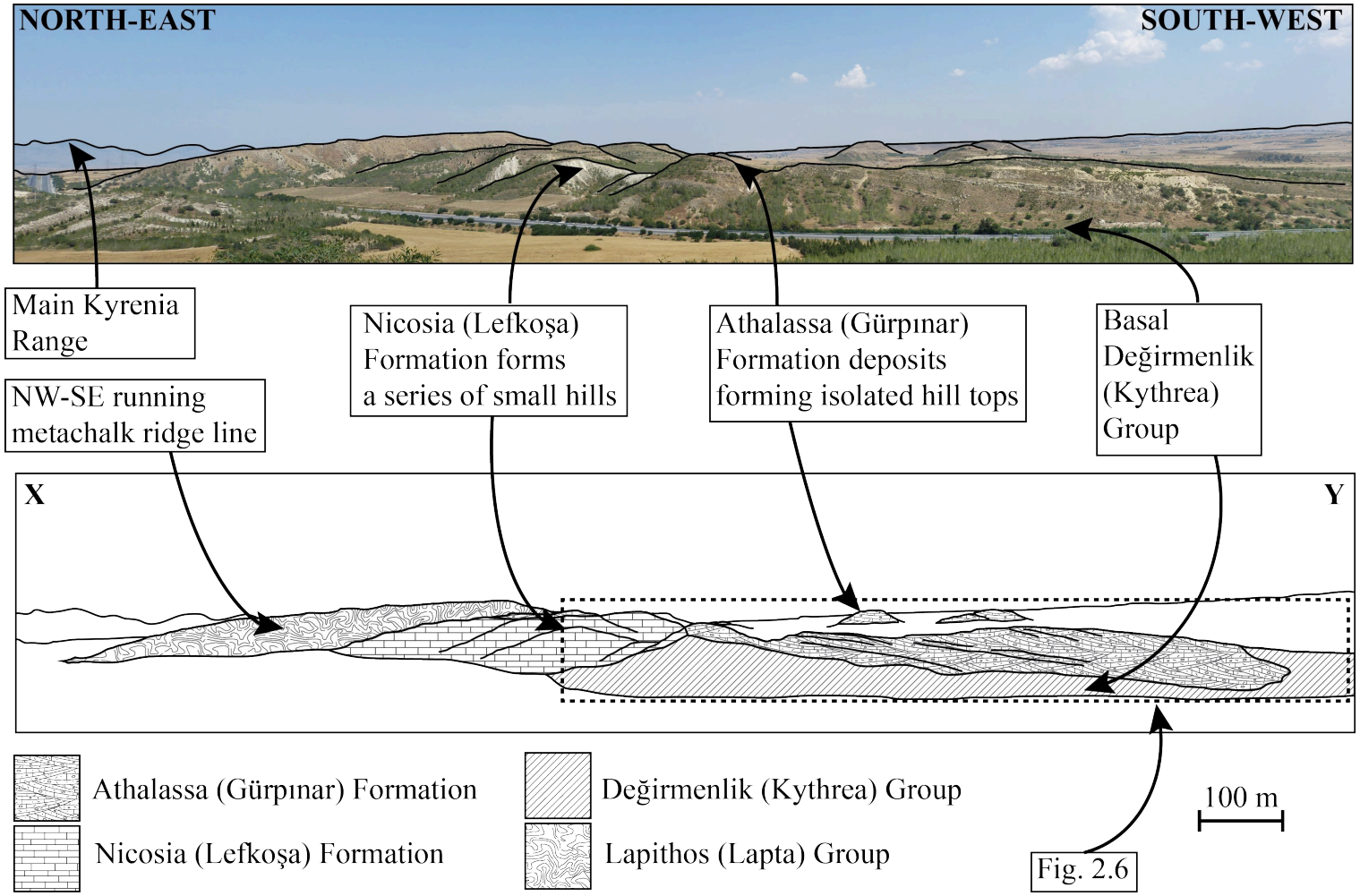

Figure 2.5: Photograph and schematic section showing the key geological relationships between Pliocene shallow-marine sediments on the underlying geology around the Ovgos (Dar Dere) fault zone. See Figure 2.4 for the location of this section.

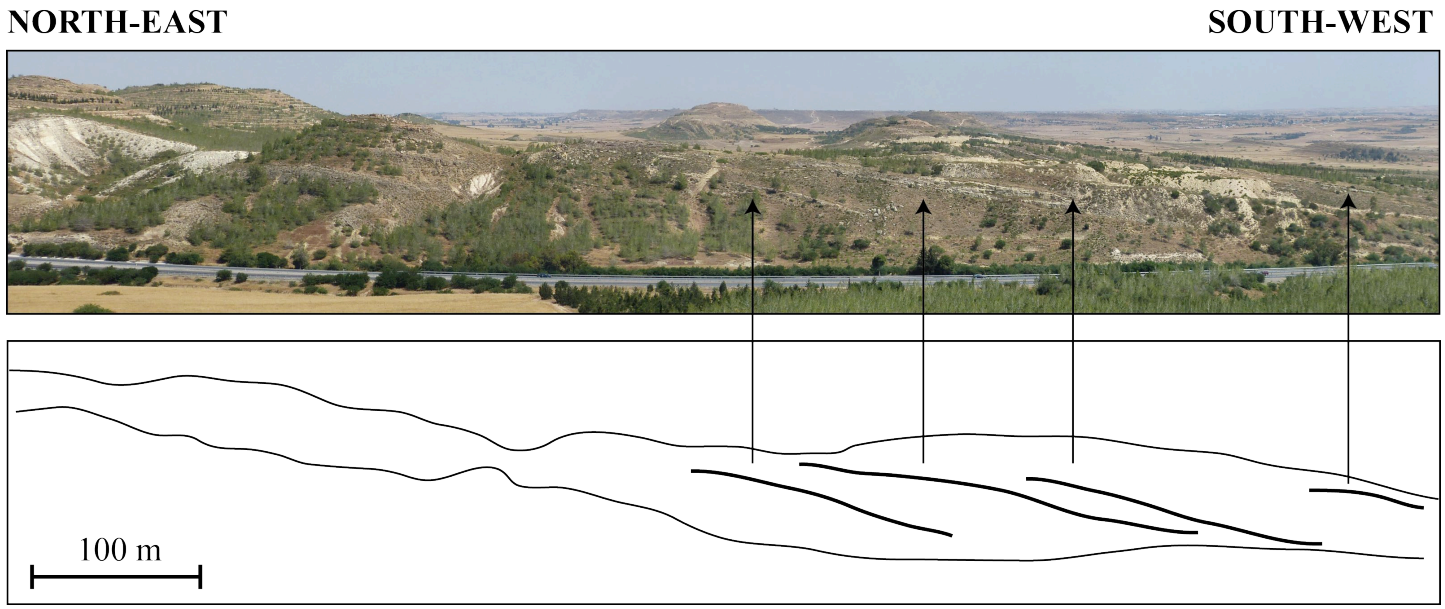

Figure 2.6: Photograph of the Athalassa (Gürpınar) Formation showing bedding dipping down to the southwest. The location of the section is show in Figure 2.5.

Section 1

The first section is of the sedimentary contact between the Nicosia (Lefkoşa) and the Athalassa (Gürpınar) Formations to the southwest of the chalk ridgeline (location is shown on Figure 2.4). The section is representative of the Pliocene deposits on the eastern side of the Güzelyurt (Morphou)-Lefkoşa (Nicosia) road (Fig. 2.4). Two sedimentary sections are shown in Figure 2.7, which represent the Athalassa (Gürpınar) Formation.

Section 1 (a) is made up of a basal matrix-supported conglomerate with well-rounded clasts, this is overlain by a coarsening-upwards grainstone with occasional conglomerate channels. Conformably overlying this unit is a cross-bedded grainstone. The basal conglomerate is rich in both biogenic and clastic material. The biogenic clasts include casts of reworked *Tarbellastraea* coral (Miocene aged, as described by Mertz-Kraus *et al.* (2008)) (Fig. 2.7 Photo (a)), pecten and oncoids; the clastic material is predominantly chalk that has been heavily bored (Fig. 2.7 Photo (b)), the matrix is made up of a fine grained grainstone. The basal conglomerate is erosionally overlain by a fine- to coarse-grained grainstone, interbedded with channels of conglomerate with well-rounded clasts ranging in size from 1 cm to 3 cm. The unit coarsens upwards into a cross-bedded grainstone, which is ca. 2 m thick. The cross-bedded upper grainstone is made up of several 50 to 100 cm-thick units. The cross-bedding is always dipping at $>30^o$ and have both easterly and westerly palaeoflow directions.

Section 1 (b) is made up of a fine-grained grainstone with a ca. 1 m-thick conglomerate bed in the upper part of the section (Fig. 2.7). The grainstone and conglomerate lithologies are similar to those described in Section 1 (a). The lower grainstone unit thickens to >10 m towards the southwest (Fig. 2.5).

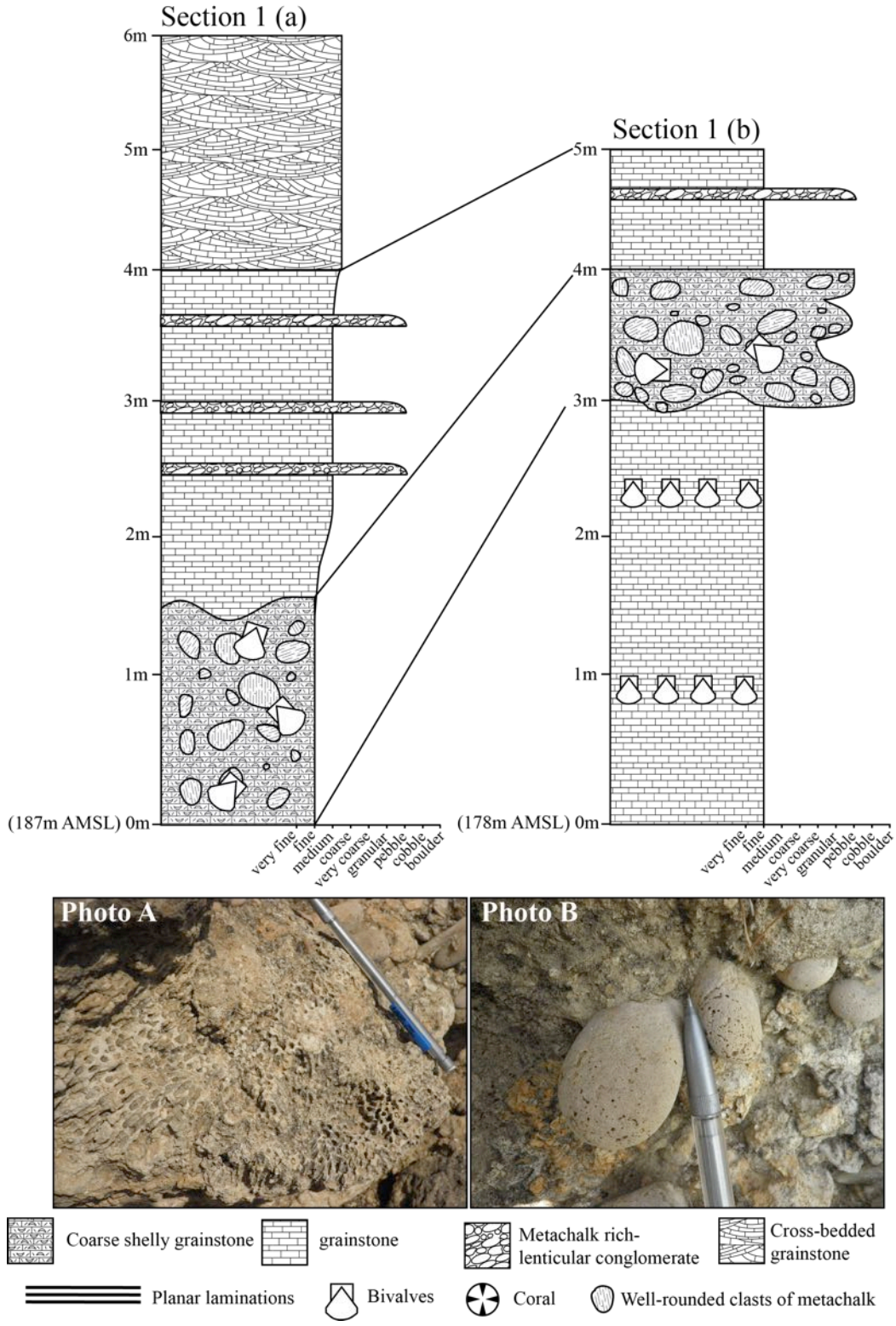

Figure 2.7: Logged sedimentary sections and photographs of the Athalassa (Gürpınar) Formation (locations shown on Figure 2.4). Photographs A and B show a reworked Miocene-aged coral (*Tarbellastrae*) and bored pebbles, respectively.

Section 2

Section 2 is from an Athalassa (Gürpınar) Formation to the northwest, and is north of the Güzelyurt (Morphou)-Lefkoşa (Nicosia) road (Fig. 2.4). The associated deposits form a low-angle surface that dips southwestwards away from the chalk ridge. The surface is made up of the Athalassa (Gürpınar) Formation, in Section 2 (a) (Fig. 2.8), whereas Section 2 (b) also represents a deposit from the Athalassa (Gürpınar) Formation which underlies section 2 (a) but is laterally discontinuous.

Section 2 (a) is a ca. 18 m-thick, coarse- to fine-grained grainstone with occasional conglomerate beds made up of a mixture of carbonate and clastic clasts (Fig. 2.8). The sedimentary structures within the grainstone include trough cross-bedding and laminations. The cross-bedding foresets generally dip at $<30^o$ are <50 cm thick. The laminated sections separating the cross-bedded units are <30 cm thick. The grainstone grains are poorly sorted, ranging from fine to coarse, and are sub-angular. The conglomerate beds are matrix-supported and contain well-rounded 1 cm to 30 cm-sized clasts. The lower conglomerate bed contains both carbonate and clastic clasts, whereas the the upper conglomerate bed contains only clastic clasts. The carbonate clasts include pecten shells ranging in size from 5 cm to 10 cm, and also reworked oncoids. The clastic material is predominantly chalk with occasional reworked clasts of grainstone. The chalk in both conglomerate beds is often heavily bored.

Section 2 (b) is best exposed along the southwestern edge of the Athalassa (Gürpınar) Formation surface (Fig. 2.4). The deposit is made up of a coarse- to fine-grained grainstone, a shell-rich grainstone and a conglomerate bed. The grainstone varies from poorly sorted with trough cross-bedding, to fine- to medium-grained and planar laminated. Part of the way up the section there is a continuous shell-rich grainstone bed with large pecten shells and well-preserved corals. The upper grainstone is poorly-sorted and varies from fine- to coarse-grained and contains clasts of chalk that vary in size from 1 cm to 30 cm. Clasts in the upper conglomerate are well-rounded and matrix-supported, ranging size from 1 cm to 5 cm; the bed is ca. 30 cm-thick. Clasts are composed of both clastic and carbonate material. The clastic material includes diabase, jasper, plagiogranite, sandstone, serpentinite, quartz, reworked grainstone and chalk; whereas the bioclastic clasts are dominantly pecten shells. Both the clasts and pecten shells throughout the section show signs of boring.

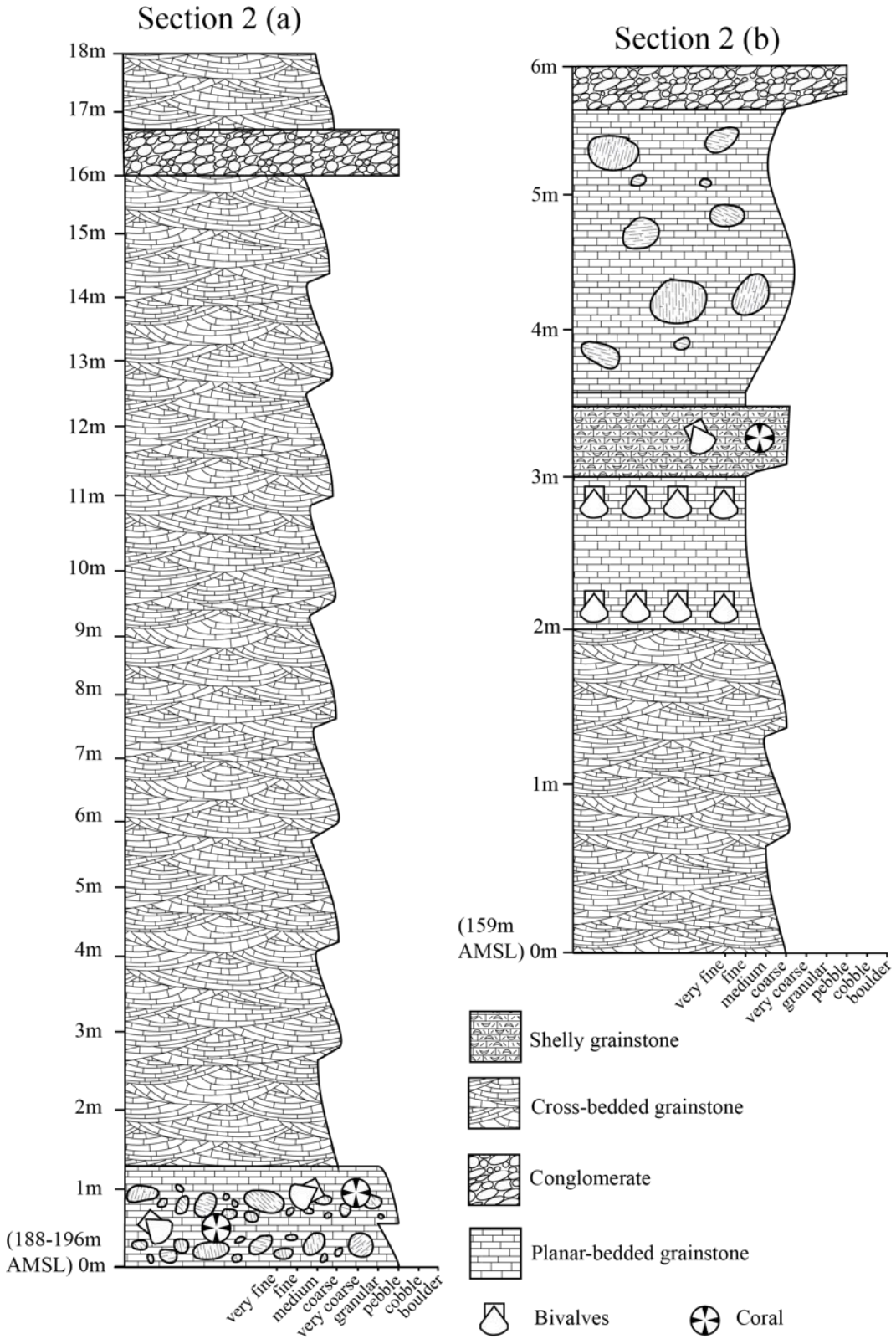

Figure 2.8: Sedimentary logs from the Athalassa (Gürpınar) Formation east of Güzelyurt (Morphou) town (Fig. 2.4). The sedimentary logs are from the southwest-dipping Athalassa (Gürpınar) Formation surface.

Section 3

Section 3 is found directly north of Mevlevi town and represents the Athalassa (Gürpınar) Formation (Fig. 2.9). The lower ca. 7 m of the deposit is laterally discontinuous; whereas the upper part forms a NE-trending surface that gently dips down to the southwest.

The basal section comprises two units, firstly a lower planar-bedded grainstone, and secondly, a poorly-sorted shelly grainstone. The basal grainstone is fine- to coarse-grained and contains large carbonate fragments including reworked *Chlamys larteti* (Miocene-aged mollusc, as described by Reed (1935)), oncoids and gastropods (Fig. 2.9, Photos A, B). The bivalves range in size from 1 cm to 15 cm and gastropods are ca. 1 cm in length. The contact between the lower grainstone unit and the middle shelly-grainstone is a sharp horizontal boundary (Fig. 2.9, Photo C) with vertical burrowing into the lower unit. The shelly grainstone is poorly sorted and comprises ca. 0.5 cm-sized gastropods and fragmented bivalve shells. The unit shows poorly preserved bedding structures on a 2 cm to 3 cm scale. The lower-bedded grainstone and the shelly grainstone are grain supported and well lithified with a carbonate cement (Fig. 2.9, Photo D). Extensive burrowing is preserved throughout the deposit (Fig. 2.9, Photo E).

The upper deposit conformably overlies the entire lower section as an approximately 8 m-thick cross-bedded grainstone (Fig. 2.9 Photo F). The dip of the cross-bedding ranges from 30^o to ca. 40^o in the form of ca. 2 m-thick units. The cross-bedding has a palaeoflow direction towards the northwest. The upper grainstone deposit forms the main southwest-dipping surface and can be clearly correlated with various isolated deposits to the northeast (Fig. 2.4). The surface ranges from ca. 110 m AMSL in this section to over 300 m AMSL to the northeast. The surface is composed of cross-bedded grainstone, varying in thickness from 8 m to 15 m; the lower deposit is discontinuous northwards (Fig. 2.4).

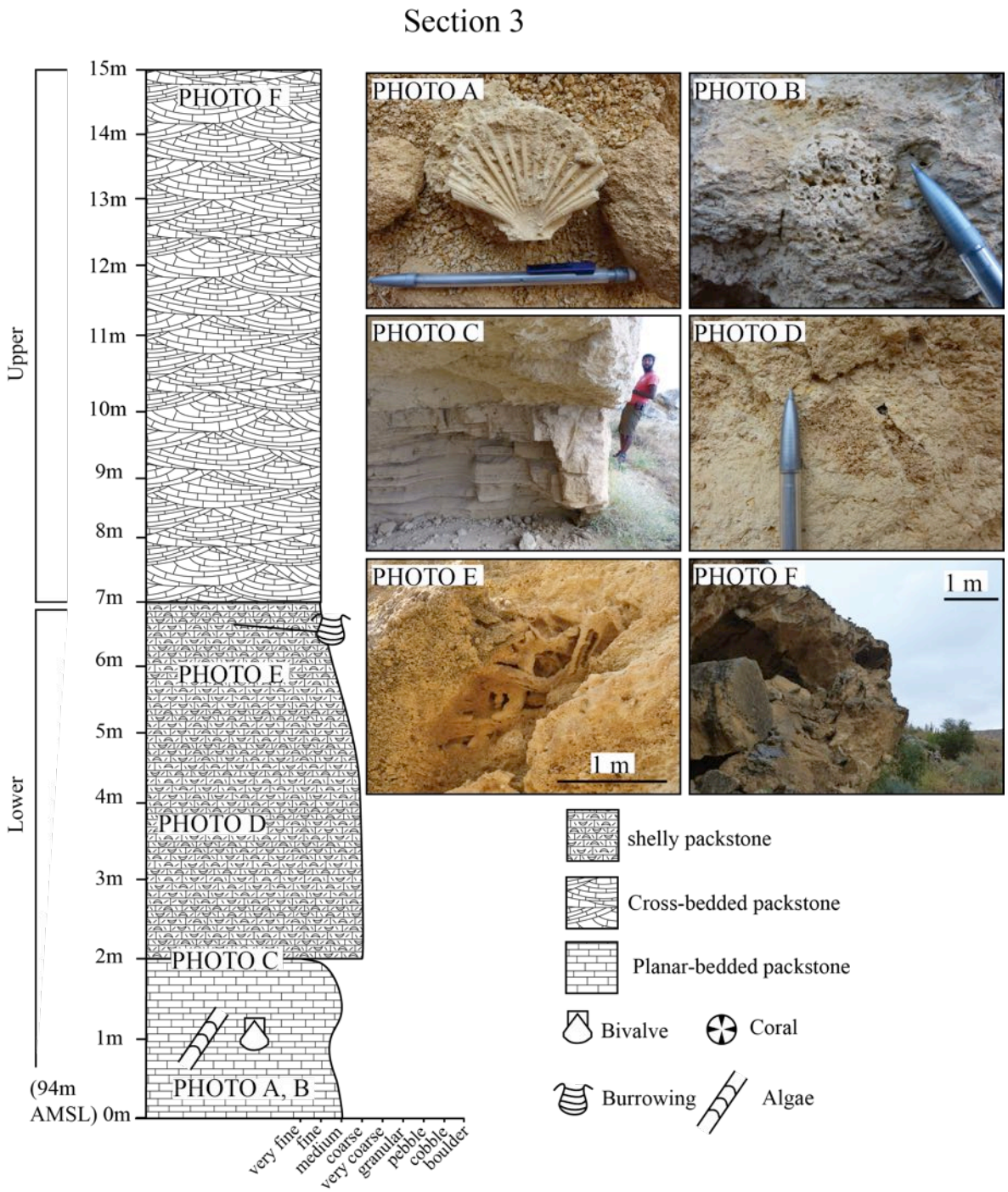

Figure 2.9: Sedimentary log and photographs of the Athalassa (Gürpınar) Formation just outside Mevlevi. Photograph (a) reworked bivalve; (b) well-preserved oncoids; (c) planar-lamination in the lower unit and a sharp erosional contact between the lower and middle unit; (d) coarse-fossiliferous rock with a cemented surface; (e) horizontal burrows preserved within the central section due to preferential weathering; and (f) Large, low-angle cross-bedding within the upper unit.

Section 4

Section 4 is found at the northeast edge of the Pliocene deposits and represents the contact between the Athalassa (Gürpınar) Formation and the chalk ridgeline (Fig. 2.4). The deposit forms part of the NE-trending surface prevoiously described. The chalk ridge forms a topographic high which the Pliocene deposit were deposited against, although exposed contacts between the two chalk and Pliocene deposits are rare. The Pliocene-chalk contact described here is at 295 m AMSL. Further to the northeast the Athalassa (Gürpınar) Formation grainstone is preserved as an isolated platform at nearly 350 m AMSL, where it unconformably overlies the Kythrea (Değirmenlik) Group (Harrison *et al.*, 2004; McCay and Robertson, 2012b).

Section 4 includes an unconformity between the Athalassa (Gürpınar) Formation grainstone and chalks of the Lapithos (Lapta) Group (Fig. 2.10). The Athalassa (Gürpınar) Formation grainstone is well cemented and has poorly preserved trough cross-bedding and planar bedding. The grainstone at this locality is less than 1 m thick, the thinnest observed along this surface. The chalk bedding is steeply dipping towards the north. Occasionally, the chalk has been fragment along bedding planes to produce elongate clasts (Fig. 2.10). The chalk clasts range from 1 cm to 1 m, with a modal clast size of ca. 10 cm. The clasts of chalk within the grainstone are heavily bored (Fig. 2.10).

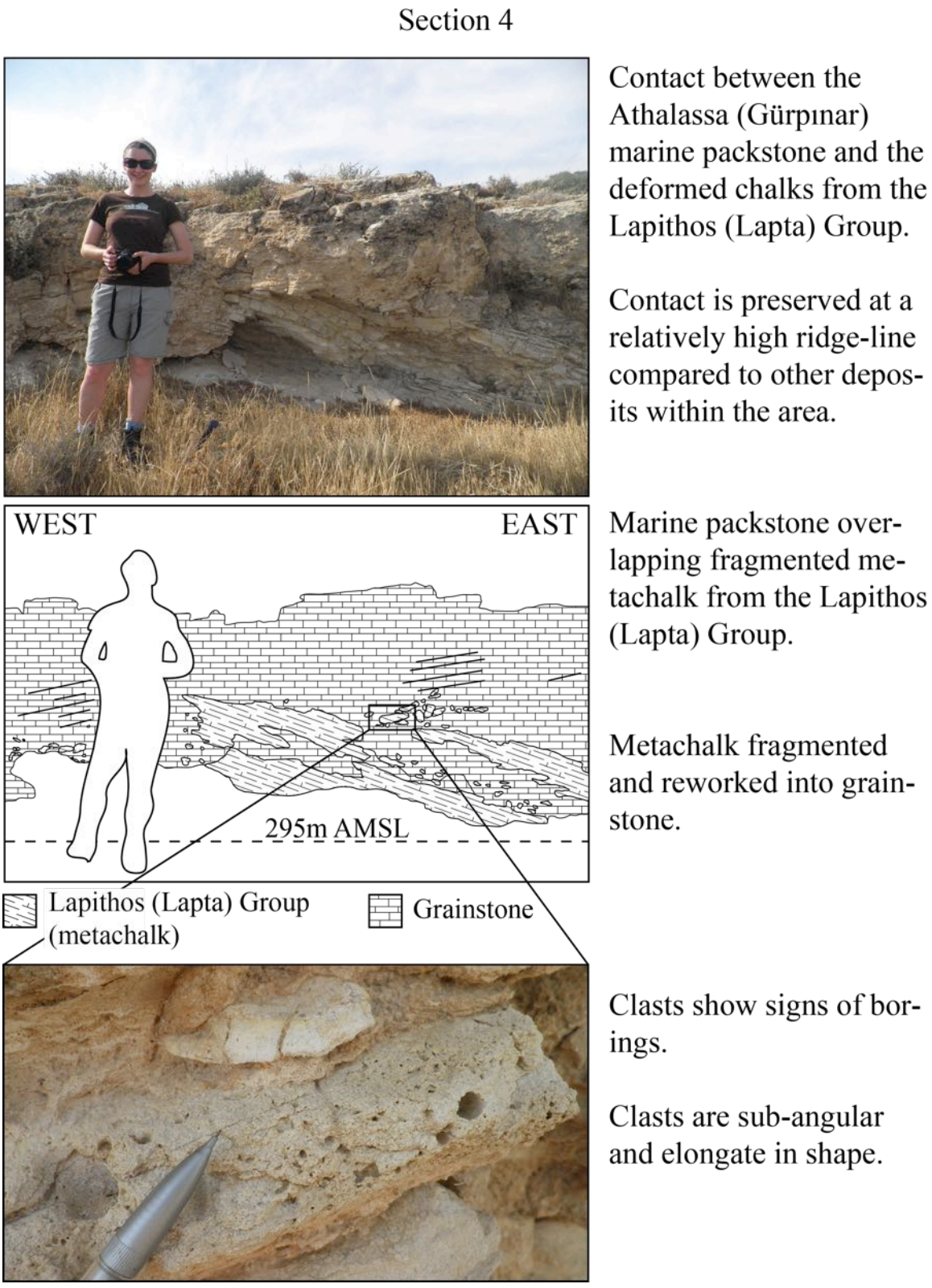

Figure 2.10: Photographs and schematic section of the Athalassa (Gürpınar) Formation contact with chalks of the Lapithos (Lapta) Group.

Section 5

Section 5 is from a road section through a major Athalassa (Gürpınar) Formation deposit that runs from Mevlevi towards the southwest for over 8 km (Fig. 2.4). The Athalassa (Gürpınar) Formation making up this surface unconformably overlies the Kythrea (Değirmenlik) Group, without the Nicosia (Lefkoşa) Formation beneath. The deposit varies in thickness from ca. 8 m at Section 5 to less than 1 m thick in several areas to the southwest.

The Athalassa (Gürpınar) Formation exposed south of Mevlevi is a ca. 8 m thick and ca. 500 m long grainstone deposit (Fig. 2.11). The deposit exhibits three depositional phases; the first is on the eastern end of the section, the second is in the central part, and the third forms the western half of the section (Fig. 2.11 Photo (a)). Each section is separated by a near-vertical erosional surface. The first section at the eastern end of the deposit comprises low-angle ($<30^o$) cross-bedding and laminated grainstone. The cross-bedding within this first unit dips towards both the east and west (Fig. 2.11, Photos (d, e)). Interbedded within this section are small conglomerate layers made up of well-rounded, 1 cm to 10 cm-sized clasts of chalk (Fig. 2.11, Photos (h, i)). The central section forms a near-vertical contact with the eastern section and comprises a poorly sorted, matrix-supported breccia. Clasts within the breccia are grainstone and are sub-angular and range in size from 1 cm to 50 cm (Fig. 2.11, Photos (f, g)). The western section is made up of five parallel 1-2 m-thick units, each of which is made up of a series of cross-bedded units. The cross-bedding foresets dip at $<30^o$ and have a general palaeoflow direction towards the east. Between each cross-bedded section is a laminated section, which is less than 50 cm thick. The cross-bedded sections are all gently dipping towards the west (Fig. 2.11, Photos (b, c)).

Figure 2.11: Photographs and schematic drawings from the Athalassa (Gürpınar) Formation along the motorway section immediately east of Mevlevi (Fig. 2.4). Photograph (a) overview photograph of the entire 40 m-long road section; (b)-(c) central part of the section; (d)-(e) eastern part of the section; (f)-(g) conglomerate of reworked grainstone from the central section; and (h)-(i) lenticular conglomerate made up of chalks within the eastern part of the section.

2.2.2 Gazimağusa (Famagusta) city

Gazimağusa (Famagusta) city is at the eastern end of the Mesaoria (Mesarya) Plain in northern Cyprus (Fig. 2.12). The Athalassa (Gürpınar) Formation is mapped as a series of isolated deposits between Gazimağusa (Famagusta) city and Geçitkale (Lefkoniko) town (Constantinou, 1995). The following section describes three areas around Gazimağusa (Famagusta) city; firstly, just outside the village of Köprülü (Kouklia); secondly, northwest of Gazimağusa (Famagusta) city in the Mesaoria (Mesarya) Plain between the villages of Sandallar (Santalaris) and Alaniçi (Peristerona); and thirdly, a series of deposits along the road between Geçitkale (Lefkoniko) and Iskele (Trikomo) towns. These deposits represent a range of Late Pliocene depositional environments within this area.

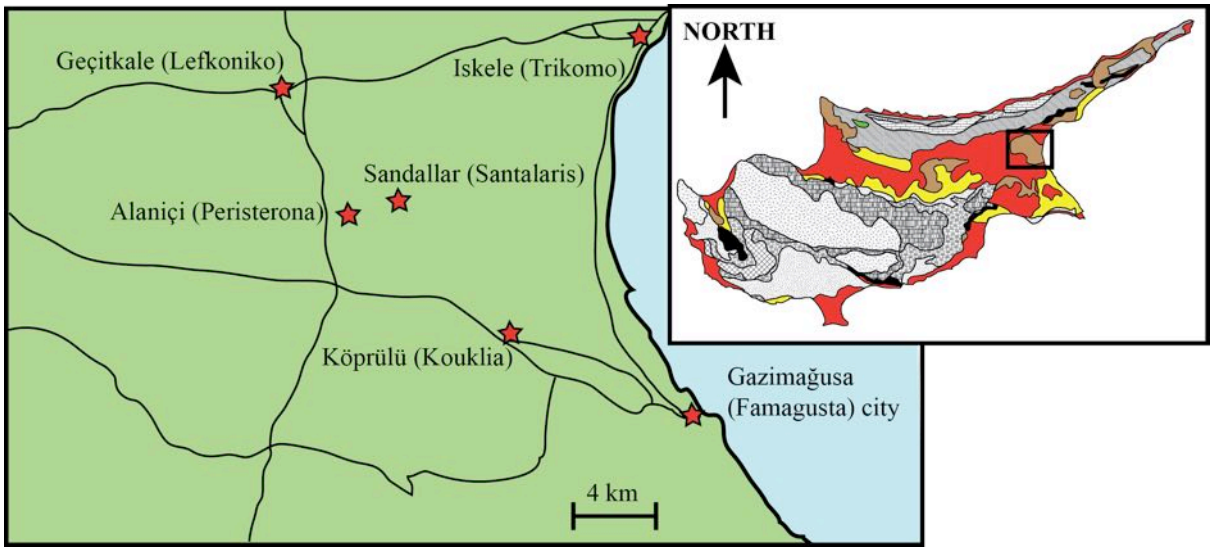

Figure 2.12: Map of the key localities on the western end of the Mesaoria (Mesarya) Plain in northern Cyprus.

Köprülü (Kouklia) village

Köprülü (Kouklia) village is ca. 5 km northwest of Gazimağusa (Famagusta) city (Fig. 2.12). This deposit represents the Athalassa (Gürpınar) Formation and is part of a ca. 3 km-long N-S orientated surface. Exposure of the entire section is due the recent excavation of a small quarry.

The basal part of the deposit is a ca. 1 m-thick fine-grained grainstone (Fig. 2.13, Photo D). The basal grainstone is overlain by a continuous clast-supported conglomerate bed made up of well-rounded clasts of chalk, diabase, radiolarite and chert (Fig. 2.13, Photo C). Conformably overlying the conglomerate are a series of cross-bedded and parallel-bedded sections with horizons rich in carbonate and clastic clasts (Fig. 2.13, Photos A, B). Overlying the entire section is a ca. 3 m-thick cross-bedded grainstone thickening southward to over 10 m thick. The cross-bedding within the upper grainstone changes from ca. 30 cm-thick foresets at the base of the section to foresets at the top that are ca. 2 m thick. The foreset angle changes from significantly less than 30^o at the base to nearly 40^o at the top. The palaeoflow direction in the upper grainstone is always towards the north. The basal grainstone deposits have small-scale compressional buckle folding in the upper beds, which could have been caused by deformation associated with the Ovgos (Dar Dere) fault zone that runs east-west to the north of this area (McCay and Robertson, 2012b).

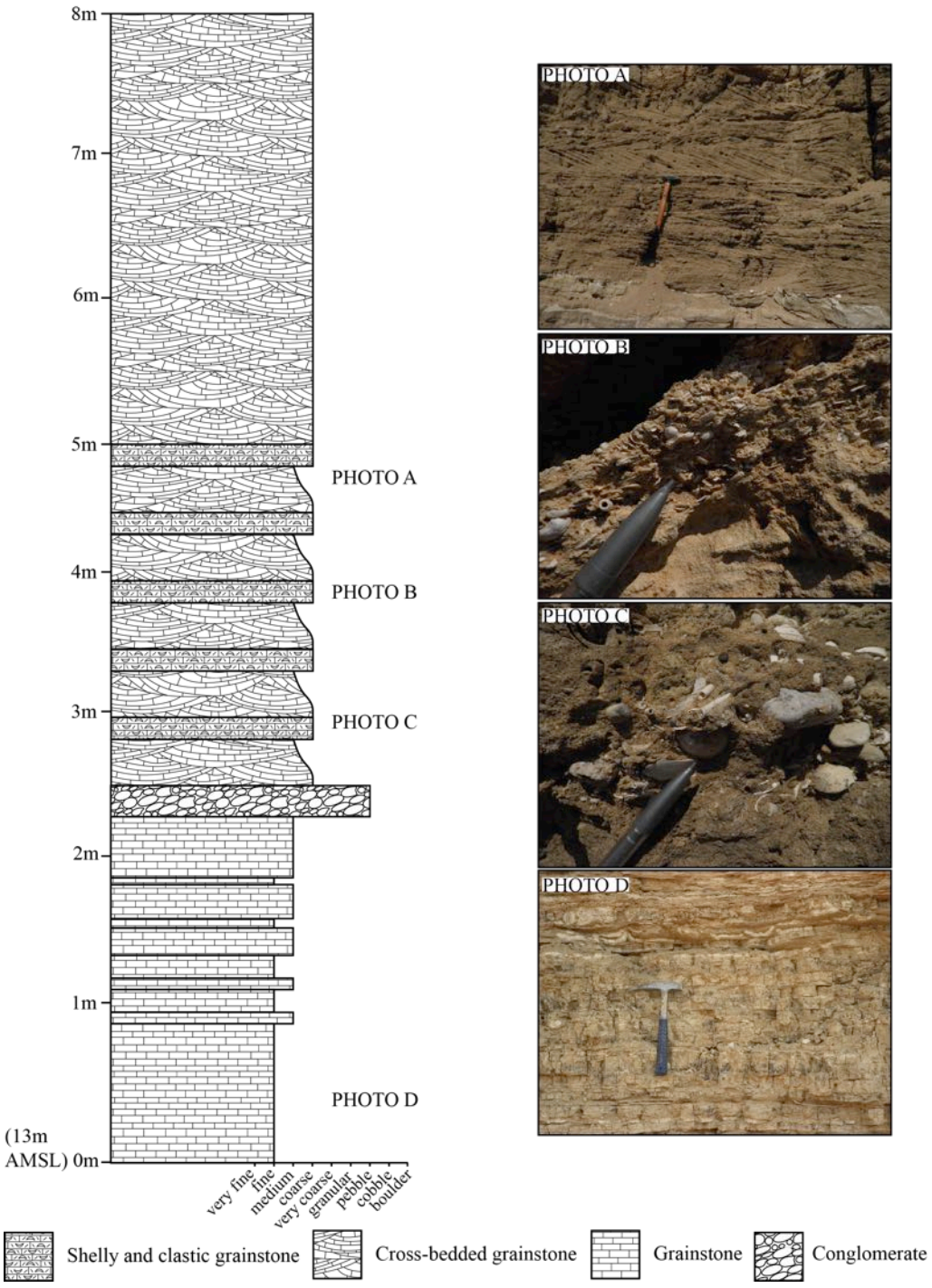

Figure 2.13: Sedimentary log and photographs of the Nicosia (Lefkoşa) and Athalassa (Gürpınar) Formations outside the town of Köprülü (Kouklia). Photograph (a) low-angle cross-bedding and laminations; (b) reworked shell-rich beds; (c) well-rounded clast and shell-rich beds; and (d) lower unit of marls within small-scale buckle folding in the upper beds.

Sandallar (Santalaris) to Alaniçi (Peristerona) villages

The deposits between the villages of Sandallar (Santalaris) to Alaniçi (Peristerona) are part of a large Pliocene section mapped between Geçitkale (Lefkoniko) and Iskele (Trikomo) towns, and surrounding Gazimağusa (Famagusta) city (Constantinou, 1995)(Fig. 2.12). The Pliocene deposits between Sandallar (Santalaris) to Alaniçi (Peristerona) villages were found within a recently exposed quarry section.

Two sections are described from small quarries just outside the two villages; each quarry dissects the current surface exposing the underlying geology. The deposit outside Sandallar (Santalaris) village is a ca. 8 m-thick section comprising a series of interbedded fine- and coarse-grained grainstone deposits with occasional conglomerate channels and large reworked blocks of grainstone. The grainstone varies from fine- to medium-grained and contains well preserved 5 cm to 10 cm-sized pecten and oyster shells. The fossiliferous grainstone in the lower part of the section are composed of casts of gastropod and bivalve shells (Fig. 2.14, Photos C, D). Overlying the fossiliferous bed is a ca. 2 m-thick chalk deposit with large blocks of grainstone, and conglomerate lenses. The conglomerate lenses contain well-rounded clasts, ranging in size from 1 cm to 10 cm, that comprise chalk, diabase, serpentinite, quartz and shell fragments. The grainstone is erosively overlain by a ca. 1 m-thick poorly bedded grainstone with conglomerate lenses (Fig. 2.14, Photo A). The conglomerate lenses are compositionally the same as the lower conglomerates however, the clasts are slightly bigger, from 1 cm to 15 cm. The upper part of the deposit is made up of a ca. 50 cm-thick fine-grained grainstone and a ca. 2.5 m-thick medium-grained grainstone.

The deposit outside Alaniçi (Peristerona) village is made up of a fine- to coarse-grained grainstone (Fig. 2.14). The lower ca. 2.5 m of the section are made up of interbedded fine- to coarse-grained grainstone beds with no preserved sedimentary structures. The middle part of the section is made of a series of fining-upward medium- to fine-grained grainstone beds. The upper part of the deposit shows a return to thickly-bedded sequence fine- to coarse-grained grainstone. The upper grainstone beds contain well-preserved pecten and oyster shells, burrowing features (Fig. 2.14, Photo B) and rare clasts of chalk, radiolarite and metacarbonate.

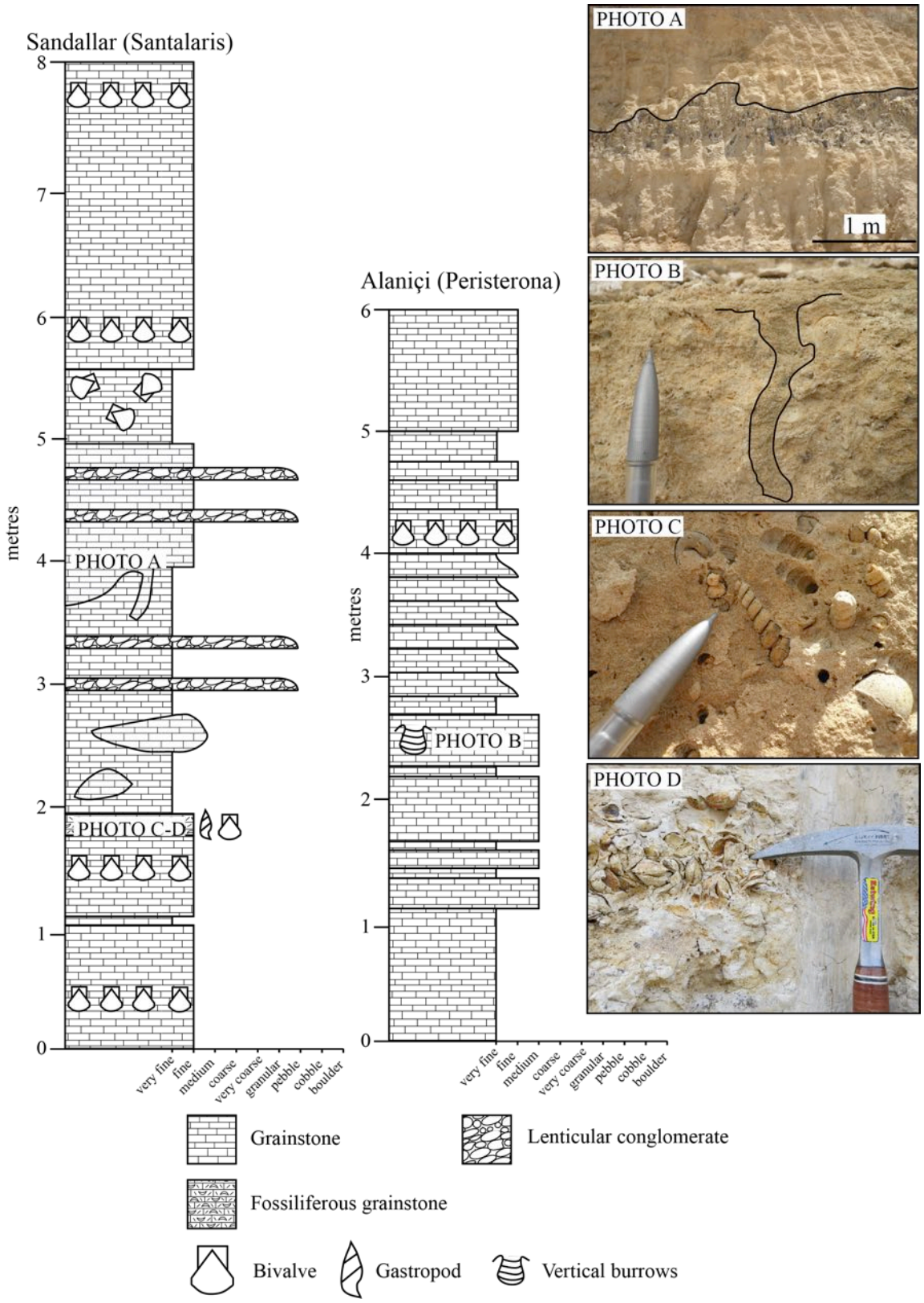

Figure 2.14: Sedimentary logs and photographs through the Nicosia (Lefkoşa) and Athalassa (Gürpınar) Formations at Sandallar (Santalaris) and Alaniçi (Peristerona), west of Gazimağusa (Famagusta). Photographs illustrating various key components from the logs, (a) erosional surface between chalk and grainstone; (b) burrowing within the grainstone; and (c,d) casts of gastropod and bivalve shells, respectively.

Geçitkale (Lefkoniko) town

The Pliocene deposits near Geçitkale (Lefkoniko) town are exposed to the east of the town as a series of sections along the Geçitkale (Lefkoniko)-Iskele (Trikomo) road (Fig. 2.12). The Geçitkale (Lefkoniko)-Iskele (Trikomo) road runs along the northern edge of the mapped Pliocene deposits (Constantinou, 1995).

Figure 2.15 shows a series of sedimentary logs from the Pliocene deposits exposed along the Geçitkale (Lefkoniko)- Iskele (Trikomo) road. The deposits are comprise a basal cross-bedded and laminated grainstone, with an overlying poorly-sorted, sub-angular, clast-supported conglomerate. The lower grainstone deposit varies in thickness from less than 2 m to over 4 m thick (Fig. 2.15). The cross-bedded packages are ca. 50 cm thick with foresets dipping at $<20^o$ (Fig. 2.15, Photo A). The cross-bedded sections are separated by laminated sections that are ca. 30 cm-thick (Fig. 2.15 Photo B). The palaeoflow direction of the cross-bedding is either toward the northeast or the southwest. The upper conglomerate erosively overlies the grainstone, with areas of major downcutting. The conglomerate unit is poorly bedded and has a poorly developed imbrication (Fig. 2.15, Photos C, D).The clasts within the conglomerate include chalk, quartz, chert, metacarbonate breccia, serpentinite and metacarbonate.

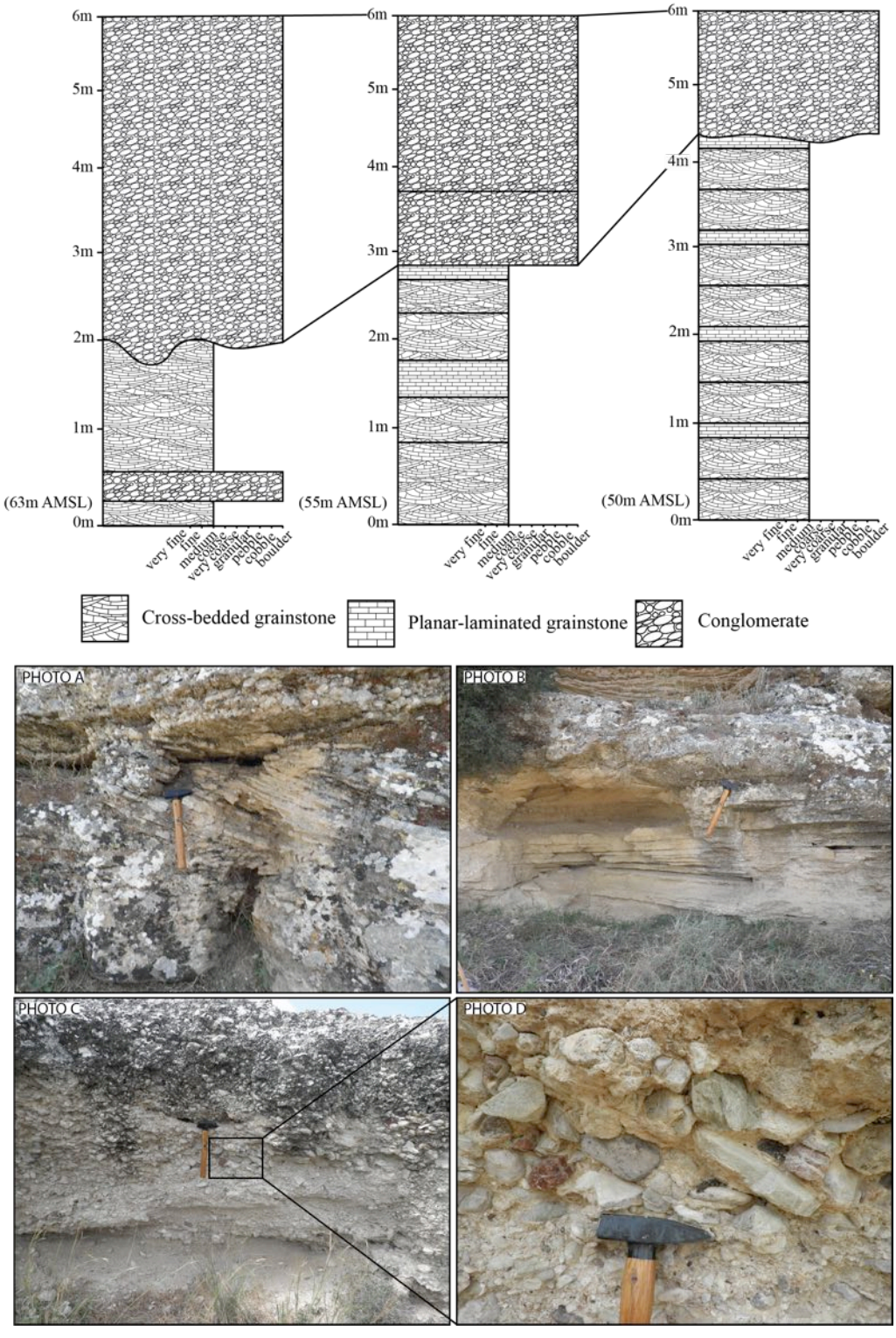

Figure 2.15: Sedimentary logs and photographs of the Athalassa (Gürpınar)-Fanglomerate Formation contact exposed southeast of Geçitkale (Lefkoniko). Photograph (a) large-scale cross-bedding within the lower grainstone; (b) planar laminations and cross-stratification within the lower grainstone; (c) upper conglomerate; and (d) clast imbrication within the upper conglomerate.

2.2.3 Kaleburnu (Galinopori) village

Kaleburnu (Galinopori) is a small village on the Karpaz (Karpas) Peninsula, ca. 2.5 km inland from the southern coast (Fig. 2.1). The basal geology in the area comprises the Kythrea (Değirmenlik) Group, unconformably overlain by the Athalassa (Gürpınar) Formation (Fig. 2.1). The Athalassa (Gürpınar) Formation forms a nearly continuous deposit from the northern to the southern coast of the peninsula in this area (Constantinou, 1995). Two sedimentary sections are presented within this area; firstly, Section 1 is from within the village; and secondly, Section 2 is immediately south of the village, from a small isolated hill (Figs. 2.16, 2.17, Photos A).

The Pliocene deposits within this area comprise a combination of planar-bedded and cross-bedded grainstone deposits (Figs. 2.16, 2.17, Photos B, C). Both sections have a 4-5 m-thick fine-grained grainstone containing 5 cm to 10 cm-sized pecten and oyster shells. In both sections, the basal grainstone is conformably overlain by a thick-bedded grainstone unit. In Section 1, the thick-bedded grainstone sequence directly overlies the fine-grained grainstone as a series of 1-2 m-thick fining upwards beds (Fig. 2.16). The thick grainstone bed contains rip-up clasts of marl (Figs. 2.16, 2.17, Photo D). The upper ca. 5 m of Section 1 is made up of a series of ca. 1 m-thick cross-bedded grainstones (Fig. 2.16), with well-preserved, 1 cm to 2 cm-sized bivalve shells (Fig. 2.17, Photo E) and horizontal burrowing (Fig. 2.17, Photo F). The cross-bedding foresets dip at $<20^o$ and have varying palaeoflow directions. In contrast, the grainstone in Section 2 forms a series of ca. 1 m-thick fining-upward beds conformably overlying the basal grainstone. The upper part of the section comprises interbedded fine- to coarse-grained beds of grainstone (Figs. 2.16, 2.17, Photo B).

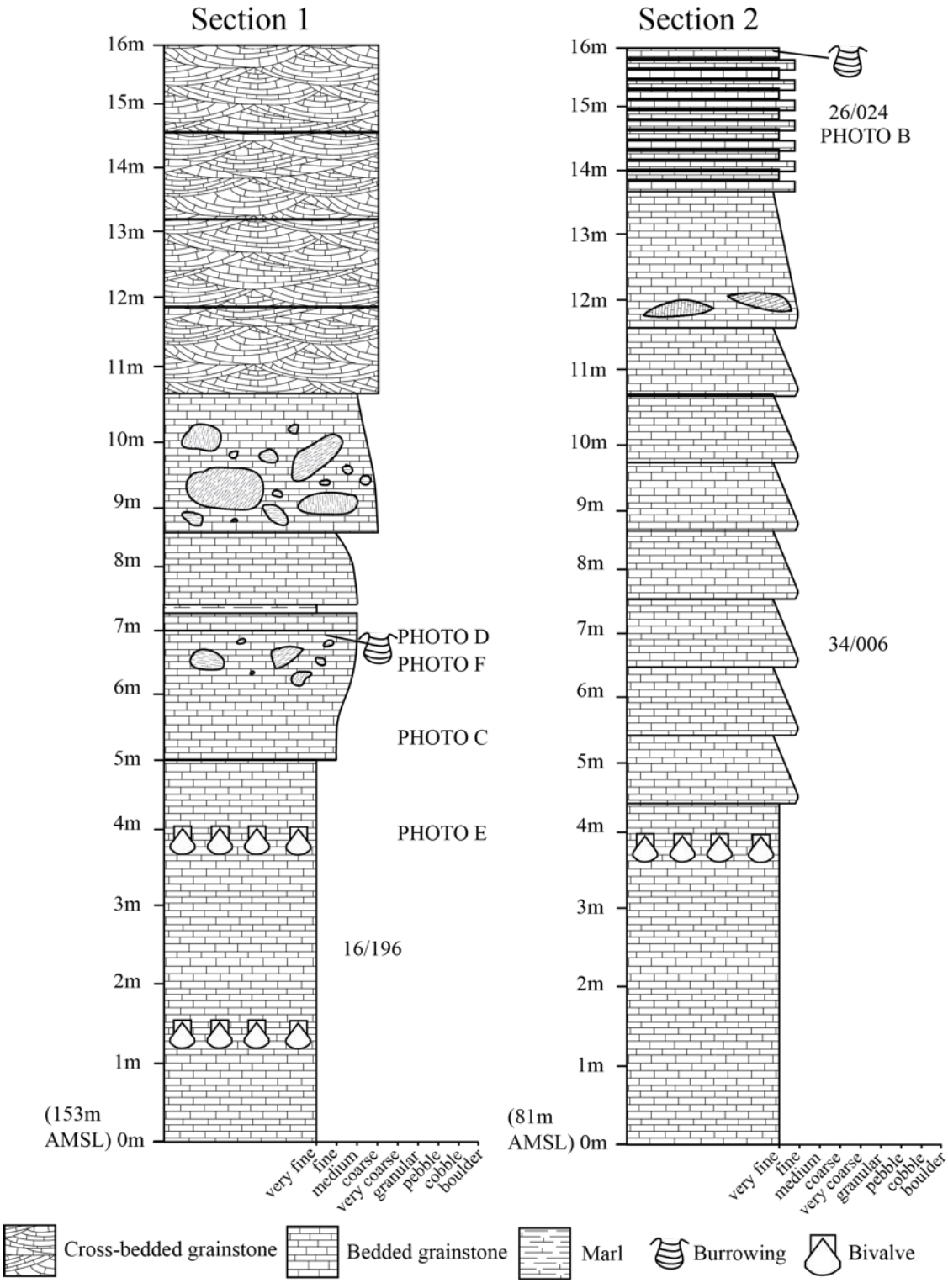

Figure 2.16: Sedimentary logs through the Nicosia (Lefkoşa) and Athalassa (Gürpınar) Formations within the small town of Kaleburnu (Galinopori), Karpaz (Karpas) Peninsula.

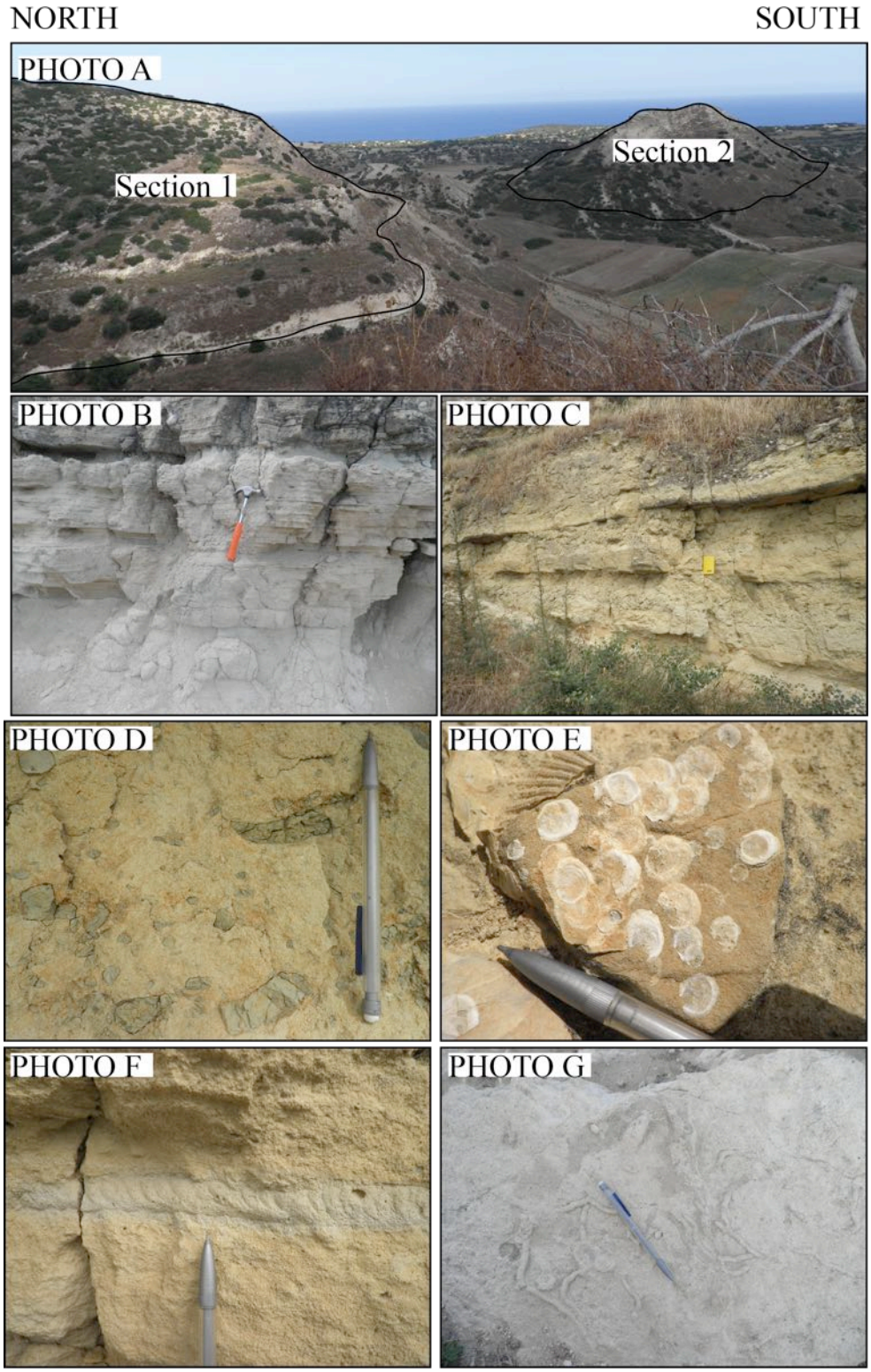

Figure 2.17: Photographs showing the Kaleburnu (Galinopori) town area and of key sedimentary features of the Athalassa (Gürpınar) Formation. Photograph (a) overview of the two sedimentary sections; (b) Bedded grainstone (c) fining-up beds within the grainstone; (d) reworked clasts of marl; (e) bivalve shells; (f) cross-section through well-preserved Cruziana ichnofacies; and (f) Cruziana ichnofacies preserved on the horizontal bedding surface.

2.3 Kalkanlı (Kapouti) Member

The Kalkanlı (Kapouti) Member is introduced here as a new subdivision of the Athalassa (Gürpınar) Formation. The Athalassa (Gürpınar) Formation accumulated within the Mesaoria (Mesarya) seaway between the Kyrenia Range and the Troodos Massif during the Late Pliocene to Early Pleistocene (McCallum and Robertson, 1995a). These Late Pliocene to Early Pleistocene deposits within the Mesaoria (Mesarya) Basin represent the change from marine to non-marine depositional setting (McCallum and Robertson, 1995a; Kinnaird *et al.*, 2011; Weber *et al.*, 2011). The timing and processes associated with the transition from marine to non-marine environments are poorly documented around the Kyrenia Range. The Kalkanlı (Kapouti) Member is represented by several deposits previously mapped as the Athalassa (Gürpınar) Formation that are preserved on the northern edge of the Mesaoria (Mesarya) Basin (Constantinou, 1995).

The Kalkanlı (Kapouti) Member occurs within ca. 10 km of the main spine of the Kyrenia Range. The deposits are rarely preserved within the central part of the Kyrenia range. The deposits are well represented at the eastern and western ends of the range. The type locality for the Kalkanlı (Kapouti) Member is in east around the town of Kalkanlı (Kapouti). Other deposits are exposed in eastern end of the range near the village of Balalan (Platanissos).

2.3.1 Kalkanlı (Kapouti) town

Kalkanlı (Kapouti) is a small town near the western end of northern Cyprus, ca. 5 km north of Güzelyurt (Morphou) town (Fig. 2.4). The Kalkanlı (Kapouti) Member forms a ca. 10 km-long surface, from ca. 3.5 km east of the town. The deposit is dipping gently down to the western coast. Several sections are studied from the Kalkanlı (Kapouti) Member surface in this area at varying heights above modern sea-level (Fig. 2.18).

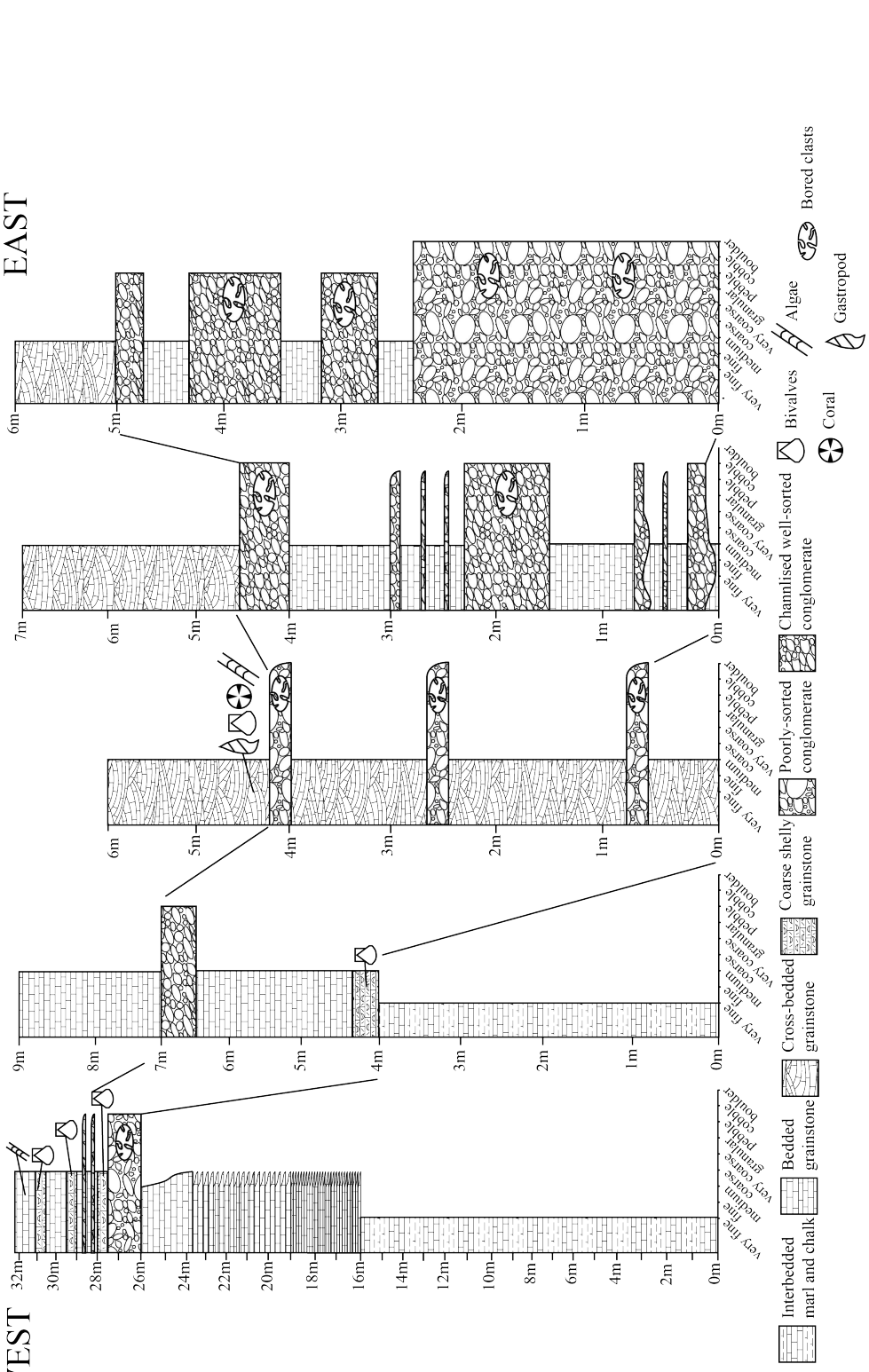

Figure 2.18: Sedimentary logs through deposits of the Nicosia (Lefkoşa) Formation and the Kalkanlı (Kapouti) Member around the town of Kalkanlı (Kapouti). The heights above modern sea-level (AMSL) given for each section are taken from the base of each deposit.

The deposits can be divided into two groups; firstly, deposits west of Kalkanlı (Kapouti) town (Fig. 2.18, Sections 1-3), and secondly, deposits east of Kalkanlı (Kapouti) town (Fig. 2.18, Sections 4, 5). Sections 1 and 2 are made up of a combination of interbedded chalks and marls, planar-bedded grainstone beds and conglomerates (Fig. 2.18). The basal chalk thickens from ca. 4 m to ca. 16 m-thick westwards away from Kalkanlı (Kapouti) town for ca. 2 km (Fig. 2.18). In both Section 1 and 2, the interbedded chalks and marls are conformably overlain by a planar-bedded grainstone of varying thickness. Section 1 includes planar-bedded grainstone, ca. 16 m-thick, with the lower ca. 8 m being made up of normally-graded, 1 cm to 16 cm-thick beds, overlain by a ca. 2 m-thick, normally-graded bed. Conformably overlying the bedded grainstone in Section 1 is ca. 1.5 m-thick clast-supported conglomerate with well-rounded clasts. The conglomerate is made up of clasts ranging in size from 1 cm to 50 cm, and include clasts of sandstone, metacarbonate, serpentinite, chert, basalt, grainstone and occasional shell fragments. The clasts within the conglomerate show signs of major boring (Fig. 2.19. Photos A, B). Overlying the conglomerate bed, there is an interbedded sequence of fossifilerous grainstone and medium-grained grainstone. The fossiliferous grainstone is rich in bivalve shell casts (Fig. 2.19, Photo C). Conglomerate channels of a similar composition to the lower conglomerate bed are also found within the grainstone beds within this interbedded sequence of fossiliferous grainstone and grainstone. The upper deposit of Section 1 is made up of a ca. 1 m-thick planar-bedded grainstone rich in oncoids with a "cauliflower-type" structure (Fig. 2.19, Photo D)(Djamali *et al.*, 2006). The grainstone deposit in Section 2 is significantly thinner than in Section 1, at only ca. 5 m thick. The grainstone at the base of Section 2 is bivalve rich and grades into a planar-bedded, ca. 5 m-thick grainstone with a conglomerate horizon of the same clast composition as in Section 1.

Section 3 forms the surface upon which Kalkanlı (Kapouti) town is built. Section 3 comprises a cross-bedded grainstone that is ca. 6 m thick and interbedded with conglomerate lenses (10 cm to 40 cm thick) and fossiliferous horizons. The clasts within the conglomerate lenses range from 1 cm to 15 cm in size and are dominantly composed of metacarbonate with occasional clasts of serpentinite, chert and basalt. The fossiliferous material includes casts of corals (Fig. 2.19, Photo E), calcareous algae (Fig. 2.19, Photo F), gastropods and bivalves. The deposit unconformably overlies steeply eastward-dipping, interbedded sandstones and mudstones of the Kythrea (Değirmenlik) Group. The deposit of Section 3 makes up the ca. 2 km-long surface, upon which Kalkanlı

(Kapouti) town is built.

Directly east of Kalkanlı (Kapouti) town there are a series of isolated surfaces which can be correlated with the Kalkanlı (Kapouti) town surface (Fig. 2.4) as represented by Sections 4 and 5 (Fig. 2.18). Sections 4 and 5 comprise interbedded planer- and cross-bedded grainstone and lenticular- to planar-bedded conglomerate. The conglomerate forms a series of beds and lenses of varying thickness from ca. 5 cm to ca. 2 m thick (Fig. 2.20, Photos A, B, C). The conglomerates are clast supported and contain well-rounded clasts, ranging in size from 1 cm to 10 cm. Compositionally, they are composed of metacarbonate, chalk, serpentinite, jasper, basalt and K0 terrace breccia (Sec. 3.6.2)(Fig. 2.20 Photo D). Some of the conglomerate clasts are heavily bored (Fig. 2.20, Photo E), these are found within most conglomerate beds. Conformably overlying the interbedded grainstone and conglomerate deposits in both Sections 4 and 5 is a 1-3 m-thick cross-bedded grainstone. Foresets dip at $<30^o$ and form ca. 50 cm sections within the deposit.

The various deposits can be correlated along the dissected east-west surface which dips gently downwards to the western coast. The upper part of Section 1 correlates to the upper part of the surface comprising Sections 2 to 5 further west, respectively. The interbedded grainstones, fossiliferous grainstone and conglomerates make up the Kalkanlı (Kapouti) Member; whereas the interbedded chalks and marls from Sections 1 and 2 are from the Nicosia (Lefkoşa) Formation.

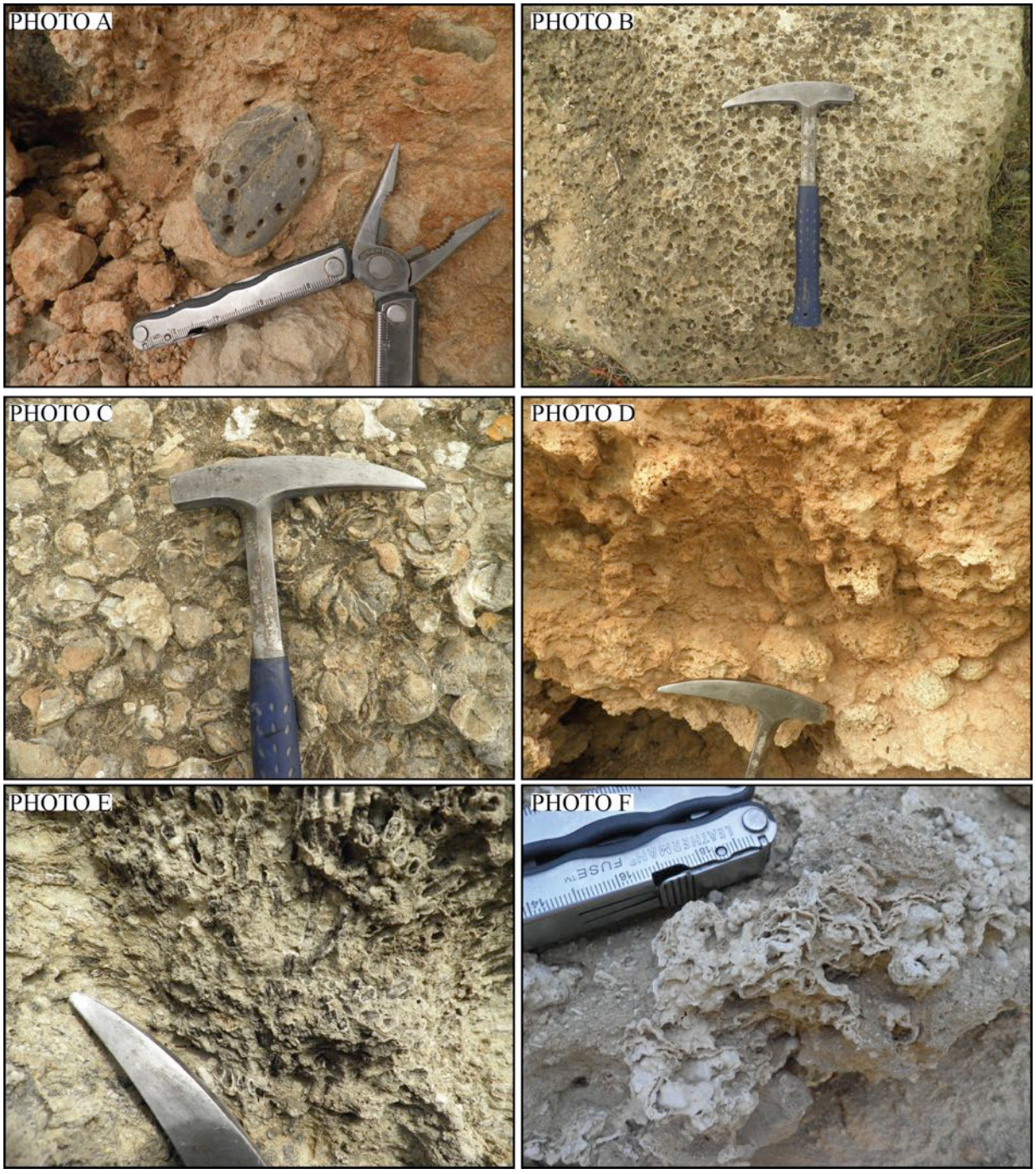

Figure 2.19: Photographs of various biogenic features in the Kalkanlı (Kapouti) Member near Kalkanlı (Kapouti) town. Photograph (a) bored clast of metacarbonate from the Trypa (Tripa) Group (Section 1); (b) heavily bored, reworked clast of grainstone (Section 1); (c) decalificed bivalve shells (Section 1); (d) Oncoids from the highest deposit (Section 1); (e) reworked casts of coral (Section 3); and (f) encrusting algae (Section 3).

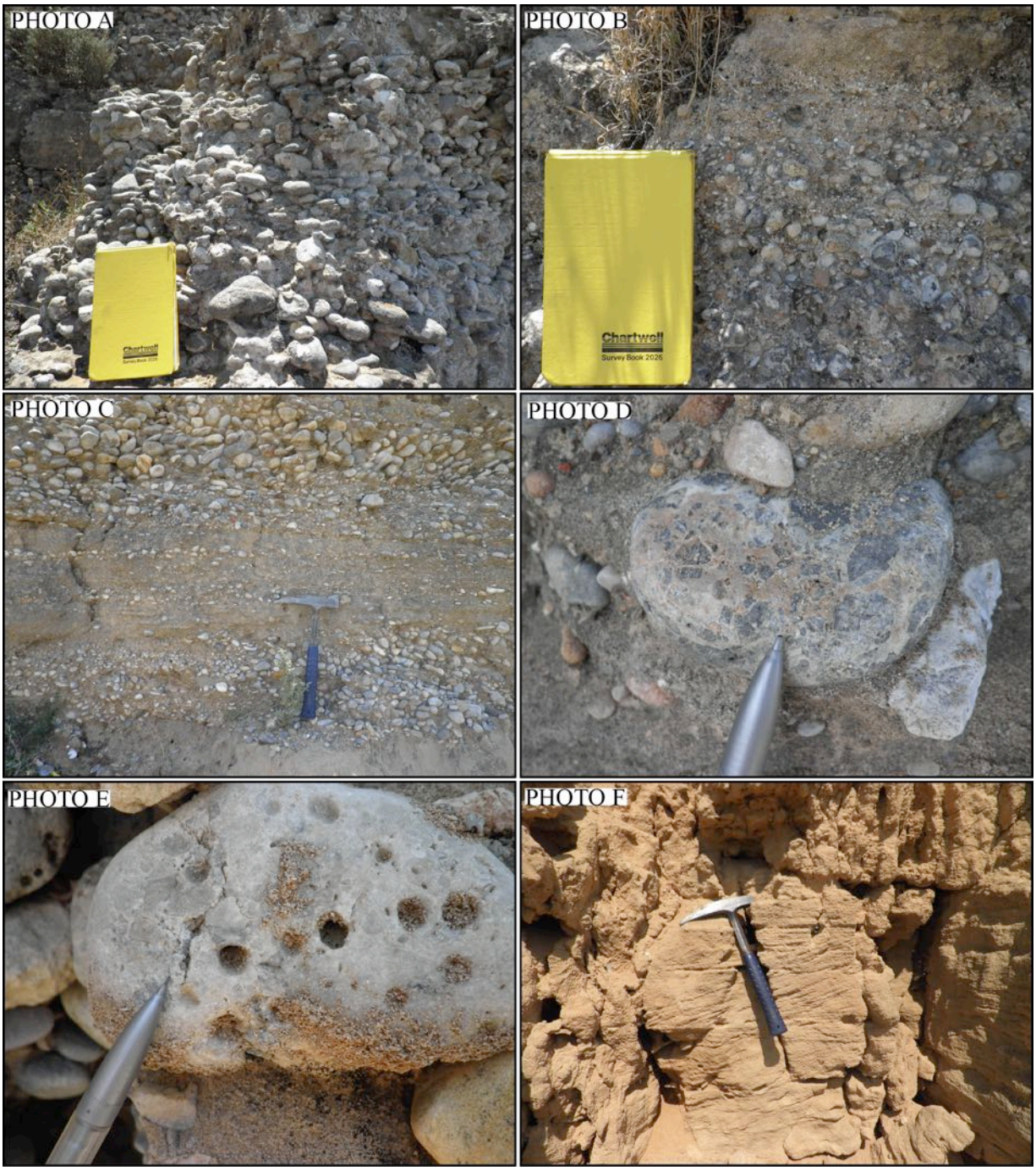

Figure 2.20: Photographs of various fluvial features from the Kalkanlı (Kapouti) Member, near Kalkanlı (Kapouti) town. Photograph (a) clast-supported basal conglomerate with well-rounded clasts (Section 4); (b) normal grading within conglomerate (Section 4); (c) conglomerate lenses significantly varying in thickness (Section 4); (d) reworked clasts of K0 breccia (Section 4); (e) bored clasts (Section 4); and (f) small-scale cross-bedding within capping grainstone (Section 4).

2.3.2 Balalan (Platanissos) village

Balalan (Platanissos) is a small village near the western end of the Kyrenia Range. In contrast to Kalkanlı (Kapouti) town, the village is perched on the main range. The Pliocene deposits within this area were mapped as the Athalassa (Gürpınar) Formation, which covers the flanks of the range in this area (Constantinou, 1995)(Fig. 2.1). The Pliocene section forms the hillside that the village is built upon.

The base of the deposit at Balalan (Platanissos) village is comprise a ca. 14 m-thick sequence of interbedded chalks and marls (Fig. 2.21). This is conformably overlain by a ca. 4 m-thick, interbedded section of conglomerate and grainstone. The conglomerate contains poorly sorted, sub-angular clasts, composed of both clastic and carbonate material. The clastic material within the conglomerate includes basalt, serpentinite, radiolarite and chert; the carbonate material includes bivalves, gastropods, serpulid worms and calcareous algae (Fig. 2.21, Photos D, F). The clasts and shells in the conglomerate are heavily bored (Fig. 2.21, Photo E). Conformably overlying the conglomerate is a ca. 6 m-thick poorly-sorted medium-grained shelly grainstone, rich in bivalves, gastropods and calcareous algae. The shelly grainstone deposit fines upwards into a ca. 14 m-thick medium- to fine-grained grainstone with planar bedding; this is interbedded with occasional ca. 20 cm-thick conglomerate lenses in the upper part of the section. The planar-bedded grainstone is conformably overlain by another ca. 1 m-thick bed of shelly grainstone, with large well-preserved and reworked *Macrochlamys* (Micoene aged, such as described by Bojar *et al.* (2004)) and calcareous algae (Fig. 2.21, Photos B, C) The upper part of the deposit is composed of a ca. 14 m-thick planar cross-bedded grainstone with abundant horizontal burrows (Fig. 2.21, Photo A). The cross-bedding foresets dip from 30^o to ca. 45^o. The section unconformably overlies deformed pillow lava, radiolarite and serpentinite from the Kalograi- Ardana (Bahçeli-Ardahan) Formation (Constantinou, 1995; McCay and Robertson, 2012b).

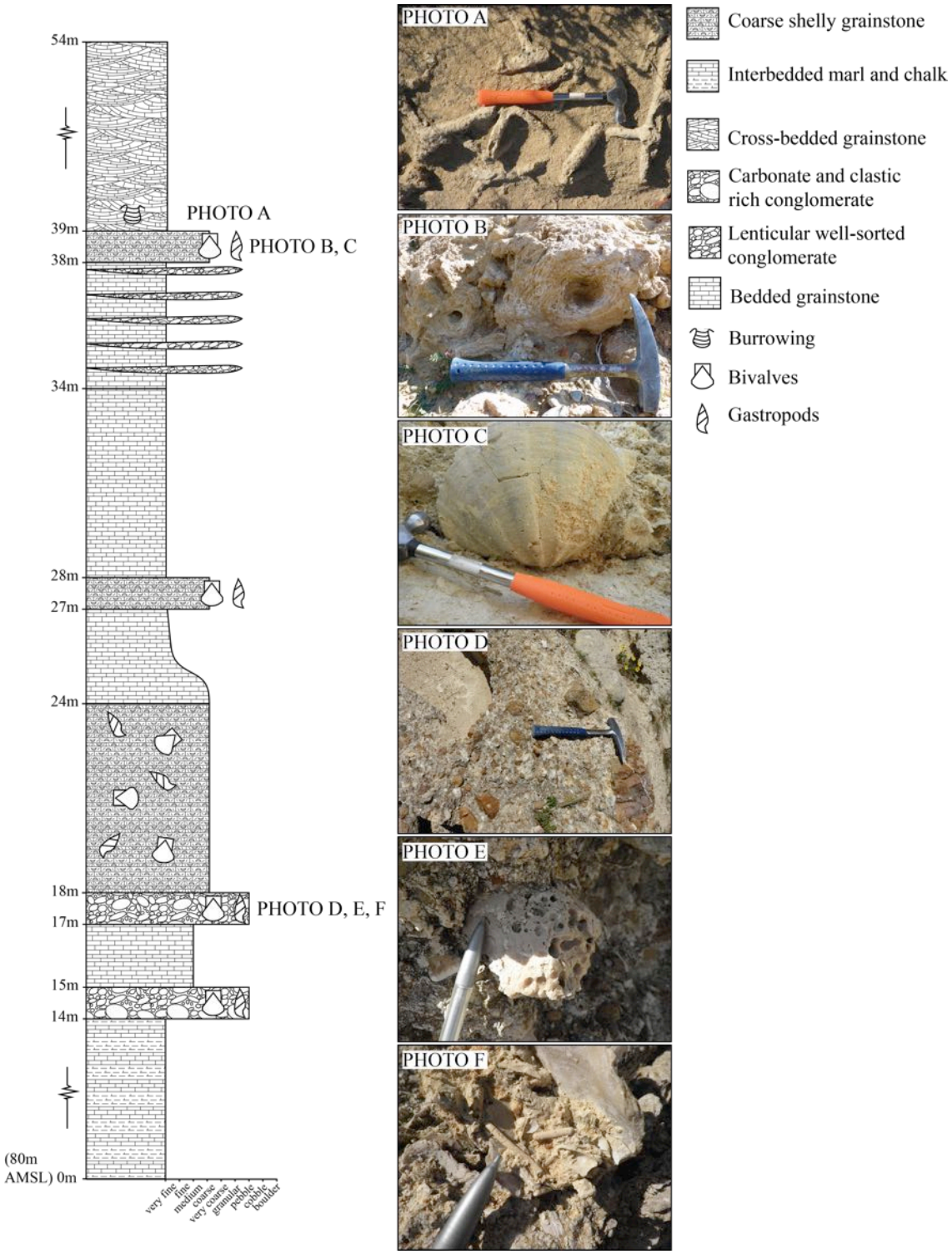

Figure 2.21: Sedimentary log and photographs of deposits from the Nicosia (Lefkoşa) Formation and the Kalkanlı (Kapouti) Member at the village of Balalan (Platanissos). Photograph (a) well-preserved horizontal burrows; (b) reworked fragments of algae; (c) reworked Miocene-aged *Macrochlamys*; (d) reworked clasts of basalt within the conglomerate beds; (e) heavily bored clast; and (f) conglomerate bed rich in reworked biogenic debris.

2.4 Grainstone palaeocurrent data

Palaeocurrent data were measured from cross-bedded grainstones in the Athalassa (Gürpınar) Formation across northern Cyprus. The data were separated into two groups: one, grainstones with cross-bedding structures that have shallow (<30°) foreset dips forming <50 cm-thick units. Two, grainstone deposits with cross-bedding units that dip at >30° and form 1 m to 2 m-thick units.

The palaeocurrent data is plotted on a rose-diagram as shown in Figure 2.22. The low-angle cross-bedded grainstone shows a large variation in palaeocurrent directions. However, there is a general flow direction towards the northeast. In contrast, the high-angle cross-bedded grainstone has palaeocurrent directions either northwards or southwards.

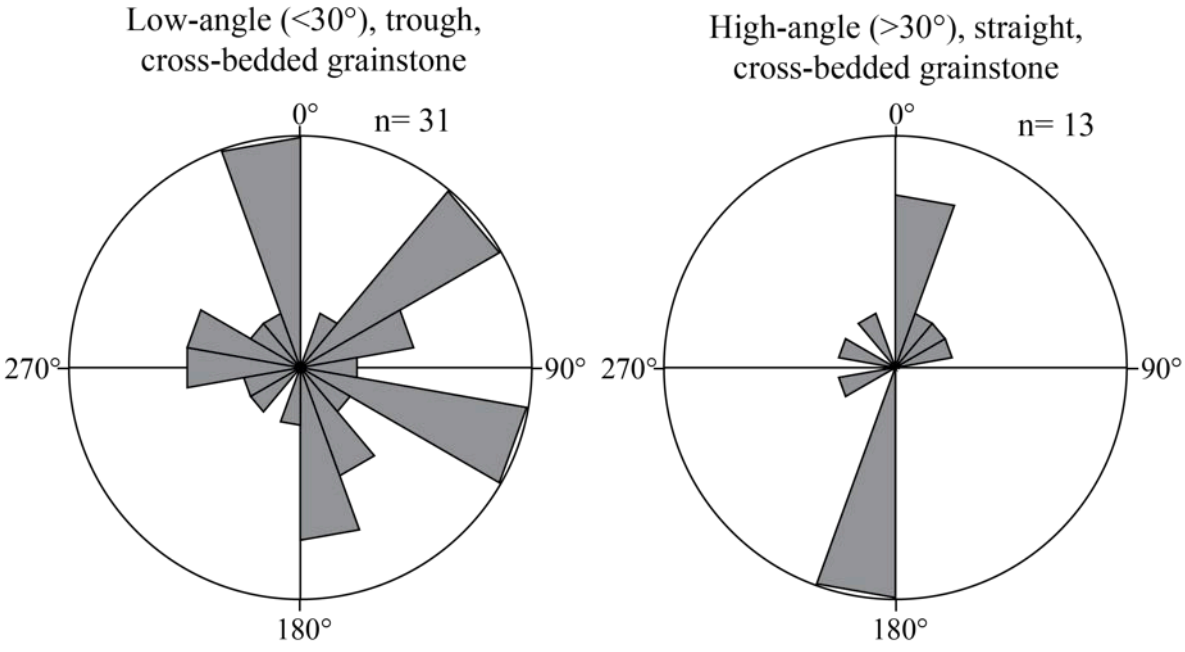

Figure 2.22: Palaeocurrent data from various grainstone facies of the Athalassa (Gürpınar) Formation.

2.5 Petrography

The petrographic analysis will focus on lithologies of the Nicosia (Lefkoşa) and Athalassa (Gürpınar) Formations and the Kalkanlı (Kapouti) Member within three key regions around northern Cyprus. Firstly, the western part of the Mesaoria (Mesarya) Plain, near Güzelyurt (Morphou) town; secondly, in the eastern part of the Mesaoria (Mesarya) Plain, outside Gazimağusa (Famagusta) city; and thirdly, on the Karpaz (Karpas) Peninsula (Fig. 2.1).

2.5.1 Microfossils

The Nicosia (Lefkoşa) and Athalassa (Gürpınar) Formations and the Kalkanlı (Kapouti) Member deposits are rich in both planktonic and benthic foraminifera. The foraminifera can be used to help interpret the depositional environment. The identifications were carried out at family level, for the planktonic foraminifera by Professor Kemal Tasli and for the benthic foraminifera by Professor Nurdan Inan of Mersin University, Turkey.

The dominant foraminifera within the chalks and marls of the Nicosia (Lefkoşa) Formation are *Globigerinidae* (Fig. 2.23(a-c)), Late Eocene to Recent planktonic foraminifera. *Globigerinidae* are also found as a minor component in the Athalassa (Gürpınar) Formation and the Kalkanlı (Kapouti) Member. Several other families of planktonic foraminifera including *Nodosariidae* and *Rotaliidae* occur in relatively minor proportions (Fig. 2.23(d-f)). The planktonic foraminifera make up 90% of the chalks; whereas, only 10% of the marls. The remainder of the marls is composed of fine grained carbonate mud. Occasional benthic foraminifera (*Lenticulina*) are also preserved within the chalks.

The Athalassa (Gürpınar) Formation and the Kalkanlı (Kapouti) Member deposits are rich in benthic foraminifera. *Miliolida* and *Neorotalia* are the dominant benthic foraminifera preserved within the grainstone deposits (Fig. 2.24(a, b)). *Peneroplidae* is only found in the Athalassa (Gürpınar) Formation deposits on the Karpaz (Karpas) Peninsula (Fig. 2.24(c)). *Anomalina*, *Textulariidae*, *Rotaliidae*, *Eponides*, *Valvulina* and *Elphidium* formas comprise relatively small proportion of the benthic foraminifera preserved within the Athalassa (Gürpınar) Formation and the Kalkanlı (Kapouti) Member

deposits (Fig. 2.24(d- j)).

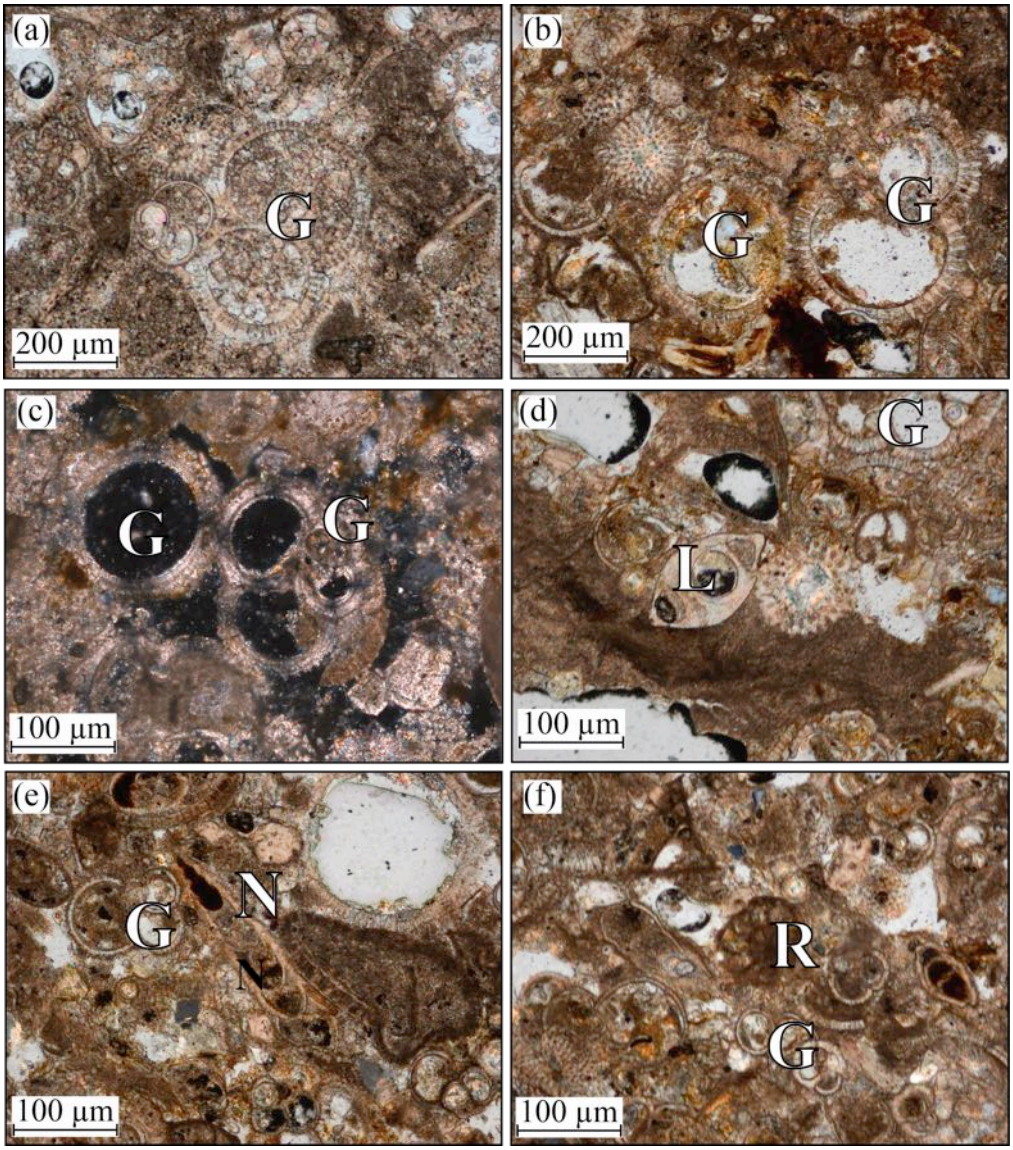

Figure 2.23: Photomicrographs of planktonic foraminifera from interbedded marls and chalks from the Nicosia (Lefkoşa) Formation. The photomicrographs include: (a) *Globigerinidae* [G]; (b) *Globigerinidae* [G]; (c) *Globigerinidae* [G]; (d) *Lenticulina* [L] (benthic foraminfera) and *Globigerinidae* [G]; (e) *Globigerinidae* [G] and *Nodosariidae* [N]; and (f) *Rotaliidae* [R] and *Globigerinidae* [G].

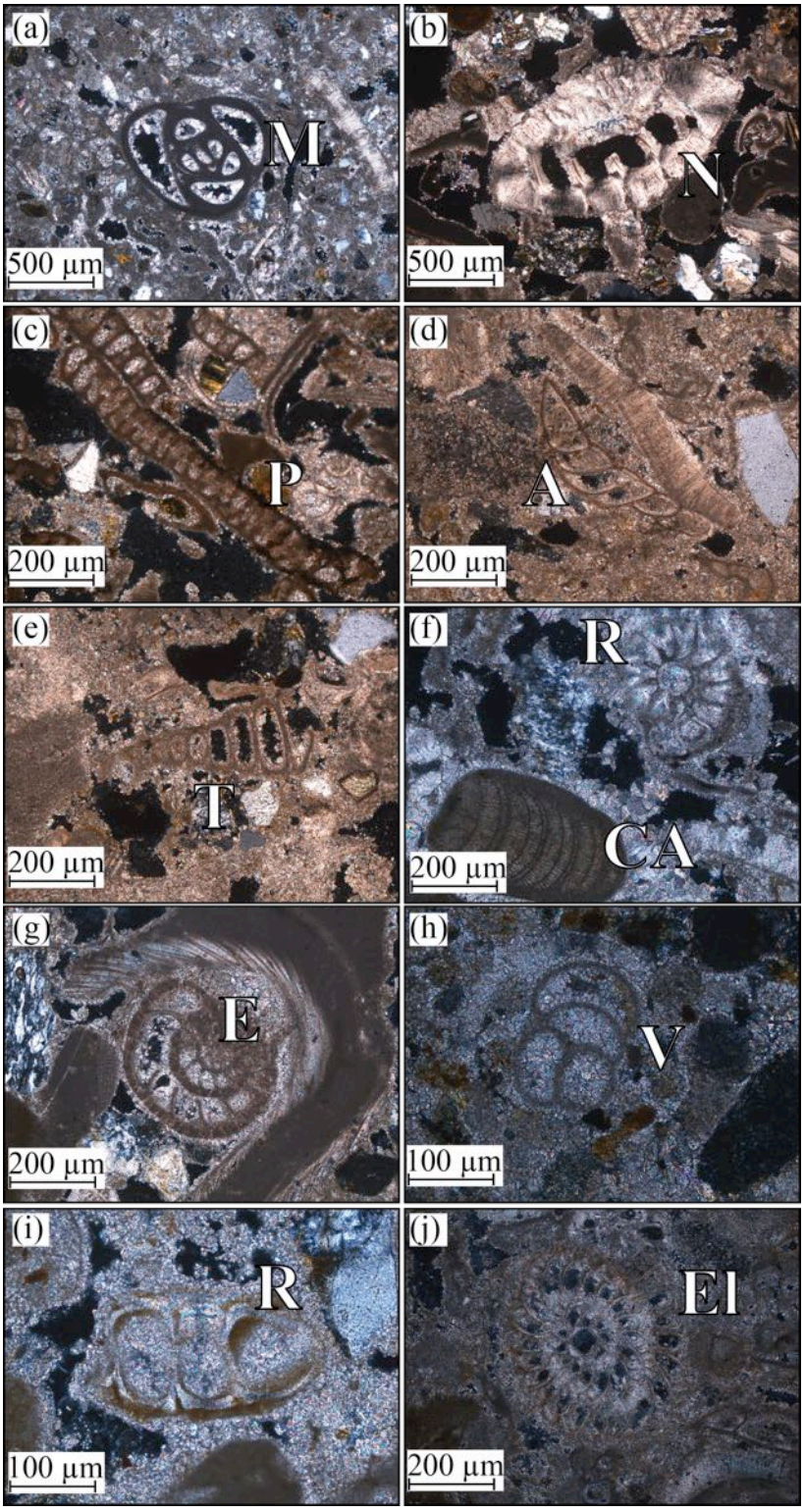

Figure 2.24: Photomicrographs of benthic foraminifera from the Athalassa (Gürpınar) Formation deposits from the Mesaoria (Mesarya) Plain and the Karpaz (Karpas) Peninsula. The photomicrographs include: (a) *Miliolida* [M]; (b) *Neorotalia* [N]; (c) *Peneroplidae* [P]; (d) *Anomalina* [A]; (e) *Textulariidae* [T]; (f) *Rotaliidae* [R] and calcaerous red algae [CA]; (g) *Eponides* [E]; (h) *Valvulina* [V]; (i) *Rotaliidae* [R]; and (j) *Elphidium* [El].

2.5.2 Carbonate and clastic grains

The grainstone of the Athalassa (Gürpınar) Formation is made up of carbonate and clastic material. The foraminifera within the Pliocene deposits were discussed in the previous section. The following description focuses on the *in situ* and reworked carbonate material and terrigenous derived clastic material. Section 2.6 will describe the spatial variations of the carbonate and clastic components.

The carbonate clasts are predominantly composed of calcareous red algae, echinoderms, bivalve fragments, bryozoa and benthic foraminifera (Fig. 2.25(a-c)). The calcareous red algae forms a rudstone (Dunham, 1962) at several localities (Fig. 2.25(a)), where the deposit is dominated by calcareous red algae. Hollow, circular, to oval-shaped carbonate clasts are preserved in most deposits and range from fully to partially fragmented (Fig 2.25(e)). The hollow grains comprise a layered micrite inner section ($<$ 200 μm-thick) and a thick acicular calcitic outer section (ca. 400 μm-thick). The inner micritic section shows a faint layered structure (Fig. 2.25(f)) suggesting a microbial algal encrustation (rather than a a diagenetic cement). Examples of such microbial (algal) encrustation are seen on echinoderm plates (Fig. 2.25(g)) and as reworked fragments (Fig. 2.25(h)). The outer section is an acicular isopachous calcitic cement. The reworked echinoderm plates often have a speckly texture possibly due to bacterial alteration (Fig. 2.25(i, j)). Ostracods and bryozoa also occur as minor components in several deposits.

Reworked clasts form a major constituent of the Pliocene grainstone deposits and can be divided into groups: 1) clastic material and 2) carbonate grains. Clastic material includes mono and polycrystalline quartz (Fig. 2.25(k)), chert, serpentinite, diabase, metacarbonate and feldspar. The reworked carbonate is dominantly benthic and planktonic foraminifera and calcareous red algae (Fig. 2.25(k-m)). Foraminifera that were reworked from older deposits have chambers infilled with a different cement compared to the host rock (Fig 2.25(k, l)). The reworked calcareous red algae form well-rounded grains (Fig. 2.25(m)); well-rounded, reworked clasts of grainstone, chalk and marl also occur as a minor constituant within the grainstone deposits (Fig. 2.25(n, o)).

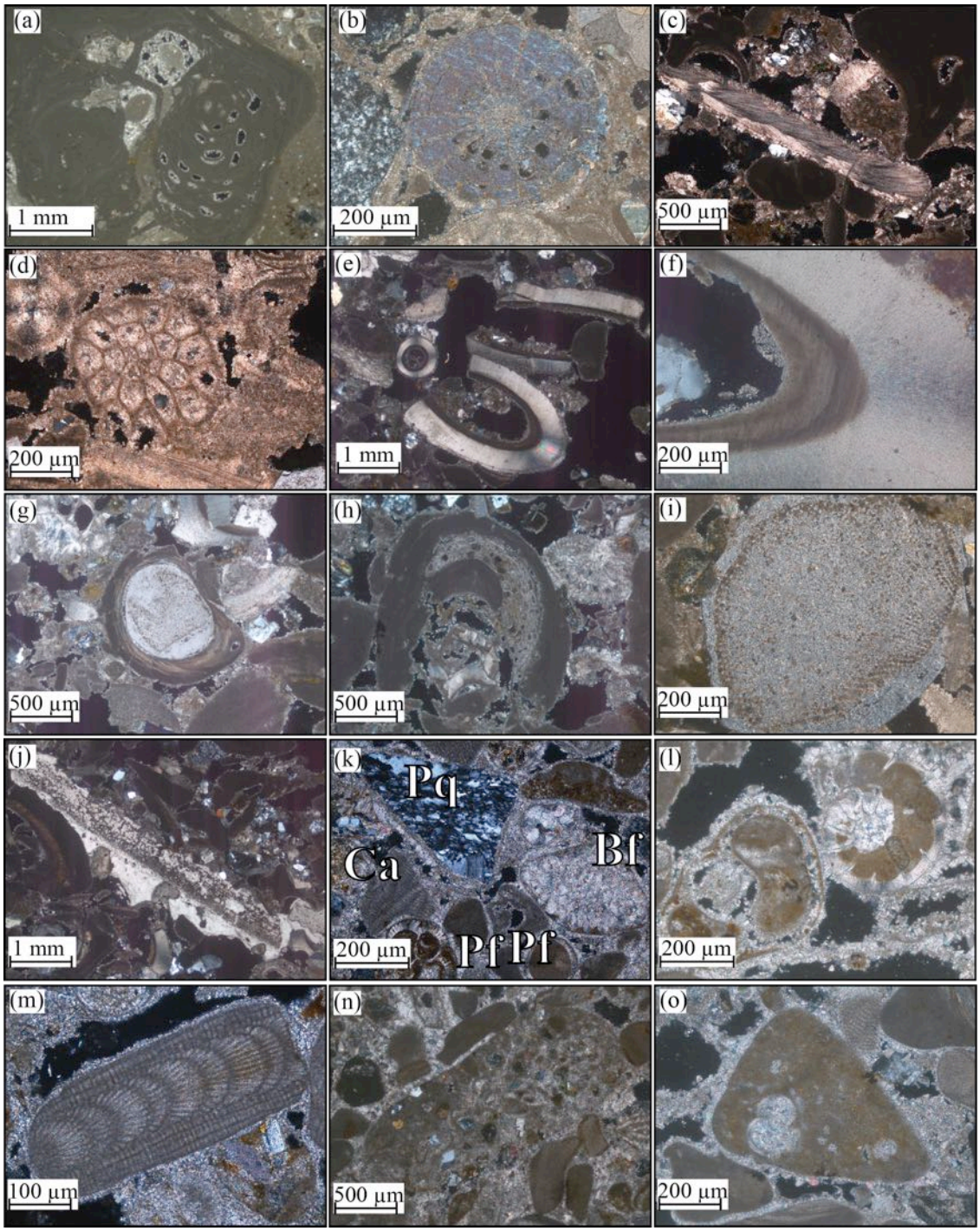

Figure 2.25: Photomicrographs of carbonate and clastic grains in the Athalassa (Gürpınar) Formation deposits in northern Cyprus. The photomicrographs include:(a) calcareous red algae; (b) echinoderm plate; (c) bivalve fragment; (d) bryozoa; (e) reworked carbonate algae with fibrous cement; (f) faint algal structure coated by fibrous carbonate cement; (g) echinoderm with encrusting algae; (h) reworked clast of algae with encrusting calcareous red algae; (i) echinoderm plate with algal overgrowth; (j) echinoderm plate with algal overgrowth; (k) polycrystalline quartz [Pf], calcareous red algae [Ca], benthic foraminifer [Bf] and planktonic foraminifera [Pf]; (l) reworked benthic foraminifera with microbic cement infilling chambers; (m) reworked grain of calcareous red algae; (n) reworked grain of grainstone; and (o) reworked grain of marl with planktonic foraminifera.

2.5.3 Kalkanlı (Kapouti) Member

The Kalkanlı (Kapouti) Member comprises a grainstone (Dunham, 1962), with both carbonate and clastic grains (Fig. 2.26 (a)). The carbonate grains include calcareous red algae, *Miliolida* (benthic foraminifera), *Neorotalia* (benthic foraminifera) (Fig. 2.26 (b, c, d)), crinoids and bivalve shell fragments. The clastic grains are dominantly monocrystalline quartz and metacarbonate (Fig. 2.26(e, f)). In addition, reworked carbonate and clastic-rich grainstone (Fig. 2.26 (g, h)) and reworked planktonic and benthic foraminifera (Fig. 2.26 (i, j)) are also found within the Kalkanlı (Kapouti) Member grainstone. The grainstone has a sparite cement which coats all of the grains and partially infills pore space (Fig. 2.26). Both the carbonate and clastic grains are well rounded and well sorted (Fig. 2.26 (a)).

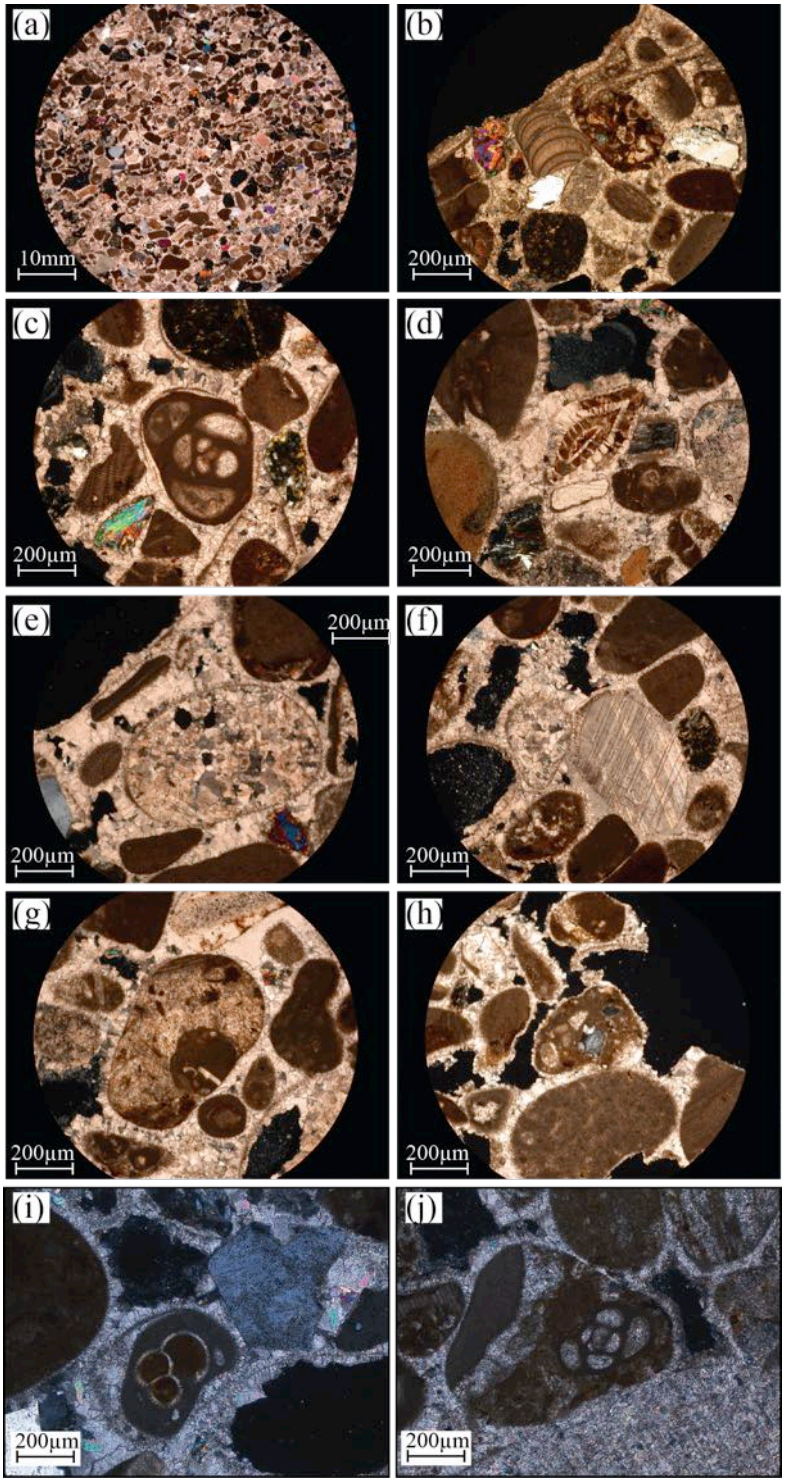

Figure 2.26: Photomicrographs of the Kalkanlı (Kapouti) Member outside the town of Kalkanlı (Kapouti) town. The photomicrographs include: (a) overview of the well-rounded and well-sorted grains; (b) reworked grains of calcareous red algae, grainstone and quartz; (c) *Miliolida* (benthic foraminifera); (d) *Neorotalia* (benthic foraminifera); (e) reworked grain of carbonate; (f) reworked grain of metacarbonate; (g) reworked grain of grainstone; (h) reworked grain of grainstone with quartz; (i) reworked pelagic carbonate grain; and (j) reworked grainstone grain with *Miliolida* benthic foraminifera.

2.5.4 Diagenesis

The grainstone deposits of the Athalassa (Gürpınar) Formation are generally grain supported, with ca. 10% to 20% carbonate cement. The carbonate cement is predominantly a microcrystalline carbonate (micrite) cement (Fig. 2.27(a)). In addition, in several deposits, the cement is a fine sparite (Fig. 2.27(b)). The carbonate cement forms a granular mosaic with a microcrystalline carbonate coating of the grains and infilling of pore space. The pore-filling cement varies from nearly 90% of the pore space to only 10% (Fig. 2.27(a-d)). In a small number of sections, micritic envelopes have formed, which envelop single and multiple grains (Fig. 2.27(e, f)).

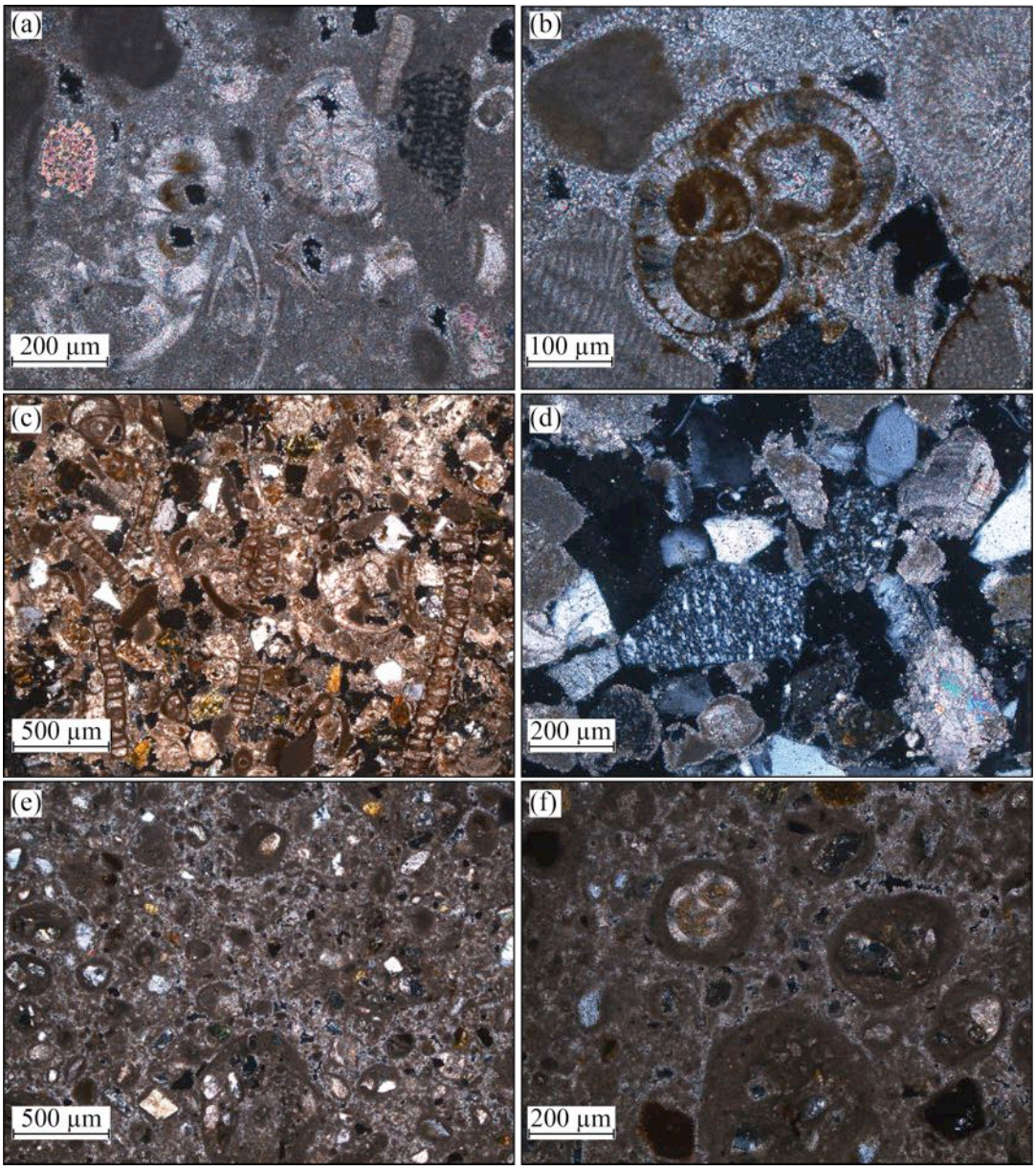

Figure 2.27: Photomicrographs showing various diagenetic features in the Athalassa (Gürpınar) Formation from the Mesaoria (Mesarya) Plain and the Karpaz (Karpas) Peninsula. The photomicrographs include: (a) micritic cement coating grains and infilling pore space; (b) fine sparite cement coating grains and partially infilling chambers of reworked planktonic foraminifera; (c) meniscus (fine sparite) cement; (d) mono and polycrystalline quartz with minimal carbonate cement from deposits outside Gazimağusa (Famagusta) city; (e) micritic envelopes, coating grains with fine-sparite partially infilling pore space; and (f) planktonic foraminifera and clastic material within micritic envelopes.

2.6 Point-count data

The Athalassa (Gürpınar) Formation dominantly comprises grainstone of a varying composition of carbonate and clastic material. An understanding of the spatial variation within the carbonate material can be helpful when interpreting the depositional environment of the Athalassa (Gürpınar) Formation in northern Cyprus. Point-count data from the grainstone and rudstone deposits in northern Cyprus are presented here.

Point-count data were collected from 27 samples within the Mesaoria (Mesarya) Plain and the Karpaz (Karpas) Peninsula. 400 points were counted for each sample from the following categories: monocrystalline quartz, polycrystalline quartz, chert, metamorphics, volcanics, feldspar, sedimentary lithics, calcareous red algae, benthic foraminifera, planktonic foraminifera, bivalve fragments, echinoderms, bryozoa, calcareous algae and ostracods. The data are plotted in the following categories: calcareous red algae, benthic foraminifera, planktonic foraminifera, echinoderms, bivalves, clastic grains and other carbonate grains. The clastic grains encompasses silicic material and reworked lithic fragments, such as from volcanic and sedimentary rocks. The 'other carbonate grains' encompasses carbonate material, which forms a minor component of the rock and are commonly reworked, these grains include: bryozoa, calcareous algae and ostracods. The point-count data are presented in two diagrams: firstly, data from several different deposits from localities across northern Cyprus (Fig. 2.28); secondly, from deposits outside Güzelyurt (Morphou) town (Fig. 2.29).

The point-count data from across northern Cyprus (Fig. 2.28) show a clear regional variation in carbonate composition between grainstone deposits. The key components which significantly vary include: clastic, calcareous red algae, benthic foraminifera and planktonic foraminifera. The proportions of the benthic foraminifera, planktonic foraminifera, calcareous red algae and clastic grains show the substantial variation across the Athalassa (Gürpınar) Formation. Three distinct depositional zones can be identified from the point count data: firstly, areas rich in planktonic foraminifera; secondly, areas rich in benthic foraminifera; and thirdly, areas rich in calcareous red algae. The planktonic foraminifera-rich (>50%) deposits are found north of Kalkanlı (Kapouti) town and from the lower part of the Kalkanlı (Kapouti) Member grainstone. These deposits are rich in benthic foraminifera (15% to >50%) and with a minor planktonic foraminifera (12% to 25%) component are found in the eastern Mesaoria (Mesarya) Plain and on the eastern tip and coast of the Karpaz (Karpas) Peninsula. The calcare-

ous red algae-rich (45% to 70%) deposits are found on the Karpaz (Karpas) Peninsula. In all regions the clastic grain component of the deposits significantly varies from >50% to <5%.

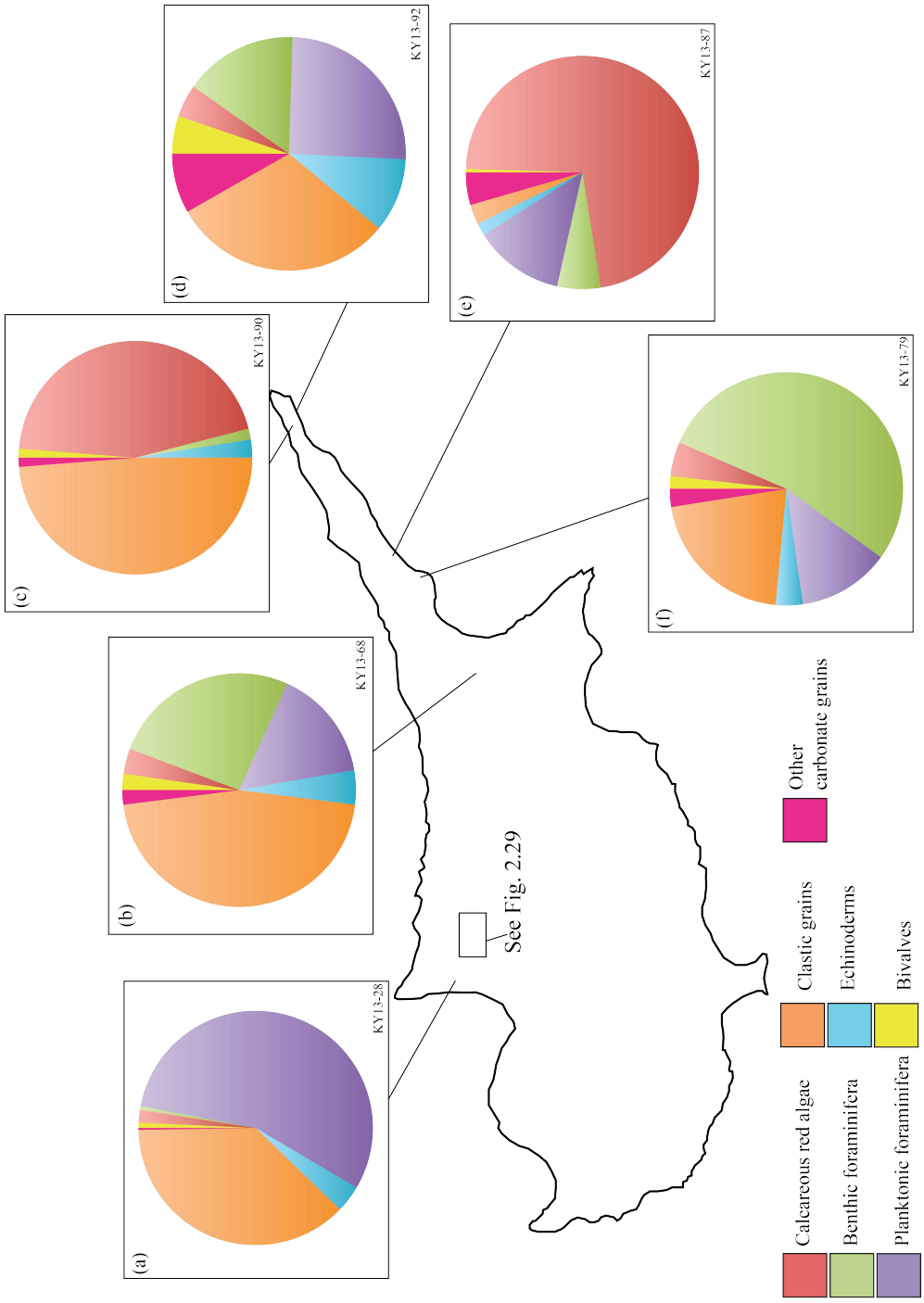

Figure 2.28: Point count data for grainstone deposits throughout northern Cyprus (see text for discussion).

A more focused point-count study carried out on the deposits east of Güzelyurt (Morphou) town reflects the excellent preservation and the clear field relationships of these deposits (Fig. 2.29). The point-count data indicate the preservation of three compositional groups within this area: firstly, benthic and planktonic foraminifera-rich deposits (ca. 50%); secondly, calcareous red algae-rich deposits (40% to 75%); and thirdly, clastic grain-rich deposits (ca. 70%). Deposits rich in benthic and planktonic foraminifera are found in the southeast of the area (Fig. 2.29(e, f)), as isolated deposits. The calcareous red algae-rich deposits (Fig. 2.29(d, g)) are preserved further northwest relative to the foraminifera rich deposits and stratigraphically overlie the foraminifera-rich deposits. Finally, the clastic-rich deposits are found at the stratigraphically highest levels in the southwest area of the map (Fig. 2.29(a-c, h)).

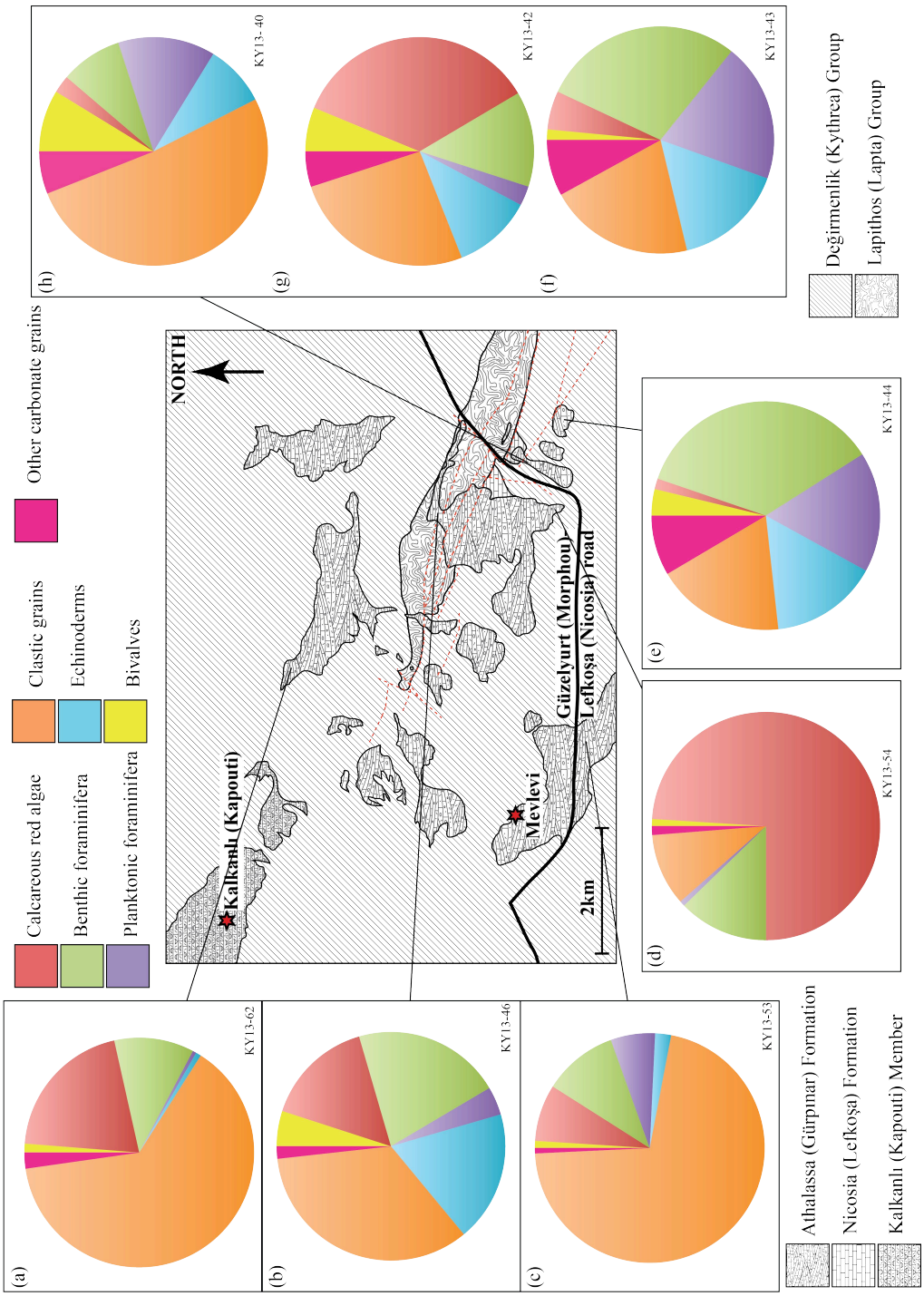

Figure 2.29: Point count data from grainstone deposits outside Güzelyurt (Morphou) town (see text for discussion).

2.7 Facies

Figures 2.30, 2.31 and 2.32 summarise the facies and the interpreted depositional environments of the Pliocene deposits.

2.7.1 Nicosia (Lefkoşa) Formation

The Nicosia (Lefkoşa) Formation is represented by two different facies (Fig 2.30). The formation predominantly consists of interbedded chalk (A1) and marl (A2). The interbedded chalks and marls are rich in Pliocene to Pleistocene planktonic foraminifera indicating a pelagic environment within the Mesaoria (Mesarya) Basin and the Karpaz (Karpas) Peninsula area. The variation from chalk to marl is attributed to variations in productivity of the surface water, which are primarily controlled by variations in nutrients, salinity, surface temperatures and clastic input. Examples of interbedded chalks and marls which represent variation in the productivity of surface waters are also found in southern Italy (Thunell *et al.*, 1991).

Nicosia (Lefkoşa) Formation

Facies code	Facies	Description	Depositional evironment
A1	Chalk	Fine-grained deposit completely comprised of planktonic foraminifera. Occasional well-preserved bivalves.	Low-energy nutrient ***rich*** pelagic environment
A2	Marl	Fine-grained mudstone with poorly-preserved planktonic foraminifera.	Low-energy nutrient ***poor*** pelagic environment

Figure 2.30: Summary of the facies described from the Nicosia (Lefkoşa) Formation on the northern side of the Mesaoria (Mesarya) Plain.

2.7.2 Athalassa (Gürpınar) Formation

The Athalassa (Gürpınar) Formation is represented by seven different facies, which are distinguished based upon lithology, carbonate composition and sedimentary structures (Fig. 2.31). The following section is a discussion of the facies observed from the Atha-

lassa (Gürpınar) Formation deposits in northern Cyprus.

The B1 to B4 facies preserved within western end of the Mesaoria (Mesarya) Basin can be interpreted as representing a cool-water carbonate ramp (Pedley and Carannante, 2006)(Fig. 2.31). The key characteristic of the B1 facies is the abundance on benthic foraminifera and clastic grains and the well-preserved Cruziana ichnofacies, which indicates an open-marine environment with a detrital grain input from a non-marine source. The B1 facies forms a 2 m to10 m-thick horizontal deposit overlying the Nicosia (Lefkoşa) Formation and is preserved within the Mesaoria (Mesarya) Plain at several localities that are ca. 12 km south of the Kyrenia Range, and also on the Karpaz (Karpas) Peninsula. The B2 facies overlies the B1 facies at several localities but is not seen continuously across all of the B1 facies deposits. The B2 facies is composed of fragmented calcareous red algae with a small amount of detrital clastic grains surrounded by micritic cement. The abundance of calcareous red algae and the thick planar bedding of the B2 facies suggests that the deposit represents an outer carbonate ramp environment below the storm wave level (Burchette and Wright, 1992; Pedley and Carannante, 2006).

The B3 facies overlies the B1 or B2 facies within the Mesaoria (Mesarya) Plain and on the Karpaz (Karpas) Peninsula. The B3 facies is characterised by a grainstone with low-angle (<30°) trough cross-bedding and planar laminations. The trough cross-bedding and laminations suggest periods of wave controlled deposition and periods of low-energy sedimentation. The composition of the carbonate material within the B3 facies is dominated by molluscs, echinoderms, bryozoan and calcareous algae with occasional benthic foraminifera and ostracods. The grains are moderately well-rounded indicating reworking due to wave action within a mid- to upper-carbonate ramp environment (Pedley and Carannante, 2006).

The B4 facies is preserved as discontinuous beds within the B3 facies within the Mesaoria (Mesarya) Basin. The deposit comprises well-rounded to sub-rounded clasts within a matrix-supported conglomerate. Clast composition varies spatially across the Mesaoria (Mesarya) Basin from chalk-dominanted in the west to metacarbonate-dominanted in the east. The rounding of clasts suggests reworking in a high-energy environment prior to redeposition within an upper-carbonate ramp environment.

The B5 facies is found conformably overlying the B3 deposit within the Mesaoria

(Mesarya) Plain and on the Karpaz (Karpas) Peninsula. The B5 grainstone is composed of carbonate and clastic grains. However, unlike the B3 facies, the B5 grainstone has a high proportion of clastic to carbonate grains. The sedimentary structures include high angle (>30°) planar cross-bedded units forming ca. 2 m-thick depositional units. The increased proportion of clastic grains in the high-angle planar cross-bedding suggests that the B5 facies represents an aeolian environment (Frébourg *et al.*, 2008). In most cases the B5 facies overlies the the B3 facies horizontally. However, rarely a near vertical contact is exposed and the two facies are separated by a breccia deposit (B6 facies). The B6 facies is composed of sub-angular clasts of grainstone, which range in size from 1 cm to 50 cm. The poorly sorted and angular nature of the clasts suggests a minimal transport distance. The clasts are grainstone, suggesting reworking of the B3 facies grainstone to make the B6 facies breccia.

Athalassa (Gürpınar) Formation

Facies code	Facies	Description	Depositional evironment
B1	thick-bedded grainstone	Packstone comprises dominantly **benthic foraminifera** and clastic grains. Sedimentary structures include laminations and centimetre-scale bedding.	Open-marine basin.
B2	thick-bedded rudstone	Packstone comprises dominantly **calcareous red algae** and clastic grains. Sedimentary structures include laminations and centimetre-scale bedding.	Outer-carbonate ramp.
B3	Low-angle trough cross bedded grainstone	Packstone comprises carbonate and clastic grains. Sedimentary structures include cross-bedding with forsets <30°.	Mid-carbonate ramp.
B4	Conglomerate	Well-rounded to sub-angular clasts within a matrix-supported conglomerate. Clast composition varies depending on local geology. The matrix is a grainstone.	Erosion of underlying lithologies in a terrestrial environment, reworking into a shallow-marine environment.
B5	High angle planar cross-bedded grainstone	Packstone comprises carbonate and clastic grains. Sedimentary structures include ca. 2 m-thick cross-bedded units with a forset dip between 30°- 45°.	Dune deposits reflecting an east-west palaeowind system running parallel to the Kyrenia Range.
B6	Breccia	Poorly sorted breccia comprised of rework clasts of grainstone.	Erosion within a non-marine environment.

Figure 2.31: Summary of the facies described from the Athalassa (Gürpınar) Formation on the northern side of the Mesaoria (Mesarya) Plain.

2.7.3 Kalkanlı (Kapouti) Member

The Kalkanlı (Kapouti) Member is preserved near the Kyrenia Range within the Mesaoria (Mesarya) Plain and also overlying the main range on the Karpaz (Karpas) Peninsula. The Kalkanlı (Kapouti) Member is the stratigraphically upper part of the Athalassa (Gürpınar) Formation and represents a marine environment, proximal to the Kyrenia Range.

The C1 and C2 facies are grainstone deposits ranging from medium to coarse grained, with a grain composition dominantly made up of carbonate grains, but with a small proportion of clastic grains (Fig. 2.32). The carbonate grains include molluscs, calcareous algae, bryozoa, serpulid worms and solitary corals, which are indicative of an upper-carbonate ramp environment (Pedley and Carannante, 2006). The sedimentary structures include low-angle cross-bedding and planar centimetre-scale bedding, indicating an environment varying between wave controlled and low-energy sedimentation involving sediment settling from the water column.

The C3 and C4 facies form 1 m to 2 m thick continuous beds and are seen at various points within the C1 and C2 facies. In the western end of the Mesaoria (Mesarya) Plain the C3 and C4 facies are found within the upper part of the Kalkanlı (Kapouti) Member sequence. However, at Balalan (Platanissos) village the C4 facies deposits occur throughout the sequence. The C3 facies is rich in algal-coated grains (oncoids) within a fine-grained grainstone and can be termed an oncolite (Teichert, 1970; Peryt, 1981) or an oncoid floatstone (Dunham, 1962)(Fig. 2.32). The presence of oncoids can can be used as an environmental indicator, suggesting an intertidal to subtidal marine depositional environment (Flugel, 2004); an example being the Palaeocene- Eocene Flagstaff oncolitic beds, Utah (Weiss, 1969) and the Late Quaternary deposits of the Zarand Basin, central Iran (Djamali *et al.*, 2006). The abundance of a mono-species *in situ* oyster shells within facies C4 suggests a low-energy open-marine lagoonal setting (Fig. 2.32).

The C5 facies is a conglomerate composed of both clastic and carbonate material (Fig. 2.32). The clasts are sub-angular and range in size from 1 cm to 30 cm derived from the local underlying geology. For example, at Balalan (Platanissos) village the clasts are dominantly basalt and radiolarite and occasional Miocene aged bivalves, whereas near Kalkanlı (Kapouti) village the clasts are mainly metacarbonate. The car-

bonate clasts include large bivalve shells, serpulid worms, gastropods and coral. The conglomerate shows no sign of sedimentary sorting, suggesting minimal transportation from the source.

The C6 facies is another conglomeratic deposit, however, this can be distinguished from the C5 facies based upon sedimentary characteristics (Fig. 2.32). The C6 facies conglomerate contains well-rounded and well-sorted clasts ranging in size from 1 cm to 10 cm, mainly composed of metacarbonate rock. The conglomerate is clast supported and contains <10% matrix of unlithified carbonate and clastic sand. The well organised nature of the C6 facies conglomerate suggests a well developed fluvial drainage system. Numerous clasts within the C6 facies conglomerate show significant borings indicating that the clasts have spent some time within a shallow marine environment.

Kalkanlı (Kapouti) Member

Facies code	Facies	Description	Depositional evironment
C1	Bedded grainstone	Packstone comprised of carbonate and clastic grains. Sedimentary structures include centimetre-scale bedding.	Low-energy coastal lagoon on a carbonate shelf.
C2	Low-angle cross-bedded grainstone	Grainstone comprised of carbonate and clastic grains. Sedimentary structures include cross-bedding with forsets <30º.	Carbonate shelf open to wave action with variable palaeocurrent directions.
C3	Oncoid floatstone (Oncolite)	Grainstone with well preserved oncolites.	Inter-tidal to sub-tidal shallow-marine environment.
C4	Oyster floatstone	Decalcified monospecies oysters within a fine-grained grainstone	Low energy lagoonal environment. Single species of bivalve suggests stressed environment.
C5	Conglomerate with terrigenous and carbonate clasts	Conglomerate with poorly-sorted clasts of locally sourced clastic material and large bivalve shells.	Local reworking of terrigenous material down-slope into a shallow-marine environment; incorporating carbonate debris.
C6	Conglomerate with well-rounded clasts	Conglomerate with well-rounded and occasionally bored clasts of metacarbonate	Fluvial conglomerate deposited during sea-level lows.

Figure 2.32: Summary of the facies described from the Kalkanlı (Kapouti) Member on the northern side of the Mesaoria (Mesarya) Plain.

2.8 Discussion

The Pliocene sediments of northern Cyprus are best preserved within the Mesaoria (Mesarya) Plain and on the Karpaz (Karpas) Peninsula. The deposits represent the Mesaoria (Mesarya) seaway that separated the Kyrenia Range from the Troodos Massif. The Pliocene sediments in northern Cyprus document a change from a marine to a non-marine environment during the earliest emergence of the Kyrenia Range. This chapter has presented new data from the Pliocene deposits in northern Cyprus to better understand the timing and processes associated with the initial emergence of the Kyrenia Range.

Depositional model

The deposits of the Nicosia (Lefkoşa) Formation in northern Cyprus are composed of interbedded chalks and marls, rich in planktonic foraminifera and some benthic formaminifera. The Early Pliocene deposits can be correlated between the northern and the southern sides of the Mesaoria (Mesarya) Plain (Lord *et al.*, 2000; Harrison *et al.*, 2004). The continuity of these deposits around much of Cyprus suggests an open-marine environment surrounded the Kyrenia Range and Troodos Massif landmasses. The lack of Pliocene marine deposits in the central Kyrenia Range is because of uplift or because the range was above sea-level during the Early Pliocene.

Conformably overlying the Nicosia (Lefkoşa) Formation in northern Cyprus is the Athalassa (Gürpınar) Formation. The Athalassa (Gürpınar) Formation includes the Kalkanlı (Kapouti) Member, which is preserved on the flanks of the Kyrenia Range. The Athalassa (Gürpınar) Formation represents a shallow-marine setting within the Mesaoria (Mesarya) Basin, following the open-marine environment represented by the Nicosia (Lefkoşa) Formation. The Athalassa (Gürpınar) Formation represents a cool-water carbonate ramp at the western end of the Mesaoria (Mesarya) Basin. The nature of the facies that comprise this cool-water carbonate ramp suggest that the environment was affected by changes in sea-level (Fig. 2.33). The oldest part of the carbonate ramp sequence is the benthic foraminiferal-rich grainstone and calcareous red-algal rudstone (Fig. 2.33(a)), representing the deepest environment associated with the carbonate ramp, ranging from 50 m to100 m water depth (Pedley and Carannante, 2006; Nalin and Massari, 2009). The carbonate ramp shallowed towards the northeast, where coral

and molluscs were the dominant organisms. This environment underwent a rapid fall in sea-level, as represented by onlapping foresets within the benthic foraminiferal-rich grainstone and the bioclastic conglomerate (Fig. 2.33(b)). The deposition of the grainstone with trough cross-bedding and planar laminations that overlies the entire sequence represents a relative rise of sea-level (Fig. 2.33(c)). Lagoonal facies and oncolites are preserved in the shallow, northwest part of the carbonate ramp. The youngest part of the entire sequence is the carbonate aeolianite and fluvial deposits that represent a non-marine environment in the northwest. A fall in sea-level exposed the entire carbonate sequence and resulted in major aeolian erosion, forming an overlying aeolianite deposit (Fig. 2.33(d)).

The palaeocurrent data from the marine grainstone facies have a heavily varied palaeocurrent direction, with a a slight trend towards the north and northeast. This north and northwest palaeocurrent direction could be a consequence of large scale dominant storm events generating a northwesterly current, up ramp towards the Kyrenia Range, as seen in the Lower Pleistocene sequences in Rhodes, Greece (Hansen, 1999). The large scatter seen in the marine grainstone palaeocurrent data, is potentially caused by local coastal processes, as seen in southern Italy (Nalin and Massari, 2009). In contrast, the aeolian grainstones either have a northward or more commonly southward palaeocurrent direction. The aeolian grainstone palaeocurrent could be indicative of local winds within the Mesaoria (Mesarya) Plain. McCallum and Robertson (1995a) presented palaeocurrent data from a range of grainstone facies from the Athalassa Formation on the southern side of the Mesaoria Plain. This work showed a dominant palaeocurrent towards the south, which was attributed to major storm events during the Late Pliocene-Early Pleistocene with a prevailing wind direction towards the south. The difference in palaeocurrent data between deposits on the northern and southern side of the range, suggest that the palaeocurrents in the marine and aeolian environments in northern Cyprus were controlled by relatively local processes compared to the Mesaoria (Mesarya) Basin as a whole.

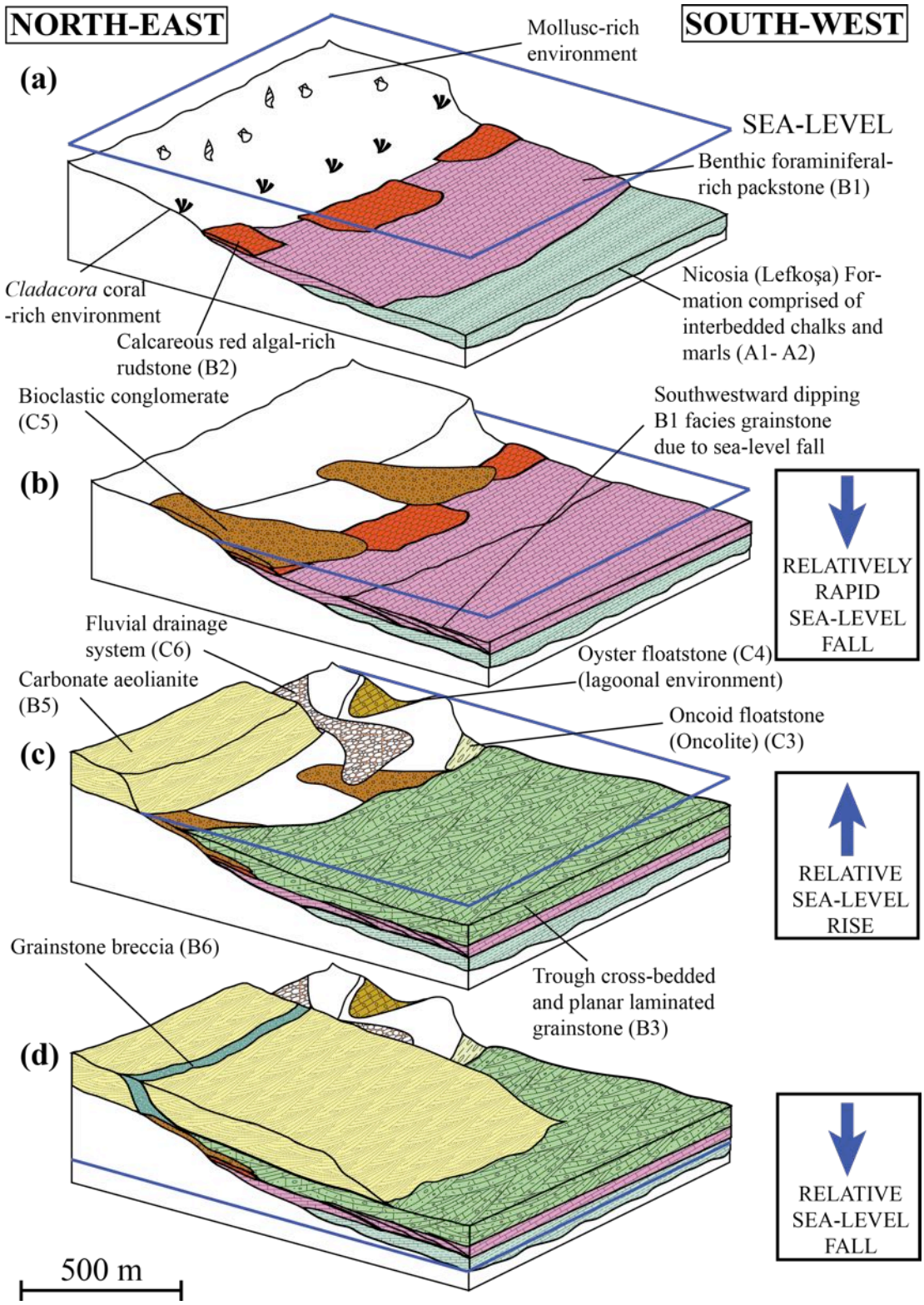

Figure 2.33: Depositional model for the southern side of the Kyrenia Range during the Late Pliocene to Early Pleistocene. Facies labels and descriptions are shown in Figures 2.31 and 2.32.

2.9 Conclusions

1. The transition from the Nicosia (Lefkoşa) Formation to the Athalassa (Gürpınar) Formation represents a shallowing-upward marine environment.

2. The Athalassa (Gürpınar) Formation within the eastern Mesaoria (Mesarya) Basin represent various facies within a cool-water carbonate ramp.

3. The Kalkanlı (Kapouti) Member represents a transition from marine to non-marine environments on the northern margin of the Mesaoria (Mesarya) Basin.

4. Discontinuous Athalassa (Gürpınar) Formation deposits in the eastern Mesaoria (Mesarya) Basin and the Karpaz (Karpas) Peninsula represent a shallow marine environment surrounding the Kyrenia Range, and may represent various parts of a cool-water carbonate ramp.

5. Sedimentary relationships indicate a major regression event, followed by a transgression and then a regression finally, probably caused by the Pleistocene uplift of the Kyrenia Range.

Chapter 3

Continental alluvial depositional systems in northern Cyprus

3.1 Introduction

The depositional controls on fluvial systems in compressional tectonically-active mountain ranges is currently a dynamic field of research. The closure of the Tethys ocean resulted in the uplift of numerous European and Asian mountain belts. These mountain ranges are natural laboratories for the study of fluvial drainage systems that are controlled by tectonic uplift and climatic change (Lavé and Avouac, 2001; Suresh *et al.*, 2007; Wegmann and Pazzaglia, 2009). The interaction between tectonic and climatic controls on fluvial systems within active mountain chains is at the forefront of this research (Starkel, 2003; Kober *et al.*, 2013). To understand these fluvial systems a range of scientific disciplines must be used including sedimentology and geomorphology. Furthermore, an array of dating techniques can also be used including cosmogenic dating, optically stimulated luminescence (OSL) and Uranium-series dating. This chapter focuses on the sedimentology of the K0 to K5 terraces in the Kyrenia Range.

The general descriptions of the Kyrenia Range terraces by Ducloz (1964) and Knup (1965) hint towards a change in the sedimentology of the continental deposits with height, on the southern flanks of the range (chapter 2). However, since the work of Ducloz (1964) and Knup (1965) no follow-up study has been carried out to understand, in detail, the evolving alluvial depositional systems on the southern flanks of the range.

In southern Cyprus a general description and classification of the Pleistocence Qua-

ternary terraces was produced by Poole and Robertson (1991). Their study focused on the fluvial terraces associated with the uplift of the Plio-Pleistocene cover of the Troodos Massif. Using the fluvial terraces are approximately correlated with the marine terraces around the southern coastline of Cyprus (Poole and Robertson, 2000). Both fluvial and marine terraces in southern Cyprus are defined as F1 to F4.

More recently, studies have been carried out on specific catchments in southern Cyprus. The Vasilikos Valley catchment has received significant attention due to its excellent preservation and exposure of deposits (Gomez, 1987). Gomez (1987) studied the entire Vasilikos Valley and correlated the Pleistocene fluvial systems with the Kyrenia Range fluvial terraces as defined by Ducloz (1972). Waters *et al.* (2010) focused on the Vasilikos Valley deposits on the southern coastline and completed an in-depth study of the multiple fluvial systems and their possible responses to climatic change. Finally, Schirmer *et al.* (2010) studied the fluvial systems during the Early Pleistocene, focusing on a deposit within the Apalos Formation on the northern flanks of the Troodos Massif. This study used detailed sedimentology and magnetostratigraphy to help understand the fluvial responses to tectonic uplift.

Until now, follow-up studies on the preliminary work of Baroz, Knup and Ducloz have not been carried out on the fluvial deposits on the southern flanks of the Kyrenia Range, until now. The following chapter presents new field data on the alluvial deposits on the southern side of the range. The data aims to infer the fluvial responses to the tectonic uplift of the Kyrenia Range.

3.2 Taşkent (Vouno) Member

The deposits associated with the Taşkent (Vouno) Member are found at the highest points within the main spine of the Kyrenia Range. (Ducloz, 1964; Ducloz, 1965; Ducloz, 1972; Baroz, 1979). The K0 terrace breccia was deposited into continental depositional environment (Ducloz, 1964; Baroz, 1979); consequentially, the central Kyrenia Range must have been above sea-level prior to the first uplift-related terrace deposit. Ducloz (1972) describes a series of lacustrine deposits preserved within the central Kyrenia Range and groups these deposits with the K0 terrace. The lacustrine deposits described by Ducloz (1972) are relatively rare and are currently unaccessible due to the

military bases.

3.2.1 South side of Beşparmak (Pentadaktylos) mountain

The Taşkent (Vouno) Member deposit is preserved on the southern side of the Kyrenia Range, parallel to Beşparmak (Pentadaktylos) Mountain (Fig. 3.1). The deposit is within a series of steeply-dipping thrust fault, between the Lapithos (Lapta) and Trypa (Tripa) Groups (McCay and Robertson, 2012b; Robertson *et al.*, 2013). The Plio-Quaternary deposits within this area unconformably overlie both the Değirmenlik (Kythrea) and Lapithos (Lapta) Groups. The Lapithos (Lapta) Group forms a east-west chalk ridgeline and has bedding steeply dipping to the south, parallel to the contact with the Kythrea (Değirmenlik) Group mudstones (Fig. 3.2 (a)).

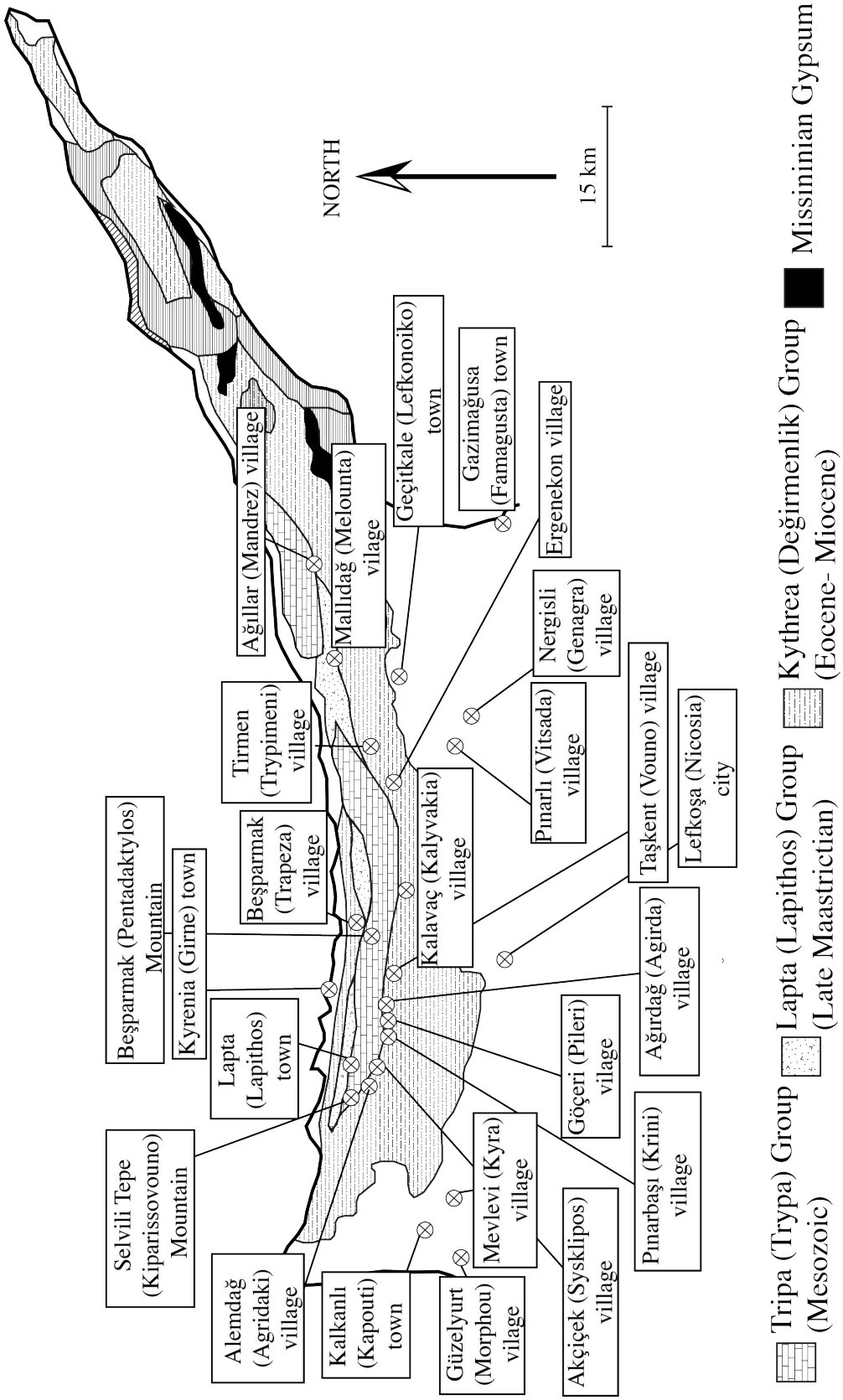

Figure 3.1: Simplified geological map of northern Cyprus showing the key localities discussed within this chapter.

The K0 terrace deposit (chapter 2) forms a gently-dipping northward surface from the Lapithos (Lapta) Group chalk ridgeline back towards the Kyrenia Range (Fig. 3.2 (a)). The western fringes of the K0 surface are unconformably overlain by the Taşkent (Vouno) Member (Fig. 3.2 (b)). The Taşkent (Vouno) Member forms a continuous deposit for ca. 1 km, running east-west parallel to the range.

Two representative sections from the Taşkent (Vouno) Member deposit within this are presented (Fig. 3.3). Both sections are composed of interbedded chalk, mudstone and conglomerate. Section A is made up of a basal conglomerate, conformably overlying the conglomerate is an interbedded sequence of laminated chalks and mudstone. Finally the entire Section is covered by another conglomerate. The conglomerate clasts are poorly-sorted, matrix-supported, sub-angular and are composed of reworked chalk and caliche. The basal conglomerate has clasts ranging from 1 cm to 4 cm, whereas, in the upper conglomerate the clasts range from 5 cm to 20 cm with rare 40 cm-sized clasts. The mudstone deposit directly overlying the basal conglomerate contains well-preserved bivalve shell fragments. The interbedded chalks and mudstones also contain well-preserved non-marine gastropod shells throughout.

Section B comprises a ca. 3 m-thick basal mudstone, followed by a ca. 3 m-thick sequence of interbedded mudstones and chalks; finally the upper part of the section is a ca. 1 m-thick conglomerate, which is similar in character to the upper conglomerate in Section A (Fig. 3.3). The central interbedded sequence of chalks and mudstone contains well-preserved, non-marine gastropod shells which are 1- 10 mm in size.

The middle and upper parts of the two sections can be correlated for ca. 1.5 km running parallel to the range. The middle part of the section varies in thickness from 3 m to 5 m, whereas the upper conglomerate ranges from 50 cm to ca. 2 m. The conglomerates deposits form a series laterally discontinuous beds throughout the entire deposit.

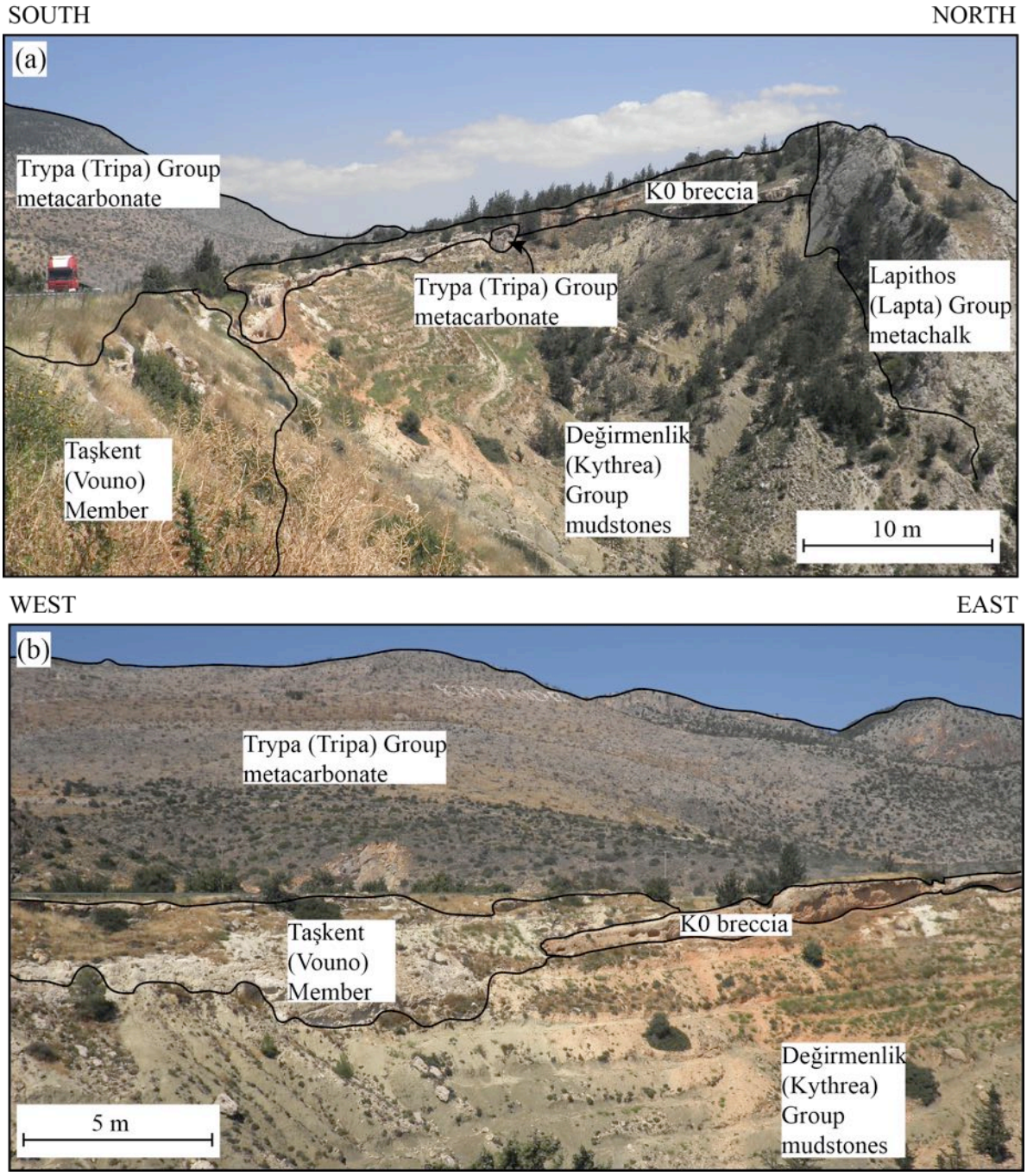

Figure 3.2: Annotated photographs showing features of the Taşkent (Vouno) Member on the southern side of the Kyrenia Range, parallel to Beşparmak (Pentadaktylos) Mountain. Photographs (a) North-south section showing the relationship of the Taşkent (Vouno) Member and K0 breccia to older geology; and (b) East-west section showing the sedimentary relationship between the Taşkent (Vouno) Member and the K0 breccia.

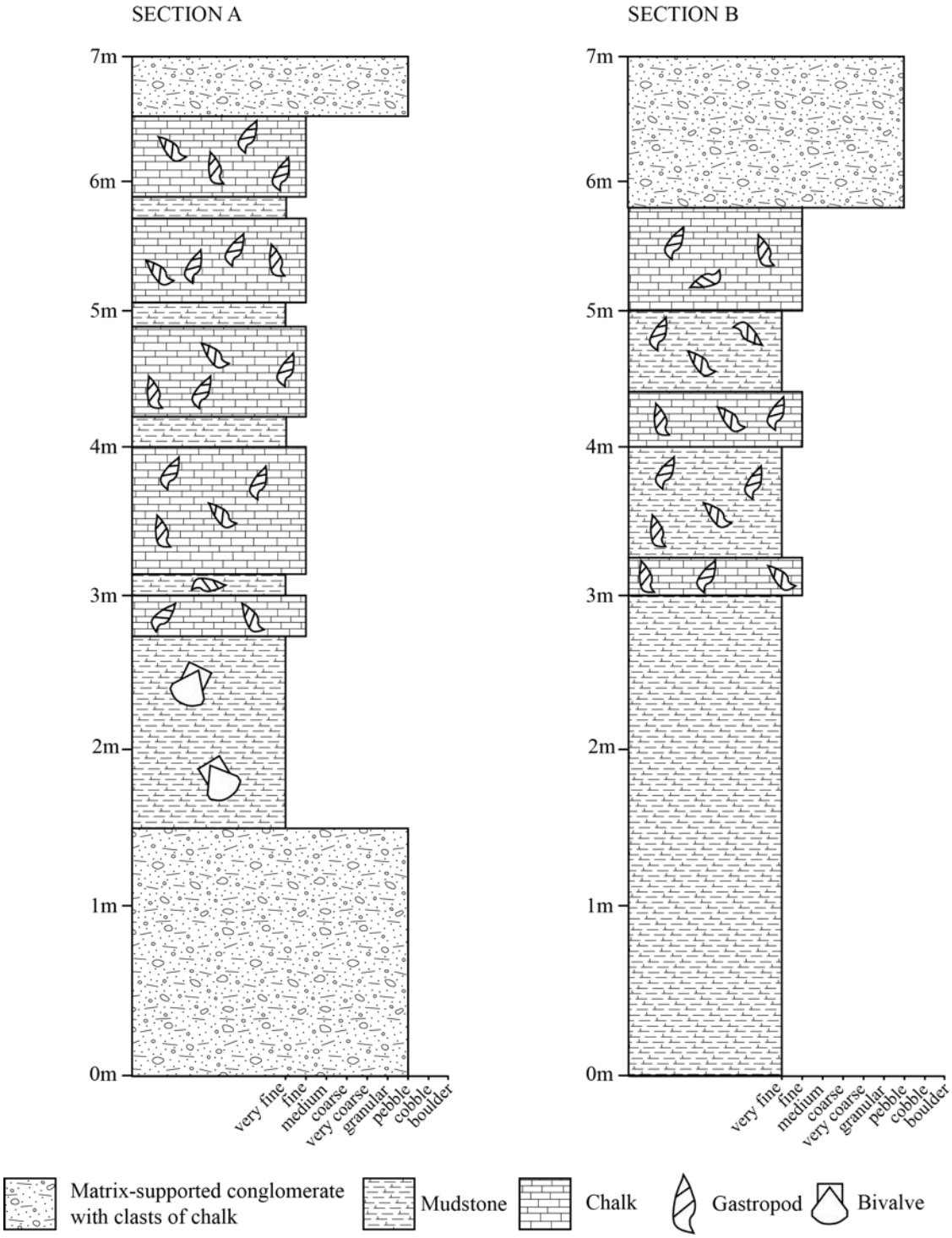

Figure 3.3: Sedimentary logs through the Taşkent (Vouno) Member on the southern side of the Kyrenia Range, parallel to Beşparmak (Pentadaktylos) Mountain.

3.3 K0 and K1 terrace deposits on the northern and southern flanks of the Kyrenia Range

The K0 and K1 terraces form the highest Pleistocene deposits within the Kyrenia Range, mapping has shown that the deposits are preserved on the northern and southerns flanks of the range (Ducloz, 1964; Knup, 1965). The following sections present new field sedimentology data from the K0 and K1 terrace deposits. The aim of the work is to understand the depositional environment represented by the two terraces and furthermore, to understand how the depositional environment varies between and within the terraces. A series of key localities are presented, illustrating the range of deposits that were found within the two terraces.

3.3.1 Selvili Tepe (Kiparissovouno) mountain

Selvili Tepe (Kiparissovouno) is the highest peak in the Kyrenia Range, at 1024 m AMSL (above modern sea-level), and is on the western end of the mountain range (Fig. 3.1). The main peak comprised Trypa (Tripa) Group metacarbonate, with the flanks of the mountain being made up of the Lapithos (Lapta) and Kythrea (Değirmenlik) Groups (Fig. 3.4). Major NE-SW faults have been mapped within the Trypa (Tripa) Group; these heavily dissect and structurally weaken the metacarbonate (Constantinou, 1995). The Trypa (Tripa) Group metacarbonate forms a prominent cliff line at the contact with the Lapithos (Lapta) Group on both the northern and southern sides of the range. The metacarbonate cliffs are ca. 200 m high on both sides of Selvili Tepe (Kiparissovouno). The Trypa (Tripa) Group deformed metacarbonates are much harder and, therefore, less susceptible to erosion than the lithologies that comprise the Lapithos (Lapta) and Dęgirmernlik (Kythrea) Groups.

Figure 3.4 shows the distribution of the Quaternary terrace deposits on the western tip of the Kyrenia Range. The youngest terraces (K2-K5) can be seen to run parallel to the coastline, whereas the K0 deposits are more proximal to the Trypa (Tripa) Group metacarbonates. The outcrop is intermittent on both the northern and southern sides of the range. K0 deposits are found at ca. 400 m AMSL.

No K1 terrace deposits are found within this area, however, the S1 surface can be

identified on both the northern and southern sides of the range. On the northern side of the range the S1 surface is less than 250 m wide (in the N-S direction) and grades directly into a prominent S2 surface. In contrast, on the southern side of range the S1 surface is up to 500 m wide but again lacks any deposits. No equivalent K0 or K1 deposits are preserved on the western tip of the range. The only Quaternary terraces that are preserved in this area are K3 age and younger and will be discussed in the following chapter.

The K0 deposits preserved around Selvili Tepe (Kiparissovouno) Mountain are made up of breccias with poorly-sorted and angular clasts. Clasts within this breccia range in size from 1 cm to 2 m, with blocks up to 20 m. The thickness of the deposit is difficult to accurately constrain as the basal unconformity is not always visible however, the thickness appears to vary between ca. 1 m to 20 m.

The K0 deposit has two components; firstly, a well-consolidated lower section and secondly, a poorly-consolidated upper section. The lower component makes up >80% of the K0 deposit, and the upper component makes up <20%. The matrix of the lower component is fine-grained mudstone that has undergone varying extents of consolidation, from well-consolidated to moderately consolidated (Fig. 3.4). The upper K0 component is a similar breccia however, it has no matrix. The upper component forms a patchy deposit which overlies the lower breccia.

The S0 surface is steep on both the northern and southern sides of Selvili Tepe (Kiparissovouno). The S0 and S1 surfaces dip away from the main range, with the slope angle reducing away from the range, on both the northern and southern sides of Selvili Tepe (Kiparissovouno) Mountain. The K0 deposits are found on this steep S0 surface, therefore this surface pre-dates the deposit. The dip of the terrace surface after S2 becomes relatively uniform and does not significantly change.

The majority of the K0 deposit is well-consolidated due to a carbonate cement infilling the space between the clasts. Tufa covers the outer surface of the deposits and the surface of the Trypa (Tripa) Group metacarbonate cliff lines. The surface breccia contains <10% of a fine-grained matrix and is poorly-consolidated.

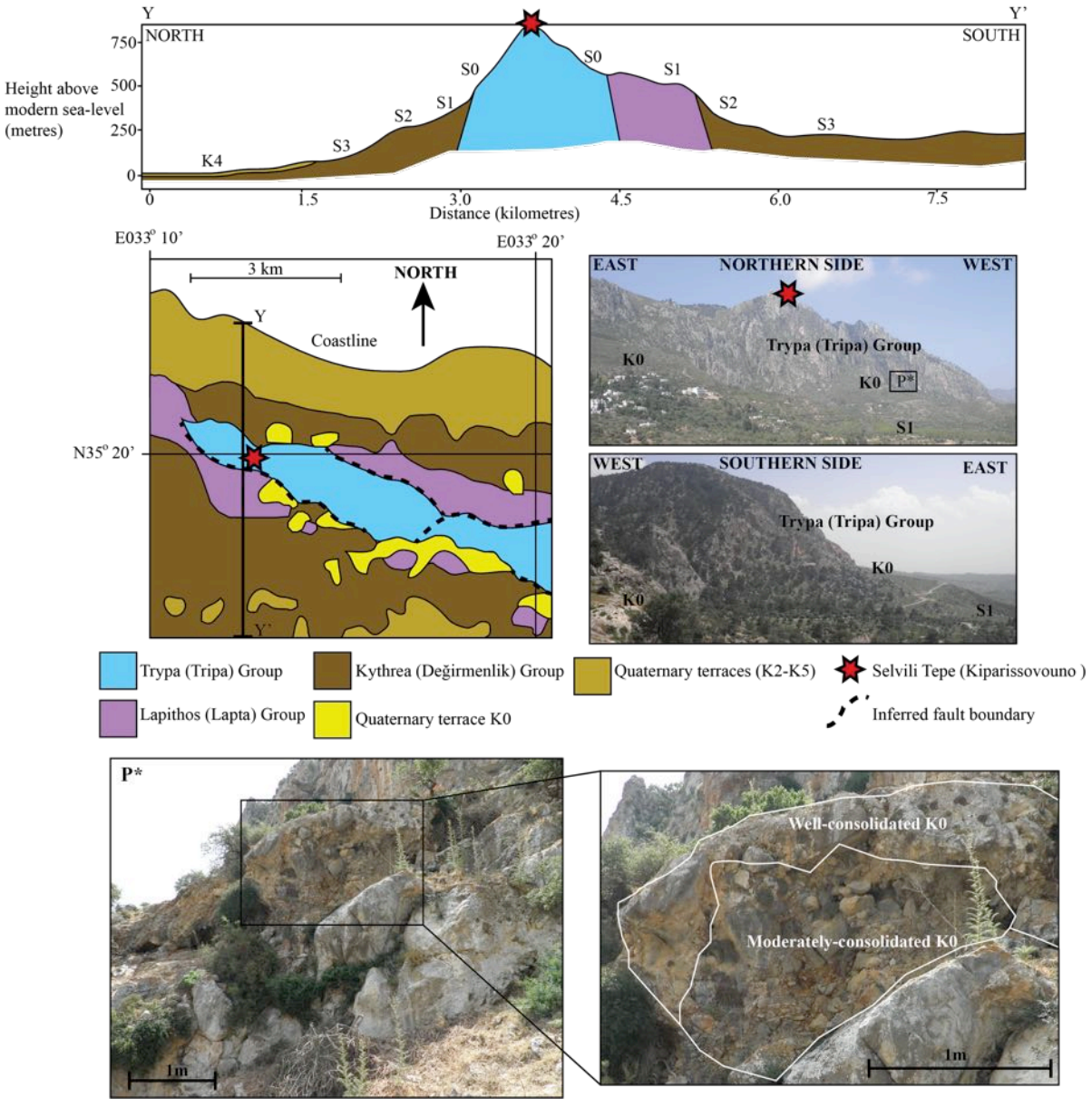

Figure 3.4: Simplified geological map and cross-section of the region around Selvili Tepe (Kiparissovouno) Mountain with photographs of the northern and southern flanks of the range (geological map adapted from the Geological Survey Department, Cyprus (Constantinou, 1995)).

3.3.2 Alemdağ (Agridaki) to Akçiçek (Sysklipos) villages

The towns Alemdağ (Agridaki) to Akçiçek (Sysklipos) are found ca. 4 km to the east of Selvili Tepe (Kiparissovouno) Mountain (Fig. 3.1). The height of the range is <800 m AMSL, which is 200 m lower than Selvili Tepe (Kiparissovouno) Mountain to the west (Fig. 3.5). The K0 terrace in this area is ca. 1.5 km wide and less than 1 km long. The terrace is composed of a K0 component. The K0 deposit stretches from the boundary of the Trypa (Tripa) and Kythrea (Değirmenlik) Groups southwards away from the main range. The boundary of the Trypa (Tripa) and Kythrea (Değirmenlik) Groups can be clearly distinguished by a large metacarbonate cliff line, which marks the start of the K0 deposit. The K0 deposit in this area is a clast-supported breccia with poorly-sorted and angular clasts ranging in size from 1 cm to 2 m. The matrix is a fine-grained mudstone. The deposit is ca. 6 m thick at its most southern margin.

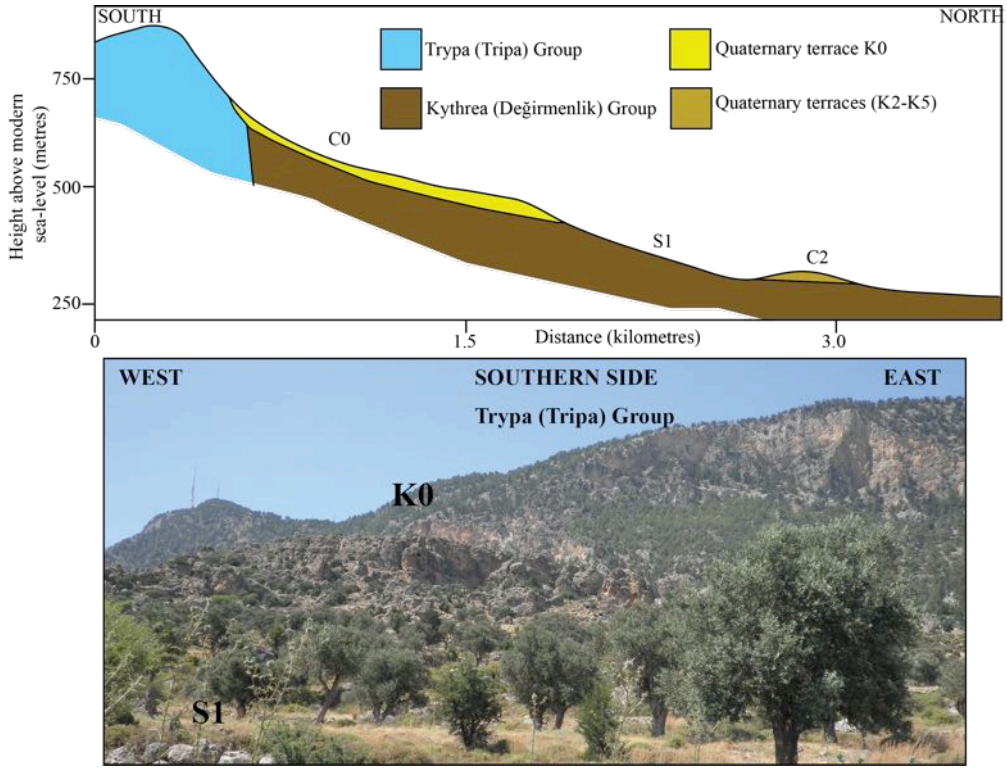

Figure 3.5: Cross-section showing the simplified subsurface geology and the overlying Quaternary terrace deposits, between Alemdağ (Agridaki) and Akçiçek (Sysklipos).

3.3.3 Lapta (Lapithos) town

Lapta (Lapithos) is a small town on the northern side of the Kyrenia Range, which is ca. 20 km west of Kyrenia (Girne) (Fig. 3.1). The modern town stretches from the coastline up into the main range. The height of the range here is <750 m AMSL, significantly lower than Selvili Tepe (Kiparissovouno) Mountain to the west. The main range comprises Trypa (Tripa) Group metacarbonate; with significant outcropping Lapithos (Lapta) Group on the northern side of the range (Fig. 3.6). The large amount of Lapithos (Lapta) Group rocks results in a more gentle topography compared to that around Selvili Tepe (Kiparissovouno) Mountain.

No major K0 deposits are preserved on the northern side of the range; however, the S0 surface is clearly visible overlying the Lapithos (Lapta) Group. There is a continuous surface between S0 and S1, dipping down to the K2 terrace deposits. The S0-S1 surfaces have a combined N-S width of ca. 1 km.

A change in surface geology from predominantly Trypa (Tripa) Group metacarbonate to both Trypa (Tripa) and Lapta (Lapithos) Group results in a gentler topography across the range. The height of the range in this area is still significantly less than around Selvili Tepe (Kiparissovouno) Mountain. The S0 surface gently dips away from the main range on the northern side of the range (Fig. 3.6).

3.3.4 Göçeri (Pileri) village

Göçeri (Pileri) is a small village on the southern side of the Kyrenia Range, roughly parallel with Lapta (Lapithos) (Fig. 3.1). The Trypa (Tripa) Group on this southern side of the range is in contact with the Dęgirmernlik (Kythrea) Group, with only a small amount of Lapta (Lapithos) Group outcropping (Fig. 3.6). The S0 surface within this area is well-preserved, extending from the Trypa (Tripa) Group cliff line southwards, dipping steeply away from the range. Younger fluvial systems have dissected the terraces surfaces in an north-south orientation. The K0 deposit can be found northeast of the town, ca. 0.5 km off the E-W running road.

The deposit near Göçeri (Pileri) village is ca. 15 m thick and is a breccia with poorly-sorted, angular clasts composed of metacarbonate from the Trypa (Tripa) Group. Clasts

within this unit range in size from 1 cm to 2 m, with blocks up to 10 m. The matrix is a fine-grained, well-cemented mudstone. The base of this section is at ca. 405 m AMSL. The degree of consolidation of the K0 breccia varies from well consolidated to moderately consolidated. Conformably overlying the K0 breccia is an unconsolidated breccia with no matrix, this deposit is only preserved at the base of the Trypa (Tripa) Group cliffs.

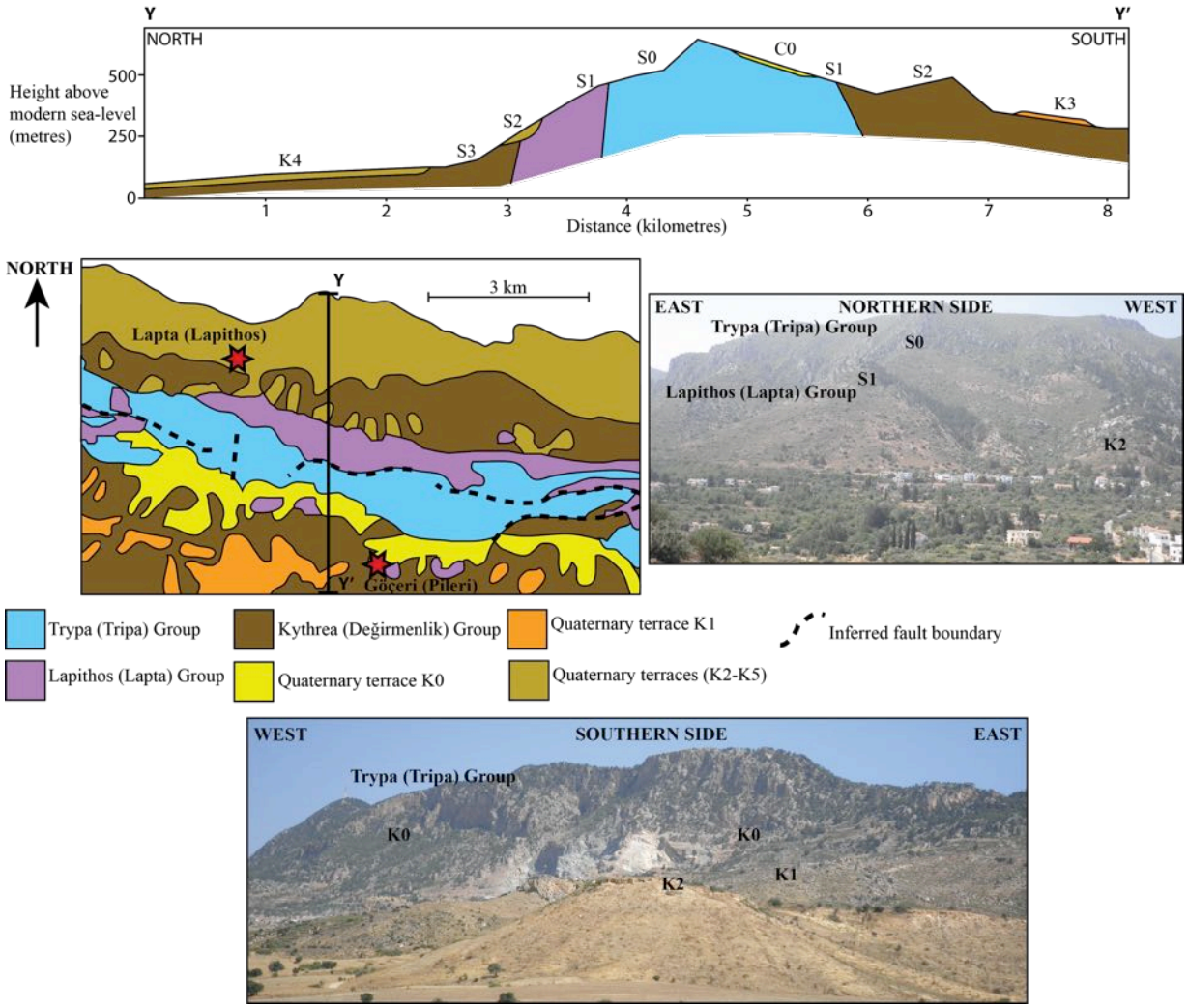

Figure 3.6: Simplified geological map and cross-section of the region surrounding Lapta (Lapithos) and Göçeri (Pileri) with photographs of the northern and southern flanks of the range (geological map adapted from the Geological Survey Department, Cyprus (Constantinou, 1995)).

3.3.5 Pınarbaşı (Krini) village

Pınarbaşı (Krini) is a village on the southern side of the Kyrenia Range, ca. 4 km further east of Göçeri (Pileri) (Fig. 3.1). The range height is just below 800 m AMSL. The Trypa (Tripa) Group is unconformably and vertically overlain by the Kythrea (Değirmenlik) Group on the southern flank of the range (Fig. 3.7). The K0 deposit horizontally overlies the contact. The K0 deposit forms a ca. 1 km-wide terrace which dips steeply down to the K1 terrace (Fig. 3.7).

The K0 deposit is a matrix-supported breccia, poorly sorted and angular clasts. Clasts range in size from 1 cm to 2 m (Fig. 3.7(b)). The clasts are dominantly made up of Trypa (Tripa) Group, deformed metacarbonate, no Lapta (Lapithos) Group derived clasts were found. Karst weathering can be seen extensively on the surface of the deposit and infilling large spaces between clasts (Fig. 3.7 (b, c)).

The K1 deposit is a clast-supported conglomerate with moderately-sorted subangular clasts. Clasts range from 1 cm to 20 cm and are composed of reworked Trypa (Tripa) Group metacarbonate and K0 breccia. The matrix is a fine-grained, poorly-consolidated mudstone. The K1 deposit is ca. 1 m thick and less than ca. 50 m wide; forming isolated deposits at the foot of the K0 terrace.

Figure 3.7 (a) shows the reworked K0 breccia on the S1 surface. The K0 deposit on this surface is composed of a combination of K0 breccia, karst weathered material and Trypa (Tripa) Group metacarbonate. Clasts on the surface range in size from 1 cm to 5 m. This deposit is not consolidated and is found the foot of the K0 terrace deposit.

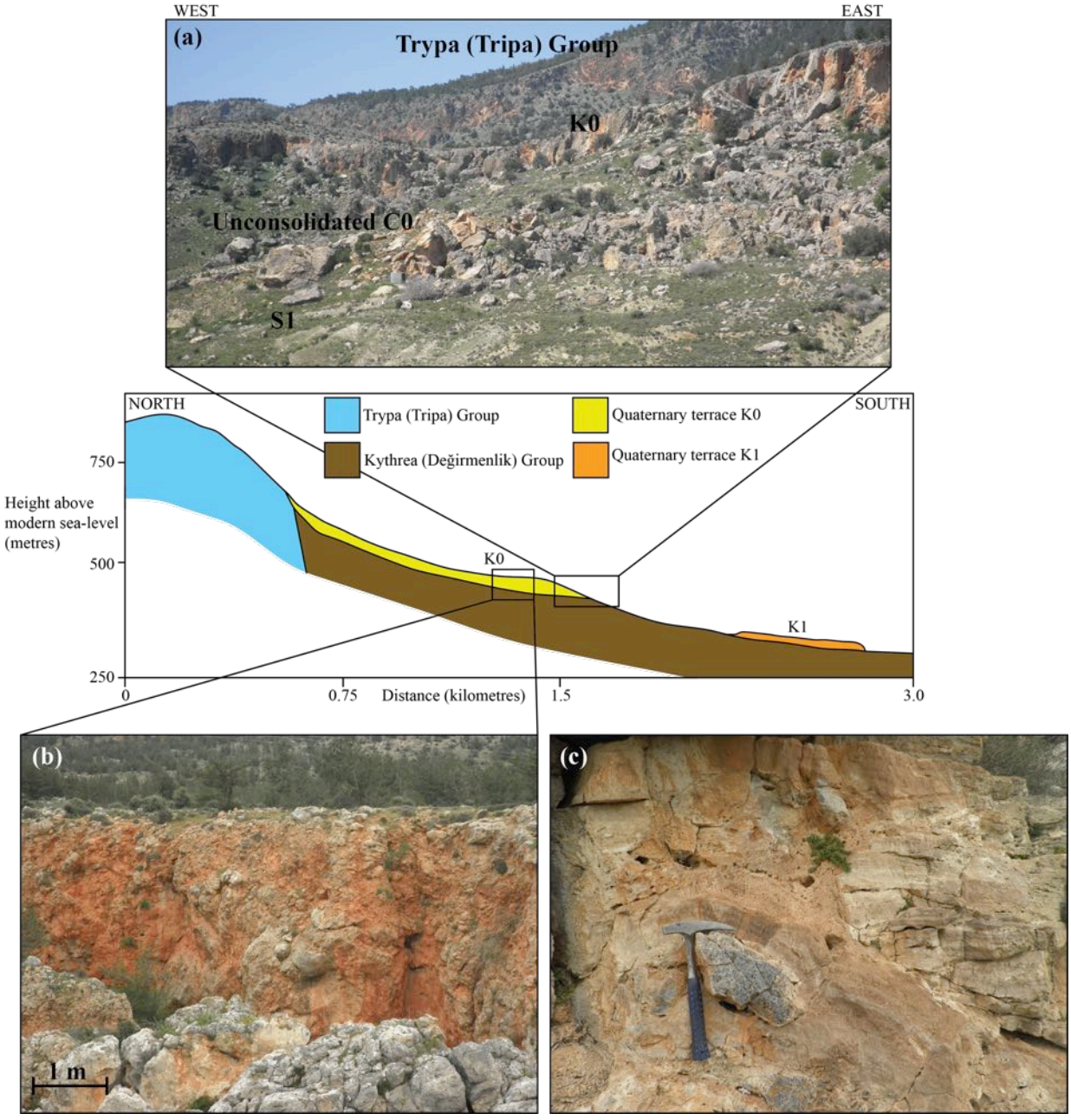

Figure 3.7: Cross-section of the southern side of the Kyrenia Range east of Pınarbaşı (Krini). Photographs from the K0 and K1 deposits from the cross-section. (a) The K0 deposit, and the steeply dipping S1 surface down to the south, with unconsolidated K0 on S1; (b) K0 breccia deposit; and (c) karst weathering of the K0 breccia.

3.3.6 Beşparmak (Pentadaktylos) Mountain (Fig. 3.1)

Beşparmak (Pentadaktylos) is the "mountain of five-fingers"; geologically each finger is as a result of parallel faults dissecting the Trypa (Tripa) Group metacarbonate (Fig. 3.8). The mountain is slightly offset from the main range, ca. 0.5 km further north.

Figure 3.8 shows a geological map of the region around Beşparmak (Pentadaktylos). The mountain itself is composed of Trypa (Tripa) Group metacarbonate with parallel NE-SW faults and E-W faults (Ducloz, 1964). The Trypa (Tripa) Group metacarbonate is surrounding by Lapithos (Lapta) Group rocks on it's northern and southern flanks. The Lapithos (Lapta) Group is unconformably overlain by the Kythrea (Değirmenlik) Group. Unconformably overlying these transitions are the K0 and K1 terrace deposits.

K0 is preserved on steep surfaces on the northern and southern flanks of the range and within fault controlled topographic lows in the range (Ducloz, 1964). Beşparmak (Pentadaktylos) has E-W faults on its northern and southern flanks and on both sides there is an associated K0 deposit.

The K0 deposit is a matrix-supported breccia with poorly-sorted angular clasts (Fig. 3.9 (b)). Clasts within this breccia range in size from 1 cm to 2 m. No sedimentary structures or sorting are visible within the deposit. The lower boundary of the deposit is an erosional unconformity with the Lapithos (Lapta) and the Kythrea (Değirmenlik) Groups. The thickness of the deposit varies from 4 m to 15 m. The maximum thickness is difficult to constrain in this area due to limited exposure.

Figure 3.8 (c) is a photograph of a quarry exposing the Trypa (Tripa) Group and the K0 deposit contact (on a N-S profile). The outcrop is ca. 30 m high and ca. 60 m wide, exposing the Trypa (Tripa) Group in the middle of the section and K0 on the northern and southern flanks of the outcrop. The Trypa (Tripa) Group metacarbonate is extensively fractured, with fractures infilled with tufa. The unconformity between the K0 and the Trypa (Tripa) Group on the northern side of the outcrop is gently northwards dipping; in contrast, the boundary on the southern side is steeply southwards dipping. The K0 deposit in this area is well-consolidated and ranges from 10 m to 20 m thickness.

The K0 terrace deposits are exposed along the main road up to Beşparmak (Pen-

tadaktylos) on the northern side of the range. Figure 3.9 shows two photographs of the K0 deposit exposed along the road. Figure 3.9 (a, b) shows the basal erosional unconformity between the Lapithos (Lapta) Group and the K0 deposit. The thickness of the K0 breccia varies within this section from <1 m to nearly 3 m; this is representative of the highly variable erosional surface that K0 was deposited on. Figure 3.9 (b-c) show a photograph and sketch of the K0 deposit exposed along the Beşparmak (Pentadaktylos) road. The K0 breccia deposit is well-consolidated, matrix supported and contains angular clasts.

The K1 deposit is well-preserved in the region north of Beşparmak (Pentadaktylos) (Fig. 3.8). The K1 deposit is seen on the northern side of a small hill south of Arapköy (Klepini) town. Figure 3.10 shows a section through the K1 deposit at Arapköy (Klepini). The deposit is a matrix-supported conglomerate made up of poorly-sorted, sub-angular clasts with a mudstone matrix and palaeosol beds (Fig. 3.10(a)). The deposit on the top of the hill is heavily altered to caliche (Fig. 3.10(b)). Clasts within the conglomerate are a combination of Trypa (Tripa) Group metacarbonate and K0 breccia (Fig. 3.10 (d)).

The K1 terrace conglomerate continues down the northern side of the hill until it is overlain by an aeolian grainstone (Fig. 3.10 (a,c)). The K1 aeolian grainstone is 2 m to 3 m thick and continuous for ca. 600 m northwards, underlying Arapköy (Klepini) village. The grainstone is composed of a combination of carbonate and clastic grains. The carbonate grains include gastropods, benthic foraminifera and red algae. The clastic grains include mono- and poly-crystalline quartz, feldspar, chert and igneous clasts. The grains are sub- to well-rounded and well-sorted. A micro-sparite cement (<100 microns thick) coats the carbonate and clastic grains, but does not infill the pore space.

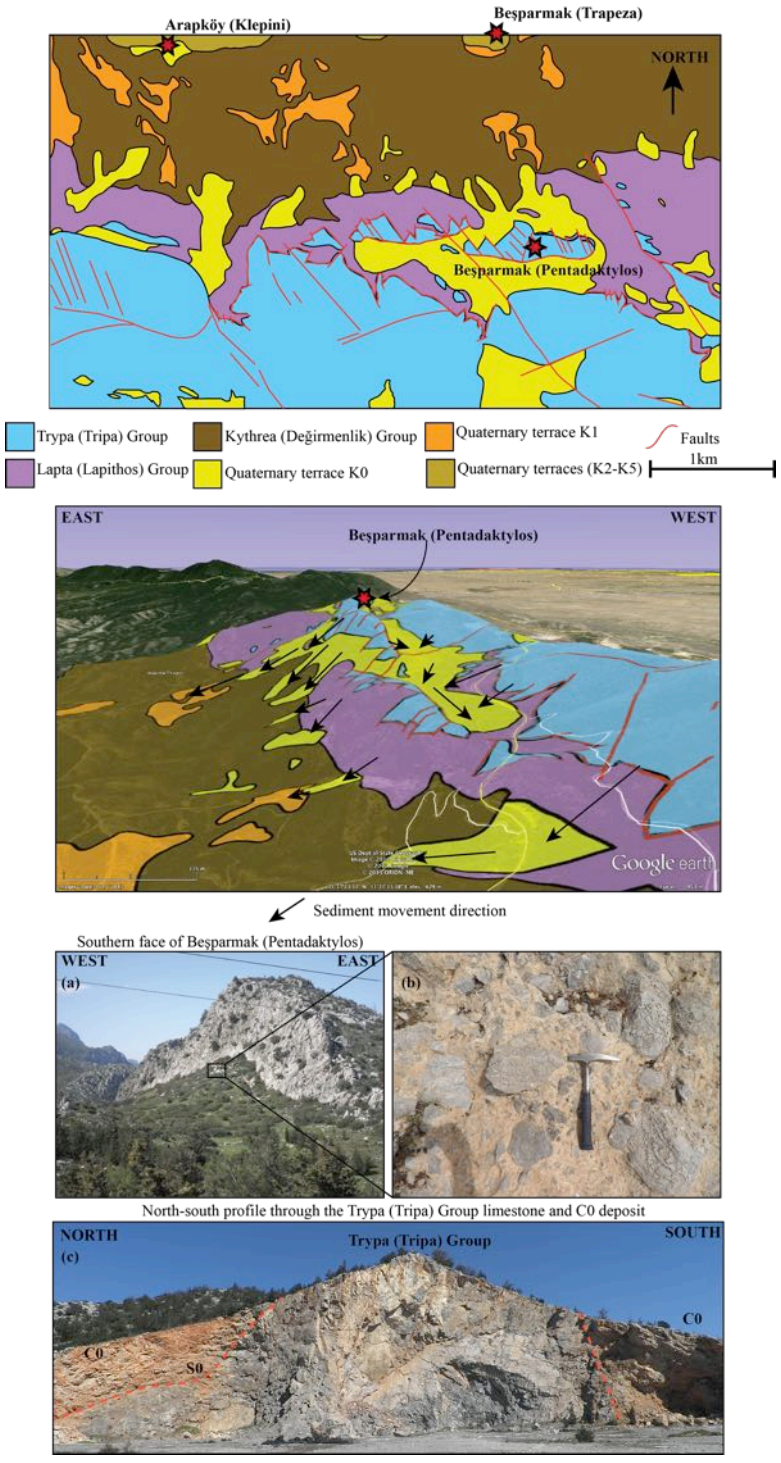

Figure 3.8: Geological map of the region surrounding Beşparmak (Pentadaktylos)(adapted from Ducloz, 1964), overlain on Google Earth topography. (a) Photographs of the southern side of Beşparmak (Pentadaktylos); (b) associated K0 deposit; (c) quarry through the Trypa (Tripa) Group and K0 deposit.

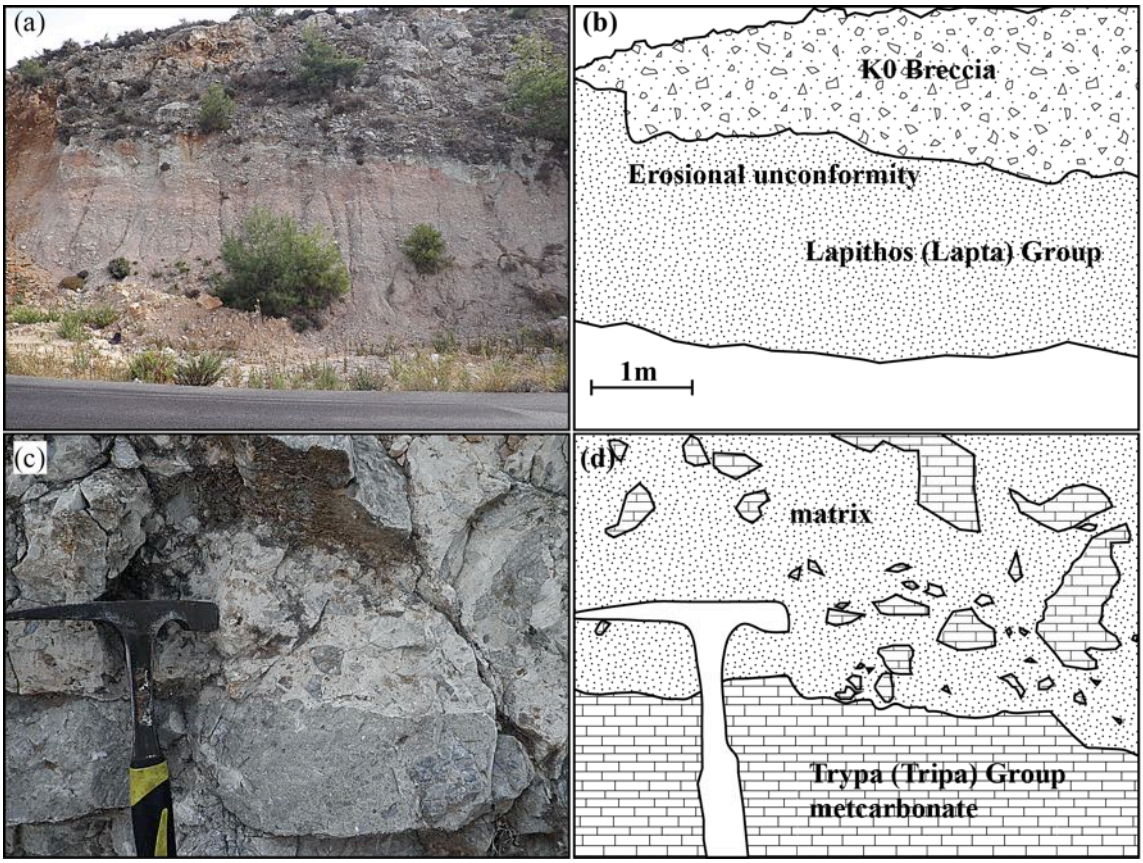

Figure 3.9: Photographs and schematics illustrating the K0 erosional unconformity with the Lapithos (Lapta) Group (a-b) and the K0 breccia (c-d).

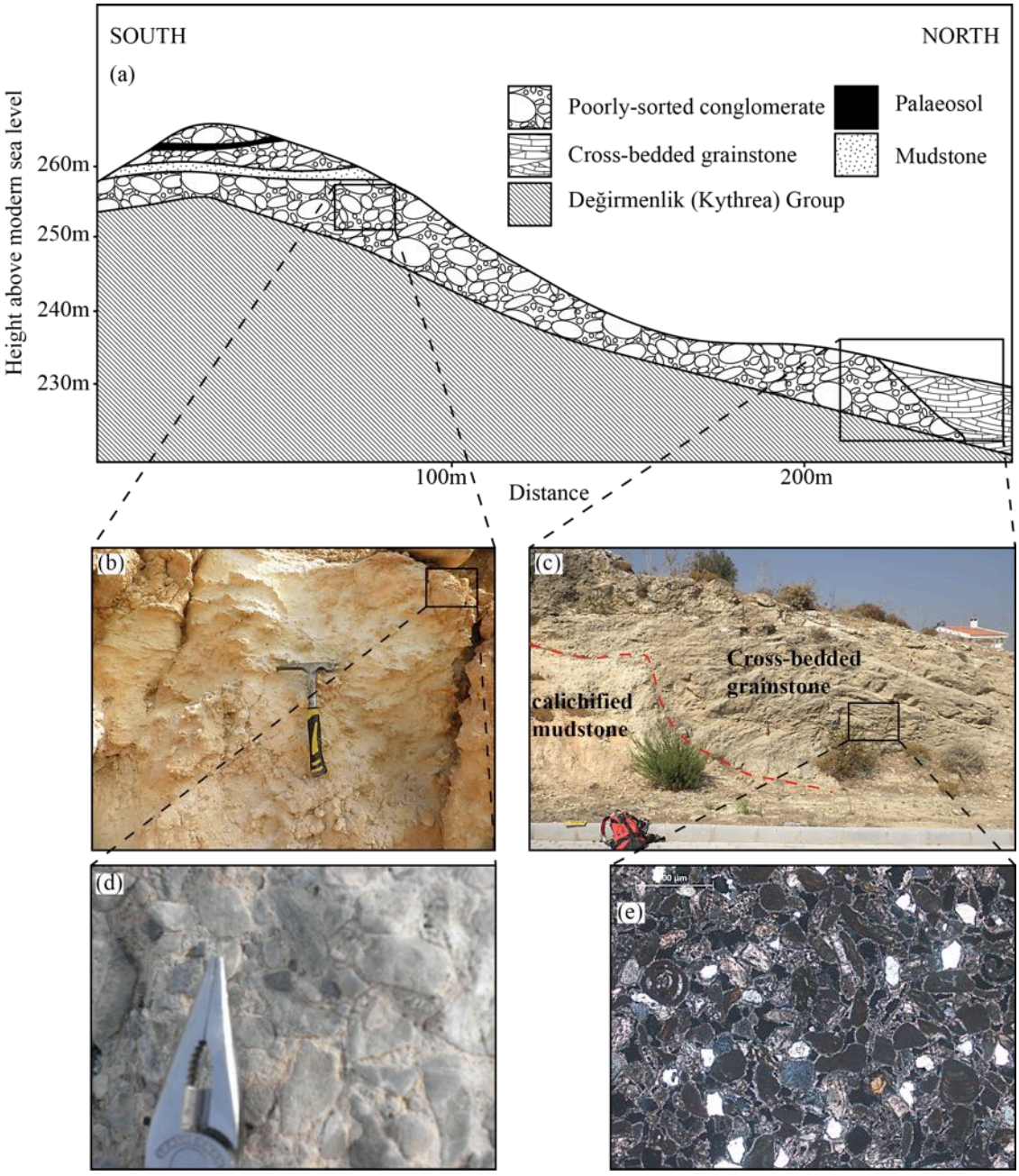

Figure 3.10: Cross-sections and photographs through the K1 terrace deposit at Arapköy (Klepini). (a) cross-section through the K1 deposit; (b) calcified K1 deposit; (c) K1 conglomerate and aeolinite contact; (d) clasts of K0 breccia within K1 conglomerate; and (e) photomicrograph of the K1 aeolian grainstone.

3.3.7 Beşparmak (Trapeza) village

Beşparmak (Trapeza) is a small village ca. 1 km north of Beşparmak (Pentadaktylos) Mountain (Fig. 3.1). The K1 terrace deposit is found on the southern edge of the town. Excellent exposure of the K2 terrace (K2 and M2 components) is found on the northern edge of the town, as discussed in the following chapter.

Figure 3.11 shows a cross-section from Beşparmak (Pentadaktylos) mountain down to the K2 terrace deposit and a log through the terrace. The K2 terrace is composed of a ca. 3 m-thick aeolian grainstone with a thin, pale brown palaeosol half-way through the sequence. The grainstone is well-sorted, sub-rounded to well-rounded and medium grained. Within the grainstone are well-rounded, poorly-sorted (2 cm to 20 cm) clasts of Trypa (Tripa) Group metacarbonate, chalk, metabasalt and sandstone.

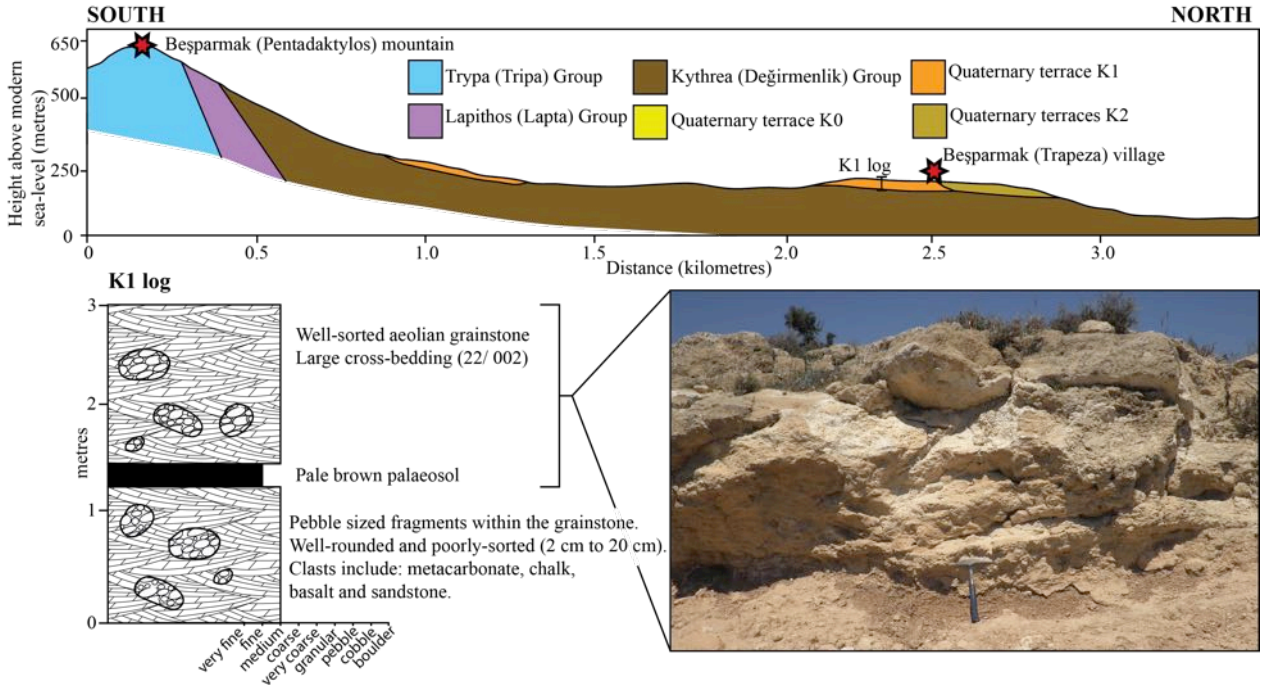

Figure 3.11: Cross-section from Beşparmak (Pentadaktylos) mountain down to Beşparmak (Trapeza) village (adapted from Ducloz (1972)). The log and photographs are from a K1 deposit north of the town.

3.3.8 Kalacaç (Kalyvakia) village

Kalacaç (Kalyvakia) is small village on the southern side of the range, ca. 7 km further east of Beşparmak (Pentadaktylos) Mountain (Fig. 3.1). The K0 and K1 deposits are preserved directly north of the village, parallel to the main range.

Figure 3.12 shows a geological map of the region north of Kalacaç (Kalyvakia) village, illustrating the significant K0 and K1 deposits. The map shows the K0 deposits associated with the Trypa (Tripa) Group metacarbonates. The K0 terrace forms a series of northward-dipping surfaces. The K1 terrace deposits are found immediately downslope of the K0 terrace deposits.

The K0 terrace is made up of a moderately-consolidated breccia with poorly-sorted, angular clasts. Clasts range in size from 1 cm to 1 m. The clasts comprise Trypa (Tripa)) Group metacarbonate and Lapithos (Lapta) Group chalks.

S1 forms a ca. 2.5 km-wide, southward-dipping continuous surface from S0 down to S2 (Fig. 3.12). The K1 deposit is a poorly-consolidated conglomerate with poorly- to moderately-sorted, sub-angular clasts. Clasts range in size from 1 cm to 20 cm and comprise Trypa (Tripa) Group metacarbonate, Lapithos (Lapta) Group chalk and K0 breccia. The K1 deposit is ca. 1 m thick and forms a continuous terrace deposit for ca. 2 km, in the north-south direction.

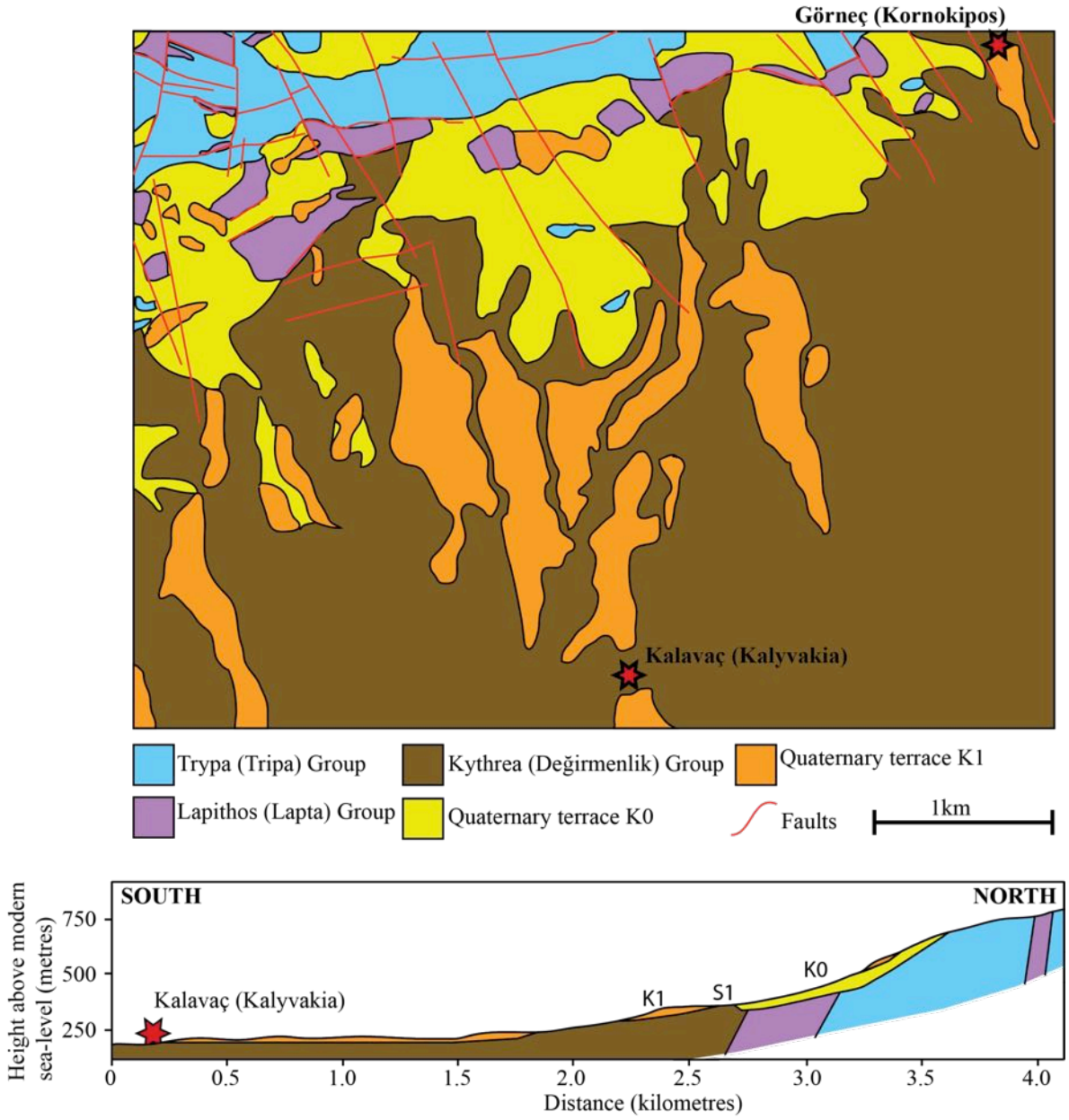

Figure 3.12: Geological map (adapted from Knup (1965)) and cross-section showing the K0 and K1 deposits north of Kalacaç (Kalyvakia).

3.3.9 Tirmen (Trypimeni) village

Tirmen (Trypimeni) is a small village on the southern side of the range, ca. 10 km east of Kalacaç (Kalyvakia) (Fig. 3.1). The terrace deposit is preserved ca. 1 km east of the village. The basement geology of the main range within this region belongs to the Lapithos (Lapta), Değirmenlik (Kythrea) and KalograiaArdana (Başhelı-Ardahan) Groups. No Trypa (Tripa) Group metacarbonate crops out in this area. The Lapithos (Lapta) Group dominates the highest points of the range in this area, which is significantly lower than the Trypa (Tripa) Group dominated areas at ca. 450 m AMSL.

The only component of the K0 terrace found within this area is the S0 surface (Fig. 3.13 (a)). The S0 surface is a steep surface dipping southwards from the highest points of the range down to the K1 terrace deposits. The S0 surface is formed on the Lapithos (Lapta) Group, and ends at the unconformity with the Kythrea (Değirmenlik) Group.

The K1 terrace form a southward-dipping surface away from the main range at ca. 240 m AMSL (Fig. 3.13 (a)). The surface is continuous in an E-W direction for ca. 1 km, except for where younger erosion dissects the terrace surface. The K1 deposits are ca. 3 m thick and form a isolated terrace platforms, 5 m to 10 m wide and 30 m to 50 m long.

The K1 terrace deposit is a matrix- to clast-supported conglomerate with poorly-sorted, sub-angular clasts (Fig. 3.13 (b,c)). Clasts range in size from 1 cm to 30 cm and are composed of chalk, chert and metabasalt. The deposit is both matrix supported and clast supported in parts. The matrix-supported areas are poorly-sorted with clasts ranging from 1 cm to 30 cm in size, with angular, unsorted clasts. By comparison, clast-supported areas show signs of sorting with grain sizes ranging from 1 cm to 5 cm, with signs of normal grading (Fig. 3.13 (c)) and northward imbrication.

3.3.10 Mallıdağ (Melounta) village

Mallıdağ (Melounta) is a small village on the southern side of the central Kyrenia Range (Fig. 3.1). The basement geology in this area is dominanted by the Lapithos (Lapta) and Kalograia-Ardana (Başhelı-Ardahan) Groups. The highest points of the range within this area are at ca. 450 m AMSL, half the height of Selvili Tepe (Kiparissovouno)

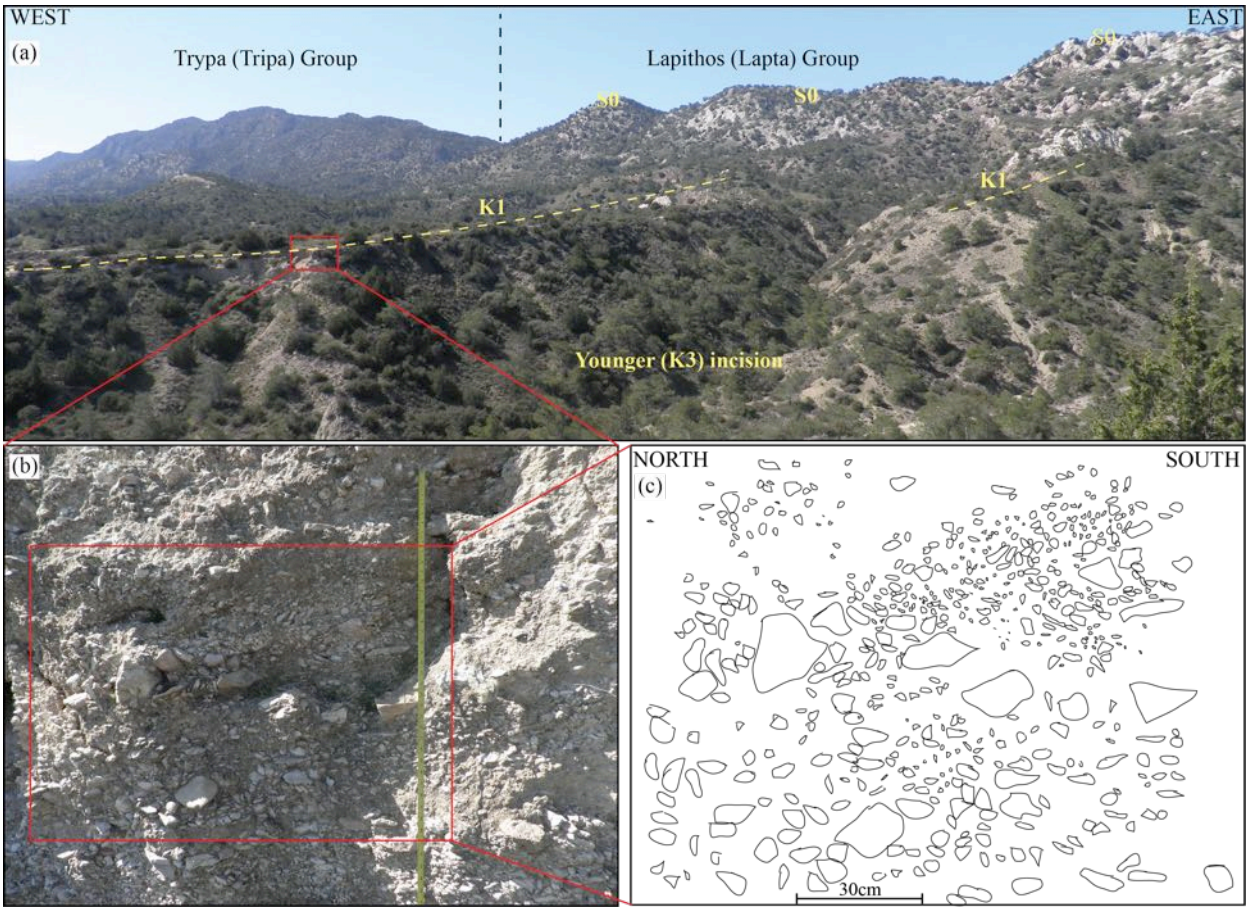

Figure 3.13: Photographs and sketch of the K1 deposits east of Tirmen (Trypimeni) village.

Mountain at the western end of the Kyrenia Range.

The K1 deposit in this region is similar to the K1 deposit at Tirmen (Trypimeni). The S1 surface dips southwards from the main range, with the K1 deposit exposed at ca. 340 m AMSL. The K1 deposit is a ca. 10 m-thick conglomerate with sub-angular clasts, dominantly composed of chalk, with occasional sandstone, metabasalt and chert. Clasts range in size from 1 cm to 1 m, with a average clast size of 3 cm to 5 cm. The clasts are elongate and planar in shape, similarly to the K1 deposits near Tirmen (Trypimeni).

The matrix is a fine-grained pink-coloured mudstone comprising ca. 20% of the deposit. Similar to the K1 deposit at Tirmen (Trypimeni), the deposit is mainly clast-supported but with small areas of matrix-supported conglomerate. The clast-supported

areas of the deposit show signs of poorly-developed normal-grading and bedding structures.

Figure 3.14: Photographs of the K1 terrace deposit east of Mallıdağ (Melounta). Photography (a) overview photograph of the K1 deposit; (b) K1 conglomerate with a range of sub-angular clast sizes; (c) clast-supported K1 conglomerate; and (d) matrix-supported K1 conglomerate

3.4 Fluvial drainage systems on the southern side of the Kyrenia Range

The Pleistocene terrace deposits on the southern flank of the Kyrenia Range were mapped by both Ducloz (1964) and Knup (1965); these bodies of work, described the terraces as being composed of gravel deposits. No further work had been carried on these terrace deposits to understand the depositional environment represented by the gravel deposits. The following section presents new field sedimentology data on the K2-K5 terrace deposits on the southern flank of the Kyrenia Range and from the Mesaoria (Mesarya) Plain.

3.4.1 K2

S2 surface

The K2 terrace forms a discontinuous surface running parallel to the main Kyrenia Range. The surface is at ca. 300 m to 400 m AMSL, with occasional K2 deposits preserved. The large height range of the terrace surface reflects the large variation in height of the range, with the highest parts of the terrace surface at the western end of the range. The K2 deposits unconformably overlie the steeply-dipping mudstones and sandstones of the Kythrea (Değirmenlik) Group. The S2 surface forms a continuous, ca. 1 km to 2 km-wide surface running parallel to the range. This surface is heavily dissected by younger fluvial erosion running perpendicular to the range (N-S). The S1-S2 boundary is a continuous southward-dipping surface. Incision by the K3 terrace has resulted in a series of isolated K0-K2 terrace tongues extending southward from the range.

K2 terrace deposits

The K2 terrace deposits are sporadically preserved along the southern side of the Kyrenia Range. Due to the large amount of younger fluvial downcutting and reworking of the K2 deposits, the deposits are preserved as isolated terrace platforms on the southern flank of the range. Correlation of the terrace deposits is based upon their relative height above sea-level and the relationship between the S1 and S2 surfaces.

Ağıllar (Mandrez) village

Ağıllar (Mandrez) village is at the eastern end of the range ca. 10 km northeast of Geçitkale (Lefkonoiko) (Fig. 3.1). The K2 deposit is exposed along a road section north of the village. The section is ca. 1.5 m thick and <10 m long. The terrace surface is ca. 1.5 km wide and is part of a continuous S2 surface running parallel to the Kyrenia Range.

The deposit is made up of a series of lenses of conglomerate within a light-brown mudstone (Fig. 3.15). The lenses range from 10 cm to 50 cm wide and from 1 m to nearly 5 m long. The clasts within the lenses are sub-angular, moderately-sorted and range in size from 1 cm to 30 cm with an average clast size of ca. 5 cm. The conglomerates are clast-supported, although the deposits contain approximately <10% matrix. The clasts are dominantly composed of chalk. The lenses are interbedded with a light-brown, structureless, heavily-weathered mudstone. Outsized clasts ranging in size from 4 cm to 10 cm are found within the mudstone.

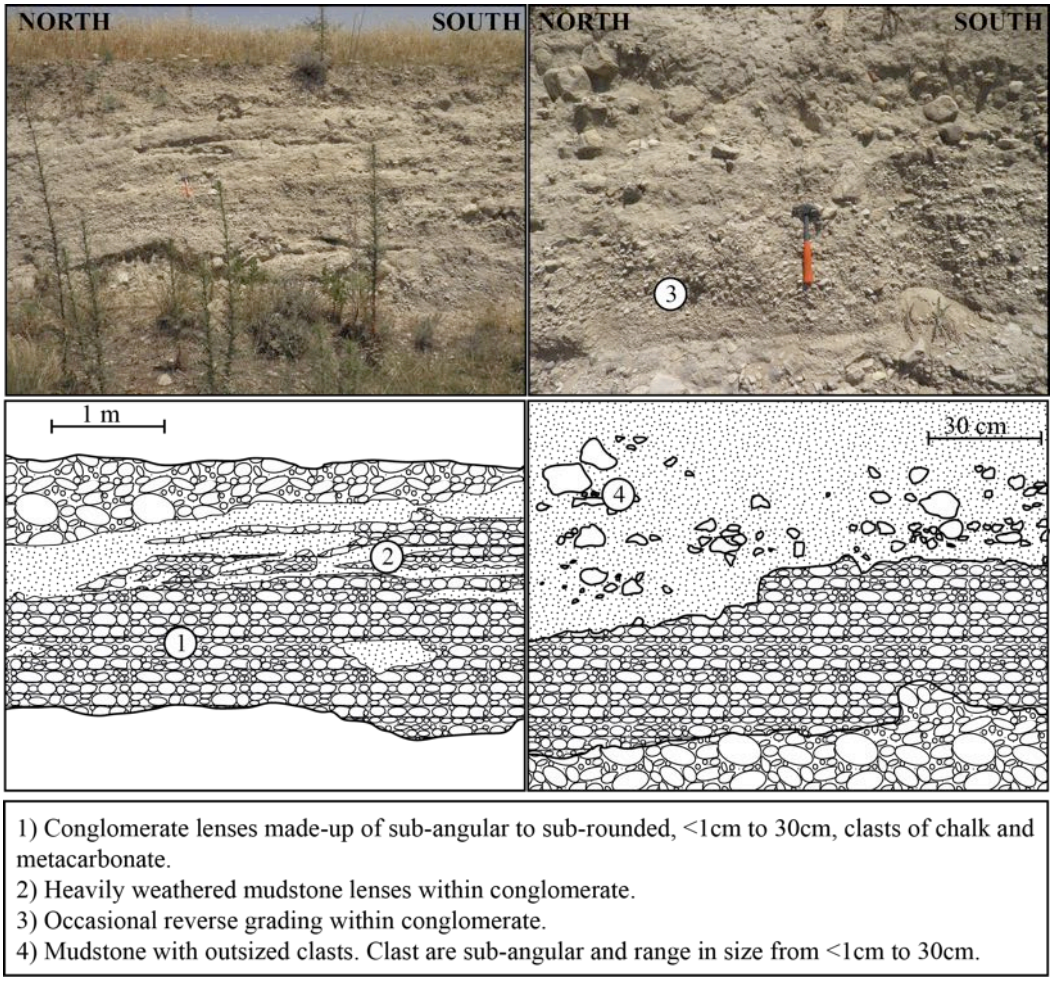

Figure 3.15: Photographs and sketches of the K2 deposit near Ağıllar (Mandrez) village.

3.4.2 K3

S3 surface

The K3 terrace forms a major terrace surface on the southern flanks of the range. The S2-S3 surface is a major stepped boundary with a significant drop in topographic height and this feature can be clearly identified along the length of the range. The K3 terrace forms a major erosive surface truncating older terraces and cutting back into the main range. The S3 surface forms an almost continuous terrace surface from the main range out into the Mesaoria (Mesarya) Plain. The surface varies in width from 1-3 km, depending on the extent of erosion of the older and higher terraces.

K3 terrace deposits

Ağırağ (Agirda) village

Ağırağ (Agirda) village is located in the central Kyrenia Range, directly north of Lefkoşa (Nicosia) (Fig. 3.1). The village is situated at the base of the Kyrenia Range and the K3 deposit is preserved to the north of the village along the road to Kömürcü.

The deposit is at the most northerly edge of the S3 surface, where the terrace surface has downcut through the older K2 terrace. The deposit is exposed in a road section just outside the main village. Figure 3.16 is a schematic sketch through the K3 deposit, illustrating the sedimentary relationships between the various lithologies. The deposit is composed of both mudstone and conglomerate. The mudstone ranges from being cross-laminated to massive and structureless. The conglomerate clasts are sub-angular and poorly-sorted, with clast sizes ranging from 1 cm to 20 cm. The conglomerate deposits vary in composition and structure. The clasts within the southernmost conglomerate are predominantly metacarbonate (Trypa (Tripa) Group) whereas, the clasts within the northern conglomerate are predominantly metachert and metaradiolarite (Lapithos (Lapta) Group). The northerly conglomerate is structureless with no sedimentary sorting of the clasts. In contrast, the southerly conglomerate shows some sedimentary organisation into lenses.

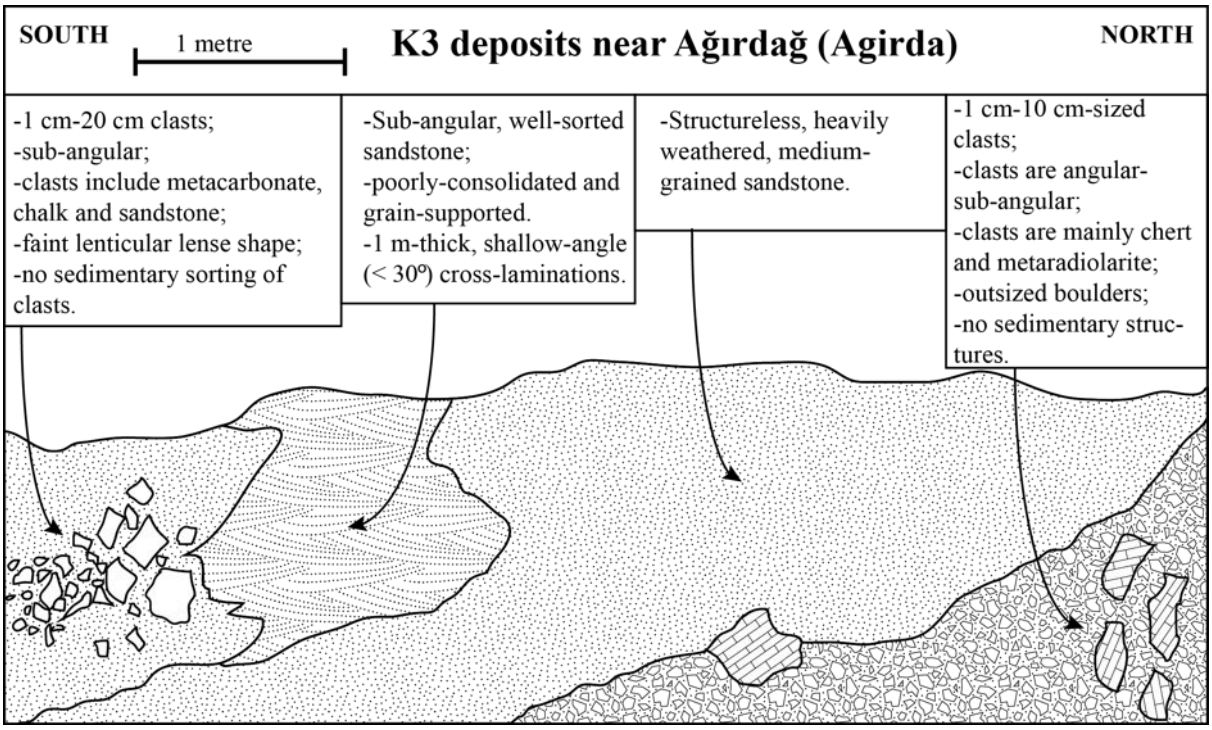

Figure 3.16: Schematic sketch through the K3 deposit south of Ağırağ (Agirda) village.

Ergenekon village village

The small village of Ergenekon is on the southern side of the central Kyrenia Range, to the east of Ağırağ (Agirda) village (Fig. 3.1). The village is situated at the base of the Kyrenia Range. The deposit is exposed in a small quarry ca. 2 km to the south of the village, along the main approach road. The terrace forms a continuous surface for ca. 2 km, from Ergenekon village southwards.

The K3 deposit unconformably overlies a sequence of interbedded brown and white mudstones of the Kythrea (Değirmenlik) Group (Fig. 3.17). The basal erosive unconformity varies in height from ca. 215 m to ca. 220 m AMSL. The K3 deposit ranges in thickness from 1 to 3 m within the small quarry. The lower 2 m of the section is dominantly made up of bedded conglomerate, whereas the upper 1 m is mudstone. The lower conglomerate section is well-sorted and contains sub-angular to sub-rounded clasts. The clasts within the conglomerate beds are either pebble (1 cm to 20 cm sized clasts) or boulder (>15 cm sized clasts) sized, with no sedimentary sorting is seen within each bed. The conglomerate is clast-supported, with <10% matrix. Mudstone lenses are also

occasionally preserved within the conglomerate beds. Clasts are predominantly chalk with additional clasts of metaradiolarite, sandstone, metacarbonate, and rip-up clasts of Kythrea (Değirmenlik) Group mudstone. Conformably overlying the 2 m-thick conglomerate is a 1 m-thick layer of heavily-weathered, structureless, grey-brown mudstone.

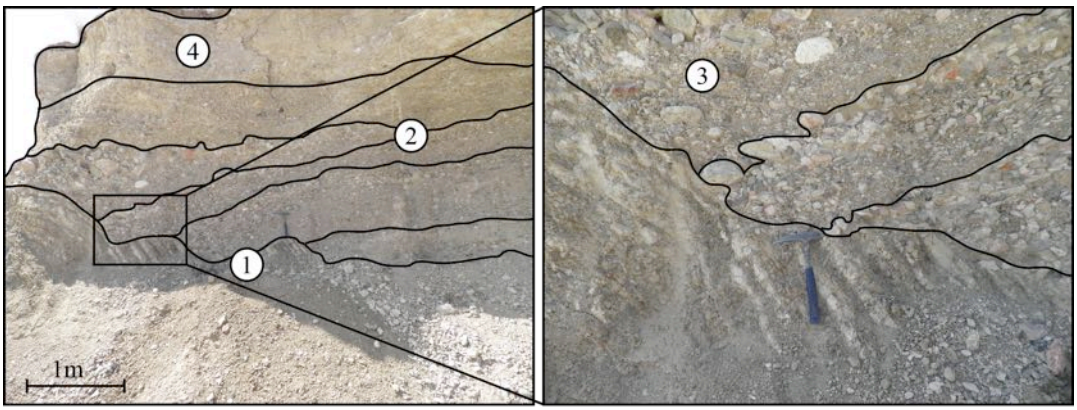

1) Erosional unconformity with the Kythrea (Değirmenlik) Group.
2) Channelised conglomerate with multiple phases. Conglomerate clasts are sub-angular and range in size from 1 cm to 30cm.
3) The conglomerate is clast-supported with <10% matrix. Individual conglomerate channels are reverse graded. Compositionally, the clasts include chalk, radiolarite, sandstone, metacarbonate and rip-up clasts of Kythrea (Değirmenlik) Group mudstone
4) Overlying the entire sequence is a heavily weathered mudstone with occasional outsized clasts.

Figure 3.17: Annotated photographs of the K3 terrace deposit ca. 2km south of Ergenekon village.

3.4.3 K4

S4 surface

The K4 terrace forms a relatively continuous surface with the K3 terrace and extending down into the Mesaoria (Mesarya) Plain. The boundary between the two terraces is unclear owing to younger alluvium and agricultural developments on both terraces. The S4 surface runs parallel to the Kyrenia Range within the Mesaoria (Mesarya) Plain. Nevertheless, the K4 terrace can be distinguished using relative terrace height and numerous differences in the sedimentology of the deposits.

K4 terrace deposits

Three representative K4 deposits are described from localities along the range. The differing sedimentology at each of the localities illustrate the variation in sedimentary characteristics of the K4 terrace deposits on the southern flank of the range.

Kalkanlı (Kapouti) village

Kalkanlı (Kapouti) is small village in the western end of Kyrenia Range (within the orange-growing province) near Güzelyurt (Morphou), in western northern Cyprus (Fig. 3.1). The Dar Dere (Ovgos) fault zone runs to the north of Kalkanlı (Kapouti) village, parallel to the Kyrenia Range (McCay and Robertson, 2012b). The Dar Dere (Ovgos) fault zone deforms the basal geology (McCay and Robertson, 2012b) resulting in differential erosion by the K4 drainage systems, in contrast to older terraces where the basal geology is mostly uniform.

Figure 3.18 shows a profile through an east-west trending valley north of the Dar Dere (Ovgos) fault zone. The valley extends for ca. 11 km, from Yılmazköy (Skylloura) town to Kalkanlı (Kapouti), before widening and continuing for a further ca. 10 km westward to the coast. The profile is from a section directly north of Kalkanlı (Kapouti) village across a ca. 2 km-wide gully. The K4 deposits are preserved at the edges of the gully and have been exposed by a younger fluvial system.

The two K4 deposits are composed of interbedded lenticular conglomerate and mudstones (Fig. 3.18). The K4 deposit on the southern side of the gully is composed of mudstone interbedded with conglomerate. The entire K4 deposit erosively overlies steeply-dipping interbedded sandstones and mudstones from the Kythrea (Değirmenlik) Group. The conglomerates vary from lacking sedimentary organisation to lenticular in shape and reverse graded. The clasts within the conglomerate are sub-angular and range in size from 1 cm to 20 cm. These clasts are predominantly chalk and metacarbonate. Within the conglomerate are lenses of unlithified sand with fine parallel laminations.

The K4 deposit on the northern side of the gully can be sub-divided into two units, a lower brown mudstone with interbedded conglomerate and an upper red structureless mudstone (Fig. 3.18). The two units are separated by a horizontal erosional surface. The conglomerate in the lower unit is structureless, poorly-sorted and contains sub-

angular clasts of a similar composition to the deposit on the southern side of the gully. Occasional outsized clasts are found within the mudstone. The upper red mudstone is structureless, without interbedded conglomerate.

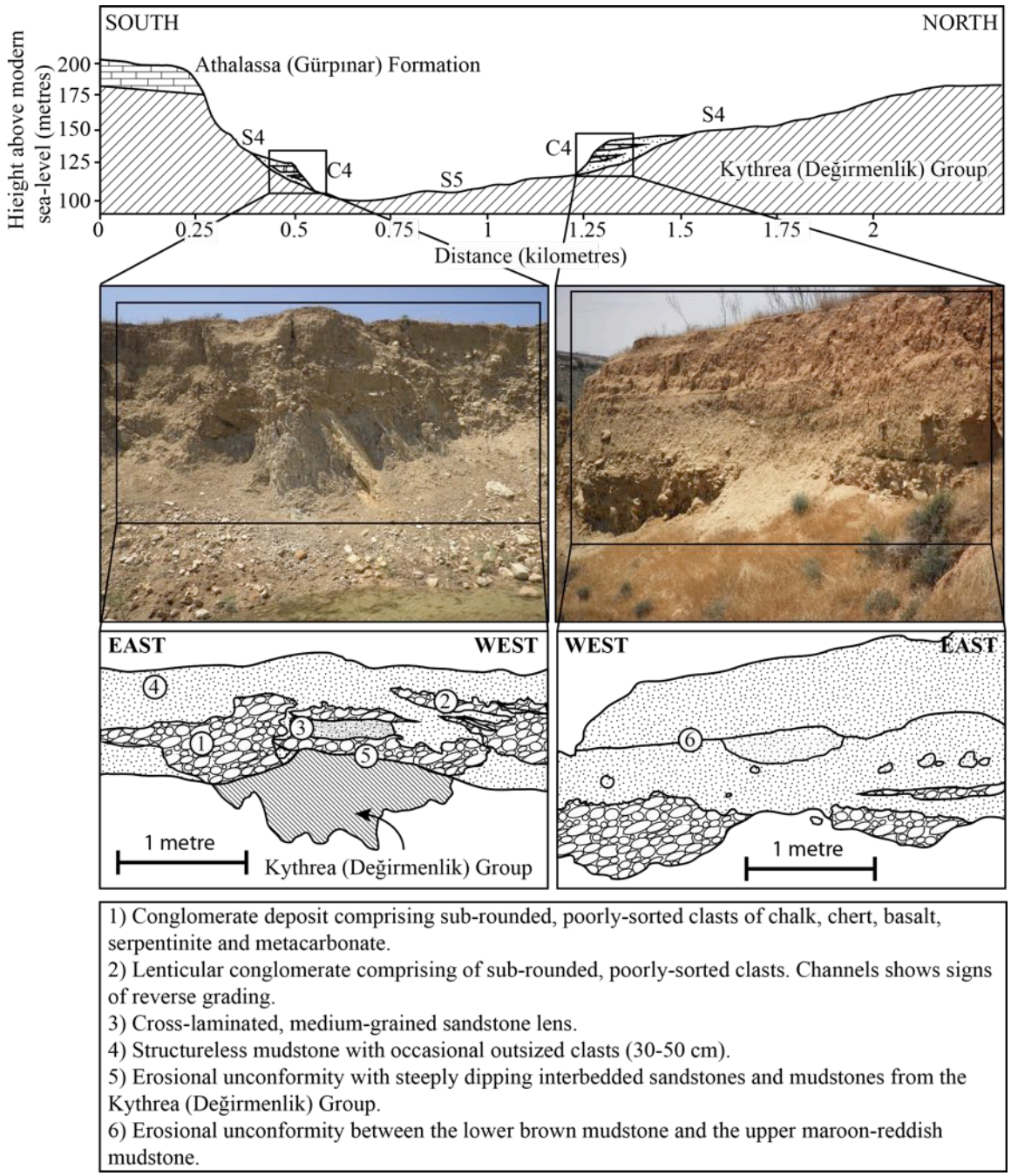

Figure 3.18: Profile, photographs and schematic sketches through the K4 deposit in the east-west trending valley north of Kalkanlı (Kapouti).

Mevlevi (Kyra) village

Mevlevi (Kyra) is small village to the southeast of Kalkanlı (Kapouti), ca. 5 km east of Güzelyurt (Morphou) town (Fig. 3.1). The deposit is preserved along the Güzelyurt (Morphou)-Lefkoşa (Nicosia) motorway at a junction ca. 6 km to the east of Mevlevi (Kyra) village.

The deposit can be sub-divided into two sections, a lower brown-mudstone interbedded with conglomerate lenses and outsized boulders; and an upper red-mudstone with poorly-developed conglomerate channels and outsized boulders (Fig. 3.19). The conglomerate lenses within the lower mudstone are made up of moderately-sorted, subangular, chalk clasts. The boundary between the lower and the upper deposits is an erosional surface that can be clearly identified from the different colours of the two mudstones. The upper mudstone contains conglomerate lenses, but without sedimentary organisation.

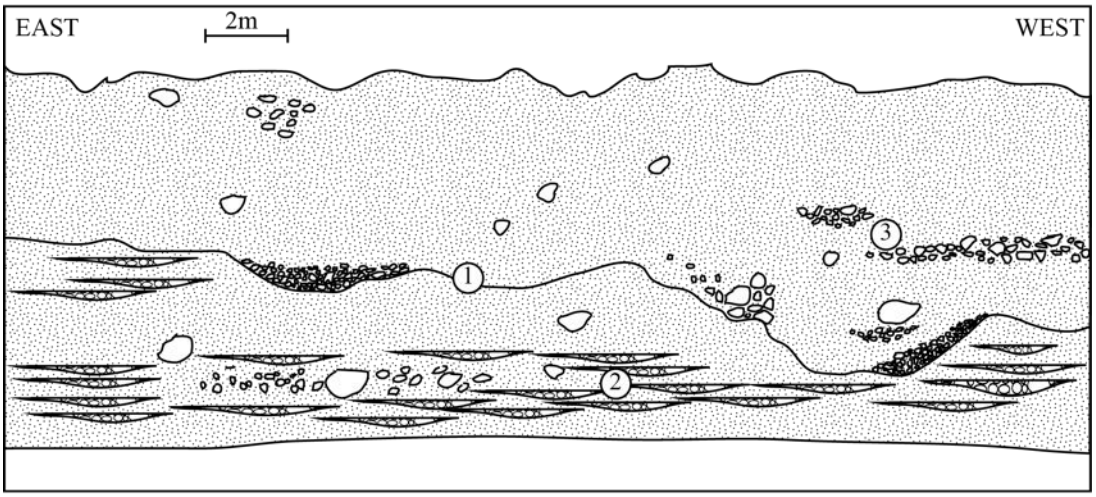

1) Horizontal erosional surface with mudstone.
2) Lenticular conglomerate channels. Clasts are sub-angular, moderately-sorted (1 cm to 10cm) and include chalk, grainstone and Kythrea (Değirmenlik) Group mudstone. Poor-developed eastward imbrication direction. Channels are ca. 20 cm thick and range in length from 20 cm to several metres.
3) Mudstone with occasional outsized clasts and small conglomerate lenses. Clasts are sub-angular and range in size from 1cm to 20cm. The clasts are compositionally similar to the lower unit.

Figure 3.19: Photograph and field sketch of the K4 deposit preserved, ca. 6km west of Mevlevi (Kyra), along the main road.

Geçitkale (Lefkonoiko) town

Geçitkale (Lefkonoiko) is a small town in the east of northern Cyprus, ca. 30 km east of Lefkoşa (Nicosia) city (Fig. 3.1). The K4 terrace deposit is exposed along numerous road cuttings along the east-west trending Lefkoşa (Nicosia)-İskele (Trikomo) road. The K4 terrace is exposed directly east of the town.

The Dar Dere (Ovgos) fault zone in the eastern region of northern Cyprus is inferred to curve towards the north-west, following the curvature of the range and heading offshore before the Karpaz (Karpas) peninsula (McCay and Robertson, 2012b). The Dar Dere (Ovgos) fault zone has a limited surface expression within this region, resulting in the fault zone having a minor influence of the K4 drainage system.

The K4 deposit unconformably overlies heavily deformed mudstone of the Kythrea (Değirmenlik) Group (Fig. 3.20). The K4 deposit is composed of a clast-supported conglomerate with poorly-sorted and sub-rounded clasts predominantly composed of chalk. The entire section is composed of conglomerate with no mudstone preserved. The conglomerate is subdivided into channels of different clast size (Fig. 3.20). The deposits doesn't show any signs of sedimentary organisation. This deposit is exposed numerous road cuttings along the east-west trending Lefkoşa (Nicosia)-İskele (Trikomo) road.

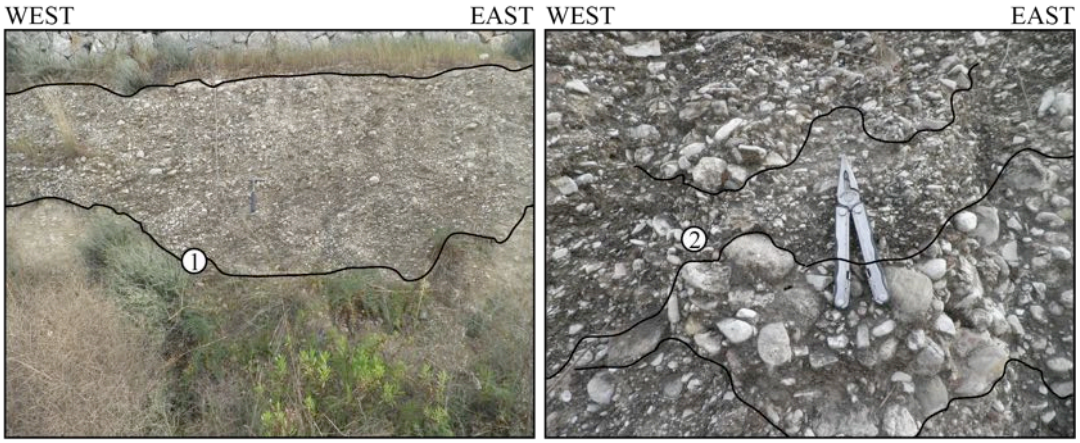

1) Erosional unconformity between the K4 deposit and deformed mudstones of the Değirmenlik (Kythrea) Group. The thickness of the K4 deposit is <2.
2) K2 conglomerate with sub-rounded clasts of chalk. The conglomerate can be sub-divided into conglomerate lenses which are moderately sorted. Clasts range in size from <1cm to 10cm. The entire unit is clast-supported with ca. 20% mudstone matrix. No sedimentary sorting or structures occur within any channel.

Figure 3.20: Annotated photographs of the K4 deposit preserved as a road section at the main junction to the west of the Geçitkale (Lefkonoiko) town.

3.4.4 K5

S5 surface

The K5 terrace forms a continuous surface, together with the K4 terrace, with a gradual drop in height further south into the Mesaoria (Mesarya) Plain. The K5 terrace is found within the central Mesaoria (Mesarya) Plain and forms a continuous east-west surface ca. 10 km south of the main Kyrenia Range.

K5 deposits

Exposure of the K5 deposits is relatively rare, owing to the large amount of agricultural development on the terrace surface on the Mesaoria (Mesarya) Plain. Small quarries in the east of northern Cyprus expose fresh sections through the K5 deposit. Two localities represent the depositional environment of the K5 terrace on the southern side of the Kyrenia Range.

Pınarlı (Vitsada) village

Pınarlı (Vitsada) is a small village in the east of northern Cyprus, ca. 30 km east of Lefkoşa (Nicosia) city along the Lefkoşa (Nicosia)-İskele (Trikomo) road (Fig. 3.1). The K5 deposit is exposed directly south of the village in a small quarry which dissects the terrace surface.

The K5 deposit comprises two major components, a lower conglomerate with an overlying sandstone (Fig. 3.21). The lower conglomerate is composed of well-rounded, well-sorted clasts of metacarbonate, chalk, metabasalt, serpentine, radiolarite and chert. The conglomerate has no obvious sedimentary structures and doesn't show any signs of sedimentary sorting. Within the conglomerate deposit are lenses of planar-laminated sandstone. The upper sandstone unit has poorly-preserved, low-angle cross-bedding. The unit appears to conformably overly the lower conglomerate deposit.

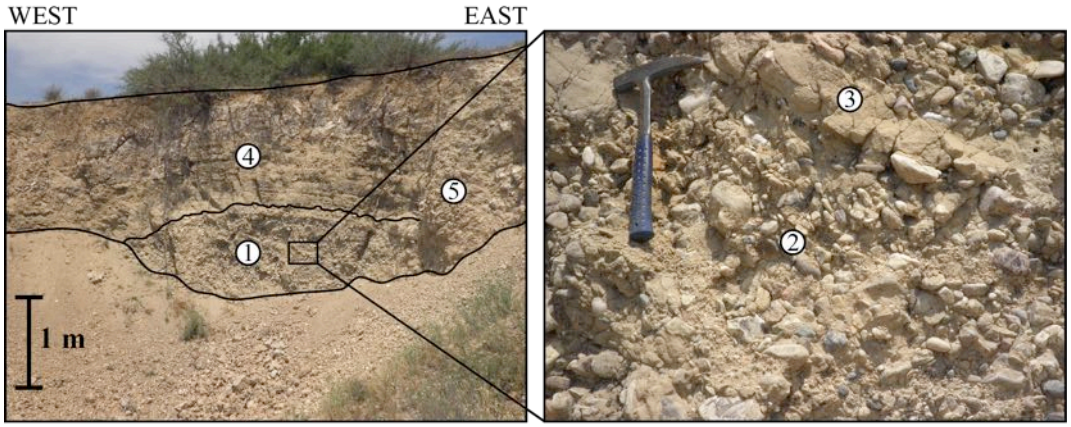

1) The conglomerate unit makes up the lower 2 m of the section, although due to weathering it is unclear how continuous the unit is.
2) The clasts within the lower conglomerate are well-rounded, well-sorted (3 cm to 10 cm) and comprised of metacarbonate, chalk, basalt, serpentinite, radiolarite and chert.
3) Lenses of sand are preserved within the conglomerate. The lenses are <20 cm thick and up to 1 m long. The sand is medium-grained, well-sorted and has poorly preserved parallel laminations.
4) Overlying the entire unit is a large cross-bedded sandstone. This unit appears to be continuous beyond this outcrop. The upper section is approximately 2m thick.

Figure 3.21: Annotated photographs from the K5 deposit from a small quarry to the south of Pınarlı (Vitsada) village.

Nergisli (Genagra) village

Nergisli (Genagra) is small village ca. 3 km to the southeast of Pınarlı (Vitsada) village (Fig. 3.1). The K5 deposit is exposed in a small quarry to the northwest of the village. The quarry exposes the terrace surface which in the surrounding area is obscured by agricultural land use.

The K5 deposit at Nergisli (Genagra) is predominantly composed of a thick conglomerate unit (Fig. 3.22). The deposit can be sub-divided into three sections, firstly a structured conglomerate, secondly structureless conglomerate, and thirdly lenses of finely laminated unlithified sand. The structured conglomerate sections (Fig. 3.22) form elongate channels that are moderately sorted with clasts ranging from 1 cm to 5 cm. In contrast, the structureless areas of the conglomerate are poorly sorted with clasts ranging in size from 1 cm to 20 cm. The entire conglomerate deposit comprises well-rounded of clasts of chalk, metacarbonate, sandstone, serpentinite, radiolarite and chert. The unlithified sand forms lenses within the conglomerate with fine parallel laminations.

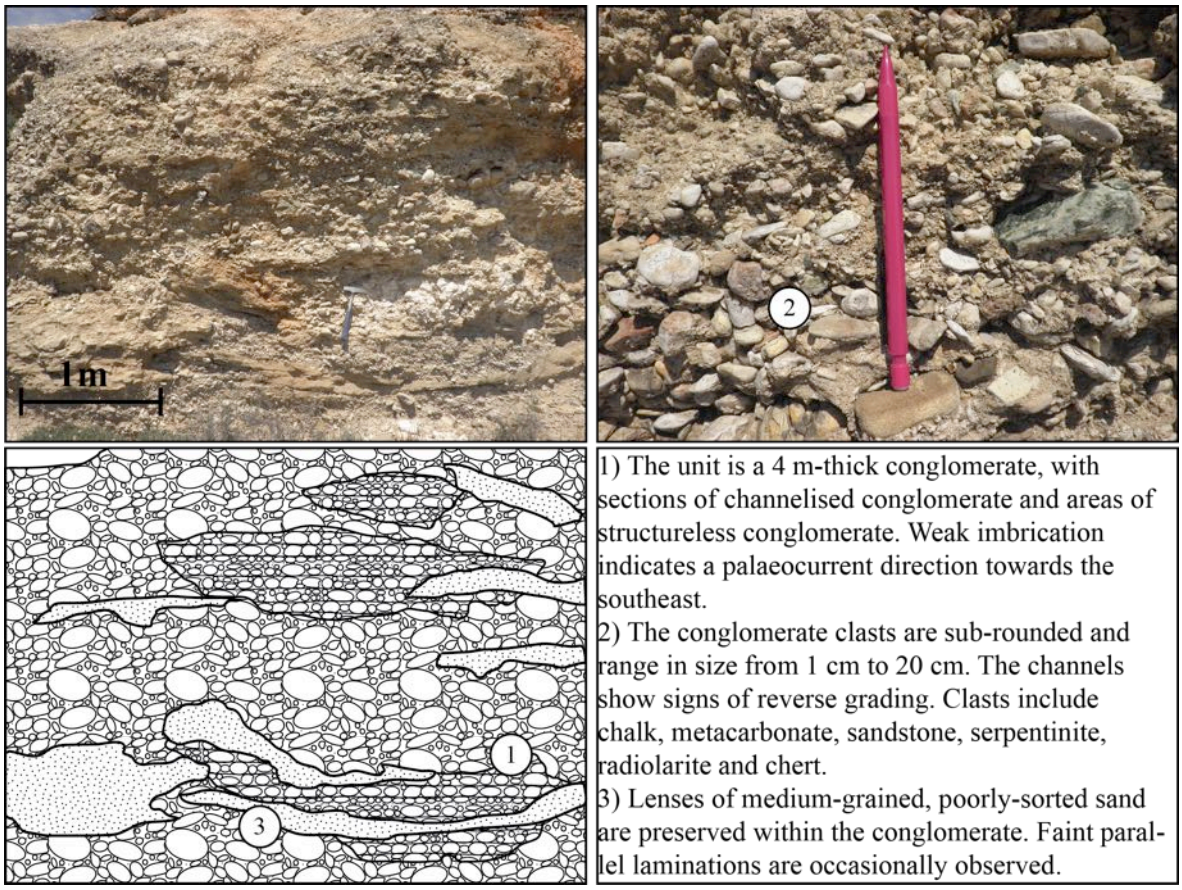

Figure 3.22: Photographs and schematic sketches of the K5 deposit preserved to the west of the small village Nergisli (Genagra).

3.5 Facies

The non-marine facies preserved on the flanks of the Kyrenia Range represent a range of depositional environments, reflecting tectonic, climatic and eustatic influences. The oldest Plio-Pleistocene non-marine deposit preserved in northern Cyprus is the Taşkent (Vouno) Member which is composed of interbedded mudstone, chalk and conglomerate (Fig. 3.23). The D1 conglomerate facies is made up of matrix-supported conglomerate with sub-angular clasts that are dominantly chalk and with occasional outsized clasts (ca. 40 cm). The outsized clasts of mainly composed of metacarbonate. The combination of sub-angular clasts, matrix support and the lack of sedimentary organisation suggests that this deposit did not undergo significant transportation but instead was eroded and deposited locally. The D1 facies conglomerate is interpreted as a colluvial

deposit formed by down-slope reworking.

The D2 and D3 facies represent interbedded chalks and mudstones respectively (Fig. 3.23). The D2 chalk facies is rich in mollusc shells (1 mm to 10 mm sized), which are dominantly composed of gastropods with occasional bivalves. The D3 mudstone facies is made up of a fine grained, poorly lithified mud with occasional mollusc shell fragments. The D2 and D3 facies form an interbedded sequence with the D1 colluvial facies preserved in both the lowest and uppermost parts of the deposit. The D1-D3 sequence is interpreted as a lacustrine deposit, comparable to Fucino Basin in Central Italy (Cavinato *et al.*, 2002) and Lake Bonneville, Northern Utah, USA (Lemons and Chan, 1999).

Facies	Description	Geometry	Interpretations	Terraces
D1- Chalk conglomerate (colluvium)	Matrix-supported conglomerate with clasts of sub-angular chalk, which range in size from 1 cm to nearly 20 cm, with occasional 40 cm-sized blocks of metacarbonate.	The conglomerate forms a horizontal bed ranging in thickness from 40 cm to 1.5 m. Conglomerate deposits are preserved at the base and at the uppermost part of the deposit.	The conglomerate represents slope reworking of locally derived material into a lacustrine environment.	Taşkent (Vouno) Member
D2- Chalk	Fine-grained chalk with 1-3 mm-sized gastropods.	The chalks beds are ca. 50 cm-thick and interbedded with the D3 facies.	Periods of high biogenic productivity within a lacustrine environment.	
D3- Mudstone	Light brown mudstone with occasional bivalve fragments.	The mudstone forms ca.15 cm-thick beds, which are interbedded with the D2 facies.	Periods of low biogenic activity within a lacustrine environment.	

Figure 3.23: Summary of the non-marine facies from the highest uplifted points of the Kyrenia Range and on the southern flank of the Kyrenia Range (part 1 of 3).

The D4 facies is extensively preserved along the Kyrenia Range on both its northern and southern flanks, except at the extreme western and eastern ends of the range. The D4 facies only occur where the Trypa (Tripa) Group metacarbonate outcrops. The D4 facies is composed of a breccia with angular clasts ranging in size from 1 cm to 2 m, and with blocks up to 20 m in size. The D4 facies is therefore described as a megabreccia, based upon the Udden-Wentworth grain-size classification (Udden, 1914;

Wentworth, 1922; Folk *et al.*, 1970; Blair and McPherson, 1999)(Fig. 3.24). The clasts are dominantly composed of metacarbonate. The deposit ranges from matrix supported proximal to the range, evolving to clast supported further away from the range. The thickness of the deposit ranges from 1 m to 10 m, thinning away from the range. The matrix is made up of a fine-grained well-lithified mudstone. The megabreccia has no signs of sedimentary sorting of the clasts. The deposit is extensively covered by tufa precipitation, coating the surface of the deposit and infilling cracks within the deposit. The D4 facies represents a proximal slope talus deposit (Sanders *et al.*, 2009), formed by a period of major erosion of the metacarbonate core of the range.

The D5 conglomerate facies is composed of sub-angular clasts of metacarbonate and D4 megabreccia facies, ranging in size from 1 cm to 1 m (Fig. 3.24). The D5 facies is poorly exposed on both the northern and southern flanks of the range but where visible is found proximal to the D4 megabreccia facies deposits. The D5 conglomerate ranges in thickness from <1 m to nearly 2 m. The D5 conglomerate facies is interpreted as a colluvial deposit formed downslope of the D4 megabreccia facies.

The D6 angular-grained conglomerate (Fig. 3.24) is only preserved between the villages of Tirmen (Trypimeni) and Mallıdağ (Melounta) (Fig. 3.1) on both the northern and southern flanks of the range. The deposit is best preserved <1 km away from the main range, forming a discontinuous surface running parallel to the range. The conglomerate is clast-supported and made up of sub-angular to elongate clasts of chalk. Clasts range in size from 1 cm to 1 m, with an average clast size of ca. 5 cm. The matrix is made up of a fine- to medium-grained, poorly-lithified pink mudstone. Structures within the deposit range from 50 cm-thick imbricated beds to metre-thick sections with no sedimentary organisation. The D6 facies conglomerate is interpreted as a cohesive debris flow deposit (Postma, 1986; Coussot and Meunier, 1996; Hungr *et al.*, 2001).

The D7 facies is preserved within the K1 terrace on the northern flank of the range and the K5 terrace within the Mesaoria (Mesarya) Plain. The D7 facies is composed of a grainstone deposit (Fig. 3.24), which is made up of siliciclastic, clastic and bioclastic grains. The grainstone contains high-angle >30°-dipping planar foresets. The grainstone is well-sorted, fine- to medium-grained and contains well-rounded grains. The D7 grainstone facies is interpreted as representing an aeolian depositional environment (Frébourg *et al.*, 2008). A more detailed discussion of the grainstone facies is presented

in the following chapter.

The D8 to D12 facies are preserved with the K2-K5 terraces on the southern flank of the Kyrenia Range and within the Mesaoria (Mesarya) Plain. The D8 facies is a fine-grained to medium-grained mudstone (Fig. 3.25), varying in colour from browny-grey to browny-red. In general, the mudstone shows no sedimentary structures, except for occasional channel-shaped features that are visible on erosional surfaces within the mudstone. The channel structures contain 1 cm to 5 cm-sized clasts that are sub-angular and well sorted and outsized clasts of metacarbonate, chalk, chert, sandstone and mudstone, range in size from 5 cm to 30 cm. The D8 mudstone facies is interpreted as a low-energy flood plain deposit with occasional erosive channels forming, similar to Palaeocene deposits in the Beartooth Range, in Wyoming and Montana (DeCelles *et al.*, 1991), within a fluvial distributary system (Nichols and Fisher, 2007).

The D9 facies conglomerate forms lenticular-shaped deposits interbedded with the D8 mudstone facies. The lens dimensions range from 5 cm to 40 cm-thick and 1 m to nearly 10 m-long, with well-sorted clasts within each lens. The composition of the clasts include metacarbonate, chalk, chert, basalt, D4 megabreccia, sandstone and mudstone. The relative proportions of clasts types varies significantly between the deposits. The conglomerate lenses are interpreted as high-energy channelised, muddy debris-flow deposits (Coussot and Meunier, 1996), similar to deposits on the Beartooth Range, Wyoming and Montana (DeCelles *et al.*, 1991), within a fluvial distributary system (Nichols and Fisher, 2007).

The D10 facies is a conglomerate with sub-angular to well-rounded clasts, ranging in size from 1 cm to 20 cm. The D10 conglomerate facies forms 1 m to 3 m-thick deposits, which are composed of 30 cm to 1 m-thick beds. The conglomerate beds are well-sorted and exhibit well-preserved normal grading and imbrication. The D10 conglomerate facies is comparable to the Plio-Pleistocence deposits within the Himalayan foreland basin, India (Thomas *et al.*, 2002; Kumar *et al.*, 2003). The composition of the clasts is the same as in the D9 conglomerate facies. Poorly lithified sand lenses are preserved within the conglomerate, with poorly preserved parallel laminations within the K4 and K5 terraces. Furthermore, the K4 terrace D10 conglomerate facies are occasionally overlain by the D7 aeolian grainstone facies. The rounding and organisation of the clasts within the conglomerates suggests persistent stream flow. The deposits represent high-energy, fluvial, sheet flood deposits (Thomas *et al.*, 2002; Kumar *et al.*,

2003), draining away from the Kyrenia Range into the Mesaoria (Mesarya) Plain before heading to the coast.

The D11 conglomerate is composed of sub-angular to well-rounded clasts, ranging in size from 1 cm to 40 cm. The clasts are compositionally the same as those in the D9 and D10 conglomerates. The conglomerate forms 1 m to 3 m-thick discontinuous beds within with D8-D9 facies. The conglomerate doesn't show any signs of sedimentary sorting or structures. The D11 facies is interpreted as slope colluvium, which is comparable to the basal colluvium around Lake Eğirdir in the Taurus Mountains, Turkey, (Nemec and Kazanci, 1999). The colluvium represents a local slope reworking of the D9 and D10 conglomerate facies within fluvial drainage systems.

The D12 facies is pale-brown palaeosol, which is preserved within the K1 terrace. The palaeosol facies represents periods of landscape stability (Kraus, 1999). The palaeosol facies is discussed further in the following chapter.

Facies	Description	Geometry	Interpretations	Terraces
D4- Megabreccia	The deposit ranges from matrix supported to clast supported. Clasts are angular and range in size from 1 cm to 2 m with blocks up to 20 m. The clasts are dominantly comprised of metacarbonate with occasional fragments of tufa. In several localities the deposit is heavily covered and infilled by tufa precipitation.	The deposit ranges in thickness from 1 m to nearly 10 m. The breccia is thickest near the metacarbonate cliff, thinning away from the cliff. The breccia is found at the base of metacarbonate cliffs within the main Kyrenia Range. The deposit is absent from the eastern and eastern ends of the range.	Slope talus formed by fault-scarp degradation.	K0
D5- K1 colluvium	Conglomerate with sub-angular clasts ranging in size from 1 cm to 1 m. The clasts are composed of metacarbonate, metacarbonate breccia and reworked tufa.	The deposits are preserved proximal to the D1 breccia facies. The conglomerate deposit is ca. 1 m-thick.	Local reworking of the D1 conglomerate facies.	K1
D6-Angular grained conglomerate	Clast-supported conglomerate comprised of clasts that range in size from 1 cm to 10 cm. The clasts are sub-angular and elongate. The composition of the clasts is dominantly chalk.	The deposit is preserved on a series of surfaces that dip gently away from the main range and range in width from 100 m to 200 m. The deposits range from 1 m to 5 m thick.	Cohesive debris-flow deposit.	K1
D7- High-angle planar cross-bedded grainstone	Well sorted, fine to medium grained grainstone. Grains comprise clastic and carbonate material. The grains are well-rounded in shape.	1 m to 2 m-thick units of planar cross-bedding. Cross-bedded units are separated by 30 cm-thick units of laminated grainstone. The palaeoflow direction of the cross-bedding E-W tending (parallel to the coastline).	Onshore dune field.	K1, K5

Figure 3.24: Summary of the non-marine facies at the topographically highest parts of the range and the southern side of the Range (part 2 of 3).

Facies	Description	Geometry	Interpretations	Terraces
D8- Fine grained mud-stone	Fine- to medium-grained browny-grey to browny-red mudstone.	Massive and structure-less deposit	Low-energy deposition within a flood plain with occasional low-energy channels.	K2- K5
D9- Lenticular conglomerate (Alluvium)	Conglomerate clasts that are sub-angular and well-sorted, ranging in size from 1 cm to 20 cm. Clasts are moder-ate- to well-sorted within the lenticular-shaped beds. The clasts are mainly composed of metacarbonate but also contain chalk, basalt, chert, metacarbonate breccia, sandstone and mudstone.	The conglomerate deposits are preserved as lenticular-shaped beds within a mud-stone. The lenses range in size from 5 cm to 40 cm thick and from 1 m to nearly 10 m long. Poorly developed normal grading is often observed.	Conglomerate channels representing rapid phases of high energy debris flow style depo-sition.	K2- K5
D10- Bedded conglomerate (Alluvium)	The conglomerate clasts, are sub-angular to well-rounded, well-sorted and range in size from 1 cm to 20 cm. The composition of the clasts is the same as in the D9 facies.	The conglomerate deposits form continu-ous beds ranging in thickness from 30 cm to 1 m. The beds are well sorted and have well preserved normal grading.	Cohesive, high-energy fluvial deposition.	K2- K5
D11- Conglomerate (Colluvium)	Conglomerate contain-ing sub-angular clasts ranging in size from 1 cm to 40 cm. The clasts comprise chalk, chert, basalt, serpentinite and metacarbonate.	The conglomerate deposit ranges in thick-ness from 1 m to nearly 3 m thick. The clasts are poorly sorted and show no signs of sedi-mentary organisation.	Reworking of conglom-erate downslope within a fluvial drainage system.	K2- K5
D12- Palaeosol	Fine-grained pale brown palaeosol. Cali-che is preserved in several horizons.	The palaeosols form continuous horizontal beds within the mud-stone and conglomer-ate deposits.	Preserved ancient soil horizon.	K1

Figure 3.25: Summary of the non-marine facies at the topographically highest parts of the range and the southern side of the Range (part 3 of 3).

3.6 Discussion

3.6.1 Taşkent (Vouno) Member

The Taşkent (Vouno) Member was initially described by Ducloz (1972) as part of the Karka (K0) terrace; however, due to the unique stratigraphy of the formation and its major difference from the K0 deposits it has been separated from the Pleistocene terrace system in this study. The deposits described by Ducloz (1972) are found associated with the K0 terrace deposits, proximal to the main range. However, most of these localities are currently inaccessible or vegetation-covered except on the southerly side of Beşparmak (Pentadaktylos) mountain. This locality presents excellent preservation of the Taşkent (Vouno) Member deposit and a key sedimentary relationship with the K0 megabreccia.

The Taşkent (Vouno) Member is composed of interbedded conglomerate, mudstone and chalk, representing a lacustrine environment. On the eastern edge of the deposit the chalks are interbedded with the K0 megabreccia. Interbedded relationship of the deposits indicates that the K0 megabreccia was deposited into a non-marine lacustrine environment.

3.6.2 K0-K1 non-marine terraces

K0 megabreccia formation process

The D4 megabreccia facies is a product of massive fault-scarp degradation processes related to the Trypa (Tripa) Group metacarbonate. This type of mass-wasting is often seen associated with major surface fault activity (Leeder *et al.*, 1991; Cavinato *et al.*, 2002). This hypothesis was tested by extensive searching for activation features on "older" fault surfaces within the Trypa (Tripa) Group metacarbonate. No evidence was found to suggest any activation surfaces on these faults during the Pleistocene.

The D4 megabreccia facies outcrop is related to the exposed Trypa (Tripa) Group metacarbonate, which make up the central portion of the Kyrenia Range (Fig. 3.1). The megabreccia facies is only preserved proximal to the metacarbonate cliffs, at the highest areas of the range and is not found within any of the lower, younger terraces.

The megabreccia represents a major phase of erosion and mass-wasting of the Trypa (Tripa) Group metacarbonate, which did not continue throughout the Pleistocene. The megabreccia represents a period of unique depositional conditions that were relatively short lived.

Three key factors, based upon field observations, are suggested to have controlled the deposition of the megabreccia facies:

1. The difference in hardness of the metacarbonate relative to the Lapithos (Lapta) and Kythrea (Değirmenlik) Groups lithologies.
2. Existing major fractures and faults within the metacarbonate (from previous deformation events).
3. A phase of rapid uplift.

The deposition of the megabreccia is as a result of a combination of the above factors and not each one individually. The Trypa (Tripa) Group metacarbonate is significantly harder than the lithologies that comprise both the Lapithos (Lapta) and Kythrea (Değirmenlik) Groups, resulting in a slower erosion rate of the metacarbonate when compared to the Lapithos (Lapta) and Kythrea (Değirmenlik) Groups. Older deformation events had left the Trypa (Tripa) Group metacarbonate riddled with cross-cutting fractures and faults mapped by both Ducloz (1964) and by Knup (1965)); therefore erosion results in the fragmentation of metacarbonate clasts ranging in size from 10 cm to 10 m. A combination of lithological hardness differences and heavy faults and fractures alone would only have caused "normal" slope erosion; therefore, major uplift is inferred to accentuate the process. Figure 3.26 is a model for how this process could have worked. The rapid uplift drove increased erosion rates, particularly of the relatively soft Kythrea (Değirmenlik) Group mudstones and sandstones, resulting in slope destabilisation (Fig. 3.26 (b-c)). Mass wasting of the Trypa (Tripa) Group metacarbonate occured to form the D4 megabreccia facies (Fig. 3.26 (d)). Failure along the older faults and fractures within the Trypa (Tripa) Group metacarbonate resulted in blocks from 10 cm to ca. 10 m in size. The final stage included karstic weathering and tufa precipitation onto the surface and within the megabreccia deposit (Fig. 3.26 (e)).

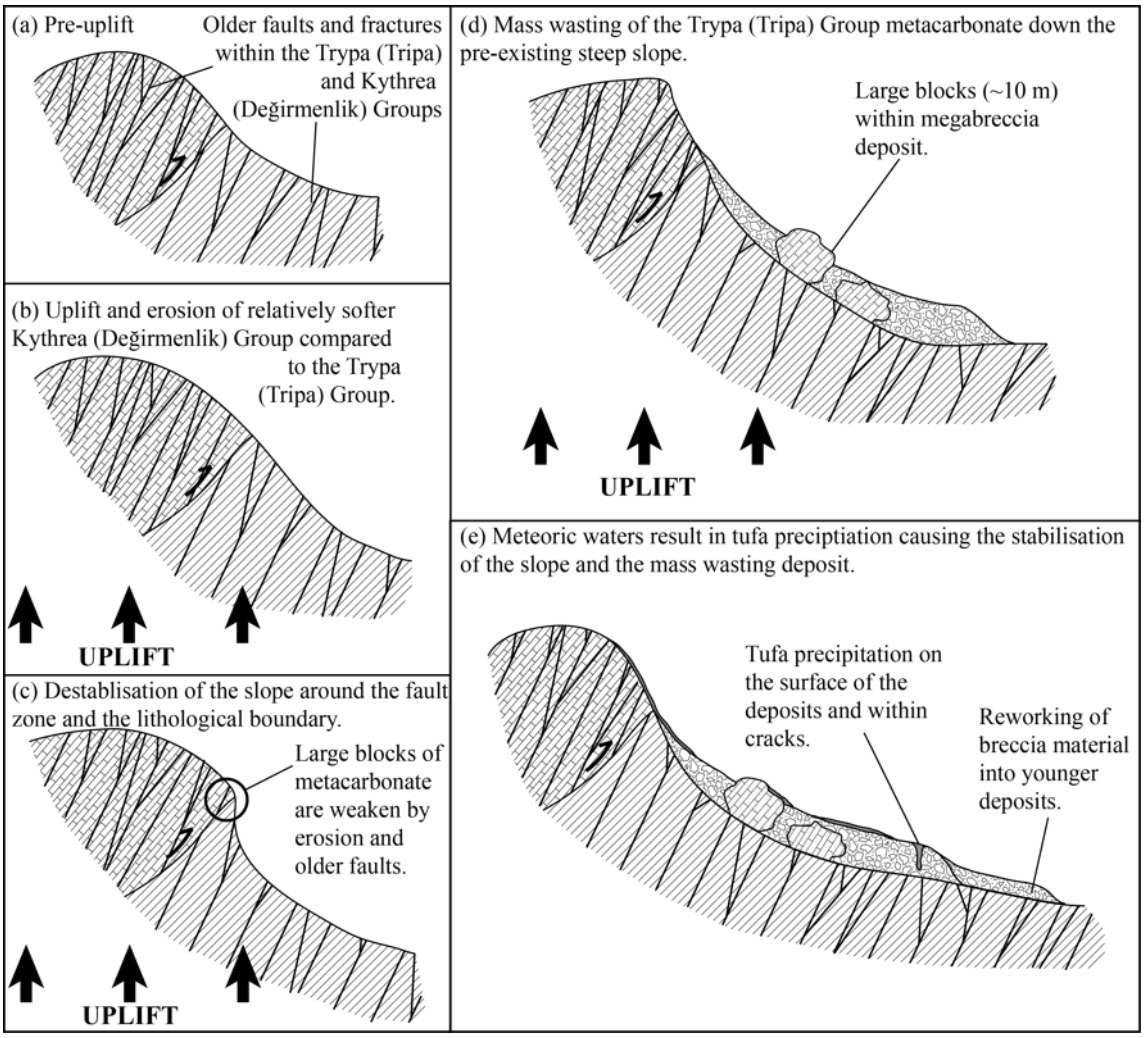

Figure 3.26: Schematic diagram showing the process of fault scarp degradation that drives the deposition of the K4 megabreccia facies.

K1 terrace depositional model

Two K1 facies conglomerate deposits were identified; firstly a colluvial deposit (D5 facies); and secondly, a debris-flow deposit (D6 facies). The D5 colluvial facies is interpreted as the result of downslope reworking of the D4 megabreccia. The colluvial deposit contains reworked D4 facies including eroded tufa, indicating that the colluvial deposit formed after the megabreccia had finished accumulating. At several localities on the northern side of the range, the D5 colluvium facies is overlain by aeolian grainstone (D7 facies). The aeolian grainstone facies is composed of reworked bioclastic and clastic material, which was formed from the reworking of an uplifted Pleistocene marine

deposits (discussed in the following chapter).

The D6 debris flow facies is found within areas of the range where the underlying rocks are made up of the Lapithos (Lapta) Group chalks rather than Trypa (Tripa) Group metacarbonate (Fig. 3.1). The D6 facies represents high-energy, debris flow deposits, which flowed away from the range. The D6 facies was deposited on a relatively flat surface and not within channels or valleys, and therefore, represents deposition prior to major fluvial erosion. No sedimentary relationships are preserved between the D6 conglomerate facies and the D4 megabreccia facies therefore, the relative ages of the deposits are unknown. The D6 conglomerate was either deposited contemporaneously with the megabreccia deposits or shortly after. The D6 conglomerates represent high-energy deposition, and is interpreted as representing the response of areas of the range that are not comprised of metacarbonate to rapid uplift.

Figure 3.27 illustrates the relationship between the D4, D5 and D7 facies. The K0 terrace megabreccia deposit forms a surface dipping steeply away from the range. The K1 terrace colluvium conglomerate is represented by discontinuous deposits downslope of the megabreccia deposit. The palaeocoastline was likely to have been within ca. 2 km of the main range, where the aeolian grainstones were deposited, overlying the K1 terrace colluvium.

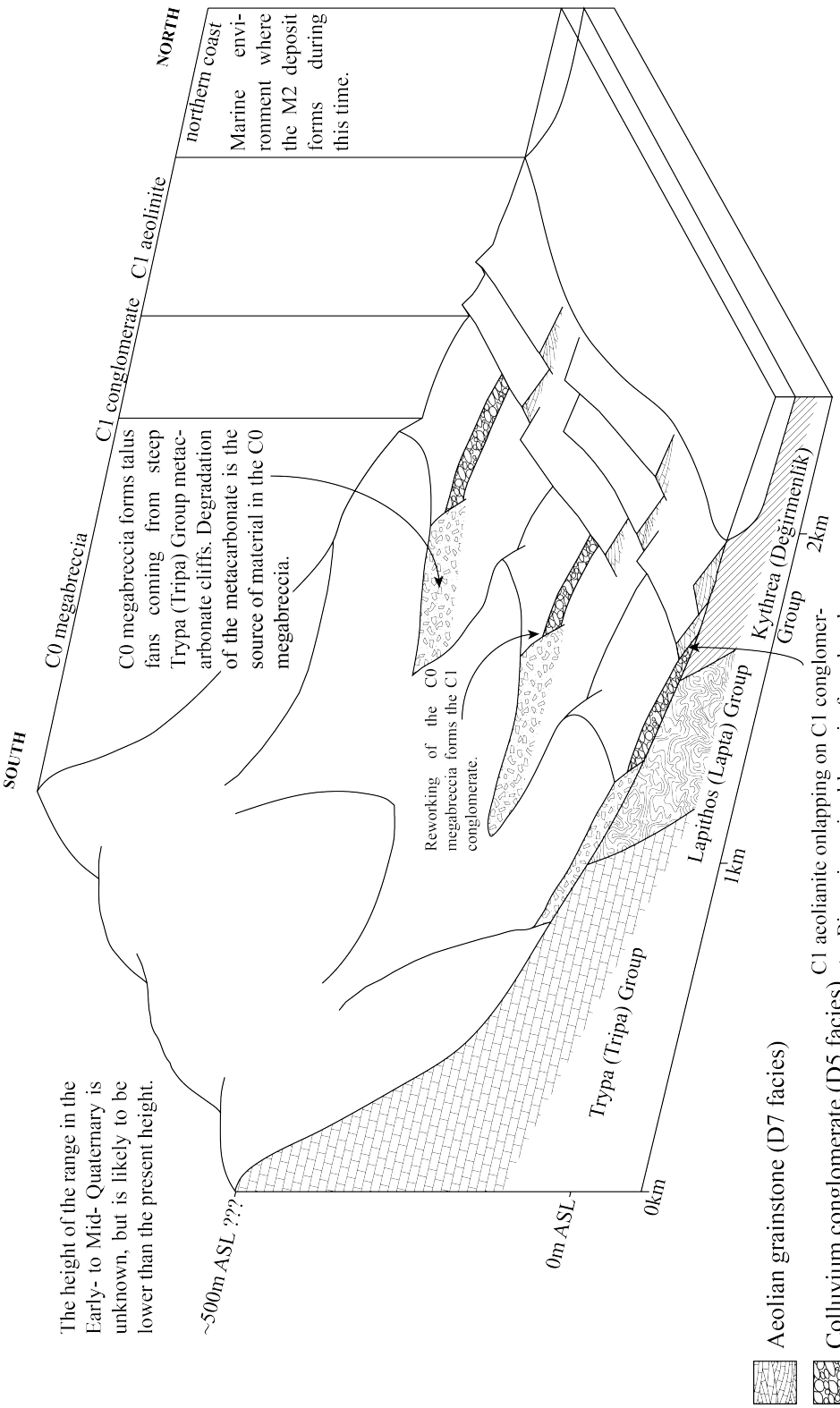

Figure 3.27: Block diagram showing the depositional environment of the K0 and K1 terraces.

3.6.3 Southern side fluvial depositional systems

The Pleistocene terrace deposits on the southern side of the Kyrenia Range represent a series of erosional fluvial systems. The older deposits are preserved highest and closest to the Kyrenia Range, whereas the the younger deposits are further away from the range, on the Mesaoria (Mesarya) Plain.

The K2 depositional system is preserved within ca. 2 km of the main Kyrenia Range and forms a continuous surface compared to the K1 terrace, dipping southward away from the range. Due to erosion by younger fluvial systems it is unclear how far this terrace prograded away from the main range. The K3 terrace forms a major geomorphological feature on the southern side of the range. A major phase of downcutting formed a major break in the terrace height of nearly 100 m between the S2 and S3 surfaces. Discontinuous isolated K3 deposits are preserved at the northern most end of the terrace. The K4 terrace forms a continuous surface, with the K3 terrace dipping away from the Kyrenia Range into the Mesaoria (Mesarya) Plain. Unlike older drainage systems, the K4 fluvial systems were controlled by the underlying rock type and structures. At the western end of northern Cyprus the K4 fluvial system is strongly influenced by the Dar Dere (Ovgos) fault zone. The N-S fluvial system was deflected towards the west due to the Dar Dere (Ovgos) fault zone. The K5 terrace is preserved within the Mesaoria (Mesarya) Plain, at over 10 km away from the range. The boundary between the K4 and K5 terraces is a southward dipping surface, with the K5 terraces at a slightly lower height above sea-level. Exposure of the K5 terrace deposits is relatively rare, but minor occurances within the Mesaoria (Mesarya) Plain provide the opportunity to study the associated terrace deposits.

The K2-K5 terraces are composed of flood-plain mudstone, channelised mudstone (D8 facies), bedded conglomerate (D10 facies) and channelised conglomerate (D9 facies). The deposits preserved within the upper K2 and K3 terraces come from drainage systems that are proximal to the range, in contrast, the deposits preserved within the K4 and K5 lower terraces come from the distal components of the drainage system. The deposits preserved within the upper terraces represent high-energy, braided stream deposits with persistent stream flow, comparable to the alluvial terraces in the southern Himalayas, India (Thomas *et al.*, 2002; Suresh *et al.*, 2007).

The K4-K5 fluvial deposits of the lower terraces include high-energy, braided stream

deposits and flood plain deposits with occasional channels and channelised conglomerate deposits. High-energy, braided stream deposits are preserved parallel to the main range within the Mesaoria (Mesarya) Plain, representing a high-energy intermediate zone within a fluvial drainage system (Nichols and Fisher, 2007). In contrast, the fluvial deposits within the eastern and western regions of the Mesaoria (Mesarya) Plain are composed of interbedded mudstone and channelised conglomerate. The interbedded D8 mudstone and D9 channelised conglomerate facies represent a flood plain with occasional high-energy conglomerate channels, and is, therefore, interpreted as the distal component of a fluvial drainage system (Nichols and Fisher, 2007). The facies making up the fluvial drainage system are comparable to those in similar environments within the Himalayas (Thomas *et al.*, 2002; Kumar *et al.*, 2003; Suresh *et al.*, 2007), Montserrat fan delta, Spain (Burns *et al.*, 1997) and southern Cyprus (Gomez, 1987; Poole and Robertson, 1998; Waters *et al.*, 2010). The distribution of the fluvial deposits within the lower terraces suggests high energy, N-S drainage from the range into the Mesaoria (Mesarya) Plain, followed by low-energy drainage towards the eastern and western coasts.

3.7 Conclusions

1. The Taşkent (Vouno) Member represent a non-marine, lacustrine environment during deposition of the K0 megabreccia.

2. The K0 terrace is composed of a megabreccia representing a relatively short-lived phase of rapid uplift.

3. The K2-K5 terraces on the southern side of the Kyrenia Range represent fluvial drainage systems.

4. The transition between the K2 to K3 terraces represents a major phase of fluvial downcutting.

Chapter 4

Sedimentology and morphology of the marine and non-marine terrace deposits on the northern flank of the Kyrenia Range

4.1 Introduction

The understanding of Cenozoic coastal terrace sequences is an active global research field. Research in ongoing on the coast of Iran and Syria (Reyss *et al.*, 1998; Dodonov *et al.*, 2008), the Gibraltar Straits area (southern Spain) (Zazo *et al.*, 1999), the Hatay-Samandağ coast, southern Turkey (Doan *et al.*, 2012), the island of Bermuda (Hearty, 2002) and also in the Gulf of Corinth (Leeder *et al.*, 2003). These are all areas of significant tectonic uplift where the geological evolution is controlled by the interplay of tectonics and sea-level change.

Eustatic sea-level has varied throughout the Quaternary, related to variations in global ice volume during glacial cycles (Imbrie *et al.*, 1984; Chappell and Shackleton, 1986; Shackleton, 1987; Siddall *et al.*, 2006). The rate and amplitude of eustatic sea-level cycles has increased from the Early to Late Cenozoic (Siddall *et al.*, 2006)(Fig. 4.2). The increased rate of sea-level change during the Early Pleistocene to Recent directly influences the morphology of coastal terraces. Numerous studies have used isotopic data from foraminifera from various oceans as a proxy for global sea-level during the

Pleistocene (Siddall *et al.*, 2006)(Fig. 4.1).The scale of individual sea-level cycles (Marine Isotopic Stages (MIS)) has a significant influence on the morphology of individual terraces (Pedoja *et al.*, 2014)(Fig. 4.3).

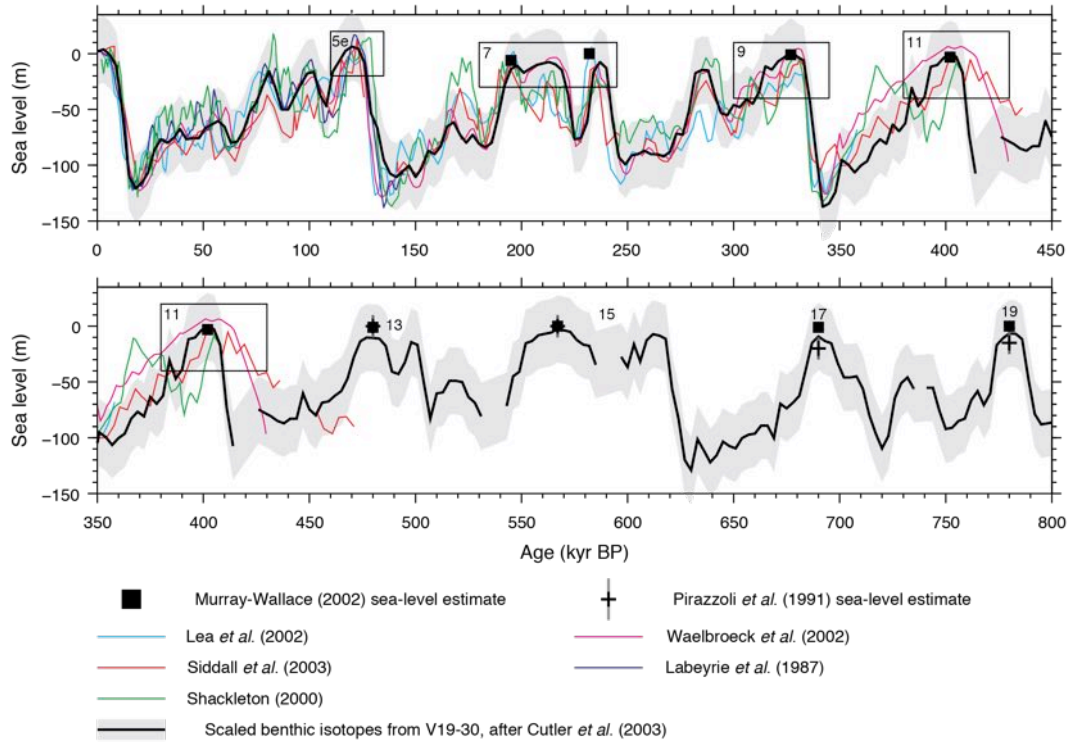

Figure 4.1: Continuous global sea-level estimates from various sources for the Middle to Late Pleistocene (Siddall *et al.*, 2006).

The other controls affecting the morphology of coastal terrace sequences include (i) coastal influences and (ii) continental processes. Coastal processes are dominated by sea-level related controls such as maximum and minimum sea-levels related to glacial cycles. Continental controls are influenced by climate and include aeolian processes, alluvial fan development, meteoric erosion (chemical weathering) and fluvial erosion (Fig. 4.3).

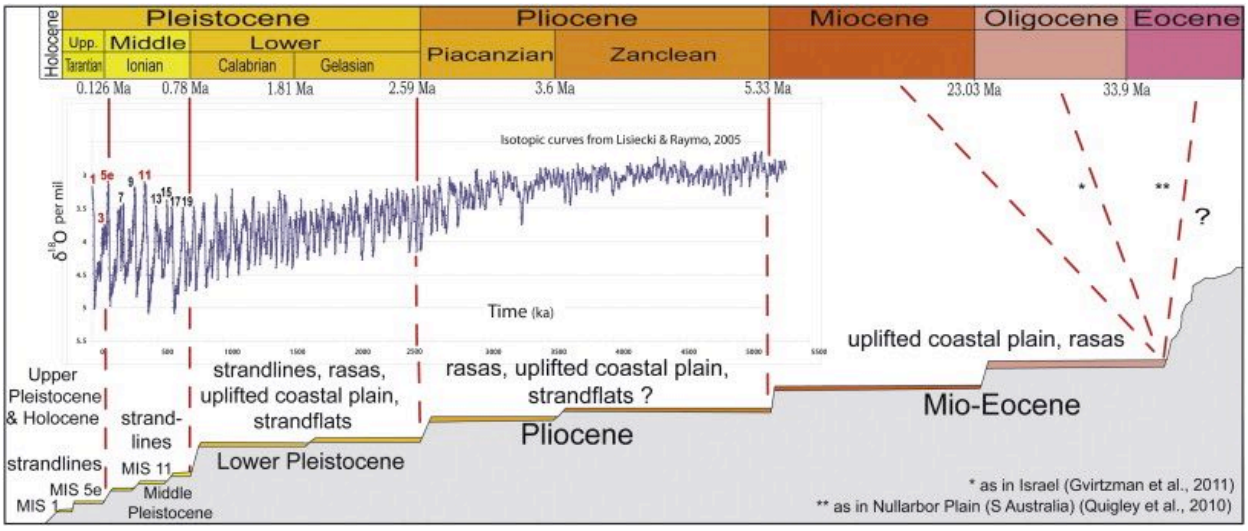

Figure 4.2: The geomorphological terrace occurrence related to eustatic sea-level change during the Cenozoic (Pedoja *et al.*, 2014).

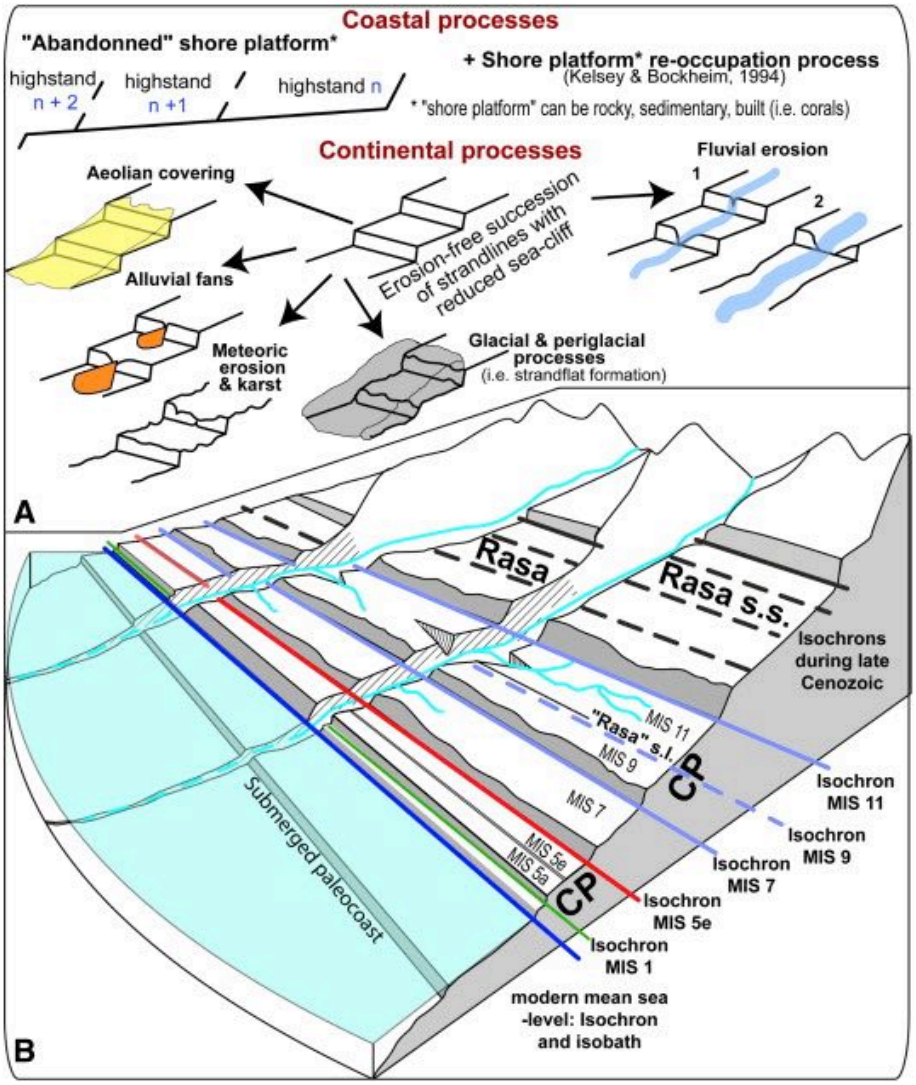

Figure 4.3: The processes and geomorphology of Middle to Late Pleistocene coast development (Pedoja *et al.*, 2014): (a) coastal and continental processes that affect Pleistocene coasts; and (b) the general geomorphology of coasts as a result of coastal and continental processes.

The morphology of coastal Pleistocene terraces is directly controlled by the rate of uplift (Pedoja *et al.*, 2011). Pedoja *et al.* (2011) presents five models (A-E) showing how the morphology of the MIS 5 (Marine Isotopic Stage 5) marine terrace can vary depending upon the rate of uplift (Fig. 4.4). The model presented by Pedoja *et al.* (2011) is based upon a synthesis of 809 sites from 829 published studies representing a range of global tectonic settings. A first observation from these models is that the greater the uplift, the higher the terrace will be relative to modern sea-level (Fig. 4.4). Secondly, the width and shape of the terrace may vary with different rates of uplift. Higher uplift rates result in a wider terrace which may preserve the effect of subtle variations in uplift rate (Fig. 4.4). The rate of uplift is controlled by a number of factors including, eustasy, glacio-hydro-isostasy, dynamic topography and plate tectonics (Pedoja *et al.*, 2011).

The Kyrenia Range in the north of Cyprus forms an east-west, concave, ca. 160 km-long mountain range; with the northern side exposed to the Mediterranean Sea and the southern side to the Mesaoria (Mesarya) plain with the Troodos Mountains to the south. The Quaternary deposits form a veneer on the flanks of the northern and southern sides of the mountain range. The Mesaoria (Mesarya) seaway separated the Kyrenia Range from the Troodos mountains until the Late Pliocene (McCallum and Robertson, 1995b); since its closure the southern side of the Kyrenia Range has been a non-marine environment. In contrast, the northern side of the Kyrenia Range has been exposed to the Mediterranean Sea throughout its Plio-Pleistocene geological history.

The previous work of Baroz (1979) shows a general description of the stratigraphy of the various terrace deposits on the flanks of the Kyrenia Range (see chapter 2). The processes shaping northern Cyprus during the Pleistocene are documented within the evolving depositional environments. A detailed study on the sedimentology of the marine and non-marine deposits on the northern flanks of the Kyrenia Range will shed light upon the larger scale controls, such as tectonic uplift, global sea-level change and climatic change. The following section of the thesis presents a detailed description of the sedimentology and morphology of the Quaternary terraces on the northern side of the Kyrenia Range to aid the understanding of the processes involved in the shaping of the Kyrenia Range during the Pleistocene.

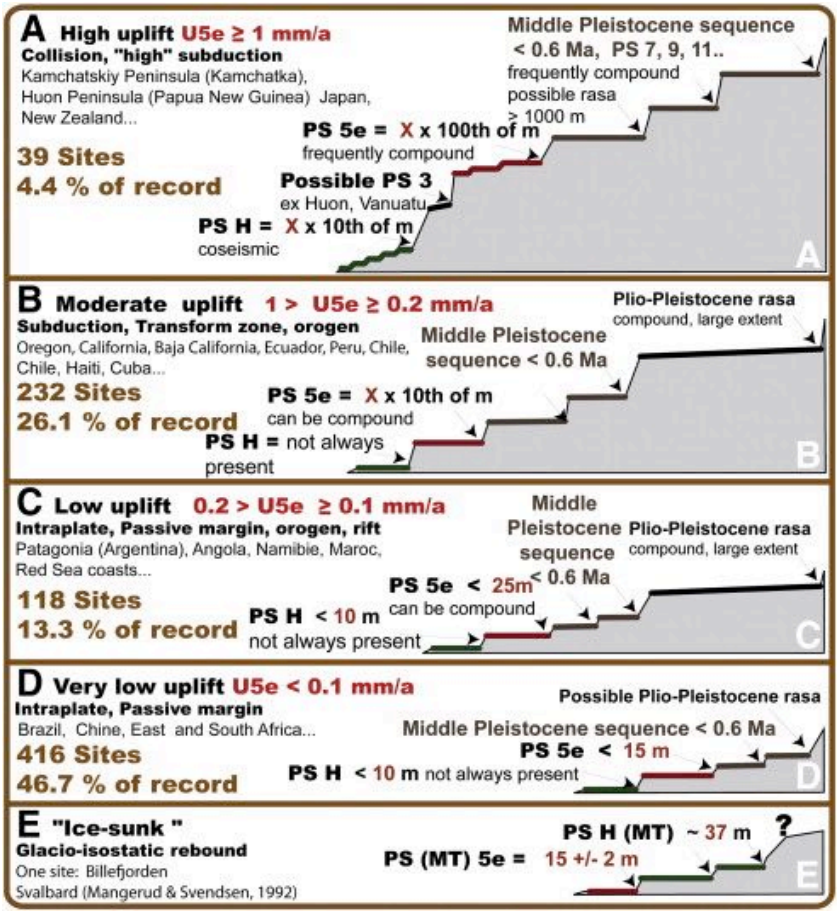

Figure 4.4: Morphological classification of Pleiestocene shorelines based upon tectonic uplift rates; four models (A-D) are presented based on decreasing uplift rates from 1mm/a to <0.1mm/a. A fifth model (E) is presented based upon eustatic rebound rather than tectonic process. (Pedoja *et al.*, 2011)

4.2 The Lower terraces

The lower terraces on the northern flank of the Kyrenia Range include the K2-K5 terraces. The following section describes a series of key localities from each terrace. The terraces represent a series of marine and non-marine environments (Ducloz, 1972). The new field sedimentology and petrography further describes the types of marine and non-marine environments and how the various depositional settings are related.

4.3 Field sedimentology of the K2 terrace deposits

The K2 terrace forms a major terrace step on the northern side of the Kyrenia Range. The base of the terrace varies from between ca. 150 m and ca. 200 m AMSL (above modern sea-level). Preservation of the terrace deposit is fairly poor however, the terrace surface can always be found on the northern side of the range. The K2 surface has been heavily dissected by younger fluvial systems, forming a series of isolated platforms that comprise the K2 terrace.

The boundary between the K1 and K2 terrace deposits forms a single northward-dipping surface. No step is observed between the two terraces on the northern side of the range. Due to the poor preservation of the K1 terrace deposits the sedimentary relationship between the two terraces is rarely seen.

Several key localities of the K2 terrace are described below to demonstrate the depositional environments associated with this major terrace. The localities are described geographically from west to east, starting with Lapta (Lapithos) in the east and ending on the western end of the range at Kaplıca (Davlos) (Fig. 4.5).

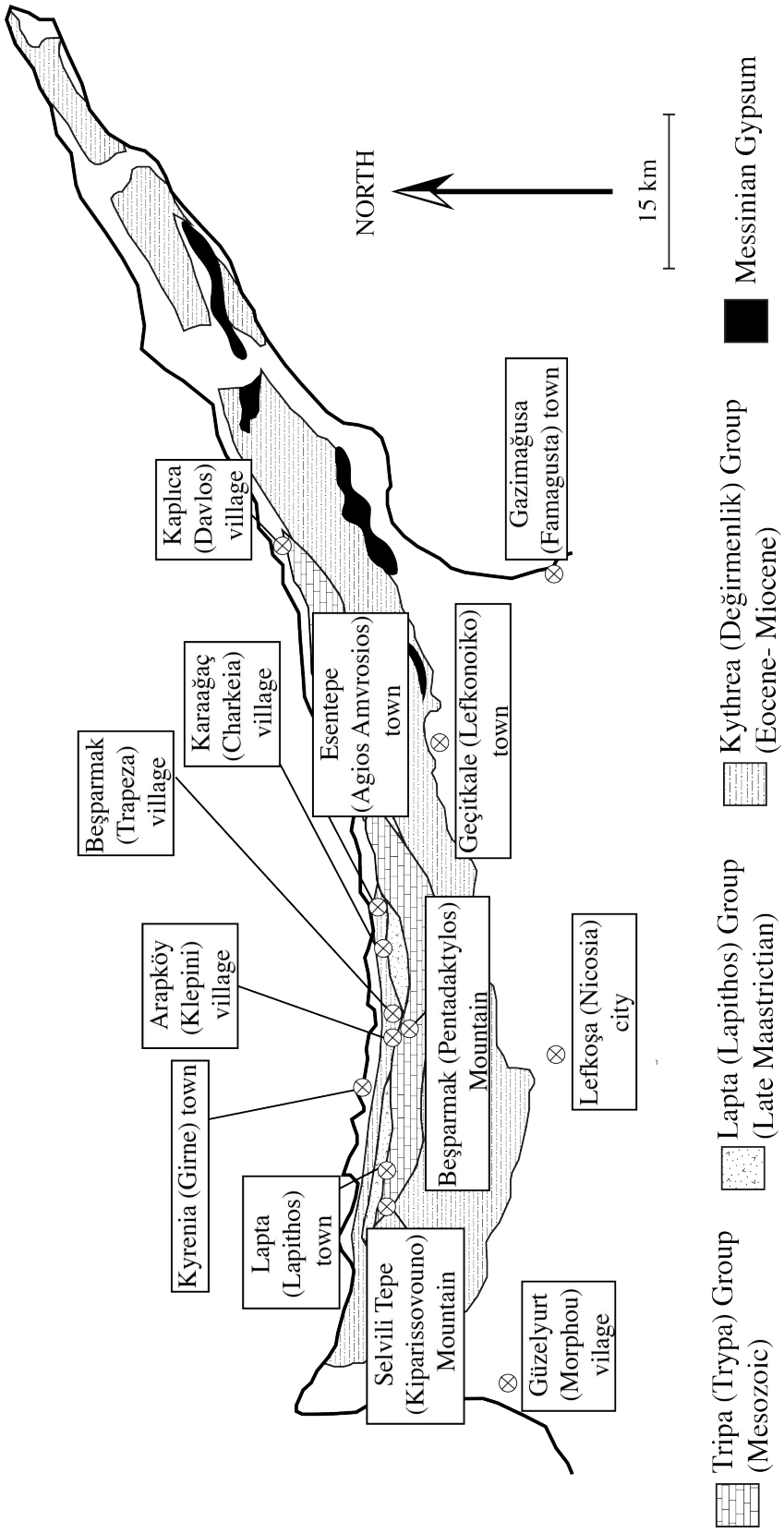

Figure 4.5: Simplified geological map of northern Cyprus showing the K2 terrace localities.

4.3.1 Lapta (Lapithos) town

The old town centre of Lapta (Lapithos) (Fig. 4.5) is built at the base of the K2 terrace. The modern town extends from the terrace down to the coast. The town is the site of one of a number of thermal springs in northern Cyprus which source water from aquifers within the metacarbonate (Tripa (Trypa) Group) (Burdon, 1955). The S2 surface is a prominent feature around Lapta (Lapithos), however the K2 terrace deposits are relatively sparse.

Poorly preserved exposures of the K2 terrace are located to the south-east of the town. The exposed section is only found along a dirt road leading out the town into the main Kyrenia Range. The terrace surface can be clearly identified as part of a continuous east-west surface which trends parallel to the main range. Figure 4.6 is a log through the K2 terrace deposit near Lapta (Lapithos) town.

The K2 terrace deposit near Lapta (Lapithos) town can be divided into two units, a lower ca. 9 m-thick grainstone and an upper ca. 21 m-thick grainstone (Fig. 4.6). The base of the deposit erosively overlies steeply-bedded mudstones and sandstones of the Kythrea (Değirmenlik) Group. The lower grainstone comprises poorly-sorted, medium- to coarse-grained grainstone. This lower unit is full of small cave structures (1 m wide and 2 m deep) which are exposed at the surface; these have been used as graves during Neolithic times (Gjerstad *et al.*, 1934). The upper grainstone is made up of a well-sorted, medium-grained grainstone. The surface of the deposit is covered in a younger tufa precipitate. The precipitation of tufa has resulted in preservation of modern flora on the surface of the deposit.

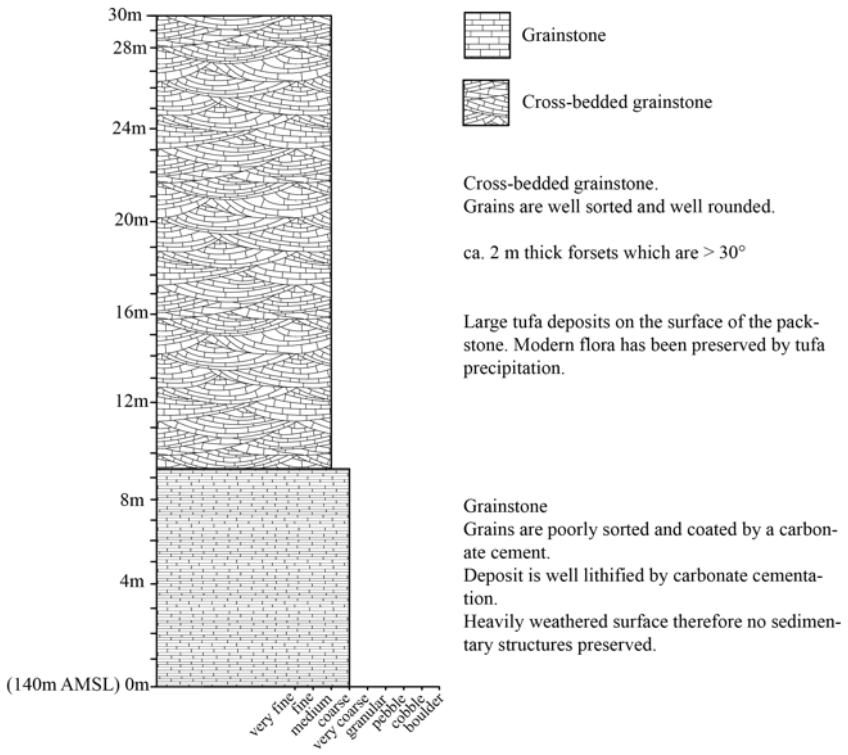

Figure 4.6: Sedimentary log through the K2 terrace deposits near the town of Lapta (Lapithos) (N35 20.079' E033 11.618').

4.3.2 Arapköy (Klepini) village

Arapköy (Klepini) town (Fig. 4.5) is built on the K1-K2 terrace surface. Exposure of the K2 terrace deposit is found along the northern side of Arapköy (Klepini) town. Figure 4.7 is a log from the section exposed along the road on the north-western side of the town. The exposure runs in a north to south orientation and from lower to higher along the road.

The K2 terrace deposit is composed of a basal grainstone overlain by a mudstone interbedded with conglomerate lenses (Fig. 4.7). The basal grainstone deposit erosively overlies mudstones of the Kythrea (Değirmenlik) Group, and is composed of a fine-grained, well-sorted, heavily-cemented grainstone. Overlying the marine deposit is the non-marine deposit, which is composed of a mudstone with interbedded conglomerate lens and multiple laterally continuous palaeosol horizons.

The conglomerate lenses are interbedded with a structureless mudstone. Conglom-

erate lens dimensions vary from 3 cm by 40 cm at the lowest and most northern edge of section, to 60 cm by 5 m at the top and most southern part of the section. Clasts sizes also vary from 1 cm to 5 cm at the bottom of the sequence, and from 1 cm to 30 cm near the top of the sequence (Figure 4.7). In general, the channels get wider and thicker towards the top of the section. Throughout the section the clasts within the conglomerate lens are well-sorted and normally-graded.

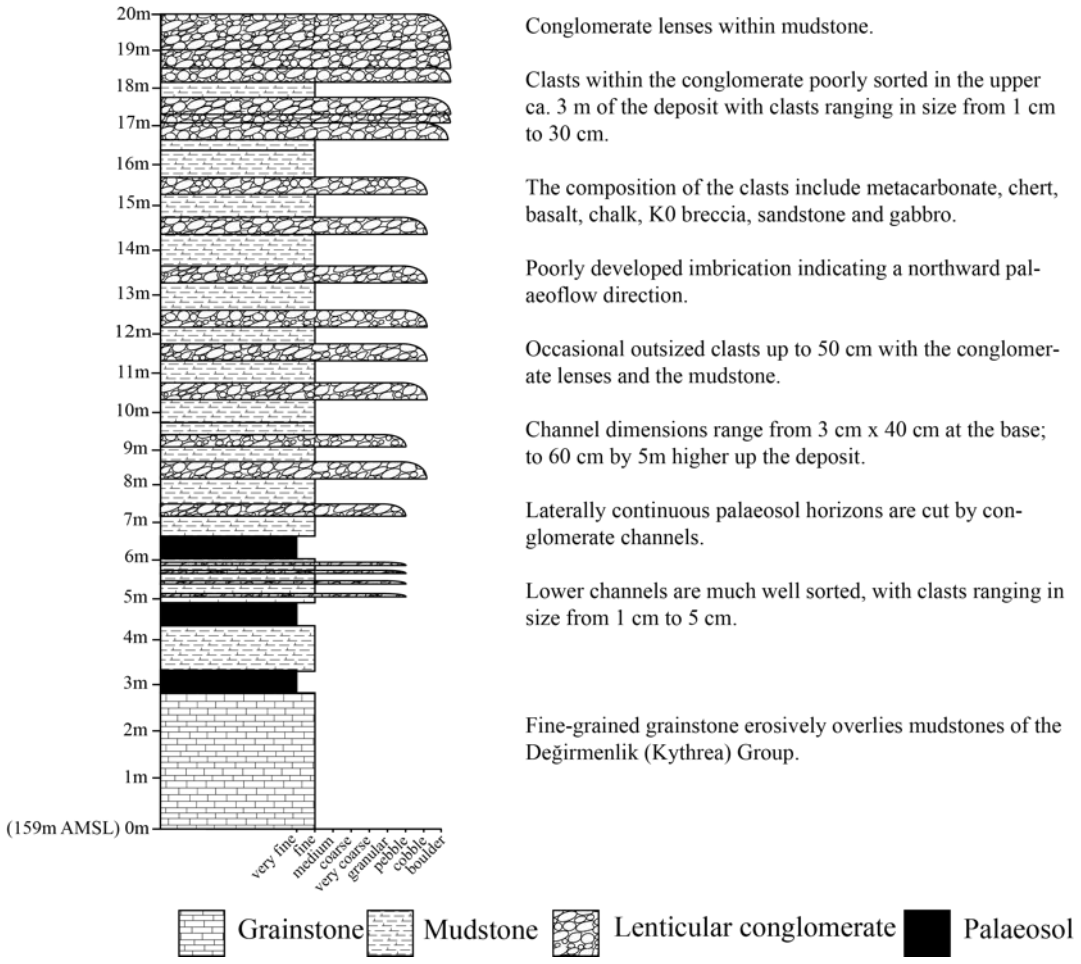

Figure 4.7: Sedimentary log through the K2 terrace deposit north of the town of Arapköy (Klepini) (N35 18.819' E033 25.550').

4.3.3 Beşparmak (Trapeza) village

Beşparmak (Trapeza) is a small village at the base of Beşparmak (Pentadaktylos) Mountain (Fig. 4.5). The K2 terrace deposit is exposed on the northern side of the village,

at the top of a series of switch-backs on the road leading to the village.

The K2 terrace deposit associated with Beşparmak (Trapeza) village is composed of a basal grainstone overlain by a mudstone interbedded with conglomerate lenses. The basal grainstone erosively overlies steeply bedded mudstones and sandstones of the Kythrea (Değirmenlik) Group.

The basal grainstone is ca. 75 cm-thick and is fine- to medium-grained and well-lithified with a carbonate cement. The grainstone is heavily weathered and has no visible sedimentary structures. Directly overlying the lower grainstone is a mudstone interbedded with conglomerates lenses and palaeosols (Fig. 4.8). The entire mudstone and conglomerate deposit is ca. 14 m thick and forms a 300 m-wide terrace deposit. The lower grainstone tapers out southwards towards the main range.

The conglomerate lenses are wider at the base, gradually becoming thinner further up the section. The basal lenses are 2 m to 3 m (wide) by 4 m to 5 m (thick) and are heavily down-cutting, further up section the channels become more elongate (10 cm by 8 m) and are parallel with no cross-cutting relationships.

Clasts within the conglomerate are sub-angular and poorly-sorted at the base of the section, gradually becoming better sorted upwards through the deposit. Compositionally, the clasts are predominantly metacarbonate but also occasional clasts of chalk, chert and metabasalt. Clasts range in size from 1 cm to 10 cm with poorly developed normally grading within the lenses. The lower channels contain occasional outsized clasts of up to ca. 40 cm in diameter.

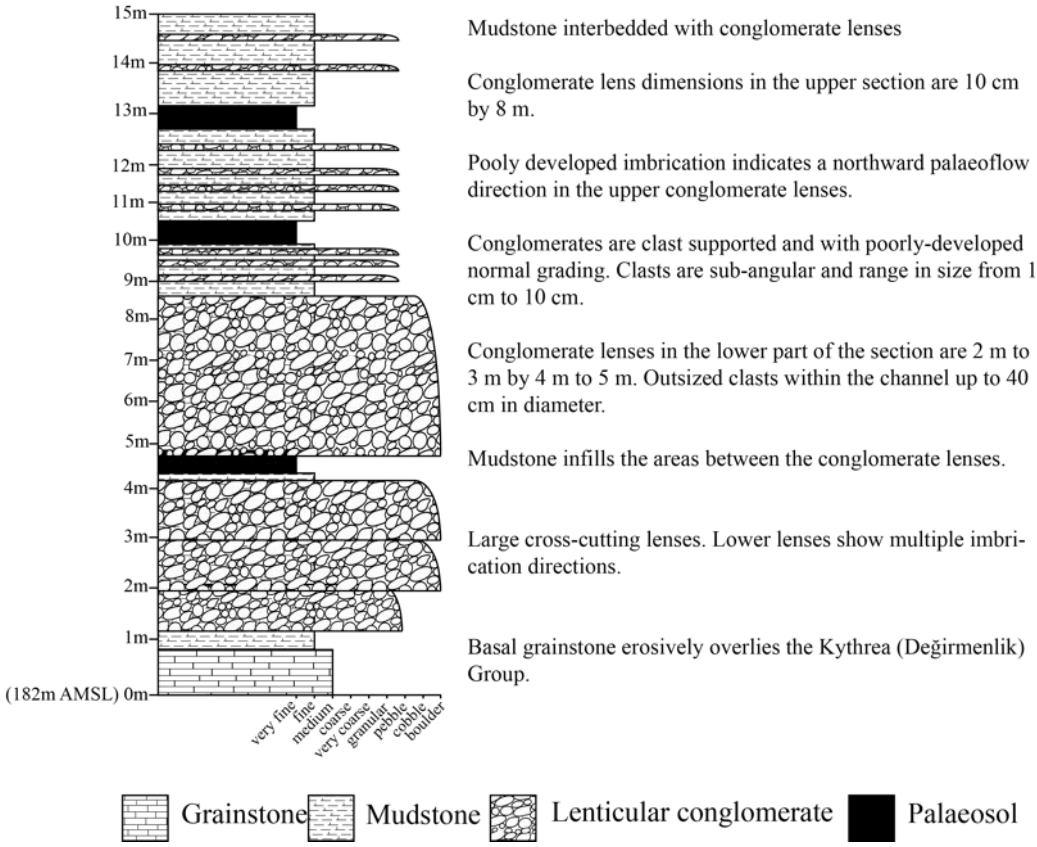

Figure 4.8: Sedimentary log through the K2 terrace deposits near the town of Beşparmak (Trapeza) (N35 18.571' E033 28.150').

4.3.4 Karaagaç (Charkeia) town

Karaagaç (Charkeia) is a small town ca. 3 km west of Esentepe (Agios Amvrosios) (Fig. 4.5). The K2 deposit is exposed along the cliff line which runs parallel to the main town, across a small gully.

The K2 terrace at Karaagaç (Charkeia) is made up of a basal grainstone overlain by interbedded mudstones, palaeosols and lenticular conglomerates. The basal grainstone erosively overlies steeply bedded mudstones and sandstones of the Kythrea (Değirmenlik) Group. The basal grainstone is ca. 2 m-thick and the overlying mudstone, sandstone, palaeosol and conglomerate deposit is ca. 17 m-thick.

The basal grainstone is a fine- to medium-grained and well cemented. The grainstone grains are poorly-sorted and sub-angular in nature. Reworked bivalve and gas-

tropod shells are found within the deposit. The grainstone deposit is heavily weathered and poorly preserved therefore no sedimentary features are observed.

Directly overlying the grainstone deposit is a mudstone deposit with conglomerate lenses and palaeosols. The conglomerate lenses are generally 20 cm by 2 m and contain clasts ranging in size from <1 cm to 15 cm, with an average clast size of ca. 5 cm. Clasts are sub-angular and normally-graded within the lenses. Compositionally, the lenses are made up of metacarbonate, chert and chalks. Directly overlying the unit is an interbedded poorly lithified mudstone and palaeosol deposit. The mudstone has no clear sedimentary structures. The palaeosols are a dark-brown colour. The sand and palaeosol deposit is overlain by a major conglomerate unit made up of several cross-cutting conglomerate lenses with clasts ranging in size from 1 cm to 3 cm. The upper part of the unit is another mudstone deposit interbedded with conglomerate lenses. Well-developed flower-shaped caliche structures are found in patches within the middle sand deposit.

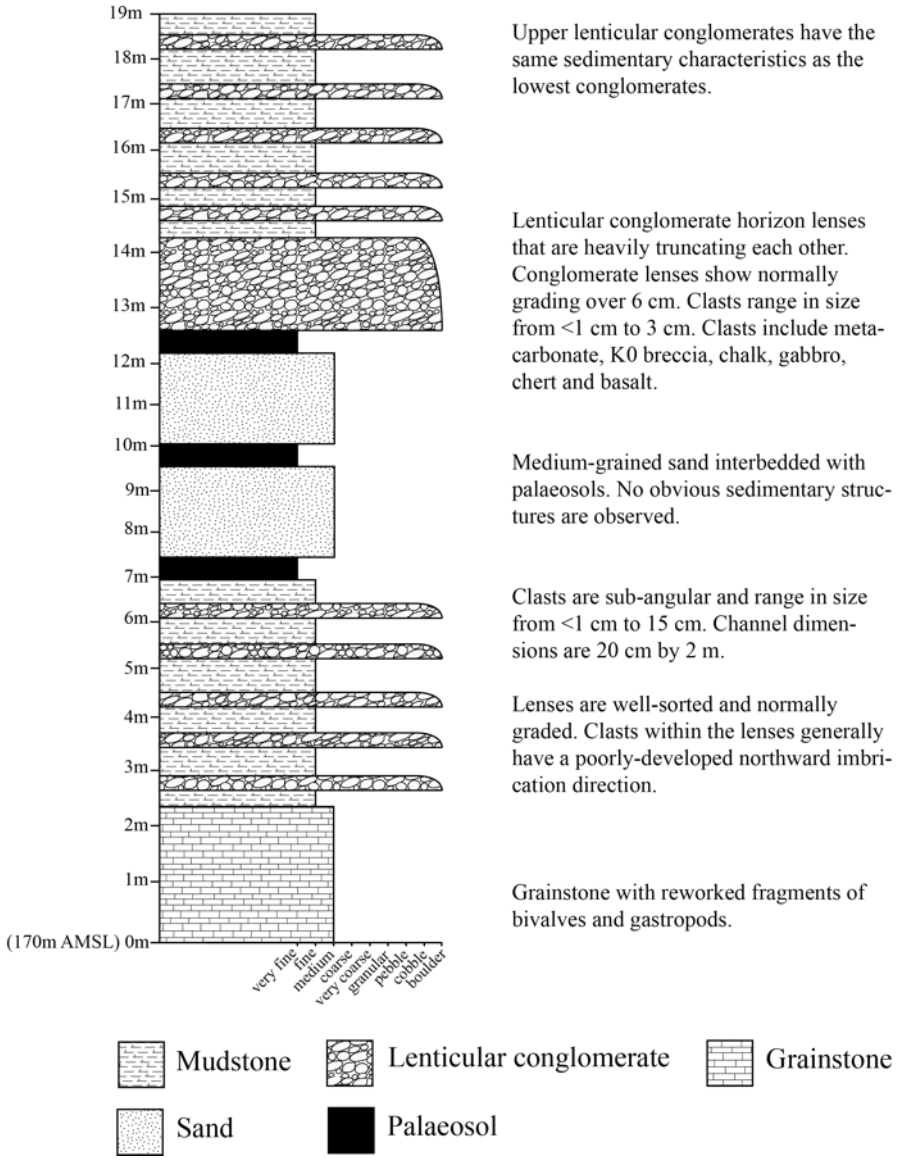

Figure 4.9: Sedimentary log through the K2 terrace deposits near the town of Karaagaç (Charkeia) (N35 19.701' E033 33.459').

4.3.5 Esentepe (Agios Amvrosios) town

Esentepe (Agios Amvrosios) is a large town in the central part of the Kyrenia Range (Fig. 4.5). The K2 terrace deposit is exposed on the western side of the town, and is composed of a mixture of grainstone, mudstones, lenticular conglomerates and palaeosols.

The base of the section is a 2 m-thick fine- to medium-grained well-cemented grainstone. Conformably overlying the grainstone is a dark-brown palaeosol, passing directly into a poorly lithified mudstone, interbedded with a series of conglomerate lenses. The lens dimensions are 10 cm by 8 m. The conglomerate lenses are relatively uniform throughout the deposit. The clasts within the conglomerate lense are sub-angular and range in size from 1 cm to 10 cm, with a modal clast size of ca. 5 cm. The clasts are predominanyly metacarbonate with minor amount of clasts comprising chalk, chert and metabasalt.

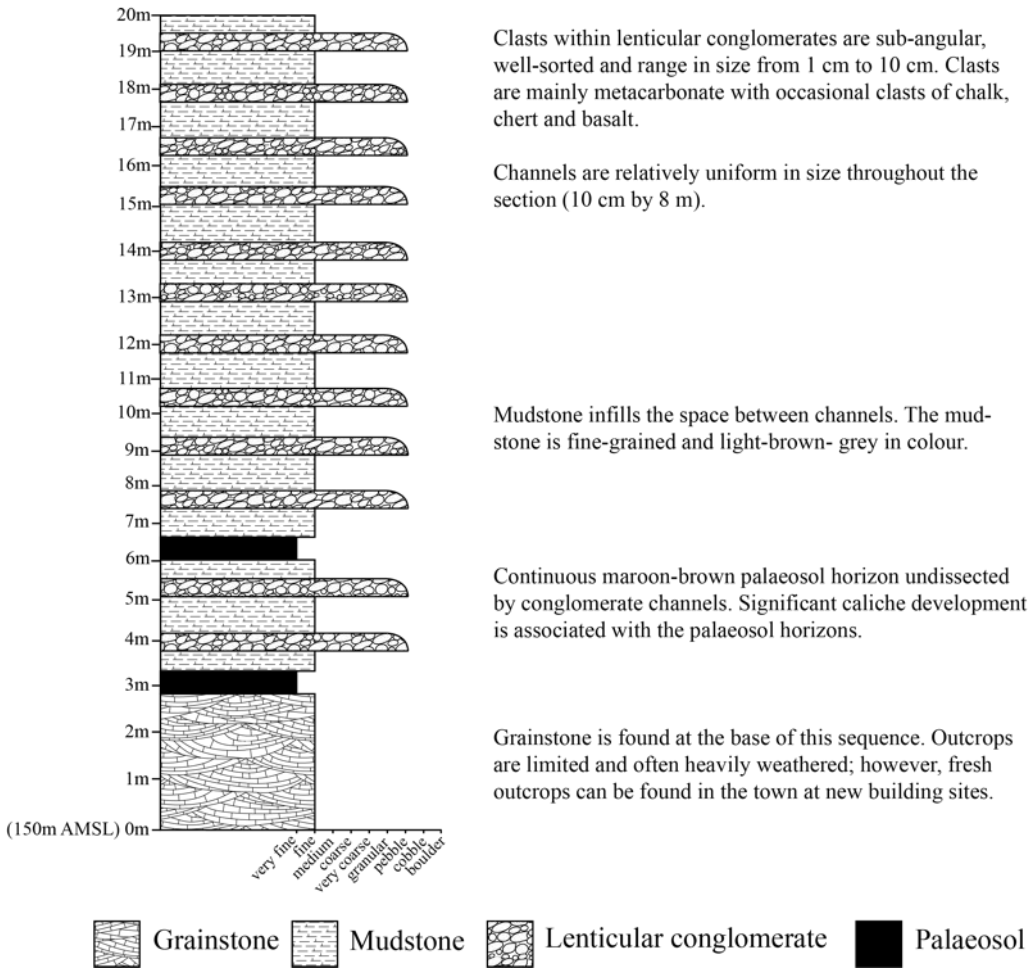

Figure 4.10: Sedimentary log through the K2 terrace deposits near the town of Esentepe (Agios Amvrosios) (N35 20.237' E033 34.953').

4.3.6 Kaplıca (Davlos) village

Kaplıca (Davlos) is a small village on the central-eastern part of the Kyrenia Range (Fig. 4.5). The main town is found just inland from the coast and on the southern side of the main road. The K2 deposit is exposed ca. 500 m south of town along a road that leads to Kantara Castle.

The K2 terrace at Kaplıca (Davlos) comprises a basal grainstone deposit overlain by a mudstone interbedded with conglomerate lenses (Fig. 4.11). The basal grainstone erosively overlies mudstones and sandstones of the Kythrea (Değirmenlik) Group. The interbedded mudstone and conglomerate deposit can be traced back ca. 600 m towards

the main range. The basal grainstone deposit tapers out southwards, within ca. 10 m, towards the main range.

The base of the unit is composed of a medium- to coarse-grained well-lithified grainstone which ranges in thickness from 1 m to 2 m, dependent upon the height of the basal unconformity. Directly overlying this is a cross-bedded, moderately-lithified grainstone with occasional thin conglomerate lenses and a palaeosol. The dimensions of the conglomerate lenses within the grainstone are ca. 5 cm by 1 m. The conglomerate clasts are well-sorted, sub-angular and range in size from 1 cm to 5 cm.

The upper part of the deposit is composed of a mudstone with interbedded conglomerate lenses and occasional palaeosols. The conglomerate lenses and clast size become larger further up-section and further inland. Conglomerate lenses in the lower part of the sequence are 5 cm by 1 m; but increase to 30 cm by 5 m in the upper part of the sequence. The clast size also increases from <5 cm in the lower grainstone to nearly 15 cm in the uppermost part of the section. Progressing up-section, the relationship between the conglomerate lenses changes from no clear interaction between the lenses to downcutting of older lenses by younger lenses.

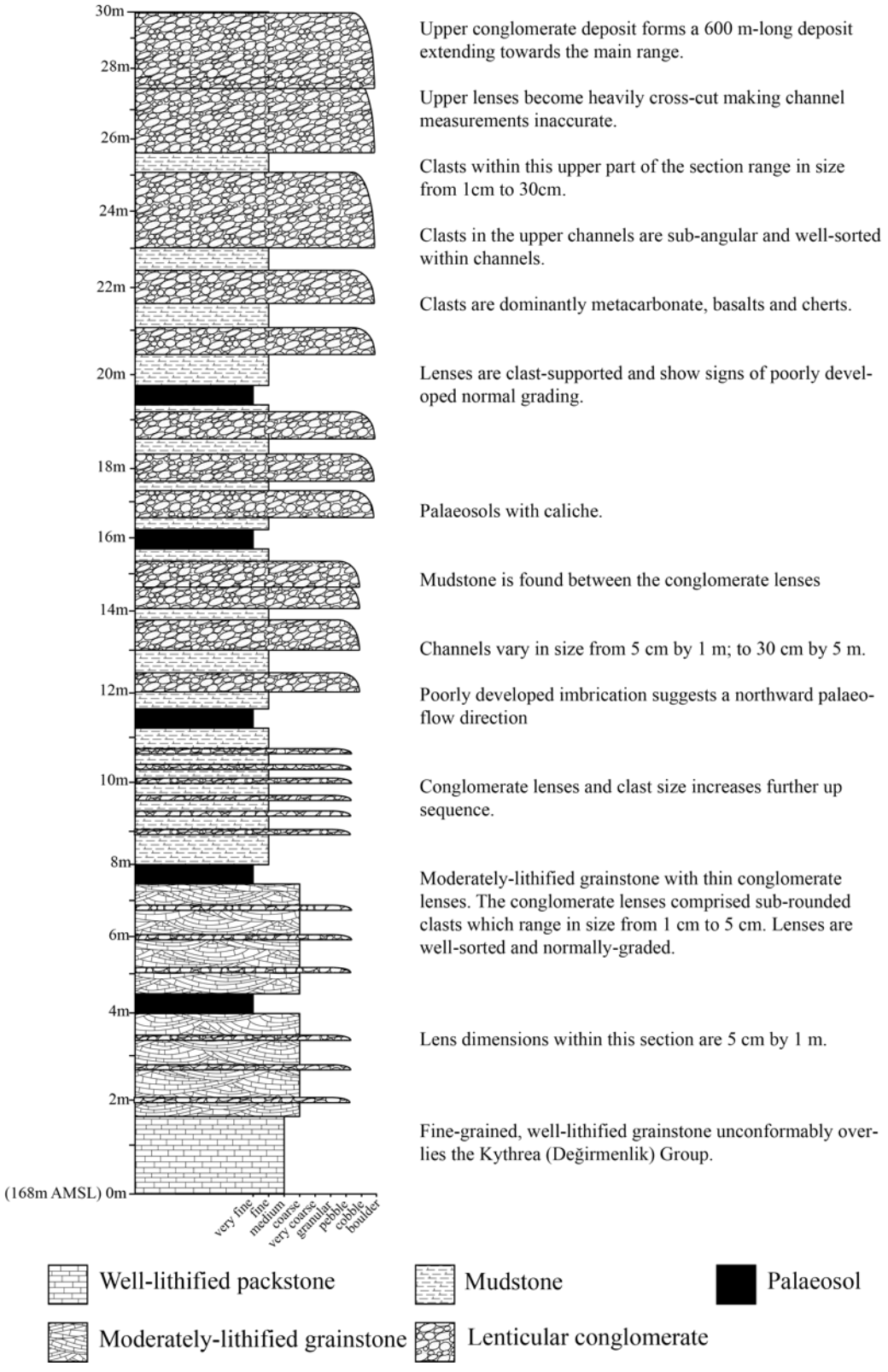

Figure 4.11: Sedimentary log through the K2 terrace deposits near the town of Kaplıca (Davlos) (N35 24.966' E033 54.273').

4.4 Field sedimentology of the K3 terrace deposits

The K3 terrace on the northern side of the Kyrenia Range forms a discontinuous surface gently dipping northwards away from the range. The boundary between the K2 and K3 terrace is marked by a significant drop in height, this allows for a clear identification of the boundary between the K2 and K3 terrace systems.

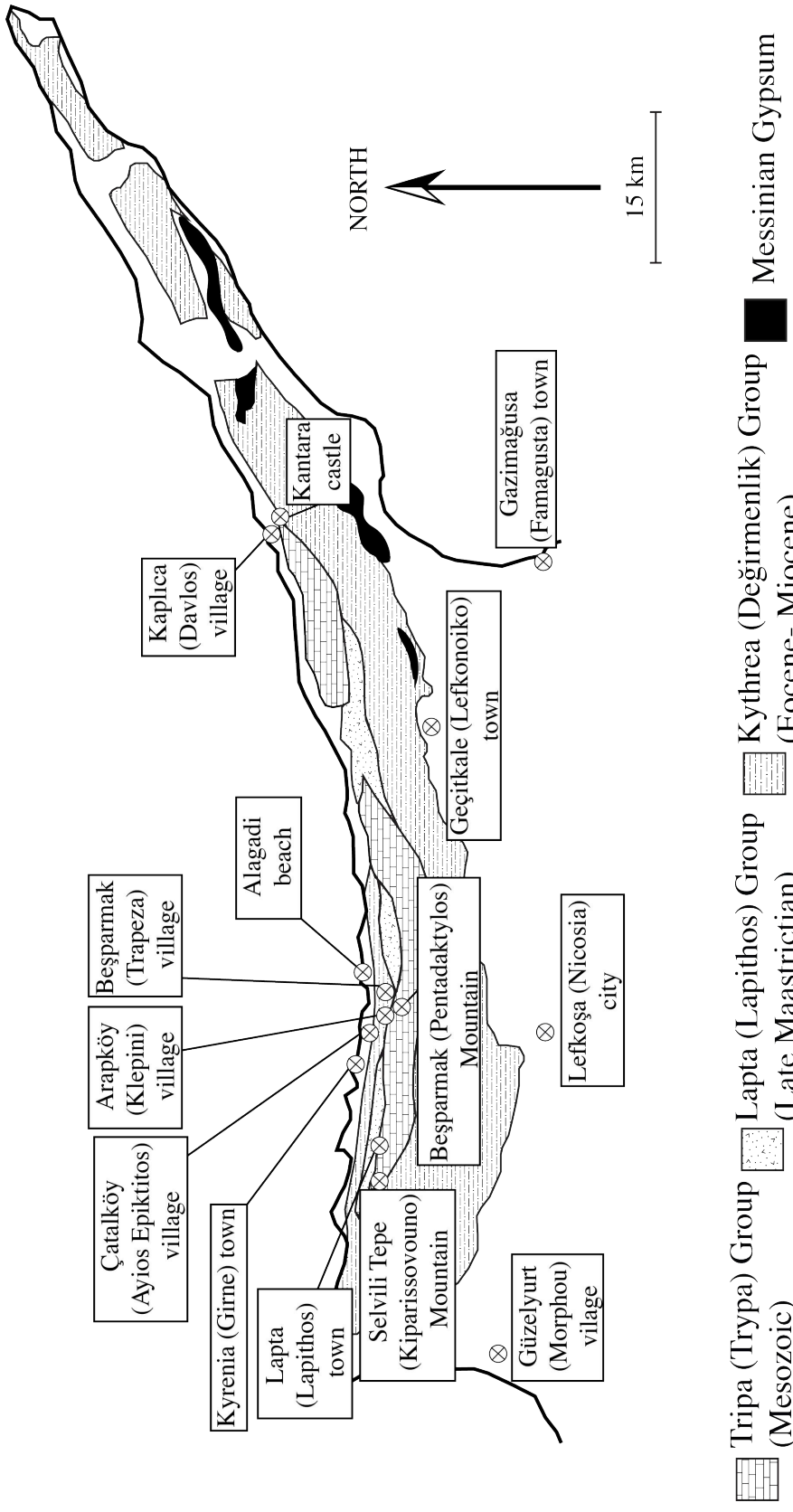

Figure 4.12: Simplified geological map of northern Cyprus showing the K3 terrace localities.

4.4.1 Çatalcöy (Ayios Epiktitos) town

Çatalcöy (Ayios Epiktitos) town is in the central Kyrenia Range, ca. 9 km west of Girne (Kyrenia) town (Fig. 4.12). The old town centre is over 1 km from the coast, while the modern town continues from there all the way to the coast. The stratigraphy of the K3 deposit in the town centre was originally described by Baroz (1979). Two K3 deposits will be described within the this area; firstly, the original section in the town centre as described by Baroz (1979) and secondly, a section exposed in ca. 1 km to the east of the town centre (Fig. 4.13).

The deposit at Çatalcöy (Ayios Epiktitos) village is made of a grainstone and conglomerate deposit (Fig. 4.13(a)). The basal grainstone becomes less lithified from the bottom to the top of the deposit. Directly overlying the grainstone is a conglomerate with well-rounded and well-sorted clasts. The clasts are dominantly made up of metacarbonate, probably sourced from the Tripa (Trypa) Group, with occasional clasts of chalk, basalt and chert from the Lapithos (Lapta) Group. Conformably overlying the conglomerate is a ca. 3 m-thick poorly-lithified grainstone with well-sorted and well-rounded grains.

The second K2 deposit outside the Çatalcöy (Ayios Epiktitos) old town centre, is a mudstone with interbedded conglomerate lenses and palaeosol horizons (Fig. 4.13(b)). Poorly-developed imbrication within the conglomerate lenses suggests a northward palaeocurrent direction. The clasts are sub-angular and range in size from 1 cm to 6 cm. The channels range from clast-supported to matrix-supported. The composition of the clasts includes, metacarbonate, chalk, chert and igneous clasts. The palaeosols are ca. 30 cm thick and a dark-red to light-brown in colour. This deposit is exposed by a younger fluvial system which has eroded a new valley.

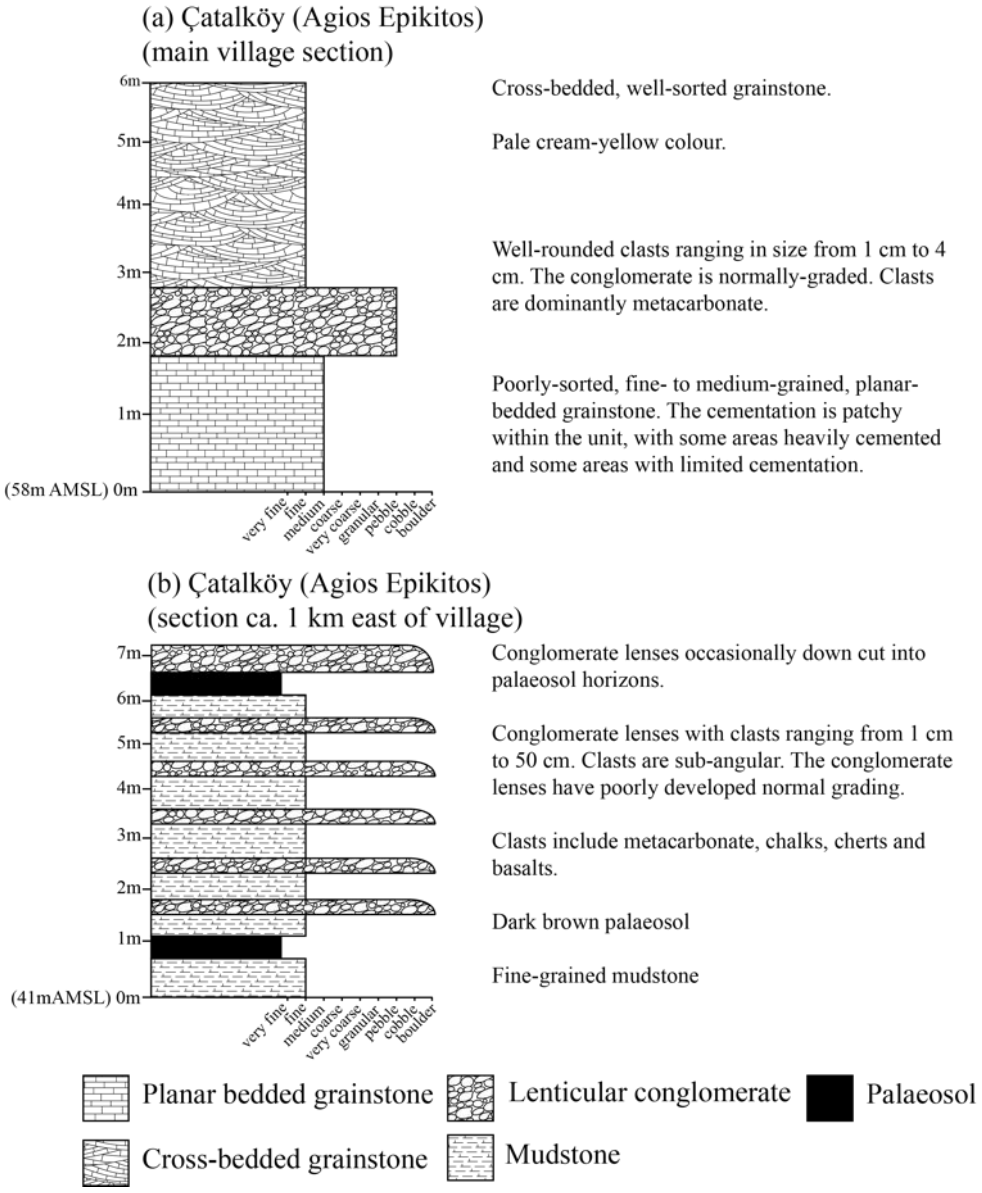

Figure 4.13: Sedimentary logs through the K3 terrace exposed at Çatalcöy (Ayios Epiktitos) town ((a) N35 19.417' E033 23.338' (b) N35 19.132' E033 23.596').

4.4.2 Arapköy (Klepini) village

The K3 terrace deposit exposed at Klepini (Arapkóy) village (Fig. 4.12) is found on a series of northward-dipping surfaces, on the northern side of the town. The logged deposit (Fig. 4.14) comes from the most easterly of three surfaces. The terrace surface dips northward and merges with the K4 terrace which continues towards the coast. The boundary between the K2 and K3 terraces is marked by a significant drop in height above sea-level from 159m AMSL to 127m AMSL. The stepped relationship between the K2 and K3 terrace, as seen at Arapköy (Klepini)(Fig. 4.14), is continuously visible from Selvili Tepe (Kiparissovouno) to Kaplıca (Davlos), within the central Kyrenia Range.

The K3 deposit is composed of a basal grainstone, overlain by a mudstone interbedded with conglomerate lenses and a palaeosol (Fig. 4.14). The basal grainstone is well lithified by a carbonate cement and contains well-sorted and well-rounded grains. The grainstone deposit is ca. 1 m thick on most southern end of the terrace and increases to nearly ca. 4 m thick northwards towards the coast. The interbedded mudstone, conglomerate and palaeosol are only found on the southern end of the terrace and do not continue laterally northwards towards the coast. The conglomerate forms a series of 30 cm by 2 m lenses within the mudstone. The conglomerate lenses contain sub-angular clasts which range is size from 1 cm to 50 cm. The conglomerate lenses show no sign of sedimentary sorting although the outcrop is poorly exposed.

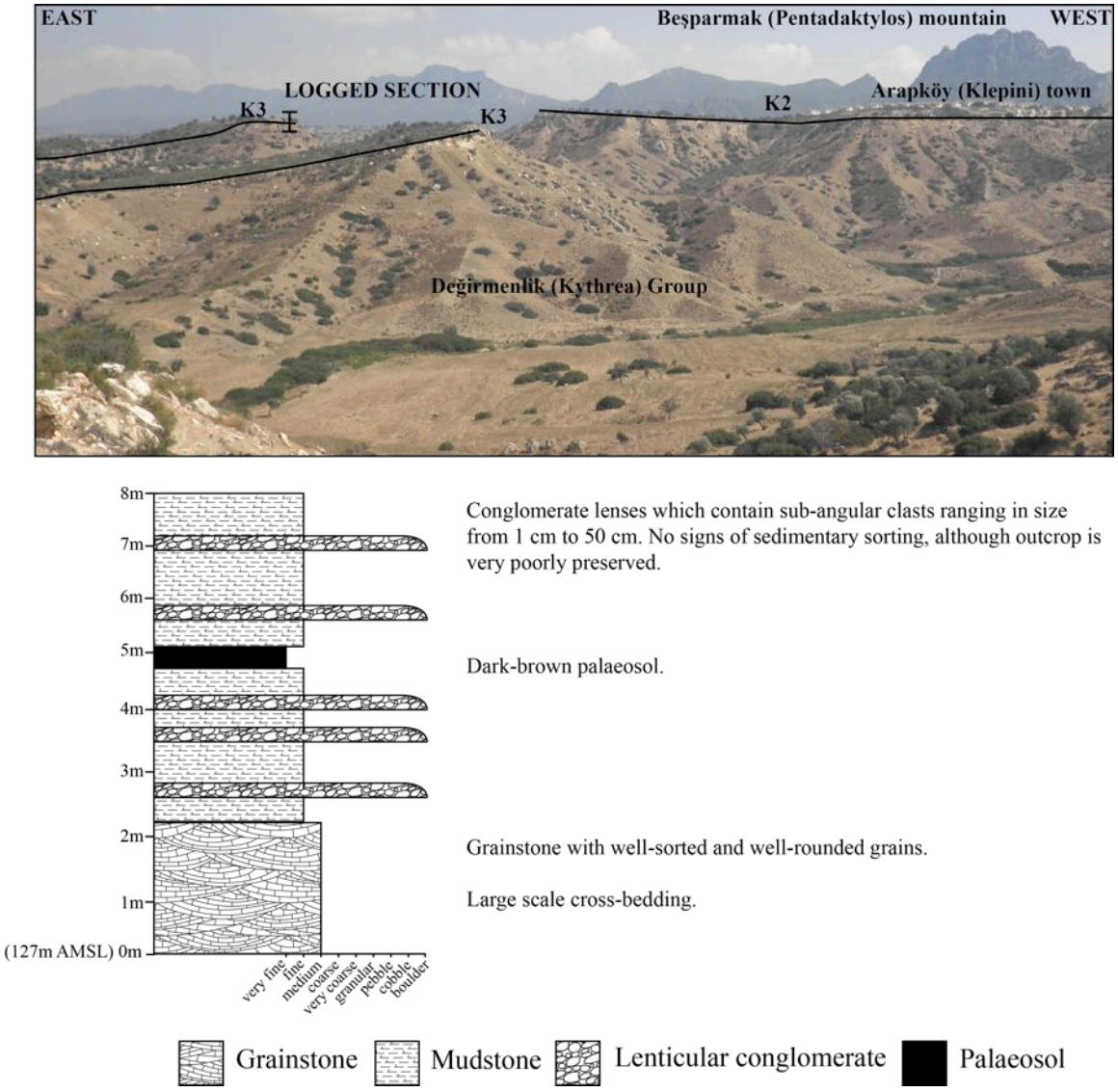

Figure 4.14: Sedimentary log and photograph of the K3 terrace exposed to the north of Arapköy (Klepini) town (N35 18.964' E033 26.495').

4.4.3 Beşparmak (Trapeza) village

The K3 terrace forms a northward-dipping surface extending from Beşparmak (Trapeza) village (Fig. 4.12) down towards the northern coast. Two K3 terrace deposits are described, firstly a more easterly deposit directly north of the village, and secondly, a westerly deposit on an isolated hill to the northwest of the village (Fig. 4.15).

The more westerly deposit forms a terrace surface which continues for over ca. 1 km towards the northern coast. Figure 4.15 shows a log through the deposit on the most southerly and topographically highest end of the terrace surface. The deposit is composed of a mixture of interbedded mudstones, lenticular conglomerates and palaeosols. This deposit unconformably overlies mudstones of the Kythrea (Değirmenlik) Group. The width of the terrace surface increases from ca. 40 m at the southern end to nearly ca. 1 km on the northern end, and eventually merging into the K4 terrace.

The more easterly K3 deposit outcrops at the base of the K2 deposit at the northern end of the Beşparmak (Trapeza) village. No sedimentary contact is preserved between the K2 and the K3 terrace deposits. There is a clear step down in topographic height from the base of the K2 terrace deposit (ca. 182 m AMSL) to the base of the younger K3 terrace deposit (ca. 120 m AMSL). The K3 terrace deposit in this area is a 6 m-thick deposit of grainstone. The grainstone grains are well-sorted, fine- to medium-grained and well-rounded. The grainstone deposit contains ca. 1.5 m-thick cross-bedded units with straight foresets (Fig. 4.15). The cross-bedded units are separated by ca. 50 cm-thick beds of laminated grainstone (Fig. 4.15). The terrace surface and deposit continue for over ca. 1 km, with a distal deposit that outcrops near Alagadi beach (Sec. 4.5.6).

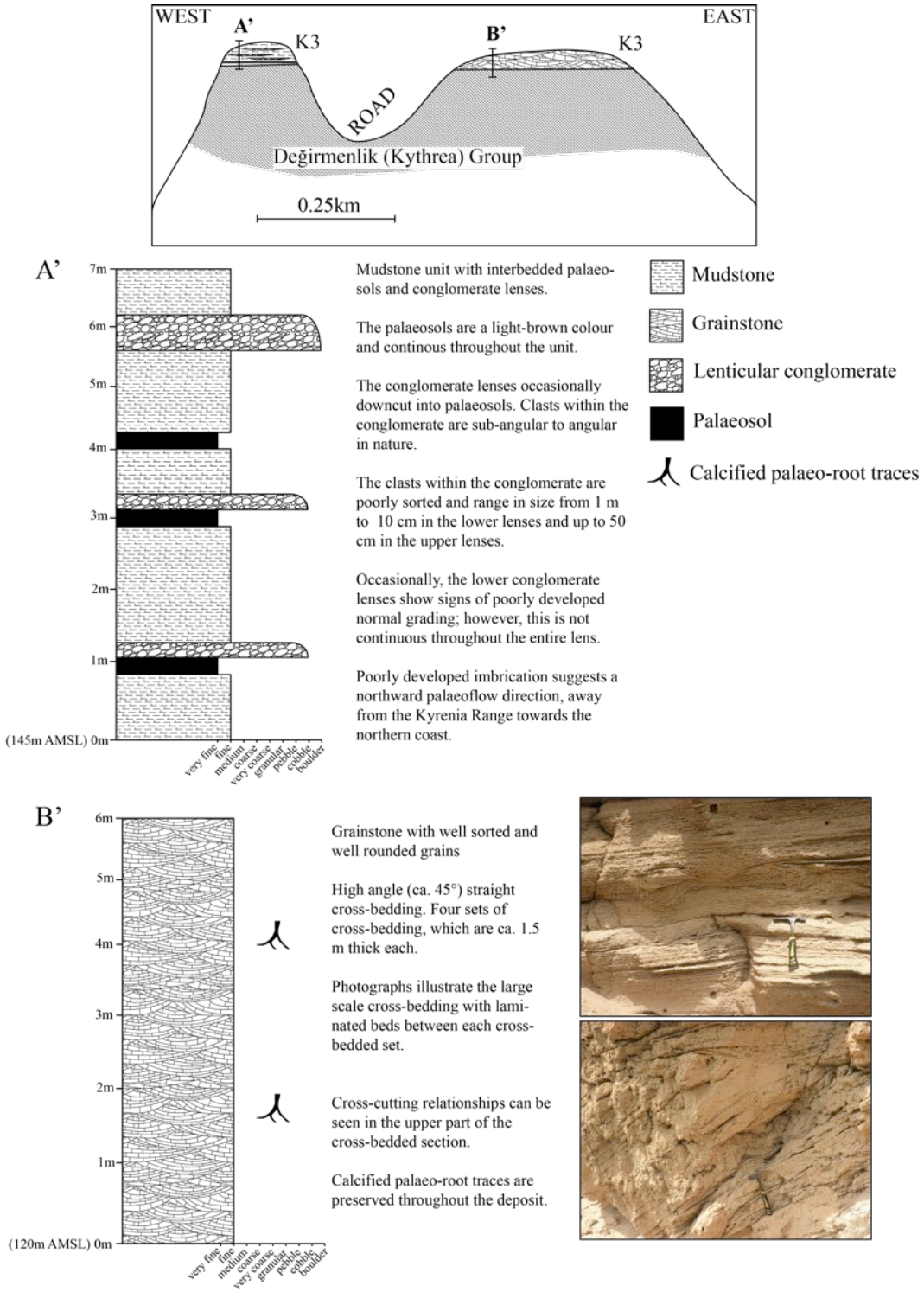

Figure 4.15: Sedimentary logs K3 terrace deposits north of Beşparmak (Trapeza) village ((A') N35 18.900' E033 27.898' (B') N35 18.969' E033 28.317').

4.4.4 Alagadi Beach

This K3 deposit is found ca. 1 km directly south of Alagadi beach (Fig. 4.12). The deposit forms the northern-most outcrop of the K3 terrace surface which is also exposed directly north of Beşparmak (Trapeza) town (previous section). The K3 terrace preserved here is composed of a ca. 3 m-thick grainstone. The grainstone is fine- to medium-grained and the grains are well-sorted and well-rounded. The sedimentary features include ca. 30 cm-thick beds of low-angle (<30°) cross-bedding and fine-laminations (Fig. 4.16). Palaeo-roots are preserved throughout the grainstone deposit. The basal unconformity of this unit is at ca. 80 m AMSL.

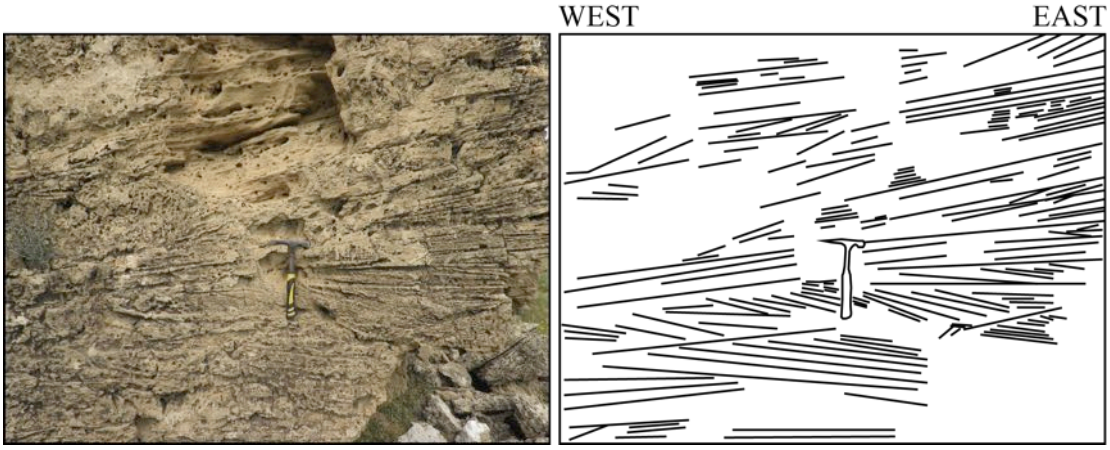

Figure 4.16: Photograph and sketch of the K3 terrace deposit that is exposed directly south of Alagadi Beach (N35 19.384' E033 28.873').

4.4.5 Kaplıca (Davlos) town

Kaplıca (Davlos) town is located near the eastern end of Kyrenia Range, ca. 60 km further east of Girne (Kyrenia) town and directly north of Kantara castle (Fig. 4.12). The K3 deposit is exposed to the southeast of the town. The section exposes the contact between the K3 deposit and the underlying interbedded mudstones and sandstones of the Kythrea (Değirmenlik) Group. The unconformity between the K3 terrace and the Kythrea (Değirmenlik) Group is only exposed on a vertical surface. The original sub-horizontal contact, as seen elsewhere, is not exposed at this locality.

The K3 deposit associated with Kaplıca (Davlos) town comprises a combination of interbedded conglomerates, mudstones and cross-bedded grainstones (Fig. 4.17). The base of the deposit is composed of a conglomerate with poorly-sorted and sub-angular clasts with a medium-grained sandstone matrix (Fig. 4.17 (1)). The conglomerate clasts range in size from ca. 1 cm to 30 cm. Furthermore, the basal conglomerate contains ca. 50 cm-sized blocks of mudstone of the underlying Kythrea (Değirmenlik) Group.

Overlying the basal conglomerate is a ca. 2 m-thick mudstone (Fig. 4.17 (2)). The mudstone contains poorly preserved planar bedding, which gently dips northwards. Within the upper part of the mudstone deposit is a thin wedge of conglomerate, which has similar sedimentary characteristics to the lower basal conglomerate.

Directly overlying the mudstone and conglomerate is a medium-grained sandstone with occasional high-angle (>30°) cross-bedding structures interbedded with conglomerate lenses (Fig. 4.17 (3)). The dimensions of the conglomerate lenses are ca. 30 cm by 5 m. The clasts within the lenses range in size from 1 cm to 10 cm and are poorly sorted and show signs of poorly-developed normal grading.

The uppermost deposit is a grainstone, which is deposited conformably over the top of the entire section (Fig. 4.17 (4)). The grainstone has a fine- to medium-grain size and contains well-rounded and well-sorted grains. Furthermore, the grainstone contains high angle (>30°) cross-bedding structures, which are 1 m to 2 m thick.

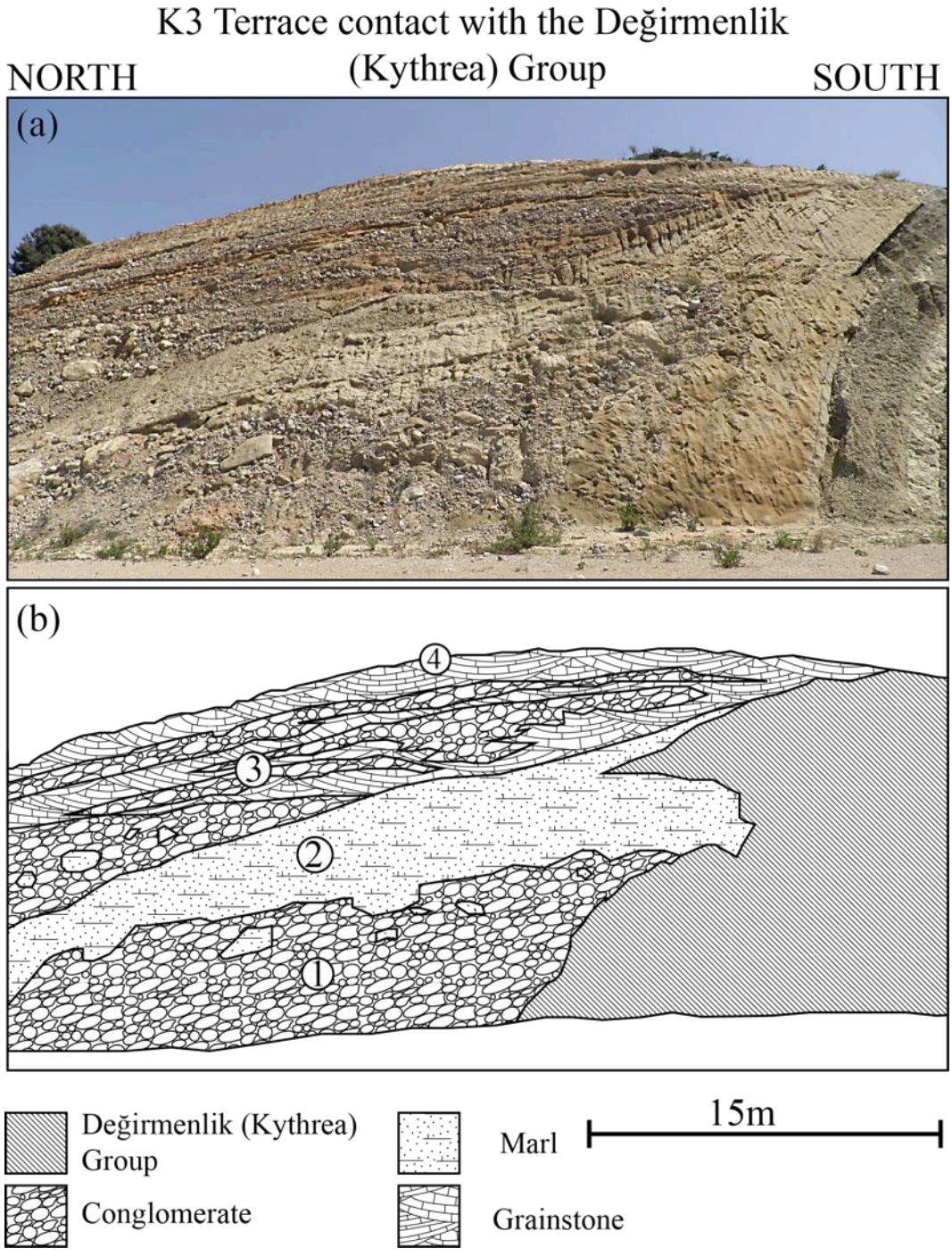

Figure 4.17: Photograph and sketch of the K3 terrace deposit that is exposed southeast of Kaplıca (Davlos), further explanations of diagram are given in text (N35 25.306' E033 54.465').

4.5 Field sedimentology of the K4 terrace deposits

The K4 terrace is the best preserved terrace on the northern side of the Kyrenia Range and forms a major surface extending along the entire length of the range. Unlike the older terraces, the K4 terrace forms a nearly continuous terrace surface along the northern coast of Cyprus. The excellent preservation of the K4 terrace deposit provides an excellent opportunity to study a complex terrace depositional system.

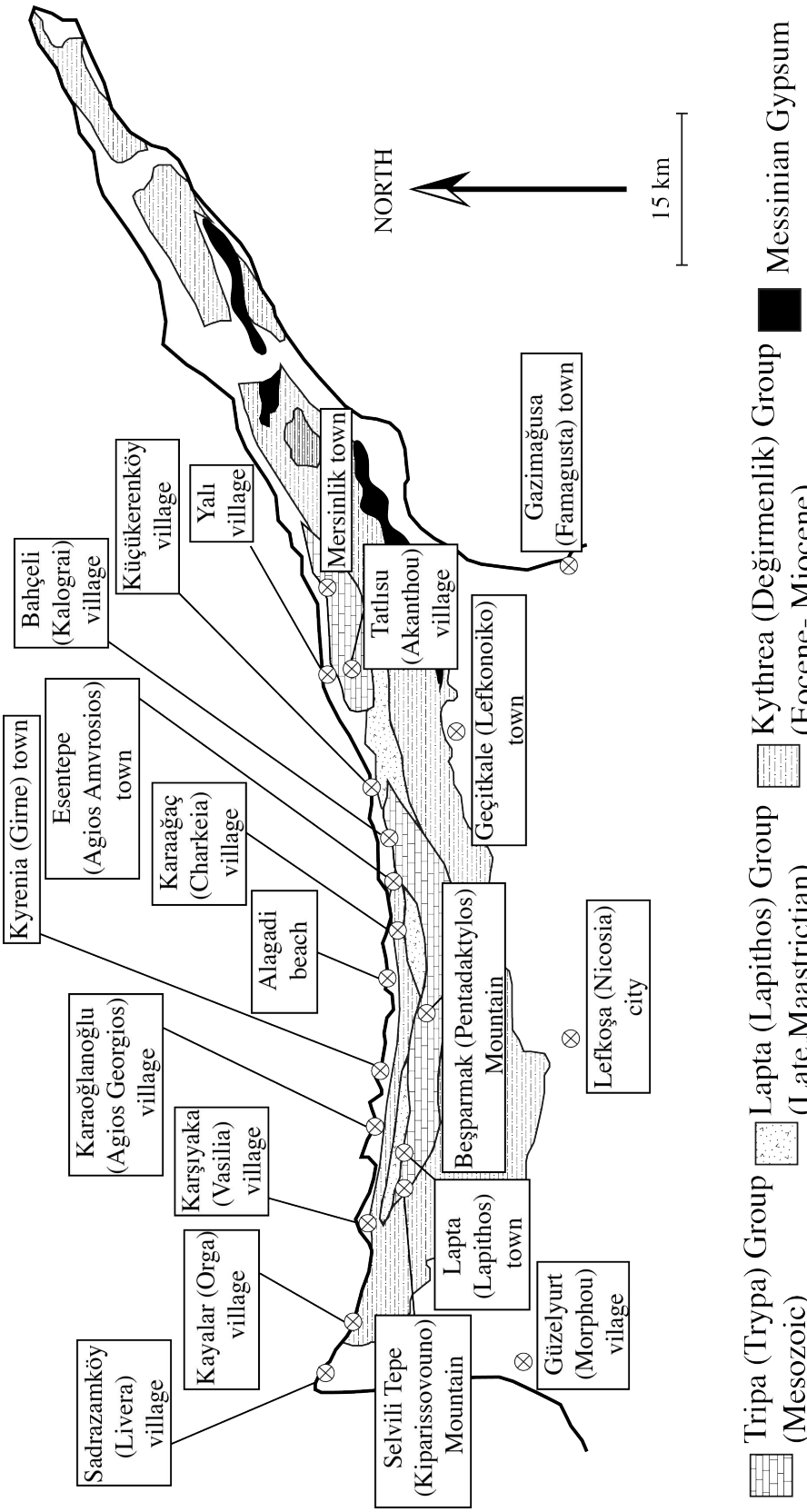

Figure 4.18: Simplified geological map of northern Cyprus showing the K4 terrace localities.

4.5.1 Sadrazamköy (Livera) village

The small village of Sadrazamköy (Livera) is found near the north-western tip of the island (Fig. 4.18). The western peninsula of northern Cyprus has a maximum height above modern sea-level of ca. 170 m. The underlying geology of the area is dominanted by the Lapithos (Lapta) and Kythrea (Değirmenlik) Groups with occasional blocks of Tripa (Trypa) Group. The K4 terraces forms a continuous surface from the coast inland for ca. 1 km. The best exposure of the terrace deposits is found at the coast.

The logged section is located in a small embayment ca. 4 km east of Sadrazamköy (Livera) village (Fig. 4.19). The deposit is composed of a series of interbedded grainstone beds with varying grain size and grain composition. The base of the unit is a ca. 30 cm-thick conglomerate, which erosively overlies steeply-bedded mudstones of the Kythrea (Değirmenlik) Group. The conglomerate contains clasts that are sub-rounded and poorly-sorted, and range in size from 1 cm to 50 cm. Overlying the conglomerate is ca. 30 cm-thick medium-grained grainstone with low angle ($<30°$) trough cross-bedding. Erosively overlying the grainstone deposit is a ca. 1 m-thick conglomerate with clasts ranging in size from 1 cm to 10 cm and well-developed normal grading within ca. 30 cm-thick beds. The clasts within both conglomerate deposits are composed of metacarbonate, basalt, chalk, chert, reworked grainstone, serpentinite and mollusc shells. The conglomerate deposit is overlain by a ca. 1 m-thick fine-grained grainstone with poorly preserved horizontal burrowing. The grainstone deposit is overlain by a ca. 50 cm-thick bedded grainstone deposit. The beds within the grainstone are ca. 10 cm-thick and contain well-preserved normal grading. The grainstone is dominantly composed of gastropods and bivalves.

The upper ca. 2 m of the deposit is a medium-grained, well-sorted grainstone (Fig. 4.19). The grainstone contains ca. 1 m-thick straight crossbeded units, with foresets dipping at $>30°$. Calcified palaeo-root traces are preserved throughout the upper grainstone deposit.

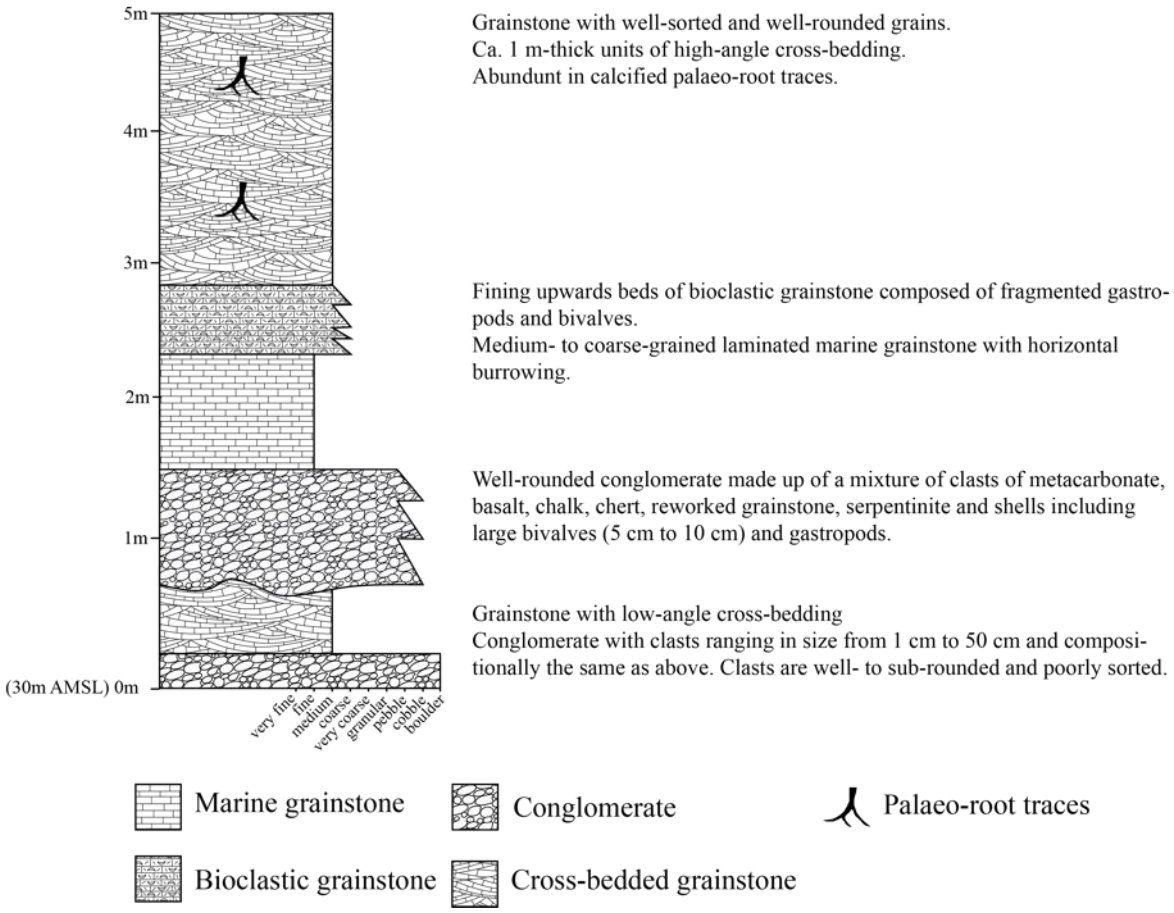

Figure 4.19: Sedimentary log through the K4 terrace deposit at Sadrazamköy (Livera) (N35 22.132' E032 59.820').

4.5.2 Kayalar (Orga) village

Kayalar (Orga) is small village east along the coast from Sadrazamköy (Livera)(Fig. 4.18). The K4 terrace deposit is preserved on the eastern end of the village along a road section. Figure 4.20 is a sedimentary log of the K4 terrace deposit which is composed of interbedded sandstone, grainstone, mudstone, conglomerates and palaeosols. The entire sequence is ca. 9 m-thick at the coast. The upper ca. 5 m of the deposit extends inland for 1 km, and the lower ca. 4 m of the deposit tapers out inland within ca. 100 m.

The lower ca. 5 m part of the deposit is composed of interbedded marl and bioclastic conglomerate (Fig. 4.20). The base of the deposit is a ca. 40 cm-thick laterally continuous conglomerate deposit. The conglomerate clasts are well-rounded and com-

posed of metacarbonate, chalk, chert, metabasalt and reworked shelly-debris including pectens and oysters (Fig. 4.21(a, f, g)). Large clasts within the conglomerate deposit are covered in borings and encrusting serpulid worm casts (Fig. 4.21(c)). Directly overlying the conglomerate is a ca. 2 m-thick medium- to fine-grained marl with poorly preserved ca. 10 cm-thick beds with normal grading (Fig. 4.21(b)). Outsized clasts ranging in size from 1 cm to 30 cm are found within the marl unit. Several 2 m to 3 m-sized blocks of grainstone are also found within the marl, the blocks are occasionally heavily bored (Fig. 4.21(e)). Overlying the sandstone deposit is a bioclastic conglomerate, which is rich in reworked shells including large (5 cm to 10 cm) bivalves, gastropods, serpulid worms and *in situ* solitary *Cladocora* coral (Fig. 4.21(d)). The conglomerate also contains well-rounded clastic material including metacarbonate, chalk, chert, serpentinite, diabase, gabbro, mudstone and sandstone. The conglomerate is overlain by a ca. 50 cm-thick marl unit, which the has the same sedimentary characteristics as the lower marl unit.

The upper ca. 5 m of the deposit is made up of interbedded mudstone, conglomerate lenses and palaeosols (Fig. 4.20). The conglomerate clasts range in size from 1 cm to 10 cm and vary from being sub-angular to sub-rounded. The composition of the clasts include metacarbonate, chalk, chert and metabasalt, but contain no carbonate shells (Fig. 4.21(h)). Palaeosols are preserved in the uppermost part of the deposit.

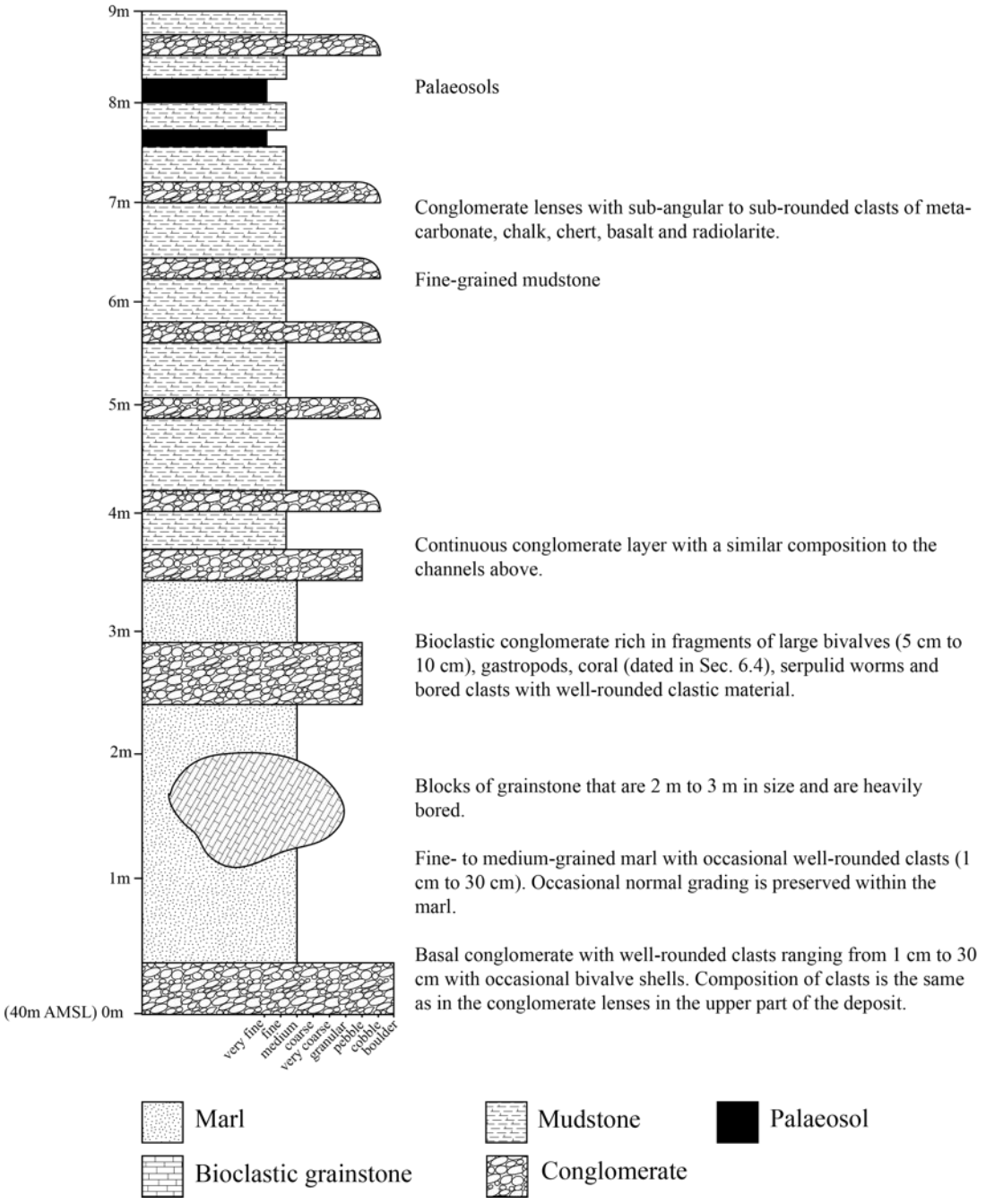

Figure 4.20: Sedimentary log through the K4 terrace deposit at Kayalar (Orga) (N35 21.458' E033 02.814').

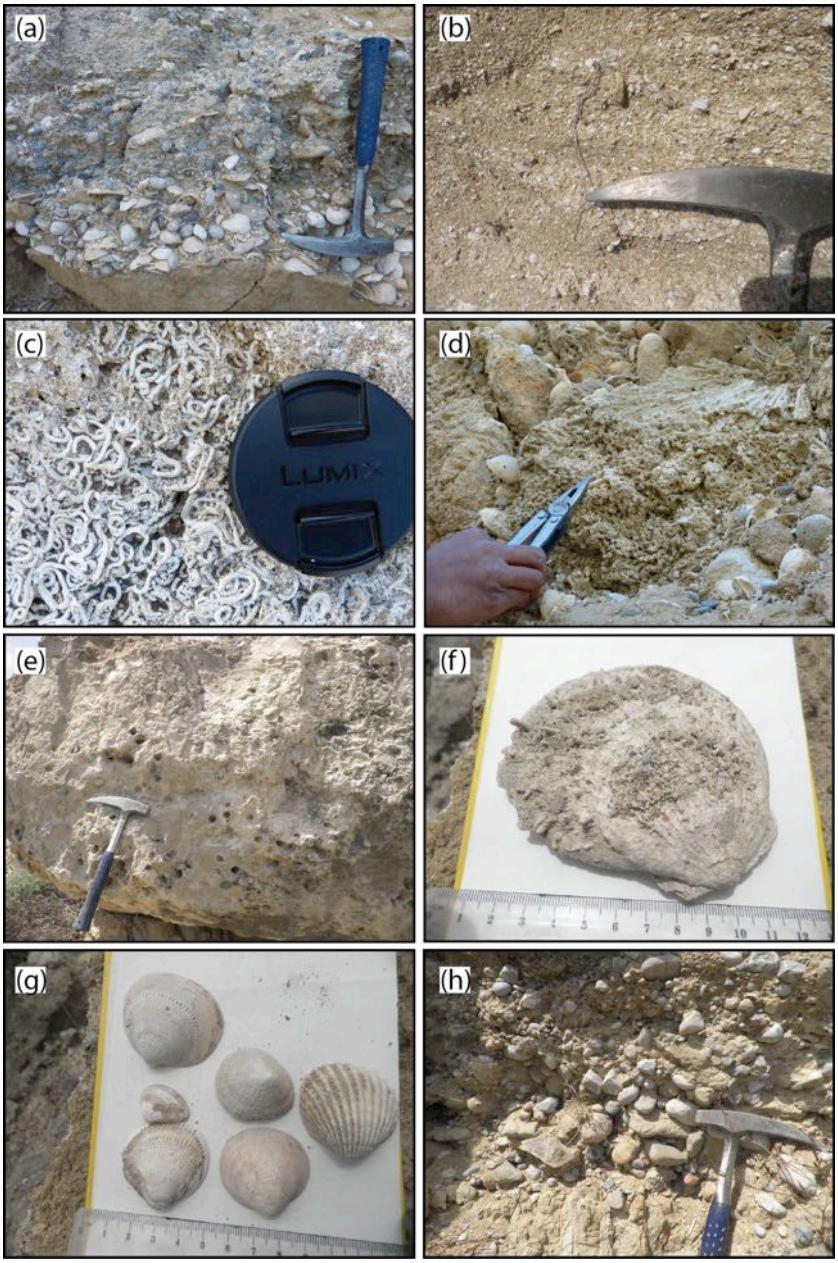

Figure 4.21: Photographs of the marine deposit with the K4 terrace deposit near Kayalar (Orga): (a) conglomerate rich in reworked shells with normally graded and well-rounded clasts; (b) medium to fine grained marl, showing signs of normal grading and reworking of shell fragments; (c) serpulid worm tubes encrusting a boulder, this is common within this sequence; (d) locally reworked solitary *Cladocora* coral; (e) borings within grainstone boulders; (f) *Spondylus*; (g) mollusc shells range in size from ca. 2 cm to ca. 5 cm in width, including *Glycymeris cardium*, on the right hand side; and (h) sub-rounded clasts that are composed of metacarbonate, metabasalt and chalk from the upper part of the deposit.

4.5.3 Karşıyaka (Vasilia) village

The K4 terrace near Karşıyaka (Vasilia) village is at the base of Selvili Tepe (Kiparissovouno) Mountain on the western end of the Kyrenia Range (Fig. 4.18). This area marks the start of the central Kyrenia Range and first major appearance of the Trypa (Tripa) Group. The only exposure of the K4 terrace deposit in this area is found near the coast directly north of the Karşıyaka (Vasilia) village.

The K4 terrace deposit is composed of a grainstone deposit with varying grain size and sedimentary structures (Fig. 4.22). The lower ca. 1.8 m grainstone deposit is poorly-sorted and medium- to coarse-grained. The lower-most grainstone contain ca. 10 cm-thick beds with well-developed normal grading. Directly overlying the lower grainstone is ca. 30 cm-thick coarse-grained grainstone deposit, rich in reworked carbonate material including bivalves, gastropods, algae and coral.

The uppermost part of the deposit is made up of a well-sorted, fine- to medium-grained grainstone with a palaeosol horizon (Fig. 4.22). Calcified palaeo-root traces are observed throughout the upper ca. 2 m of the grainstone deposit. This upper grainstone forms the upper terrace surface and continues both along the coast and inland. The lower grainstone tapers southward, away from the modern coast. The upper grainstone continues along the coast, varying in thickness from less than 2 m-thick to up to 6 m-thick thick, dipping northwards below modern sea-level.

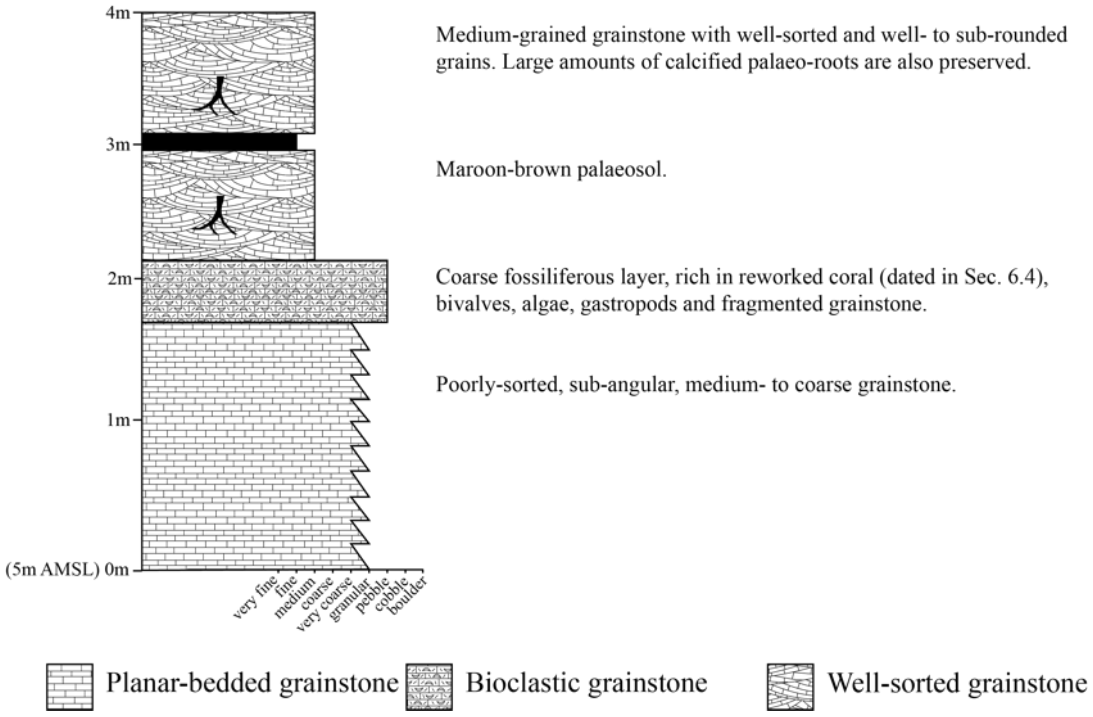

Figure 4.22: Sedimentary log through the K4 terrace deposit at the coast directly north of Karşıyaka (Vasilia) village (N35 21.627' E033 08.277').

4.5.4 St. Fanourios Church, Karaoğlanoğlu (Agios Georgios) village

St. Fanourios Church, Karaoğlanoğlu (Agios Georgios) is located directly north of Alsancak (Karavas) town, ca. 4 km further east of Lapta (Lapithos)(Fig. 4.18). The K4 terrace deposit is a ca. 8 m-thick grainstone deposit with varying grain size and sedimentary structures (Fig. 4.23).

The lower ca. 3.5 m grainstone is coarse-grained, sub-rounded and poor- to moderately-sorted. The preserved sedimentary structures include low-angle (<30°) cross-bedding, ripples and parallel laminations (Fig. 4.23(d, e). Each cross-bedded unit is ca. 20 cm thick and the parallel laminated and ripple units are < 10 cm-thick. In the uppermost part of this section parallel laminations become the dominant sedimentary structure (Fig. 4.23(c)).

The uppermost ca. 3m-thick grainstone is fine- to medium-grained and well-sorted. The unit contains large, high-angle (>30°) cross-bedding. Calcified palaeo-root traces

also become abundant within the upper ca. 2 m of the unit (Fig. 4.23(b)). Vertebrate fossils of pygmy hippopotamus bones are also preserved within the upper grainstone (Baroz, 1979)(Fig. 4.23(a)). The bones are well-cemented into the grainstone.

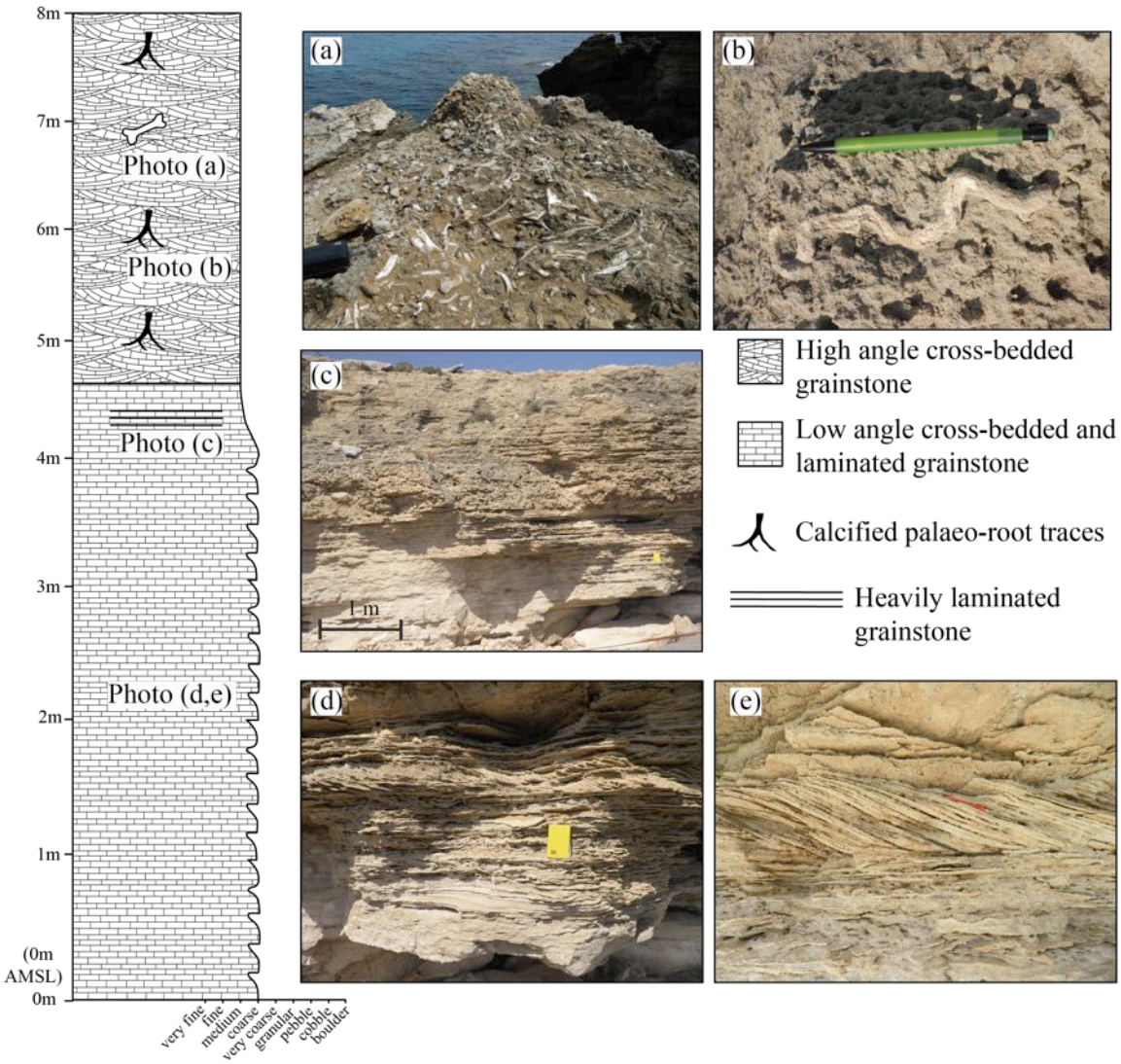

Figure 4.23: Sedimentary log and photographs through the K4 terrace deposit at the coast north of Alsancak (Karavas). Photographs include: (a) pygmy Hippopotamus bones; (b) calcified palaeo-rooting; (c) laminated grainstone; (d) cross-bedding, ripples and laminations within lower most grainstone unit; and (e) low-angle cross-bedding (N35 20.927' E033 15.764').

4.5.5 Girne (Kyrenia) town

There are numerous K4 deposits exposed within and around Girne (Kyrenia) town (Fig. 4.18). The deposit described here was originally described and illustrated by Dreghorn (1978) and is located ca. 1 km to the east of Girne (Kyrenia) castle. The deposit is a ca. 4 m-thick grainstone deposit at the coast, however further inland it reaches nearly ca. 10 m-thick.

The K4 terrace deposit associated with Girne (Kyrenia) town is made up of a basal coarse-grained grainstone and upper medium-grained grainstone (Fig. 4.24). The basal grainstone varies in thickness from 20 cm to nearly 1 m. The deposit is rich in well-preserved shell fragments which include bivalves, gastropods and coral. The deposit is overlain a ca. 3 m-thick well-sorted, medium-grained grainstone with high-angle (>30°) cross-bedding and calcified palaeo-root traces preserved throughout.

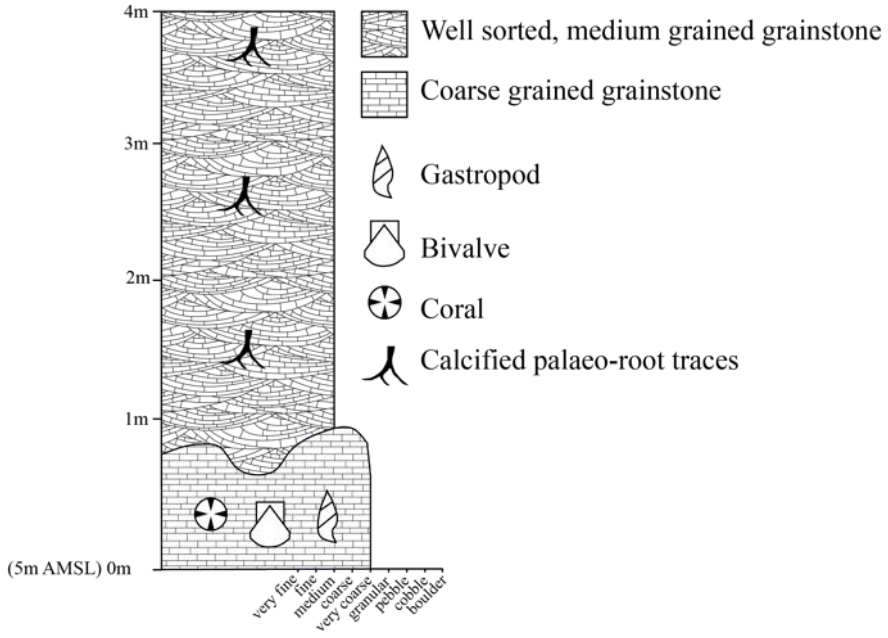

Figure 4.24: Sedimentary log through the K4 terrace deposit to the east of Girne (Kyrenia) town (N35 20.284' E033 20.092').

4.5.6 Alagadi town and beach

The exposure of the K4 terrace between Girne (Kyrenia) and Alagadi is limited owing to the large amount of modern development along the northern coast (Fig. 4.18). The K4 terrace forms a major surface in the Alagadi area (Fig. 4.25). The best exposures of the terrace deposit are found, firstly along the coast, and secondly, in road sections along the main coastal road. Three logged sections are presented from the K4 terrace exposures along the coast, together with a schematic sketch of the K4 terrace deposits exposed along the coast near Alagadi town (Fig. 4.26).

The K4 terrace exposures along the coast are made up of grainstone and conglomerate deposits. At the base of the K4 terrace deposit is a conglomerate unit, varying in thickness from 20 cm to 1 m (Fig. 4.26). The basal conglomerate erosively overlies sandstones of the Kythrea (Değirmenlik) Group. The basal conglomerate clasts are poorly-sorted and sub-angular and range in size from 30 cm to 1 m. The clasts are composed of mudstone, sandstone, metacarbonate, bivalves, gastropods, algae and fragmented coral. Overlying the basal conglomerate is a poorly-sorted, well-cemented grainstone unit. This lower grainstone contains rare fragments of large bioclasts including bivalves, calcareous algae and corals. The sedimentary features within the lower grainstone include small-scale, low-angle (<30°) cross-bedding and parallel laminations. The most westerly marine grainstone deposit is interbedded with conglomerate lenses with pebble-sized clasts, which are compositionally similar to the basal conglomerate. The upper 1 m to 3 m of the coastal K4 terrace deposit is composed of a well-sorted, well-rounded, well-cemented grainstone. This upper grainstone unit is rich in calcified palaeo-root traces and occasionally contains high-angle (>30°) cross-bedding with straight foresets.

The basal grainstone and conglomerate deposit tapers out southwards within ca. 100 m of the coast, whereas the upper, well-sorted, grainstone deposit thickens and continues inland. The upper grainstone unit is exposed along the main coastal road and varys in thickness from 2 m to nearly 10 m. This K4 terrace surface continues southward and merges with the K3 terrace.

Directly south of Alagadi town there is a road-cut section which exposes the base of the K4 terrace (Fig. 4.26). The deposit is at ca. 20 m AMSL, which is the same height above sea-level as the base of the K4 terrace at the coast. The deposit is made

up of a combination of interbedded conglomerates, grainstone and palaeosols (Fig. 4.26 (b)). The basal ca. 6 m of the deposit is made up of a planar bedded conglomerate with discontinuous horizons of well-sorted, medium-grained grainstone. The conglomerate clasts are well-rounded, well-sorted and range in size from 1 cm to 5 cm. Bedding within the conglomerate ranges in thickness from 10 cm to 15 cm and shows signs of poorly-developed normal grading. Clasts within the conglomerate are predominately composed of metacarbonate with minor amounts of chert, metabasalt and chalk. The conglomerate clasts show well-developed imbrication in both easterly and westerly directions (parallel to the coast).

The grainstone within the conglomerate is poorly-lithified and contains ca. 30 cm-thick units of poorly-preserved low-angle (<30°) cross-bedding. Further up the section the grainstone beds become thicker and the conglomerate beds thinner. The uppermost section is a ca. 1 m-thick grainstone deposit with high-angle (>30°) and ca. 1 m-thick cross-bedding. A laterally continuous palaeosol horizon is also seen within the uppermost part of the deposit. The basal unconformity between the K4 terrace and mudstones of the Kythrea (Değirmenlik) Group is only exposed on the eastern end of the section and varies in height from 20 to 28 m AMSL (Fig. 4.26).

Metre-sized boulders of well-rounded, medium-grained grainstone are found at the eastern end of the section within the well-rounded conglomerate (Fig. 4.26(b)). The large grainstone boulders are found below the upper grainstone deposit and are therefore from an older grainstone deposit.

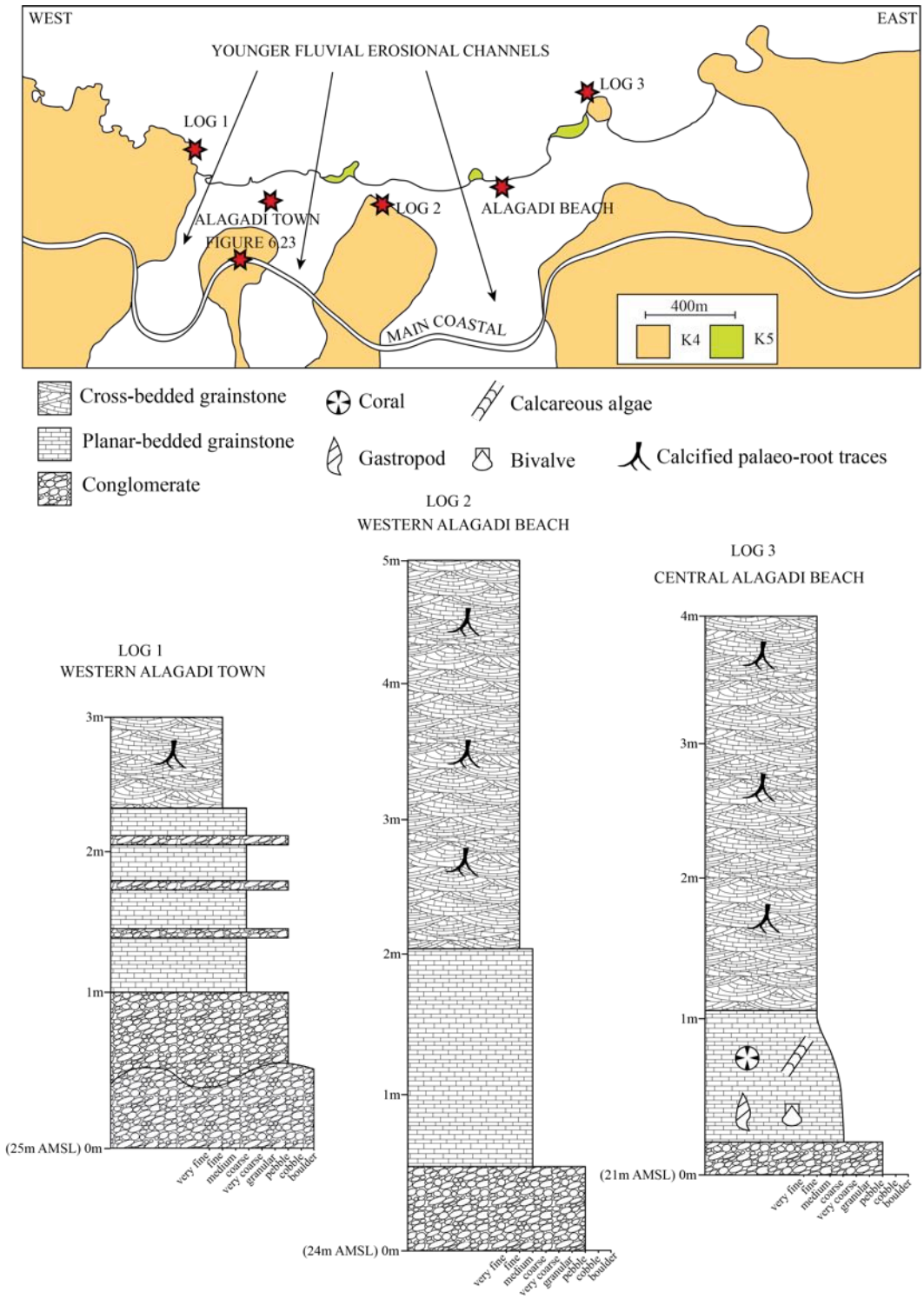

Figure 4.25: Simplified geological map and sedimentary logs of the K4 terrace deposits surrounding Alagadi beach ((Log 1) N35 20.034' E033 28.094'; (Log 2) N35 19.892' E033 28.676'; (Log 3) N35 20.138' E033 29.342').

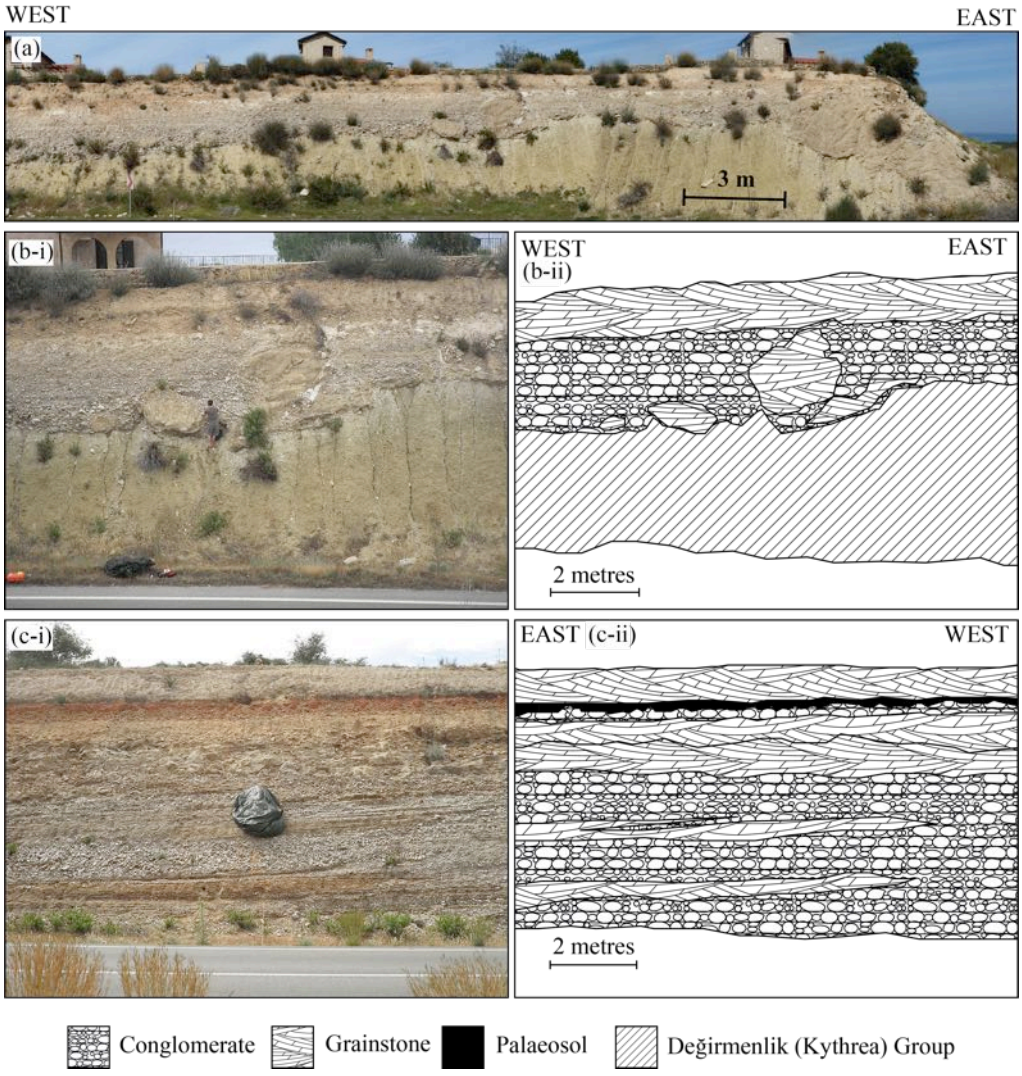

Figure 4.26: Photographs and stetches of the K4 terrace deposit exposed along the main coast road directly east of Alagadi village. Photograph (a) is a view of the eastern third of the outcrop; photograph (b-i) and sketch (b-ii) provide more detail on the eastern end of the outcrop; and finally photograph (c-i) and sketch (c-ii) are from the central part of the outcrop (N35 19.768' E033 28.241').

4.5.7 Karaagaç (Charkeia) village

The K4 terrace deposit associated with Karaagaç (Charkeia) village (Fig. 4.18) is exposed on the coast directly north of the village. The K4 terrace deposit is a continuation of the terrace deposit exposed at Alagadi beach, ca. 2 km to the west. The deposit is best exposed along the coast within this area and additional outcrops occur along the main coastal road. Figure 4.27 is a cross-section and sedimentary logs through the coastal section. The section preserved shows multiple interacting depositional environments within the K4 terrace.

The K4 terrace deposit preserved within this area is made up of interbedded medium-grained grainstone, coarse-grained grainstone and conglomerate. Figure 4.27 shows a cross-section through K4 terrace deposit exposed at the coast. A younger fluvial channel has eroded through the K4 terrace to expose the section. The lower ca. 2 m of the outcrop on the eastern side of the gully is composed of a poorly-sorted grainstone with coarse-grained bioclastic-grainstone layers. The coarse-grained bioclastic-grainstone is made up of bioclasts, including bivalves, gastropods and coral. In contrast, the lower ca. 4 m of the deposit on the western side of the gully is a coarse-grained grainstone with conglomerate lenses and rip-up clasts of the grainstone (Fig. 4.27). The conglomerate lenses contain sub- to well-rounded clasts, ranging in size from 1 cm to 10 cm. The clasts are made up of metacarbonate and chalk. In addition, on the western side of the gully there is a ca. 1 m-thick conglomerate lens inter-fingering with the lower grainstone, which tapers out in a westerly direction. The conglomerate lens contains ca. 20 cm-thick beds, within which the clasts are well sorted and normally graded.

Directly overlying the basal interbedded grainstone, grainstone and conglomerate on both sides of the gully is a ca. 2 m-thick, well-sorted, fine- to medium-grained grainstone, rich in calcified palaeo-root traces. The uppermost grainstone unit continues inland from the coast, for ca. 1 km; in contrast, the lower part of the sequence is discontinuous inland.

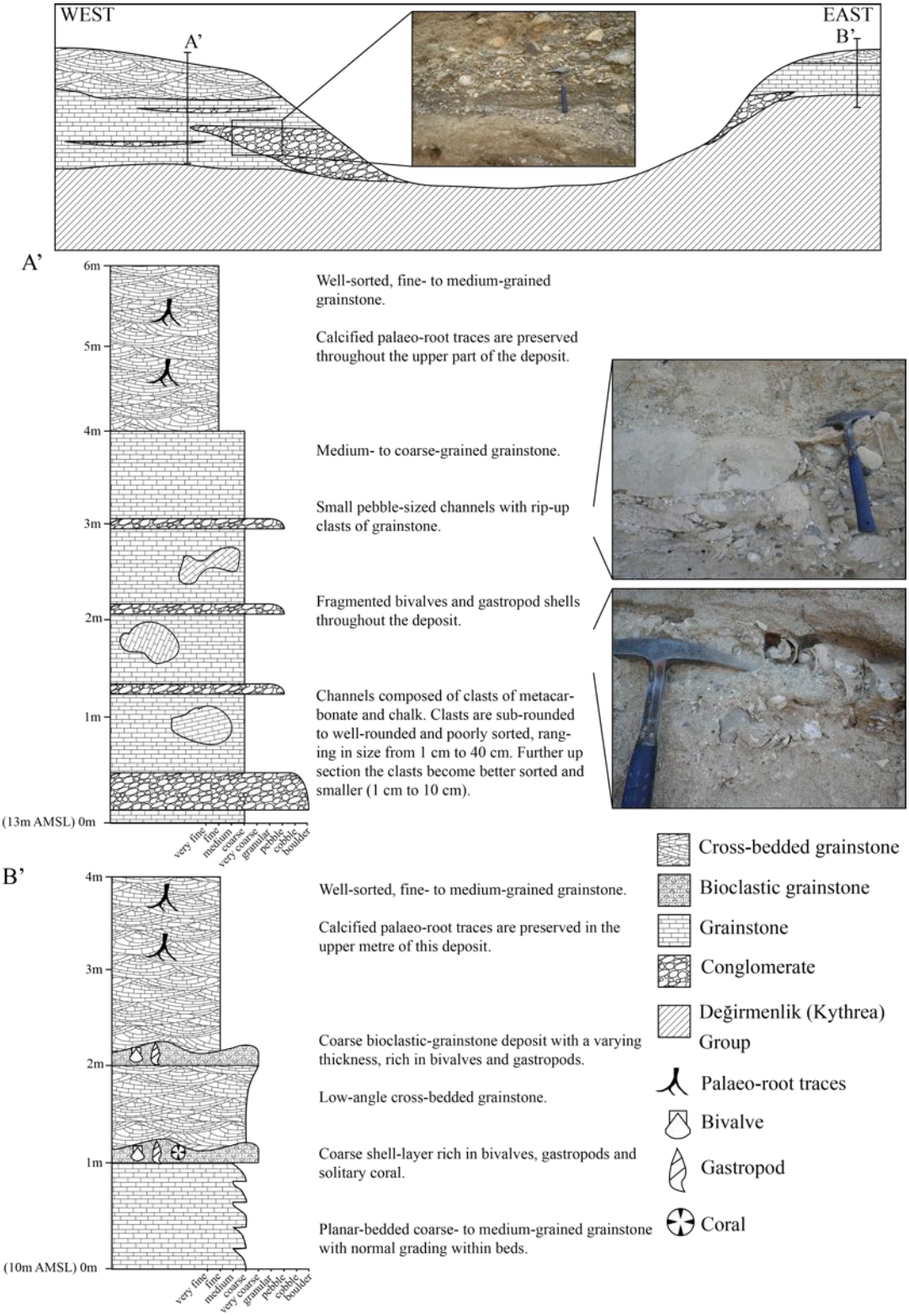

Figure 4.27: Sedimentary log through the K4 terrace deposit at the coast directly north of Karaagaç (Charkeia) (N35 20.671' E033 31.884').

4.5.8 Esentepe (Agios Amvrosios) town

Esentepe (Agios Amvrosios) is a large town further east along the coast from Karaagaç (Charkeia)(Fig. 4.18). The town stretches from the coast upwards towards the Kyrenia Range. Two K4 terrace deposits are described around Esentepe (Agios Amvrosios); firstly, a road-cut section exposed along the coastal road at the turning for Esentepe (Agios Amvrosios)(Fig. 4.28); and secondly, a coastal deposit just off the old coastal road, less than 1 km east of Esentepe (Agios Amvrosios)(Fig. 4.29).

The K4 deposit preserved along the main coastal road is composed of a cross-bedded gravel (Fig. 4.29(c)) with a boulder-conglomerate unit and a grainstone unit and overlain by a mudstone interbedded with conglomerate lenses. The cross-bedded gravel makes up the lower ca. 7 m of the deposit. The clasts within the gravel are well-sorted (0.5 cm to 3 cm) and sub-rounded to well-rounded. The gravel is clast supported and contains less than 10% matrix, which is a medium-grained, poorly-lithified sand. The gravel clasts are dominantly metacarbonate with occasional clasts of chalk. The cross-bedding in the gravel forms 20 cm to 50 cm-thick units, becoming thicker further up the deposit, with foresets that dip at $<20°$.

Within the lower part of the deposit is a ca. 1 m-thick laterally continuous conglomerate with boulders ranging in size from 1 cm to nearly 2 m (Fig. 4.29(c)). The clasts are well-rounded and are composed of either a cross-bedded gravel or a coarse-grained grainstone. The conglomerate boulders are clast supported but still have ca. 10% matrix, which is composed of a coarse gravel. Well preserved solitary coral are found within the grainstone blocks (Fig. 4.29(c,d)). Bioclastic material such as serpulid worm casts, bivalves and gastropods are also found within both the matrix and the grainstone clasts. The grainstone and gravel boulders are well lithified by a carbonate cement.

Within the upper part of the gravel is a fine- to medium-grained, well-cemented grainstone, which is rich in biogenic debris, including bivalves, gastropods and solitary coral. The grainstone deposit is laterally continuous throughout the section.

Finally, overlying the grainstone deposit is a ca. 12 m-thick mudstone interbedded with conglomerate lenses. The clasts in the conglomerate are compositionally similar those in the lower gravel unit; however, they are significantly larger (1 cm to 40 cm).

The lenses significantly vary in size from 20 cm to 1 m-thick and from 1 m to 10 m-long. The clasts are sub-angular and have poorly-developed normal grading within the lenses. The lower part of the section contains ca. 1 m by 2 m downcutting lenses. Whereas, within the upper the part of the deposit the lenses are ca. 40 cm by 5 m. The conglomerate lenses are surrounded by a fine mudstone that makes up 30 % to 40% of the deposit.

The second K4 deposit in this area is preserved along the old coastal road along the coast to the northeast of Esentepe (Agios Amvrosios)(Fig. 4.29). The K4 terrace deposit is a grainstone of varying clast size, clast composition and sedimentary structures. The lower ca. 3 m of the section is composed of a poorly-sorted, medium- to coarse-grained, well-cemented grainstone. The deposit also contains beds of coarse grainstone that are predominantly composed of gastropod shells with occasional bivalves. The grainstone beds exhibit well-developed normal grading with rip-up clasts of well-cemented grainstone (Fig. 4.29). Pebble-sized clasts (0.5 cm to 2 cm) of metacarbonate and chalk are also found within the lower part of the section.

Overlying the lower grainstone unit is a ca. 3 m-thick well-sorted, fine- to medium-grained grainstone, with ca. 1 m-thick units of cross-bedding. The foresets within the cross-bedding dip at >30°. Calcified palaeo-root are also found throughout the upper part of the deposit. The upper grainstone deposit forms a continuation of the terrace surface inland for ca. 1 km.

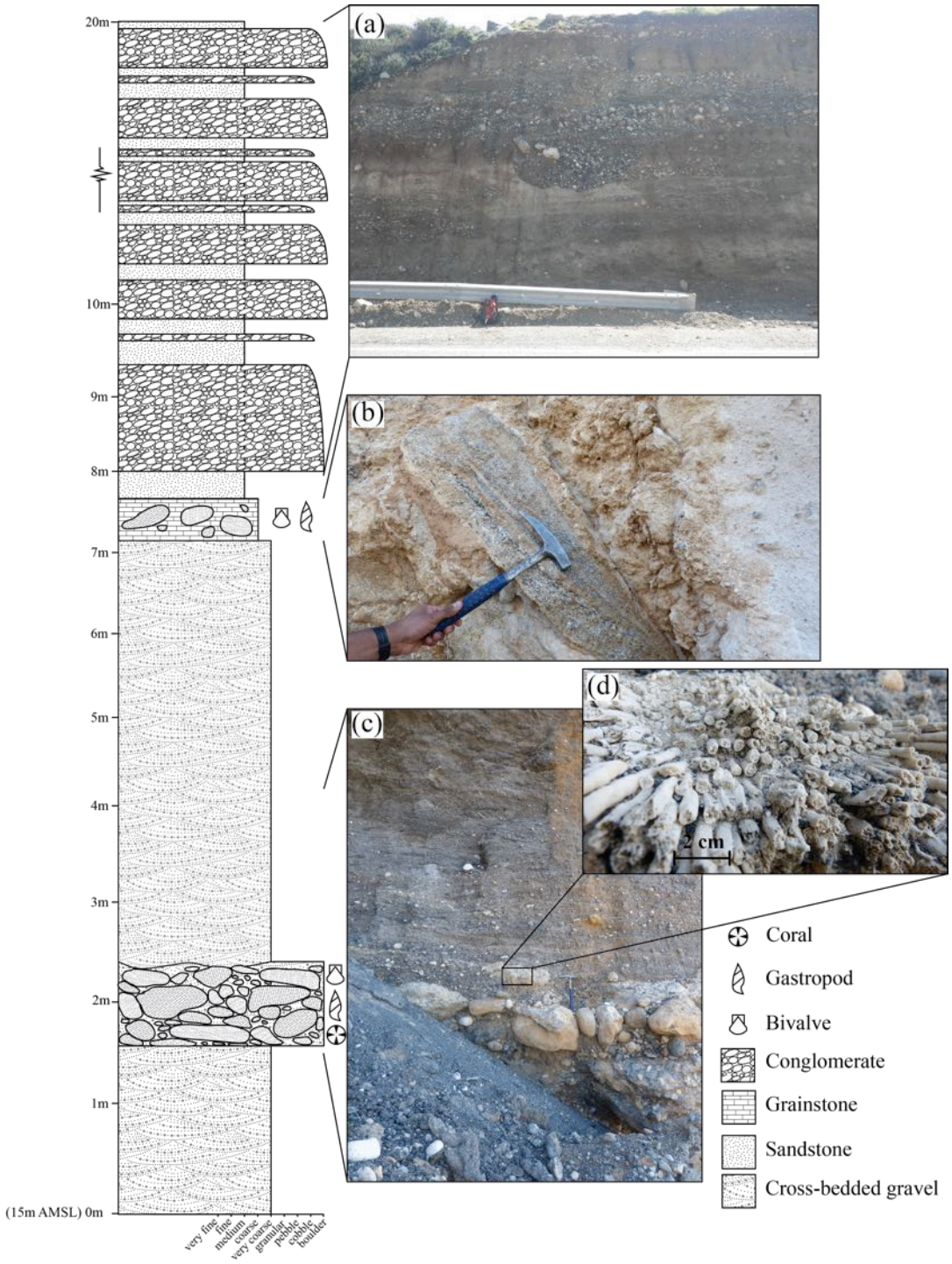

Figure 4.28: Sedimentary log through the K4 terrace deposit exposed along the main coastal road directly north of Esentepe (Agios Amvrosios) (N35 20.870' E033 34.372').

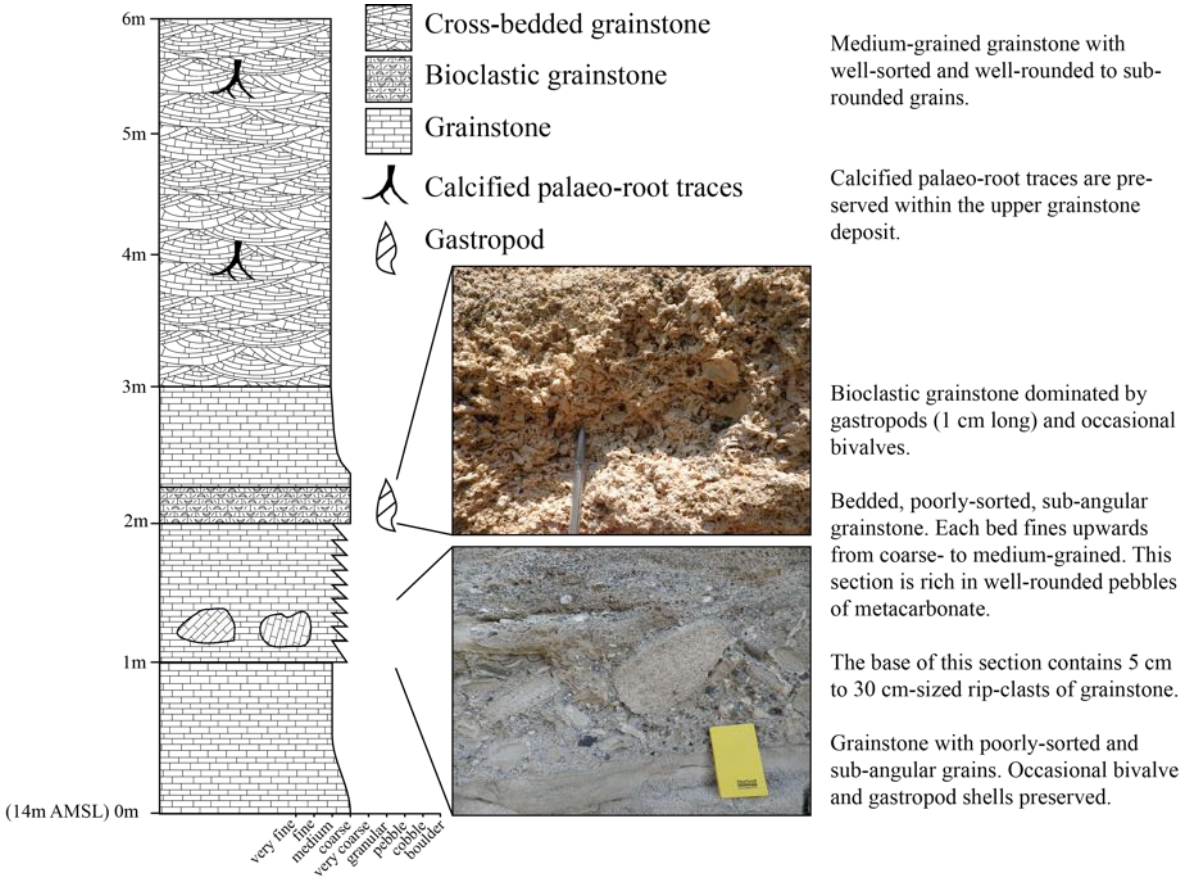

Figure 4.29: Sedimentary log through the K4 terrace deposit exposed along the old coastal road to the north-east of Esentepe (Agios Amvrosios) (N35 21.153' E033 35.235').

4.5.9 Bahçeli (Kalograi) village

The K4 terrace continues as a single surface to the east of Esentepe (Agios Amvrosios). Two K4 deposits are preserved near Bahçeli (Kalograi)(Fig. 4.18); firstly, directly north of the town at the coast, and secondly, along the main east-west coastal road. The K4 terrace deposit at the coast is ca. 4 m-thick coarse grained grainstone deposit interbedded with conglomerate lenses (Fig. 4.30). The grainstone grains are poorly-sorted and sub-angular to sub-rounded. The conglomerate lenses are made up of clasts ranging in size from 1 cm to 5 cm. Cross-bedding structures are preserved within the conglomerate lenses. The cross-bedding forms ca. 30 cm-thick units with foresets that dip at $<20°$ (Fig. 4.30). This unit also contains large (ca. 30 cm) rip-up clasts of grainstone in the upper metre of the section.

The second K4 terrace deposit is preserved along the main coastal road, on the eastern side of the turning for Bahçeli (Kalograi). The deposit is made up of mudstone, interbedded with conglomerate lenses and several palaeosol horizons (Fig. 4.31). The lower part of the deposit is a mudstone plus two palaeosols; the entire unit varies in thickness from 4 m to over 10 m. Directly overlying this is a mudstone, interbedded with conglomerate lenses. The two deposits are separated by an erosional contact which dips eastwards at ca. 45°.

The upper part of the deposit continues towards the west for over 1 km, forming a K4 terrace surface that is nearly 1.5 km wide. Conglomerate clasts within the deposits are sub-angular, well-sorted and range in size from 1 cm to 20 cm with an average clast size of ca. 5 cm. The conglomerate lenses are ca. 20 cm-thick and vary in length from 4 m to 10 m. The entire K4 terrace deposit ranges in thickness from ca. 10 m at the peripheries (Fig. 4.31) to nearly 20 m further to the east. Occasional conglomerate deposits, further west and within the lower part of the deposit, contain clasts that are well-sorted and well-rounded, containing $<10\%$ matrix.

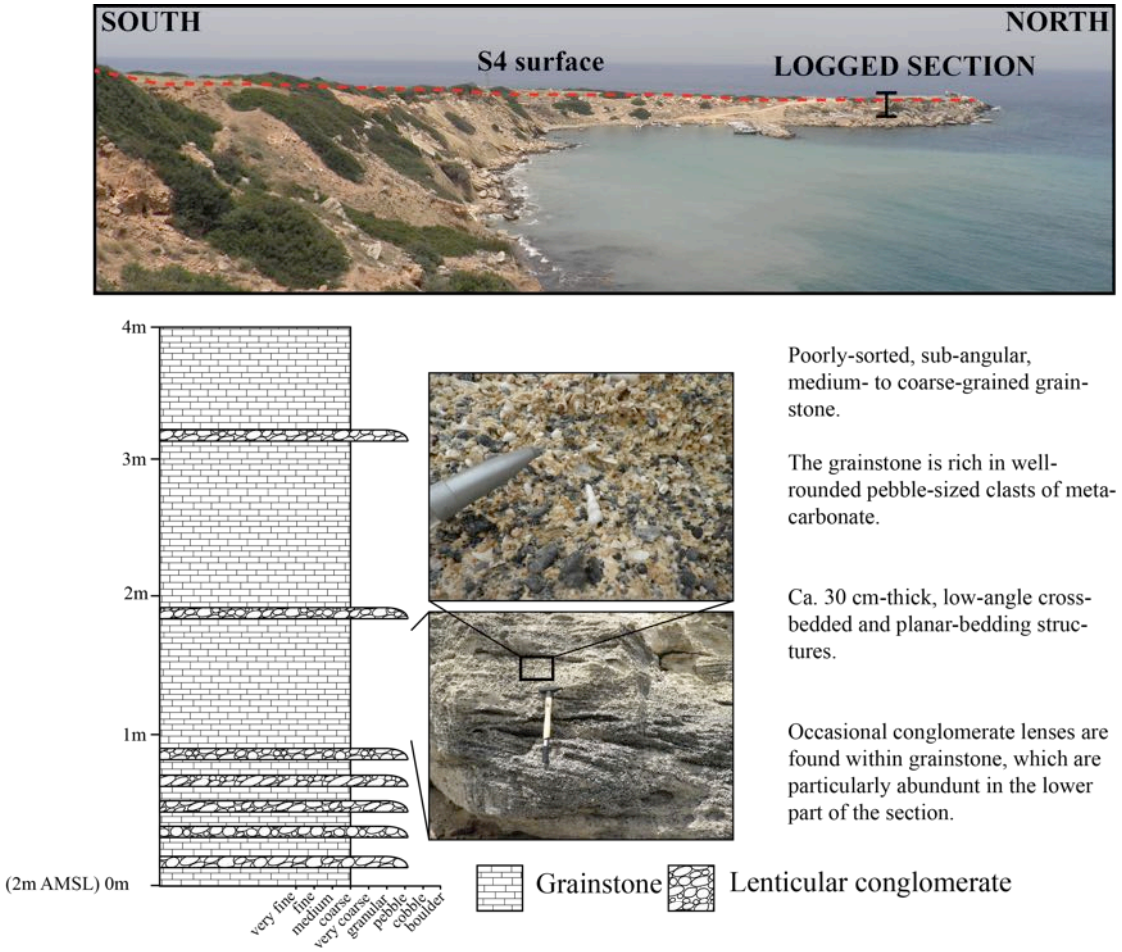

Figure 4.30: Sedimentary log through the K4 terrace deposit exposed at the coast to the north-west of Bahçeli (Kalograi) village (N35 21.578' E033 36.486').

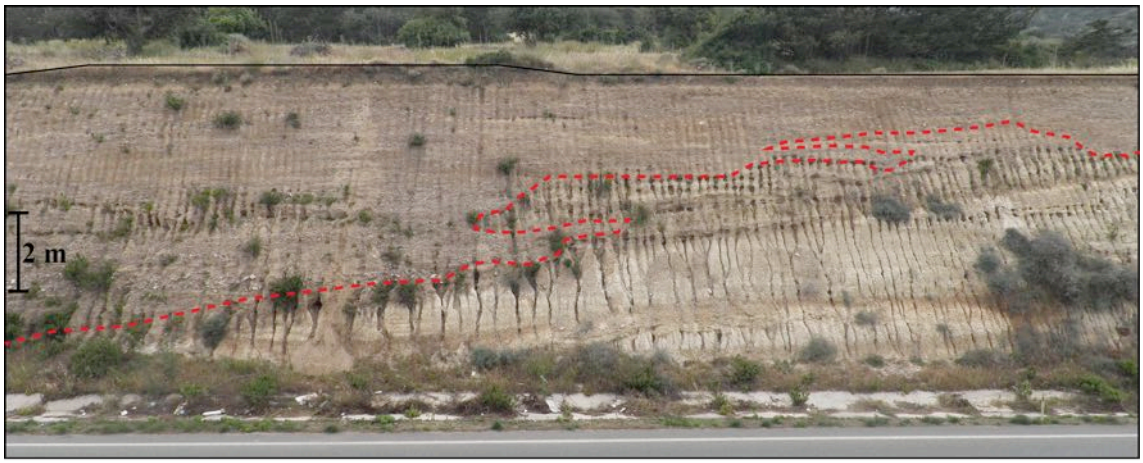

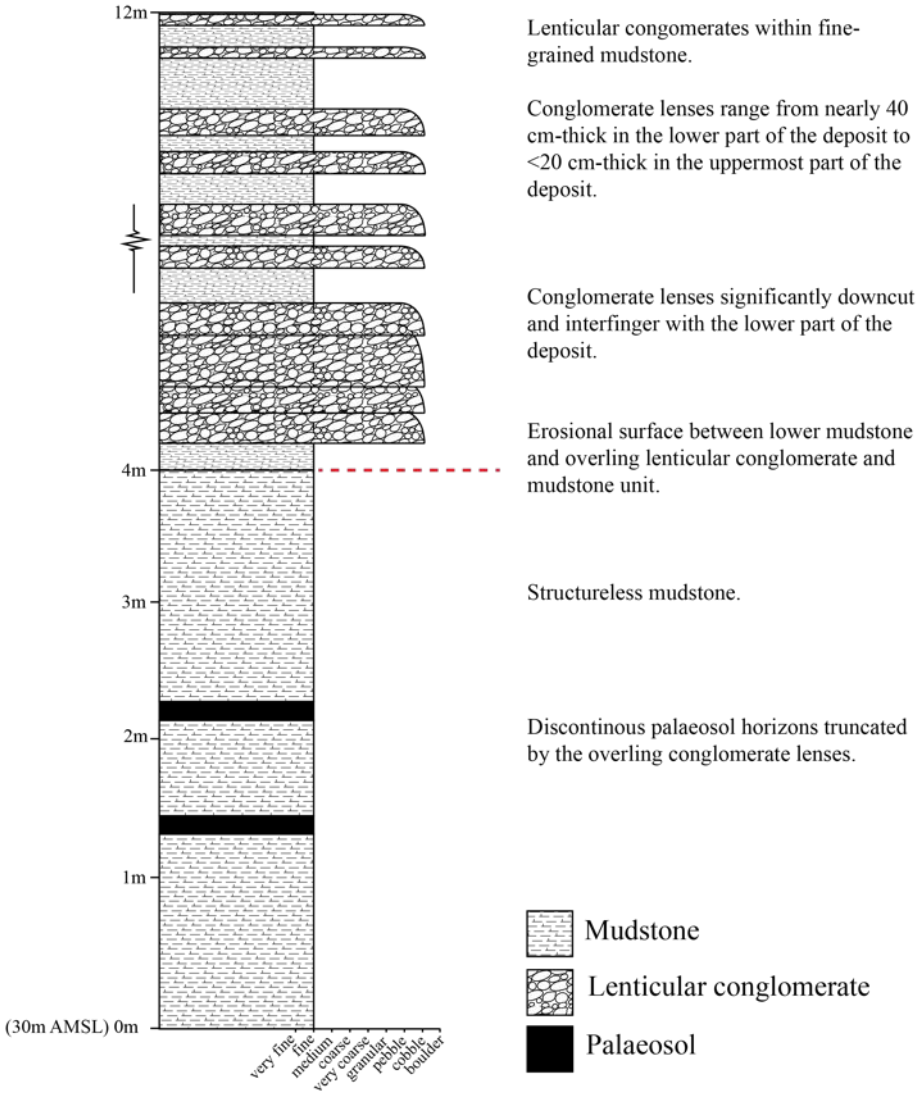

Figure 4.31: Sedimentary log through the K4 terrace deposit exposed along the main coastal ride directly north of Bahçeli (Kalograi) village (N35 21.222' E033 38.141').

4.5.10 Küçükerenköy village

Küçükerenköy was described by Baroz (1979) as the type locality of the Kyrenia (Girne)(K4) terrace (Fig. 4.18). The section is best exposed along the coast within this area and is composed of a ca. 7 m-thick grainstone deposit with varying sedimentary structures. The lower ca. 3 m of the deposit is a poorly-sorted, coarse-grained grainstone with discontinuous beds of bioclastic grainstone. Pecten and oyster shells, ranging in size from 2 cm to nearly 10 cm, are found within this lower grainstone unit (Fig. 4.32). Overlying the basal unit is a by ca. 3 m-thick coarse- to medium-grained grainstone deposit with sedimentary structures such as parallel laminations, low-angle ($<20°$) cross-bedding and normally-graded bedding. The section is overlain by a ca. 1 m-thick fine- to medium-grained grainstone with calcified palaeo roots preserved in the uppermost metre of the deposit.

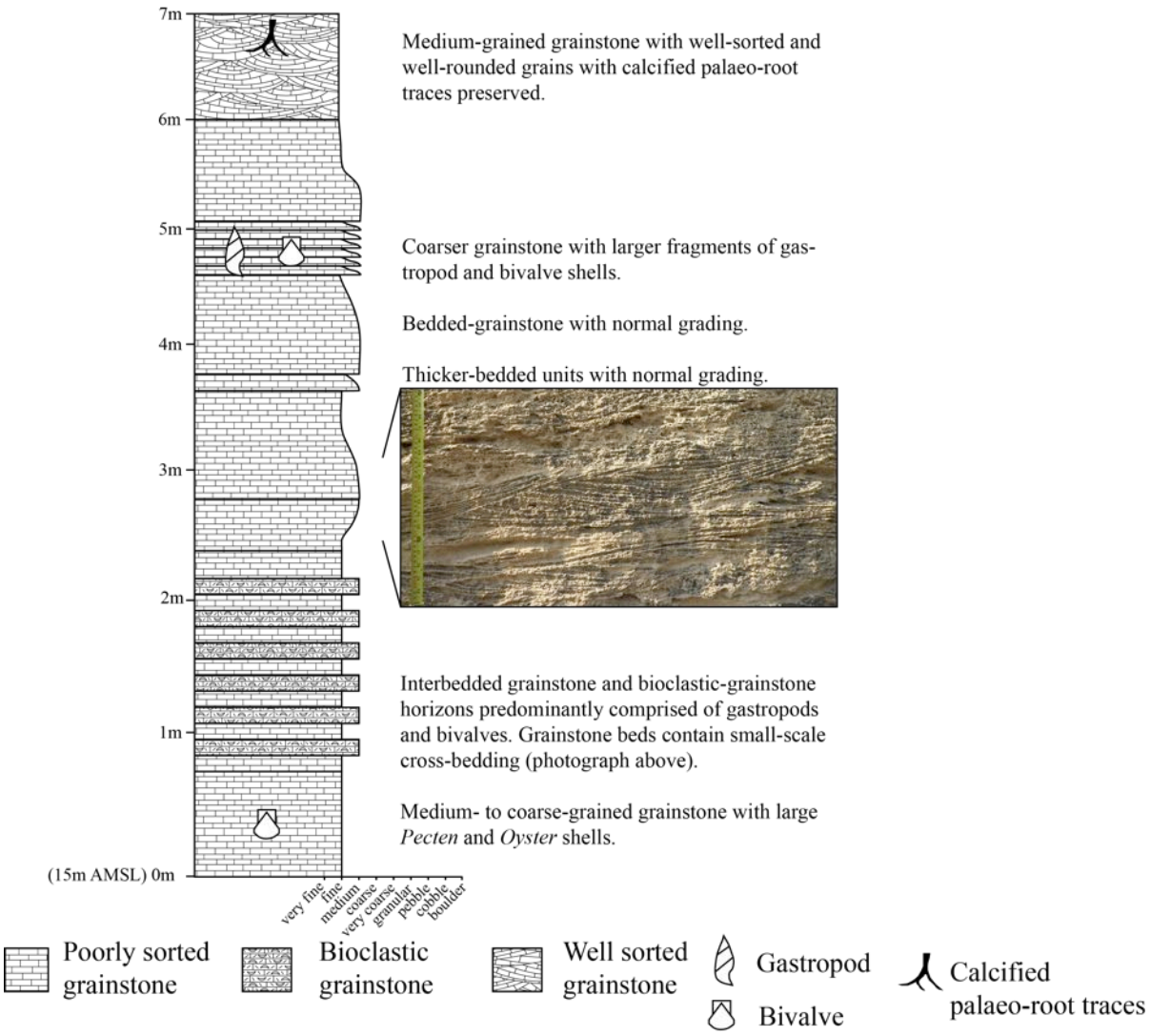

Figure 4.32: Sedimentary log and photographs through the K4 terrace deposit exposed at the coast at Küçükerenköy village (N35 21. 849' E033 40.160').

4.5.11 Tatlısu (Akanthou) village

The village of Tatlısu (Akanthou) is ca. 8 km further east along the coast from Küçükerenköy village (Fig. 4.18). The K4 terrace deposit is best exposed along the coast from the small village of Yalı north of Tatlısu (Akanthou).

Figure 4.33 is a cross-section and sedimentary log of the K4 terrace deposit preserved at the coast. The lower part of the deposit is a ca. 2 m-thick coarse-grained grainstone, which sits unconformably on the Kythrea (Değirmenlik) Group at ca. 15 m AMSL. The basal grainstone contains bioclastic debris such as bivalves, gastropods and solitary coral. Rip-up clast of sandstones of the Kythrea (Değirmenlik) Group and coarse-grained grainstone are found within the basal unit.

Directly overlying the lower grainstone unit is a ca. 40 cm-thick palaeosol and 3 m to 5 m-thick grainstone (Fig. 4.33). The grainstone is well-sorted and fine- to medium-grained. 1 m to 2 m-thick cross-bedding, with foresets dipping at >30°. The uppermost part of the deposit forms a surface that dips northward and continues below the modern sea-level. The distribution of the upper grainstone deposit along the coast in this area will be described in more detail in Section 4.6.7.

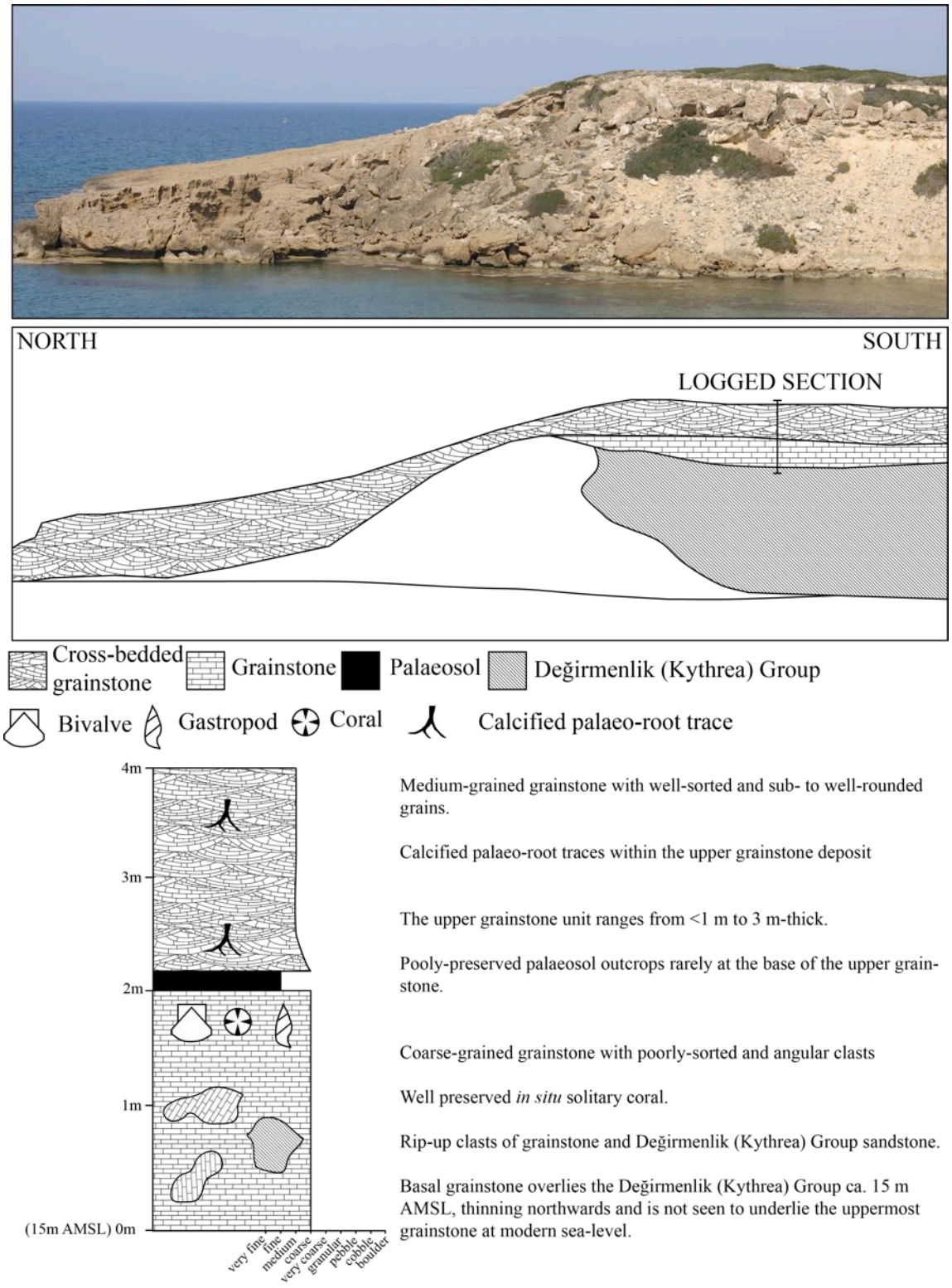

Figure 4.33: Sedimentary log and photographs through the K4 terrace deposit, exposed at the coast along the old coast road north of Tatlısu (Akanthou) village (N35 24.5209' E-33 45.509').

4.5.12 Mersinlik town

The K4 terrace deposit described is exposed along the old coastal road ca. 2.5 km to the west of Mersinlik town (Fig. 4.18). This K4 terrace deposit includes multiple lithologies incoporating key sedimentary contacts, which can be used for interpreting a more detailed depositional history.

Figure 4.34 shows a schematic section through the K4 terrace exposed within this area. The K4 terrace is cut by a younger fluvial channel, which exposes a three-dimensional section through terrace deposit. The terrace deposit is composed of mud-stone, conglomerate lenses, palaeosols and grainstone deposits. The oldest part of the terrace system is exposed on either side of the valley and is made up of a grainstone, rich is bioclastic material including solitary corals, bivalves and gastropods. The grainstone unit is a discontinuous deposit, tapering out southwards away from the coast.

Overlying the basal grainstone is a mudstone unit interbedded with conglomerate lenses and several palaeosols. The conglomerate lenses are made up of clasts that are sub-angular, ranging in size from 1 cm to 10 cm, and composed of metacarbonate of the (Trypa (Tripa) Group). The conglomerate lenses are well-sorted and have poorly-developed normal grading. Three palaeosol horizons were observed, two at the base of the section and one at the top of the mudstone deposit. Directly overlying the mudstone and conglomerate unit is a 2 m to 3 m-thick medium-grained, well-sorted grainstone deposit, forming a continuous terrace deposit inland and along the coast. The upper grainstone unit contains ca. 2 m-thick cross-bedding with foresets that dip at $>30°$.

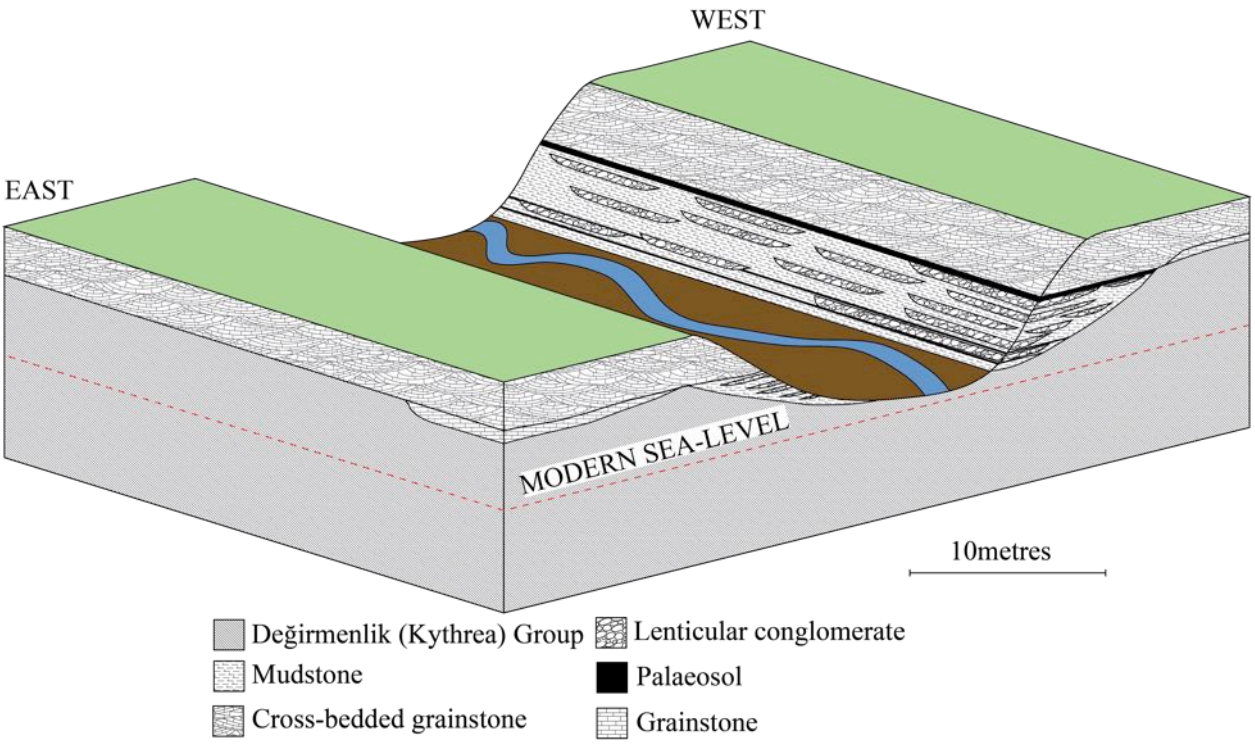

Figure 4.34: Schematic section through the K4 terrace deposit, to the north-west of Mersinlik village along the old coastal road (N35 24.761' E033 48.659').

4.6 Field sedimentology of the K5 terrace deposits

The K5 terrace deposits are found along the northern coast of northern Cyprus. Unlike the previous terraces, the K5 deposits do not form a major terrace surface. The geomorphological development of this terrace is limited. However, due to its relatively young age, sedimentary preservation of the terrace deposit is excellent. The deposits record subtle events related to the evolution of the Kyrenia Range during the Pleistocene, more so than the older terrace deposits.

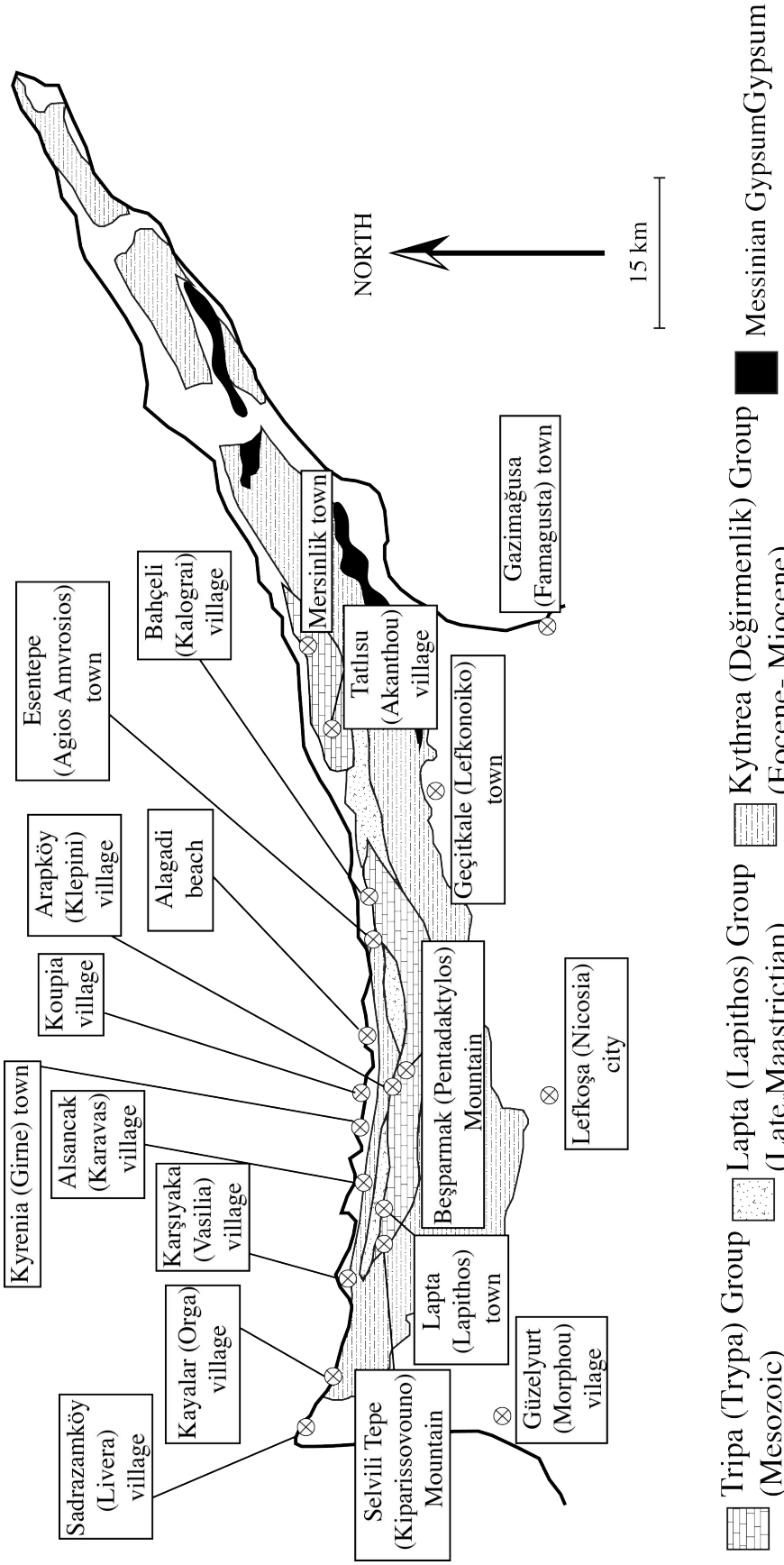

Figure 4.35: Simplified geological map of northern Cyprus showing the K5 terrace localities.

4.6.1 Sadrazamköy (Livera) village

The K5 terrace deposit at Sadrazamköy (Livera) is located just over 1 km to the north-east of the village at the coast (Fig. 4.35). The K5 terrace deposit is a ca. 6 m-thick grainstone deposit (Fig. 4.36). The grainstone is dominantly well-sorted and fine- to medium-grained with abundant calcified palaeo-root preserved and ca. 1 m-thick cross-bedding with foresets that dip at >30°. Part way up and at the top of the deposit is a planar-bedded grainstone unit. The grainstone part way up the deposit is coarse grained and rich in fragmented bivalve and gastropod shells, and rip-up clasts of grainstone (Fig. 4.36). The upper grainstone deposit is fine grained and well cemented and contain *Cladacora* solitary corals in abundance (Fig. 4.36). In general, the corals are exposed on the surface of deposit and have been mostly de-calcified.

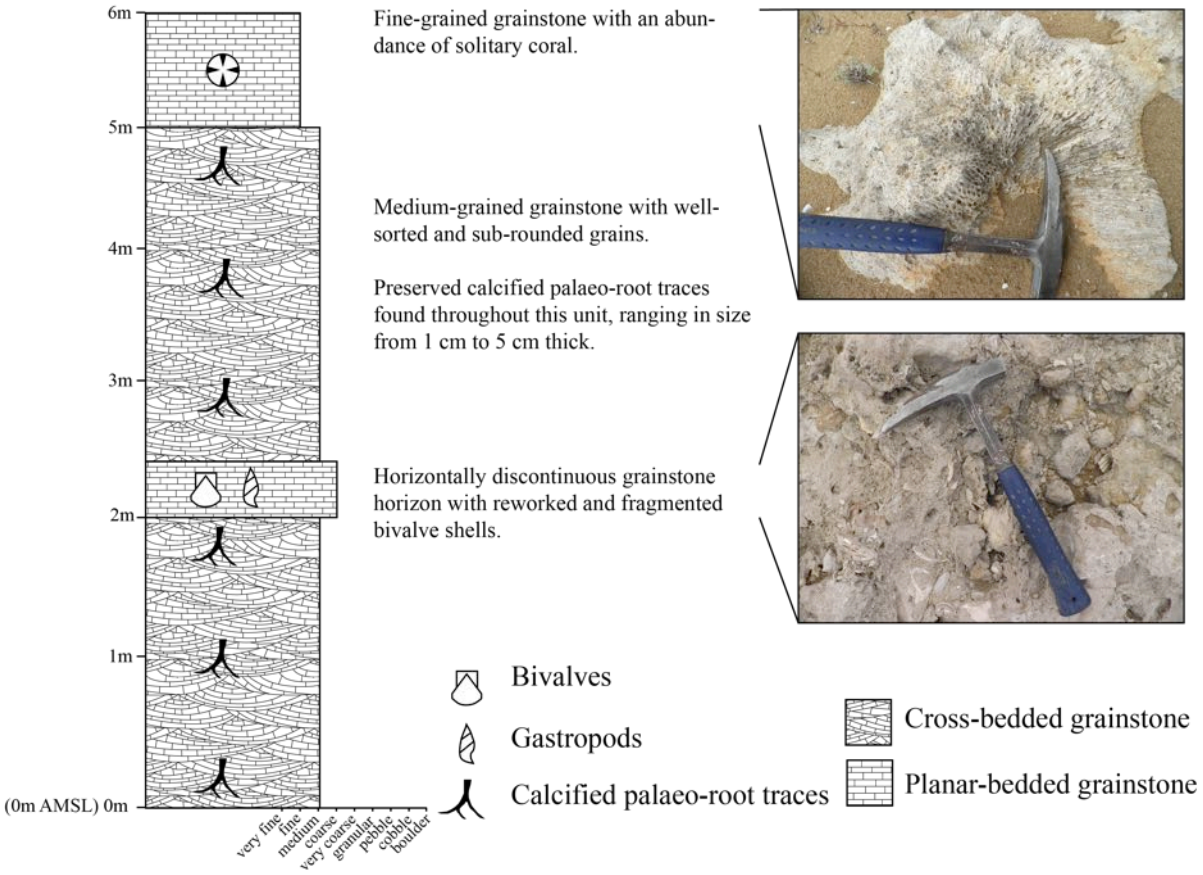

Figure 4.36: Sedimentary log and photographs through the K5 terrace deposit, at the coast near Sadrazamköy (Livera) (N35 23. 261' E033 57.782').

4.6.2 Kayalar (Orga) village

Figure 4.37 shows the K5 deposit along the coast to the east of Kayalar (Orga)(Fig. 4.35). These deposits are made up of the fine- to medium-grained grainstone, with 2 m to 3 m-thick, high-angle (>30°) trough cross-bedding and an abundance of calcified palaeo-root traces. The grainstone deposits range in thickness from 1 m to 6 m, but are mostly 5 m to 6 m thick. The deposits often dip northwards below the modern sea-level.

The K5 deposits along this stretch of coast are isolated and discontinuous. Figure 4.37 shows a profile of the K4 (Sec. 4.5.2) and the K5 deposits north of the village of Kayalar (Orga). The base of the K4 deposit is at ca. 40 m AMSL, whereas the base of the K5 deposit is just below modern sea-level. The K5 grainstone forms at the base of a steep northward-dipping slope. The deposits in general dip seawards (north). The coast within this area is dominanted by K4 terrace deposits which continue inland for ca. 1 km.

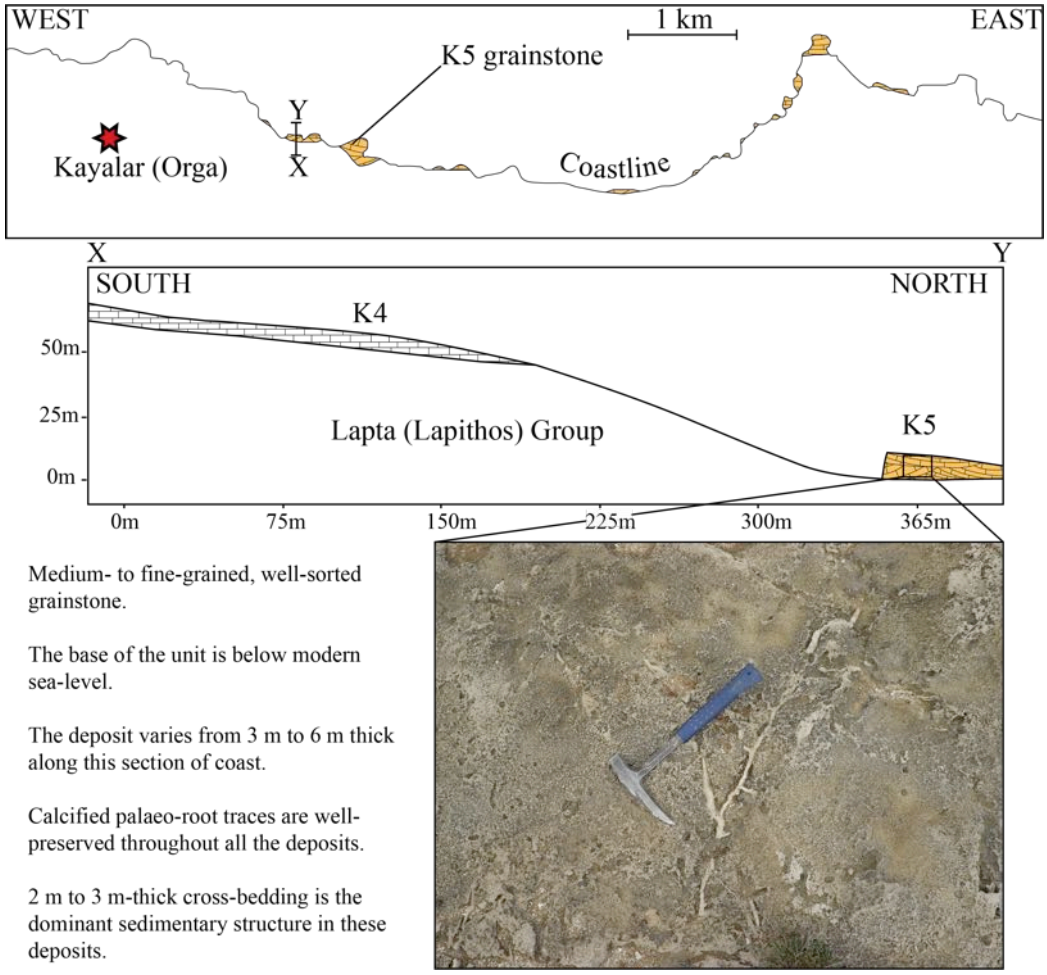

Figure 4.37: Map, cross-section and photograph of the K5 deposits along the coast from Kayalar (Orga) (N35 21.513' E033 02.939').

4.6.3 Alsancak (Karavas)

The K5 terrace deposit at Alsancak (Karavas) is found directly north of the town along the coast (Fig. 4.35). The deposit is composed of a grainstone with a conglomerate lens (Fig. 4.38). The lower ca. 2 m of the deposit is a medium-grained, well-sorted grainstone. Ca. 1 m-thick cross-bedding with foresets dipping at >30° are found within the lower grainstone. The lower grainstone is overlain by an ca. 80 cm-thick coarse-grained grainstone with bivalves, gastropods and encrusting algae present (Fig. 4.38). The coarse-grained grainstone is overlain by a ca. 70 cm-thick grainstone with similar sedimentary characteristics to the basal grainstone.

The entire grainstone deposit is overlain by a mudstone with a large conglomerate lens. The conglomerate is made up of poorly sorted, sub-angular clasts of metacarbonate and chalk. The clasts within the conglomerate range in size from 1 cm to 10 cm. No sedimentary sorting or structures are found within the conglomerate.

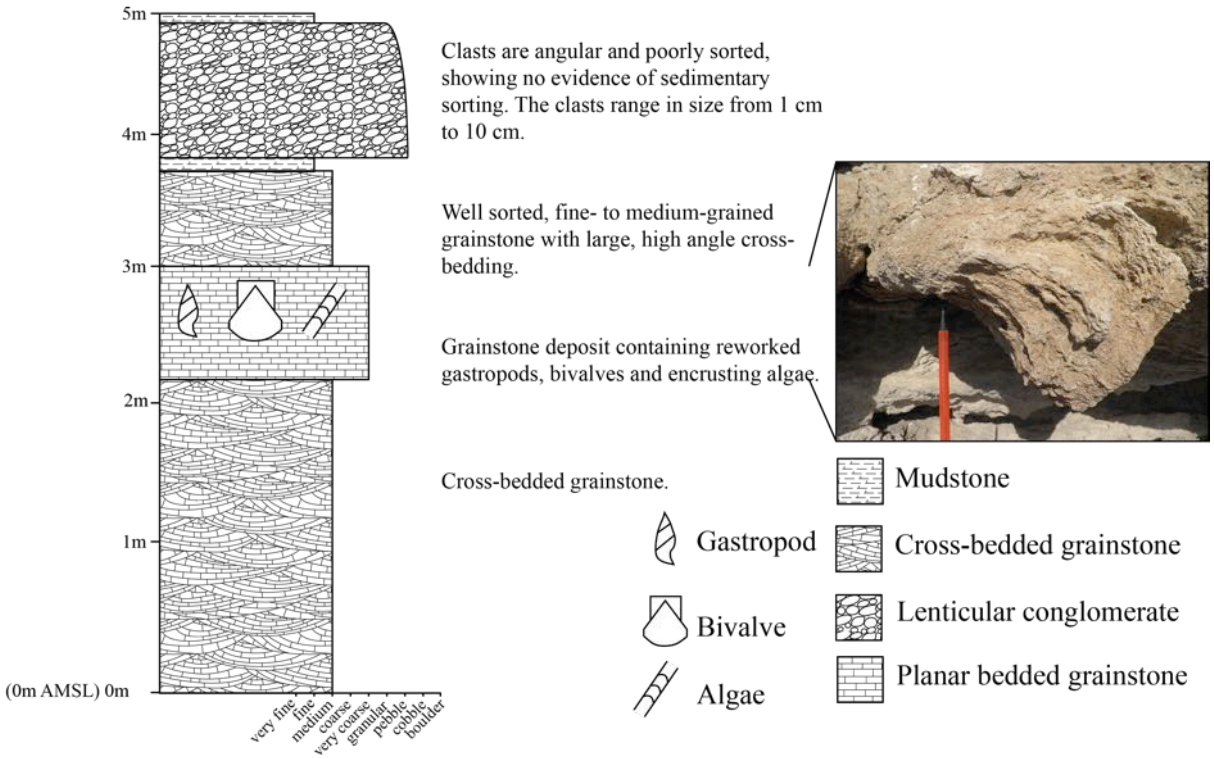

Figure 4.38: Sedimentary log and photographs of the coastal deposit directly north of Alsancak (Karavas) town (N35 20.872' E033 15.918').

4.6.4 Arapköy (Klepini) (Koupia)

The K5 deposit near Arapköy (Klepini) is exposed directly north of the town at the coast, ca. 3 km west of Alagadi beach (Fig. 4.35). The locality was previously a Greek village called Koupia but is presently abandoned. The exposed deposit was described by Baroz (1979) as the type locality of the K5 (Koupia) terrace. Baroz (1979) produced a cross-section through the K4 and K5 deposits within this area; since then the new coastal road has exposed more of the relationships than were previously visible. Figure 4.39 shows a new cross-section through the K4 and K5 terrace deposits within this

area.

The K4 terrace is dominantly made up of a ca. 5 m-thick grainstone deposit with a basal palaeosol and conglomerate. The new coastal road exposes the basal conglomerate, which can only be found at the northern end of the terrace deposit. The conglomerate deposit is less than 1 m-thick; the clasts within it are well-rounded and well sorted. The composition of the clasts is predominantly metacarbonate and chalk. The base of the conglomerate sits directly on the Kythrea (Değirmenlik) Group at ca. 30 m AMSL.

The K5 terrace deposit is found on the coast directly north of the previously described K4 deposit(Fig. 4.39). The deposit is dominantly comprised of a medium-grained grainstone with a thin-discontinuous bed of grainstone with bioclastic debris (Fig. 4.39, Photo 2). The K5 grainstone forms a 1 m to 2 m-thick deposit along the coast, which dips northwards below modern sea-level. The K5 grainstone has ca. 1 m-thick trough cross-bedding and abundant calcified palaeo-root traces. The bioclastic grainstone is found discontinuously within the medium-grained grainstone at ca. 2 m AMSL (Fig. 4.39). The bioclastic debris is composed of fragmented shells including bivalves and gastropods, with rip-up of clasts of grainstone (Fig. 4.39, Photo 3). The K5 grainstone at the coast has been eroded by the modern sea to form wave-cut platforms.

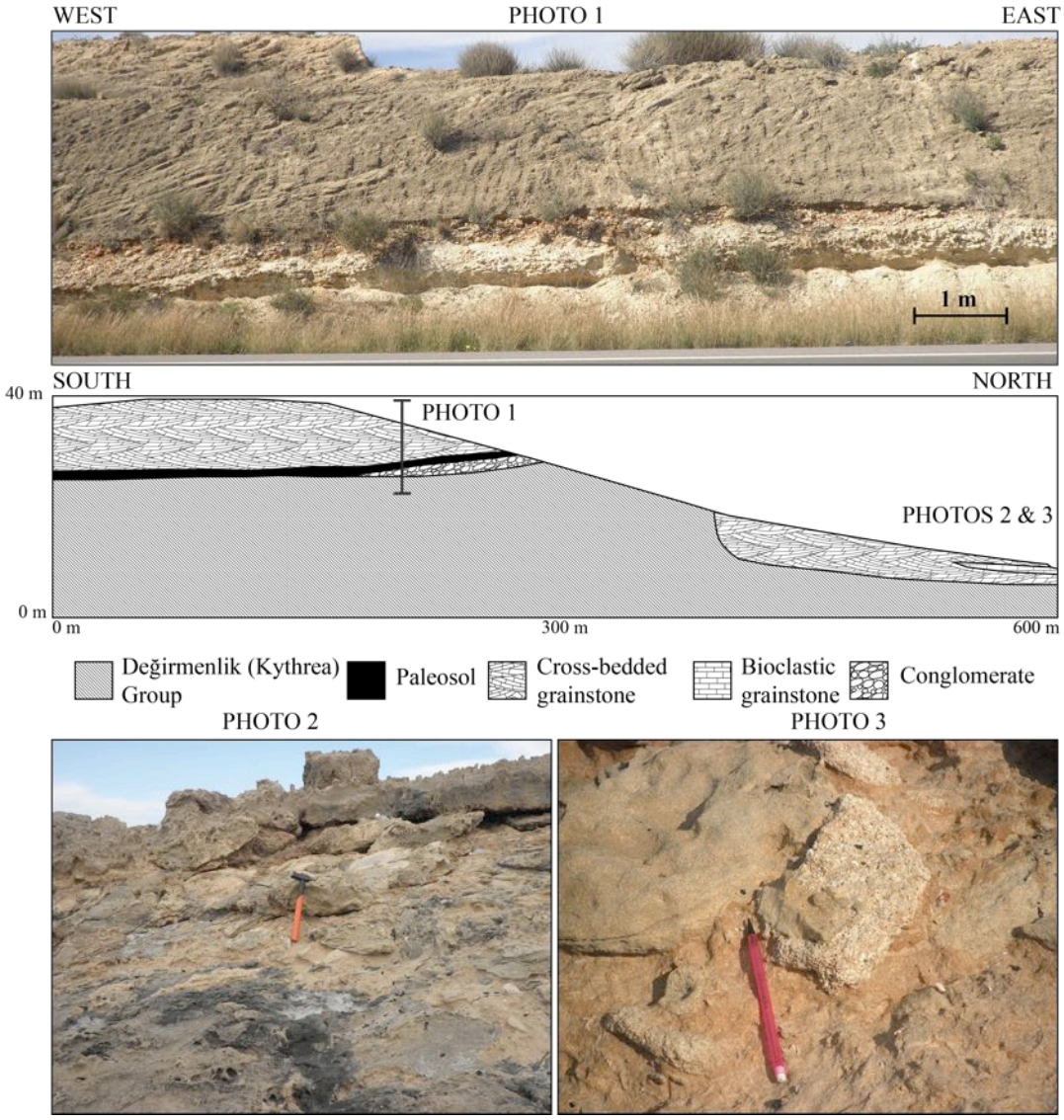

Figure 4.39: Schematic section and photographs of the K4 and K5 terrace deposits at the old village of Koupia which is located on the coast directly north of Arapköy (Klepini). Photograph 1) an overview of the K4 terrace deposit; 2) grainstone bed rich in bioclastic debris; and 3) rip-up clasts of bioclastic grainstone (N35 20.191' E033 26.929').

4.6.5 Alagadi beach (Fig. 4.35)

The K5 terrace at Alagadi beach is located in the centre of the Alagadi turtle beach (Fig. 4.25). The deposit comprises a ca. 3 m-thick grainstone deposit with varying sedimentary structures and grain size (Fig. 4.40). The basal unconformity is with sandstones of the Kythrea (Değirmenlik) Group at ca. 4 m AMSL. The terrace forms an isolated deposit and cannot be connected with any inland terrace deposit or surface.

The base of the deposit comprises a 20 cm to 30 cm-thick discontinuous medium-grained, well-sorted, poorly-consolidated grainstone. Erosively overlying the basal grainstone is a poorly-sorted bioclastic grainstone. The bioclastic grainstone is rich in bioclastic debris including bivalves, gastropods, algae and solitary corals. Rip-up clasts of Kythrea (Değirmenlik) Group sandstone are abundant within this deposit. The thickness of the bioclastic grainstone range from 20 cm to 50 cm.

Overlying the bioclastic grainstone is a coarse- to fine-grained grainstone. At the base of the grainstone unit there are abundant ca. 20 cm-thick units of low angle (<20°) cross-bedded and parallel laminations (Fig. 4.40). Parallel laminations become the dominant structure further up the grainstone unit. The grainstone in the upper ca. 1 m of the deposit is well sorted and fine grained. The upper grainstone ranges in thickness from 1 m to nearly 3 m thick. Cross-bedding is the dominant structure within this upper unit, forming ca. 1 m-thick cross-bedded units. Calcified palaeo-root traces are also found throughout the uppermost part of the deposit.

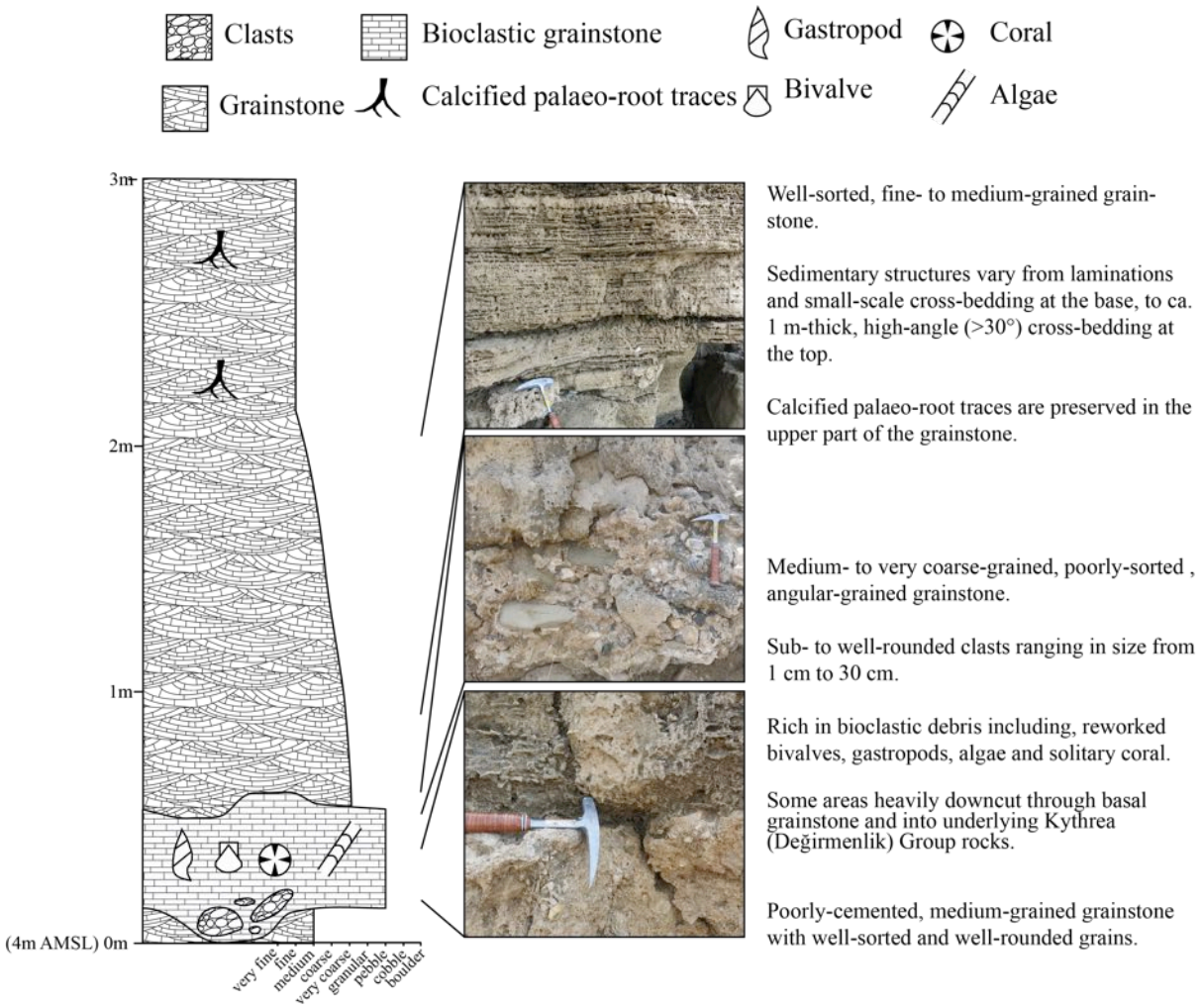

Figure 4.40: Sedimentary log and photographs from the K5 terrace deposit at Alagadi beach (N35 20.074' E033 29.286').

4.6.6 Esentepe (Agios Amvrosios)

K5 terrace deposits are not exposed between Alagadi beach and Esentepe (Agios Amvrosios) (Fig. 4.35). However K4 terrace deposits are exposed at the coast. The K5 deposit at Esentepe (Agios Amvrosios) is preserved to the north-east of the town, at the start of the old coastal road.

The K5 terrace deposit is made up of a grainstone overlain by a mudstone interbedded with conglomerate lenses (Fig. 4.41). The basal grainstone is well-sorted, fine- to medium-grained, with high-angle (>30°) cross-bedding. Calcified palaeo-root traces

are preserved in abundance throughout. The basal unconformity with the Kythrea (Değirmenlik) Group is below modern sea-level. The deposit is isolated and does not form part of a continuous inland terrace.

Directly overlying the grainstone is a 3 m to 4 m-thick mudstone, interbedded with conglomerate lenses. The clasts within the conglomerate are composed of metacarbonate, chalk and reworked gravel (Fig. 4.41). The conglomerate clasts are sub-rounded to well-rounded and are poorly sorted, ranging in size from 1 cm to 30 cm. The lenses are well sorted and have poorly developed normal grading. The clasts within the lenses become increase in size (1 cm to 15 cm) the upper parts of the mudstone deposit.

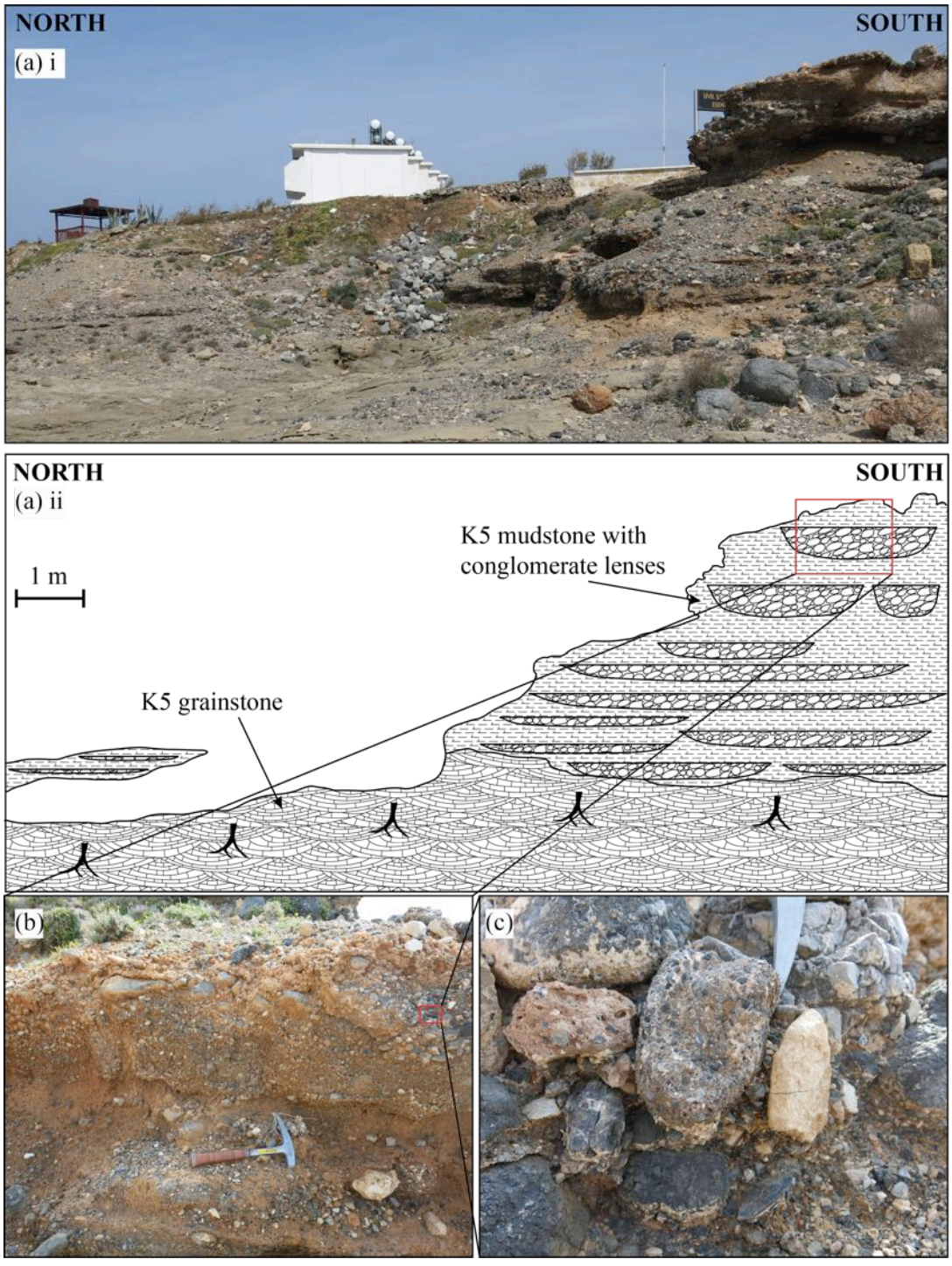

Figure 4.41: Schematic section and photographs of the K5 terrace deposit along the old coast road, to the north-east of Esentepe (Agios Amvrosios) Photograph (a)(i-ii) overview photograph and sketch of the K5 deposit; (b) uppermost part of the interbedded mudstone and conglomerate deposit; and (c) reworked clasts of gravel facies and metacarbonate (N35 21.037' E033 35.023').

4.6.7 Bahçeli (Kalograia) to Tatlısu (Akanthou) and onto Mersinlik (Fig. 4.35)

Beyond Esentepe (Agios Amvrosios), no K5 deposits are preserved for nearly 2 km. The next K5 deposits are found between Bahçeli (Kalograia) and Mersinlik. Figure 4.42 shows a simplified map of the K5 terrace deposits along this stretch of coast. The deposits are made up of 1 m to 6 m-thick well-sorted fine- to medium-grained grainstone with 1 m to 2 m-thick units of trough cross-bedding with foresets dipping at >30°. Calcified palaeo-root traces are also preserved throughout the deposits.

The deposits are found at isolated localities along the coast, with no continuous terrace surface inland. The base of the deposit is never exposed with grainstone continuing below modern sea-level. Depending on the inland topography, the deposit is either restricted to the coast or continues inland for 20 m to 30 m (Fig. 4.42). Where the topography inland of the deposit is steep the grainstone is restricted to the coast however, when the inland topography gradually dips northward, the grainstone extends southwards (Fig. 4.33; Fig. 4.42).

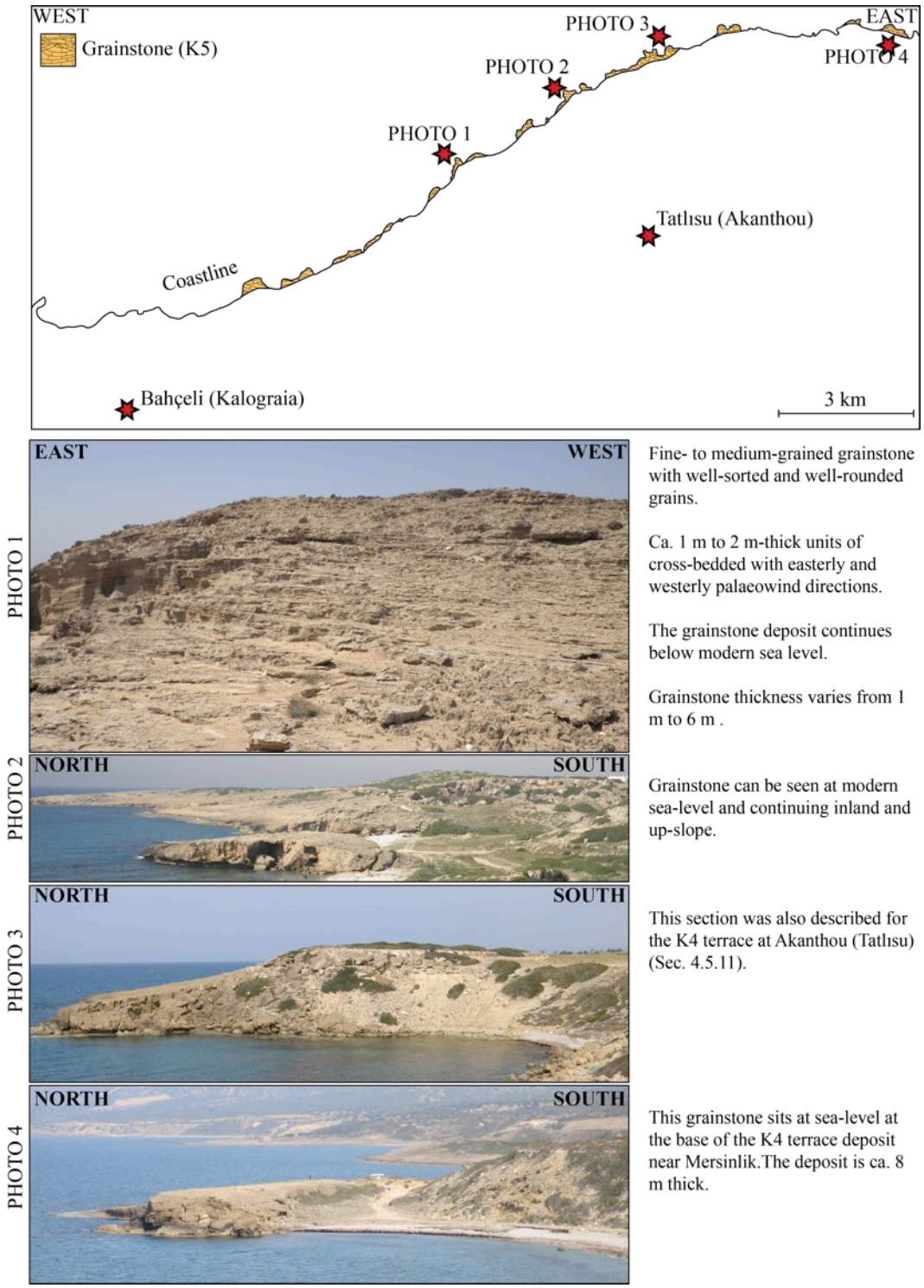

Figure 4.42: Geological sketch map and photographs of the K5 terrace deposits along the coast east of Bahçeli (Kalograia).

4.7 Petrography

Grainstone deposits are exposed within all of the terrace systems on the northern flank of the Kyrenia Range. In the previous section, field descriptions were presented, including grain size, sorting, rounding and larger-scale sedimentary structures. Further details of the composition, size and rounding of the grains are presented from petrological analysis.

The grainstone deposits are lithified carbonate sands, which can be generally described as calcarenite (Grabau, 1904). The term grainstone (Dunham (1962)) is used to describe these deposits because of several factors, including: 1) the grains within the deposit are not bound together during deposition, the unit is therefore allochthonous; 2) the unit is grain supported; 3) the interstitial space between the grains is partially infilled with a sparry-carbonate cement (occasionally the cement is micritic; this will be discussed later).

Field descriptions show that the grainstone deposits range from fine- to coarse-grained with sub-angular to well-rounded grains. From the petrography it is possible to be more specific concerning grain size and rounding. The grains range from 100 μm (0.1 mm)(fine grained), up to 3 mm (coarse grained). The size of the grains is not controlled by the composition; both the bioclastic and clastic grains vary in size equally. In contrast, the roundness of the grains does seem to vary with composition. The bioclastic grains are sub-rounded to well-rounded, whereas the clastic grains are generally sub angular.

4.7.1 Carbonate grains

The carbonate grains are fragmented and rarely preserved in their complete form, except for the benthic foraminifera. The most common carbonate grains are echinoderm plates and calcareous red algae (Fig. 4.43(a,b)). The calcareous red algae are always found as reworked, well-rounded grains. Calcareous green algae (Fig. 4.43(c)) are preserved in several deposits and are heavily fragmented.

Numerous families of benthic foraminifera are also found within the deposits. The most common include *Miliolida* and *Neorotalia* (Fig. 4.43(c, d)). Minor proportions of

several other types of benthic foraminifera are also found including *Peneroplidae* and *Textulariidae* (Fig. 4.43(e, f)).

Minor amounts of other carbonate grains are also found including bivalves, particularly oyster fragments (Fig. 4.43(g, h)), calcareous algae (Fig. 4.43(i, j)) bryozoa, ostracods, gastropods and planktonic foraminifera. These carbonate grains form a relatively minor proportion (<10%) of the carbonate material in all the grainstone deposits.

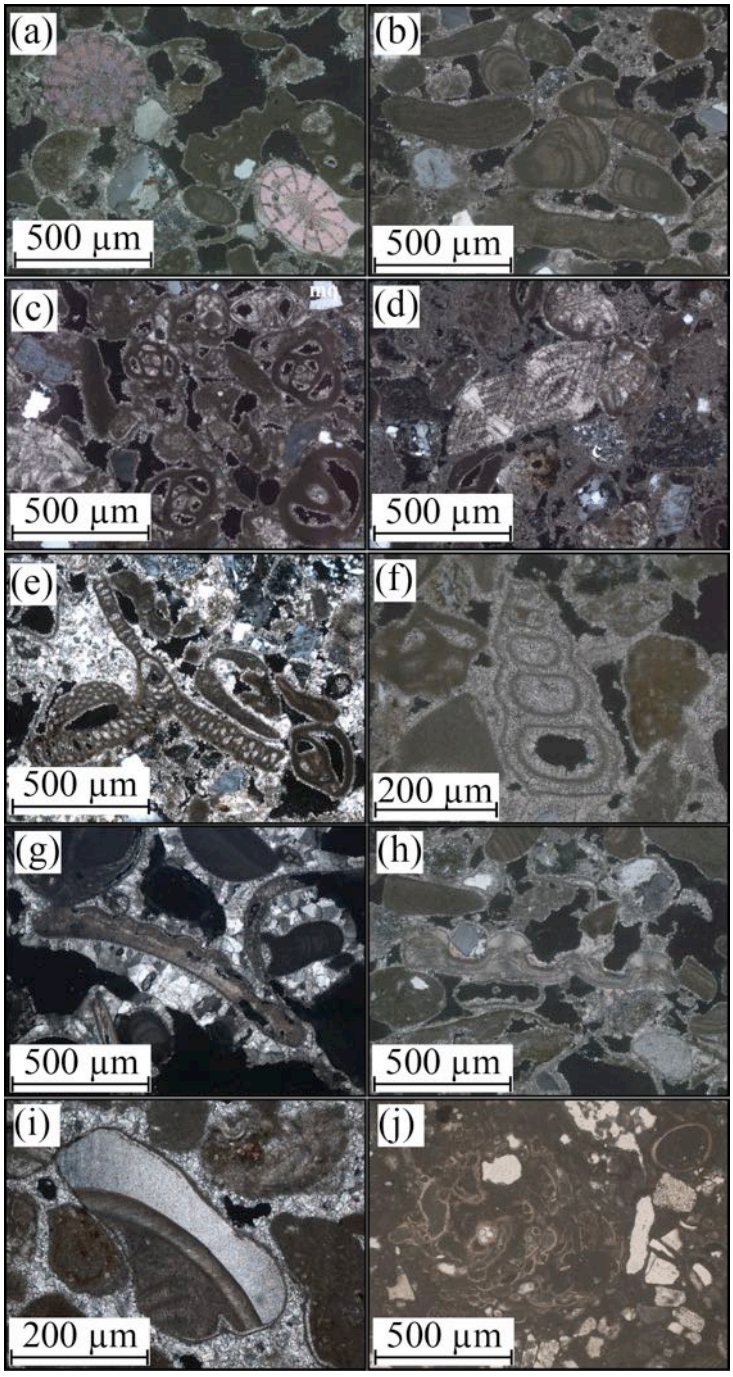

Figure 4.43: Photomicrographs of carbonate grains from grainstone deposits on the northern flank of the Kyrenia Range. The photomicrographs include: (a) echinoderm plates; (b) reworked and well-rounded calcareous red algae; (c) *Miliolida* benthic foraminifera; (d) *Neorotalia* benthic foraminifera; (e) *Peneroplidae* benthic foraminifera; (f) *Textulariidae* benthic foraminifera; (g) pecten shell fragment; (h) oyster shell fragment; (i) reworked algae (as described in Section 2.7.2); and (j) algae.

4.7.2 Clastic grains

The clastic grains are found in all of the grainstone deposits on the northern flank of the Kyrenia Range. The clastic grains include material that is composed of silicic material and reworked rock fragments.

Silicic material in the grainstone deposits is dominantly composed of monocrystalline quartz, polycrystalline quartz, plagioclase, chert and diabase (Fig. 4.44(a-e)). Reworked rock fragments include metacarbonate, grainstone and foraminifera-rich marl (Fig. 4.44(f-h)). The relative amounts of silicic grains and reworked rock fragments varies significantly between the grainstone deposits; this will be explored further using point-count data in Section 4.7.6.

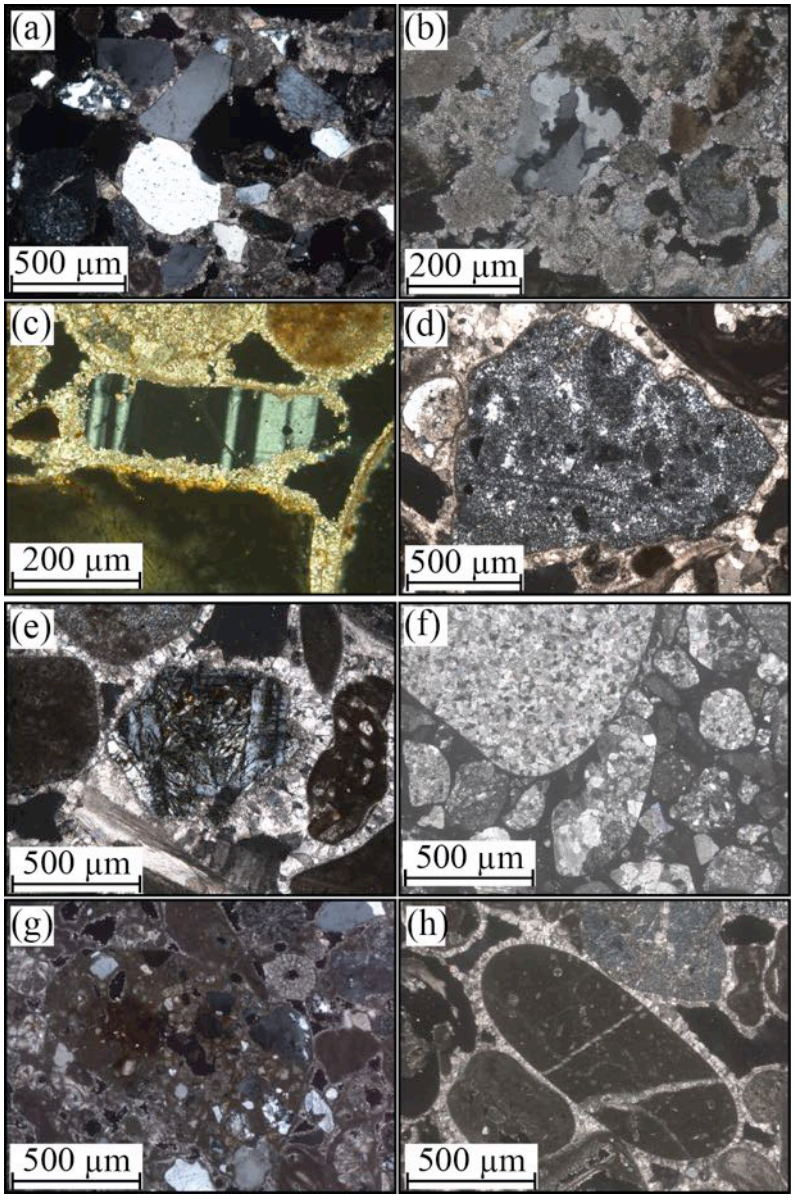

Figure 4.44: Photomicrographs of clastic grains from grainstone deposits on the northern flank of the Kyrenia Range. Photomicrographs include: (a) monocrystalline quartz; (b) polycrystalline quartz; (c) plagioclase; (d) chert; (e) diabase; (f) metacarbonate; (g) grainstone; and (h) foraminifera-rich marl.

4.7.3 Diagenesis

The lithification of the grainstone deposits on the northern flank of the Kyrenia Range is due to the precipitation of carbonate cement. The carbonate cement within the grainstone deposits is dominantly composed of sparite; however, several deposits have a micritic cement. In the case of deposits with a sparite cement, the cement coats all the grains but only partially infills the pore space. In contrast, in the deposits with a micritic cement the cement completely infills the pore space.

4.7.4 Oxygen and carbon isotopic data from grainstone cements

Sampling method

Representative grainstone samples were selected from the K1 to K5 terraces on the northern side of the Kyrenia Range (Table. 4.1).

Sample	Terrace	Locality	Section
KY12-63	K1	Arapköy (Klepini)	3.3.6
KY12-36	K2	Davlos (Kaplıa)	4.3.6
KY12-62	K3	Arapköy (Klepini)	4.4.2
KY12-33	K4	Karşıyaka (Vasilia)	4.5.3
KY12-40	K5	Mersinlik	4.6.7
KY11-19	K4 (1)	Küçükerenköy	4.5.10
KY12-32	K4 (2)	Karşıyaka (Vasilia)	4.5.3

Table 4.1: Terraces and samples used for stable δ^{18}O and δ^{13}C isotopic analysis.

Results

The δ^{18}O and δ^{13}C isotopic data are expressed in relation to the Vienna standard from the PeeDee Formation of South Carolina (VPDB). The carbon and oxygen isotopic ratios are expressed in parts per thousand (‰). The data from Pleistocene terraces on the northern flank of the Kyrenia Range are shown in Table 6.2 and Figure 4.45.

The grainstone deposits have negative oxygen and carbon isotope ratios. The most negative carbon isotopic ratios are generally associated with the most negative oxygen isotopic ratios. The range in values of the carbon isotopic ratios (3.438) is significantly larger than for the oxygen isotopic ratios (1.484)(Table 6.2).

Terrace	**δ^{13}C V-PDB (‰)**	**δ^{18}O V-PDB (‰)**
K1	-6.853	-4.484
K2	-4.251	-4.453
K3	-6.598	-4.515
K4	-6.574	-3.540
K5	-4.191	-3.031
K4 (1)	-3.626	-3.249
K4 (2)	-7.064	-4.340
Range →	3.438	1.484

Table 4.2: δ^{18}O and δ^{13}C stable isotopic data from grainstone deposits on the northern flank of the Kyrenia Range.

4.7.5 Discussion

To understand the diagenetic environments in which the grainstone cements formed, the oxygen and carbon data were plotted, first, in a generalised isotope field graph, and secondly, in comparison with Bermuda beach aeolianites (Fig. 4.45). The data plots within or near the meteoric cement field (Fig. 4.45(a)), which initially suggests that the cements formed within a vadose rather than a phreatic diagenetic environment. The δ^{13}C ratio is within the range of meteoric cements; however, several of the δ^{18}O ratios are outside of the fields for meteroic cements suggested by Hudson (1977) and Nelson and Smith (1996).

The Pleistocene geology of Bermuda has provided an excellent opportunity to study the depositional and diagenetic processes associated with coastal lithified carbonate sands (Gross, 1964; Hearty, 2002). Figure 4.45(b) compares Kyrenia stable isotope data with Pleistocene aeolianites in Bermuda (Gross, 1964). The Kyrenia data has δ^{13}C within the Bermuda aeolianite range; however, the δ^{18}O ratio is slightly low, indicating subtly different subsurface water conditions.

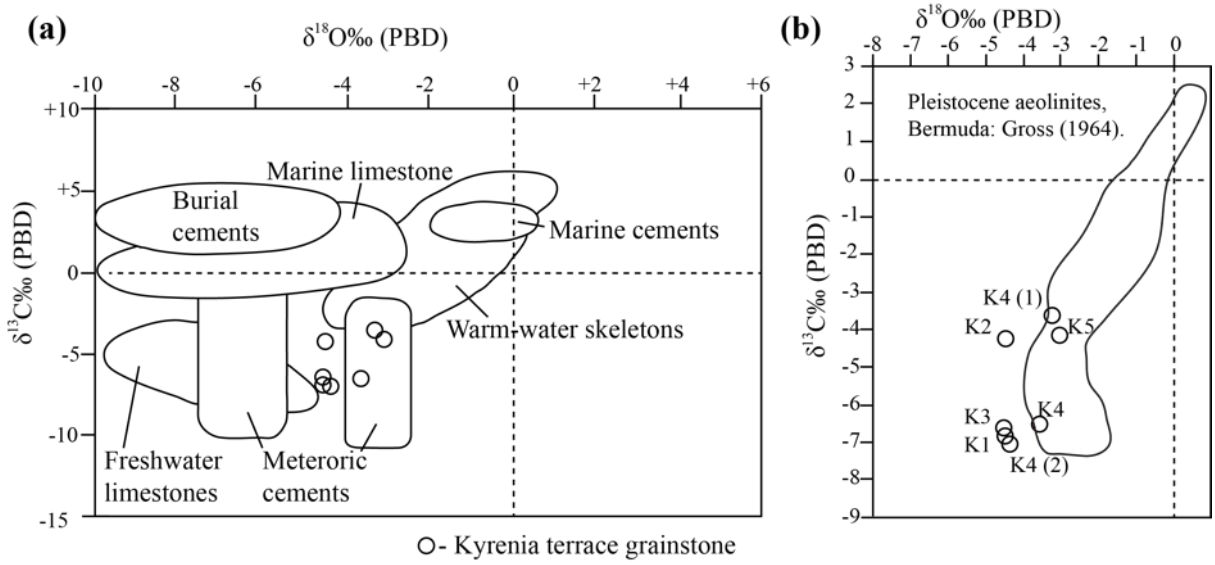

Figure 4.45: δ^{18}O and δ^{13}C plots from carbonate cement from Quaternary marine and aeolian grainstones from northern Cyprus; (a) adapted from Hudson (1977); and Nelson and Smith (1996); and (b) Pleistocene aeolianite field adapted from data in Gross (1964).

4.7.6 Grainstone point-count data

The composition of the grains within the grainstone deposits includes an array of types of carbonate and clastic grains, as previously described. Field observations have also indicated an array of sedimentary structures within the grainstone deposits, suggesting that the grainstone deposits represent a range of depositional processes. Point counting was carried out on grainstone deposits with a range of sedimentary structures, from the K2 to K5 terraces on the northern flank of the Kyrenia Range.

Point-count data were collected from 23 grainstone deposits from the K2 to K5 terraces. Samples were selected from grainstone deposits that contain either low-angle (<30°) cross-bedding, laminations and centimetre-scale bedding, or 1-2 m-thick units of high angle (>30°) cross-bedding.

Figures 4.46 and 4.47 graphically represent the point-count data from the K2-K5 terrace grainstone deposits. Figure 4.46 shows the point-count data from low-angle cross-bedded grainstone deposits, whereas Figure 4.47 shows the point data from high-angle cross-bedded grainstone deposits. The point-count data shows that the main

constituents of the varying grainstone facies include: monocrystalline quartz, calcareous red algae, polycrystalline quartz, chert, benthic foraminifera and reworked clastic grains. The proportions of each grain type significantly varies between deposits from <10% up to 30% to 50%.

The low-angle cross-bedded and laminated grainstone facies is made up of ca. 50 % clastic grains, such as monocrystalline and polycrystalline quartz and chert. The remaining grains are composed of calcareous red algae, benthic foraminifera and echinoderm plates. In comparison, the high-angle cross-bedded grainstone facies generally contains ca. 70 % clastic material with ca. 30 % calcareous red algae, benthic foraminifera and echinoderm plates.

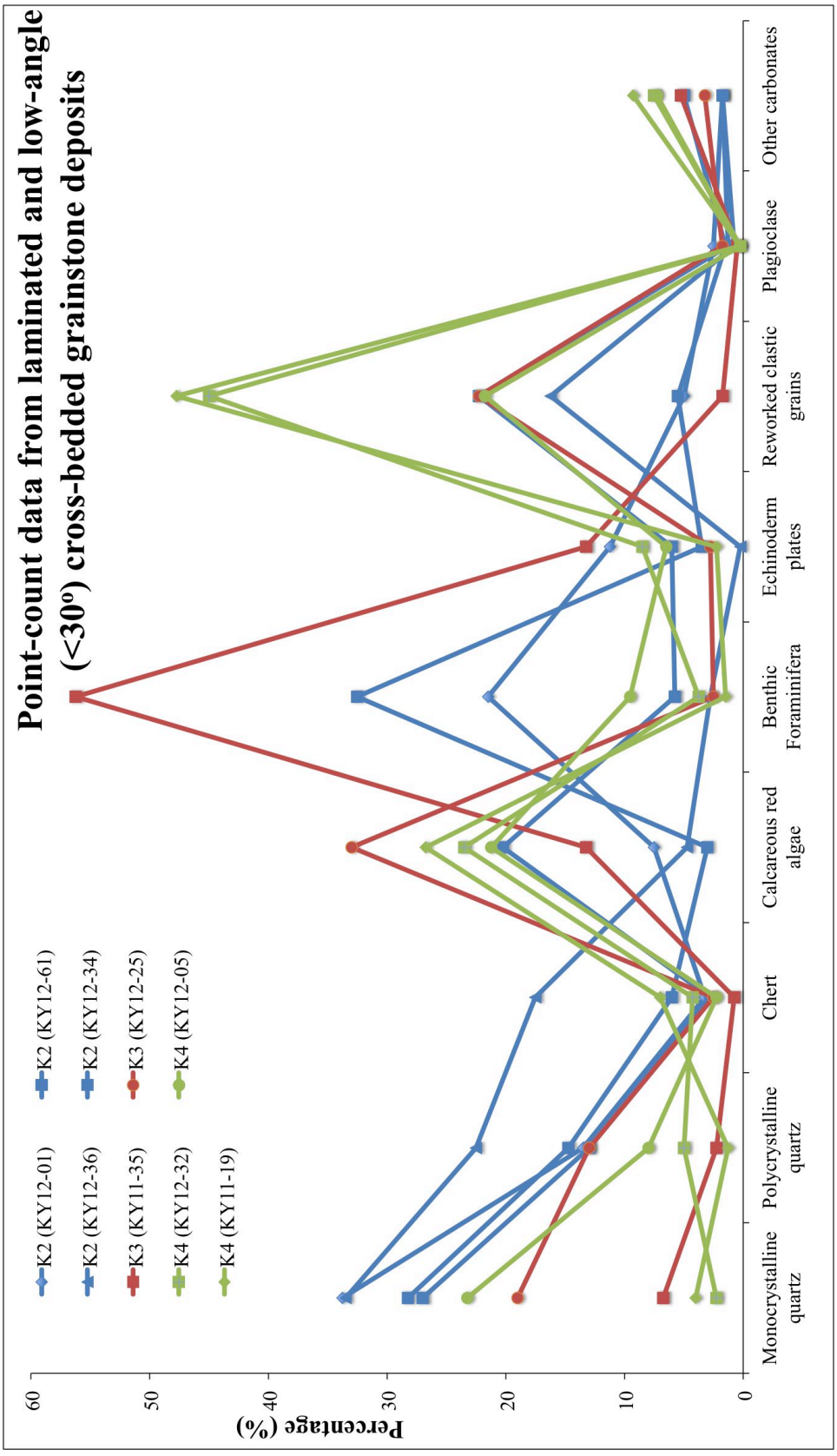

Figure 4.46: Point count data from K2 to K5 terrace grainstone deposits with sedimentary structures that include low-angle (<30°) cross-bedding, laminations and centimetre-scale bedding with normal grading.

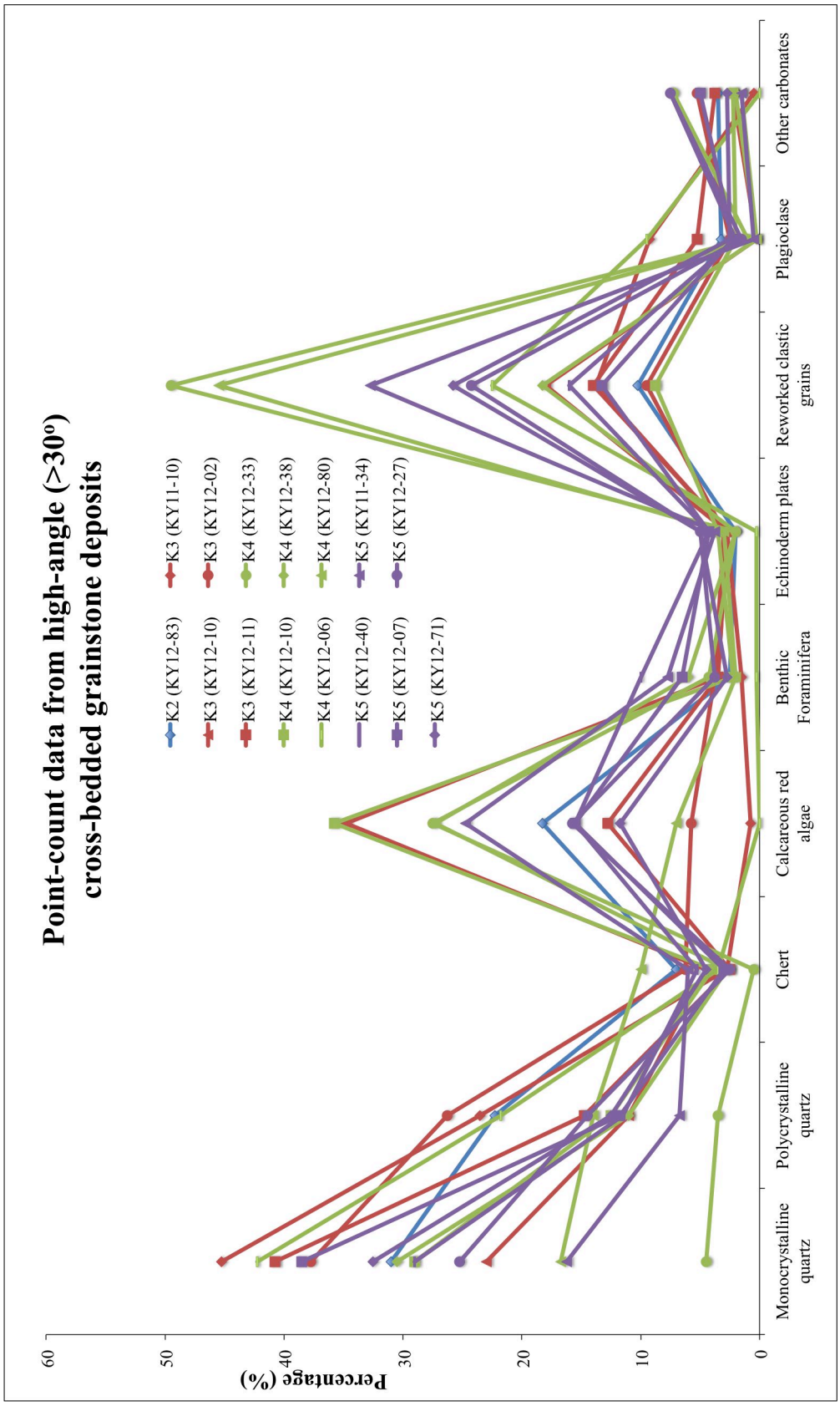

Figure 4.47: Point count data from K2 to K5 terrace grainstone deposits, which contain 1 m to 2 m-thick units of high-angle (>30°) cross-bedding.

4.8 Facies

The K2 to K5 terrace deposits on the northern side of the Kyrenia Range are made up of a series of grainstone, conglomerate, mudstone and palaeosol deposits. The range of facies associated with each of these deposits is discussed in the following section.

4.8.1 Grainstone deposits

Numerous grainstone facies form a major part of the K2 to K5 terrace deposits on the northern flank of the Kyrenia Range. Variations in grain composition, grain sorting and sedimentary structures are directly related to depositional processes. A summary of the various grainstone facies is now presented to constrain the various depositional environments represented.

Figures 4.48 and 4.49 summarise the various grainstone facies observed within the K2 to K5 terrace deposits. The grainstone facies preserved in the uppermost terraces (K2 and K3) are dominantly the E1 facies (Fig. 4.48). The E1 facies are preserved locally at the base of the terrace deposit and unconformably overlie the Kythrea (Değirmenlik) Group. The E1 facies deposits are well cemented and >40% of the facies comprises benthic foraminifera. The preserved E1 facies deposits are <2 m thick and laterally discontinouous, tapering out southwards towards main range. The E1 grainstone facies represent an offshore open-marine environment (Pedley and Grasso, 2002; Pedley and Carannante, 2006; Cornée *et al.*, 2012).

The E2 and E3 grainstone facies are observed within the K3 to K5 terraces. The E2 and E3 facies are are defined by laminations and low-angle (<30°) cross-bedding (Fig. 4.48). Compositionally, the grains making up the two facies are composed of varying amounts of clastic and bioclastic material. The E2 and E3 facies form 20 cm to 50 cm-thick interbedded units; in several localities ca. 3 m-thick deposits of E2 facies are observed. The E2 facies represent periods of relatively low-energy deposition of reworked bioclastic and clastic material. In contrast, the E3 facies represents a high-energy wave-dominated depositional setting. The interbedded E2 and E3 grainstone facies represent a shoreface or inner carbonate ramp environment (Clifton *et al.*, 1971; Pedley and Grasso, 2002).

The E4 and E5 facies are only preserved within the K4 terrace deposits at the coast (Fig. 4.48). The E4 facies is a bedded coarse-grained packstone deposit with well-developed normal grading. The packstone grains are composed of clastic and bioclastic material. The well-developed normal grading suggests rapid deposition by flow processes; in addition the large grain size of the packstone deposit suggests a relatively high-energy event. Rip-up clasts are often preserved within these deposits and are composed of the underlying lithologies further suggesting a short-lived, high-energy event. The combined features described within the E4 facies suggests that the packstone deposits represent short-lived high-energy storm events resulting in shallow-water tempestite deposits (Aigner, 1982). The normal grading of the grainstone with shallow-marine fauna and rip-up clasts are the key features that indicate a tempestite deposit, similar to the deposits from the Pleistocene carbonate shelf in Israel (Buchbinder and Zilberman, 1997) and the Lower Pleistocene deposits in Rhodes, Greece (Hansen, 1999).

The E5 packstone facies forms 5 cm to 10 cm-thick beds comprised dominantly of mollusc shells. The mollusc shells are predominantly gastropods with occasional bivalve shell fragments. The beds are well sorted with shells ranging from 0.5 cm to 1 cm in size, with no evidence of sedimentary grading. The dominance of mollusc shells within these deposits and the lack of sedimentary structures suggests a low-energy, lagoonal environment, similar to the shallowing carbonate lagoonal facies of the Sabkha Boujmel Formation in southeast Tunisia (Lakhdar *et al.*, 2006).

The E6 and E7 grainstone facies (Fig. 4.49) are observed within the K2 to K5 terraces on the northern flank of the range. The grainstone deposits making up the E6 and E7 facies are well sorted, medium- to fine-grained and contain well-rounded grains. Both grainstone facies contain abundant calcified palaeo-root traces. Both grainstone facies comprises >70% clastic grains. Reworked bioclastic material comprise <30% of the grains and include calcareous red algae, benthic foraminifera and echinoderm plates. The main distinction between the E6 and E7 facies is the shape and scale of the cross-bedding foresets. The E6 facies contains 1 m to 2 m-thick planar cross-bedding whereas, the E7 facies contains 1 m to 3 m-thick trough cross-bedding. The E6 planar cross bedding forms regular bedforms, whereas the E7 trough cross-bedding forms cross-cutting bedforms. The E6 facies cross bedding indicates palaeo-flow direction either towards the east or towards the west, parallel to the coast. In contrast, the E7 cross bedding has a large variation of palaeo-flow directions. The foresets in the E7 facies have a rela-

tively high angle of dip (ca. 45°), in contrast to the foresets in the E6 facies (30° to 45°).

The E6 and E7 grainstone facies represent carbonate aeolianite deposits from the K1 to K5 terraces on the northern flank of the Kyrenia Range (the K1 terrace grainstone is described in the Secction 3.4.4). The recognition of variations in sedimentological elements at various scales can be used to distinguish between a high-energy tidal environment and an aeolian environment (Frébourg *et al.*, 2008). A number of features can distinguish an aeolian environment (Frébourg *et al.*, 2008), including:

1. large foresets (>1 m-thick)
2. high-angle foresets (>30°)
3. landward-dipping foresets
4. root traces
5. vertebrate footprints or fossils
6. restriction to grainstone facies
7. well-rounded particles
8. mixed bioclasts representing different environments
9. planktonic and benthic foraminifera with micritic-filled chambers
10. vadose meniscus cements.

The list of facies characteristics as described by Frébourg *et al.* (2008), is based upon the study of 600 sections from present day, Holocene and Pleistocene deposits in Sardinia, Crete, southern Cyprus, Tunisia, Morocco, Australia and California. The aeolian grainstone characteristics are all observed in the E6 and E7 facies from the K1-K5 terraces.

Facies	Description	Geometry	Interpretations	Terraces
E1- Well cemented grainstone	Well-cemented grainstone. Compositionally these contain large amount of benthic foraminifera.	The deposit is generally <2 m thick and often unconformably overlies pre-Pleistocence unit.	The large amount of benthic foraminifera suggests an open marine environment.	K2-K3
E2- Laminated grainstone	Fine-grained and well-cemented grainstone. Compositionally the grainstones have varying proportions of clastic and bioclastic material.	Parallel laminations; forms 30-50 cm-thick units. Occasionally, laminated units are nearly 3 m-thick.	Periods of low energy sedimentation of reworked bioclastic and clastic material. The depositional environment was a shoreface zone.	K3-K5
E3- Low-angle cross-bedded grainstone	Medium- to coarse-grained grainstone that is compositionally similar to facies E1.	20 cm to 30 cm-thick crossbedded units dipping at <30° in multiple directions.	Wave-dominant in a shoreface environment.	K3-K5
E4- 5 cm to 10 cm-thick bedded packstone	Coarse-grained, clastic and bioclast-rich packstone. Clastic material is mainly metacarbonate and the bioclastic material are reworked mollusc shells. Occasionally within these beds there are rip-up clasts of basal lithologies or older lithified grainstones.	5 cm to 10 cm-thick beds with well-developed normal grading.	Shoreface environment with high energy currents transporting reworked clastic and bioclastic material. This is likely to represent short-lived storm events.	K4
E5- Mollusc-rich packstone	Packstone comprising >90% mollusc shells, predominantly 0.5 cm to 1 cm-sized gastropods.	5 cm to 10 cm-thick beds that are well sorted but with no sedimentary grading developed.	Lagoonal environment with relatively highly stressed marine conditions.	K4

Figure 4.48: Summary of the E1 to E5 grainstone facies from the K2 to K5 terraces on the northern flank of the Kyrenia Range (part 1) as described in Section 4.8.1.

Facies	Description	Geometry	Interpretations	Terraces
E6- High-angle planar cross-bedded grainstone	Well-sorted, fine- to medium-grained grainstone. (The composition of the grains is the same as the A5 facies). Calcified palaeo-root traces are preserved throughout the deposit.	1 m to 2 m-thick planar cross beded units. Cross-bedded units are separated by 30 cm-thick units of laminated grainstone. The palaeoflow direction of the cross-bedding is either toward the west or towards the east (parallel to the coast).	Onshore dune field with a palaeowind direction running parallel to the coast.	K2-K4
E7- 1 m to 3 m-thick trough cross-bedded grainstone	Medium- to fine-grained grainstone. Calcified palaeo-root traces are often preserved throughout the deposit. The grains are dominantely composed of siliciclastic and clastic material but also contain a minor component of bioclastic material.	1 m to 3 m-thick units of trough cross-bedding with forests that dip at over 30°. The palaeoflow direction varies significantly within and between the deposits.	Onshore dune field with multiple palaeowind directions.	K5

Figure 4.49: Summary of the E6 and E7 grainstone facies from the K2 to K5 terraces on the northern flank of the Kyrenia Range (part 2)as described in Section 4.8.1.

4.8.2 Mudstone, conglomerate and palaeosol deposits

The second major component of the K2 to K5 terraces on the northern flank of the range are interbedded mudstone, conglomerate and palaeosol deposits (Fig. 4.50, 4.51). The most common deposit within all the terraces is the F1 facies, which is a fine-grained, massive, structureless mudstone (Fig. 4.50). The fine grained nature of the F1 facies represents a low-energy depositional environment, such as a flood plain or overbank deposit within a fluvial system (Nichols and Fisher, 2007). Mudstone overbank deposits are well preserved in the Quaternary alluvial fans and terraces of the Himalayas, India (Thomas *et al.*, 2002; Suresh *et al.*, 2007).

The F2 and F3 conglomerates form lens-shaped beds within the F1 mudstone facies. The F2 and F3 conglomerate facies are both composed of sub-angular clasts of metacarbonate, chalk, basalt, chert, metacarbonate breccia, sandstone and mudstone. The F2 and F3 facies differ in the size of clasts and the dimensions of the lenses. The clasts within the F2 facies range from 1 cm to 20 cm, whereas those within the F3 facies range in size from 1 cm to 40 cm. The lenses within the F2 facies range in thickness from 10 cm to 40 cm and in length from 1 m to nearly 10 m. In contrast, the lenses within the F3 facies range in thickness from 1 m to 2 m and in length from 2 m to 4 m. In general, the F2 lenses are thin and elongate, whereas the F3 facies are short and thick. The F2 conglomerates lenses are well sorted, clast supported and show signs of poorly-developed normal grading. The F3 conglomerate lenses are generally organised in 10 cm to 30 cm-thick beds with well-sorted clasts. Outsized clasts, up to 40 cm in diameter, are preserved in both the F2 and F3 conglomerate facies. Both the F2 and F3 conglomerate facies have poorly developed clast imbrication indicating a general palaeo-flow direction away from the range.

The F2 and F3 conglomerate facies represent high-energy, channelised, muddy, debris-flow deposits (Coussot and Meunier, 1996), similar to those in the Beartooth Range in Wyoming and Montana, USA (DeCelles *et al.*, 1991). The sub-angular nature of the clasts and the lack of sedimentary grading within the lenses suggests rapid deposition with a short transportation distance. The elongate nature of the F2 facies lense suggests these deposits are mainly controlled by deposition. In contrast, the thick nature of the F3 facies suggests that these deposits require major incision prior to deposition. Both the F2 and F3 facies represent high-energy channels within a fluvial drainage system (Nichols and Fisher, 2007). The interbedded F1 to F3 facies are

comparable to drainage systems in numerous other regions including the Quaternary evolution of the Himalayas (Thomas *et al.*, 2002; Starkel, 2003) and the Montserrat fan delta, Spain, an Eocene aged fluvial system that responded to changes in sea-level (Burns *et al.*, 1997).

The F4 palaeosol facies is found interbedded within the F1 to F3 facies, and occasionally within the E7 facies (Fig. 4.50). The palaeosols are fine grained and range from 20 cm to 40 cm in thickness. The palaeosols range in colour from light-brown to dark reddish-brown and occasionally to dark red. A number of the palaeosol horizons have well developed caliche formation. Palaeosol (or fossil soils) form during periods of relative landscape stability (Kraus, 1999). Further analysis could be carried out on palaeosols in order to correlate them with either glacial or interglacial climatic conditions e.g. clay minerals, major and minor element ratios, carbon isotopes and numerous other factors (Sheldon and Tabor, 2009). However, for the purposes of this thesis the palaeosols are inferred to indicate periods of landscape stability (low-erosion conditions) and help correlate between terrace deposits (Section 4.9).

The F5 facies is a 7 m-thick cross-bedded gravel with sub-rounded to well-rounded clasts, ranging in size from 1 cm to 5 cm (Fig. 4.50). The facies is only preserved as part of the K4 terrace near the coast. The cross bedding forms 30 cm to 50 cm-thick units that have a cross-cutting relationship. Outsized clasts are preserved within the deposit, ranging in size from 10 cm to 30 cm. The clasts are mainly composed of metacarbonate but more rare clasts of chalk, chert and basalt are also present.

The F5 facies represents a Gilbert-type delta deposit (Gilbert, 1885, 1890; Bates, 1953) with a number of the typical features present including: homopycnal inflow by non-marine fluvial systems into an offshore environment, coarse gravels with foresets and fine sand and silt within the gravel. The evidence for homopycnal inflow are cross-cutting gravel foresets running parallel to the coast, indicating deposition in response to fluvial-tidal interactions (Bates, 1953; Colella *et al.*, 1987).

Interbedded with the F5 gravel facies is the F6 conglomerate facies (Fig. 4.51), forming a 2 m-thick laterally continuous bed. The F6 conglomerate is clast supported and is poorly sorted with clasts from 1 cm to nearly 2 m in size. The largest (metre-sized) clasts are made up of grainstone whereas the smaller (centimetre-sized) clasts are made up of metacarbonate, chert, chalk and basalt. The clasts are all sub-angular

to sub-rounded. The grainstone clasts contain well-preserved biogenic material such as *in situ* corals, molluscs and serpulid worms. The poorly sorted nature of the deposit suggests that it is locally reworked; also, the abundance of marine biota suggests a reworked marine horizon. Therefore, the F6 conglomerate facies represents a reworked marine horizon within the F5 Gilbert-type delta facies.

The F7 conglomerate facies (Fig. 4.51) is preserved within the K4 and K5 terraces proximal to the northern coast. The F7 conglomerate facies is matrix supported and is composed of sub-rounded to well-rounded clasts, ranging in size from 10 cm to 30 cm and also containing rip-up clasts of packstone and grainstone, metacarbonate, chalk, chert and basalt. The conglomerate matrix is made up of a medium-grained to coarse-grained grainstone. The deposit is always preserved in association with the E4 grainstone facies. The F7 facies conglomerate represents high-energy storm events that result in rip-up clasts of the semi-lithified E2-E4 grainstone facies and reworking of clastic material from the onshore environment.

The F8 conglomerate facies (Fig. 4.51) is only preserved within the K4 terrace proximal to the northern coast. The conglomerate facies is a planar-bedded conglomerate, varying in thickness from 2 m to nearly 7 m, with well-rounded clasts. The clasts range in size from 1 cm to 10 cm and are well rounded and well sorted within each bed. The clasts are mainly metacarbonate but chalk, chert, sandstone and mudstone are also present. The conglomerate is clast supported but has a medium-grained, poorly-lithified, carbonate sand matrix. The conglomerate beds range in thickness from 10 cm to nearly 1 m and are laterally continuous within the deposits. Interbedded within the deposit are poorly lithified E1 and E3 grainstone facies with occasional overlying E6 facies grainstone and palaeosol deposits. Well-developed clast imbrication suggests a westerly palaeocurrent direction, parallel to the coast. Large, 1 m to 3 m-sized blocks of well-sorted and medium-grained grainstone are occasionally preserved within the lower part of the F8 conglomerate facies deposit.

The F8 conglomerate facies represents an upper-shoreface depositional environment (Bourgeois and Leithold, 1984). A number of key features can be used to interpret the F8 facies environment, including the well-rounded nature of the clasts, the interbedded grainstone facies, the tabular sheet-form nature of the conglomerate beds, the thickness of the conglomerate beds, the clast-supported nature of the beds and the size of

conglomerate clasts (Clifton, 1973; Bourgeois and Leithold, 1984).

The interbedded F9 and F10 facies (Fig. 4.51) are preserved within the K4 terraces near the northern coast. The F9 bioclastic conglomerate facies is mostly less than 50 cm thick and is composed of well-rounded clasts of clastic and bioclastic material. The clastic material includes varying amounts of reworked metacarbonate, mudstone, chert, diabase and serpentinite. The bioclastic material includes *in situ* and reworked *Cladocora* coral, bivalves (including *Spondylus*), gastropods, calcareous algae and serpulid worm tubes. Trace fossils are also preserved within the F9 facies in the form of occasional heavily bored clasts. The F10 facies is a fine- to medium-grained marl with poorly preserved, ca. 10 cm-thick beds with normal grading. The marl deposit contains 1 cm to 30 cm-sized, well-rounded outsized clasts and occasional 2 m to 3 m-sized blocks. The outsized clasts are composed of metacarbonate, chalk, chert, serpentinite and diabase, whereas the large blocks are always fine to medium grained grainstone. The observed combination of *Cladocora* coral and the mollusc *Spondylus* represent warm water conditions, as described in south east Sicily during the Early Pleistocene (Pedley and Grasso, 2002).

Reworked and *in situ* solitary *Cladocora* coral are preserved in numerous K4 marine deposits. *Cladocora* coral are also preserved within the Athalassa deposits in northern Cyprus (Sec. 2.7.2) and southern Cyprus (McCallum, 1989), and within the Pleistocene marine terraces in southern Cyprus (Poole *et al.*, 1990). Modern examples are found off the coasts of Israel, Italy and Morocco (Zibrowius, 1980). Álvarez-Pérez *et al.* (2005) describe *Cladocora* coral that live at depths at 23 m to 219 m below sea-level in the Straits of Gibraltar, with most specimens being found between 114 m to 219 m below sea-level. Therefore, the presence of *Cladocora* corals within the stratigraphy suggests a marine environment that was at least 100 m deep.

The interbedded F9 and F10 facies represent a marine transgression causing reworking of older well-rounded conglomeratic deposits. The marine transgression resulted in an open-marine environment that was deep enough for solitary coral to grow. The marine transgression resulted in the reworking of the older grainstone deposit into large blocks within the marl unit.

Facies	Description	Geometry	Interpretations	Terraces
F1- Fine-grained mud-stone	Fine-grained to medium-grained mud-stone	Massive and structure-less deposit	Low-energy deposition within a fluvial envi-ronment.	K2-K5
F2- Clast-supported conglomerate (<40 cm-thick lenses)	Conglomerate with sub-angular clasts ranging in size from 1 cm to 20 cm. Clasts are moderately to well sorted within lenticular shaped beds. The clasts are mainly metacar-bonate but include chalk, basalt, chert, metacarbonate breccia, sandstone and mud-stone.	Conglomerate forms lenticular shaped beds within the mudstone. Lenses range in size from 10 cm to 40 cm-thick and from 1 m to nearly 10 m long. Poorly-developed normal grading is often observed.	Conglomerate channels representing pulses of deposition during derbis flows events.	K2-K5
F3- Clast-supported conglomerate (>1 m-thick lenses)	The clasts within the conglomerate range in size from 1 cm to 40 cm and are sub-angular to angular in shape. The clasts are composi-tionally the same as the F2 facies (above).	Conglomerate within lenticular-shaped beds that are 1 m to 2 m-thick and 2 m to 4 m-long. The lenses are made up of 10-30 cm-thick beds that are moderately to well sorted.	High-energy channels that caused major incision within a fluvial depositional environ-ment.	K2-K4
F4- Palaeosol	Fine-grained palaeosol ranging in colour from dark-maroon to red. Caliche is preserved in several horizons.	The palaeosols form horizontally continuous beds within the mud-stone and conglomer-ate deposits.	Preserved soil horizons represent a period of landscape stability.	K2-K4
F5- Cross-bedded gravel	Conglomerate with clasts ranging in size from 1 cm to 5 cm. Beds within the con-glomerate are well sorted. Clasts are sub-rounded to well-rounded in shape. Clasts are dominantly composed of metacar-bonate of the Tripa (Trypa) Group.	Low-angle, 30 cm to 50 cm-thick, cross-bedded units. Outsized clasts range in size from 10 cm to 30 cm are occasionally pre-served.	Gilbert-type deltaic environment.	K4

Figure 4.50: Summary of the F1 to F5 mudstone, conglomerate and palaeosol facies from the K2 to K5 terraces on the northern flank of the Kyrenia Range (part 1) as described in Section 4.8.2.

Facies	Description	Geometry	Interpretations	Terraces
F6- Grainstone boulder conglomerate	Conglomerate clast size range from 1 cm to nearly 2 m. The clasts are dominantly well-cemented grainstone. The grainstone contains well preserved corals, molluscs and serpulid worm tubes. The clasts are generally elongate.	The deposit is ca. 1 m thick (2 m-sized clasts are elongate and orientated parallel to bedding). The facies forms a horizontally continuous bed within the F5 facies.	Offshore marine in a younger high-energy environment such as a deltaic or fluvial system.	K4
F7- Conglomerate with reworked clastic and bioclastic material.	Conglomerate clasts are composed of reworked grainstone and packstone, metacarbonate, chalk, chert and basalt. The deposit contains a medium-grained to coarse-grained, well-lithified carbonate sand matrix. Clasts range from 1 cm to 30 cm and are sub- to well-rounded.	The deposit forms 30 cm to 50 cm-thick beds within the lower parts of the E2, E3 and E4 grainstone facies.	Storm deposits reworking lithified grainstone and inputing clastic material from onshore.	K4-K5
F8- Conglomerate with well-rounded clasts.	Clast-supported conglomerate with well-rounded, imbricated clasts. The clasts range in size from 1 cm to 10 cm and are well sorted. The clasts are compositionally the same as the F3 facies.	Conglomerate comprises a series of parallel, 20 cm to 30 cm-thick beds. The conglomerate is generally interbedded with E1 and E3 grainstone facies.	Upper shoreface depositional environment	K4
F9- Conglomerate is made up of well-rounded clastic and *in situ* biogenic material.	Conglomerate that ranges from clast to matrix supported and is composed of well-rounded clastic and biogenic material. The clastic material includes metacarbonate, mudstone, chert, diabase and serpentinite. The biogenic material includes: *in situ* coral, pectens and oysters, gastropods, calcareous algae and serpulid worm tubes.	Conglomerate forms laterally-continuous beds within the deposit, ranging from 2 to 5 m-long. The deposit ranges in thickness from 30 cm to 1 m. Interbedded with the F10 marl facies.	Maximum flooding surface, reworking older conglomerate facies and depositing biogenic material.	K4
F10- Marl	Fine to medium grained marl. The marl contains reworked, 1 cm to 2 cm-sized mollusc shells. Outsized clasts range in size from 1 cm to 30 cm.	The marl deposit ranges in thickness from 50 cm to 2 m. The marl is often interbedded with the F9 conglomerate facies.	Low-energy marine environment.	K4

Figure 4.51: Summary of the mudstone, conglomerate and palaeosol facies from the K2 to K5 terraces on the northern flank of the Kyrenia Range (part 2) as described in Section 4.8.2.

4.9 Correlations of sedimentary deposits within each terrace system

The terraces were originally mapped as geomorphological features according to height above sea level (Ducloz, 1964; Baroz, 1979). While remaining largely valid, this approach does not take account of the sedimentary deposits associated with each terrace. In many areas the sedimentary stratification dips significantly seawards, such the terraces of the same age may occur at different topographical levels. An example of this is the K3 terrace, which comprises deposits that range from 30 to 70 m AMSL (as described by Baroz, (1979)); however, the later mapping of Knup (1965) distinguished these deposits as different terraces.

The terrace deposits, as described in the previous sections, can be correlated to help define the depositional environments represented by each terrace system. The terraces form discontinuous surfaces on the northern side of the Kyrenia Range making stratigraphic correlations difficult based of direct sedimentary relationships, particularly for the older terraces. Figures 4.52 to 4.54 summarise logs from all of the terrace deposits with a comparison of their heights above modern sea-level.

Recognition of terraces makes use of a combination of: 1) height above modern sea level; 2) relative height change compared to surrounding terraces; 3) sedimentology of terrace deposits; and 4) sedimentary relationships between terrace deposits. This terrace correlation method depends upon the preservation quality of the terrace deposits. The lower K4 and K5 terraces comprises well-preserved deposits along the northern flank of the range. However, the older K2 and K3 terraces are less well preserved, therefore less key sedimentary relationships are observed within these upper terrace systems. Consequently, a larger error is associated with the older terraces when making correlations based upon height above sea-level, terrace facies and sedimentary relationships.

A number of issues are clear with a facies based correlation method including diachronous deposits within each terrace system and faulting related to uplift, which could offset contemporaneous deposits. Equivalent facies within each terrace could be of different ages, for example fluvial deposition is unlikely to be contemporaneous within each terrace system. However, in the lower terraces several key relationships are ob-

served such as interbedded fluvial and marine deposits, which can be used to constrain the relative timings of deposition. Secondly, although faulting related to uplift is a possibility for offsetting terrace deposits, no evidence of Pleistocene-aged faulting in the Kyrenia Range was observed.

4.9.1 K2

The K2 terrace forms a major, discontinuous terrace surface running east-west, parallel to the Kyrenia Range, between 140 m and 180 m AMSL (Fig. 4.52). K2 terrace deposits are only found on a few of the terrace surfaces; the other correlated surfaces have no preserved deposits. The preserved deposits represent a range of marine (M2) and non-marine (C2) environments. The basal parts of the sections are mostly made up of marine deposits conformably overlain by non-marine deposits. The non-marine deposits range from fluvial to aeolian environments.

The marine deposits (M2) that can be correlated within the K2 terrace representing an open-marine environment and the oldest part of the K2 terrace system. Palaeosol horizons are found within several of the K2 fluvial deposits, allowing a correlation of these deposits. The aeolian deposits predate the fluvial system because the aeolianite underlies the fluvial system at numerous localities (Fig. 4.52: Agios Amvrosis (Esentepe) and Davlos (Kaplıca)).

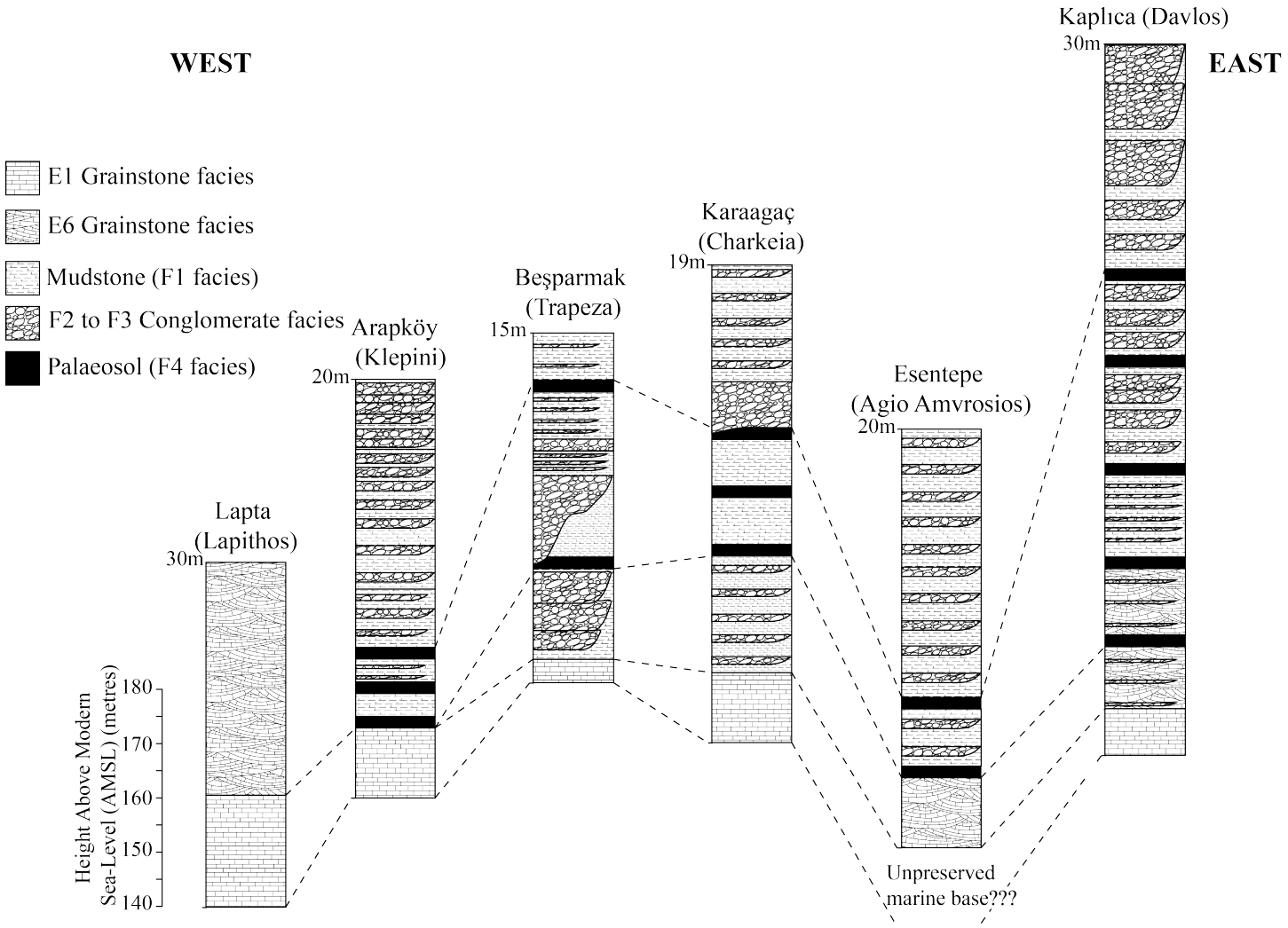

Figure 4.52: Summary logs from the K2 terrace deposits on the northern flank of the Kyrenia Range, with heights above modern sea-level from the base of each section shown by the scale of the left and the deposit thickness labeled on each log. Interpreted correlations are marked by the dashed lines.

4.9.2 K3

The K3 terrace deposits show a significant variation in height above modern sea-level, ranging from 40 m to nearly 150 m AMSL (Fig. 4.53). The K3 terrace forms a northward-dipping surface between the K2 and K4 terraces, resulting in a large variation in the height of these terrace deposits. Agios Epikitos (Çatalköy) is the only locality where the basal marine deposit of the K3 terrace is preserved, at ca. 58 m AMSL. The non-marine deposits are made up of both fluvial and aeolian facies. The Agios Epikitos (Çatalköy) deposit shows a transition from marine grainstone to aeolian grainstone; whereas, the Arapköy (Klepini) section shows a transition from aeolianite to fluvial deposits. These two localities indicate a similar environment of deposition to the K2 terrace, with aeolian deposits directly following marine deposits and, in turn directly followed by fluvial deposits.

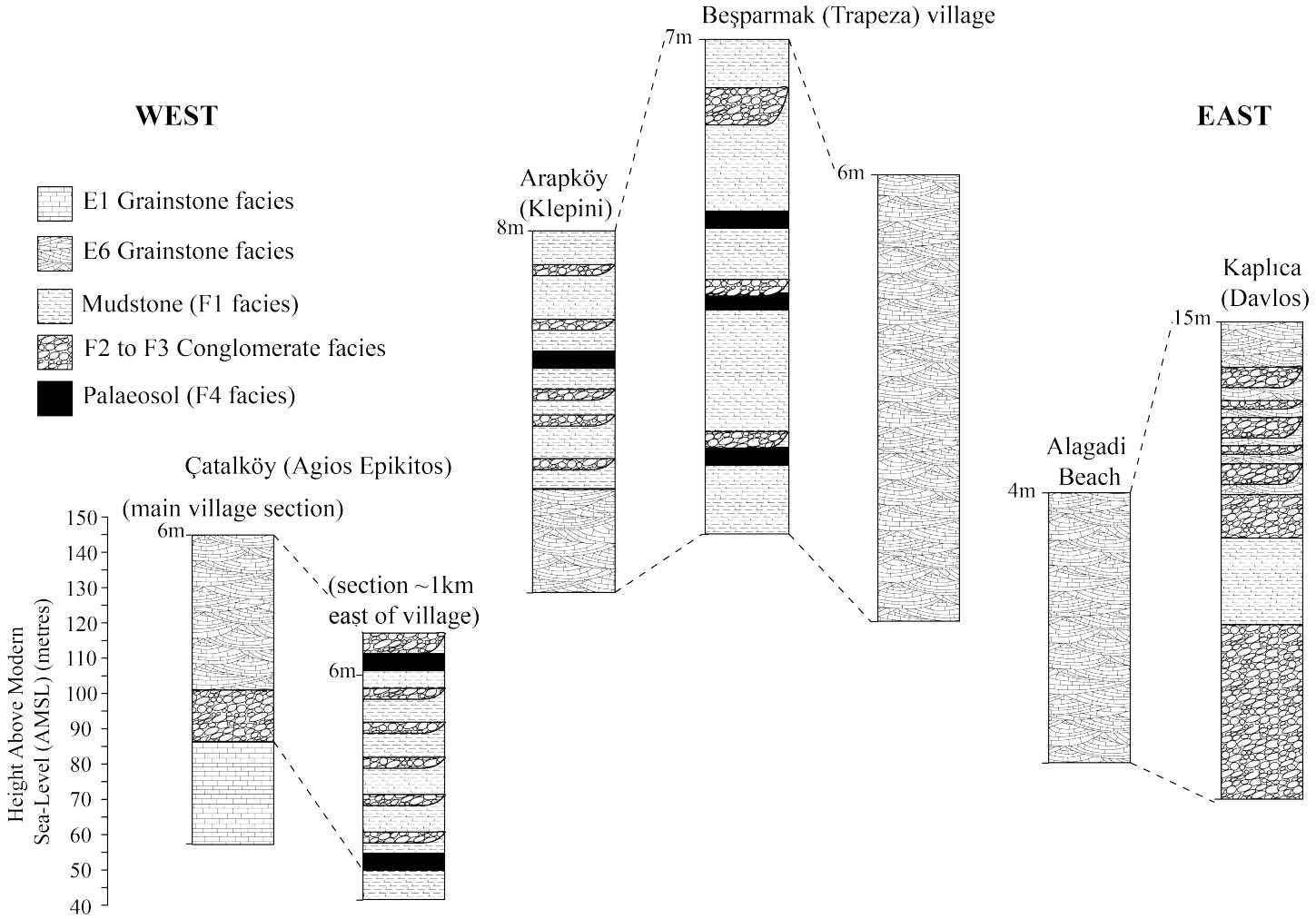

Figure 4.53: Summary logs from the K3 terrace deposits on the northern flank of the Kyrenia Range, with heights above modern sea-level from the base of each section shown by the scale of the left and the deposit thickness labeled on each log. Interpreted correlations are marked by the dashed lines.

4.9.3 K4

The K4 terrace is the most extensively preserved terrace system in the north of Cyprus. The terrace surface is discontinuous along the northern coast. The terrace is dissected by younger fluvial channels forming gullies that expose the three-dimensional structure of the terrace. The deposits include marine facies ranging from shallow-marine, to beach, to deltaic systems. The non-marine deposits represent aeolian to fluvial depositional environments. The basal marine deposits range in height from 0 to ca. 40 m AMSL (Fig. 4.54).

The K4 marine grainstone deposits form the basal part of the terrace at the lowest heights above sea-level (<15 m AMSL), proximal to the northern coast. Interbedded with the marine grainstone deposits are the deltaic deposits (Fig. 4.54: Charkeia (Karaağaç) and Esentepe (Agios Amvrosios)). Inland at several localities, are well-preserved beach deposits (Alagadi beach) at equivalent heights above sea-level to the coastal marine grainstone, implying that these can be correlated as contemporaneous environments.

The non-marine deposits represent aeolian and fluvial environments. In most examples, the aeolian deposits conformably overlie the marine grainstone at the coast and continue inland between 1-2 km. The fluvial deposits are preserved at the same height as the aeolian grainstone deposits and conformably overlie the coastal deltaic deposits (Fig. 4.54: Esentepe (Agios Amvrosios)). The K4 deposit at Mersinlik indicates a later stage of aeolianite development that conformably overlies the fluvial deposit.

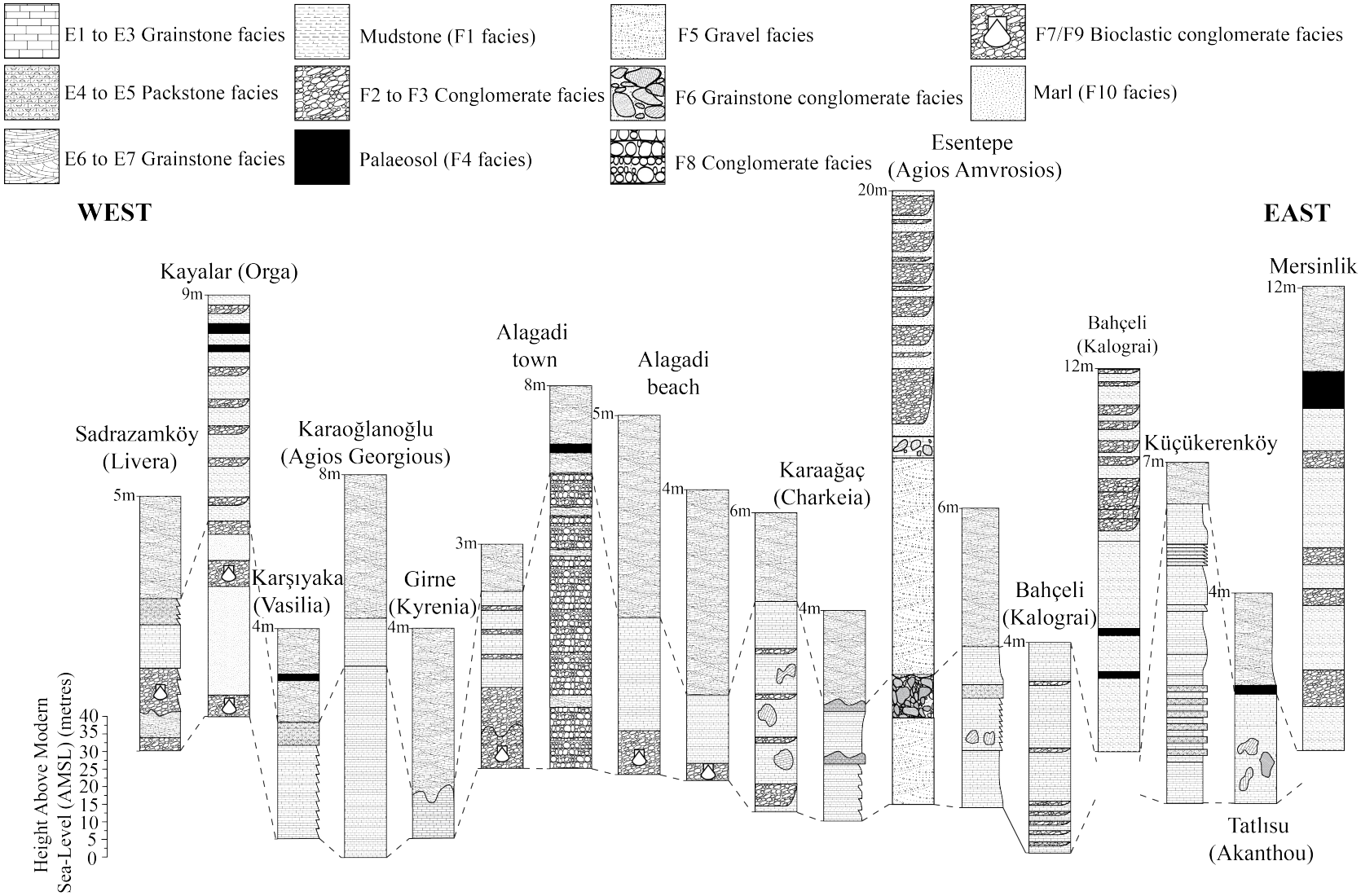

Figure 4.54: Summary logs from the K4 terrace deposits on the northern flank of the Kyrenia Range, with heights above modern sea-level from the base of each section shown by the scale of the left and the deposit thickness labeled on each log. Interpreted correlations are marked by the dashed lines.

4.9.4 K5

The K5 terrace is dominantly made up of carbonate aeolianite (C5), which occurs discontinuously along the northern coast, between 0 and 5 m AMSL. At several localities, a marine deposit (M5) is preserved as a marine transgression within the C5 aeolianite. The lack of continuity of the K5 terrace along the coast reflects patchy deposition rather than erosion. At a few localities the C5 aeolianite overlies the K4 terrace (Sec. 4.6.7, Fig. 4.42), but elsewhere the base of the aeolianite is below modern sea-level.

4.10 Discussion

4.10.1 Terrace depositional systems

Each of the individual terraces (K2 to K5) represents a complex depositional system that was active during the Pleistocene. New data on the Pleistocene sediments on the northern flank of the Kyrenia Range are used to describe how the depositional environment responded to tectonic and eustatic controls.

The K2 to K5 Pleistocene terraces on the northern flank of the Kyrenia Range are composed of both marine and non-marine deposits. The marine deposits within the K2 to K3 terraces are represented by grainstone deposits; in contrast in the K4 and K5 terraces the marine deposits include both grainstone deposits and bioclastic conglomerates. The non-marine deposits in the K2 to K5 terraces include both aeolian and fluvial facies. The marine deposits form the base of all the terraces and are conformably overlain by the non-marine deposits. The basal marine deposits forms a thin discontinuous deposit at the northern end of the K2 to K4 terrace systems. In contrast, the non-marine deposits generally form a thicker deposit, which varies in width from 100 m to >1 km.

The marine deposits in the K2 and K3 terraces is only exposed at a few localities as a poorly preserved grainstone deposit. The grainstone facies preserved within the K2 and K3 terraces contain a large proportion of benthic foraminifera, implying an open-marine environment. The benthic-foraminifera-rich grainstone facies in the K2 and K3 terrace deposits are overlain by non-marine deposits. The marine deposits within the lower K4 and K5 terraces represent a range of marine and coastal environments. In several localities the base of the marine deposit comprises a bioclastic conglomerate. The basal bioclastic conglomerate is composed of bioclastic material, including heavily reworked solitary corals, mollusc shells, calcareous algae and clastic material including semi-lithified grainstone, packstone and reworked lithologies from the Trypa (Tripa), Lapithos (Lapta) and Kythrea (Değirmenlik) Groups. This basal bioclastic conglomerate represents a conglomerate lag, which is reworking material from a maximum flooding surface.

Directly overlying the conglomerate lag is a well-preserved grainstone deposit, which represents a shoreface environment. The grainstone deposit is often rich in reworked cal-

careous red algae, benthic foraminifera and echinoderm plates. The range of reworked biogenic material indicates that the deposits that were formed in an offshore (relatively deeper marine) environment and were later reworked by wave action to form shoreface grainstone facies. The coastal marine deposits within the lowest terraces represent a regressive sequence following a major transgressive phase.

At several localities lagoonal grainstone facies are preserved, interbedded with shoreface grainstone facies. The lagoonal facies are dominated by molluscs, dominantly gastropods with occasional bivalves. This facies represents a small coastal lagoon within the K4 terrace.

Non-marine deposits are extensively preserved within all of the K2 to K5 terraces on the northern flank of the Kyrenia Range. The deposits range from aeolian facies to fluvial depositional systems. The aeolian-grainstone deposits are composed of clastic and bioclastic material, indicating reworking of the older Pleistocence marine deposits, and underlying lithologies. Sedimentary structures vary throughout the terrace sequence; the upper terraces (K2 and K3) tend to be planar cross-bedded, whereas the lower terraces (K4 and K5) are generally trough cross-bedded. The planar cross-bedding indicates a planar dune-crest, whereas the trough cross-bedding indicates a sinuous dune-crest, both dune crests run approximately parallel to the range. The sinuous trough cross-bedded aeolianite facies is most commonly preserved in the K5 terrace, near the present day coast.

The K5 terrace is dominantly made up of a trough cross-bedded carbonate aeolianite. The K5 carbonate aeolianite is preserved discontinuously along the northern coast and represents a major phase of aeolian deposition. The base of the aeolianite deposit is often below modern sea-level, indicating a relative increase in sea-level since the deposition of the aeolianite. The K5 aeolianite is generally restricted to the coast but occasionally continues inland for up to ca. 100 m.

Carbonate aeolianites are commonly found during the Pleistocene at mid-latitudes within arid to semi-arid environments (Brooke, 2001). Equivalent deposits from the Pleistocene have been identified as part of coastal terrace studies in Syria (Dodonov *et al.*, 2008), southern Italy (Zecchin *et al.*, 2004), southern Spain (Zazo *et al.*, 1999), Bermuda (Hearty, 2002) and southern Cyprus (Poole and Robertson, 2000). In most of these examples the carbonate aeolianite overlies a marine deposit, representing a similar

a relationship to that observed in northern Cyprus.

Fluvial systems are preserved in the K2 to K5 terraces on the northern flank of the range. Several fluvial drainage systems have been identified throughout all the terraces; these include those at Arapköy (Klepini), Beşparmak (Trapeza), Karaagaç (Charkeia), Esentepe (Agios Amvrosios) and Kaplıca (Davlos). The fluvial systems are composed of mudstone deposits interbedded with channelised conglomerates and palaeosols. The mudstone deposits are fine-grained and structureless and form <1 m-thick beds between conglomerate channels. The channels range in length from 1 m to 8 m and in thickness from 30 cm to ca. 2 m. The clasts within all of the conglomerate channels are sub-angular and range in size from 1 cm to 30 cm; this suggests the depositional energy was similar within all of these deposits. The deposits represent the proximal to medial zone of a relatively small (<5 km wide) fluvial distributary system (Nichols and Fisher, 2007).

The fluvial systems at the most northerly edge of the K4 terrace are occasionally interbedded with the marine and lagoonal grainstone facies. The relationships between the fluvial drainage systems are preserved as small conglomerate channels within the lagoonal grainstone facies or as deltaic deposits. The conglomerate channels within the lagoonal facies represent the coastal output of the drainage systems of the K4 terrace marine environment. The deltaic deposit preserved at Esentepe (Agios Amvrosios) represents the coastal component of the major drainage system of the K4 terrace. Part way up the deltaic deposit there is a reworked marine grainstone deposit with well-preserved *in situ* solitary coral indicating a maximum flooding surface caused by a major marine transgression. Within the the upper part of the deltaic gravel deposit there is a second marine-grainstone deposit representing a second marine transgression. The upper marine deposit is overlain by a fluvial facies deposit representing a non-marine environment. The deltaic deposit at Esentepe (Agios Amvrosios) responded to numerous changes in sea-level including transgressive phases with low clastic input that allowed marine fauna to accumulate, followed by a major marine regression causing a switch to non-marine, fluvial deposition.

The K2 to K4 terraces form a series of separate depositional systems, which include marine, aeolian and fluvial facies. The K5 terrace is dominantly composed of carbonate aeolianite facies with occasional well-preserved interbedded marine and fluvial facies. The K2 to K4 terraces each represent a regressive sequence from a marine to a non-marine depositional environment. The marine deposits formed during the time of the

previous terrace, i.e. the marine deposits associated with the K3 terrace formed during the deposition of the K2 non-marine facies. The marine deposits were uplifted above sea-level and reworked into the coastal carbonate aeoliante contemporaneously with the deposition of fluvial facies (Fig. 4.55). This process was "frozen" and preserved within the terrace prior to the uplift of the younger marine horizon, which restarts the process again within a younger terrace (Fig. 4.56). The final product is a series of regressive sedimentary sequences preserved within each terrace system.

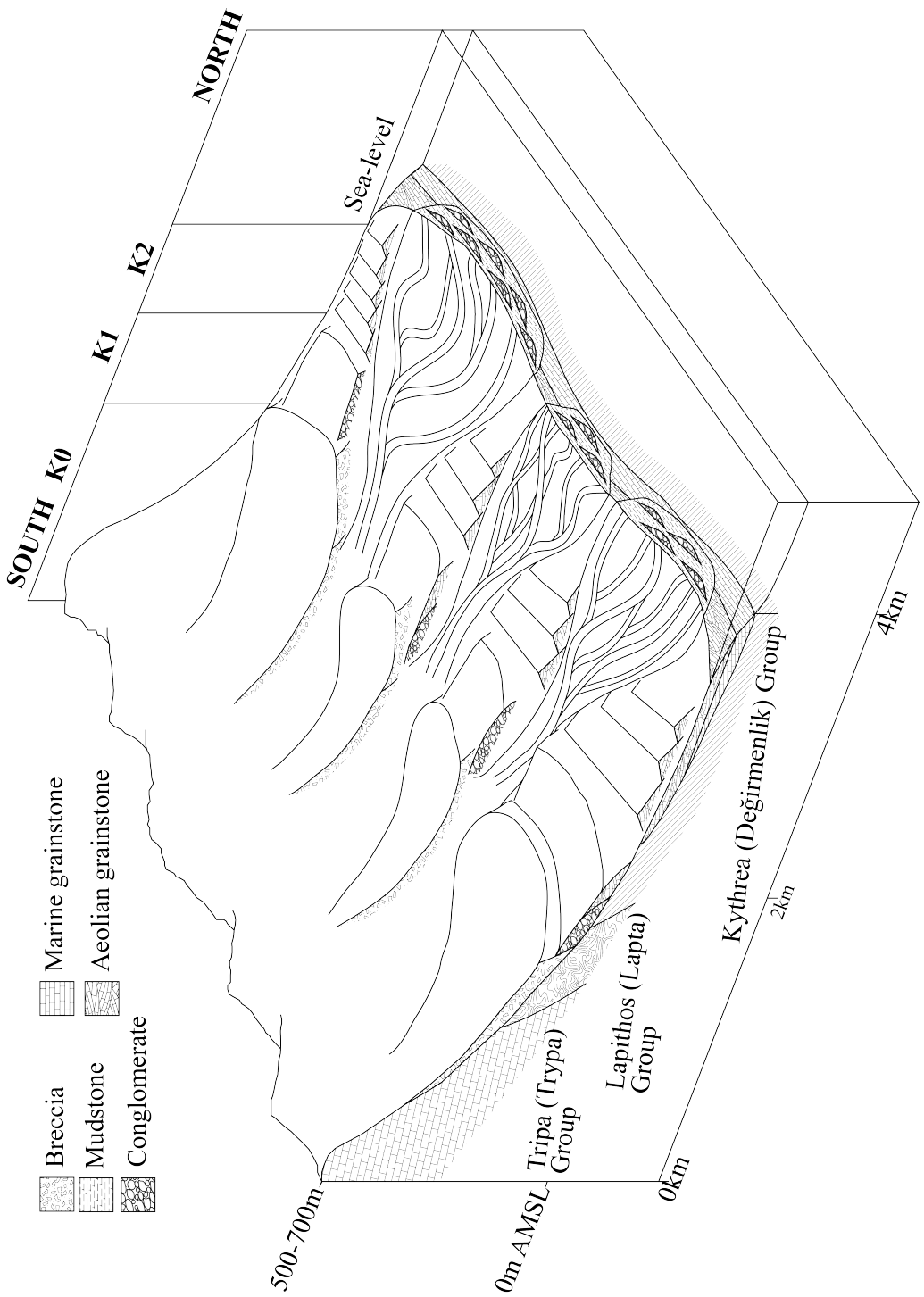

Figure 4.55: Block diagram showing the depositional environment of the K2 terrace.

Figure 4.56: Block diagram showing the depositional environment of the K4 terrace.

4.11 Conclusions

1. The K2 to K5 terraces are composed of both marine and non-marine facies.
2. The marine facies comprise grainstone deposits representing open-marine, shoreface and lagoonal environments.
3. Bioclastic conglomerates contain well-preserved solitary corals representing the maximum flooding surfaces resulting from marine transgressions.
4. Non-marine environments include aeolian deposits and fluvial drainage systems.
5. The aeolian deposits comprise reworked marine grainstone and aeolian-derived basal sediment.
6. The fluvial systems comprise conglomerate channels and flood plain deposits.
7. The conglomerate channels range from short-lived, high-energy debris-flow deposits to more developed channels that formed over longer periods of time.
8. Occasionally, the coastal component of the fluvial systems are preserved as deltaic deposits or channels with the lagoonal environment.
9. Within each terrace, a marine transgression and a later marine regression have been preserved and subsequently uplifted.

Chapter 5

Optical luminescence data from the K4 and K5 terrace deposits in northern Cyprus

5.1 Introduction

Field investigations show that the deposits associated with the K4 and the K5 terrace systems have a patchy distribution along the northern coast, occasionally extending up to ca. 1 km inland. Previously, the terraces were correlated and assigned to temporal subdivisions mainly based on their height above modern sea level (Ducloz, 1964; Baroz, 1979). In principle, terraces of the same relative age can occur at different topographic heights above sea level in different outcrops. It is also possible that faulting could have offset terraces of different ages. For example, the K5 terrace deposits are discontinuously exposed along the coast, which could either be caused by patchy deposition, variable preservation, or by the effects of faulting. Prior to any quantitative work on the timing of uplift of the terraces it is, therefore, essential to establish the basic sedimentary characteristics and the lateral correlations of the two terrace systems.

Marine and non-marine terraces are presented locally along the northern and southern flank of the range. These terraces were partially mapped and roughly correlated along both flanks of the range by Ducloz (1964), again based mainly on relative topographic height. However, the terrace deposits are patchily exposed and spatially

isolated within each terrace system.

This chapter aims to use new field luminescence data (Sec. 1.4.2) from the K4 and K5 terraces to further develop the sedimentary interpretations from the previous chapters. In addition, as a tool for correlating the K4 and K5 terrace deposits on the northern and southern flanks of the range. The following section presents a brief summary of the sedimentology of the nine sections (Fig. 5.1) selected for luminescence analysis. This is followed by a description of the portable luminescence results from each section. The sedimentary logs are presented alongside the luminescence profiles for clearer comparisons in later sections. The nine sections were selected to represent the range of deposits observed within the K4 and K5 terraces, which include marine and non-marine grainstone facies, fluvial deposits and palaeosols. The range of lithologies is required because quantitative correlations of terraces must account for the various facies observed within each terrace system.

5.2 Terrace deposits

Within the K4 and K5 terrace systems nine sections were selected encompassing a wide range of sediment types that are located along the coast some distance inland and also on the southern flank of the Kyrenia Range (Fig. 5.1). For each section, the higher-level K4 terrace deposits are described first, followed by the K5 terrace deposits, where present, moving from west to east. Unless otherwise stated the grainstone deposits are lithified and have a carbonate cement.

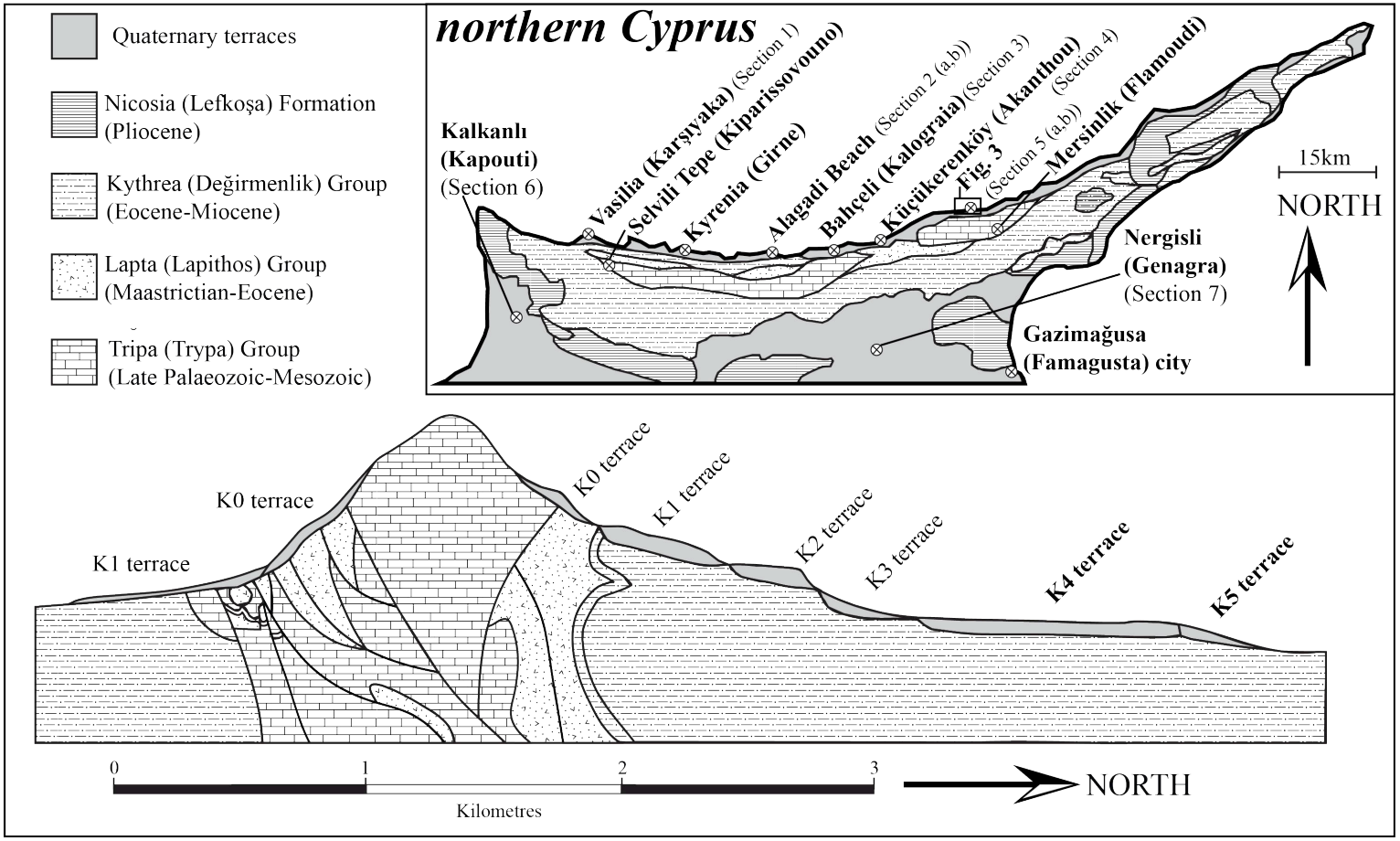

Figure 5.1: Simplified geological cross-section through the central part of the Kyrenia Range (based on Baroz (1979), Robertson and Woodcock (1986) and McCay and Robertson (2013)) showing the relative positions of the Pleistocene terraces. The inset sketch shows a summary geological map of northern Cyprus with the main localities and towns marked.

5.2.1 Section 1. Vasilia (Karşıyaka) (Sec. 4.5.3)

The section is preserved near the village of Vasilia (Karşıyaka) on the western end of the Kyrenia Range, directly north of the highest mountain in the Kyrenia Range, Selvili Tepe (Kiparissovouno). The K4 terrace deposits are mostly composed of a grainstone deposit that is ca. 4 m thick. The basal 2 m of the section are planar-bedded, medium- to coarse-grained grainstone. Bedding varies in thickness from 5 cm to 10 cm. Overlying this is a 0.5 m thick unit of bioclastic debris, with fragments of pectens, oysters, bivalves, calcareous algae and occasional *Cladocoracaespitosa* (solitary coral). This, in turn, is overlain by ca. 1.5 m of poorly-bedded, massive grainstone with abundant, cemented plant-root traces.

The grainstones are predominantly composed of bioclastic grains such as bivalves, gastropods, benthic foraminifera and calcareous red algae. Volumetrically subordinate lithic fragments include chert, monocrystalline quartz, polycrystalline quartz, reworked bioclastic fragments (e.g. calcareous algae), gastropods, bivalve shell fragments and minor amounts of feldspar. The shells are calcitic with micrite-filled chambers. Pore spaces between the grains are infilled with a both micrite and sparite cement.

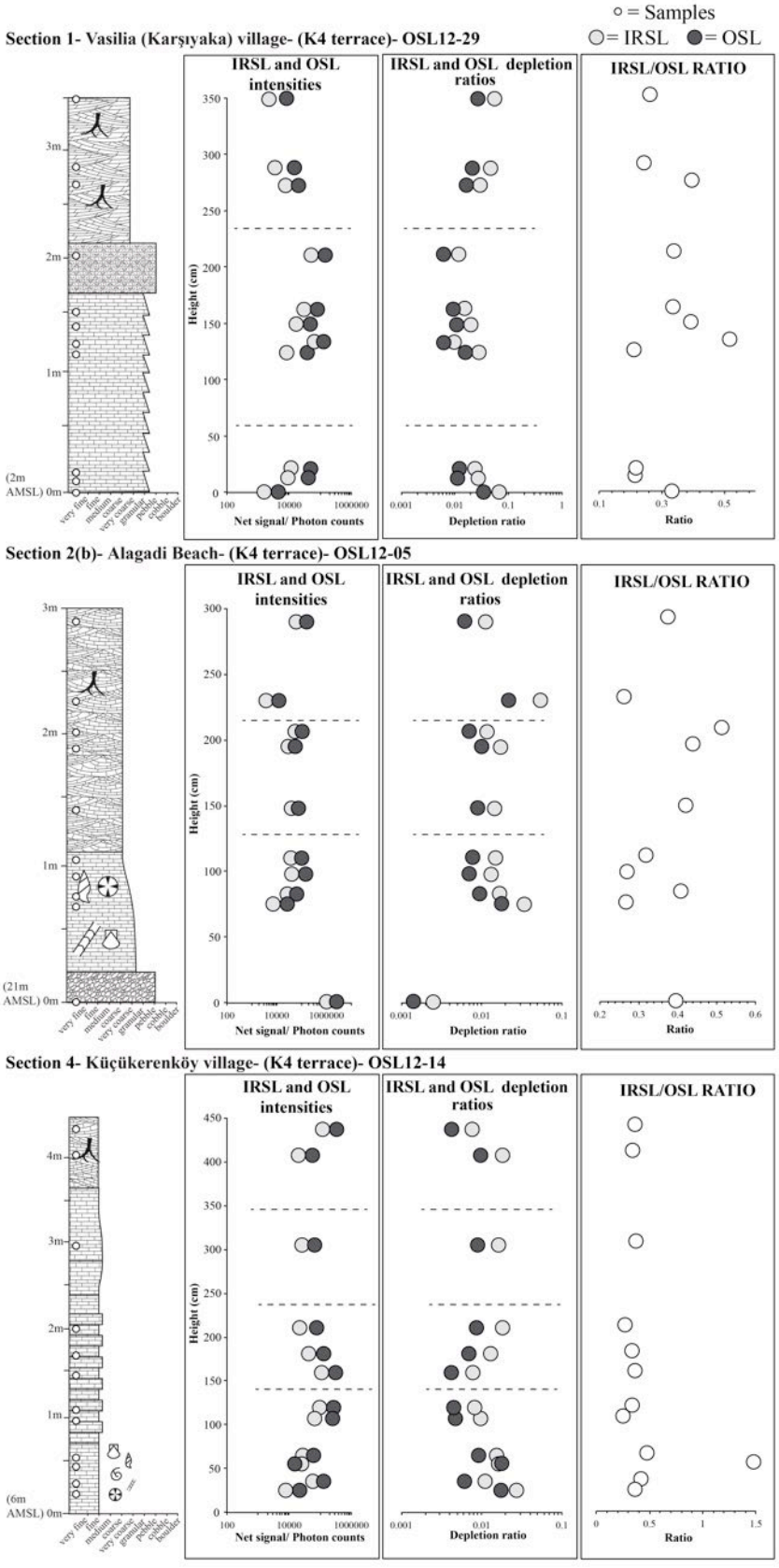

Figure 5.2: Sedimentary logs and portable luminescence profiles from grainstone deposits of the K4 terrace on the northern flank of the Kyrenia Range. Luminescence packages are marked on the IRSL and OSL profiles by dashed horizontal lines. (Key to sedimentary logs is shown in Figure 5.3).

5.2.2 Section 2: Alagadi beach (Sec. 4.5.6)

Located 15 km east of Girne (Kyrenia) town, Alagadi beach (Fig. 5.1), provides an excellent opportunity to study the relationship between the K4 and K5 terrace deposits. Two sections were studied: first, a deposit slightly above modern sea level (AMSL) and secondly a deposit ca. 15 m AMSL (Figs. 5.2, 5.3). The upper deposit was previously mapped as part of the K4 terrace, whereas the lower deposit was shown as part of the K5 terrace (Ducloz, 1964). The upper deposit continues inland for ca. 2 km, whereas the lower deposit is restricted to the coast.

Lower deposit-K5 terrace (Section 2(a))

This is a 4 m-thick grainstone sequence that overlies calcareous mudstones and sandstones of the Kythrea (Değirmenlik) Group (Fig. 5.3). An erosional unconformity between the two units is located at 2 m AMSL. The grainstone contains planar-bedded sedimentary structures, especially in the lower half of the deposit. In addition, rounded- to sub-rounded pebbles (<0.5 mm in size) are present. Bioclastic clasts comprise red algae, bryozoa, gastropods, benthic foraminifera and peloids. A subordinate volume of the rock is made up of monocrystalline quartz (Fig. 5.4(a)), chert (Fig. 5.4(b)), polycrystalline quartz (Fig. 5.4(c)), reworked benthic foraminifera and feldspar (Fig. 5.4(d)). In general, the grainstone has around 30% pore space. Cementation is mainly a microsparitic coating of grain boundaries and the partial infilling of pore space.

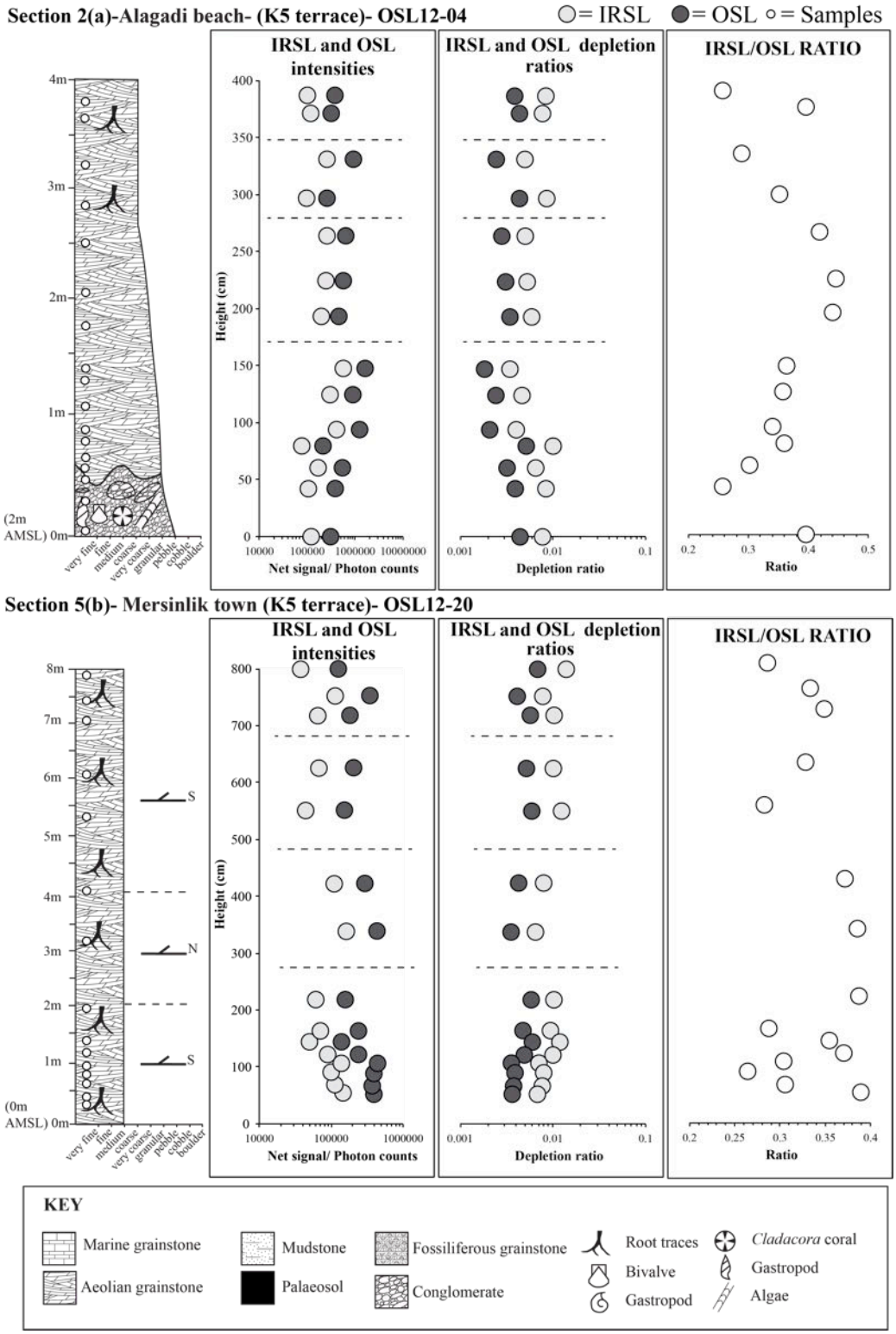

Figure 5.3: Sedimentary logs and portable luminescence profiles from grainstone deposits of the K5 terrace on the northern flank of the Kyrenia Range. Luminescence packages are marked on the IRSL and OSL profiles by dashed horizontal lines.

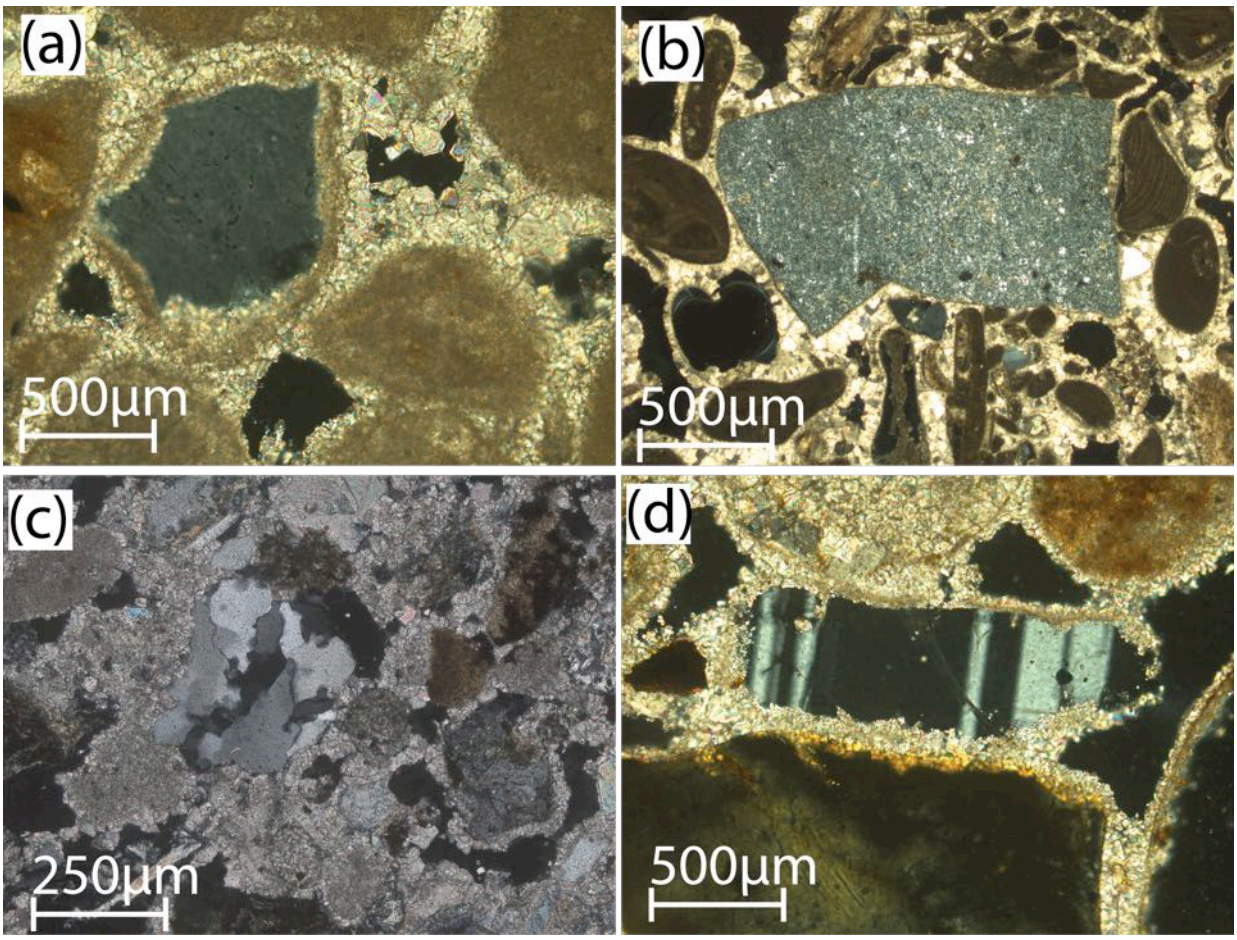

Figure 5.4: Photomicrographs of grainstone deposits of the K4 terrace: (a) monocrystalline quartz coated in a micritic and fine sparitic cement; (b) detrital chert surrounded by reworked biogenic fragments; (c) polycrystalline quartz coated by a sparitic cement; (d) detrital plagioclase grain.

Higher deposit- K4 terrace (Section 2(b))

This deposit comprises a basal conglomerate (ca. 30 cm thick) rich in bioclastic debris, notably bivalves, oysters and occasional *Cladocora* corals. This is followed by grainstone, ca. 4 m thick, making up the remainder of the section (Fig. 5.2). The sediments are structureless and contain calcified root traces that are abundant in the upper part of the section.

5.2.3 Section 3: Bahçeli (Kalograia) (Sec. 4.5.9)

The K4 terrace deposit is exposed as a 200 m-long road section that is located ca. 1 km east of Bahçeli (Kalograia) village (Fig. 5.1). The K4 terrace surface has been previously mapped in this area as continuing inland for at least 1 km (Knupp, 1964). The exposed section is divisible into a lower mudstone unit, ca. 4 m thick, and an upper lenticular-bedded conglomerate unit, ca. 8 m thick (Fig. 5.6). The lower unit includes two prominent palaeosols. The upper lenticular conglomerate unit erosively overlies the lower unit at ca. 45°, dipping eastwards. The lenticular conglomerate is composed of clasts of metacarbonates, basalt, cherts and pelagic carbonates. The clasts are mostly sub-angular and range in size from <1 cm to 15 cm, with a modal clast size of ca. 5 cm. The individual conglomerate lenses are continuous for several metres along the length of the section and vary in thickness from 10 cm to 30 cm. Sedimentary structures are poorly developed within the lenses, with poorly-develop normal-grading of the clasts.

5.2.4 Section 4: Küçkerenköy village (Sec. 4.5.10)

This coastal exposure represents the type locality of the K4 terrace (Baroz, 1979). An erosional contact with the underlying Miocene sandstone and mudstone is exposed at ca. 6 m AMSL. The section is made up of fine-grained to coarse-grained grainstones, ca. 4 m thick (Fig. 5.2). The lower 3.5 m of the deposit comprise a fine- to coarse-grained grainstone, with poorly sorted, sub-angular grains. The higher 1 m comprise well-sorted, medium-grained grainstones, with abundant calcified root traces.

The grainstone is dominated by bioclastic debris including red algae, bryozoa, corals, bivalves and gastropods. There are also monocrystalline quartz, chert, reworked grainstone fragments, detrital pelagic carbonate, polycrystalline quartz, dia-

base/microgabbro and minor amounts of feldspar present. Grains are sub-rounded to well-rounded and range in size from <0.5 mm to 3 mm. The cement is mainly microsparite (>80% of the sediment volume), which is developed along the grain boundaries, whereas sparite infills pore spaces (<20% of the sediment volume). In places, there is a bed contain bivalves (pectenids), gastropods and rare *Cladacora* coral fragments.

5.2.5 Section 5: Mersinlik village (Sec. 4.5.12)

The deposit is exposed ca. 3 km west of Mersinlik village along the main and old coastal roads (Fig. 5.5, 5.1). The deposits along the main road form part of the K4 terrace system, whereas the deposits along the coastal road form part of the K5 terrace system.

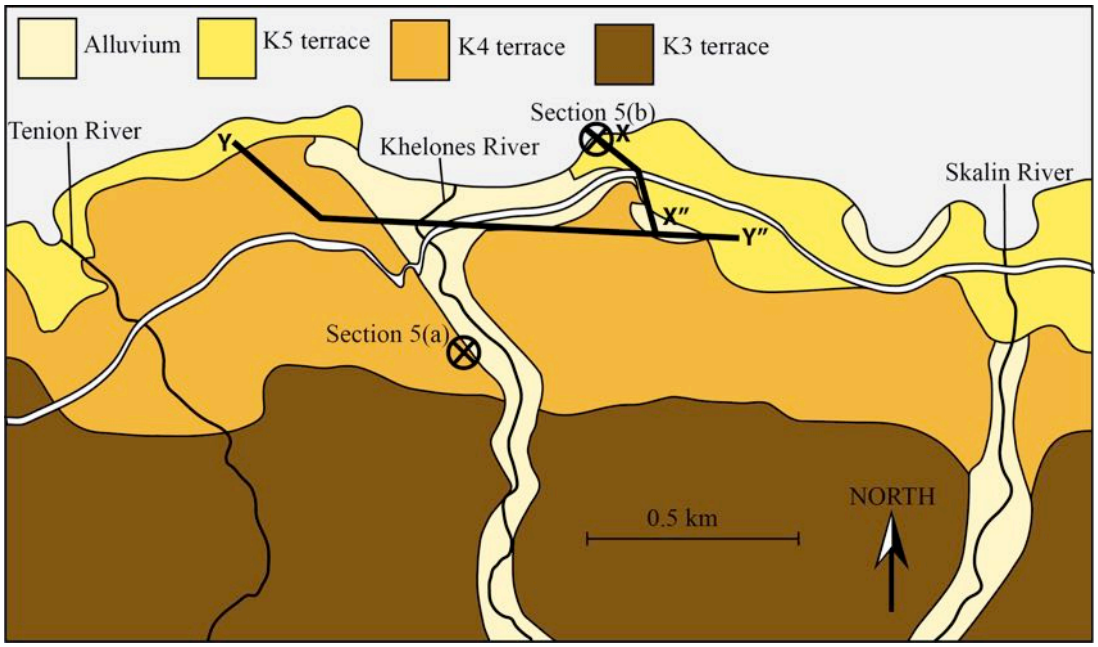

Figure 5.5: Outline geological map of the area west of Mersinlik (Flamoudi) village showing the exposed Pleistocene terrace (modified from Ducloz, 1963). Lines X-X and Y-Y refer to the cross-sections shown in Figure 5.7.

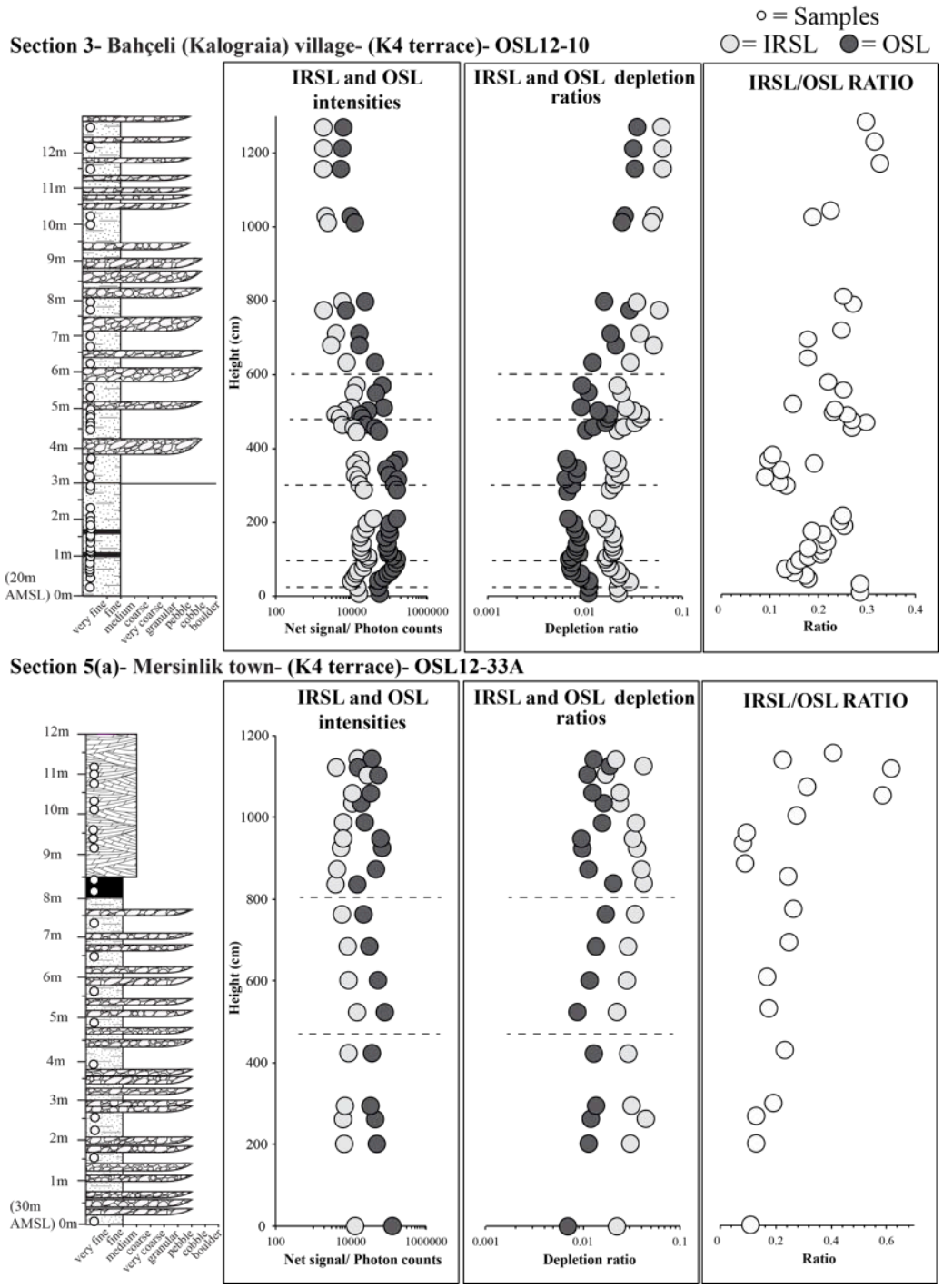

Figure 5.6: Sedimentary logs and portable luminescence profiles from mudstone and lenticular conglomerate deposits of the K4 and K5 terraces on the southern side of the Kyrenia Range. Luminescence packages are marked on the IRSL and OSL profiles by dashed horizontal lines. (Key to sedimentary logs shown in Figure 5.3).

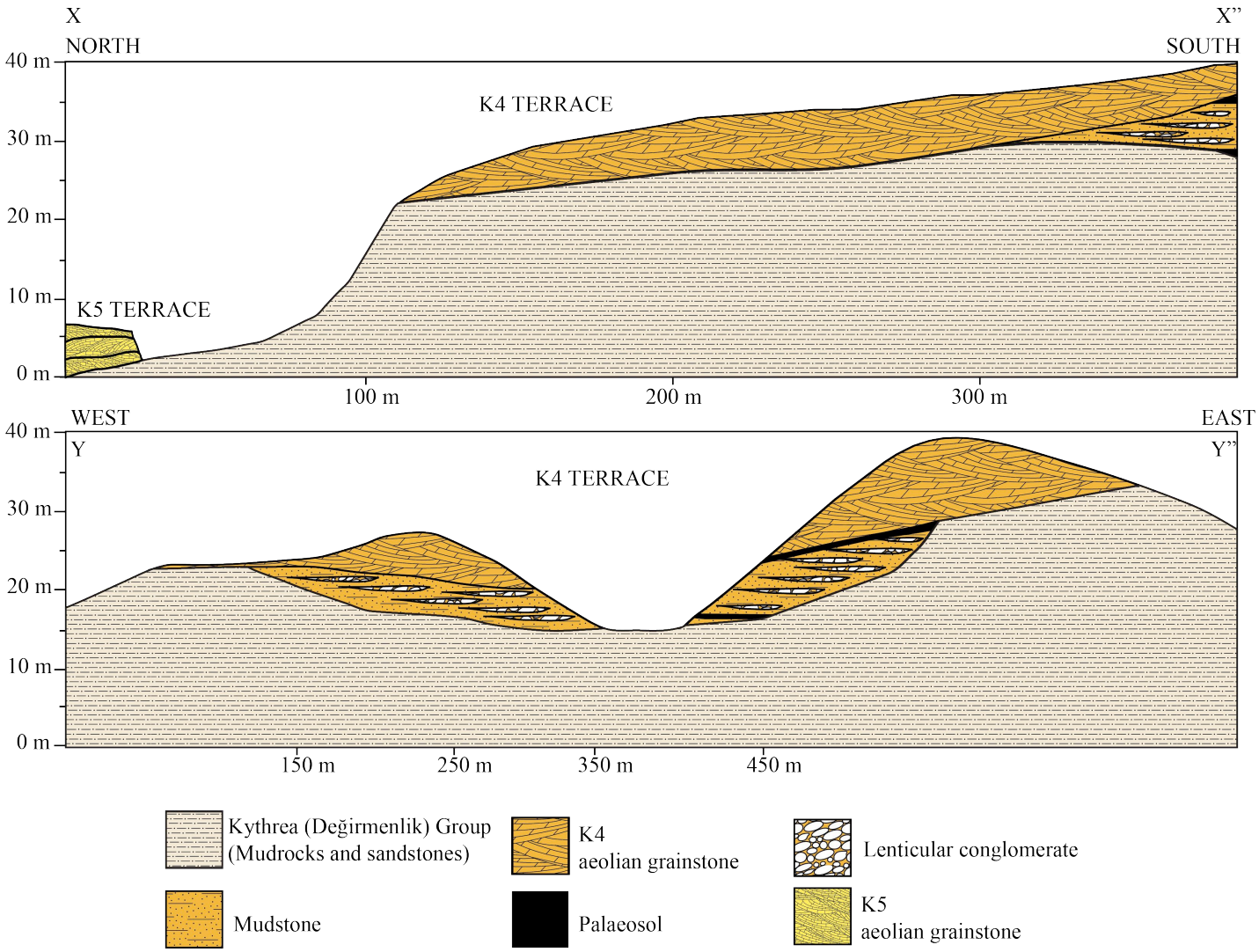

Figure 5.7: N-S and E-W cross-sections through the K4 and K5 terrace deposits near Mersinlik (Flamoudi) (see Fig. 5.1 for section locations).

Section 5(a)

The K4 terrace deposit comprises lenticular conglomerates, mudstones, palaeosols and aeolianites (Fig. 5.6). The lower 8 m-thick, nearly 100 m-wide section is made up of lenticular conglomerate, mudstone and several palaeosols. Conglomerate lenses, ca. 30 cm thick, are continuous for several metres laterally and are intercalated with fine-grained mudstone. The conglomerate is dominated by sub-angular clasts of deformed metacarbonate rocks of the Trypa (Tripa) Group, <1 cm to 10 cm in size, locally showing westerly-directed imbrication. Overlying the conglomerates is a well-developed dark maroon-coloured palaeosol, 1 m-thick, followed by ca. 3 m of aeolianite. The aeolianite exhibits a series of foresets, dipping at ca. 40° towards the west.

Section 5(b)

The K5 terrace deposit occurs along the coast very close to modern sea level. A ca. 8 m-thick sequence of cross-bedded, bioclastic grainstone is commonly exposed (Fig. 5.3). The grains in the grainstone are <0.5 mm in size and sub-rounded, and dominantly composed of red algae, gastropods, benthic foraminifera, peloids and bivalves. Monocrystalline quartz, polycrystalline quartz, chert, recrystallized shells and feldspar are also present. Microsparite coats all of the grains but only infills the smallest pores (ca. 20% by volume). The remaining pore space (ca. 80%) is filled with microsparite.

Key facies relationships are shown in Figure 5.7. The fluvial deposits of the K4 terrace are overlain by aeolianite deposits, representing two depositional phases within this terrace system. The cross-section X-X" shows the relationship of the aeolianites of the K4 terrace system (ca. 35 m AMSL) to the aeolianites of the K5 terrace system (ca. 0 m AMSL).

5.2.6 Section 6: Kalkanl (Kapouti) section (Sec. 3.4.3)

Mapping by Ducloz (l963) and by Knupp (1964) was restricted to the central Kyrenia Range. The Pleistocene terrace deposits of the western, eastern and southern flanks of the range have not previously been defined in terms of relative ages. However, two terrace deposits from the southern side of the range are used here to document non-

marine depositional environments during the Pleistocene.

Section 6 is from a large gully to the south-west of the Kyrenia Range (Fig. 5.1). These sediments are shown on the Cyprus Geological Survey Map (Constantinou, 1995) as Pleistocene, but were not assigned a specific terrace name. Specifically, the section is near Kalkanl (Kapouti), within an east-west-trending gully to the north of the village of this name. The deposits are mainly lenticular, clast-supported conglomerates, interbedded with mudstones (Fig. 5.8). The clasts are 1 cm to 10 cm in size, sub-angular, poorly sorted and dominated by metacarbonate of the Trypa (Tripa) Group. The matrix is fine-grained, maroon-coloured mud, forming a 1 m-thick layer between lenticular conglomerates (Fig. 5.8).

5.2.7 Section 7: Nergisli (Genagra) (Sec. 3.4.4)

Section 7 is just outside Nergisli (Genagra) village, north-west of Gazimagusa (Famagusta) (Fig. 5.1). This deposit is also outwith the area mapped by Ducloz (1963) and by Knupp (1964); it was inferred to be a Pleistocene terrace deposit but no specific terrace name was assigned. A small quarry near the north-western edge of the village exposes interbedded medium-grained sand and lenticular, clast-supported conglomerate (Fig. 5.8). The conglomerate clasts are sub-rounded and range from 1 cm to 10 cm in size. The clasts are predominantly sandstone, pelagic carbonate, chert, basalt, diabase and microgabbro. Clast imbrication indicates palaeoflow towards the south. The grains within the interbedded sands are mostly angular.

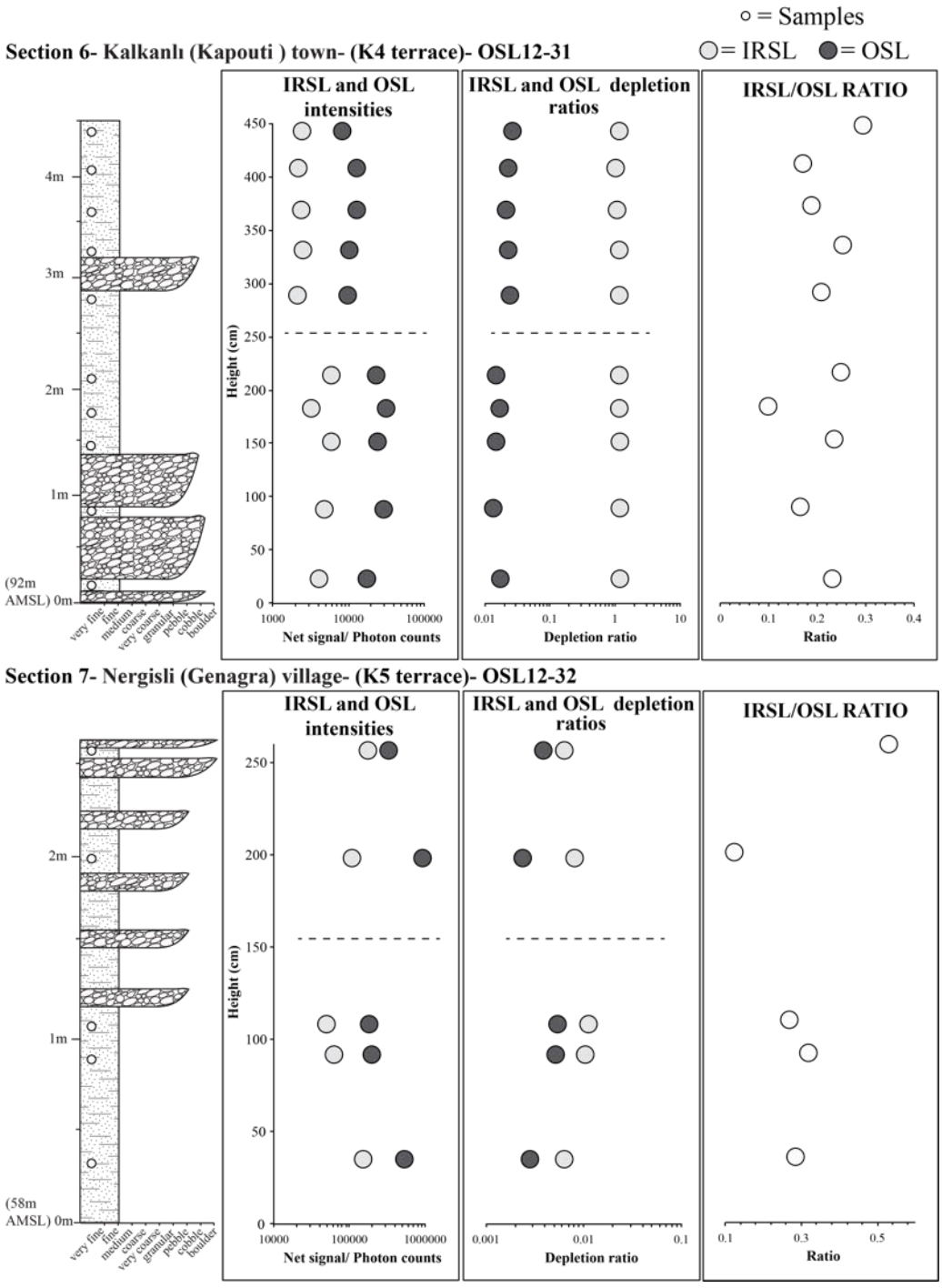

Figure 5.8: Sedimentary logs and portable luminescence profiles from mudstone and lenticular conglomerate deposits of the K4 and K5 terraces on the southern side of the Kyrenia Range. Luminescence packages are marked on the IRSL and OSL profiles by dashed horizontal lines. (Key to sedimentary logs shown in Figure 5.3).

5.2.8 Grainstone composition

The grainstone grains have varying proportions of carbonate and siliciclastic grains, influenced by the depositional environment and sediment provenance. The relative amount of quartz and feldspar, and therefore the depositional setting and provenance, are significant for luminescence analysis. Point count data were collected from five marine and aeolian grainstone deposits from both the K4 and K5 terraces. Four hundred grains were counted per sample in the following categories: monocrystalline quartz, polycrystalline quartz, feldspar, chert, volcanic grains, metamorphic grains, sedimentary grains, calcareous red algae, bivalve fragments, calcareous algae, benthic foraminifera, echinoderm fragments, gastropods, bryozoa and ostracods (Fig. 5.9).

Monocrystalline quartz within the K4 terrace marine grainstones makes up <5 %; whereas in the K4 and K5 terrace aeolian grainstones this ranges from 15-30 %. Polycrystalline quartz in both K4 and K5 terrace marine and aeolian grainstones is <15 %. The feldspar content in all of the grainstone deposits is <5 %. The reworked metamorphic grains, which include metamorphic quartz, ranges from <5 % to 15 %. Reworked sedimentary grains, which commonly include monocrystalline quartz, range from 5 % to nearly 45 %. The carbonate grains are dominantly reworked calcareous red algae with a minor component of benthic foraminifera and echinoderm fragments (with algal encrustations).

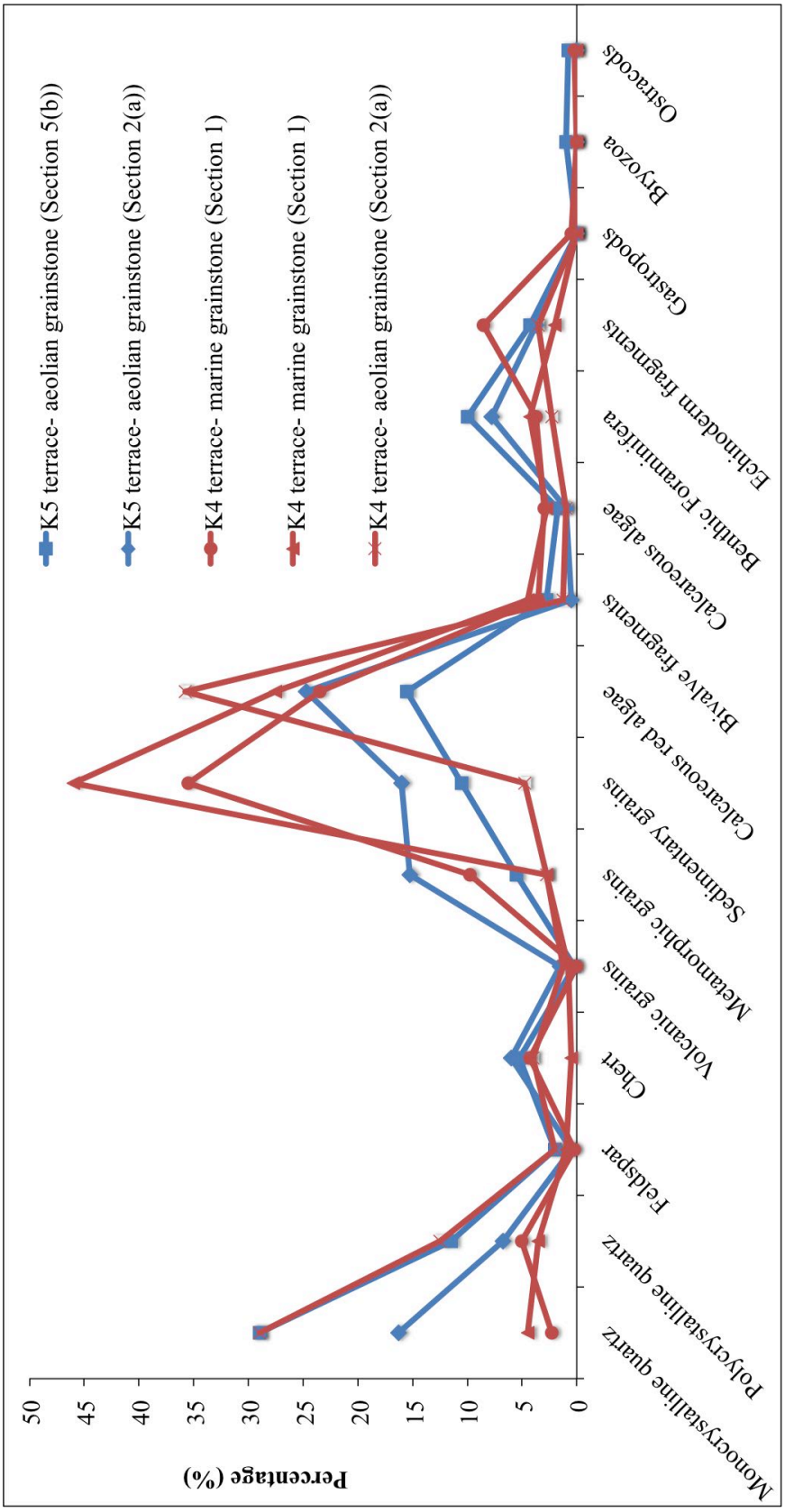

Figure 5.9: Point count data from marine and aeolian grainstone deposits along the northern coastline of Cyprus from the K4 and K5 terraces.

5.3 Luminescence field profiling results

The following section describes the results from the field based luminescence of profiling of the previously described sections. The technique and methodology are described in Section 1.4.2.

5.3.1 Sampling

A set of 107 samples where collected from the nine sections described above (see Fig. 5.1). The sample set from the K4 terrace system includes both marine and aeolian deposits (3 localities) and also fluvial deposits (3 localities). The K5 terrace system sample set comprises two marine/aeolian deposits (2 localities) and one fluvial deposit (1 locality). Samples were collected every 10 cm to 1 m through each stratigraphic section to gain a representative sample set through each section.

5.3.2 Results

Net IRSL and OSL signal intensities, their depletion indices, and the IRSL: OSL ratios were calculated (after background subtraction) for all samples. All of the samples yielded measureable luminescence signals that exceeded system backgrounds. The data was then plotted relative to height in their respective sedimentary sequence, as shown in Figures 5.2, 5.3, 5.6 and 5.8 (see also Tables 7.1-7.9). All of the samples exhibited brighter OSL than IRSL intensities. The OSL and IRSL intensities exhibit a strong correlation; i.e. for the samples that emitted a relatively dim blue signal the corresponding red signal was also dim (Fig. 5.10). The mineral assemblage in both the K5 and K4 deposits is dominated by quartz (from a variety of sources) and carbonate bioclasts, with subordinate feldspar. Point count data shows that both the aeolian and the marine grainstones are rich in quartz grains but contain only a minor feldspar component. This point count data suggests that the luminescence signal comes from a similar set of minerals from all the various facies of the K4 and K5 terraces.

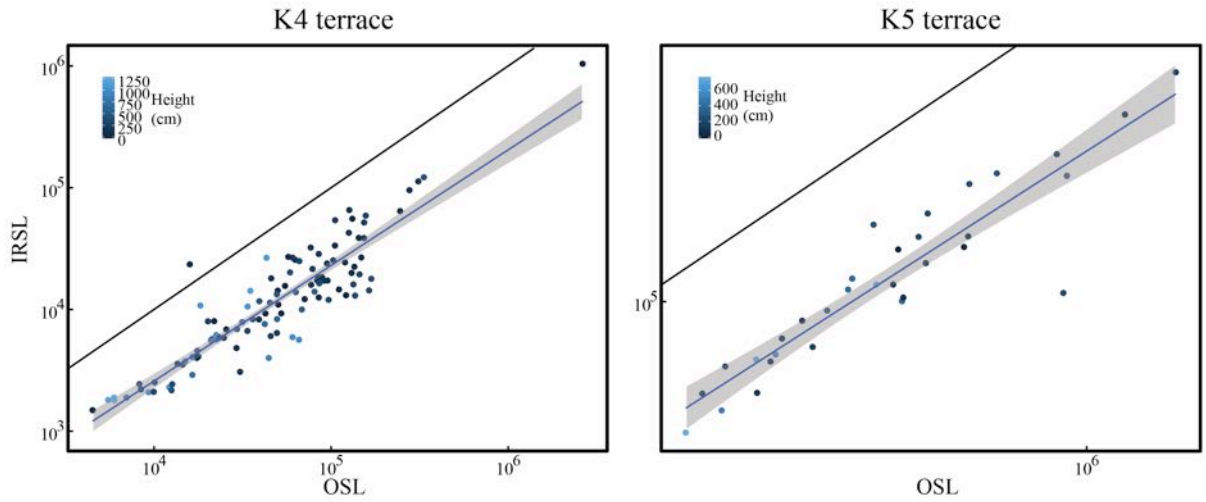

Figure 5.10: Scatter plots showing infra-red stimulated luminescence (IRSL) versus optically stimulated luminescence (OSL). The heights shown by the shading of the dots. Both plots show that the IRSL and OSL signals in both terraces are directly related. The OSL signal is generally higher than the IRSL signal, as shown by the offset of the data relative to the identity line.

The luminescence proxy variables measured by the portable unit are influenced by: (i) sediment grain-size and colour, (ii) the total radiation dose that the sediment has been exposed to during burial, (iii) the sensitivity (brightness) of the luminescence signal of the minerals present, (iv) the degree of signal resetting through sunlight exposure that the sediment has experienced prior to deposition, and (v) the post-depositional age of the sediment. A number of these variables can be constrained by sedimentological observations, as summarised above. Local variations in grain characteristics (variable (i)) were taken into consideration when interpreting signal intensities; however, no correlation was noted between grain characteristics and signal intensities.

Variable (ii) was accounted for by *in situ* gamma dose rate measurements that were made at a number of localities, encompassing both marine and fluvial deposits, and from terraces on either side of the range (Table 7.10). Within the K5 terrace, the measured in situ gamma dose rates varied between 0.6 to 0.9 mGy a^{-1}. In contrast, within the K4 terrace sections, these values range between 0.3-1.8 mGy a^{-1}. Some lithological control was noted in the grainstone deposits (Sections 1 and 5(b)) with gamma dose rate recorded that vary between 0.5 mGy a^{-1} and 1.0 mGy a^{-1}. While in the mudstones and the palaeosols, gamma dose rates ranged from 0.5 mGy a^{-1} to 1.8 mGy

a^{-1}. When comparing signal intensities in the K4 and K5 terrace deposits in adjacent areas only sediments of similar composition were utilised, thereby taking account of local variations in environmental dose rates.

For variable (iii) any difference in the mineral composition is likely to have an important influence on the sensitivity (brightness) of the luminescence signal. This sensitivity is likely to fluctuate, given the varied provenance of the Kyrenia Range sediments and the potential for multiple sediment transport pathways prior to deposition. Despite this, the variations in signal intensities are low and the IRSL: OSL ratio is similar for samples from within the individual sections of both the K4 and K5 depositional systems.

The available petrographic information indicates that the relative mineralogical composition of the light-sensitive minerals (e.g. quartz; feldspar) remains relatively constant throughout the different sections sampled. This reflects the fact that the main source of the detrital minerals was the terrigenous sediments of the Kythrea (Değirmenlik) Group, which unconformably underlies the Pleistocene terrace deposits along both flanks of the range. The composition of these deposits remains broadly similar throughout the Kyrenia Range, which reflects long-distance sedimentary transport from southern Turkey by gravity-flow processes (McCay and Robertson, 2012a).

A key observation is that the sections through the K4 and the K5 terrace deposits exhibit very different averaged IRSL and OSL intensities. The K4 terrace deposits have signal intensities of between 10^3-10^6 photon counts, whereas the K5 terrace deposits exhibit intensities generally greater than 106 photon counts (Figs. 5.2, 5.3). Notably, the terrestrial deposits in the south show similar ranges in luminescence intensities to their inferred counterparts in the north (Fig. 5.8).

A number of discrete sedimentary units within the K4 and the K5 terrace deposits are characterised by a specific set of luminescence features: (i) within the K4 terrace deposits the net IRSL signal ranges between 10^4 and 10^3 photon counts in the aeolianites and between 10^5 and 10^4 photon counts in the marine deposits, (ii) OSL signal intensities range between 10^5 and 10^3 photon counts in the aeolianites and between 10^5 and 10^4 photon counts in the marine deposits (Figs. 5.2, 5.3). Within the K5 terrace deposits, the net IRSL signal ranges between 10^5 and 10^4 photon counts for the aeolian deposits, and 10^5 photon counts for the marine deposits. OSL signal intensities are on

the order of 10^5 photon counts for both the aeolianites and the marine deposits.

The K4 fluvial terrace deposits on the northern flank of the range deposit exhibit IRSL signal intensities ranging from 10^4 to 10^3 photon counts. The OSL signal intensities are an order of magnitude higher than the IRSL signal intensities, ranging from 10^5 to 10^4 photon counts (Fig. 5.6). A similar order of magnitude difference is also recorded in the K4 terrace deposits on the southern side of the range (Section 6; Fig. 5.8). In addition, a number of discrete units can be distinguished based upon either normal or reversed signal patterns (Fig. 5.6, 5.8) on both sides of the range.

For the fluvial sections, the overall range in IRSL signal intensities is between 10^4 and 10^3 photon counts, and for OSL signal intensities the range is between 10^6 and 10^3 photon counts (Fig. 5.6, 5.8). The aeolian grainstones that overlie the fluvial sequence near Mersinlik have an IRSL intensity ranging from 10^3 to 10^4 photon counts; OSL signal intensities from this locality are ca. 10^4 photon counts (Fig. 5.6). The aeolianite signal intensities from the inland section are similar to the coastal aeolianites from the K4 terrace deposit.

Several packages of sediment can be identified within the luminescence profiles; these reflect marked changes in the luminescence signal intensity or a change from increasing to decreasing luminescence intensity or vice versa (Figs. 5.2, 5.3, 5.6 and 5.8). The packages are occasionally defined by lithological boundaries but generally do not correspond to identifiable changes in lithology. This suggests that the variation of the luminescence characteristics is due either to a variation in the depositional processes or to changes in the sediment provenance.

IRSL and OSL bleaching profiles for the K4 and the K5 sediments are shown in Figure 5.11. The IRSL and OSL signals are completely removed following fifty minutes of exposure (i.e. signal levels become indistinguishable from background levels): 70-80% of the IRSL and OSL signals are lost within the first 30 minutes, and the remaining 30-20% of signal is then lost in the following 60 minutes of exposure. This is promising luminescence behaviour, implying that the luminescence signals are susceptible to bleaching, suggesting that the material may have been well-bleached at the time of deposition. Interestingly, the bleaching profiles reveal a trend in bleaching susceptibility from the K4 aeolianites (easily bleached), through the K4 fluvial deposits to the K5

aeolianites, which are more difficult to bleach.

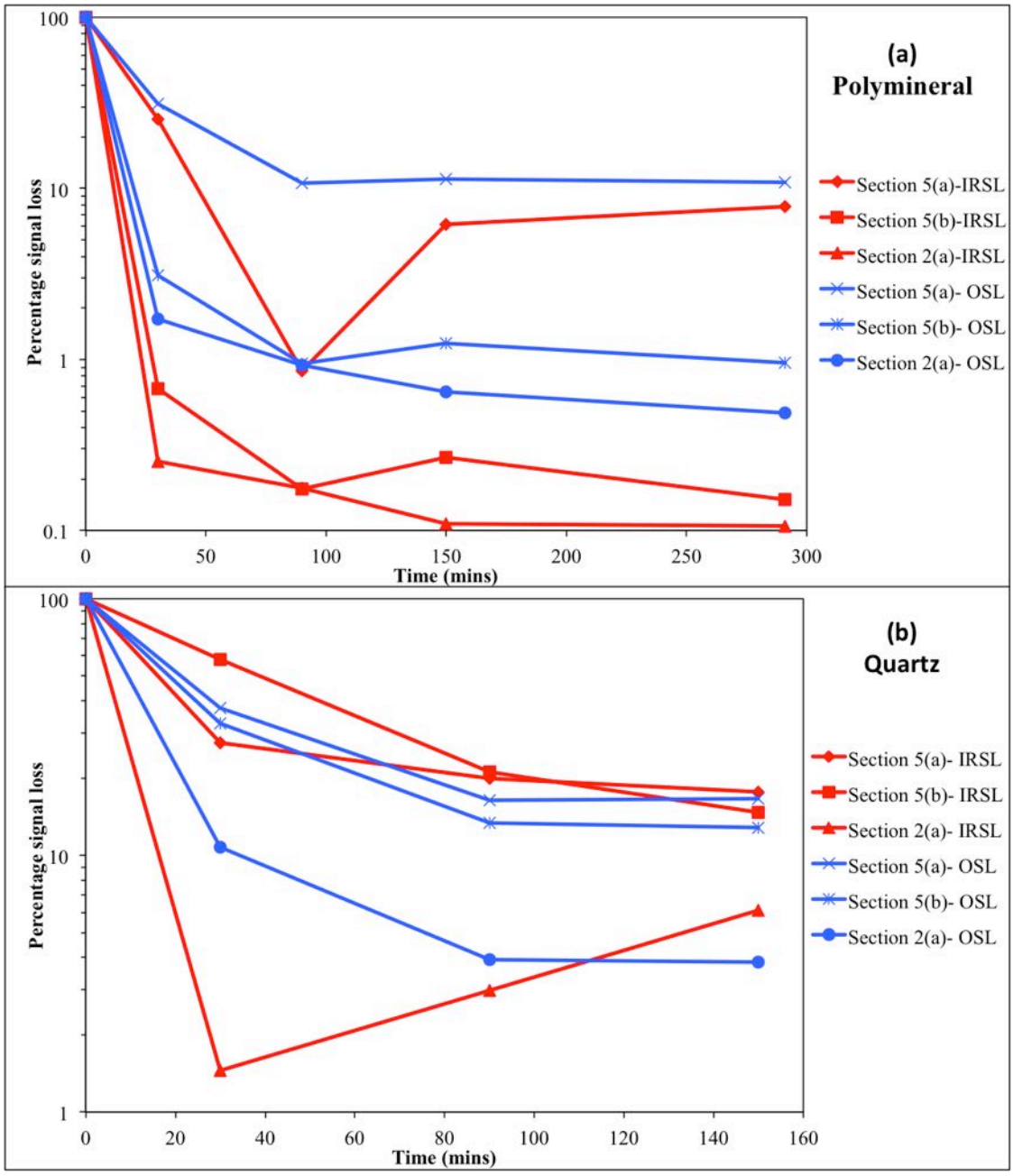

Figure 5.11: Bleaching data from polymineral and quartz aliquots averaged from Section 5(a), Section 5(b) and Section 2(a). The samples represent an even spread through each section. Samples were exposed under natural light conditions and then measured with the portable OSL reader at specific time intervals.

5.4 Discussion and interpretation

The K4 terrace is 2 km to 3 km wide and continuous for the ca. 150 km length along the Kyrenia Range. In comparison, the K5 terrace is <100 m wide and discontinuous along the length of the range. The K4 terrace deposits are 10-20 m-thick, whereas the K5 terrace deposits are <8 m-thick.

Three depositional environments can be identified within the two terrace systems exposed near the northern coast: littoral-marine, aeolian and fluvial. Each of these depositional environments are represented in both of the terrace systems. Both K4 and K5 terrace systems on the northern side of the range exhibit an overall regressive sedimentary sequence.

The K4 terrace represents a variable, multi-facies depositional system. The succession begins with a basal conglomerate and passes upwards through shallow-marine grainstones and then into coastal aeolianites. Fluvial deposits are channelled into the marine and aeolian deposits at various places along the length of the northern flank of the range. The uppermost component of the K4 terrace depositional system is an addditional aeolianite that transgresses all of the other facies. In contrast, littoral marine and aeolianite depositional environments characterise the K5 terrace system on the northern side of the range.

The terrace deposits along the southern flank of the range are exclusively non-marine. The southern-side terraces represent a series of cross-cutting drainage systems. The southern-side drainage systems were deposited penecontemporaneously with the marine and continental terraces on the northern side of the range.

The K5 deposits are known to be younger than the K4 terrace deposits along both the northern and southern flanks of the range. This is inferred as the younger sediments depositionally overlie or crosscut the older sediments at many locations. The K5 terrace deposits appear to represent a much shorter time interval than the K4 terrace deposits. This is because the K5 deposits are thinner, more homogeneous and localised along the coast, in contrast with the K4 deposits, which are thicker, lithologically more variable, form episodically, and extend as transgressive sheets up to several kilometres inland. The inference that the K4 terrace represents a longer period of time than the K5 terrace is supported by the luminescence proxy data. Not withstanding the different lithological

units, depositional mechanisms and environmental setting of the two terrace systems there is a greater range in signal intensities within the K4 terrace than in the K5 terrace.

The ages of the sediments in the different sections of the terraces can be inferred to be broadly similar in cases where the luminescence signals are similar. On this basis, the distributions of the K4 terrace deposits and the K5 terrace deposits that were originally recognised based on regional mapping of associated geomorphological surfaces (Ducloz, 1964; Knupp, 1964) are now generally confirmed from the combination of sedimentological and optical luminescence data presented here. In addition, the fluvial terraces on the southern flank of the range can now be correlated with marine and non-marine terraces on the northern flank of the range.

The luminescence profiles through the fluvial terraces on the northern side of the range are indicative of three sediment packages with specific luminescence characteristics (Figs. 5.6, 5.8). The packages represent sediment that underwent subtly different sedimentary histories, resulting in subtly differently luminescence signals. The different packages of sediment are likely to be the product of an episodically changing depositional system.

The IRSL and OSL intensities show a progression from the largest intensities at the base, to the lowest intensities at the top. This is expected for a normal age progression in which lower, stratigraphically older sediments have had longer to accumulate luminescence signals *in situ*. The relative decrease in the luminescence intensity of each section suggests that, within individual sections, the primary control of luminescence intensity is likely to be age.

The K4 and K5 terrace deposits on the northern side of the range are characterised by specific luminescence characteristics. The K4 terrace deposits have IRSL intensities of between 10^4 to 10^3 photon counts, whereas the K5 terrace IRSL signal intensities range from 10^6 to 10^5 photon counts. The K4 terrace OSL intensities are 10^5 to 10^4 photon counts, whereas the K5 terrace intensities are 10^6 to 10^5 photon counts. The IRSL and OSL signal intensities therefore indicate an order of magnitude difference between the K4 and K5 terrace deposits. A similar pattern of hugely different luminescence signals is present within the two terraces studied along the southern flank of the range. Given the known stratigraphic and sedimentological relationships between the terraces, this relationship must be due to some combination of differences in mineralogy,

depositional process and/or diagenesis, all of which could affect internal luminescence characteristics. As noted earlier, the petrographical evidence does not indicate any major difference in mineralogy between the two terrace systems, although local differences exist within and between individual sections. The contrasts in signal intensity encompass a range of depositional environments within both the K4 and K5 terrace systems, suggesting that the luminescence differences are not facies dependent.

A further factor that could explain the intensity relationship is the sensitivity (i.e. luminescence efficiency) of the sediment incorporated into each terrace. The intensity of the OSL signal from a quartz grain is a function of the size of the total radiation exposure to which it has been exposed since burial (luminescence in-growth), together with the efficiency with which this radiation dose is expressed as emitted photons during the measurement process. This efficiency (sensitivity), varies between quartz types, and may also vary within a single type of quartz grain depending upon the number of phases of deposition and reworking (Pietsch *et al.*, 2008). Sedimentary processes can influence the sensitivity of a deposit, i.e. the sensitivity tends to increase with additional phases of deposition and reworking (Pietsch *et al.*, 2008). The high signal associated with the K5 terrace could have been caused by a high sensitivity as a result of multiple phases of sediment reworking from the K4 terrace into the K5 terrace.

Figure 5.12 shows a schematic model to account for the phases of reworking, depositional pathways and potential sediment sources of the two terrace deposits. The K4 terrace is a multi-phase system with a basal marine grainstone, overlain by an aeolianite, which has been subsequently down-cut into by a fluvial system; finally in some areas, this entire sequence was overlain by a younger aeolianite. In contrast, the K5 terrace is represented by a single relatively simple phase of aeolian deposition. The Eocene-Miocene Kythrea (Değirmenlik) Group is the main source of the identifiable quartz and feldspar within the two terrace deposits. The luminescence characteristics of the two sediment deposits are very different, which could be a consequence of the different sedimentary histories. Figure 5.12 illustrates the reworking of sediment from the Kythrea (Değirmenlik) Group into the K4 terrace deposits and finally into the K5 aeolianites. The first phase of reworking involved the initial erosion of the Kythrea (Değirmenlik) Group into the grainstone at the base of the K4 terrace within a marine environment. The second phase indicates the erosion of the K4 marine grainstone into the overlying beach and dune deposits. Phase three shows the erosion of the oldest K4 terrace aeolianite in response to fluvial downcutting into younger dune systems.

The final fourth phase shown is the erosion of all of the deposits into the coastal K5 terrace aeolianite. The sediment that was finally deposited in the K5 terrace and has therefore, potentially experienced at least four phases of reworking and redeposition. A comparable process can also be envisaged for the southern side of the Kyrenia Range in which multiple phases of fluvial reworking took place from the K4 deposits to the K5 deposits. The end-product of such processes would be a much higher sensitivity of the quartz and feldspar grains within the topographically lower terrace compared to the higher terrace, resulting in the higher observed IRSL and OSL signal intensities in the younger terrace deposits.

5.5 Conclusions

A combination of sedimentology and portable OSL data provide a good understanding of the evolving depositional environments of the K4 and K5 terrace systems. On the northern flank of the Kyrenia Range, both terraces represent an overall regressive sedimentary sequence, with the K4 terrace deposits being much more diverse than those of the K5 terrace system. The terrestrial component within the K4 terrace comprises a combination of fluvial and aeolian deposits.

The portable OSL reader facilitated the rapid analysis of 107 samples, enabling comparisons within and between the individual sediment packages on both flanks of the Kyrenia Range. IRSL and OSL intensities are distinct for each terrace, allowing a quantitative correlation of the terrace deposits on the northern and southern sides of the range. Furthermore, the IRSL and OSL intensity profiles are suggestive of multiple depositional episodes with different packages of sediment showing contrasting luminescence characteristics. The luminescence profiles through the fluvial deposits on both flanks of the range are consistent with sedimentary interpretations of an episodically changing depositional system. The luminescence profiles suggest that the fluvial system represents up to three or four major phases of deposition. The specific luminescence characteristics show that the different terrace deposits in spatially distinct and separate areas can be confidently correlated for the first time.

The net signal intensities obtained for the younger, K5 terrace sediments are generally an order of magnitude larger than those in the older, K4 deposits. The differences

in signal intensity may be explained by multiple episodes of reworking of the K4 terrace deposits. These processes increased the sensitivity of the sediment and resulted in the higher intensities in the K5 terrace luminescence profiles.

The luminescence characteristics of the marine to non-marine Pleistocene terrace deposits, as obtained using the portable OSL reader, can be used to laterally correlate the different terrace sedimentary sequences on both the northern and southern flanks of the Kyrenia Range. Field luminescence profiles can be used in tandem with field sedimentary information to help interpret the depositional processes.

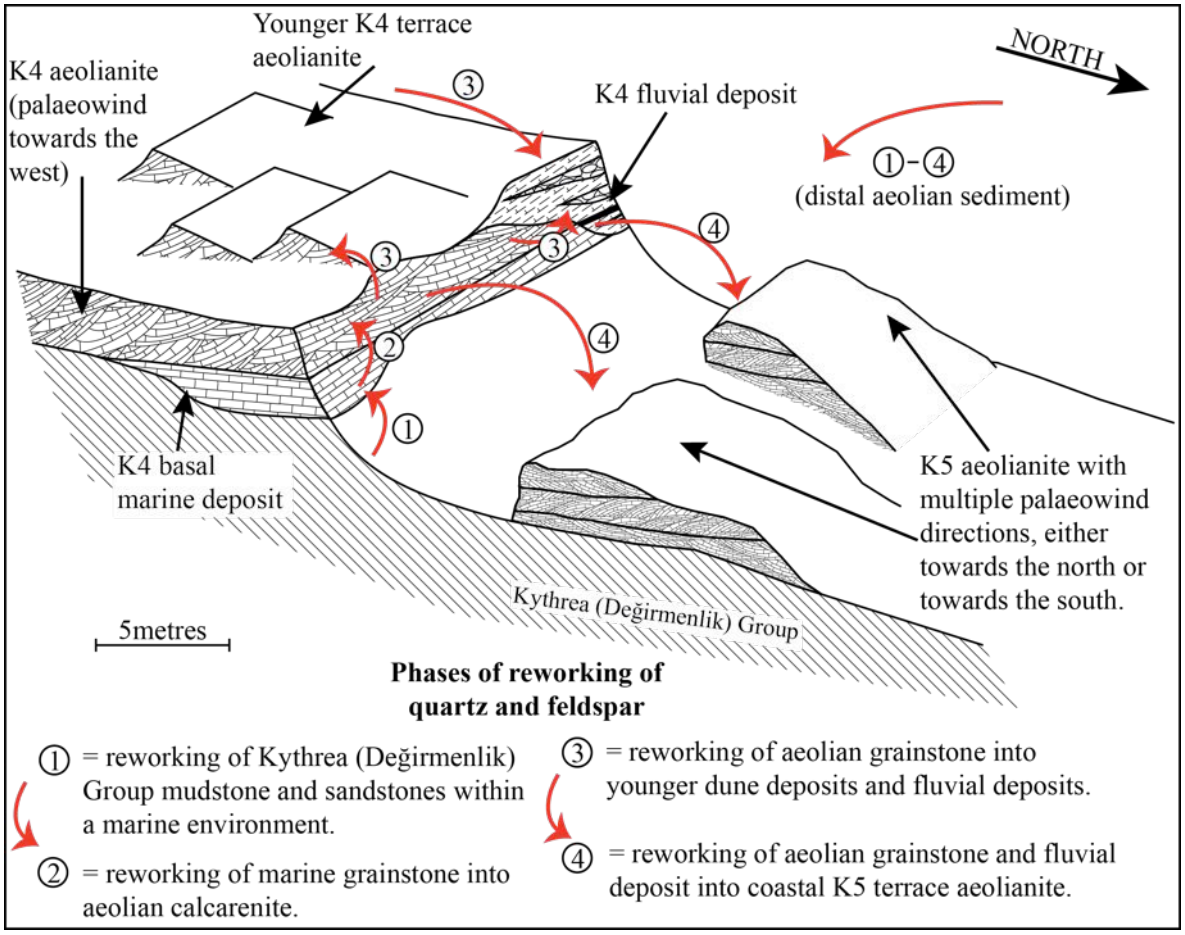

Figure 5.12: Schematic section based on field sedimentology and luminescence profiling, illustrating the sedimentary relationships and inferred phases of reworking of sediment between the K4 and the K5 terrace deposits. The K4 terrace has a diverse range of depositional environments, from littoral marine to aeolinite and fluvial. The K5 terrace is shown as patchy aeolinite that was deposited downslope of the K4 terrace.

Table 5.1: Luminescence profiling data from Section 1 (OSL12-29) at Karşıyaka (Vasilia) from the K4 terrace (N35 21.627 E033 08.277).

Lithology	Height (cm)	IRSL	Error	IRSL depletion	Error	OSL	Error	OSL depletion	Error	IRSL/OSL ratio	Error
grainstone	0.0	1487	48	1.01	0.07	4492	73	1.06	0.03	0.331	0.012
grainstone	13.1	9267	100	1.20	0.03	42527	208	1.16	0.01	0.218	0.003
grainstone	20.6	10950	108	1.22	0.02	50278	225	1.36	0.01	0.218	0.002
grainstone	124.1	8271	96	1.19	0.03	39125	200	1.53	0.02	0.211	0.003
grainstone	133.2	65482	258	1.25	0.01	126652	356	1.10	0.01	0.517	0.003
grainstone	148.5	17999	137	1.25	0.02	45862	216	1.15	0.01	0.392	0.004
grainstone	162.1	28537	171	1.26	0.02	85118	293	1.35	0.01	0.335	0.002
grainstone	210.7	51758	230	1.29	0.01	153537	393	1.21	0.01	0.337	0.002
grainstone	273.0	7983	93	1.25	0.03	20138	144	1.17	0.02	0.396	0.005
grainstone	288.0	3519	66	1.21	0.05	14499	124	1.20	0.02	0.243	0.005
grainstone	349.0	2203	54	1.13	0.06	8433	96	1.18	0.03	0.261	0.007

Table 5.2: Luminescence profiling data from Section 2(b) (OSL12-05) at Alagadi beach from the K4 terrace (N35 20.138 E033 29.342).

Lithology	Height (cm)	IRSL	Error	IRSL depletion	Error	OSL	Error	OSL depletion	Error	IRSL/OSL ratio	Error
grainstone	1.0	1041579	1023	1.26	0.00	2633073	1624	1.15	0.001	0.396	0.000
grainstone	75.4	6853	103	1.13	0.03	25565	171	1.31	0.02	0.268	0.004
grainstone	83.2	25558	171	1.24	0.02	62597	258	1.15	0.01	0.408	0.003
grainstone	98.2	38682	206	1.24	0.01	143290	383	1.27	0.01	0.270	0.002
grainstone	110.4	33444	194	1.28	0.01	105063	330	1.23	0.01	0.318	0.002
grainstone	148.1	32205	190	1.21	0.01	76617	284	1.19	0.01	0.420	0.003
grainstone	194.8	26588	174	1.30	0.02	60550	253	1.18	0.01	0.439	0.003
grainstone	206.6	54027	240	1.27	0.01	105300	330	1.12	0.01	0.513	0.003
grainstone	230.0	3570	86	1.12	0.05	13574	132	1.12	0.02	0.263	0.007
grainstone	289.8	58902	250	1.30	0.01	156860	401	1.19	0.01	0.376	0.002

Table 5.3: Luminescence profiling data from Section 4 (OSL12-14) at Küçkerenköy from the K4 terrace (N35 21.849 E033 40.160).

Lithology	Height (cm)	IRSL	Error	IRSL depletion	Error	OSL	Error	OSL depletion	Error	IRSL/OSL ratio	Error
grainstone	25.1	8009	91	1.18	0.03	21835	149	1.25	0.02	0.367	0.005
grainstone	36.3	55561	237	1.26	0.01	131705	364	1.10	0.01	0.422	0.002
grainstone	55.7	23464	154	1.22	0.02	15904	128	1.08	0.02	1.475	0.015
grainstone	65.8	27014	166	1.23	0.02	57270	240	1.10	0.01	0.472	0.004
grainstone	107.0	64206	256	1.22	0.01	245219	495	1.16	0.005	0.262	0.001
grainstone	119.5	95386	310	1.26	0.01	276970	527	1.17	0.004	0.344	0.001
grainstone	159.3	112643	338	1.30	0.01	310654	559	1.17	0.004	0.363	0.001
grainstone	181.7	42577	208	1.30	0.01	125836	355	1.21	0.01	0.338	0.002
grainstone	210.9	21487	148	1.30	0.02	78476	281	1.22	0.01	0.274	0.002
grainstone	305.4	24936	159	1.26	0.02	66092	258	1.14	0.01	0.377	0.003
grainstone	407.2	20142	144	1.27	0.02	58596	243	1.15	0.01	0.344	0.003
grainstone	437.0	121763	349	1.31	0.01	333976	578	1.21	0.004	0.365	0.001

Table 5.4: Luminescence profiling data from Section 2(a) (OSL12-04) at Alagadi beach from the K5 terrace (N35 20.138 E033 29.342).

Lithology	Height (cm)	IRSL	Error	IRSL depletion	Error	OSL	Error	OSL depletion	Error	IRSL/OSL ratio	Error

grainstone	0.0	119104	360	1.27	0.01	301546	558	1.17	0.004	0.395	0.001
grainstone	42.1	100387	332	1.26	0.01	389017	631	1.20	0.004	0.258	0.001
grainstone	60.2	164232	418	1.26	0.01	545472	746	1.17	0.003	0.301	0.001
grainstone	79.3	75540	292	1.27	0.01	210654	470	1.15	0.005	0.359	0.002
grainstone	93.8	414537	652	1.26	0.00	1215820	1107	1.13	0.002	0.341	0.001
grainstone	124.2	306639	563	1.25	0.00	858179	932	1.13	0.002	0.357	0.001
grainstone	147.0	571434	763	1.28	0.00	1576657	1260	1.16	0.002	0.362	0.001
grainstone	192.9	195403	453	1.28	0.01	443644	673	1.13	0.003	0.440	0.001
grainstone	223.7	244420	504	1.27	0.01	548902	748	1.12	0.003	0.445	0.001
grainstone	263.3	265151	525	1.27	0.01	631718	801	1.12	0.003	0.420	0.001
grainstone	296.4	93419	321	1.25	0.01	265347	525	1.11	0.004	0.352	0.001
grainstone	331.1	260111	520	1.25	0.01	903712	957	1.15	0.002	0.288	0.001
grainstone	371.0	119104	360	1.27	0.01	301546	558	1.17	0.004	0.395	0.001
grainstone	386.5	100387	332	1.26	0.01	389017	631	1.20	0.004	0.258	0.001

Table 5.5: Luminescence profiling data from Section 5(b) (OSL12-20) at Mersinlik from the K5 terrace (N35 24.761 E033 48.659).

Lithology	Height (cm)	IRSL	Error	IRSL depletion	Error	OSL	Error	OSL depletion	Error	IRSL/OSL ratio	Error

grainstone	54.0	148668	387	1.29	0.01	381496	619	1.14	0.004	0.390	0.001
grainstone	67.0	113826	339	1.27	0.01	371789	611	1.15	0.004	0.306	0.001
grainstone	90.0	103119	322	1.27	0.01	391614	627	1.21	0.004	0.263	0.001
grainstone	107.0	133994	368	1.26	0.01	439466	664	1.18	0.004	0.305	0.001
grainstone	122.0	86498	296	1.43	0.01	233570	485	1.18	0.005	0.370	0.001
grainstone	144.0	49702	226	1.28	0.01	140142	376	1.14	0.006	0.355	0.002
grainstone	164.0	70849	268	1.24	0.01	246359	498	1.18	0.005	0.288	0.001
grainstone	219.0	61082	249	1.26	0.01	157597	399	1.15	0.006	0.388	0.002
grainstone	338.0	163614	406	1.30	0.01	423453	652	1.16	0.004	0.386	0.001
grainstone	423.0	109640	333	1.29	0.01	295214	544	1.15	0.004	0.371	0.001
grainstone	551.0	43750	212	1.28	0.01	154710	395	1.17	0.006	0.283	0.002
grainstone	625.3	66895	261	1.25	0.01	203815	453	1.15	0.005	0.328	0.001
grainstone	718.5	64410	256	1.30	0.01	184636	431	1.20	0.006	0.349	0.002
grainstone	753.4	113757	339	1.29	0.01	341088	585	1.19	0.004	0.334	0.001
grainstone	798.2	36957	196	1.30	0.01	128795	360	1.22	0.007	0.287	0.002

Table 5.6: Luminescence profiling data from Section 3 (OSL12-10) at Bahçeli (Vasilia) from the K4 terrace (N35 21.222 E033 38.141).

Lithology	Height (cm)	IRSL	Error	IRSL depletion	Error	OSL	Error	OSL depletion	Error	IRSL/OSL ratio	Error
Mudstone	10.0	15601	137	1.24	0.02	54901	241	1.22	0.01	0.284	0.003
Mudstone	27.0	14262	124	1.23	0.02	49935	226	1.19	0.01	0.286	0.003
Mudstone	41.0	9275	102	1.28	0.03	52271	231	1.22	0.01	0.177	0.002
Mudstone	53.0	12154	115	1.21	0.02	70861	268	1.19	0.01	0.172	0.002
Mudstone	60.0	12528	117	1.26	0.02	85140	293	1.27	0.01	0.147	0.001
Mudstone	69.0	14575	125	1.23	0.02	110701	334	1.23	0.01	0.132	0.001
Mudstone	79.0	19946	145	1.25	0.02	130504	363	1.25	0.01	0.153	0.001
Palaeolsol	90.0	22404	153	1.26	0.02	135283	369	1.31	0.01	0.166	0.001
Palaeolsol	101.0	26690	166	1.27	0.02	147932	386	1.34	0.01	0.180	0.001
Palaeolsol	109.0	24334	159	1.29	0.02	119865	348	1.26	0.01	0.203	0.001
Mudstone	117.0	18405	140	1.27	0.02	88742	300	1.26	0.01	0.207	0.002
Mudstone	125.0	17260	134	1.28	0.02	95482	310	1.26	0.01	0.181	0.002
Mudstone	134.0	17294	133	1.23	0.02	83366	290	1.21	0.01	0.207	0.002
Mudstone	144.0	18241	137	1.27	0.02	84465	292	1.19	0.01	0.216	0.002
Mudstone	159.6	15927	128	1.22	0.02	77069	279	1.23	0.01	0.207	0.002
Mudstone	170.8	17238	133	1.23	0.02	91241	303	1.25	0.01	0.189	0.002
Palaeolsol	181.9	23841	156	1.24	0.02	94786	309	1.19	0.01	0.252	0.002
Palaeolsol	196.1	25294	161	1.29	0.02	102775	321	1.23	0.01	0.246	0.002
Palaeolsol	209.3	38557	198	1.29	0.01	153212	392	1.29	0.01	0.252	0.001
Mudstone	288.2	19396	142	1.22	0.02	144609	381	1.21	0.01	0.134	0.001

Mudstone	300.6	16043	129	1.24	0.02	133548	366	1.31	0.01	0.120	0.001
Mudstone	316.0	14323	122	1.17	0.02	163732	405	1.27	0.01	0.087	0.001
Mudstone	332.0	11985	113	1.20	0.02	96728	312	1.27	0.01	0.124	0.001
Mudstone	348.2	16379	130	1.27	0.02	85641	294	1.23	0.01	0.191	0.002
Mudstone	359.4	12989	116	1.21	0.02	136538	370	1.22	0.01	0.095	0.001
Mudstone	371.5	17842	135	1.27	0.02	168540	411	1.32	0.01	0.106	0.001
Mudstone	450.0	13311	118	1.23	0.02	49358	224	1.17	0.01	0.270	0.003
Mudstone	460.0	11676	112	1.27	0.02	39275	200	1.18	0.01	0.297	0.003
Mudstone	470.0	5696	81	1.15	0.03	21215	148	1.15	0.02	0.268	0.004
Mudstone	480.0	4573	74	1.15	0.04	17536	135	1.12	0.02	0.261	0.005
Mudstone	490.0	4096	70	1.07	0.04	17794	137	1.13	0.02	0.230	0.004
Mudstone	500.0	6885	88	1.21	0.03	29380	174	1.14	0.01	0.234	0.003
Mudstone	510.0	9980	104	1.25	0.03	68296	263	1.18	0.01	0.146	0.002
Mudstone	550.0	11365	111	1.21	0.02	45110	214	1.15	0.01	0.252	0.003
Mudstone	569.7	13853	121	1.24	0.02	63171	253	1.19	0.01	0.219	0.002
Mudstone	632.9	7588	92	1.23	0.03	42184	207	1.19	0.01	0.180	0.002
Mudstone	682.9	2900	62	1.18	0.05	16437	132	1.25	0.02	0.176	0.004
Mudstone	710.9	4063	70	1.17	0.04	16461	132	1.14	0.02	0.247	0.005
Mudstone	772.9	1886	52	1.08	0.06	6985	88	1.14	0.03	0.270	0.008
Mudstone	797.9	5677	81	1.20	0.03	22551	154	1.14	0.02	0.252	0.004
Mudstone	1011.9	2291	56	1.05	0.05	12176	114	1.26	0.02	0.188	0.005
Mudstone	1028.9	2088	54	1.02	0.05	9304	100	1.19	0.03	0.224	0.006
Mudstone	1156.9	1804	52	1.08	0.06	5505	80	1.10	0.03	0.328	0.011

Mudstone	1212.9	1885	52	1.11	0.06	5938	83	1.11	0.03	0.317	0.010
Mudstone	1268.9	1792	52	1.06	0.06	5955	83	1.21	0.03	0.301	0.010

Table 5.7: Luminescence profiling data from Section 5(a) (OSL12-33A) at Mersinlik from the K4 terrace (N35 24.761 E033 48.659).

Lithology	Height (cm)	IRSL	Error	IRSL depletion	Error	OSL	Error	OSL depletion	Error	IRSL/OSL ratio	Error
Mudstone	0.0	13066	119	1.22	0.02	121384	350	1.21	0.01	0.108	0.001
Mudstone	200.0	6404	86	1.16	0.03	49402	225	1.22	0.01	0.130	0.002
Mudstone	263.0	6036	85	1.50	0.04	45541	216	1.24	0.01	0.133	0.002
Mudstone	294.0	6653	88	1.18	0.03	33651	186	1.20	0.01	0.198	0.003
Mudstone	423.0	8308	98	1.23	0.03	36084	193	1.20	0.01	0.230	0.003
Mudstone	522.0	13982	123	1.28	0.02	80612	285	1.24	0.01	0.173	0.002
Mudstone	599.0	8325	98	1.21	0.03	49507	225	1.27	0.01	0.168	0.002
Mudstone	683.0	7871	95	1.21	0.03	31459	180	1.16	0.01	0.250	0.003
Mudstone	763.0	5578	82	1.17	0.03	20947	149	1.18	0.02	0.266	0.004
Palaeosol	838.0	3741	70	1.14	0.04	14997	127	1.20	0.02	0.249	0.005
Palaeosol	874.0	3994	72	1.12	0.04	44404	213	1.19	0.01	0.090	0.002
grainstone	922.0	5628	83	1.24	0.04	65816	258	1.20	0.01	0.086	0.001

grainstone	948.0	5916	84	1.15	0.03	60499	248	1.16	0.01	0.098	0.001
grainstone	987.0	6159	86	1.23	0.03	22410	154	1.15	0.02	0.275	0.004
grainstone	1037.4	10760	109	1.18	0.02	18246	139	1.09	0.02	0.590	0.007
grainstone	1058.7	10558	108	1.17	0.02	33740	187	1.13	0.01	0.313	0.004
grainstone	1103.0	26550	167	1.31	0.02	43140	210	1.13	0.01	0.615	0.005
grainstone	1121.0	3963	71	1.15	0.04	17387	137	1.16	0.02	0.228	0.004
grainstone	1140.0	14215	124	1.24	0.02	34963	190	1.15	0.01	0.407	0.004

Table 5.8: Luminescence profiling data from Section 6 (OSL12-31) at Kalkanlı (Kapouti) from the K4 terrace (N35 15.168' E033 02.830').

Lithology	Height (cm)	IRSL	Error	IRSL depletion	Error	OSL	Error	OSL depletion	Error	IRSL/OSL ratio	Error
Mudstone	23.0	4035	69	1.19	0.04	17524	135	1.13	0.02	0.230	0.004
Mudstone	89.0	4813	75	1.19	0.04	29195	173	1.18	0.01	0.165	0.003
Mudstone	152.0	5844	81	1.20	0.03	24762	160	1.16	0.01	0.236	0.004
Mudstone	184.0	3068	62	1.17	0.05	30591	177	1.46	0.02	0.100	0.002
Mudstone	214.0	5882	82	1.17	0.03	23404	155	1.14	0.02	0.251	0.004
Mudstone	288.9	2103	54	1.12	0.06	9952	104	1.16	0.02	0.211	0.006
Mudstone	331.4	2517	57	1.12	0.05	10073	105	1.12	0.02	0.250	0.006

Mudstone	368.6	2428	57	1.09	0.05	12665	116	1.18	0.02	0.192	0.005
Mudstone	407.6	2165	54	1.05	0.05	12541	115	1.23	0.02	0.173	0.005
Mudstone	442.8	2435	57	1.17	0.05	8258	95	1.13	0.03	0.295	0.008

Table 5.9: Luminescence profiling data from Section 7 (OSL12-32) at Nergisli (Genagra) from the K5 terrace (N35 13.198' E035 13.198').

Lithology	Height (cm)	IRSL	Error	IRSL depletion	Error	OSL	Error	OSL depletion	Error	IRSL/OSL ratio	Error
Mudstone	34.9	151478	391	1.26	0.01	534027	731	1.05	0.003	0.284	0.001
Mudstone	91.3	63430	254	1.27	0.01	198633	447	1.15	0.01	0.319	0.001
Mudstone	108.8	49970	226	1.25	0.01	185461	432	1.13	0.01	0.269	0.001
Mudstone	198.9	106812	328	1.33	0.01	887413	942	1.11	0.002	0.120	0.000
Mudstone	256.4	179427	425	1.31	0.01	336352	581	1.11	0.004	0.533	0.002

Table 5.10: Background gamma readings for five K4 and K5 terrace deposits.

Locality	Height (cm)	Gamma (m/Ga)	Error	Lithology
Section 1				
OSL12-29	0.0	0.44	0.013	Marine grainstone
K4	130.0	0.36	0.010	Marine grainstone
terrace	250.0	0.43	0.011	Aeolian grainstone
Section 5(b)				
(OSL12-20)	0.0	0.55	0.011	Aeolian grainstone
K5 terrace	400.0	0.71	0.011	Aeolian grainstone
	500.0	0.62	0.010	Aeolian grainstone
	700.0	0.89	0.016	Aeolian grainstone
Section 5(a)				
(OSL12-33A)	200.0	1.77	0.028	Palaeosol
K4	423.0	0.48	0.009	Mud
terrace	922.0	1.08	0.019	Palaeosol
	1037.4	0.55	0.010	Aeolian grainstone
Section 6				
(OSL12-31)	0.0	0.32	0.016	Mud
K4	200.0	1.04	0.016	Mud
terrace	450.0	0.31	0.017	Mud
Section 7				
(OSL12-32)	0.0	0.68	0.011	Sand
K5 terrace	100.0	0.55	0.009	Sand
	200.0	0.72	0.011	Sand

Chapter 6

Quantitative dating of Plio-Pleistocene deposits in northern Cyprus

6.1 Introduction

The aims of quantitative dating were to try and constrain the rates and timings of uplift of the Kyrenia Range, and to understand how the interplay of tectonic, eustatic and climatic processes affected the depositional environments during the Plio-Pleistocene time. Both marine and non-marine deposits in northern Cyprus were dated from both before and after major uplift.

Dating of uplifted Mediterranean regions has proved an invaluable tool in understanding sedimentary and tectonic processes. Examples of such studies include research on the Gulf of Cornith where uranium-series dating has been extensively used to help understand the uplift of fault blocks (Dia *et al.*, 1997; Leeder *et al.*, 2003). Coastal terrace studies in Italy have used OSL dating, combined with sedimentology, to constrain the uplift rates of coastal terraces (Ferranti *et al.*, 2006). Magnetostratigraphy has been used to understand the development of carbonate aeolian systems in Mallorca (Nielsen *et al.*, 2004). Recently, strontium dating was used in Cyprus to develop a detailed stratigraphy of the Kythrea (Değirmenlik) Group, during the Eocene to Miocene tectonic history of northern Cyprus (McCay *et al.*, 2012). It was also used to understand the timings and processes associated with sapropel formation during the Middle

Miocene (Taylforth *et al.*, 2014). U-series, OSL and magnetostratigraphy have been used successfully to date the Plio-Pleistocene cover of the Troodos Massif to understand the timing and rate of uplift (Poole *et al.*, 1990; Kinnaird *et al.*, 2011; Kinnaird and Robertson, 2013). These studies will be discussed in more detail later in this chapter.

The dating techniques utilised in this study include strontium isotopes, magnetostratigraphy, uranium series and optically stimulated luminescence (OSL). Each of the techniques used proved to be problematic for a number of different reasons, including financial limitations, limited datable material and poor-quality samples. As a consequence of this, only a limited number of dates were provided by each technique. Each of these techniques are discussed below, followed by the results from each technique. A synthesis of the dating results is presented at the end of the chapter.

6.2 Strontium isotope dating

6.2.1 Samples

Samples were selected from the Athalassa (Gürpınar) Formation with the aim of dating the shallow-marine environment fringing the Kyrenia Range prior to major uplift (Table 6.1). *In situ* oyster shells and grainstone samples were selected from the upper part of the Athalassa (Gürpınar) Formation. These samples were selected because they represent the late-stage, marine environment within the Mesaoria (Mesarya) Basin, prior to subaerial exposure.

6.2.2 Results

The $^{87}Sr/^{86}Sr$ ratios, errors and ages are presented in Tables 6.2 and 6.3. The resultant strontium ages are mostly Middle to Late Miocene, with one of the Athalassa (Gürpınar) Formation grainstones giving an early Pleistocene age. The Miocene ages vary from the Middle Miocene to the Miocene-Pliocene boundary. The samples older than 12 Ma are from localities that are near or south of the Ovgos (Dar Dere) fault zone. The samples with ages from 6 to 9 Ma are from localities on both side of the Ovgos (Dar Dere) fault zone. Finally, the Pleistocene age comes from a sample on the

Sample	Region	Material	Formation	Grid reference
KYSR-01	Sandallar (Santalaris)	*Ostrea gryphaea*	Athalassa (Gürpınar)	N35 13.089' E033 48.756'
KYSR-02	Sandallar (Santalaris)	*Ostrea gryphaea*	Athalassa (Gürpınar)	N35 13.089' E033 48.756'
KYSR-03	Sandallar (Santalaris)	*Ostrea gryphaea*	Athalassa (Gürpınar)	N35 13.089' E033 48.756'
KYSR-04	Sandallar (Santalaris)	*Ostrea gryphaea*	Athalassa (Gürpınar)	N35 13.089' E033 48.756'
KYSR-05	Sandallar (Santalaris)	*Ostrea gryphaea*	Athalassa (Gürpınar)	N35 13.089' E033 48.756'
KYSR-06	Sandallar (Santalaris)	*Ostrea gryphaea*	Athalassa (Gürpınar)	N35 13.089' E033 48.756'
KY13-45	Güzelyurt (Morphou)	Grainstone	Athalassa (Gürpınar)	N35 11.764' E033 07.668'
KY13-50	Güzelyurt (Morphou)	Grainstone	Athalassa (Gürpınar)	N35 12.014' E033 07.004'
KY13-52	Güzelyurt (Morphou)	Grainstone	Athalassa (Gürpınar)	N35 11.205' E033 05.423'
KY13-80	Kaleburnu (Galinopori)	Grainstone	Athalassa (Gürpınar)	N35 22.724' E034 04.977'
KY13-82	Kaleburnu (Galinopori)	Grainstone	Athalassa (Gürpınar)	N35 30.970' E034 18.781'

Table 6.1: Samples and localities used for strontium dating.

Karpaz (Karpas) Peninsula and is part of a deposit stretching from the northern to southern coast.

6.2.3 Discussion

The Early to Late Miocene and Early Pleistocene ages all appear to be statistically correct ages (Table 6.3). The older Miocene ages of both the oyster shells and grainstone samples could be either, due to reworking from the Miocene Pakhna Formation in southern Cyprus (Eaton and Robertson, 1993; Lord *et al.*, 2000) or as a result of increased fluvial run-off into the Mesaoria (Mesarya) Seaway from the Kyrenia Range and Troodos Massif, which could reduce the $^{87}Sr/^{86}Sr$ ratio and give an anomalously older date (Fig. 1.1).

Sample	**$^{87}Sr/^{86}Sr$**	**% Standard Error**	**LOWESS age (Ma)**	**LOWESS lower age range (Ma)**	**LOWESS upper age range (Ma)**
KYSR-01	0.708768	0.0014	15.25	15.13	15.35
KYSR-02	0.708926	0.0014	8.53	7.97	8.88
KYSR-03	0.708987	0.0014	6.1	6.06	6.14
KYSR-04	0.70872	0.0013	15.9	15.81	15.99
KYSR-05	0.709005	0.0013	5.8	5.75	5.86
KYSR-06	0.708983	0.0015	6.15	6.11	6.20
KY13-45	0.70897	0.0015	6.48	6.40	6.56
KY13-50	0.708829	0.0012	12.37	12.05	12.63
KY13-52	0.708699	0.0015	16.34	16.24	16.46
KY13-80	0.709106	0.0012	1.478	1.425	1.532
KY13-82	0.708916	0.0012	9.03	8.72	9.33

Table 6.2: $^{87}Sr/^{86}Sr$ Isotopes results, standard percentage error and age (Ma) based upon the LOWESS marine Sr-isotope curve produced by McArthur *et al.* (2001).

The early Pleistocene date is from a whole-rock grainstone sample in the Karpaz (Karpas) Peninsula (KY13-80). This grainstone deposit is rich in benthic and planktonic formaminifera and is, therefore, interpreted as part of an open-marine environment, i.e. the deepest part of the carbonate ramp system (Sec. 2.7.2). The age range of sample KY13-80 covers 0.4 Ma (Table 6.3), within the Calabrian and Early Pleistocene.

Sample	LOWESS age (Ma)	Calculated age range	Difference in age range	Epoch	Stage
KYSR-01	15.25	14.96-15.49	0.55	Miocene	Langhian
KYSR-02	8.53	7.54-9.33	1.79	Miocene	Tortonian
KYSR-03	6.1	5.92-6.53	0.61	Miocene	Messinian
KYSR-04	15.9	15.76-16.26	0.50	Miocene	Langhian-Burdigalian
KYSR-05	5.8	5.57-6.01	0.44	Miocene	Messinian
KYSR-06	6.15	5.97-6.5	0.53	Miocene	Messinian
KY13-45	6.48	6.19-6.98	0.79	Miocene	Messinian
KY13-50	12.37	11.57-13.03	1.46	Miocene	Tortonian-Serravallian
KY13-52	16.34	16.07-16.65	0.58	Miocene	Burdigalian
KY13-80	1.478	1.313-1.717	0.40	Pleistocene	Calabrian
KY13-82	9.03	8.24-9.6	1.36	Miocene	Tortonian

Table 6.3: Strontium isotope dates with respective epochs and stages.

6.3 Magnetostratigraphy

6.3.1 Samples

Table 6.4 shows all of the samples collected from northern Cyprus for this study. 20 sites were selected (PM12-01 to PM12-20); from each site 5 cores (Samples A-E) were drilled from the selected deposit. The Athalassa (Gürpınar) Formation sites were selected to represent deposits on the eastern and western end of the Mesaoria (Mesarya) Plain and on the Karpaz (Karpas) Peninsula. The terraces sites selected to represent a profile of K1 to K5 in the central Kyrenia Range. The cores were drilled at each site with a petrol drill and the orientation of each core was measured with a brunton compass. The drilled cores were ca. 2.5 cm wide, ranging in length from 5 cm to 10 cm. Each core was cut into 2.5 cm segments to allow for multiple analysis of each sample. Site PM12-07 was removed from the list because the samples were damaged during transport to the UK. Sites PM12-03 and PM12-19 were selected to carry out remagnetisation tests, as described by Butler (1992). A total of 85 cores from 17 sites from Nicosia (Lefkoşa), Athalassa (Gürpınar) and Fanglomerate Formations in northern Cyprus were used for magnetostratigraphy analysis.

Site (sam.)	Grid reference	Height (m AMSL)	Terr. or form.	Date and time	AF demag.	Thermal demag.
PM12-13 (A-E)	N35 18.180' E033 26.398'	241	K1	02/05/12 12.45	✓	✓
PM12-11 (A-E)	N3518.659' E033 25.726'	167	K2	02/05/12 09.53	✓	
PM12-12 (A-E)	N35 18.728' E033 25.778'	151	K3	02/05/12 13.37	✓	
PM12-04 (A-E)	N35 21.467' E033 08.524'	6	K4	29/04/12 16.29	✓	
PM12-20 (A-E)	N35 20.044' E033 27.185'	2	K5	05/05/12 14.36	✓	
PM12-05 (A-E)	N35 28.720' E034 05.838'	158		30/04/12 12.49	✓	
PM12-06 (A-E)	N35 28.747' E034 05.966'	194	Kalkanlı (Kapouti)	30/04/12 14.51	✓	✓
PM12-18 (A-E)	N35 15.384' E033 02.534'	142		04/05/12 15.01	✓	✓
PM12-02 (A-E)	N35 13.089' E033 48.761'	41		28/04/12 14.55	✓	
PM12-08 (A-E)	N35 15.988' E033 48.993'	50		01/05/12 12.12	✓	✓
PM12-09 (A-E)	N35 15.967' E033 48.947'	65		01/05/12 15.00	✓	✓
PM12-10 (A-E)	N35 10.410' E033 50.722'	28	Athalassa (Gürpınar)	01/05/12 18.36	✓	✓
PM12-14 (A-E)	N35 39.892' E034 34.441'	21		03/05/12 15.31	✓	
PM12-15 (A-E)	N35 11.069' E033 06.140'	151		04/05/12 11.17	✓	✓
PM12-16 (A-E)	N35 10.961' E033 04.789'	130		04/05/12 12:00	✓	✓
PM12-01 (A-E)	N35 13.086' E033 48.748'	35	Nicosia (Lefkoşa)	28/04/12 14.15	✓	✓
PM12-17 (A-E)	N35 15.334' E033 02.625'	94		04/05/12 14:00	✓	✓
PM12-03 (A-E)	N35 16.476' E033 26.106'	611	Neptunian dyke	29/04/12 11.57	✓	
PM12-19 (A-E)	N35 17.351' E033 26.981'	343	Congl. test	05/05/12 11.58	✓	

Table 6.4: Palaeomagnetic samples (AF demag.= Alternating field demagnetisation; Thermal demag.= Thermal demagnetisation)

6.3.2 High-temperature magnetic susceptibility results

Two samples were selected for magnetic susceptibility tests, PM12-02A and PM12-08A from the Nicosia (Lefkoşa) and Athalassa (Gürpınar) Formations respectively. The two samples are composed of chalk and grainstone facies, representing the two lithologies sampled for this study.

Figure 6.1 shows the plotted high temperature magnetic susceptibility results for samples PM12-02A and PM12-08A. Several key observations are made from the high temperature susceptibility plot, firstly that the all the values are strongly negative; secondly, a rapid change in the magnetic susceptibility between 560-600^{o}C is observed within sample PM12-08A; and thirdly, sample PM12-02A shows only a slight change in magnetic susceptibility at 560-600^{o}C. The negative magnetic susceptibility indicates a diamagnetic material; i.e. the sample developed a weakly induced magnetic field, which is characteristic of non-magnetic minerals such as quartz and calcite (Butler, 1992). The rapid change of susceptibility at 560-600^{o}C is characteristic of the Curie temperature of magnetite, which is at ca. 580^{o}C (Dunlop and Özdemir, 1997).

High-temperature magnetic susceptibility experiments show that both the chalk (PM12-02A) and grainstone (PM12-08) deposits are weakly magnetic, containing a minor amount of magnetite.

6.3.3 Thermal demagnetisation results

Samples that showed stable magnetic components during thermal demagnetisation were selected for magnetostratigraphy. Figure 6.2 shows an example of the data from two samples selected for magnetostratigraphy plotted on demagnetisation curves and Zijderveld vector plots (Zijderveld, 1967). The samples show a good reduction in magnetic signal intensity with temperature, with no induced magnetic signal (Fig. 6.2(a-b)). The Zijderveld vector plots show unstable magnetic signal at low temperatures, but this is removed at higher temperatures (>400^{o}C)(Fig. 6.2(c-d)). The magnetic component used for calculating inclination and declination from each sample comes from the stable high temperature magnetic component (400-590^{o}C)(Fig. 6.2(e-f)).

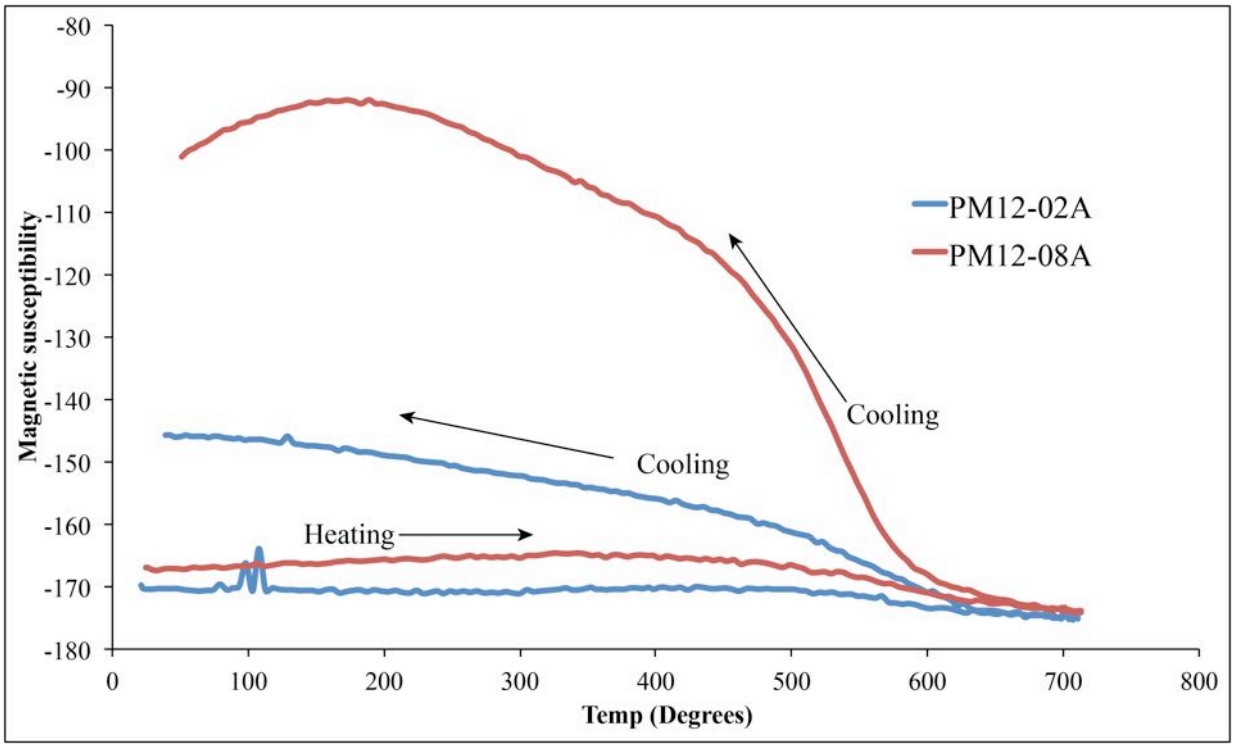

Figure 6.1: Plotted high temperature magnetic susceptibility results from samples PM12-02A and PM12-08A. Temperature is measure in degrees celsius and magnetic susceptibility is unitless.

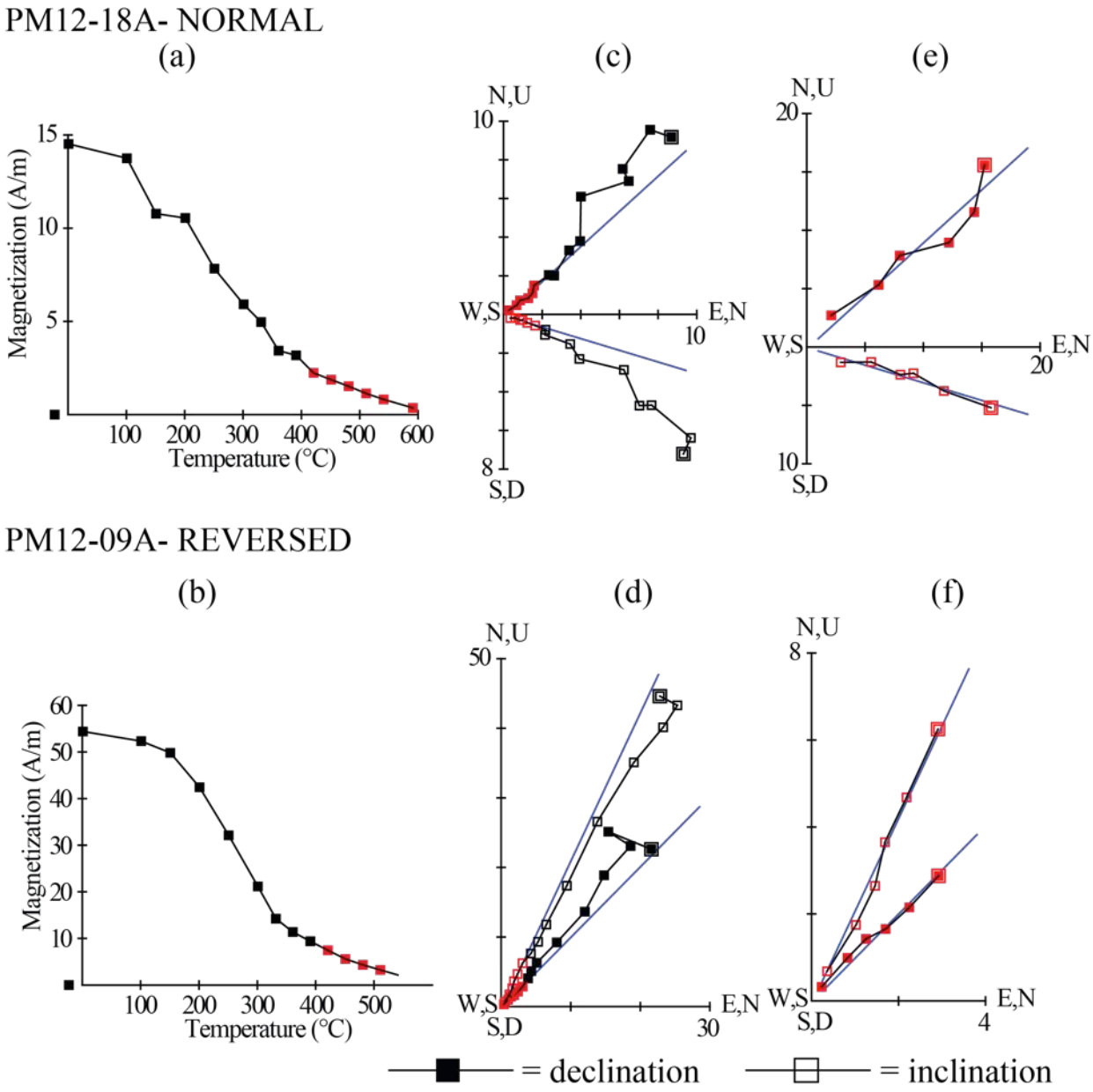

Figure 6.2: Demagnetisation plots from a normal and reversed polarity sample. Graphs (a-b) demagnetisation profiles from 0-590^{o}C; (c-d) Zijderveld vector plots (Zijderveld, 1967) showing the low-temperature, unstable component with the higher-temperature, stable component marked by red points; and (e-f) Stable magenetic component plotted on Zijderveld vector plots. (Data was plotted using PuffinPlot (Lurcock and Wilson, 2012))

6.3.4 Discussion

The final palaeomagnetism results are shown in Table 6.5 and Figure 6.3. All of the successful data was acquired from deposits of the Athalassa (Gürpınar) Formation; none of the samples from the Nicosia (Lefkoşa) or Fanglomerate Formation or remagnetisation tests gave usable data. The low magnetic signal strength results from samples of these formations suggests little or no magnetic material. Five samples were collected from each site, four of these gave usable data (Table 6.5).

The final inclinations and declinations suggest a combination of normal and reversed polarities within the Athalassa (Gürpınar) Formation (Table 6.5). The sample that indicates a reversed polarity has a southern hemisphere (90-270^o) declination and negative inclination. In contrast, the samples with a normal polarity have a northern hemisphere declination and a positive inclination.

Fisher distribution statistics were used to assess and calculate mean inclination and declination values for each site. The $\alpha 95$ value represents the radius on an equal-area plot of 95% confidence ideally, this number should be as small as possible. The k value is a Fisher precision parameter ranging from 0 to ∞, the higher values indicating increased precision of calculated means. The low $\alpha 95$ and high k values for sites PM12-09 and PM12-10 suggests statistically robust data. Site PM12-18 has relatively high $\alpha 95$ and low k values suggesting a less reliable data set. The large scatter of inclination values is possibly due to local sedimentary processes such are currents controlling grain deposition (reviewed by Kodama, 2012). The influence of sedimentary processes on inclination values is also seen in southern Cyprus (Kinnaird *et al.*, 2011).

Sample	**Facies**	**Height (m AMSL)**	**PCA**		**Fisher**				**Richter *et al.* (1998)**	**Magnetic polarity**
			dec.	**inc.**	**dec.**	**inc.**	**α95**	**k**		
PM12-09 A	Thick-bedded grainstone	50	166.97	-75.01	198.6	-70.7	15.8	35	A	Reversed
PM12-09 B			191.17	-71.06					A	
PM12-09 C			175.59	-73.25					A	
PM12-09 E			229.41	-55.61					A	
PM12-10 A	Laminated grainstone	31	10.5	34.2	342.2	33.9	19.0	24.3	A	Normal
PM12-10 B			331.2	25.4					B	
PM12-10 C			350.4	28.4					A	
PM12-10 D			331.5	34.6					A	
PM12-18 A	Laminated grainstone	93	48.6	13.8	50.6	38.5	71.0	2.7	B	Normal
PM12-18 B			210.1	56.5					B	
PM12-18 D			61	21.6					B	
PM12-18 E			30.2	20.2					B	

Table 6.5: Results of thermal demagnetisation of samples from the Athalassa (Gürpınar) Formation.

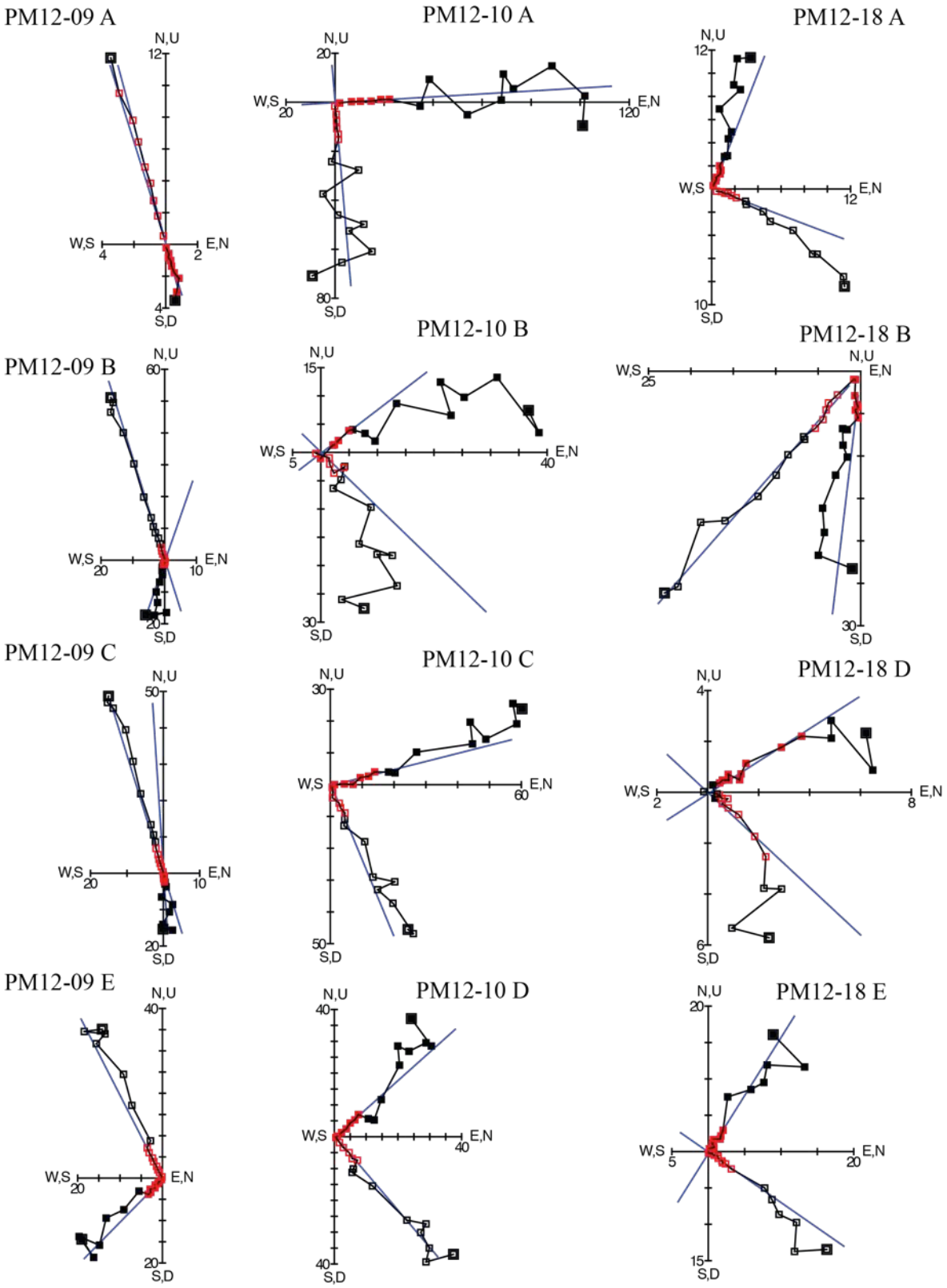

Figure 6.3: Zijderveld plots from all the results from thermal demagnetisation used to calculate inclinations and declinations. (Data was plotted using PuffinPlot (Lurcock and Wilson, 2012))

6.4 Uranium series dating

6.4.1 Samples

Eight *Cladocora* solitary coral samples were collected from the K4 terrace along the northern coast; a selection of these are shown in Figure 6.4. Corals were selected from marine deposits of the K4 terrace because these were the only coral preserved in northern Cyprus. Each sample was cut into several sub-samples and the septas were removed from each sample using a dremel drill, leaving behind the walls from each coral sample. The coral walls were used to assess the aragonite percentage of the coral, as these were likely to be less susceptible to alteration (Roberts *et al.*, 2009a). X-ray diffraction (XRD) analysis was carried out on the coral wall samples and those containing >95% aragonite were selected for U-series dating (Table 6.6).

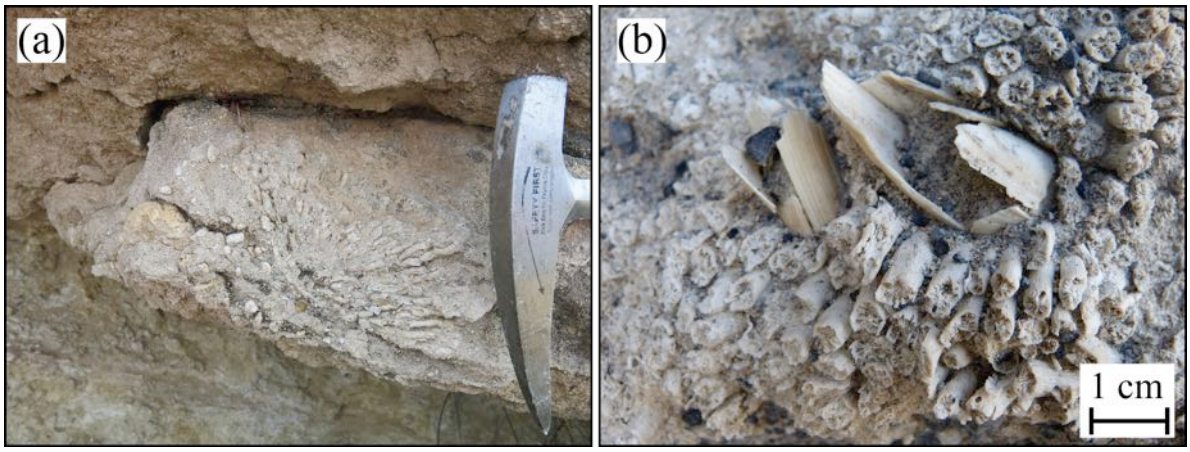

Figure 6.4: Photographs of *Cladocora* solitary corals used for U-series dating.

6.4.2 Results

Table 6.7 presents uranium and thorium isotopes and isotopic ratios from coral samples from the northern coast of Cyprus. The concentrations of the parent isotope ^{238}U are comparable with numerous previous Pleistocene U-series dating studies (Poole *et al.*, 1990; Goy *et al.*, 2003; Leeder *et al.*, 2003), indicating sufficient concentrations of the parent uranium isotope within the system. The relationship between the ^{230}Th/^{234}U and ^{234}U/^{238}U ratios can be used to determine age within a closed system (Ivanovich,

Sample	**Locality**	**Height (m)**	**Facies**	**Aragonite** (%)
KY13-19b	Karşıyaka (Vasilia) village	5	F7	98.1
KY13-94a	Tatlısu (Akanthou) village	15	F7	97.5
KY13-94b	Tatlısu (Akanthou) village	15	F7	97.5
KY 12-03	Esentepe (Agios Amvrosios) town	4	F6	99.38
KY 12-04	Esentepe (Agios Amvrosios) town	4	F6	99.85
KY11-22	Kayalar (Orga) village	40	F9	97

Table 6.6: Samples used for U-series dating

1982). Figure 6.5 is an isochron plot showing the relationship between $^{230}Th/^{234}U$ and $^{234}U/^{238}U$ ratios, up to 3 x 10^4 yrs, when secular equilibrium is reached (Ivanovich, 1982). The $^{230}Th/^{234}U$ and $^{234}U/^{238}U$ ratios from coral samples in northern Cyprus are plotted in Figure 6.5. Samples KY12-03, KY12-04 and KY11-22 have $^{230}Th/^{234}U$ ratios of <1, plotting within the datable fields defined within the isochron graph (Fig. 6.5). In contrast, samples KY13-19(b), -94(a) and -94(b) have $^{230}Th/^{234}U$ ratios of ca. 1, which indicates either that the system has reached secular equilibrium or that thorium isotopic contamination has taken place. The ^{232}Th concentrations are low enough to suggest that Thorium contamination is not a major problem in any of the samples (Table 6.7); therefore, samples KY13-19(b), -94(a) and -94(b) are likely to be in a state of secular equilibrium.

6.4.3 Discussion

Table 6.8 shows the final calculated ages of coral samples from northern Cyprus, based upon the relationship between the uranium and thorium isotopes, as derived by Ivanovich (1982). All of the coral samples produced ages from the Middle Pleistocene, with ages from 127 kyr to >350 kyr. Samples KY12-03, KY12-04 and KY11-22 can be correlated within interglacial cycles and are interpreted to represent global sea-level highs (Table 6.8). Samples KY12-03 and KY12-04 are correlated with interglacial cycles represented by the MIS (marine isotope stage) 5, and sample KY11-22 is correlated with the older MIS 7. Samples KY13-19(b), -94(a) and -94(b) represent ages

>350 ka and can be tentatively correlated with MIS 9; however a correlation with an older interglacial cycle is also possible.

Sample	^{238}**U (ppm)**	^{234}**U**/^{238}**U**	^{230}**Th**/^{234}**U**	^{232}**Th (ppb)**
KY13-19b	1.8731 ± 0.0100	1.0186 ± 0.0099	1.1192 ± 0.0401	193.64 ± 35.08
KY13-94a	2.500 ± 0.0152	0.9986 ± 0.0107	1.0610 ± 0.0380	57.93 ± 10.50
KY13-94b	2.5249 ± 0.0148	0.9952 ± 0.0102	1.0703 ± 0.0383	54.97 ± 9.96
KY12-03	2.4280 ± 0.0149	1.1052 ± 0.0109	0.7069 ± 0.0232	203.55 ± 36.88
KY12-04	2.5724 ± 0.0114	1.0961 ± 0.0093	0.7192 ± 0.0236	248.66 ± 45.05
KY11-22	2.3806 ± 0.0072	1.0946 ± 0.0051	0.9163 ± 0.0083	190.75 ± 34.48

Table 6.7: Uranium and thorium isotopes results from *Cladocora* solitary coral of the K4 terrace.

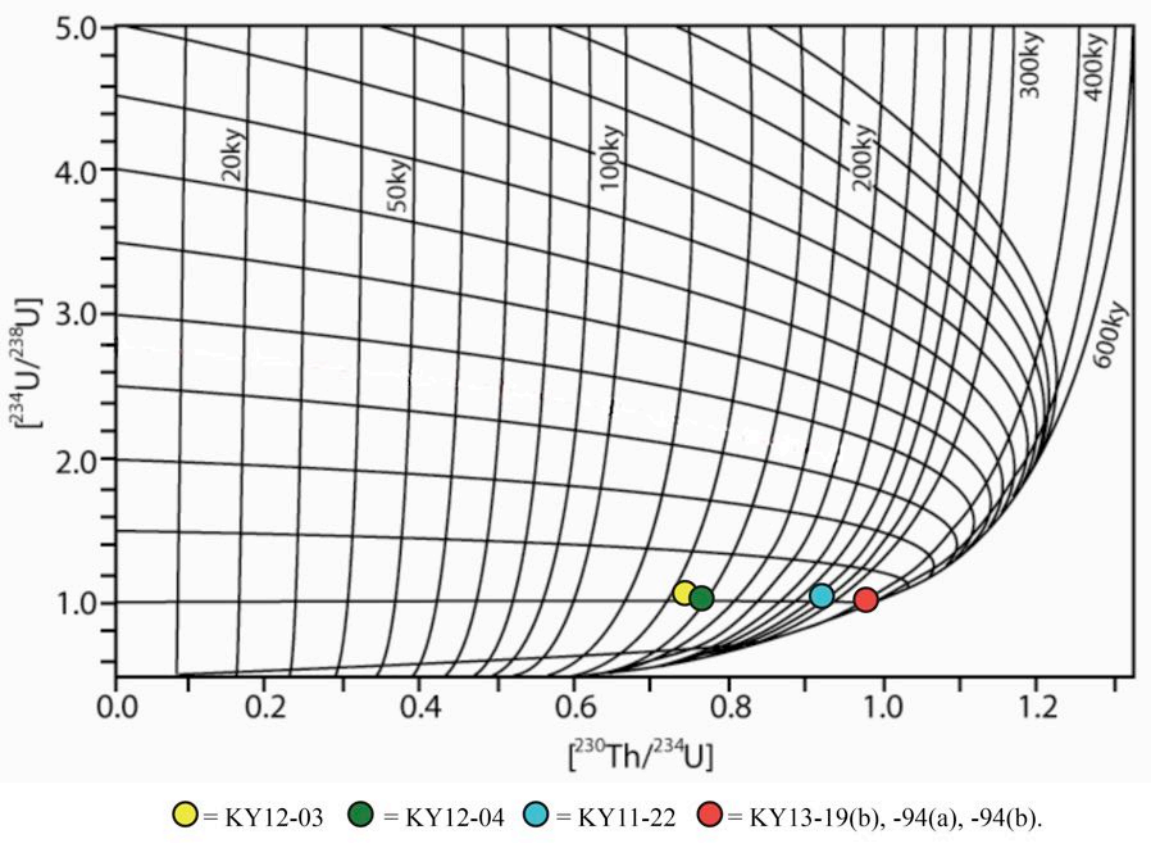

Figure 6.5: Isochron graph developed by Ivanovich (1982) to model the relationship between ^{234}U, ^{238}U and ^{230}Th.

Sample	**Age (kyr)**	**Error (kyr)**	**Stage**	**Marine isotope stage (MIS)**
KY13-19b	>350	29.3	Ionian	9?
KY13-94a	>350	5.3	Ionian	9?
KY13-94b	>350	5.2	Ionian	9?
KY 12-03	127	21.1	Ionian	5
KY 12-04	131	22.5	Ionian	5
KY11-22	243	19.5	Ionian	7

Table 6.8: Age interpretations based on U-series dating

6.5 Optically stimulated luminescence (OSL) dating

6.5.1 Samples

The maximum age for successful OSL dating varies significantly between the quartz and feldspar systems, but generally is up to 200, 000 years (Rhodes, 2011). Ducloz (1972) suggested possible ages for the K3 and K4 terraces based upon correlations with similar deposits around the Mediterranean and warm water marine fauna. The K3 terrace is associated with the classical Tyrrhenian stage (2.6-0.11 ka) and the K4 terrace with the Eutyrrhenian stage (1.3-0.11 ka). Based upon the ages suggested by Ducloz (1972), the K4 and K5 terraces were selected for dating, the K3 terrace was assumed to be out of the accepted age range for OSL dating.

To assess the luminescence characteristics of the deposits associated with the K4 and K5 terraces, field and laboratory profiling was undertaken. Details of the profiles taken during sampling are presented in Chapter 5 (Palamakumbura *et al.*, 2015).

6.5.2 Results

The results section is separated into three parts, namely: field profiling, laboratory profiling and dating results. The field profiling results are from Chapter 5 but the main conclusions from this are briefly discussed here to explain the reasoning behind the laboratory profiling.

Field profiling summary

Field profiling was carried out on seven deposits from the K4 and K5 terrace. Key inferences from this study, are:

1. The luminescence intensity varies between facies, with the highest signals coming from palaeosol deposits, followed by marine grainstone, then aeolian grainstones and finally the lowest signals from fluvial mudstones.
2. The K4 and K5 terrace deposits have distinctly different luminescence intensity characteristics.

3. The luminescence intensities of the K5 terrace deposits are an order of magnitude higher than those of the K4 terrace deposits.
4. Reworking of sediment between the K4 and K5 terraces has potentially caused an increase in sensitivity of the grains.

Laboratory profiling results

Laboratory profiling was carried out on K4 and K5 sections from Alagadi Beach and Mersinlik because the K4 and K5 terrace deposits observed are relatively close together at both localities with field relationships to confirm the relative terrace chronology. Furthermore, the terrace deposits at Mersinlik include grainstone and fluvial facies allowing the luminescence characteristics of these deposits to be assessed in laboratory.

The results from the laboratory profiling combined with field profiles are shown in Figures 6.6 and 6.7. The patterns shown within the field profiles are approximately replicated by the polymineral- and quartz-aliquot stored doses, showing similar increases and decreases in signal intensities as in the field profiling results. The stored doses for the K4 terrace are generally from 150-200 Gy, with extreme values at <40 Gy and >1000 Gy for both the polymineral and quartz aliquots. In comparison, the K5 terrace stored doses are generally <150 Gy in the polymineral aliquot and <100 Gy in the quartz aliquots. Stored dose values do not appear to follow the same patterns as the sensitivity values, suggesting that main control of stored dose is age rather than sensitivity. Sensitivities within the K4 terrace range from 60-800 Photon counts/Gy with occasional anomalously high values. In contrast, sensitivities within the K5 terrace range from 300-1000 Photon counts/Gy. A minor number of samples were not plotted in all of the graphs because they did not emit a luminescence signal.

The stored doses within the K4 terrace from both the polymineral and quartz aliquots were generally >200 Gy, which is approximately the saturation limit of quartz (Thomsen *et al.*, 2011). The high stored doses combined with low background radiation (Chapter 5, Table 5.10) suggest that these deposits are >200 ka and so are unsuitable for luminescence dating. The stored doses within the K5 terrace are significantly lower and within the accepted range for the quartz system, and hence can be reliably dated. Stored doses within the lower half of the K5 terrace deposit are generally <100 Gy, whereas in the upper half they are >100 Gy. The difference in stored doses between the lower and upper parts of the sequence is probably caused by residual signals within the

sediment in the upper part of the section, due to poor bleaching during transportation.

Based upon the laboratory profiling results, dating samples were taken from the lower part of the K5 terrace aeolianite deposits at Alagadi Beach and near Mersinlik town. The sensitivities are generally slighter higher within the K5 terrace than in the K4 terrace, indicating reworking of sediment from K4 to K5 terrace. This resulted in increased sensitivities as suggested in Chapter 5 .

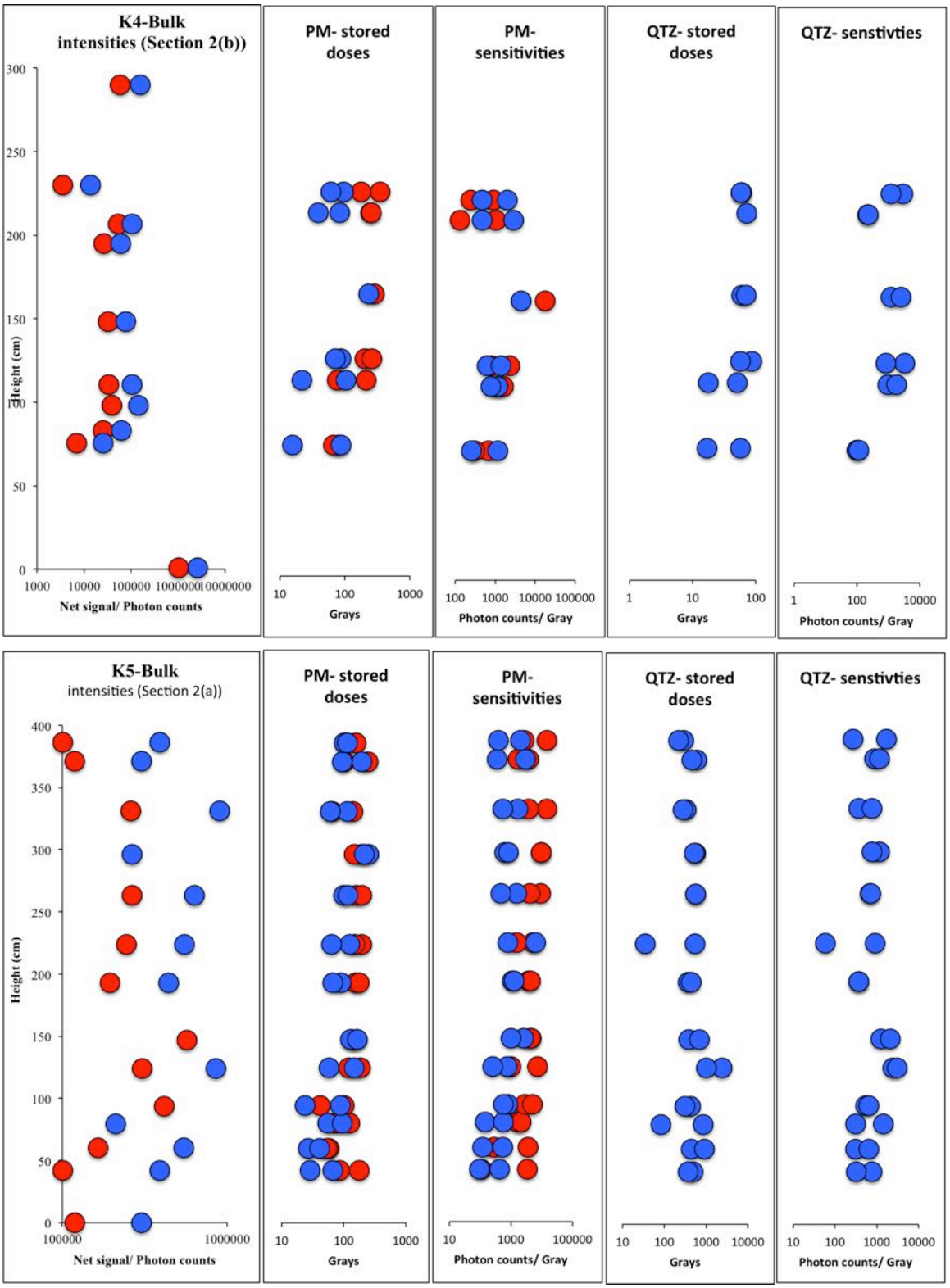

Figure 6.6: Field and laboratory profiling data from the K4 and K5 terrace deposits at Alagadi Beach. IRSL stimulation is shown by red markers and OSL stimulation is shown by blue markers.

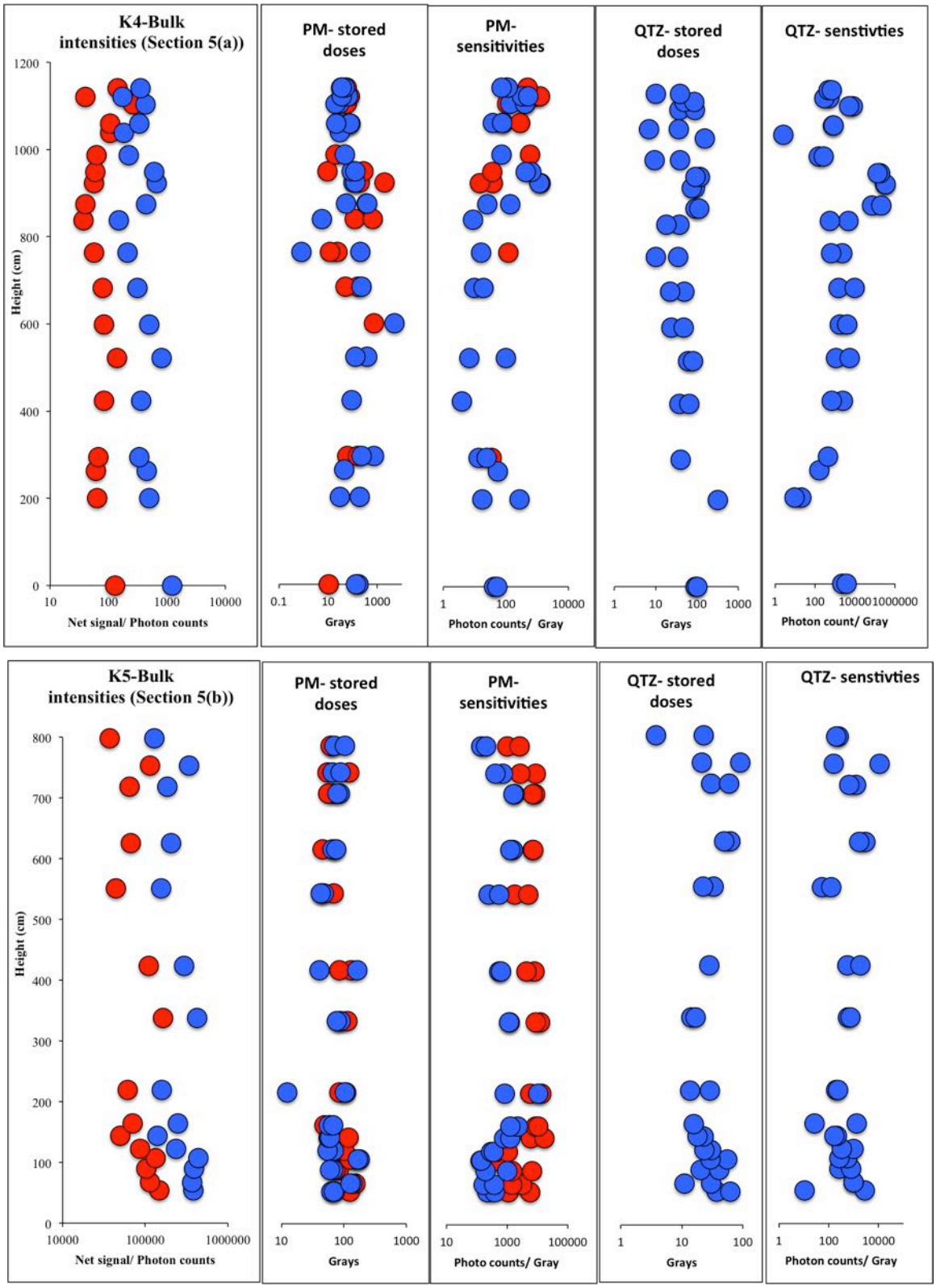

Figure 6.7: Field and laboratory profiling data from the K4 and K5 terrace deposits near Mersinlik town. IRSL stimulation is shown by red markers and OSL stimulation is shown by blue markers.

OSL dating results

Two samples were taken for dating from the K5 terrace at Alagadi Beach (KY14-01) and Mersinlik town (KY14-02) from aeolian grainstone deposits. The samples were taken from the base of each sequence, from directly above the basal unconformity because firstly, the profiles indicate that this part of the section is most suitable for dating, and secondly, a date from the base of section would constrain the oldest part of the deposit.

Dating was first attempted on quartz grains from both samples; however, this was unsuccessful due to low sensitivities and poor responses to various test doses. Following this, dating of the feldspar system was carried out using both IRSL at 50°C and post-IR IRSL at 225°C. To assess the signal fading rate over time of the feldspar system, IRSL and post-IR IRSL fading tests were carried out on 16 aliquots comprising K-feldspar grains. The fading test involved an initial IRSL and post-IR IRSL analysis and then a second analysis after 10^6 seconds. A ratio of the two IRSL and post-IR IRSL analysis results demonstrates the amount of signal decay over a given time period. Two ratios were produced of 0.93 ± 0.06 and 1.08 ± 0.08, for IRSL and post-IR IRSL respectively. The post-IR IRSL fading-test ratio suggested a more stable signal than the IRSL fading-test ratio; therefore the post-IR IRSL technique was given preference for calculating equivalent doses and age calculations. The final equivalent doses for IRSL and post-IR IRSL are plotted on radial plots in Figure 6.8. The calculated equivalent doses for IRSL at 50°C for both samples have a large spread of values. In contrast, the equivalent doses for post-IR IRSL at 225°C for both samples are better constrained. Furthermore, the error is generally higher for the equivalent doses associated with the IRSL stimulation than the post-IR IRSL. Therefore, equivalent doses of 112.0 Gy and 94.7 Gy were taken from the post-IR IRSL results to calculate the depositional age (Table 6.9).

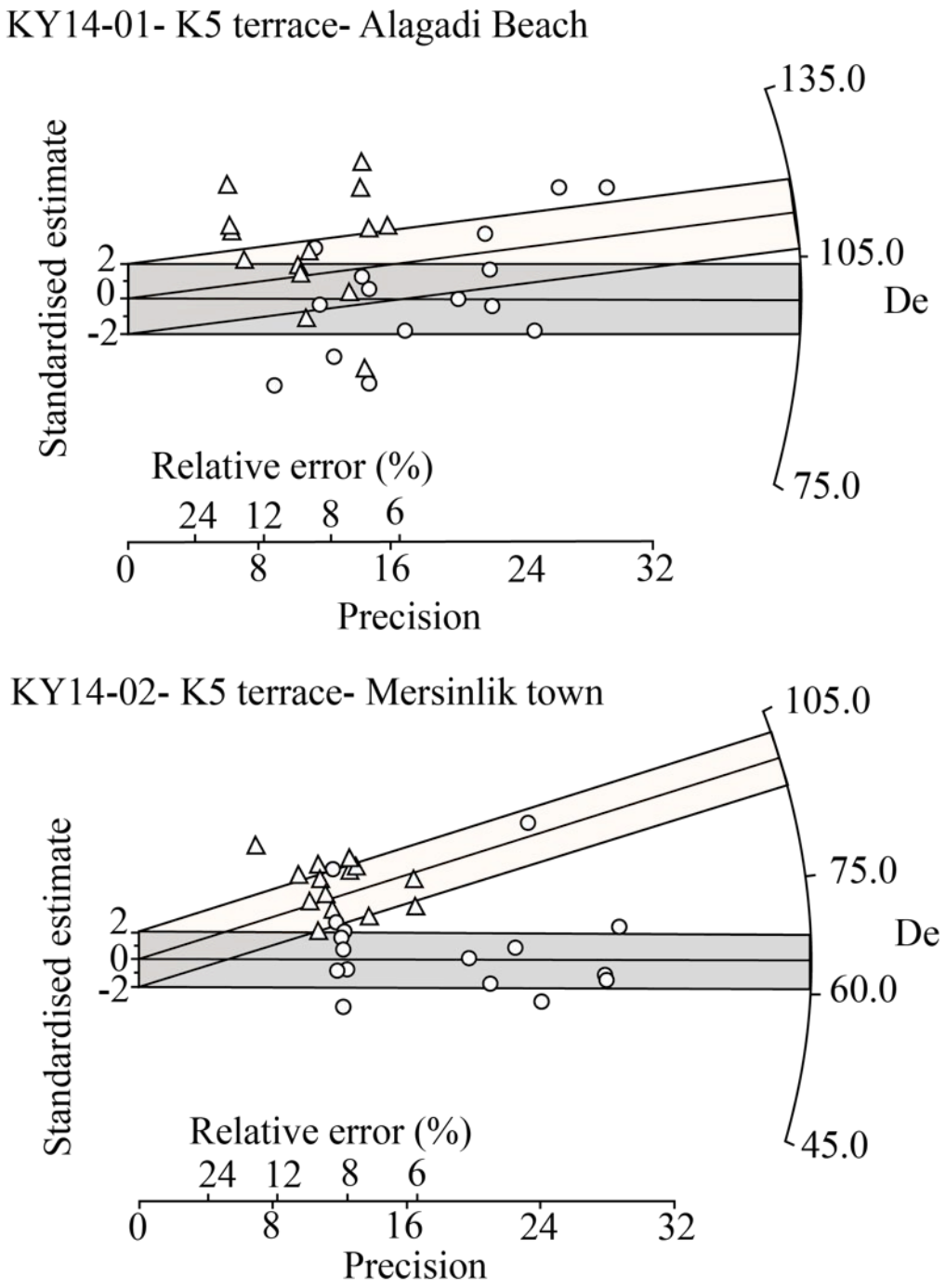

Figure 6.8: Radial plot for OSL dating from the K5 terrace (circles = IRSL 50°C D_e's; triangles = post-IR IRSL 225°C D_e's)(D_e= Equivalent dose)(Figure from OSL dating report in the appendix).

Sample	**Latitude/ Longitude**	**Dose rate (mGy/ka)**	**Stimulation type**	**Equivalent dose (D_e)(Gy)**	**OSL age (ka)**
KY14-01	N35 20.040' E033 29.239'	1.47 ± 0.09	IRSL 50°C pIR IRSL 225°C	98.8 ± 1.4 **112.0 ± 2.6**	76.1 ± 3.5
KY14-02	N35 24.817' E033 48.716'	1.76 ± 0.10	IRSL 50°C pIR IRSL 225°C	64.1 ± 0.8 **94.7 ± 2.1**	53.7 ± 2.6

Table 6.9: Optically stimulated luminescence (OSL) data from the K5 terrace aeolianite near the northern coast. Equivalent doses used for calculating the final OSL dates are shown in bold.

6.6 Discussion

The following section discusses the dating results in their geological context. Table 6.10 presents all of the newly derived dates from the Plio-Pleistocene deposits in northern Cyprus.

Technique	Facies	Environment	Date (Ma)	MIS	Glacial/ interglacial	Series	Stage
Strontium	Benthic foraminifera-rich grainstone	Open-marine Basin	1.478	48	Glacial	Early Pleistocene	Calabrian
U-series	Bioclastic conglomerate	Storm deposit	> 350	9?	Interglacial	Middle Pleistocene	Ionian
U-series	Grainstone-boulder conglomerate	Reworked-marine deposit	127	5	Interglacial	Middle Pleistocene	Ionian
U-series	Grainstone-boulder conglomerate	Uplifted-marine deposit	131	5	Interglacial	Middle Pleistocene	Ionian
U-series	Conglomerate	Maximum flooding surface	243	7	Interglacial	Middle Pleistocene	Ionian
OSL	Grainstone	Aeolianite	76.2	4	Glacial	Late Pleistocene	Tyrrhenian
OSL	Grainstone	Aeolianite	53.8	4	Glacial	Late Pleistocene	Tyrrhenian

Table 6.10: New quantitative dates from Plio-Pleistocene deposits in northern Cyprus.

6.6.1 Strontium

Strontium isotope dating produced one useful date from a benthic foraminifera-rich grainstone deposit of the Athalassa (Gürpınar) Formation. The result suggests an open-marine environment during the Early Pleistocene surrounding the Kyrenia Range, prior to major uplift.

6.6.2 Magnetostratigraphy

The magnetostatigraphy results were used to constrain the age of the Athalassa (Gürpınar) Formation during the Early Pleistocene in conjunction with strontium isotopic dating. The only reversed polarity results are from the planar-bedded grainstone that was also dated using strontium isotopes as ca. 1.4 Ma, which is a period of reversed polarity (Fig. 1.2). The other palaeomagnetic results are from shoreface environments within the upper part of the Athalassa (Gürpınar) Formation and had normal polarities. The normal polarity samples were deposited either during the Cobb Mountain (1.22-1.24 Ma), Jaramillo (0.99-1.07 Ma) or after the Matuyama-Brunhes (0.78 Ma) normal polarity chron (Fig. 1.2). Therefore, the shallow-marine shoreface environment represented by the upper part of the Athalassa (Gürpınar) Formation continued into the late Early Pleistocene.

6.6.3 U-series

The U-series dating in northern Cyprus produced four Late Pleistocene dates from marine deposits from the K4 terrace along the northern coast. Three dates can be correlated with interglacial periods during the Middle Pleistocene and the fourth date represents an older reworked marine deposit within the K4 terrace. The U-series dates come from three different marine deposits: one, a reworked marine deposit (storm event); two a maximum flooding surface at the base of the K4 terrace; three, a transgressive marine horizon within a Gilbert-type delta deposit. The first two depositional settings represent the oldest marine base of the K4 terrace (preserved within ca. 20 m of the northern coast). In contrast, the third depositional setting represents a transgressive event within the K4 terrace.

6.6.4 OSL

The OSL dating produced two successful ages for the basal part of two aeolianite deposits of the K5 terrace, which accordingly can be correlated with the MIS 4 glacial period. The K5 aeolianite deposit is preserved extensively along the northern coast, representing a major period of aeolian dune formation. The OSL dating from post-IR IRSL showed a large variation in the equivalent doses from the feldspar grains. This range of equivalent doses could be caused either by a variation in the provenance of the grains or a variation in the age of the grains. The calculated dates are correlated with a glacial period from 29-71 Ma, during this period the aeolianite grains are likely to have undergone multiple phases of reworking and deposition to produce this range of equivalent dose values.

A more detailed comparison of all the dating results combined with their geological context is presented in the final discussion (Chapter 7).

6.7 Conclusions

1. Strontium dating of the Athalassa (Gürpınar) Formation indicates an Early Pleistocene age.

2. Magnetostratigraphy of the Athalassa (Gürpınar) Formation suggest that the shallow-marine environment surrounding the Kyrenia Range lasted until the end of the Early Pleistocene.

3. U-series dates from marine deposits of the K4 terrace give Middle Pleistocene dates.

4. OSL dating of K5 aeolianite deposits give a Late Pleistocene age.

Chapter 7

Synthesis and discussion

7.1 Introduction

This chapter presents a synthesis of the sedimentology and quantitative dating results related to the uplift of the Kyrenia Range. The aim of this chapter is to discuss the larger-scale regional to global processes that have controlled the Plio-Pleistocene geological evolution of northern Cyprus.

7.2 Pre-major uplift

The pre-major uplift depositional environment in northern Cyprus is represented by the Nicosia (Lefkoşa) and Athalassa (Gürpınar) Formations. The Nicosia (Lefkoşa) Formation is a series of interbedded chalks and marls, containing planktonic foraminifera with occasional reworked benthic foraminifera (Sec. 2.7.1). The deposit represents an open-marine shelf that surrounded the Kyrenia Range during the Pliocene. Conformably overlying the Nicosia (Lefkoşa) Formation is the Athalassa (Gürpınar) Formation, including the Kalkanlı (Kapouti) Member (Sec. 2.8). The Athalassa (Gürpınar) Formation represents a shallow-marine environment that extended between the Kyrenia Range and the Troodos Massif, and was affected by relative changes in sea-level. The Kalkanlı (Kapouti) Member represents marine to non-marine environments along the northern edge of the Mesaoria (Mesarya) Basin.

7.3 Major uplift

The Taşkent (Vouno) Member accumulated during major uplift and is preserved within the core of the Kyrenia Range (Sec. 3.6.1). The deposits represent a non-marine lacustrine environment within the central range. Interbedded with the uppermost part of the Taşkent (Vouno) Member is the K0 (Karka) terrace megabreccia deposit (Sec. 3.6.2). The megabreccia deposits represent large-scale mass wasting of the Trypa (Tyripa) Group metacarbonate, during or soon after a phase of rapid uplift.

The K1 to K5 terraces represent marine to non-marine environments on the northern flank and non-marine environments on the southern flank of the range (Sec. 4.10.1). The terraces developed during the Middle to Late Pleistocene uplift of the Kyrenia Range. The field luminescence data shows that the lower terraces can be correlated along the northern and southern flanks of the range (Sec. 5.4). The K2 to K5 marine deposits represent shallow-marine environments including: nearshore open-marine (below the storm-wave base), shoreface, foreshore (beachrock) and backshore (lagoonal) environments (Sec. 4.8.1).

The K1 to K5 terrace non-marine environments include aeolian dunes and fluvial drainage systems on both flanks of the range (Sec. 4.8.1, 4.8.2). The aeolian dunes are composed of reworked marine grainstones and are often preserved conformably overlying the marine deposits. The K1 terrace fluvial systems are made up of cohesive debris-flow deposits, which are partially preserved on the northern and southern flanks of the ranges. The K2 to K5 fluvial drainage systems are made of either channelised debris flows or high-energy, fluvially controlled deposits that are interbedded with mudstones and palaeosols. On the northern flank of the range, several major drainage systems have been identified within each terrace system.The coastal component of the drainage systems on the northern flank of the range are occasionally preserved, either as Gilbert-type delta deposits or as interbedded channelised conglomerate with shoreface grainstone facies deposits. Each terrace drainage system downcuts into the older drainage systems; consequently, older terrace deposit are preserved as isolated terrace surfaces. No marine terraces are preserved on the southern flank of the Kyrenia Range, suggesting either that any marine terrace deposits were eroded by younger fluvial systems or more likely that the Mesaoria (Mesarya) Plain was never a marine environment after uplift began.

7.4 Stratigraphy

This section collates the new and previous dating and also constrain the upper and lower ages of the Pleistocene deposits of northern Cyprus. The dating of the pre-major uplift deposits was achieved using strontium isotope dating (Sec. 6.2) and the palaeomagnetism (Sec. 6.3) of the Athalassa (Gürpınar) Formation. The strontium isotope date came from a benthic foraminifera-rich grainstone from the Karpaz (Karpas) Peninsula. The dated grainstone can be correlated with the base of the carbonate ramp sequence preserved within the Mesaoria (Mesarya) Basin. The strontium isotope dating therefore demonstrates an Early Pleistocene age for the Athalassa (Gürpınar) Formation, indicating that a shallow-marine environment fringed the Kyrenia Range during this time (Fig. 7.1). Combining the strontium dating with the palaeomagnetic analysis shows that the shallow-marine environment represented by the Athalassa (Gürpınar) Formation persisted throughout the Early Pleistocene.

The uranium series (U-series) and optically stimulated luminescence(OSL) dating was carried on the K4 and K5 terraces on the northern flank of the Kyrenia Range. The U-series dating utilised corals from marine deposits within the K4 terrace (Sec. 6.4). In contrast, OSL dating was carried out on aeolian grainstone from the K5 terrace (Sec. 6.5). The K4 marine deposits are correlated with global interglacial periods while the K5 aeolianite deposits are correlated with global glacial periods (Fig. 7.1). The upper and lower age limits of the K4 and K5 terraces are constrained by U-series and OSL dating. The boundaries of the K1 to K3 terraces are based upon the inference that each terrace represents a signal interglacial-glacial cycle (see Section 7.7).

The boundaries between the Kalkanlı (Kapouti) Member, the Taşkent (Vouno) Member and the K0 terrace deposit can not be constrained by quantitative dating. However, two key sedimentary relationships within these deposits help us to understand the relative stratigraphy. The reworked fragments of K0 breccia within the Kalkanlı (Kapouti) Member (Sec. 2.3.1, Fig. 2.20, Photo D), and interbedded K0 megabreccia within the upper part of the Taşkent (Vouno) Member (Sec. 3.2, Fig. 3.2 (a)). These relationships demonstrate that the K0 megabreccia was deposited in a non-marine lacustrine environment within the central range and reworked into fluvial drainage systems within the Mesaoria (Mesarya) Plain during the earliest phase of uplift.

No new dates were obtained for the boundary between the Nicosia (Lefkoşa) and

the Athalassa (Gúrpınar) Formations. The published biostratigraphy from southern Cyprus by Lord *et al.* (2000) is therefore used to help constrain the age of this boundary. Lord *et al.* (2000) described the Nicosia (Lefkoşa) Formation as continuing into the Late Pliocene; however, based upon the newly defined Plio-Pleistocene boundary (Cohen and Gibbard, 2010) this is now within the Early Pleistocene. Lord *et al.* (2000) focused on the deposits of the southern side of the Mesaoria (Mesarya) Basin. These can be stratigraphically correlated with deposits on the northern side of the Mesaoria (Mesarya) Basin (McCallum and Robertson, 1990).

Other dating studies in northern Cyprus include OSL dating of coastal aeolianites and the use of biological environment indicators from marine deposits of the K4 terrace. Erginal *et al.* (2012) used OSL dating from coastal aeolianite deposits on the Karpaz (Karpas) Peninsula, showing ages of 1.5 Ka to 0.4 Ka, from the base to the top of the deposit. The OSL dates again show aeolian deposition during the most recent glacial period. Galili *et al.* (2012) found marine gastropods (*Persististrombus latus*) within marine deposits from the K4 terrace at the coast. This study suggested that these gastropods lived during the environmental conditions associated with marine isotopic stage (MIS) 5. The inferences of that study do have some inherent errors however, they do appear to be in agreement with the new U-series dating results.

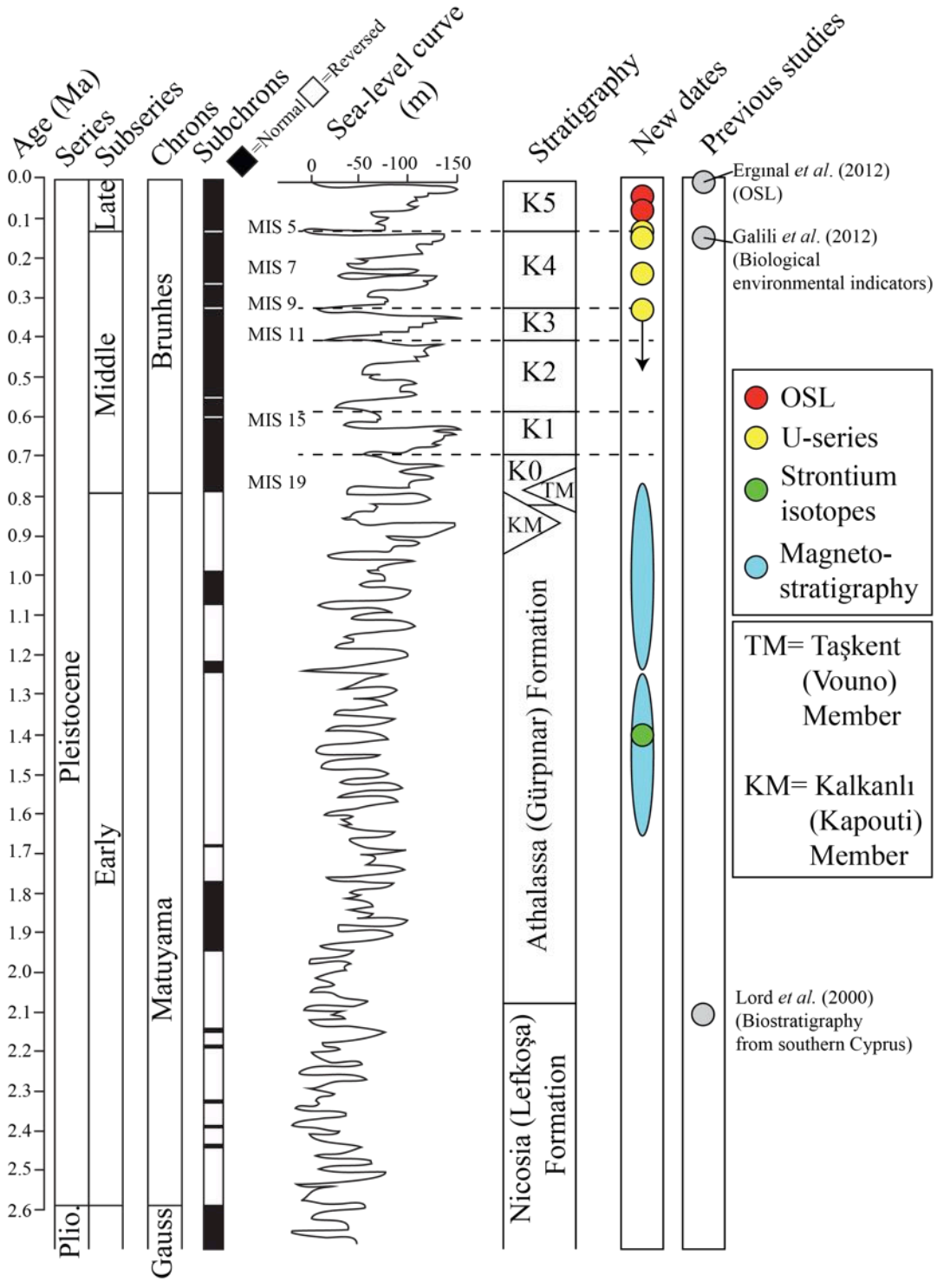

Figure 7.1: Synthesis of new and previous dating carried out on Pleistocene deposits in northern Cyprus (dates from Ducloz (1972); Lord *et al.* (2000); Erginal *et al.* (2012); Galili *et al.* (2012)).

7.5 Terrace comparison

The following section compares the deposits on the northern and southern flanks of the Kyrenia Range and the Pleistocene sedimentary cover of the Troodos Massif. The aim is to firstly, understand how the marine and non-marine environments are related along the northern and southern flanks of the Kyrenia Range. Secondly, a brief comparison is made between the Pleistocene deposits associated with both the Kyrenia Range and the Troodos Massif to compare the uplift of the two mountain ranges.

7.5.1 Northern versus southern flank deposits

Six terraces are identified on the northern and southern flanks of the Kyrenia Range, K0 to K5. The six terraces are amalgamted from previous mapping and stratigraphy carried out by Ducloz (1964, 1972), Knup (1965) and Baroz (1979). Correlation of terraces along the flanks of the range were based on: 1) height above sea-level, 2) relative height change compared to the surrounding terraces, 3) sedimentology of the terrace deposits, 4) sedimentary relationship between terrace deposits, and 5) luminescence characteristics of the lower terrace deposits. The sedimentology and sedimentary relationships of the deposits have been used alongside the previous height-based terrace differentiation system (Ducloz, 1964) to illuminate six major terrace systems.

The K0 terrace facies offer the closest comparison on the northern and southern flanks of the Kyrenia Range (Fig. 7.2). The K0 megabreccia facies has similar characteristics and is the highest terrace deposit on both the northern and southern flanks of the range.

The K1 terrace facies include colluvium and cohesive debris-flow deposits on both northern and southern flanks of the range. These deposits can be correlated around the range based on their height above sea-level and their relationship to the K0 terrace. The main variation between the northern and southern flanks of the range is the presence of aeolianite and palaeosol facies on the northern flank of the range (Fig. 7.2).

The biggest difference in depositional environments between the northern and southern flanks of the range comes from the K2 to K5 terraces. The K2 terrace on the northern flank of the range contains the first marine deposit, which is overlain by a

high-energy fluvial drainage system composed of channelised debris-flow deposits interbedded with mudstones and palaeosols (Fig. 7.2). In contrast, on the southern flank of the range, the K2 terrace is made up of a high-energy fluvial drainage system with planar-bedded and channelised conglomerate interbedded with mudstone.

The K3 terrace surface represents a major drop in height from the base of the K2 terrace to the base of K3 terrace, by ca. 100 m on both the northern and southern flanks of the range. The sedimentology of the K3 terrace is comparable to the K2 terrace deposits on the northern and southern flanks (Fig. 7.2).

The base of the K4 terrace deposit on the northern flank of the range is composed of shallow-marine and carbonate aeolianite facies, which are not found on the southern side of the range (Fig. 7.2). Interbedded and overlying the marine deposits on the northern flank of the range are a series of fluvial and deltaic deposits that are comparable to the fluvial drainage systems on the southern flank of the range. The sedimentology of the fluvial deposits on both flanks suggests a series of high-energy fluvial drainage systems flowing away from the range. The fluvial drainage systems formed deltas on the northern coast or drained into the Mesaoria (Mesarya) Plain on the south side of the range.

The K5 terrace has a number of similarities and differences between the northern and southern flanks of the range. The deposits on the northern coast are primarily composed of aeolianite facies and are occasionally overlain by fluvial deposits made up of interbedded channelised conglomerate and mudstone. In contrast, on the southern side of the range, the K5 terrace deposits are poorly-consolidated high-energy fluvial deposits that are best preserved within the Mesaoria (Mesarya) Basin. Major valleys on the northern flank that have been cut into the K4 and older terraces are likely to be associated with the K5 terrace. Deposits preserved within these valleys are poorly consolidated due to their relatively young age.

7.5.2 Northern versus southern Cyprus terraces

Two types of terrace are preserved in southern Cyprus, firstly a series of fluvial terraces, and secondly, a sequence of shallow-marine and aeolianite deposits (Poole and Robertson, 1998, 2000). Sedimentary relationship are poorly preserved between the two types

of terrace in southern Cyprus. Both terraces types are described as F0 to F4 and are loosely correlated in terms of relative age (Poole and Robertson, 1991).

The highest and oldest fluvial terraces (F0 and F1) are composed of <15 m thick poorly-sorted conglomerate with angular clasts, which are interpreted as representing streamflood or sheetflood processes (Poole and Robertson, 1998). The high-energy deposition of the F0 and F1 conglomerates was attributed to the an early phase of rapid uplift during the Early Pleistocene (Poole and Robertson, 1991). The high-energy deposition and the period of rapid uplift are represented in the Kyrenia Range by the K0 and K1 terrace deposits. Therefore, the F0 to F1 terraces in southern Cyprus can be correlated with the K0 to K1 terraces in northern Cyprus (Fig. 7.2). One major difference is that no megabreccia facies (K0 (Karka)) as seen in northern Cyprus is preserved in southern Cyprus. This is because of the unique conditions of formation for this type of deposit that occured in the Kyrenia Range were not present in the Troodos Massif. Namely, the very steep slopes generated during the uplift of the Kyrenia Range are not formed during the domal uplift of the Troodos Massif.

The F2 to F4 fluvial terraces in southern Cyprus are composed of 10 m-thick interbedded sandstones, medium-grained gravels with discontinuous silty beds (Poole and Robertson, 1998). The F2 to F4 terraces are interpreted as high-energy braided, channelised and floodplain sequences associated with the Middle to Late Pleistocene gradual uplift (Poole and Robertson, 1991). The high-energy fluvial drainage systems represented by the F2 to F4 terraces in southern Cyprus can be correlated with the fluvial drainage systems of the K2 to K4 terraces in northern Cyprus (Fig. 7.2).

The K5 terrace represents the most recent phase of fluvial deposition, which has resulted in unconsolidated conglomerate deposits within the Mesaoria (Mesarya) Basin. In southern Cyprus, this phase of recent fluvial deposition is not incorporated within the terrace nomenclature system.

Correlating the marine terraces in northern and southern Cyprus has been achieved by using U-series dating of corals within the F4 and K4 terraces. U-series dates from both F4 and K4 terraces show that marine deposits accumulated during MIS 5 (Poole *et al.*, 1990; Poole and Robertson, 1991). The K1 to K4 terraces are correlated with the F1 to F4 based on the quantitative correlation of the K4 terrace from U-series dating results (Fig. 7.2). Finally, the K5 terrace aeolianites can be correlated with the

F4 terrace because Poole and Robertson (2000) describes equivalent coastal aeolianite facies deposits in southern Cyprus as part of the F4 terrace (Fig. 7.2).

NORTHERN CYPRUS									SOUTHERN CYPRUS	
Ducloz (1964)	Northern Kyrenia Range				Southern Kyrenia Range				Poole	
	Terr.	Log	Envir.	Description	Terr.	Log	Envir.	Description	Fluv.	Mar.
Karka	K0		C0	Megabreccia	K0		C0	Megabreccia	F0	-
Klepini (Arapköy)	K1		C1 C1	Debris-flow sheets and colluvium, locally overlain by aeolianites and palaeosols.	K1		C1	Debris-flow sheets and colluvium.	F1	F1
Trapeza (Beşparmak)	K2		C2 C2 M2	Marine deposits overlain by non-marine deposits, including: aeolianites and interbedded channelised debris-flows and mudstones.	K2		C2	High-energy fluvial drainage system made up of interbedded planar-bedded conglomerates, channelised conglomerates and mudstones.	F2	F2
Ayios Epiktitos (Çatalköy)	K3		C3 C3 M3	Terrace locally downcut into the K2 terrace. Basal marine deposit is overlain by non-marine deposits, including: aeolianites and interbedded channelised debris flows and mudstones.	K3		C3	High-energy fluvial drainage system which has undergone a phase of major downcutting through older terraces. The deposit is an interbedded planar-bedded conglomerate and mudstone.	F3	F3
Kyrenia (Girne)	K4		C4 C4 C4 M4 C4 M4	Basal marine deposit overlain by non-marine deposits, including: aeolianites and interbedded channelised debris flows and mudstones. Basal non-marine deposits include transgressive marine phase.	K4		C4	Fluvial drainage system with fault-controlled segments. Deposits include channelised conglomerate, planar-bedded conglomerate, channelised mudstone and massive mudstone.	F4	F4
Koupia	K5		C5 M5 C5	Aeolianite above marine transgression preserved in the lower part of the deposit. Fluvial systems erodeed older terraces, with unconsolidated conglomerate deposits.	K5		C5	High-energy fluvial drainage system, locally overlain by aeolianite.	-	

Figure 7.2: Comparison of terrace deposits on the northern and southern flanks of the Kyrenia Range with the Pleistocene terraces on the Troodos Massif.

7.6 Climate controls

A combination of new sedimentological and quantitative dating results are used here to shed new light on the climatic controls of terrace depositional environments during the Middle to Late Pleistocene. Climatic conditions during the Late Cenozoic represent some of the most dynamic variations in Earths geological history (Siddall *et al.*, 2006; Zachos *et al.*, 2001). The dynamic Cenozoic climate is attributed to an increase in frequency and amplitude of glacial cycles related to a complex interaction of factors such as astronomical forcing (Lambeck *et al.*, 2002). The effects of such dynamic glacial cycles and climatic variations are represented by the depositional environments and their relationships with the non-marine terrace deposits in northern Cyprus. Two key depositional environments are preserved within the terraces that represent contrasting climatic conditions, including aeolian dunes and fluvial drainage systems.

The aeolian dunes are preserved within the K1 to K5 terraces on the northern flank of the Kyrenia and are likely to have formed during arid climate conditions. The OSL dating of the K5 terrace carbonate aeolianite suggests that they accumulated during the most recent glacial stage. Brooke (2001) suggests that coastal carbonate aeolianites can be intepreted to represent "warm and windy" climatic conditions. An modern analogue of such conditions is southern Australia, which has a local submarine carbonate platform to source material and a warm, windy and arid climate. The repeated preservation of carbonate aeolianites within the K1 to K5 terraces would suggest that warm, windy and arid climatic conditions occurred during the glacial stages of the Middle to Late Pleistocene.

Fluvial drainage systems are preserved within the K2 to K5 terraces on both the northern and southern flanks of the Kyrenia Range. The fluvial drainage systems comprise interbedded channelised debris-flow deposits, mudstones, palaeosols and caliche. The channelised debris-flow deposits represent episodes of high-energy depositions, while the mudstones represent overbank low-energy deposits between the channels. Evidence for this interpretation comes from the U-series dating of marine deposits interbedded with deltaic deposits of the K4 terrace. The dated deposits suggest major fluvial deposition during the MIS 5 interglacial stage. Maroon-coloured palaeosols are preserved within the lower part of the K2 to K4 terrace fluvial drainage systems (Sec. 4.9) and are interpreted as representing wet humid climatic conditions (Kraus, 1999). Mottled caliche is preserved predominantly within the palaeosols of the K2 to

K4 terraces. Arakel (1982) described mottled caliche as forming in arid environments with moderate rainfall, i.e. environments with high evapotranspiration. This type of caliche is also found in the Mojave Desert, California (Schlesinger, 1985), the coast of Israel (Magaritz *et al.*, 1979) and western Australia (Arakel, 1982). The caliche within the K2 to K4 terrace is therefore interpreted as representing a diagenetic process occurring within an arid climate with occasional precipitation.

Marine fauna assemblages preserved within marine deposits of the K4 terrace can be used to interpret climate conditions during interglacial periods. The basal marine conglomerate of the K4 terrace contain both the mollusc *Spondylus* and the coral *Cladocora*, these can be used to interpret warm water conditions (Pedley and Grasso, 2002). The *Cladocora* corals from this deposit have been dated as 243 ka, which is the interglacial marine isotope stage 7. These interpretations are in agreement with $^{18}O/^{16}O$ ratios from spelothem overgrowths in Mallorca, Spain (Vesica *et al.*, 2000) and in Israel (Bar-Matthews *et al.*, 2000), which also indicate warm climatic conditions during MIS 7.

7.7 Tectonic, climatic and sea-level processes

This sections aims to infer how tectonic, climatic and sea-level processes controlled the sedimentology and morphology of the terraces on the northern flank of the range. An attempt will be made to correlate each terrace with a specific marine isotopic stage. This approach provides approximate ages for each terrace system.

Figure 7.3 shows a simplified model for the formation of the marine and non-marine terraces on the northern flank of the Kyrenia Range. The oldest part of the each terrace on the northern flank of the range is a marine deposit, which represents a maximum flooding surface and with occasional interbedding with fluvial deposits. This suggests that the basal marine deposit and fluvial drainage systems of each terrace formed contemporaneously during an interglacial period with a global sea-level maximum (Fig. 7.3(a)). Supporting evidence comes from the U-series dating of coral (Sec. 6.4), showing that the marine deposits, which are occasionally interbedded with deltaic deposits, formed during interglacial periods. In the upper terraces (K2 and K3), only the nearshore open-marine environment are preserved (Fig. 4.48); however, in the lower terraces a larger range of marine environments are preserved. Similar processes

have been studied on Pleistocene deposits in Sicily, Italy, where it was shown that in a microtidal environment, maximum cool-water carbonate production occurred during global sea-level highs (Pedley and Grasso, 2002).

Progressing into a glacial stage caused a major sea-level drop resulting in the exposure of the marine facies and aeolian dune deposition (Fig. 7.3(b)). OSL dating of the K5 terraces shows that the aeolianites were deposited during glacial periods (Sec. 6.5). As previously discussed, this glacial period is represented by arid climatic conditions.

A marine transgression resulted in an erosive terrace step being cut into the marine and non-marine deposits at the previous interglacial-glacial cycle (Fig. 7.3(c)). Moving into the new interglacial stage resulted in another sea-level high and a maximum flooding surface with subsequent marine and fluvial deposition. The pre-existing marine and non-marine terraces are abandoned during the formation of the next terrace. This process of terrace abandonment related to tectonic uplift is also described, for example, from the fluvial terraces in the Central Makran Range, SE Iran (Kober *et al.*, 2013).

The transition from interglacial to glacial periods combined with tectonic uplift resulted in a changing climate and falling base level resulting in a large amount of fluvial downcutting, also studied by Blum and Törnqvist (2000) and Starkel (2003) (Fig. 7.3(d)). Again, contemporaneously aeolian deposition and reworking of the older marine deposit took place. The processes was repeated for the K1 to K5 terraces on the northern flank of the Kyrenia Range.

This process of terrace formation through the interaction of tectonic uplift and sea-level change was also inferred for southern Cyprus (Poole *et al.*, 1990; Poole and Robertson, 2000), the Messenia Peninsula, south Greece (Kourampas and Robertson, 2000), and Morocco, Eastern Patagonia and the Tonga Island in the Pacific Ocean (Pedoja *et al.*, 2014). This terrace formation processes implies that each terrace represents one eustatic oscillation during ongoing tectonic uplift. Based upon this terrace formation process, each terrace can be correlated with a marine isotopic stage during the Middle to Late Pleistocene.

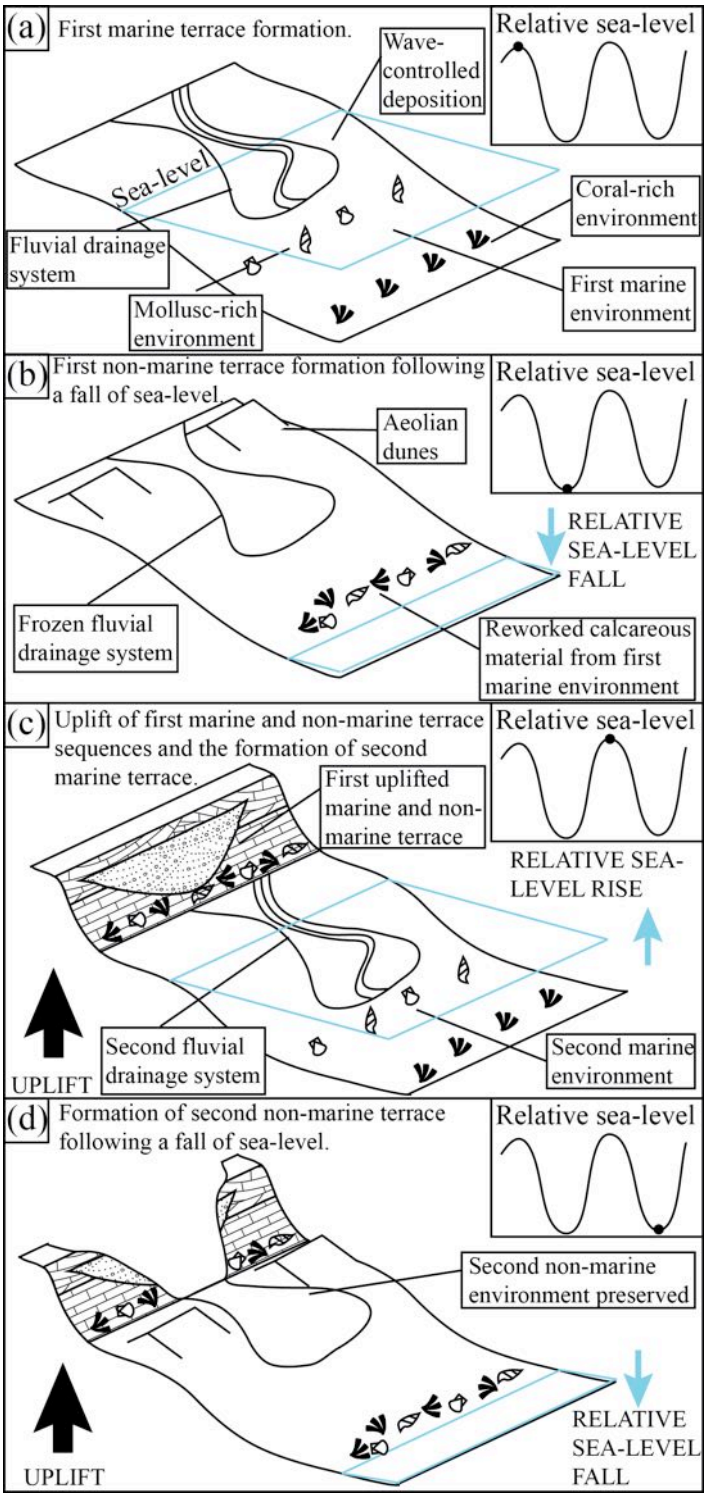

Figure 7.3: Simplified terrace formation model showing the tectonic and eustatic processes affecting the terraces on the northern flank of the Kyrenia Range.

A combination of the dating and sedimentological results can be used to correlate the K1 to K5 terraces with the global sea-level curve. Correlations are made between the dated K4 and K5 terraces with global sea-level. The K1 to K3 terraces are back correlated with the sea-level curve during the Middle to Late Pleistocene. A similar method of correlating terraces with global sea-level has previously been used in studies on the Messenia Peninsula, south Greece (Kourampas and Robertson, 2000), northern California (Merritts and Bull, 1989) and southern Italy (Dumas *et al.*, 2005).

The OSL dating was carried out on samples from the lower part of the K5 terrace aeolianite, representing the beginning of aeolian deposition during the most recent glacial period. The U-series dating of corals suggest that multiple eustatic oscillations are represented within the K4 terrace. The oldest date of >350 Ka is interpreted as being from locally reworked coral from an older marine environment. The second date of ca. 240 Ka comes from a maximum flooding surface at the base of the K4 terrace and can be correlated with MIS 7. The final U-series date from the K4 terrace is interpreted as representing a marine transgression at ca. 130 Ka, which is preserved within the coastal deltaic deposit. The combination of the quantitative dating and sedimentological studies allowed the K4 and K5 terraces to be correlated with the global eustatic sea-level curve (Fig. 7.4).

The K1 to K3 terraces are interpreted as each representing a single eustatic oscillation. There are no preserved sedimentary relationship that indicate multiple eustatic oscillations. From quantitative dating, the K4 terrace extends to MIS 9, therefore, the K3 terrace can be correlated with MIS 11 (Fig. 7.4). Marine isotope stage 11 represents one of the warmest interglacial periods during the Middle Pleistocene with sea-levels at 21 m above modern sea-level (Olson and Hearty, 2009; Roberts *et al.*, 2012).

The K1 and K2 terraces can be correlated with MIS 15 and MIS 13, respectively (Fig. 7.4). The correlation of the K1 to K5 terraces with the global sea-level curve provides an approximate age of ca. 600 ka for the formation of terrace sequence in northern Cyprus. The K0 terrace cannot be correlated with global sea-level curve as the depositional processes are dominantly controlled by tectonic uplift rather than sea-level change. The age of the K0 terrace is somewhere between 1.4 Ma (age of pre-uplift marine environment) and 0.6 Ma (age deduced for K1 to K5 terrace sequence).

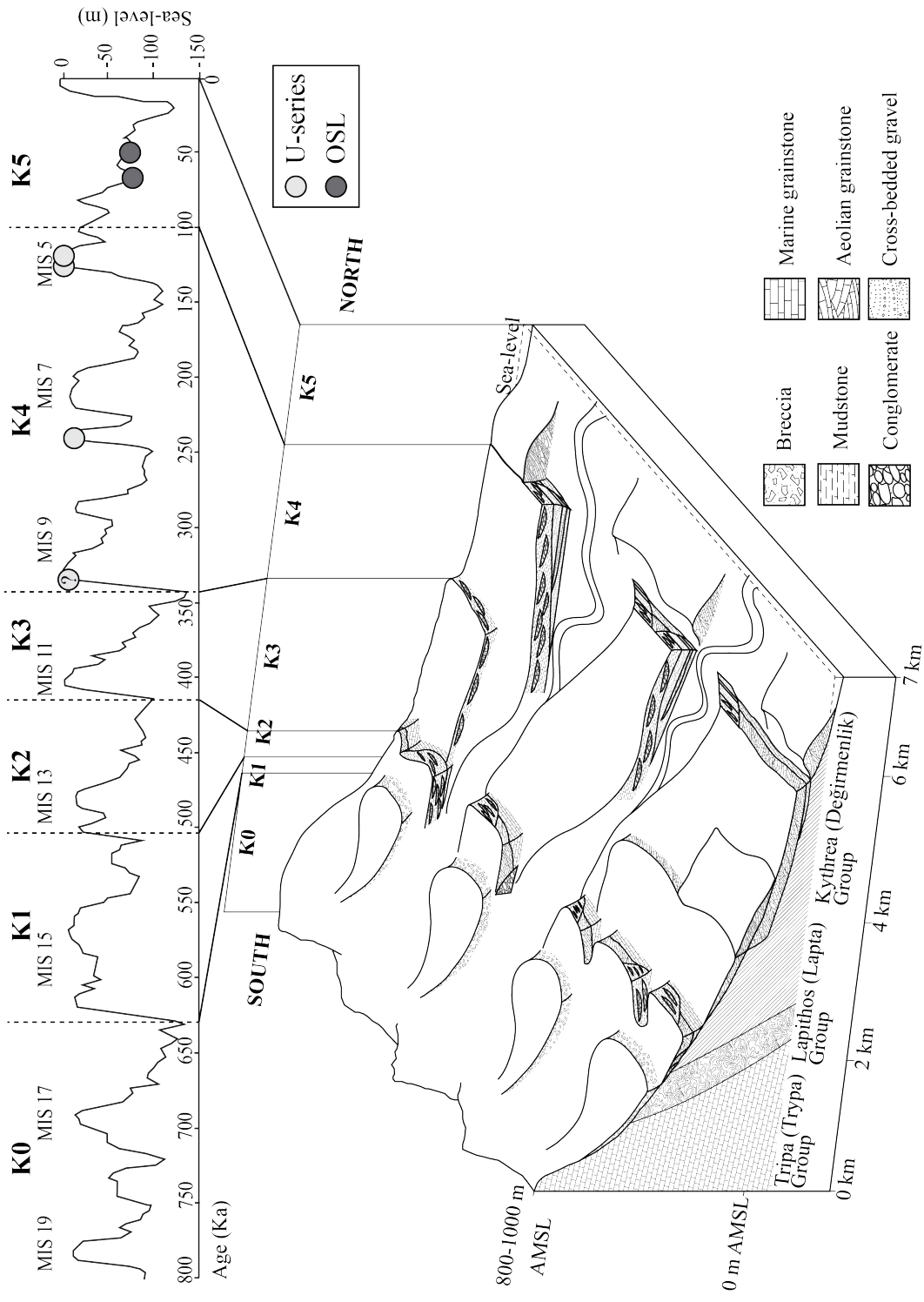

Figure 7.4: Block diagram showing depositional environments of the K0 to K5 terraces correlated with the global sea-level curve (sea-level curve is taken from Siddall *et al.* (2006)).

7.8 Terrace morphology

The discussion so far has focused on how the interaction between tectonic uplift and global sea-level change have controlled the sedimentology of each terrace system. To develop these concepts further, this section explores how varying rates of tectonic and sea-level change could control terrace morphology.

Eustasy throughout the Pleistocene was extremely dynamic, with strong variability in magnitude and duration of glacial-interglacial cycles during the Middle to Late Pleistocene (Waelbroeck *et al.*, 2002; Siddall *et al.*, 2003; Siddall *et al.*, 2006). Furthermore, tectonic uplift of the Kyrenia Range may not have been constant in rate throughout the Plio-Pleistocene. Table 7.1 explores the theoretical consequences of relative differences in tectonic uplift rate and rates of sea-level change on terrace morphology. The size and gradient of the erosional step between terraces could be controlled by the difference in tectonic uplift rate versus the rate of sea-level change; therefore, a basic interpretation of the sea-level and uplift relationship can be inferred from the profile of a coastal terrace sequence.

Tectonic uplift rate compared to eustasy	**Sedimentary sequence**	**Terrace morphology**	**Dominant control**
U > SF	Regression	Major fluvial downcutting	Tectonics and sea-level
U < SF	Regression	Gentle terrace gradient to small terrace step	Tectonics and sea-level
U > SR	Regression	Gentle terrace gradient to small terrace step	Tectonics
U < SR	Trangression	Prominent terrace step	Sea-level change

Table 7.1: Theoretical results when comparing tectonic uplift rates (U) with varying rates of either sea-level fall (SF) or sea-level rise (SR).

Four scenarios are presented in Table 7.1 involving varying rates of sea-level rise (SR) and fall (SF) compared with varying uplift rates (U). The rate of relative sea-level fall can either be slower than uplift rate (U > SF) or faster than tectonic uplift (U < SF). In both of these scenarios, the resultant sedimentary sequence is a marine regression, as a consequence of both tectonic and sea-level controls. In a scenario where U

> SF the result would be a major drop of the base level, which could drive increased fluvial downcutting resulting in major height difference between terraces. Whereas, when U < SF the fall in relative sea-level is less and does not result in major fluvial erosion.

During periods of relative sea-level rise, rates of uplift could either be greater than those of sea-level rise (U > SR) or less than the those of sea-level rise (U < SR). The resultant sedimentary sequence when rates of uplift are greater than those of sea-level rise is a marine regression. In contrast, when uplift rates are less than those of sea-level rise the sedimentary sequence would be a marine transgression. When U > SR the dominant control would likely be tectonics, whereas when U < SR the dominant control is sea-level change (Table 7.1). In the case of uplift rates that are slower than sea-level rise, the marine transgression could result in major coastal erosion forming a prominent terrace step.

Figure 7.5 shows a profile of the S1 to S5 terrace surfaces on the northern side of the central Kyrenia Range. The S1 to S2 terrace surfaces form a single continuous northward-dipping surface; this is caused by the onlapping relationship of the K1 and K2 terrace deposits. The S2 to S3 surface then forms a major step in the topography. The step is from ca. 180 m AMSL (S2) down to ca. 80 m AMSL (S3), representing a ca. 100 m break in slope. The S3 surface then forms a continuous surface down to the S4 surface at the coast. The sedimentary relationships between the S3 and S4 deposits are rarely exposed. The lowest point on the K3 terrace is at ca. 58 m AMSL; in contrast, the highest point of the K4 terrace is at ca. 40 m AMSL. Hence, there is a clear difference in height between the two terraces but the boundary is a gradual northward-dipping surface. Finally, the S4 to S5 boundary is a major step at the coast of between ca. 5 m to 10 m.

Two types of terrace surface boundary are evident along the northern coast of the Kyrenia Range; firstly, a gradual, shallow-dipping boundary, with a large drop in height over a significant distance (1 km to 2 km); and secondly, a stepped boundary with a significant drop in height over a relatively short distance (<100 m). The S1 to S2 and the S3 to S4 surface boundaries represent shallow northward-dipping boundaries; whereas the S2 to S3 and the S4 to S5 surface boundaries are stepped (Fig. 7.5).

The K2 to K4 terraces all represent regressive sedimentary sequences, which sug-

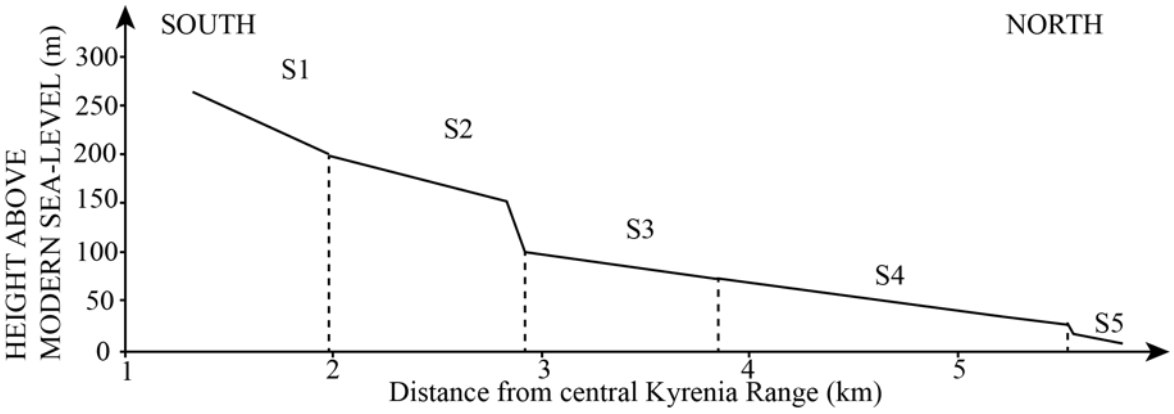

Figure 7.5: Schematic section through the S1 to S5 surfaces on the northern side of the Kyrenia Range. Surface heights are based on heights measured in the field; distance from the Kyrenia Range was measured using Google Earth, allowing estimates of surface angle.

gests that the formation of all these terraces is controlled by both sea-level and tectonic processes. The large step between the K2 to K3 and K4 to K5 terraces is likely to be a consequence of major fluvial downcutting and could, therefore, be interpreted as representing U > SF. The gentle steps represented by the K1 to K2 and K3 to K4 terraces suggest a more gradual fall of sea-level.

The K4 and K5 terraces contain preserved marine transgressions, suggesting that they both represent periods where uplift rate was lower than the rate of sea-level rise (U < SR). The K4 terrace is represented by a marine regression followed by a major marine transgression. This suggests that the K4 terrace was initially controlled by tectonics and sea-level, however, relative sea-level change eventually became the dominant control.

These suggested theoretical interpretations are compared with the global eustatic sea-level curve during the Pleistocene. Based on interpretations from Section 7.7 each terrace can be associated with a unique marine isotopic stage as follows: K1- MIS15, K2- MIS 13, K3- MIS 11, K4- MIS 9-5 and K5- MIS 4-3 (Fig. 7.4). The significant height differences between the K2 and K3 and K4 and K5 terraces is interpreted as representing faster rates of uplift than sea-level fall during MIS 11 and MIS 5 relative to MIS 15 (K1 to K2) and MIS 9-7 (K3 to K4). This observation is also made by Pedoja *et al.* (2014) who presented a synthesis of global uplifted terrace shorelines. This

worked described the interaction between tectonic uplift and eustatic sea-level change as resulting in a "sea-level barcode" during the Pleistocene. Their study identifies the MIS 5, 7, 9 and 11 as major terrace steps, which is attributed to the amplitude of the sea-level oscillations during these glacial cycles.

Previous discussions have shown that the interaction between relative sea-level change and tectonic uplift is an important process controlling the Kyrenia Range terrace sedimentology and morphology. However, clearly the variations in amplitude of relative sea-level change and rates of tectonic uplift also play a major role in shaping the terraces. The slowing uplift combined with varying amplitudes and frequencies of glacial cycles resulted in the various widths and height differences of each terrace system.

7.9 Uplift rates

Uplift rates can be calculated based on the terrace ages as deduced from sea-level correlations and terrace heights from Google Earth. The height and age used for calculating uplift rate is the difference in height and age of a terrace relative to the next youngest terrace. This method provides an estimate of uplift rate for each terrace during various times during the Middle to Late Pleistocene.

The calculated uplift rates are shown graphically in Figure 7.6. The K1 to K4 terraces show steadily decreasing uplift rate from >1 mm/yr during the Middle Pleistocene to <0.2 mm/yr during the Late Pleistocene. The uplift rate for the K0 terrace is estimated based on faster uplift rates than those used for the younger terraces, due to sedimentological interpretations that were previously discussed (Sec. 3.6.2).

To understand the relevance of the calculated uplift rates of the Kyrenia Range, a comparison is made with areas that are also undergoing Pleistocene uplift in the Eastern Mediterranean. The localities chosen for comparison geographically surround Cyprus. Importantly, the selected localities all underwent Pleistocene uplift due to local tectonic processes related to the regional convergence of the African and Eurasian plates. Table 7.2 shows uplift rates for selected regions around Cyprus during the Pleistocene. Several observations can be made based on the uplift rates across the Eastern Mediterranean; firstly, areas to the east of Cyprus have constant and slower uplift rates than

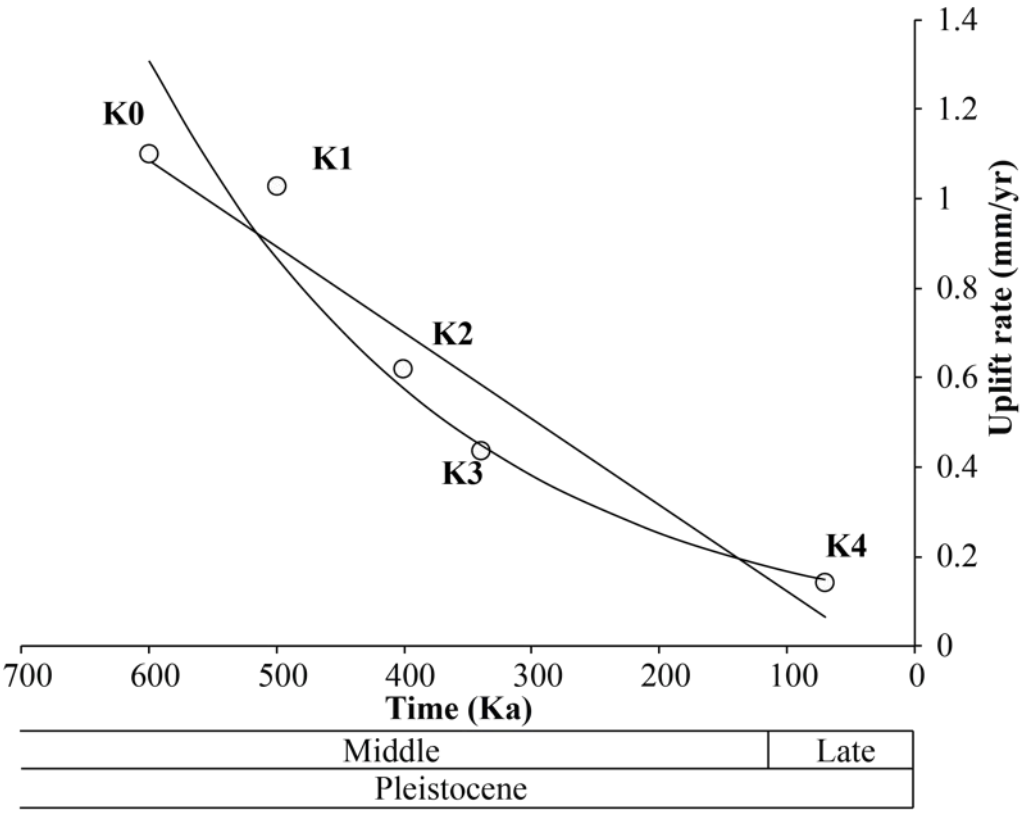

Figure 7.6: Graphical representation of uplift rates of the Kyrenia Range, northern Cyprus. Terraces ages are taken from sea-level curve correlations and heights from K0 to K5 terraces preserved near Arapköy (Klepini) town.

Cyprus during the Pleistocene. Secondly, Cyprus and the region north of Cyprus have variable uplift rates during the Pleistocene. In Cyprus and the region north of Cyprus the greatest uplift rates are generally during the Early Pleistocene, and decrease during the Middle and Late Pleistocene. The fastest uplift rates are seen in Cyprus during the Early Pleistocene.

The scales and time spans of uplift in the various case studies presented (Table 7.2) are very different, which needs to be accounted for when making any comparisons. The uplifted Troodos Massif is ca. 50 km wide, in contrast the width of the Kyrenia Range is ca. 6 km. Both the Troodos Massif and the Kyrenia Range uplifted during the Pleistocene. The uplifted southern Anatolian Plateau is ca. 150 km wide and has gradually uplifted throughout the Cenozoic but with increased uplift rates during the Pleistocene (Schildgen *et al.*, 2012, 2014). Finally, the Lebenese Coast and the Amanos Mountains

(SE Turkey) regions are ca. 200 km long and have been uplifted from the Pliocene to Recent (Gomez *et al.*, 2006; Seyrek *et al.*, 2008). Hence the uplift of mountain ranges in Cyprus represents focused uplift over a relatively short time span in comparison to other regions in the Eastern Mediterranean.

Comparison of the specific uplift rates of the Troodos Massif and the Kyrenia Range during early stages of uplift has a some uncertainty. The Troodos Massif is ca. 2000 m AMSL, whereas the Kyrenia Range is just over 1000 m AMSL at the western end of the range. This height difference is either due to differences in uplift rates or to the nature of the underlying geological processes. If the uplift rates are correct then the difference in heights of the two mountain ranges is directly related to major difference in uplift rates. Alternatively, the heavily fractured nature and narrow width of the Kyrenia Range is likely to have resulted in more material being eroded due to uplift. A consequence of this would be that if the Kyrenia Range uplifted at the same rate as the Troodos Massif it would never reach an equivalent height but would erode rapidly as it rose (i.e. resulting in the K0 (Karka) megabreccia). Therefore, during the Early Pleistocene the Kyrenia Range uplifted at either just over 1.2 mm/yr or at >2 mm/yr. Based upon either uplift rate, the Kyrenia Range is uplifting at a significantly faster rate than other areas within the Eastern Mediterranean during the Early Pleistocene.

Region	**Pleistocene**			**Reference**
	Early	**Middle**	**Late**	
Kyrenia Range	>1.2	1.0-0.4	<0.2	This study
Troodos Massif	2.4	0.5	0.5	Poole *et al.*, 1990
Southeast Cyprus	-	-	1.8	Harrison *et al.*, 2012
Anatolian Plateau	0.72-0.74	0.6-0.7	0.6-0.7	Schildgen *et al.*, 2012
Lebenese Coast	0.14	0.14	0.14	Gomez *et al.*, 2006
Amanos Mountains (SE Turkey)	0.25-0.4	0.25-0.4	0.25-0.4	Seyrek *et al.*, 2008

Table 7.2: A comparison of uplift rates (mm/yr) of the Kyrenia Range with several other regions in the Eastern Mediterranean that are undergoing uplift related to the closure of the Tethys ocean during the Pleistocene.

7.10 Tectonic model

The uplift of the Kyrenia Range has occurred within a regional-scale, plate convergence zone in the Eastern Mediterranean (Sec. 1.7). The aim of this study has been to use detailed sedimentology and quantitative dating of the sedimentary deposits of the Kyrenia Range to understand firstly, the tectonic mechanisms driving the Pleistocene uplift, and secondly, to relate the uplift of the Kyrenia Range to the large-scale, regional tectonic setting during the Pleistocene.

The earliest Plio-Pleistocene emergence of the Kyrenia Range is represented by the shallowing marine sequences preserved within the Mesaoria (Mesarya) Basin (Fig. 7.7(a)). The interbedded chalks and marls of the Nicosia (Lefkoşa) Formation are conformably overlain by the shallow-marine grainstone facies of the Athalassa (Gürpınar) Formation. The uppermost parts of the Athalassa (Gürpınar) Formation shallow-marine grainstone facies show signs of varying relative sea-level. The variations in sea-level are probably due to interglacial-glacial oscillations during the Early Pleistocene. Non-marine fluvial facies (Kalkanlı (Kapouti) Member) are interbedded with the upper Athalassa (Gürpınar) Formation suggesting that the Kyrenia Range was above sea-level during the Early Pleistocene. Equivalent non-marine fluvial deposits in southern Cyprus suggest that the Troodos Massif was also above sea-level at this point (McCallum and Robertson, 1995b; Schirmer *et al.*, 2010; Kinnaird *et al.*, 2011; Weber *et al.*, 2011).

During the late Early Pleistocene large megabreccia deposition (K0) on the northern and southern flanks of the Kyrenia Range indicates a rapid phase of tectonic uplift (Fig. 7.7(b)). In addition, the first high energy debris flow sheet flood facies are deposited in southern Cyprus related to an Early Pleistocene phase of rapid uplift (Poole and Robertson, 1998; Kinnaird *et al.*, 2011). The Kyrenia Range and the Troodos Massif underwent rapid uplift during the Early Pleistocene, approximately at the same time. No major faulting is observed in the field in northern Cyprus related to this Early Pleistocene phase of rapid uplift. The shallow-marine seaway within the Mesaoria (Mesarya) Basin persisted during the Early Pleistocene but emerged by the Middle Pleistocene. Continuing uplift during the Middle to Late Pleistocene resulted in a series of marine and non-marine terraces around the Troodos Massif and the Kyrenia Range (Fig. 7.7(c)). The Troodos Massif uplifted to ca. 2000 m AMSL, whereas the Kyrenia

Range uplifted to ca. 1000 m AMSL by the end of Late Pleistocene.

The late Early Pleistocene rapid uplift of the Troodos Massif has been shown to be related to serpentinite diapirism associated with the collision of the Eratosthenes Seamount with the Cyprus Trench (Shelton, 1993; Robertson, 1998b). The development or reactivation of deeper compressional faults within the Mesaoria (Mesarya) Basin and the Kyrenia Range (Sec. 1.7.2) has been suggested to control the Pleistocene uplift of northern Cyprus (McCallum and Robertson, 1990; Robertson, 1998a; Calon *et al.*, 2005b). The combined collision of the Eratosthenes Seamount and the domal uplift of the Troodos Massif is likely to have been a major factor driving the re-activation of pre-existing, deep, thrust faults, in turn driving the rapid surface uplift of the Kyrenia Range. Increased rates of surface uplift are also observed directly north of the Kyrenia Range on the Southern Anatolian Plateau (Schildgen *et al.*, 2012)(Table 7.2). The late Early Pleistocene uplift of the Kyrenia Range is associated with an "Early-to Middle Pleistocene tectonic transition" (Schattner, 2010), which is directly related to the Eratosthenes Seamount-trench collision. The seamount trench collision resulted in local compressional tectonics in northern Cyprus, driving the uplift of the Kyrenia Range within the Eastern Mediterranean.

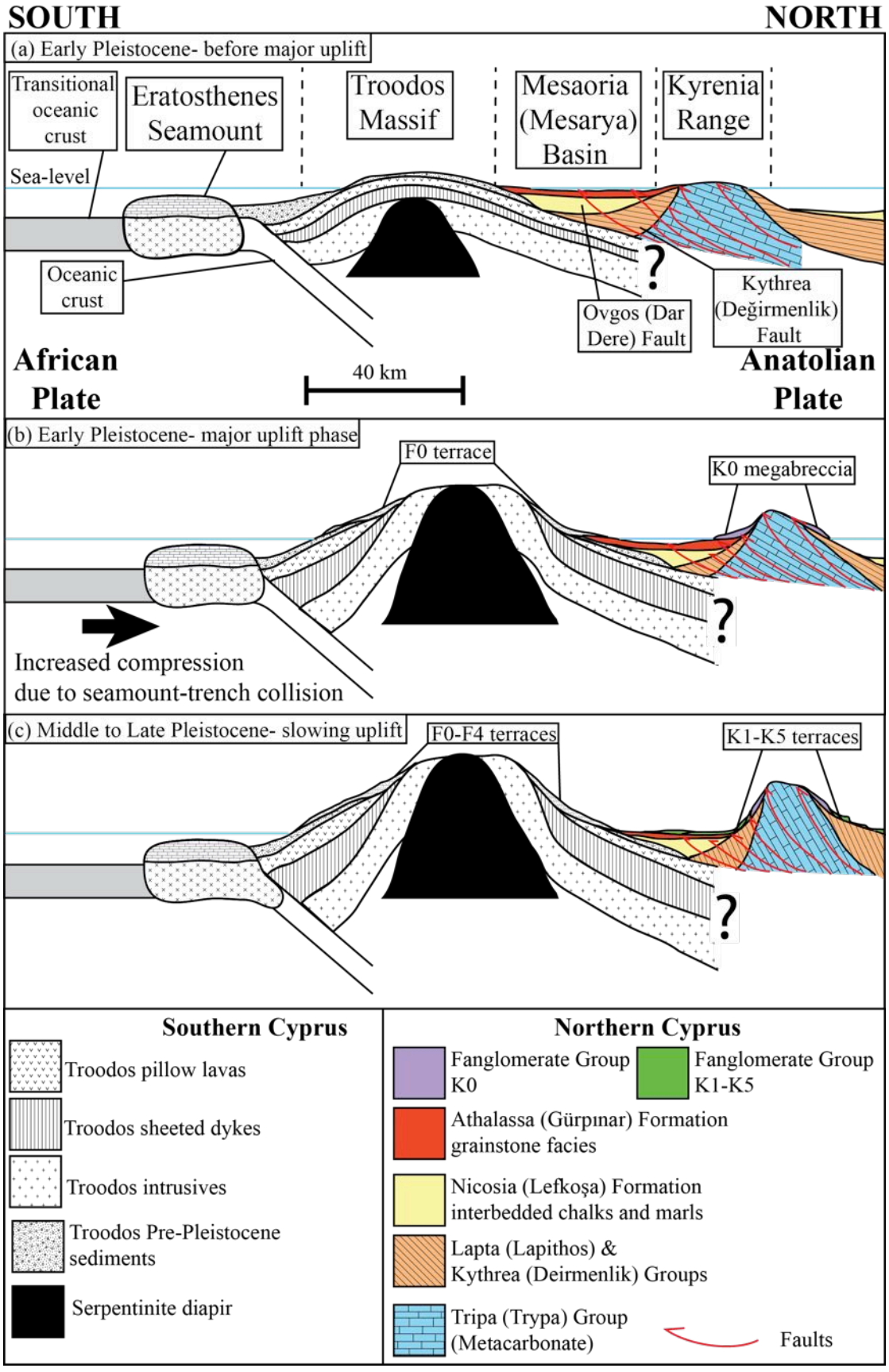

Figure 7.7: Summary tectonic diagram showing the Pleistocene uplift of Cyprus.

7.11 The coupling of tectonics, sea level and climate with sedimentation

A major aspect of this project was to understand the dynamic interaction between tectonics, sea-level change and climate change and how this controls sedimentation. To understand these processes a range of methods and techniques have been used to study the sediments associated with the uplift of various mountain ranges. Numerous studies have used geomorphological methods (e.g. digital elevation models) to map out terraces and correlate them with glacial and interglacial cycles (Bridgland and Westaway, 2008). Several such studies have focused on the Late Pleistocene development of Mediterranean terraces, including the fluvial depositional and erosional processes involved (Macklin *et al.*, 2002; Maddy *et al.*, 2008). Other studies have investigated coastal marine terraces of Late Pleistocene age to understand the interaction of tectonic uplift versus subsidence in relation to glacially controlled cyclicity (Reyss *et al.*, 1998; Zazo *et al.*, 2003; Zecchin *et al.*, 2004; Ferranti *et al.*, 2006). Larger mountain ranges outside of the Mediterranean have also been the focus of numerous studies, such as the Himalayas (Kober *et al.*, 2013), the Andes (Le Roux *et al.*, 2000) and several mountain ranges on the Island of Borneo (Hall *et al.*, 2004). These studies have focused on understanding how the interaction of tectonic uplift and climate change have controlled fluvial drainage systems.

Most uplifting mountain ranges are likely to contain a range deposition systems, although not always well preserved in the geological record. However, it is relatively rare to find studies that have focused on various depositional systems within a single area. To understand the interactions of tectonics, sea level change and climate change on sedimentation requires the study of a range of depositional systems and their interactions.

The Kyrenia Range in northern Cyprus provides a unique field laboratory for studying these processes due to the excellent preservation of a large range of depositional systems of Pliocene and Pleistocene age. The Eastern Mediterranean represents a region of dynamic tectonic activity during the Cenozoic, due to the ongoing convergence of Africa and Eurasia. This has resulted in varies tectonic processes including: subduction, strike-slip (including transpression and transtension), and collision (at different scales), together with deep-seated processes such as crustal delamination, slab break-off

and slab tearing (Faccenna *et al.*, 2006; Berk Biryol *et al.*, 2011; Schildgen *et al.*, 2012; Bartol and Govers, 2014). The interaction of these tectonic processes drives surface uplift in various areas of the easternmost Mediterranean such as in Greece (Roberts *et al.*, 2009a; Turner *et al.*, 2010) and Turkey (Schildgen *et al.*, 2012). In addition, climatic conditions during the Pleistocene varied greatly (Zachos *et al.*, 2001; Siddall *et al.*, 2006), in part related to the frequency and amplitude of glacial cycles. Hence, the combined complex tectonic setting of the Eastern Mediterranean and the dynamic climate during the Pliocene and Pleistocene make the Kyrenia Range an ideal place to study interaction of these processes.

New data from northern Cyprus shows that the Pliocene to Pleistocene uplift of the Kyrenia Range resulted in a range of depositional systems including: shallow-marine carbonate systems, fluvial-drainage networks, slope talus megabreccias, debris flows and carbonate aeolianites. Detailed facies analysis combined with quantitative dating has shown how each depositional system is controlled by allocyclic mechanisms.

Within an environment of rapid tectonic uplift the sea level and climatic signals are not preserved within the facies. The formation of the megabreccia facies along the northern and southern flanks of the Kyrenia Range represent an environment where deposition is directly controlled by tectonic uplift. This is a relatively unique case of deposition being directly controlled by crustal processes, and is an important example of the interaction of tectonics and sedimentation.

Within an environment of gradual tectonic uplift, the climate and sea level signals are well preserved within the facies. The varies facies preserved in northern Cyprus represent the various allocyclic controls of deposition. The combined terrace morphology and sedimentology can be used to understand the interaction of tectonic uplift and sea level change. Furthermore, the change in facies and facies relationships are used to describe climatic changes during glacial cycles.

To fully appreciate the tectonic, sea-level and climate controls requires the study of a range of depositional systems. Sedimentation varies between interglacial to glacial cycles from marine and fluvial deposition to aeolian dune deposition. This change in deposition represents changes in climatic conditions during interglacial cycles. Any mountain range forming during the Late Cenozoic is likely to have been strongly affected by glacial cyclicty, and therefore will require a similar method of wide reaching

sedimentology to understand the controls of deposition.

Chapter 8

Conclusions

8.1 Conclusions

- The earliest emergence of northern Cyprus is represented by a change from deep marine to shallow marine facies within the Mesaoria (Mesarya) Basin and in the Karpaz (Karpas) Peninsula, within the east of the Kyrenia Range.

- The shallow-marine facies within the Mesaoria (Mesarya) Basin represents a cool-water carbonate ramp dipping southwestwards away from the Kyrenia Range.

- The shallow-marine carbonate ramp facies preserved within the Mesaoria (Mesarya) Basin show signs of relative sea-level change with interbedded marine and non-marine facies.

- A combination of strontium isotope dating and magnetostratigraphy show that a shallow-marine environment, continued throughout the Early Pleistocene, surrounding the Kyrenia Range prior to major uplift.

- Fluvial facies are interbedded with the upper parts of the shallow-marine facies deposits of the Mesaoria (Mesarya) Basin. The detritus within the fluvial facies was derived from the Kyrenia Range, indicating a non-marine setting prior to major uplift.

- The terraces of northern Cyprus are categorised into a six terrace system that can be correlated along the northern and southern flanks of the range. The six terraces are termed K0 to K5, where K0 is the oldest and highest above modern sea-level and K5 is the youngest and lowest above modern sea-level.

- The K0 (Karka) terrace is composed of megabreccia deposits along the northern and southern flanks of the Kyrenia Range representing a phase of rapid uplift. The major uplift results in mass wasting of previously tectonically fractured lithologies.

- The K1 to K5 terraces are composed of marine and non-marine facies on the northern flank of the range and non-marine terrace facies on the southern flank of the range.

- Marine facies on the northern flank of the range represent a range of depositional environments including nearshore open-marine environments below the storm-wave base, shoreface, foreshore (beachrock), and backshore lagoonal environments.

- Non-marine environments on both flanks of the range include aeolian dunes, fluvial and deltaic drainage systems.

- Fluvial drainage systems on both flanks of the range include, channelised debris-flow deposits, bedded conglomerates, palaeosols and mudstones.

- U-series dating of several marine deposits within the K4 terrace suggest that the terrace represents a period of ca. 250,000 years from MIS 9 to MIS 5, i.e. incorporating two complete glacial cycles during the Middle Pleistocene.

- OSL dating of the K5 terrace suggests a phase of major aeolian dune deposition during the most recent glacial stage, i.e. Late Pleistocene.

- The carbonate aeolianites preserved within the K1 to K5 terraces are interpreted as representing an arid dry climate during glacial stages.

- The fluvial drainages systems are suggested to represent a humid climate with episodes of heavy rainfall during interglacial stages.

- Correlations of the K1 to K3 terraces with the Middle Pleistocene global sea-level curve based upon each terrace representing a single glacial cycle, suggest that the K1 to K5 terrace sequence was formed over ca. 600 ka.

- Uplift rates are calculated from the K0-K5 terrace during the Pleistocene. Rapid initial uplift of >1.2 mm/yr during the late Early Pleistocene is represented by the K0 terrace. Uplift rates rapidly decreased to <0.2 mm/yr towards the end of the Late Pleistocene.

- Uplift timings and rates of the Kyrenia Range are comparable to the uplift of the Troodos Massif and the southern Anatolian Plateau during the Pleistocene.

- The collision of the Eratosthenes seamount with the Cyprus Trench is suggested as the driving mechanism of the uplift of the Kyrenia Range. The seamount-trench collision resulted in a period of local compressional tectonics within the Eastern Mediterranean. This compressional setting resulted in the re-activation of deep-seated faults in northern Cyprus with the result being rapid but short lived tectonic uplift.

8.2 Future work

The initial aim of this study was to constrain the timing and rate of uplift of the Kyrenia Range through a focused study of the sedimentary cover. Several aspects of this study have shown that some further work would be useful. Firstly, the U-series and OSL dating was used to postulate a model for tectonic, sea-level and climatic interactions but could be developed further. Secondly, high-resolution digital terrain data could be used for terrace mapping and river profile modelling. Thirdly, new onshore seismic data could be used to understand the deeper structures associated Pleistocene enhanced compressional tectonics.

The combined sedimentological and dating results were used to produce a model for terrace formation related to the interaction of tectonic uplift, global eustatic sea-level change and climate change. To develop and assess this terrace formation model further more detailed dating would be required from selected deposits containing marine and non-marine sedimentary relationships. The limitations for this would be finding dating methods and material that cover the appropriate time spans.

Currently, the only digital terrain data available of northern Cyprus is the globally available NASA ASTER data set. Preliminary investigations with this data set provided limited results due to its low resolution. High-resolution data of northern Cyprus could be used to correlate the six terraces based upon the results of this thesis, and to understand uplift rates through detailed geomorphic mapping of river profiles. Previous-field based topographic studies were based on a limited stratigraphy; however, with a greatly improved understanding of the sedimentology of the terraces in northern Cyprus the terraces could be mapped using a high-resolution digital terrain data set.

Quantifying river profiles have been shown to be a successful tool for understanding tectonic uplift (Kirby and Whipple, 2001) and have been used in several case studies such as in the Himalayas (Burbank *et al.*, 1996), the Yunnan Province, China (Schoenbohm *et al.*, 2004) and in northern California (Snyder *et al.*, 2000).

To understand the deeper structure of northern Cyprus requires the application of geophysical techniques such as seismic studies. The offshore basins in the Eastern Mediterranean have been the focus of several published studies, indicating the Neogene tectonic setting of the Latakia Basin to the east of Cyprus (Calon *et al.*, 2005a), the Oligocene to recent evolution of the Mesaoria (Mesarya) Basin (Calon *et al.* (2005b)) and the Quaternary evolution of the basins around the Eastern Anatolian fault zone (Aksu *et al.*, 1992). The data from these studies have been used as an offshore analogue of the Kyrenia Range; however, a focused onshore study would be essential for understanding the deeper structures related to the Pleistocene uplift of northern Cyprus.

Bibliography

Aigner, T. (1982). Calcareous tempestites storm-dominated strati- fication in Upper Muschelkalk limestones (Middle Trias, SW Germany). In Einsele, G. and Seilacher, A., editors, *Cyclic and Event Stratification*, pages 180–198. Springer Berlin Heidelberg.

Aksu, A. E., Calon, T. J., Piper, D. J. W., Turgut, S., and Izdar, E. (1992). Architecture of Late orogenic Quaternary basins in northeastern Mediterranean Sea. *Tectonophysics*, 210:191–213.

Allan, J. R. and Matthews, R. K. (1977). Carbon and oxygen isotopes as diagenetic and stratigraphic tools: surface and subsurface data, Barbados, West Indies. *Geology*, 5:16–20.

Álvarez-Pérez, G., Busquets, P., Mol, B. D., and Sandoval, N. G. (2005). Deep-water coral occurrences in the Strait of Gibralter. In *Coldwater corals and Ecosystems*, pages 207–221. Springer Berlin Heidelberg.

Arakel, a. V. (1982). Genesis of Calcrete in Quaternary Soil Profiles, Hutt and Leeman Lagoons, Western Australia. *Journal of Sedimentary Research*, 52(1):109–125.

Bailey, R., Smith, B., and Rhodes, E. (1997). Partial bleaching and the decay form characteristics of quartz OSL. *Radiation Measurements*, 27(2):123–136.

Bailey, T., McArthur, J., Prince, H., and Thirlwall, M. (2000). Dissolution methods for strontium isotope stratigraphy: whole rock analysis. *Chemical Geology*, 167(3-4):313–319.

Bar-Matthews, M., Ayalon, A., and Kaufman, A. (2000). Timing and hydrological conditions of Sapropel events in the Eastern Mediterranean, as evident from speleothems, Soreq cave, Israel. *Chemical Geology*, 169(1-2):145–156.

Barka, A. and Reilinger, R. (1997). Active tectonics of the Eastern Mediterranean region: deduced from GPS, neotectonic and seismicity data. *Annali Di Geofisica*, 11(3):587–610.

Baroz, F. (1979). *Etude geologique dans le Pentadaktylos et la Mesaoria (Chypre Septentrionale)*. PhD thesis, Universite de Nancy.

Bartol, J. and Govers, R. (2014). A single cause for uplift of the Central and Eastern Anatolian plateau? *Tectonophysics*, 637:116–136.

Bates, C. C. (1953). Rational Theory of Delta Formation. *Bulletin of the American Association of Petroleum Geologists*, 37(9):2119–2162.

Berk Biryol, C., Beck, S. L., Zandt, G., and Özacar, a. A. (2011). Segmented African lithosphere beneath the Anatolian region inferred from teleseismic P-wave tomography. *Geophysical Journal International*, 184(3):1037–1057.

Biju-Duval, B., Letouzey, J., Montadert, L., Courrier, P., Mugniot, J. F., and Sancho, J. (1974). Geology of the Mediterranean Sea Basins. In Drake, C. A. and L, B. C., editors, *The Geology of continental margins*, pages 695–721. Springer Berlin Heidelberg.

Biju-Duval, B. and Montadert, U. (1977). Introduction to the Structural History of the Mediterranean Basins. In *Structural History of Mediterranean Basins*, pages 1–12. Technip, Paris.

Blair, T. C. and McPherson, J. G. (1999). Grain-size and textural classification of coarse sedimentary particles. *Journal of Sedimentary Research*, 69:6–19.

Blum, M. D. and Törnqvist, T. E. (2000). Fluvial responses to climate and sea-level change: a review and look forward. *Sedimentology*, 47:2–48.

Bojar, A.-V., Hiden, H., Fenninger, A., and Neubauer, F. (2004). Middle Miocene seasonal temperature changes in the Styrian basin, Austria, as recorded by the isotopic composition of pectinid and brachiopod shells. *Palaeogeography, Palaeoclimatology, Palaeoecology*, 203(1-2):95–105.

Botter-Jensen, L., Bulur, E., Duller, G. A. T., and Murray, A. S. (2000). Advances in luminescence instrument systems. *Radiation Measurements*, 32(5):523–528.

Bourgeois, J. and Leithold, E. L. (1984). Wave-worked conglomerates- depositional processes and criteria for recognition. In Koster, E. H. and Steel, R. J., editors, *Sedimentology of gravels and conglomerates*, volume 10, pages 331–343. Canadian Society of Petroleum Geologists, Memoir.

Brass, G. W. (1976). The variation of the marine 87 Sr/86 Sr ratio during Phanerozoic time: interpretation using a flux model. *Geochimica et Cosmochimica Acta*, 40(1974):721– 730.

Bridgland, D. and Westaway, R. (2008). Climatically controlled river terrace staircases: A worldwide Quaternary phenomenon. *Geomorphology*, 98(3-4):285–315.

Brooke, B. (2001). The distribution of carbonate eolianite. *Earth-Science Reviews*, 55:135–164.

Buchbinder, B. and Zilberman, E. (1997). Sequence stratigraphy of Miocene-Pliocene carbonate-siliciclastic shelf deposits in the eastern Mediterranean margin (Israel): effects of eustasy and tectonics. *Sedimentary Geology*, 112(1-2):7–32.

Burbank, D. W., Leland, J., Fielding, E., Anderson, R. S., Brozovic, N., Reid, M. R., and Duncan, C. (1996). Bedrock incision, rock uplift and threshold hillslopes in the northwestern Himalayas. *Nature*, 379(6565):505–510.

Burbidge, C., Sanderson, D., Housley, R., and Allsworth Jones, P. (2007). Survey of Palaeolithic sites by luminescence profiling, a case study from Eastern Europe. *Quaternary Geochronology*, 2(1-4):296–302.

Burchette, T. P. and Wright, V. P. (1992). Carbonate ramp depositional systems. *Sedimentary Geology*, 79:3–57.

Burdon, D. J. (1955). Groundwater in the Island of Cyprus. *The International Association of Hydrogeologists*, 1:315–323.

Burns, B. a., Heller, P. L., Marzo, M., and Paola, C. (1997). Fluvial response in a sequence stratigraphic framework; example from the Montserrat fan delta, Spain. *Journal of Sedimentary Research*, 67:311–321.

Butler, R. F. (1992). *Paleomagnetism: Magnetic Domains to Geologic Terranes*. Blackwell, Boston, MA.

Buylaert, J. P., Murray, a. S., Thomsen, K. J., and Jain, M. (2009). Testing the potential of an elevated temperature IRSL signal from K-feldspar. *Radiation Measurements*, 44(5-6):560–565.

Calon, T., a.E. Aksu, and Hall, J. (2005a). The Neogene evolution of the Outer Latakia Basin and its extension into the Eastern Mesaoria Basin (Cyprus), Eastern Mediterranean. *Marine Geology*, 221(1-4):61–94.

Calon, T., a.E. Aksu, and Hall, J. (2005b). The Oligocene-Recent evolution of the Mesaoria Basin (Cyprus) and its western marine extension, Eastern Mediterranean. *Marine Geology*, 221(1-4):95–120.

Cavinato, G. P., Carusi, C., Dall'asta, M., Miccadei, E., and Piacentini, T. (2002). Sedimentary and tectonic evolution of Plio-Pleistocene alluvial and lacustrine deposits of Fucino Basin (central Italy). *Sedimentary Geology*, 148:29–59.

Chappell, J. and Shackleton, N. J. (1986). Oxygen isotopes and sea level. *Nature*, 324:137–140.

Choi, J. H., Kim, J. W., Murray, a. S., Hong, D. G., Chang, H. W., and Cheong, C. S. (2009). OSL dating of marine terrace sediments on the southeastern coast of Korea with implications for Quaternary tectonics. *Quaternary International*, 199(1-2):3–14.

Cleintuar, M. R., Knox, G. J., and Ealey, P. J. (1977). The geology of Cyprus and its place in the East-Mediterranean framework. *Geologie en Mijnbouw*, 56:66–82.

Clifton, H. E. (1973). Pebble segregation and bed lenticularity in waveworked versus alluvial gravel. *Sedimentology*, 20:173–187.

Clifton, H. E., Hunter, R. E., and Phillips, R. L. (1971). Structures and Processes in the Non-Barred High Energy Nearshore. *Journal of Sedimentary Petrology*, 41(3):651–670.

Clube, T. M. M., Cree, K. M., and Robertson, A. H. F. (1985). Palaeorortation of the Troodos microplate, Cyprus. *Nature*.

Cohen, K. M. and Gibbard, P. L. (2010). Global chronostratigraphical correlation table for the last 2.7 million years. Technical Report 2002, International Commission on Stratigraphy.

Colella, A., De Boer, P. L., and Nio, S. D. (1987). Sedimentology of a marine intermontane Pleistocene Gilbert-type fan-delta complex in the Crati Basin, Calabria, southern Italy. *Sedimentology*, 34:721–736.

Constantinou, G. (1995). Geological map of Cyprus. Technical report, Geological survey department, Cyprus.

Cornée, J. J., Léticée, J. L., Münch, P., Quillévéré, F., Lebrun, J. F., Moissette, P., Braga, J. C., Melinte-Dobrinescu, M., De Min, L., Oudet, J., and Randrianasolo, A. (2012). Sedimentology, palaeoenvironments and biostratigraphy of the Pliocene-Pleistocene carbonate platform of Grande-Terre (Guadeloupe, Lesser Antilles forearc). *Sedimentology*, 59:1426–1451.

Cosentino, D., Schildgen, T. F., Cipollari, P., Faranda, C., Gliozzi, E., Hudáčková, N., Lucifora, S., and Strecker, M. R. (2012). Late Miocene surface uplift of the southern margin of the Central Anatolian plateau, Central Taurides, Turkey. *Bulletin of the Geological Society of America*, 124(1-2):133–145.

Coussot, P. and Meunier, M. (1996). Recognition, classification and mechanical description of debris flows. *Earth-Science Reviews*, 40:209–227.

De Vaumas, E. (1961). Further contributions to the geomorphology of Cyprus. Technical report, Annual Report of the Geological Survey Department (Cyprus).

DeCelles, P. G., Gray, M. B., Ridgway, K. D., Cole, R. B., Pivnik, D. a., Pequera, N., and Srivastava, P. (1991). Controls on synorogenic alluvial-fan architecture, Beartooth Conglomerate (Palaeocene), Wyoming and Montana. *Sedimentology*, 38(4):567–590.

Delph, J. R., Biryol, C. B., Beck, S. L., Zandt, G., and Ward, K. M. (2015). Shear wave velocity structure of the Anatolian Plate: anomalously slow crust in southwestern Turkey. *Geophysical Journal International*, 202(1):261–276.

Dia, A., Cohen, A. S., O'Nion, R. K., and Jackson, J. A. (1997). Rates of uplift investigated through 230Th dating in the gulf of Corinth (Greece). *Chemical Geology*, 138:171–184.

Dickinson, W. (1970). Interpreting detrital modes of graywacke and arkose. *Jounrary of Sedimentary Petrology*, 40(2):695–707.

Dilek, Y. and Altunkaynak, S. (2009). Geochemical and temporal evolution of Cenozoic magmatism in western Turkey: mantle response to collision, slab break-off, and lithospheric tearing in an orogenic belt. *Geological Society, London, Special Publications*, 311(1):213–233.

Dilek, Y. and Sandvol, E. (2009). Seismic structure, crustal architecture and tectonic evolution of the Anatolian-African Plate Boundary and the Cenozoic Orogenic Belts in the Eastern Mediterranean Region. *Geological Society, London, Special Publications*, 327(1):127–160.

Djamali, M., Soulié-Märsche, I., Esu, D., Gliozzi, E., and Okhravi, R. (2006). Palaeoenvironment of a Late Quaternary lacustrinepalustrine carbonate complex: Zarand Basin, Saveh, central Iran. *Palaeogeography, Palaeoclimatology, Palaeoecology*, 237(2-4):315–334.

Dodonov, A. E., Trifonov, V., Ivanova, T., Kuznetsov, V., Maksimov, F., Bachmanov, D., Sadchikova, T., Simakova, A., Minini, H., Al-Kafri, A.-M., and Ali, O. (2008). Late Quaternary marine terraces in the Mediterranean coastal area of Syria: Geochronology and neotectonics. *Quaternary International*, 190(1):158–170.

Doan, U., Koçyiit, A., Varol, B., Özer, I., Molodkov, A., and Zöhra, E. (2012). MIS 5a and MIS 3 relatively high sea-level stands on the Hatay-Samanda Coast, Eastern Mediterranean, Turkey. *Quaternary International*, 262:65–79.

Dreghorn, W. (1978). *Landforms in the Girne Range Northern Cyprus*. Ankara, Maen Tetkik we Arama Enstitusu.

Ducloz, C. (1964). Geological map of the Central Kyrenia Range. Technical report, Geological Survey Department, Government of Cyprus.

Ducloz, C. (1965). Revision of the Pliocene and Quaternary stratigraphy of the central Mesaoria. Nicosia. Technical report, The Cosmos Press, Ltd.

Ducloz, C. (1972). The geology of the Bellapais-Kythrea area of the Central Kyrenia Range. *Bulletin of the Geological Survey deparment*, 6:44–71.

Dumas, B., Guérémy, P., and Raffy, J. (2005). Evidence for sea-level oscillations by the "characteristic thickness" of marine deposits from raised terraces of Southern Calabria (Italy). *Quaternary Science Reviews*, 24(18-19):2120–2136.

Dunham, R. J. (1962). Classification of carbonate rocks according to deposition texture. *American Association of Petroleum Geologists*, 1(1):108–121.

Dunlop, D. J. and Özdemir, O. (1997). *Rock magnetism; fundementals and frontiers*. Cambridge Univeristy Press.

Eaton, S. and Robertson, A. H. (1993). The Miocene Pakhna Formation, southern Cyprus and its relationship to the Neogene tectonic evolution of the Eastern Mediterranean Simon. *Sedimentary Geology*, 86:273–296.

Elderfield, H. (1986). Isotope systematics The isotope systematics of Sr are summarized in Table I. 87 Sr is a radiogenic, Standards The Sr isotopic compositions of the commonly-used standards are listed in. *Palaeogeography, Palaeoclimatology, Palaeoecology*, 57:71– 90.

Erginal, A. E., Kiyak, N. G., and Ertek, T. A. (2012). A New Late Holocene Eolianite Record from. *Turkish Journal of Earth Sciences*, 21:407–414.

Faccenna, C., Bellier, O., Martinod, J., Piromallo, C., and Regard, V. (2006). Slab detachment beneath eastern Anatolia: A possible cause for the formation of the North Anatolian fault. *Earth and Planetary Science Letters*, 242(1-2):85–97.

Fernandes, R. M. S. (2003). The relative motion between Africa and Eurasia as derived from ITRF2000 and GPS data. *Geophysical Research Letters*, 30(16):1–5.

Ferranti, L., Antonioli, F., Mauz, B., Amorosi, A., Dai Pra, G., Mastronuzzi, G., Monaco, C., Orrù, P., Pappalardo, M., Radtke, U., Renda, P., Romano, P., Sansò, P., and Verrubbi, V. (2006). Markers of the last interglacial sea-level high stand along the coast of Italy: Tectonic implications. *Quaternary International*, 145-146:30–54.

Flugel, E. (2004). *Microfacies of Carbonate Rocks. Analysis, Interpretation and Application*. New York: Springer-Verlag.

Folk, R. L. (1974). *The Petrology of Sedimentary Rocks*. Hemphill publishing company, Texas.

Folk, R. L., Andrews, P. B., and Lewis, D. W. (1970). Detrital sedimentary rock classification and nomenclature for use in New Zealand. *New Zealand Journal of Geology and Geophysics*, 13:937–968.

Frank, P., Degering, D., Markus, F., Alexandra, H., Annette, K., Nicole, K., Matthias, K., Daniel, R., and Joel Q G, S. (2008). Luminescence dating: basics, methods and applications. *Quaternary Science Journal*, 57(1-2):95– 149.

Frébourg, G., Hasler, C.-A., Le Guern, P., and Davaud, E. (2008). Facies characteristics and diversity in carbonate eolianites. *Facies*, 54(2):175–191.

Galili, E., Sevketoglu, M., Salamon, A., Zviely, D., Mienis, H. K., Rosen, B., and Moshkovitz, S. (2012). Late Pleistocene and Holocene beach deposits and archaeological features on Cyprus and Israeli coasts, markers of sea levels and vertical earth movements. In *Rovere, A., Furlani, S., Benjamin, J., Fontana, A., Anzidei, M., Antonioli, F. (EDS). MEDFLOOD first meeting*, volume 1, pages 13–14. Commission coastal and marine processes.

Garfunkel, Z. and Derin, B. (1984). Permian-early Mesozoic tectonism and continental margin formation in Israel and its implications for the history of the Eastern Mediterranean. *Geological Society, London, Special Publications*, 17(1):187–201.

Gazzi, P. (1966). Le arenarie del flysch sopracretaceo dellAppennino modenese; correlazioni con il flysch di Monghidoro. *Mineral. Petrogra. Acta*, 12(6).

Gilbert, G. K. (1885). Gilbert's topographic features of lake shores. *The American Naturalist*, 20(7):626–628.

Gilbert, G. K. (1890). *Lake Bonnedville*. Washington, D.C.: U.S. Govt. Print. Off.

Gjerstad, E., Lindros, J., Sjöqvist, K., and Westholm, A. (1934). The Swedish Cyprus Expedition I: Finds and Results of the Excavations in Cyprus 1927-1931. Technical report, Stockholm: Swedish Cyprus Expedition.

Godfrey-Smith, D., Huntley, D., and Chen, W.-H. (1988). Optical dating studies of quartz and feldspar sediment extracts. *Quaternary Science Reviews*, 7(3-4):373–380.

Gomez, B. (1987). The Alluvial Terraces and Fills of the Lower Vasilikos Valley, in the Vicinity of Kalavasos, Cyprus. *The Royal Geographical Society (with the Institute of British Geographers) Stable*, 12(3):345–359.

Gomez, F., Khawlie, M., Tabet, C., Nasser Darkal, A., Khair, K., and Barazangi, M. (2006). Late Cenozoic uplift along the northern Dead Sea transform in Lebanon and Syria. *Earth and Planetary Science Letters*, 241(3-4):913–931.

Goy, L., Dabrio, C. J., Bardaj, T., Zazo, C., and Gonza, . (2003). Pleistocene raised marine terraces of the Spanish Mediterranean and Atlantic coasts: records of coastal uplift , sea-level highstands and climate changes. *Marine Geology*, 194(1):103–133.

Grabau, A. W. (1904). On the classification of sedimentary rocks. *American Geologist*, 33:228–247.

Gross, M. (1964). Variations in the and ratios of diagenetically altered limestones in the Bermuda Islands. *The Journal of Geology*, 72(2):170–194.

Hakyemez, Y., Turhan, N., Sonmez, I., and Sumengen, M. (2000). Kuzey Kbrs Turk Cumhuriyeti nin Jeolojisi (Geology of the Turkish Republic of Northern Cyprus). Technical report, Unpublished report of MTA (Maden Tektik ve Arama, Genel Mudurlugu Jeoloji Etutleri Diaresi, Ankara,.

Hall, J. S., Mozley, P., Davis, J. M., and Roy, N. D. (2004). Environments of formation and controls of spatial distribution of calcute cement in Plio-Pleistocene fluvial deposits, New Mexico, U.S.A. *Journal of Sedimentary Research*, 74(5):643–653.

Hansen, K. S. (1999). Development of a prograding carbonate wedge during sea level fall: Lower Pleistocene of Rhodes, Greece. *Sedimentology*, 46:559–576.

Harrison, R., Newell, W., Bathanl, H., Panayides, I., McGeehin, J., Mahan, S., zhr, a., Tsiolakis, E., and Necdet, M. (2004). Tectonic framework and Late Cenozoic tectonic history of the northern part of Cyprus: implications for earthquake hazards and regional tectonics. *Journal of Asian Earth Sciences*, 23(2):191–210.

Harrison, R., Newell, W., Panayides, I., Stone, B., Tsiolakis, E., Necdet, M., Batihanli, H., Ozhur, A., Lord, A., Berksoy, O., Zomeni, Z., Schindler, J. S., and Survey, U. S. G. (2008). Bedrock Geologic Map of the Greater Lefkosia Area, Cyprus. Technical report, U . S . Geological Survey.

Harrison, R. W., Tsiolakis, E., Stone, B. D., Lord, A., Mcgeehin, J. P., Mahan, S. A., and Chirico, P. (2012). Late Pleistocene and Holocene uplift history of Cyprus: implications for active tectonics along the southern margin of the Anatolian microplate. In Robertson, A. H. F., Parlak, O., and Ünlügenç, U. C., editors, *Geological Development of Anatolia and the Easternmost Mediterranean Region*, volume 372, pages 561–584. Geological Society, London, Special Publications.

Hearty, P. J. (2002). Revision of the late Pleistocene stratigraphy of Bermuda. *Sedimentary Geology*, 153(1-2):1–21.

Henderson, G. M., Martel, D. J., O'Nions, R. K., and Shackleton, N. J. (1994). Evolution of seawater 87Sr/86Sr over the last 400 ka: the absence of glacial/ interglacial cycles. *Earth and Planetary Science Letters*, 128:643– 651.

Henson, F. R. S., Browne, R. V., and McGinty, J. (1949). A synopsis of the stratigraphy and geological history of Cyprus. *Quarterly Journal of the Geological Society*, 105(1-4):1–41.

Hillaire-Marcel, C. (2009). The U-series dating of (biogenic) carbonates. In *IOP Conference Series: Earth and Environmental Science*, volume 5. IOP Publishing.

Hodgson, E., Morris, A., Anderson, M., and Robertson, A. (2010). First palaeomagnetic results from the Kyrenia Range terrane of northern Cyprus and their implication for the regional plate tectonic evolution of the eastern Mediterranean. In *American Geophysical Union, Fall Meeting*, volume 12, page 6449.

Howarth, R. and McArthur, J. (1997). Statistics for strontium isotope stratigraphy: a robust LOWESS fit to the marine Sr-isotope curve for 0 to 206 Ma, with look-up table for derivation of numeric age. *The Journal of Geology*, 105(4):441–456.

Hudson, J. D. (1977). Stable isotopes and limestone lithification. *Journal of the Geological Society*, 133(6):637–660.

Hungr, O., Evans, S. G., Bovis, S. G., and Hutchinson, J. N. (2001). A review of the classification of landslide flow type. *Environmental and Engineering Geoscience*, 7(3):221–238.

Huntley, D. J., Godfrey-Smith, D. I., and Thewalt, M. L. W. (1985). Optical dating of sediments. *Nature*, 313(5998):105–107.

Imbrie, J., Hays, J. D., Martinson, D. G., McIntyre, A., Mix, A. C., Morley, J. J., Pisias, N. G., Prell, W. L., and Shackleton, N. J. (1984). The orbital theory of Pleistocene climate: support from a revised chronology of the marine δ18 O record. In Berger, A., Imbrie, J., Hays, H., Kukla, G., Saltzman, B., and Dordrecht, D., editors, *Milankovitch and climate: Understanding the response to astronomical forcing*, page 269. Reidel Publishing.

Inwood, J., Morris, A., Anderson, M. W., and Robertson, A. H. (2009). Neotethyan intraoceanic microplate rotation and variations in spreading axis orientation: Palaeomagnetic evidence from the Hatay ophiolite (southern Turkey). *Earth and Planetary Science Letters*, 280(1-4):105–117.

Ivanovich, M. (1982). Uranium series disequilibria applications in geochronology. In Uranium- Series Disequilibrium. In Ivanovich, M. and Harmon, R. S., editors, *Applications to Environmental Problems*, pages 56–78. Oxford University Press.

Jaffey, N. and Robertson, A. (2005). Non-marine sedimentation associated with Oligocene-Recent exhumation and uplift of the Central Taurus Mountains, S Turkey. *Sedimentary Geology*, 173(1-4):53–89.

Jaffey, N. and Robertson, A. H. F. (2004). New sedimentological and structural data from the Ecemis Fault Zone, southern Turkey: implications for its timing and offset and the Cenozoic tectonic escape of Anatolia. *Journal of the geological society, London*, 158:367–378.

Kahle, H. G., Straub, C., Reilinger, R., McClusky, S., King, R., Hurst, K., Veis, G., Kastens, K., and Cross, P. (1998). The strain rate field in the eastern Mediterranean region, estimated by repeated GPS measurements. *Tectonophysics*, 294(3-4):237–252.

Kempler, D. (1998). Erstosthenes seamount: the possible spearhead of incipient continental collision in the Eastern Mediterreanean. In Robertson, A., Emeis, K., Richter, C., and Camerlenghi, A., editors, *Proceedings of the Ocean Drilling Program, Scientific Results*, volume 160, chapter 53, pages 709–721. IODP.

Kempler, D. and Garfunkel, Z. (1994). Structures and kinematics in the northeastern Mediterranean: A study of an irregular plate boundary. *Tectonophysics*, 234(1-2):19–32.

Kinnaird, T. and Robertson, A. (2013). Tectonic and sedimentary response to subduction and incipient continental collision in southern Cyprus, easternmost Mediterranean region. In Robertson, A., Osman, P., and Ünlügenç, U. C., editors, *Geological Development of Anatolia and the Easternmost Mediterranean Region*, volume 372, pages 585–613. Geological Society of London.

Kinnaird, T. C., Robertson, A. H. F., and Morris, A. (2011). Timing of uplift of the Troodos Massif (Cyprus) constrained by sedimentary and magnetic polarity evidence. *Journal of the Geological Society*, 168(2):457–470.

Kinnaird, T. C., Sanderson, D. C., and Bigelow, G. F. (2015). Feldspar SARA IRSL dating of very low dose rate aeolian sediments from Sandwick South, Unst, Shetland. *Quaternary Geochronology*, pages 1–7.

Kinnaird, T. C., Sanderson, D. C. W., and Woodward, N. L. (2012). Applying luminescence methods to geoarchaeology: a case study from Stronsay, Orkney. *Earth and Environmental Science Transactions of the Royal Society of Edinburgh*, 102(03):191–200.

Kirby, E. and Whipple, K. (2001). Quantifying differential rock-uplift rates via stream profile analysis. *Geology*, 29(5):415–418.

Knup, P. E. (1965). Geological map of the Central Kyrenia Range. Technical report, Geological Survey Department, Government of Cyprus.

Kober, F., Zeilinger, G., Ivy-Ochs, S., Dolati, a., Smit, J., and Kubik, P. (2013). Climatic and tectonic control on fluvial and alluvial fan sequence formation in the Central Makran Range, SE-Iran. *Global and Planetary Change*, 111:133–149.

Kodama, K. P. (2012). *Paleomagnetism of sedimentary rocks: process and interpretation*. John Wiley & Sons.

Kourampas, A. and Robertson, A. H. F. (2000). Controls on Plio-Quaternary sedimentation within an active fore-arc region: Messenia Peninsula (SW Peloponnese), S. Greece. In Panayides, I., Xenophonotos, C., and Malpas, J., editors, *Proceedings of the third international conference on the geology of the Eastern Mediterranean*. Geological Society of London.

Kraus, M. J. (1999). Paleosols in clastic sedimentary rocks: their geologic applications. *Earth-Science Reviews*, 47(1-2):41–70.

Kumar, R., Ghosh, S. K., Mazari, R., and Sangode, S. (2003). Tectonic impact on the fluvial deposits of Plio-Pleistocene Himalayan foreland basin, India. *Sedimentary Geology*, 158(3-4):209–234.

Lakhdar, R., Soussi, M., Ben Ismail, M. H., and M'Rabet, A. (2006). A Mediterranean Holocene restricted coastal lagoon under arid climate: Case of the sedimentary record of Sabkha Boujmel (SE Tunisia). *Palaeogeography, Palaeoclimatology, Palaeoecology*, 241:177–191.

Lambeck, K., Esat, T. M., and Potter, E.-k. (2002). Links between climate and sea levels for the past three million years. *Nature*, 419(6903):199–206.

Lavé, J. and Avouac, J. P. (2001). Fluvial incision and tectonic uplift across the Himalayas of central Nepal erosion. *Journal of Geophysical Research*, 106(11):26561–26591.

Le Roux, J. P., Tavares Correa, C., and Alayza, F. (2000). Sedimentology of the Rimac-Chillon alluvial fan at Lima, Peru, as related to Plio-Pleistocene sea-level changes, glacial cycles and tectonics. *Journal of South American Earth Sciences*, 13(6):499–510.

Leeder, M. R., McNeill, L. C., Collier, R. E. L., Portman, C., Rowe, P. J., and Andrews, J. E. (2003). Corinth rift margin uplift: New evidence from Late Quaternary marine shorelines. *Geophysical Research Letters*, 30(12):1611.

Leeder, M. R., Seger, M. J., and Stark, C. P. (1991). Sedimentation and tectonic geomorphology adjacent to major active and inactive faults, southern Greece. *Journal of the Geological Society*, 148:331–343.

Lemons, D. R. and Chan, M. A. (1999). Facies architecture and sequence stratigraphy of fine-grained lacustrine deltas along the eastern margin of late pleistocene Lake Bonneville, Northern Utah and Southern Idaho. *American Association of Petroleum Geologists Bulletin*, 83(4):635–665.

Lian, O. B. and Roberts, R. G. (2006). Dating the Quaternary: progress in luminescence dating of sediments. *Quaternary Science Reviews*, 25(19-20):2449–2468.

Lord, A. R., Panayides, E. U., and Xenophontos, C. (2000). A biochronostratigraphical framework for the Late CretaceousRecent circum-Troodos sedimentary sequence, Cyprus. In *Proceedings of the third International conference on the geology of the Eastern Mediterranean.*, pages 289–297. Geological Survey Department, Nicosia, Cyprus.

Lurcock, P. C. and Wilson, G. S. (2012). PuffinPlot: A versatile, user-friendly program for paleomagnetic analysis. *Geochemistry, Geophysics, Geosystems*, 13(6):1–6.

Lytras, C. S. (1962). Progress Report: The Geology of the Avolona - Yerolakkas Area. Nicosia. Technical report, The Cosmos Press, Ltd.

Macklin, M. G., Fuller, I. C., Lewin, J., Maas, G. S., Passmore, D. G., Rose, J., Woodward, J. C., Black, S., Hamlin, R. H. B., and Rowan, J. S. (2002). Correlation of fluvial sequences in the Mediterranean basin over the last 200 ka and their relationship to climate change. *Quaternary Science Reviews*, 21:1633–1641.

Maddy, D., Demir, T., Bridgland, D. R., Veldkamp, A., Stemerdink, C., van der Schriek, T., and Westaway, R. (2008). The Early Pleistocene development of the Gediz River, Western Turkey: An uplift-driven, climate-controlled system? *Quaternary International*, 189(1):115–128.

Magaritz, M., Gavish, E., Bakler, N., and Kafri, U. (1979). Carbon and oxygen isotope composition- indicators of cementation in environment in recent, Holocene, and Pleistocene sediments along the coast of Israel. *Jounrary of Sedimentary Petrology*, 49(2):0401–0411.

Matthews, R. K. and Allan, J. R. (1982). Isotope signature associated with early meteoric diagenesis. *Sedimentology*, 29:797–817.

McArthur, J. (1994). Recent trends in strontium isotope stratigraphy. *Terra Nova*, 6(4):331–358.

McArthur, J., Howarth, R., and Bailey, T. (2001). Strontium isotope stratigraphy: LOWESS version 3: best fit to the marine Sr-isotope curve for 0-509 Ma and accompanying look-up table for deriving numerical age. *The Journal of Geology*, 109(2):155–170.

Mcarthur, J. M., Howarth, R. J., and Shields, G. A. (2012). Strontium Isotope Stratigraphy. In Gradstein, F. M., Ogg, J. G., Schmitz, M., and Ogg, G., editors, *The Geologic Time Scale 2012*, pages 127–144. Elsevier, 1st edition.

McCallum, J. (1989). *Sedimentation and Tectonic of the Plio-Pleistocene of Cyprus*. PhD thesis, University of Edinburgh.

McCallum, J. E. and Robertson, A. H. F. (1990). Pulsed uplift of the Troodos Massifevidence from the Plio-Pleistocene Mesaoria basin. In *Troodos 87, ophiolite and oceanic lithosphere*, volume 1, pages 217–230. Geological Survey Department, Ministery of Agriculture and Natural Resources.

McCallum, J. E. and Robertson, A. H. F. (1995a). Late Pliocene-early Pleistocene Athalassa Formation, north central Cyprus: carbonate sand bodies in a shallow seaway between two emerging landmasses. *Terra Nova*, 7(2):265–277.

McCallum, J. E. and Robertson, A. H. F. (1995b). Sedimentology of two fan-delta systems in the Pliocene-Pleistocene of the Mesaoria Basin, Cyprus. *Sedimentary Geology*, 98:215–244.

McCay, G. and Robertson, A. (2012a). Late Eocene-Neogene sedimentary geology of the Girne (Kyrenia) Range, northern Cyprus: A case history of sedimentation related to progressive and diachronous continental collision. *Sedimentary Geology*, 265-266:30–55.

McCay, G. and Robertson, A. H. F. (2012b). Upper Miocene-Pleistocene deformation of the Girne (Kyrenia) Range and Dar Dere (Ovgos) lineaments, northern Cyprus: role in collision and tectonic escape in the easternmost Mediterranean region. In Robertson, A., Osman, P., and Ünlügenç, U. C., editors, *Geological Development of Anatolia and the Easternmost Mediterranean Region*, volume 372, pages 421–445. Geological Society, London, Special Publications.

McCay, G., Robertson, A. H. F., Kroon, D., Raffi, I., Ellam, R. M., and Necdet, M. (2012). Stratigraphy of Cretaceous to Lower Pliocene sediments in the northern part of Cyprus based on comparative 87Sr/86Sr isotopic, nannofossil and planktonic foraminiferal dating. *Geological Magazine*, pages 1–27.

McCay, G. A. (2010). *Tectonic-sedimentary evolution of the Girne (Kyrenia) Range and the Mesarya (Mesaoria) Basin, North Cyprus*. PhD thesis, University of Edinburgh.

McClusky, S., Balassanian, S., Barka, A., Demir, C., Ergintav, S., Georgiev, I., Gurkan, O., Hamburger, M., Hurst, K., Kahle, H., Kastens, K., Kekelidze, G., King, R., Kotzev, V., Lenk, O., Mahmoud, S., Mishin, A., Nadariya, M., Ouzounis, A., Paradissis, D., Peter, Y., Prilepin, M., Reilinger, R., Sanli, I., Seeger, H., Tealeb, A., Toksöz, M. N., and Veis, G. (2000). Global Positioning System constraints on plate kinematics and dynamics in the eastern Mediterranean and Caucasus.

McClusky, S., Reilinger, R., Mahmoud, S., Ben Sari, D., and Tealeb, a. (2003). GPS constraints on Africa (Nubia) and Arabia plate motions. *Geophysical Journal International*, 155(1):126–138.

Merritts, D. and Bull, W. B. (1989). Interpreting Quaternary uplift rates at the Mendocino triple junction, northern California, from uplifted marine terraces. *Geology*, 17(11):1020–1024.

Mertz-Kraus, R., Brachert, T. C., and Reuter, M. (2008). Tarbellastraea (Scleractinia): A new stable isotope archive for Late Miocene paleoenvironments in the Mediterranean. *Palaeogeography, Palaeoclimatology, Palaeoecology*, 257(3):294–307.

Moores, E. M. and Vine, F. J. (1971). The Troodos Massif, Cyprus and other Ophiolites as Oceanic Crust: Evaluation and Implications. *Philosophical Transactions of the Royal Society A: Mathematical, Physical and Engineering Sciences*, 268(1192):443–467.

Morris, a. (1996). A review of palaeomagnetic research in the Troodos ophiolite, Cyprus. *Geological Society, London, Special Publications*, 105(1):311–324.

Muñoz-Salinas, E., Bishop, P., Sanderson, D. C., and Zamorano, J.-J. (2011). Interpreting luminescence data from a portable OSL reader: three case studies in fluvial settings. *Earth Surface Processes and Landforms*, 36(5):651–660.

Munyikwa, K., Brown, S., and Kitabwalla, Z. (2012). Delineating stratigraphic breaks at the bases of postglacial eolian dunes in central Alberta, Canada using a portable OSL reader. *Earth Surface Processes and Landforms*, 37(15):1603–1614.

Murray, a. S., Buylaert, J. P., Thomsen, K. J., and Jain, M. (2009). The effect of preheating on the IRSL signal from feldspar. *Radiation Measurements*, 44(5-6):554–559.

Murray, a. S. and Wintle, a. G. (2000). Luminescence dating of quartz using an improved single-aliquot regenerative-dose protocol. *Radiation Measurements*, 32(1):57–73.

Nalin, R. and Massari, F. (2009). Facies and stratigraphic anatomy of a temperate carbonate sequence (Capo Colonna terrace, Late Pleistocene, Southern Italy). *Journal of Sedimentary Research*, 79(4):210–225.

Necdet, M. and Anl, M. (2006). The geology and geochemistry of the gypsum deposits in Northern Cyprus. *Geosound (Yerbilimleri)*, 48:49:11–49.

Nelson, C. S. and Smith, A. M. (1996). Stable oxygen and carbon isotope compositional fields for skeletal and diagenetic components in New Zealand Cenozoic nontropical carbonate sediments and limestones: a synthesis and review. *New Zealand Journal of Geology and Geophysics*, 39:93–107.

Nemec, W. and Kazanci, N. (1999). Quaternary colluvium in west-central Anatolia: Sedimentary facies and palaeoclimatic significance. *Sedimentology*, 46:139–170.

Nichols, G. J. and Fisher, J. a. (2007). Processes, facies and architecture of fluvial distributary system deposits. *Sedimentary Geology*, 195:75–90.

Nielsen, K. a., Clemmensen, L. B., and Fornós, J. J. (2004). Middle Pleistocene magnetostratigraphy and susceptibility stratigraphy: Data from a carbonate aeolian system, Mallorca, Western Mediterranean. *Quaternary Science Reviews*, 23(16-17):1733–1756.

Olson, S. L. and Hearty, P. J. (2009). A sustained +21 m sea-level highstand during MIS 11 (400 ka): direct fossil and sedimentary evidence from Bermuda. *Quaternary Science Reviews*, 28(3-4):271–285.

Palamakumbura, R. N., Robertson, A. H. F., Kinnaird, T. C., and Sanderson, D. C. W. (2015). Sedimentary development and correlation of Late Quaternary terraces in the Kyrenia Range, northern Cyprus, using a combination of sedimentology and optical luminescence data. *International Journal of Earth Sciences (Geologische Rundschau)*.

Palmar, M. R. and Elderfield, J. (1985). Sr isotope composition of sea water over the past 75 Myr. *Nature*, 314(11):526– 528.

Pearce, J. and Robinson, P. (2010). The Troodos ophiolitic complex probably formed in a subduction initiation, slab edge setting. *Gondwana Research*, 18(1):60–81.

Pedley, M. and Carannante, G. (2006). Cool-water carbonate ramps: a review. In Pedley, H. and Carannante, G., editors, *Cool-water Carbonates: Depositional Systems and Palaeoenvironmental Controls*, volume 255, pages 1–9. Geological Society, London, Special Publications.

Pedley, M. and Grasso, M. (2002). Lithofacies modelling and sequence stratigraphy in microtidal cool-water carbonates: A case study from the Pleistocene of Sicily, Italy. *Sedimentology*, 49:533–553.

Pedoja, K., Husson, L., Johnson, M. E., Melnick, D., Witt, C., Pochat, S., Nexer, M., Delcaillau, B., Pinegina, T., Poprawski, Y., Authemayou, C., Elliot, M., Regard, V., and Garestier, F. (2014). Coastal staircase sequences reflecting sea-level oscillations and tectonic uplift during the Quaternary and Neogene. *Earth-Science Reviews*, 132:13–38.

Pedoja, K., Husson, L., Regard, V., Cobbold, P. R., Ostanciaux, E., Johnson, M. E., Kershaw, S., Saillard, M., Martinod, J., Furgerot, L., Weill, P., and Delcaillau, B.

(2011). Relative sea-level fall since the last interglacial stage: Are coasts uplifting worldwide? *Earth-Science Reviews*, 108(1-2):1–15.

Peryt, T. M. (1981). Phanerozoic oncoids an overview. *Facies*, 4:197–214.

Pietsch, T. J., Olley, J. M., and Nanson, G. C. (2008). Fluvial transport as a natural luminescence sensitiser of quartz. *Quaternary Geochronology*, 3(4):365–376.

Poole, A. and Robertson, A. (1998). Pleistocene fanglomerate deposition related to uplift of the Troodos Ophiolite, Cyprus. In Robertson, A., Emeis, K.-C., and Camerlenghi, A., editors, *Proceedings 38 of the Ocean Drilling Program*, volume 160, pages 545 – 566. IODP.

Poole, A. J. and Robertson, A. H. F. (1991). Quaternary uplift and sea-level change at an active plate boundary, Cyprus. *Journal of the Geological Society*, 148(5):909–921.

Poole, A. J. and Robertson, A. H. F. (2000). Quaternary marine terrace and aeolinites in coastal south and west Cyprus: implications for regional uplift and sea-level change. In Panayides, I., Xenophontos, C., and Malpas, J., editors, *Proceedings of the Third International Conference on the Geology of the Eastern Mediterranean*, pages 105–123. Geological Survey Department, Ministry of Agriculture and Natural Resources.

Poole, A. J., Shimmield, G. B., and Robertson, A. H. F. (1990). Late Quaternary uplift of the Troodos ophiolite, Cyprus: Uranium-series dating of Pleistocene coral. *Geology*, 18:894–897.

Postma, G. (1986). Classification for sediment gravity-flow deposits based on flow conditions during sedimentation. *Geology*, 14:291–294.

Reed, F. R. C. (1935). I.Notes on the neogene faunas of Cyprus.II. *Journal of Natural History*, 15(85):1–37.

Reilinger, R., Toksoz, N., McClusky, S., and Barka, A. (2000). 1999 Izmit, Turkey eathquake was no surprise. *GSA Todat*, 10(1-6).

Reyss, J. L., Pirazzoli, P. a., Haghipour, A., Hatte, C., and Fontugne, M. (1998). Quaternary marine terraces and tectonic uplift rates on the south coast of Iran. In Reyss, J.-l., Pirazzoli, P. A., and Haghipour, A., editors, *Coastal Tectonics*, volume 146, pages 225–237. Geological Society, London, Special Publications.

Rhodes, E. J. (2011). Optically Stimulated Luminescence Dating of Sediments over the Past 200,000 Years. *Annual Review of Earth and Planetary Sciences*, 39(1):461–488.

Richter, C., Roberts, A., Stoner, J., Benning, L., and Chi, C. (1998). Magnetostratigraphy of Pliocene-Pleistocene sediments from the eastern Mediterranean Sea. In Robertson, A., Emeis, K., and Camerlenghi, A., editors, *Proceedings of the Ocean Drilling Program Scientific Results 160*, volume 160, pages 61–73. IODP.

Roberts, D. L., Karkanas, P., and Jacobs, Z. (2012). Melting ice sheets 400,000 yr ago raised sea level by 13 m: Past analogue for future trends. *Earth and Planetary Science Letters*, 357:226–237.

Roberts, G. P., Houghton, S. L., Underwood, C., Papanikolaou, I., Cowie, P. a., Van Calsteren, P., Wigley, T., Cooper, F. J., and McArthur, J. M. (2009a). Localization of quaternary slip rates in an active rift in 105 years: An example from central Greece constrained by 234U- 230Th coral dates from uplifted paleoshorelines. *Journal of Geophysical Research: Solid Earth*, 114(10):1978–2012.

Roberts, H. M. and Duller, G. a. T. (2004). Standardised growth curves for optical dating of sediment using multiple-grain aliquots. *Radiation Measurements*, 38(2):241–252.

Roberts, H. M., Durcan, J. a., and Duller, G. a. T. (2009b). Exploring procedures for the rapid assessment of optically stimulated luminescence range-finder ages. *Radiation Measurements*, 44(5-6):582–587.

Robertson, A. H., McCay, G. A., Tasli, K., and Yildiz, A. (2013). Eocene development of the northerly active continental margin of the Southern Neotethys in the Kyrenia Range, north Cyprus. *Geological Magazine*, 151(04):692–731.

Robertson, A. H. F. (1977). Tertiary uplift history of the Troodos massif, Cyprus. *Geological Society Of America Bulletin*, 12:1763–1772.

Robertson, A. H. F. (1998a). Mesozoic-Tertiary tectonic evolution of the easternmost Mediterranean area: integration of marine and land evidence. In Robertson, A. H. F., Emeis, K. ., Richter, C., and Camerlenghi, A., editors, *Proceedings of the Ocean Drilling Program, Scientific Results*, volume 160, chapter 54. IODP.

Robertson, A. H. F. (1998b). Tectonic significance of the Eratosthenes Seamount: A continental fragment in the process of collision with a subduction zone in the eastern Mediterranean (Ocean Drilling Program Leg 160). *Tectonophysics*, 298(1-3):63–82.

Robertson, A. H. F. (2000). Mesozoic-Tertiary Tectonic-Sedimentary Evolution of a South Tethyan Oceanic Basin and its Margins in Southern Turkey. In Robertson, A. and Demosthenis, M., editors, *Tectonic Development of the Eastern Mediterranean Region*, volume 173, pages 97–138. Geological Society, London, Special Publications.

Robertson, A. H. F. and Dixon, J. E. (1984). Introduction: aspects of the geological evolution of the Eastern Mediterranean. In Dixon, J. E. and Robertson, A., editors, *The Geological Evolution of the Eastern Mediterranean*, volume 17, pages 1–74. Geological Society, London, Special Publications.

Robertson, A. H. F., Osman, P., and Ustaömer, T. (2012a). Overview of the Palaeozoic neogene evolution of neotethys in the Eastern Mediterranean region (southern Turkey, cyprus , Syria). *Petroleum Geoscience*, 18(2012):381–404.

Robertson, A. H. F., Tasli, K., and nan, N. (2012b). Evidence from the Kyrenia Range, Cyprus, of the northerly active margin of the Southern Neotethys during Late CretaceousEarly Cenozoic time. *Geological Magazine*, 149(02):1–27.

Robertson, A. H. F. and Woodcock, N. H. (1986). The Role of the Kyrenia Range Lineament, Cyprus, in the Geological Evolution of the Eastern Mediterranean Area. In Reading, H. G., Watterson, J., and White, S. H., editors, *Major Crustal Lineaments and their influences on the Geological History of Continental Lithosphere*, volume 317, pages 141–177. Philosophical Transactions of the Royal Society A: Mathematical, Physical and Engineering Sciences.

Robertson, A. H. F. and Xenophontos, C. (1993). Development of concepts concerning the Troodos ophiolite and adjacent units in Cyprus. In Dilek, Y. and Newcomb, S., editors, *Ophiolite Concept and the Evolution of Geological Thought*, volume 76, pages 85–119. Geological Society, London, Special Publications.

Russell, R. (1882). On the Geology of the Island of Cyprus. *Rep. Brit. Assoc., York*, pages 2–37.

Sanders, D., Ostermann, M., and Kramers, J. (2009). Quaternary carbonate-rocky talus slope successions (Eastern Alps, Austria): Sedimentary facies and facies architecture. *Facies*, 55:345–373.

Sanderson, D. C. and Murphy, S. (2010). Using simple portable OSL measurements and laboratory characterisation to help understand complex and heterogeneous sediment sequences for luminescence dating. *Quaternary Geochronology*, 5(2-3):299–305.

Sanderson, D. C. W., Bishop, P., Houston, I., and Boonsener, M. (2001). Luminescence characterisation of quartz-rich cover sands from NE Thailand. *Quaternary Science Reviews*, 20(5-9):893–900.

Sanderson, D. C. W., Bishop, P., Stark, M. T., and Spencer, J. Q. (2003). Luminescence dating of anthropogenically reset canal sediments from Angkor Borei, Mekong Delta, Cambodia. *Quaternary Science Reviews*, 22(10-13):1111–1121.

Saucier, A. E. and Major, R. L. (1963). The Geology and Minerla Resources of the Kantara-Koma Tou Yialou Area (West Karpas Peninsula). Technical report, The Cosmos Press, Ltd, Nicosia.

Savostin, L. A., Sibuet, J. C., Zonenshain, L. P., Le Pichon, X., and Roulet, M. J. (1986). Kinematic evolution of the Tethys belt from the Atlantic Ocean to the Pamirs since the Triassic. *Tectonophysics*, 123:1–35.

Schattner, U. (2010). What triggered the early-to-mid Pleistocene tectonic transition across the entire eastern Mediterranean? *Earth and Planetary Science Letters*, 289(3-4):539–548.

Schildgen, T., Cosentino, D., Bookhagen, B., Niedermann, S., Yldrm, C., Echtler, H., Wittmann, H., and Strecker, M. (2012). Multi-phased uplift of the southern margin of the Central Anatolian plateau, Turkey: A record of tectonic and upper mantle processes. *Earth and Planetary Science Letters*, 317-318:85–95.

Schildgen, T. F., Yildirim, C., Cosentino, D., and Strecker, M. R. (2014). Linking slab break-off, Hellenic trench retreat, and uplift of the Central and Eastern Anatolian plateaus. *Earth-Science Reviews*, 128:147–168.

Schirmer, W., Weber, J., Bachtadse, V., Boudagher-fadel, M., Heller, F., Lehmkuhl, F., Panayides, I., and Schirmer, U. (2010). Fluvial stacking due to plate collision and uplift during the Early Pleistocene in Cyprus. *Central European Journal of Geosciences*, 2(4):514–523.

Schlesinger, W. H. (1985). The formation of caliche in soils of the Mojave Desert, California. *Geochimica et Cosmochimica Acta*, 49(1):57–66.

Schoenbohm, L. M., Whipple, K. X., Burchfiel, B. C., and Chen, L. (2004). Geomorphic constraints on surface uplift, exhumation, and plateau growth in the Red River region,

Yunnan Province, China. *Bulletin of the Geological Society of America*, 116(7-8):895–909.

Schwarcz, H. P. (1989). Uranium series dating of Quaternary deposits. *Quaternary International*, 1:7–17.

Sengor, A. M. C., Yilmaz, Y., and Sungurlu, O. (1984). Tectonics of the Mediterranean Cimmerides: nature and evolution of the western termination of Palaeo-Tethys. In Dixon, J. E. and Robertson, A., editors, *The Geological Evolution of the Eastern Mediterranean*, volume 17, pages 77–112. Geological Society, London, Special Publications.

Seyrek, A., Demir, T., Pringle, M., Yurtmen, S., Westaway, R., Bridgland, D., Beck, A., and Rowbotham, G. (2008). Late Cenozoic uplift of the Amanos Mountains and incision of the Middle Ceyhan river gorge, southern Turkey; Ar-Ar dating of the Düziçi basalt. *Geomorphology*, 97(3-4):321–355.

Shackleton, N. J. (1987). Oxygen isotopes, ice volume and sea level. *Quaternary Science Reviews*, 6:183–190.

Sheldon, N. D. and Tabor, N. J. (2009). Quantitative paleoenvironmental and paleoclimatic reconstruction using paleosols. *Earth-Science Reviews*, 95(1-2):1–52.

Shelton, a. W. (1993). Troodos revisited: the Mount Olympus gravity anomaly. *Geological Society, London, Special Publications*, 76(1):197–212.

Siddall, M., Chappell, J., and Potter, E. (2006). Eustatic Sea Level During Past Interglacials. *Developments in Quaternary Sciences*, 7:75–92.

Siddall, M., Rohling, E. J., Almogl-Labin, A., Hemleben, C., Meischner, D., Schmeizer, I., and Smeed, D. A. (2003). Sea-level fluctuations during the last glacial cycle. *Nature*, 423:853–858.

Snyder, N. P., Whipple, K. X., Tucker, G. E., and Merritts, D. J. (2000). Stream profiles in the Mendocino triple junction region, northern California. *GSA Bulletin*, 112(8):1250–1263.

Starkel, L. (2003). Climatically controlled terraces in uplifting mountain areas. *Quaternary Science Reviews*, 22(20):2189–2198.

Suresh, N., Bagati, T. N., Kumar, R., and Thakur, V. C. (2007). Evolution of Quaternary alluvial fans and terraces in the intramontane Pinjaur Dun, Sub-Himalaya, NW India: interaction between tectonics and climate change. *Sedimentology*, 54(4):809–833.

Taylforth, J. E., McCay, G. a., Ellam, R., Raffi, I., Kroon, D., and Robertson, A. H. F. (2014). Middle Miocene (Langhian) sapropel formation in the easternmost Mediterranean deep-water basin: Evidence from northern Cyprus. *Marine and Petroleum Geology*, 57:521–536.

Teichert, C. (1970). Oolite, oolith, ooid: discussion. *The American Association of Petroleum Geologist Bulletin*, 54(9):1748–1749.

Thomas, J. V., Parkash, B., and Mohindra, R. (2002). Lithofacies and palaeosol analysis of the Middle and Upper Siwalik Groups (Plio-Pleistocene), Haripur-Kolar section, Himachal Pradesh, India. *Sedimentary Geology*, 150:343–366.

Thomsen, K. J., Murray, A. S., and Jain, M. (2011). Stability of IRSL signals from sedimentary K-feldspar samples. *Geochronometria*, 38(1):1–13.

Thunell, R., Rio, D., Sprovieri, R., and Raffi, I. (1991). Limestone-marl couplets: origin of the early pliocene trubi marls in calabria, southern italy i. *Journal of Sedimentary Petrology*, 61(7):1109–1122.

Turner, J. A., Leeder, M. R., Andrews, J. E., Rowe, P. J., Van Calsteren, P., and Thomas, L. (2010). Testing rival tectonic uplift models for the Lechaion Gulf in the Gulf of Corinth rift. *Journal of the Geological Society*, 167(6):1237–1250.

Udden, J. A. (1914). Mechanical composition of clastic sediments. *Bulletin of the Geological Society of America*, 25:655–744.

Van Calsteren, P. and Schwieters, J. B. (1995). Performance of a thermal ionisation mass spectrometer with a deceleration lens system and post-deceleration detector selection. *International Journal of Mass Spectrometry and Ion Processes*, 146-147:119–129.

Van Calsteren, P. and Thomas, L. (2006). Uranium-series dating applications in natural environmental science. *Earth-Science Reviews*, 75(1-4):155–175.

Van der Plas, L. and Tobi, a. C. (1965). A chart for judging the reliability of point count results. *American Journal of Science*.

Vesica, P. L., Tuccimei, P., Turi, B., Fornós, J. J., Ginés, a., and Ginés, J. (2000). Late Pleistocene Paleoclimates and sea-level change in the Mediterranean as inferred from stable isotope and U-series studies of overgrowths on speleothems, Mallorca, Spain. *Quaternary Science Reviews*, 19(9):865–879.

Waelbroeck, C., Labeyrie, L., Michel, E., Duplessy, J., McManus, J., Lambeck, K., Balbon, E., and Labracherie, M. (2002). Sea-level and deep water temperature changes derived from benthic foraminifera isotopic records. *Quaternary Science Reviews*, 21(1-3):295–305.

Waters, J., Jones, S., and Armstrong, H. (2010). Climatic controls on late Pleistocene alluvial fans, Cyprus. *Geomorphology*, 115(3-4):228–251.

Weber, J., Schirmer, W., Heller, F., and Bachtadse, V. (2011). Magnetostratigraphy of the Apalós Formation (early Pleistocene): Evidence for pulsed uplift of Cyprus. *Geochemistry, Geophysics, Geosystems*, 12(1).

Wegmann, K. W. and Pazzaglia, F. J. (2009). Late Quaternary fluvial terraces of the Romagna and Marche Apennines, Italy: Climatic, lithologic, and tectonic controls on terrace genesis in an active orogen. *Quaternary Science Reviews*, 28(1-2):137–165.

Weiler, Y. (1970). Mode of occurrence of pelites in the Kythrea Flysch basin (Cyprus). *Journal of Sedimentary Research*, 40(4):1255–1261.

Weiss, M. P. (1969). Oncolites, Paleoecology, and Laramide Tectonics, Central Utah. *The American Association of Petroleum Geologist Bulletin*, 53(5):1105–1120.

Wentworth, C. K. (1922). A scale of grade and class terms for clastic sediments. *The Journal of Geology*, 30(5):377–392.

Westaway, R. O. B. (2003). Kinematics of the Middle East and Eastern Mediterranean Updated. *Turkish Journal of Earth Sciences*, 12:5–46.

Wilson, K., Litchfield, N., Berryman, K., and Little, T. (2007). Distribution, age, and uplift patterns of Pleistocene marine terraces of the northern Raukumara Peninsula, North Island, New Zealand. *New Zealand Journal of Geology and Geophysics*, 50(3):181–191.

Wintle, a. G. (1973). Anomalous Fading of Thermo-luminescence in Mineral Samples. *Nature*, 245(5421):143–144.

Wintle, A. G. and Huntley, D. J. (1982). Thermoluminescence dating of sediments. *Quaternary Science Reviews*, 1:31–53.

Yetis, C., Kelling, G., Gokcen, S. L., and Baroz, F. (1995). A revised stratigraphic framework for Later Cenozoic sequences in the northeastern Mediterranean region. *International Journal of Earth Sciences*, 84:794–812.

Zachos, J., Pagani, M., Sloan, L., Thomas, E., and Billups, K. (2001). Trends, rhythms, and aberrations in global climate 65 Ma to present. *Science*, 292(5517):686–693.

Zazo, C., Goy, J. L., Dabrio, C. J., Bardaj, T., Hillaire-Marcel, C., Ghaleb, B., González-Delgado, J.-Á., and Soler, V. (2003). Pleistocene raised marine terraces of the Spanish Mediterranean and Atlantic coasts: records of coastal uplift, sea-level highstands and climate changes. *Marine Geology*, 194(1-2):103–133.

Zazo, C., Silva, P., Goy, J., Hillaire-Marcel, C., Ghaleb, B., Lario, J., Bardaj, T., and González, a. (1999). Coastal uplift in continental collision plate boundaries: data from the Last Interglacial marine terraces of the Gibraltar Strait area (south Spain). *Tectonophysics*, 301(1-2):95–109.

Zecchin, M., Nalin, R., and Roda, C. (2004). Raised Pleistocene marine terraces of the Crotone peninsula (Calabria, southern Italy): Facies analysis and organization of their deposits. *Sedimentary Geology*, 172:165–185.

Zibrowius, H. (1980). Les Scleractiniaires de la Mediterranee et de l'Atlantique nord-oriental. *Mem Inst oceanogr*, 11:1–284.

Zijderveld, J. D. A. (1967). AC demagnetization of rocks: analysis of results. In Collinson, D. W., Creer, K. M., and Runcorn, S. K., editors, *Methods in Paleomagnetism 3*, pages 254–286. Elsevier, Amsterdam.

Appendix

Scottish Universities Environmental Research Centre

OSL dating of aeolianites from the northern coast of Cyprus

Appendix to: 'Sedimentary response to the tectonic uplift of the Kyrenia Range, northern Cyprus, in its Eastern Mediterranean tectonic setting'

February 2015

T.C. Kinnaird[1], R. Palamakumbura[2], A.H.F. Robertson[2] & D.C.W. Sanderson[1]

[1]SUERC, East Kilbride, UK
[2]School of Geosciences, University of Edinburgh, Edinburgh, UK

East Kilbride Glasgow G75 0QF Telephone: 01355 223332 Fax: 01355 229898

University of Glasgow
The University of Glasgow, charity number SC004401

The University of Edinburgh is a charitable body, registered in Scotland, with registration number SC005336

Summary

This report is concerned with optically stimulated luminescence (OSL) investigations on sediments sampled from the younger of a series of Quaternary marine terraces on the northern flank of the Kyrenia Range in northern Cyprus. The youngest marine terrace, the Koupia terrace, is patchily developed along the coastline (and never more than 100 m inland). It is tentatively correlated with oxygen isotope stage 3, dating the terrace to less than 50 Ka. The Koupia terrace was sampled at two localities for luminescence dating at Alagadi Beach (SUTL2698) and near Mersinlik town (SUTL2699).

Conventional OSL quartz and post-infra red elevated temperature infra-red stimulated luminescence (post-IR IRSL) K feldspar approaches were examined as potential methods for dating the aeolianite component of this terrace. Low OSL sensitivities, poor thermal stability at elevated temperatures and low saturation limits restrict the use of conventional quartz OSL methods. Furthermore, the local geology dominated by Permian to Middle Miocene calcareous rocks, with only subordinate volcanogenic and siliceous rocks, indicates several additional challenges, namely that (if locally derived) the sands will be comprised of low radioactivity materials, and contain little quartz and alkali feldspar. However, luminescence profiling during fieldwork, and then subsequently in the laboratory revealed stratigraphically progressive OSL and IRSL signals, indicating phases in the sediments with dating potential. While laboratory characterisation recovered some quartz, its low yields, low luminescence sensitivity and on further investigation, lack of thermal stability of the conventional OSL signals (i.e. the fast component) precluded application of quartz methods. Electron microscopy confirmed the presence of feldspars, which were separated and used for IRSL and elevated temperature post-IRSL IRSL single aliquot regeneration (SAR) dating. Fortuitously, polymineral sensitivities were a magnitude larger than their quartz equivalents, registering variations in stored dose over the dynamic range expected for these sediments. Dose rate estimates from these sands were assessed using a combination of field gamma spectrometry, high resolution gamma spectrometry (HRGS) and thick source beta counting (TSBC) reconciled with each other and with the water contents and micro-dosimetry of the model. In addition to the two dating samples, a series of 8 bulk gamma spectrometry samples were collected to permit retrospective analysis of the external gamma dose rates. The gamma dose rates were reconstructed from 7 of these giving wet gamma dose rates between 0.4 and 0.7 mGy a^{-1}, which are comparable with the measured values recorded at the sampling positions (0.4-0.5 mGy a^{-1}). Counting times for both HRGS and TSBC measurements were extended by 1 order of magnitude, resulting in overall uncertainties of <4% for these low dose rates. Internal alpha dose rates have been estimated on the basis of ICPMS analyses of comparable feldspars, and make a minor contribution to the overall dose rates from this material.

Equivalent doses were determined by IRSL from 16 aliquots of K feldspar per sample using a post-IR IRSL elevated temperature single-aliquot-regenerative (SAR) approach. The material exhibited good IRSL sensitivity and produced acceptable SAR internal quality control performance. Fading tests have been initiated. The mean ratios of sensitisation-independent stored to prompt normalised signals after 10^6 s storage are 0.93 ± 0.06 and 1.08 ± 0.08, for IRSL and post-IRSL IRSL 225°C, respectively. On the basis of these results, the IRSL SAR quality selection criteria and the expectations of the procedure, preference was given to the post-IR IRSL 225°C signals in equivalent dose determinations. Radial plotting methods revealed some

heterogeneity in the equivalent dose distributions of each sample, reflecting variable bleaching at deposition and indicating that each sample enclosed mixed-age materials. The laboratory profiles provide some measure of control on this. The basal units, which erosionally overlay the underlying marine calcarenites and grainstones, show the greatest dispersion/spread in IRSL stored dose values, and importantly, the lowest values in each profile. In contrast, the upper units are characterised by larger IRSL stored dose values with tighter distributions, reflecting faster deposition and poor to incomplete bleaching, or zeroing, of the luminescence signals. This could indicate that initially the sands were mobile, blowing freely across the freshly cut palaeo-surface, with greater scope for bleaching; and that subsequently, the sands were re-worked rapidly from older deposits. Following this reasoning through, the lowest population of equivalent doses, which presumably reflects the well-bleached component, was used in age determinations. For age determinations, the weighted mean of the equivalent dose distribution was used, as for the two dating samples, this encloses the low dose component.

Luminescence ages were calculated using standard microdosimetric models, with uncertainties that combined measurement and fitting errors from the SARA/SAR analysis, all dose rate evaluation uncertainties, and allowance for the calibration uncertainties of the sources and reference materials. The post-IR IRSL 225°C age estimates are for SUTL2698 - 76.1 ± 3.5 ka and SUTL2699 - 58.7 ± 2.6 ka.

Contents

List of figures

List of tables

1. Introduction

This report is concerned with optically stimulated luminescence (OSL) investigations on sediments sampled from the younger of a series of Quaternary marine terraces on the northern flank of the Kyrenia Range in northern Cyprus. It forms an appendix to the PhD thesis: 'Sedimentary response to the tectonic uplift of the Kyrenia Range, northern Cyprus, in its Eastern Mediterranean tectonic setting', authored by Romesh Palamakumbura. The work reported herein, may be divided into three sections, the field and laboratory luminescence profiling undertaken by the author RP, and the quantitative dating undertaken by the authors TK and RP. This report is largely concerned with the latter, but drawns upon the observations and inferences made by RP (and published in 'Sedimentary development and correlation of Late Quaternary terraces in the Kyrenia Range, northern Cyprus, using a combination of sedimentology and optical luminescence data' by 2015).

The uplift of the Troodos Massif is known from research on the Plio-Quaternary deposits exposed in the south of Cyprus. This effectively began with mapping of the deposits by the Cyprus Geological Survey Department (e.g. Bagnall, 1960) and early stratigraphical studies (Ducloz, 1964). This was supplemented by sedimentological and dating studies (Poole and Robertson, 1991; Poole and Robertson, 1998, 2000; Poole et al., 1990), allowing a tectonic-sedimentary model for the uplift to be proposed. Recently, the deposits have been dated using a combination of magnetostratigraphy (Kinnaird et al., 2011), optically stimulated luminescence (OSL) and isotopic studies (Harrison et al., 2004; Harrison et al., 2012; Kinnaird and Robertson, 2013). Different areas, for example south-eastern Cyprus (Harrison et al., 2012), central southern Cyprus (Kinnaird and Robertson, 2013) and western Cyprus (Kinnaird and Robertson, 2013; Weber et al., 2011), have distinctive tectonic and sedimentary features related to the Quaternary uplift such that individual areas need to be carefully studied before the overall regional uplift can be understood.

The Kyrenia Range is known to have undergone strong uplift during the Plio-Quaternary (Baroz, 1979; Ducloz, 1972; Robertson and Woodcock, 1986). Quaternary deposits have been mapped on both sides of the Kyrenia Range and a series of geomorphological terraces, and related deposits have been recognised (Ducloz, 1963; Knupp, 1964). As yet, these deposits remain largely undated.

1.1. Research questions

The aim of this investigation is provide the first absolute ages for deposition of the Koupia Terrace, northern Cyprus.

1.2. Luminescence background

In much luminescence dating work quartz is used as the primary dosimeter (Huntley et al., 1985; Murray and Wintle, 2000), with the initial part of the OSL signal, the 'fast' component (Bailey, 1998) used in age determination. This part of the signal is known to show little growth with dose when samples are irradiated above a few hundred Gy. This therefore limits the dating range of quartz using conventional techniques.

Luminescence signals from feldspars continue to grow to far higher doses than those from quartz; this offers the possibility of dating significantly older material providing sufficiently stable signals can be achieved. The IRSL and TL signals from feldspars are expected to respond to additional radiation up to the 1 – 5 kGy range. In a low dose rate environment, this means that there is the potential to date sediments well beyond ~ 250 ka. Unfortunately, the luminescence signals from feldspar may fade at a rate faster than expected simply from a consideration of trap depth and ambient temperature (a phenomenon termed 'anomalous fading' by Wintle, 1973). Some authors (Huntley and Lamothe, 2001; Spooner, 1992) have suggested that anomalous fading is inherent to some extent within all feldspars. However in practice, signal stability is dependent on the mineralogy of the studied feldspar (Alexander, 2007; Krbetschek et al., 1997; Krbetschek and Rieser, 1995) its geological origins (Huntley and Lamothe, 2001; Zink et al., 1995), its structural configuration (i.e. order vs disorder; Visocekas et al., 1994; Visocekas et al., 1998), and its composition (i.e. major or minor element chemistry; Huntley et al., 2007; Huntley and Lian, 2006; Spooner, 1994). Thermal fading processes are always present, regardless of whether additional proximity or tunnelling effects are also operating, and affect storage/accumulation temperatures and timescales (Sanderson, 1988a). Recent work (Buylaert et al., 2009; Thomsen et al., 2008) has suggested a new procedure based on elevated temperature post-IR IRSL measurements which can potentially produce the desired low fading rates under convenient automated conditions. They interpreted the increased signal stability of these post-IR IRSL as a consequence of the removal of unstable donor-acceptor pairs in close lattice proximity to each other during the prior IR stimulation at 50°C. In this explanation the subsequent post-IR IRSL signal is interpreted as originating in more distant pairs, which can be accessed by re-stimulating the sample at elevated temperatures. Recently, following Murray et al. (2009)'s study on preheat dependence and equivalent dose determination, Thiel et al. (2011) proposed post-IR IRSL stimulation at significantly higher temperatures to obtain higher signal intensities.

Given the expected age range of the Koupia sediments, we will assess the luminescence properties of both mineral phases, before selecting the preferred luminescence dating approach for this sediment.

1.3. Geological background

The bedrock geology of the range is largely dominated by a Permian to the Middle Miocene sedimentary assemblage of pelagic carbonates and locally derived carbonate breccias, with only subordinate sandstone turbidities derived from mixed continental, basic volcanic, neritic carbonate and pelagic lithologies. In addition, two volcanogenic sequences are exposed in the western-central Kyrenia Range: the first is a sequence of Campanian–Lower Maastrichtian(?) pelagic carbonates, silicic tuffs, silicic lava debris flows and thick-bedded to massive rhyolitic lava flows; the second sequence comprises two intervals of basaltic extrusive rocks interbedded with pelagic carbonates (Robertson et al., 2012).

Given these bedrock lithologies, it may expected, that if locally derived, the sands may be comprised of extremely low radioactivity materials, and contain little quartz and alkali feldspar.

2. Sampling

Sampling was undertaken by Romesh Palamakumbura and Alastair Robertson in XX 2014. A brief description of the samples is given in Table 2-1, together with the laboratory (SUTL) numbers assigned to each sample on arrival at the SUERC luminescence laboratories. Photographs of the sections (Fig. 2-1), together with luminescence profiling data obtained using portable OSL instrumentation (Table 2-2), accompanied sample submission.

SUTL no.	Field ID	Context	Geological significance
2698	KY14-01(a)	Alagadi Beach, Koupia	OSL12-04, Section 2a
	KY14-01(c)	5cm above	for retrospective analysis of the external gamma dose rates
	KY14-01(b)	30cm above	
	KY14-01(d)	5cm below	
	KY14-01(e)	30cm above	
2699	KY14-02 (a)	Mersinlik, Koupia	OSL12-20, Section 5b
	KY14-02 (c)	5cm above	for retrospective analysis of the external gamma dose rates
	KY14-02 (b)	30cm above	
	KY14-02 (d)	5cm below	
	KY14-02 (e)	30cm above	

Table 2-1: Sample details, including field codes, laboratory SUTL numbers and geological contexts

Palamakumbura et al. (2015) used a combination of sedimentology and optical luminescence data, obtained using portable OSL equipment, to correlate and characterise the Quaternary geomorphological terraces along both flanks of the Kyrenia Range. Of significance to this investigation, are the profiles taken through the Koupia terrace deposits at Alagadi Beach and Mersinlik (OSL12-04, section 2a and OSL12-20, section 5b, respectively), which enclose the dating samples. The field profiles are reproduced in figures 2-1 and 2-2. Both profiles reveal complex stratigraphies, with no apparent stratigraphic trends in IRSL or OSL signal intensities or their associated depletion indices, presumably indicating, in both instances, a rapid accumulation. Given that the measured gamma dose rates through the Mersinlik section were similar (table 2-2), and that the mineralogy/grain size was alike, then in this scenario, the samples which carry larger signal intensities may indicate the samples which carry luminescence residuals (poorly bleached at deposition). It is notable that with this hypothesis, the best targets for dating these deposits, would be the basal units immediately overlying the marine calcarenites and grainstones, as the overlying units would contain mixed age materials. Laboratory luminescence profiling, which provides preliminary estimates on stored dose estimates and sensitivities, will provide one means of testing this hypothesis.

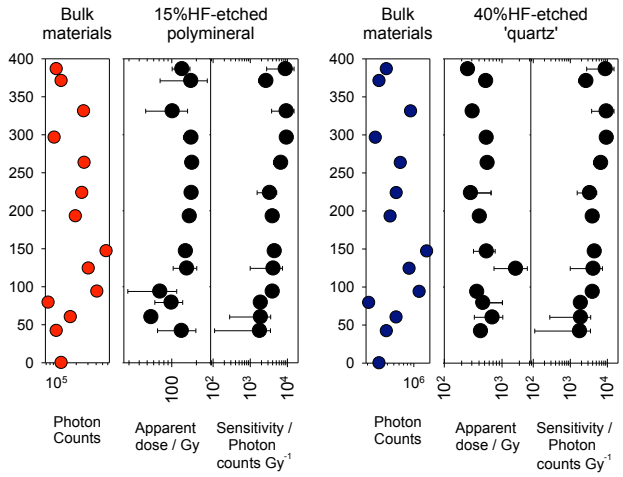

Figure 2-1: Luminescence-depth profiles for OSL12-04, Section 2a

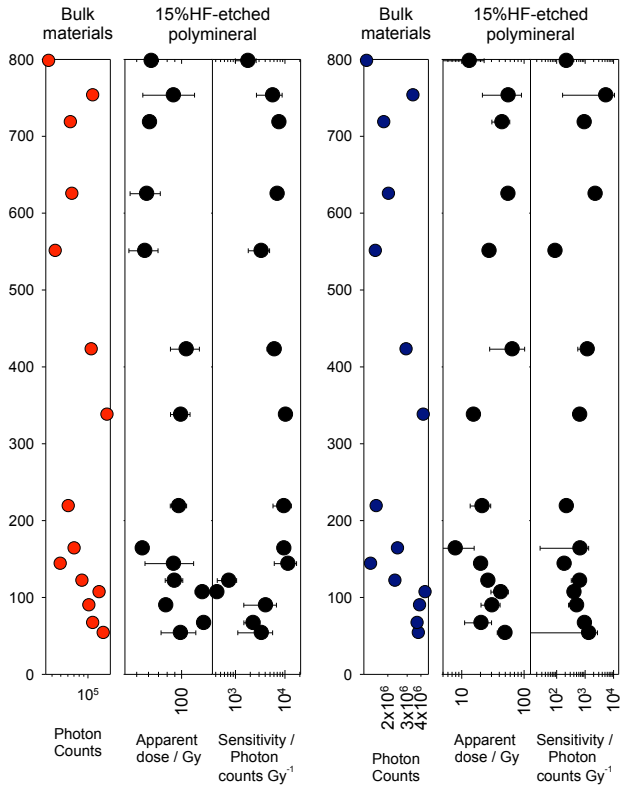

Figure 2-2: Luminescence-depth profiles for OSL12-20, Section 5b

Subsequent to the field profiling, sub-samples were subjected to calibrated luminescence screening measurements. In this procedure, paired aliquots of polymineral and 40%HF-etched 'quartz' concentrates, were subjected to a simplified two-step SAR procedure to obtain a preliminary assessment of luminescence sensitivities and apparent dose (the latter proportional to age). The respective sensitivity-depth and stored dose-depth profiles are presented in figures 2-1 and 2-2 (with their associated field profiles).

The basal units, which erosionally overlay the underlying marine calcarenites and grainstones, show the greatest dispersion/spread in IRSL stored dose values, and importantly, the lowest values in each profile. In contrast, the upper units are characterised by larger IRSL stored dose values with tighter distributions, reflecting faster deposition and poor to incomplete bleaching, or zeroing, of the luminescence signals. It is interesting to speculate why this is so. It may be that the first sands were mobile, blowing freely across this freshly cut palaeo-surface, with greater scope for bleaching; and that the subsequent sands, were more rapidly re-worked and re-deposited from older deposits. Therefore, the dating samples,fortuitously positioned at the base of each sequence, immediately above the basal unconformity, should provide a constrain on the first ingression of sands at each of the sampled localities.

It is noted that there is a positive correlation between luminescence sensitivity and apparent dose, suggesting that the luminescence intensities observed in the field profiles may also be influenced by sensitivity.

2.1. Field gamma spectrometry measurements

Field gamma spectrometry (FGS) measurements were made using a Health Physics Instruments Rainbow MCA with a 2"x 2" NaI probe. Prior to fieldwork, measurements were made using this system on the doped concrete reference pads at SUERC in order to provide cross-reference to dose-rate conversion factors established by Sanderson (1986), based on comparisons with TL dosimetry in doped blocks then at the Oxford and Risø luminescence laboratories. The spectra were calibrated to the 1457 keV peak from ^{40}K, then dose rates were determined from integral counts >450 keV, >1350 keV, and the energy integral (sum of counts times energy) across all the recorded spectrum. Using this approach yielded dose rates from the pads that were within errors of expected values. Field spectra were each measured for 300s in holes cut into representative strata, and calibrated to the 1461 keV peak from ^{40}K before calculation of dose rates. Table 2-1 shows the mean gamma dose rates recorded in-situ for strata adjacent to the dating samples.

Field no.	SUTL no.	Depth from datum / cm	FGS / mGy a^{-1}		
			as measured	geometric correction	corrected
Alagadi Beach, OSL12-04, Section 2a					
KY14-01	2698		-	-	-
Mersinlik, OSL12-20, Section 5b					
KY14-02,	2699		0.22 ± 0.03	0.50	0.43 ± 0.06

OSL12-20			(12.7%err)		

Table 2-2: In situ gamma dose rates measurements made at each of the dating sample positions, using a Health Physics Instruments Rainbow MCA with a 2"x 2" NaI probe

3. Luminescence measurements

3.1. Sample preparation

All sample handling and preparation was conducted under safelight conditions in the SUERC luminescence dating laboratories.

3.1.1. Water contents

Bulk samples were weighed, saturated with water and re-weighed. Following oven drying at 50 °C to constant weight, the actual and saturated water contents were determined as fractions of dry weight. These data were used, together with information on field conditions to determine water contents and an associated water content uncertainty for use in dose rate determination.

3.1.2. HRGS and TSBC Sample Preparation

Bulk quantities of material, weighing c. 50g, were removed from each full dating sample for environmental dose rate determinations. In addition to the two dating samples, a series of 8 bulk gamma spectrometry samples were prepared to permit retrospective analysis of the external gamma dose rates (see appendix C). All materials were placed in an oven to dry to constant weight. Approximately 50g quantities of dried material from each sample were weighed into HDPE pots for a high-resolution gamma spectrometry (HRGS) measurement. Each pot was sealed with epoxy resin and left for 3 weeks prior to measurement to allow equilibration of ^{222}Rn daughters. A further 20 g of the dried material was used in thick source beta counting (TSBC; Sanderson, 1988b).

3.1.3. Mineral preparation

The samples were subjected to standard mineral preparation procedures to concentrate sand-sized concentrates of quartz and K feldspar. Samples were disaggregated using a pester and mortar, prior to wet-sieving at 90, 150 and 250 μm. The 150-250 μm fractions were treated with 1M HCl for 10 minutes, 15% HF for 15 minutes and 1M HCl for 10 minutes, and then rinsed in acetone and de-ionised water. This etched material was then centrifuged in sodium polytungstate at densities of ~2.51, 2.58, 2.64 and 2.74 g cm^{-3}, to concentrate K feldspar (2.51-2.58 g cm^{-3}) and quartz (2.64-2.74 g cm^{-3}). The quartz subsample was then treated with 40% HF for 40 minutes, to dissolve the less chemically resistant minerals and to etch the outer part of the grains, and 1 M HCl for 10 minutes to dissolve any precipitated fluorides. The HF-etched 'quartz' and HCl-washed 'K feldspar' fractions were dispensed onto 10 mm stainless steel discs. 16 aliquots were made per sample.

3.2. Measurements and determinations

3.2.1. Dose rate determinations

Dose rates were measured in the laboratory using HRGS and TSBC. Full sets of laboratory dose rate determinations were made for all samples.

HRGS measurements were performed using a 50% relative efficiency "n" type hyper-pure Ge detector (EG&G Ortec Gamma-X) operated in a low background lead shield with a copper liner. Gamma ray spectra were recorded over the 30 keV to 3 MeV range from each sample, interleaved with background measurements and measurements from SUERC Shap Granite standard in the same geometries. Samples were counted for 500 ks. The spectra were analysed to determine count rates from the major line emissions from ^{40}K (1461 keV), and from selected nuclides in the U decay series (^{234}Th, ^{226}Ra + ^{235}U, ^{214}Pb, ^{214}Bi and ^{210}Pb) and the Th decay series (^{228}Ac, ^{212}Pb, ^{208}Tl) and their statistical counting uncertainties. Net rates and activity concentrations for each of these nuclides were determined relative to Shap Granite by weighted combination of the individual lines for each nuclide. The internal consistency of nuclide specific estimates for U and Th decay series nuclides was assessed relative to measurement precision, and weighted combinations used to estimate mean activity concentrations (Bq kg^{-1}) and elemental concentrations (% K and ppm U, Th) for the parent activity. These data were used to determine infinite matrix dose rates for alpha, beta and gamma radiation.

Beta dose rates were also measured directly using the SUERC TSBC system (Sanderson, 1988b). Sample count rates were determined with eighteen replicate 600 s counts for each sample, bracketed by background measurements and sensitivity determinations using the Shap Granite secondary reference material. Infinite-matrix dose rates were calculated by scaling the net count rates of samples and reference material to the working beta dose rate of the Shap Granite (6.25 ± 0.03 mGy a^{-1}). The estimated errors combine counting statistics, observed variance and the uncertainty on the reference value.

The dose rate measurements were used in combination with the assumed burial water contents, to determine the overall effective dose rates for age estimation. Cosmic dose rates were evaluated by combining latitude and altitude specific dose rates (0.18 ± 0.01 mGy a^{-1}) for the site with corrections for estimated depth of overburden using the method of Prescott and Hutton (1994).

3.2.2. SAR luminescence measurements

3.2.2.1 Quartz

All measurements were conducted using a Risø DA-15 automatic reader equipped with a ^{90}Sr/^{90}Y β-source for irradiation, blue LEDs emitting around 470 nm and infrared (laser) diodes emitting around 830 nm for optical stimulation, and a U340 detection filter pack to detect in the region 270-380 nm, while cutting out stimulating light (Bøtter-Jensen et al., 2000).

Equivalent dose determinations were made on sets of 16 aliquots per sample, using a single aliquot regeneration (SAR) sequence (cf Murray and Wintle, 2000). According to this procedure, the OSL signal level from an individual disc is calibrated to provide an absorbed dose estimate (the equivalent dose) using an interpolated dose-response curve, constructed by regenerating OSL signals by beta irradiation in the laboratory. Sensitivity changes which may occur as a result of readout, irradiation and preheating (to remove unstable radiation-induced signals) are monitored using small test doses after each regenerative dose. Each measurement is standardised to the test dose response determined immediately after its readout, to compensate for observed changes in sensitivity during the laboratory measurement sequence. For the purposes of interpolation, the regenerative doses are chosen to encompass the likely value of the equivalent (natural) dose (determined in the initial laboratory characterisation study, see section 3). A repeat dose point is included to check the ability of the SAR procedure to correct for laboratory-induced sensitivity changes (the 'recycling test'; Table 4-1), a zero dose point is included late in the sequence to check for thermally induced charge transfer during the irradiation and preheating cycle (the 'zero cycle'; Table 4-2), and an IR response check is included to assess the magnitude of non-quartz signals.

In the present study, 16 discs per sample were measured using 4 discs each at 4 different preheats - 200°C, 220°C, 240°C and 260°C. Regenerative dose response curves were constructed using doses of 5, 50, 100, 150 Gy (and 200Gy, for SUTL2699), with a test dose of 2 Gy.

3.2.2.2 K feldspar

All measurements were conducted on a similar Risø DA-20 automatic reader as described above, but equipped instead with a combination of Schott BG39 + Corning 7/59 + Schott GG400 filters to detect in the region 390-450 nm, and isolate the main emission of the feldspar fraction. IRSL SAR runs were undertaken on 16 aliquots of K feldspar from both SUTL2698 and 2699 (cf. Blair et al., 2005; Wallinga et al., 2000), adapted to include measurements of post-IR IRSL at 225°C and 290°C, after every regenerative dose (Blair et al., 2005, 2006; Buylaert et al., 2009; Thomsen et al., 2008). 16 discs per sample were measured using 4 discs each at 4 different preheats - 200°C, 220°C, 240°C and 260°C. Regenerative dose response curves were constructed using doses of 5, 50, 100 and 200Gy, with a test dose of 1 Gy.

Fading tests. Fading tests were performed on 16 aliquots per sample. For each sample, 8 aliquots were given a 50 Gy dose before storage; the other 8 aliquots were given a 50 Gy dose immediately after storage. Irradiations were performed using an automated Elsec irradiator, equipped with a 1.85GBq ^{90}Sr source (dose rate 1.76 Gy/min at time of the experiment). For an initial readout the samples were stored in the dark at ambient temperatures for periods ranging between 6.7 and 6.8 $\times$ 10^6 s. All aliquots were then subjected to the post-IR elevated temperature IRSLprotocol described above. Following the last readout 8 aliquots per sample were again given a 50 Gy dose, before being placed in storage for a further fading test to be conducted in the future (over 10^7 s time or longer).

3.3. Results

3.3.1. Dose rates

HRGS results are shown in Table 4-1, both as activity concentrations (i.e. disintegrations per second per kilogram) and as equivalent parent element concentrations (in % and ppm), based in the case of U and Th on combining nuclide specific data assuming decay series equilibrium.

SUTL no.	Activity Concentration[a] / Bq kg^{-1}			Equivalent Concentration[b]		
	K	U	Th	K / %	U / ppm	Th / ppm
2698A	316 ± 6	7.7 ± 0.2	5.8 ± 0.1	1.02 ± 0.02	0.62 ± 0.01	1.43 ± 0.02
2699A	341 ± 10	19.5 ± 0.7	12.4 ± 0.5	1.10 ± 0.03	1.58 ± 0.06	3.06 ± 0.12

Table 3-1: Activity and equivalent concentrations of K, U and Th determined by HRGS
[a]Shap granite reference, working values determined by David Sanderson in 1986, based on HRGS relative to CANMET and NBL standards.
[b]Activity and equivalent concentrations for U, Th and K determined by HRGS (Conversion factors based on NEA (2000) decay constants): 40K: 309.3 Bq kg^{-1} %K^{-1}, 238U: 12.35 Bq kg^{-1} ppmU^{-1}, 232Th: 4.057 Bq kg^{-1} ppm Th^{-1}.

Infinite matrix alpha, beta and gamma dose rates from HRGS are listed for all samples in Table 4-2, together with infinite matrix beta dose rates from TSBC.

SUTL no.	HRGS, dry[a] / mGy a^{-1}			TSBC, dry / mGy a^{-1}	FGS, wet / mGy a^{-1}
	Alpha	Beta	Gamma		
2698A	2.79 ± 0.04	0.98 ± 0.02 (1.7%)	0.39 ± 0.01 (1.3%)	1.05 ± 0.03	0.43 ± 0.06
2698B	6.64 ± 0.18	1.23 ± 0.03 (2.4%)	0.60 ± 0.01 (2.0%)	0.90 ± 0.03	0.43 ± 0.06

Table 3-2: Infinite matrix dose rates determined by HRGS and TSBC.
[a]based on dose rate conversion factors in Aikten (1983) and Sanderson (1987)

The water content measurements with assumed values for the average water content during burial are given in Table 4-3. The table also lists the gamma dose rate from the HRGS after application of a water content correction. Effective dose rates to the HF etched 200 μm quartz grains are given for the gamma dose rate and beta dose rate (the mean of the TSBC and HRGS data, accounting for water content and grain size).

SUTL no.	Water Content[a] / %			Effective Dose Rate / mGy a^{-1}		
	Fractional	Saturated	Assumed	Beta[b]	Gamma	Total[c,d]
2698A	2	15	10 ± 5	0.85 ± 0.06	0.39 ± 0.06	1.49 ± 0.09
2699B				0.89 ± 0.06	0.49 ± 0.07	1.63 ± 0.10

Table 3-3: Water contents, and effective beta and gamma dose rates following water correction.
[a] actual and saturated water contents were determined as fractions of dry weight.
[b] Effective beta dose rate combining water content corrections with inverse grain size attenuation factors obtained by weighting the 200 μm attenuation factors of Mejdahl (1979) for K, U, and Th by the relative beta dose contributions for each source determined by Gamma Spectrometry.
[c] includes a contribution from an internal alpha effective dose (see section 3.2.2)
[d]includes a cosmic dose contribution

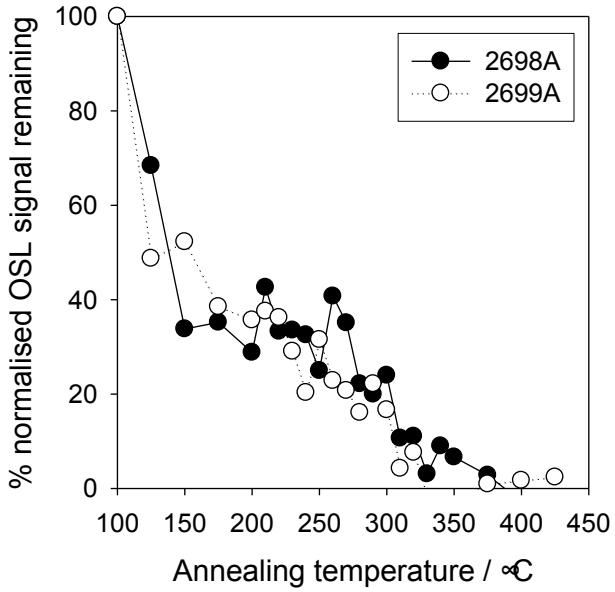

In addition to the two dating samples, a series of 8 bulk gamma spectrometry samples were collected to permit retrospective analysis of the external gamma dose rates. The gamma dose rates were reconstructed from 7 of these giving wet gamma dose rates of between 0.39 and 0.70 mGy a^{-1} (Appendix C), which are comparable with the measured values recorded at the sampling positions (0.4 – 0.5 mGy a^{-1}).

3.3.2. Internal grain dosimetery

In cases where the gamma dose rate is low, such as for the samples collected at Alagadi Beach and Mersinlik, the internal activity becomes increasingly important. The standard age model assumes certain values for the concentration of radionuclides within each grain. Here, an estimate of the internal alpha effective dose is made on an alpha efficiency of 6.7 % (based on Burbidge et al., in prep), and U and Th internal contents of 0.18 and 0.55, respectively. The internal alpha effective dose as calculated for the Cyprian samples is 0.06 ± 0.03 mGy a^{-1}.

3.3.3. Single aliquot equivalent dose determinations

3.3.3.1 Quartz

First, an attempt was made to date the quartz from Alagadi Beach and Mersinlik, using the conventional quartz OSL SAR method, which utilises the initial part of the OSL signal, the fast component. Unfortunately, the quartz had low sensitivities and responded poorly to the test dose, precluding the use of the conventional SAR procedure to date this material. The quartzes also failed other SAR quality criteria (Table 3-4). Thermal stability analyses were conducted to assess the relationship between the natural and regenerated OSL signals from this quartz (and potentially identify a more stable OSL signal). In this procedure, the OSL signal was recorded at a range of temperatures, using a short stimulation (1 s at 10% power) at a range of temperatures between 100 and 500°C. The experiment was repeated following a nominal dose of 100Gy. The results of this experiment are shown in figure 3-1. The regenerated OSL signal from both quartzes shows poor thermal stability across the entire pulsed annealing range; most quartzes show thermal stability to 200-220°C, with progressive depletion of the signals through the 220°C to 350-450°C range, and good reproducibility between the natural and regenerated curves.

Figure 3-1: Pulsed annealing curves for SUTL2698 and SUTL2699, following a 1kGy regenerative dose

SUTL No.	Sensitivity / counts Gy^{-1}	Sensitivity change / %	Recycling Ratio	Zero Dose / Gy	IRSL response / %
2698	219 ± 76	11.8 ± 4.4	1.07 ± 0.23	5.0 ± 5.0	5.7 ± 3.6
2699	209 ± 29	2.5 ± 0.5	0.79 ± 0.17	0.2 ± 0.1	8.0 ± 3.5

Table 3-4: Quartz SAR OSL quality parameters. Standard errors given.

3.3.3.2 K feldspar

The IRSL and TL signals from feldspars are expected to respond to additional radiation up to the 1 – 5 kGy range. In a low dose rate environment, this means that there is the potential to date sediments beyond ~ 250 ka. Unfortunately, the IRSL signal from feldspar may suffer from anomalous fading, and vary with temperature. Recent work (Thomson et al., 2008; Buylaert et al., 2009) has suggested a new procedure based on elevated temperature post-IR IRSL measurements which can potentially produce the desired low fading rates under convenient automated conditions.

For equivalent dose determination, data from single aliquot regenerative dose measurements were analysed using the Risø TL/OSL Viewer programme to export integrated summary files that were analysed in MS Excel and SigmaPlot. There was no evidence of significant differences in normalised OSL ratios (both in natural and regenerated dose points) between the subsets of discs pre-heated at temperatures from 200°C to 260°C. Accordingly composite dose response curves from selected discs for each sample were constructed and used to estimate equivalent dose values for each individual discs and their combined sets (Fig. 3-3; Appendix B). Dose response curves for each of the four preheating temperature groups and the combined data (using linear and weighted mean estimates), were

Figure 3-2: Dose response curves for SUTL2698
Key as follows: Composite dose response curve, black; Dose response curve following a 200°C preheat (red); a 220°C preheat (orange); a 240°C preheat (yellow); a 260°C preheat (Green)

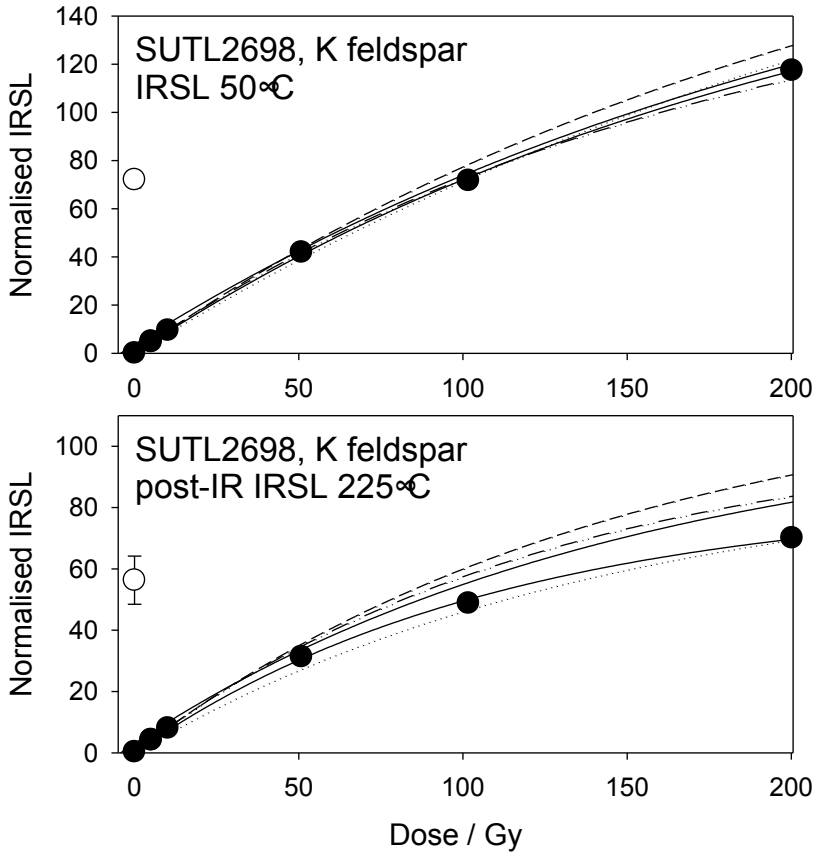

determined using an exponential fit. The equivalent dose was then determined for each aliquot using the corresponding exponential fit parameters. Table 3-5 summarises the quality evaluation checks on the SAR data (once filtered); the mean sensitivity of each aliquot and sensitivity change, the recycling ratio and zero dose response.

SUTL no.	Stimulation	Sensitivity / counts Gy^{-1}	Sensitivity change / %	Zero dose / Gy	Recycling ratio
2698	50'C IRSL	6655 ± 1040	-1.3 ± -0.3	0.10 ± 0.01	1.03 ± 0.02
	post-IRSL 225'C IRSL	27892 ± 4787	-2.2 ± -0.5	0.31 ± 0.03	0.98 ± 0.01
	post-IRSL 290'C IRSL	14343 ± 2210	0.3 ± 0.1	0.25 ± 0.11	0.95 ± 0.05
2699	50'C IRSL	3214 ± 433	1.1 ± 0.2	0.09 ± 0.04	1.07 ± 0.02
	post-IRSL 225'C IRSL	13732 ± 1968	-0.6 ± -0.1	0.31 ± 0.03	0.98 ± 0.01
	post-IRSL 290'C IRSL	3920 ± 563	1.3 ± 0.3	0.59 ± 1.07	0.86 ± 0.07

Table 3-5: K feldspar SAR IRSL quality parameters. Standard errors given

Within the SAR cycle performed here it is possible to check dose recovery from regenerated cycles. Like other dose recovery tests this suffers the limitation that it does not address potential behavioural changes associated with removal of the natural signal, and the first cycles of preheating. It does not however depend on aliquot matching. The weighted mean results for each sample in terms of recovered dose over given dose are, following IRSL 50°C stimulation, 1.11 ± 0.03 and 1.14 ± 0.02, SUTL2698 and SUTL2699 respectively, and post-IR IRSL stimulation at 225°C, 1.08 ± 0.04 and 1.16 ± 0.05, SUTL2698 and SUTL2699 respectively (Table 3-6).

SUTL No.	IRSL 50°C	post IR IRSL 225°C	post IR IRSL 290°C
2698	1.11 ± 0.03 (0.01)	1.08 ± 0.04 (0.02)	0.90 ± 0.14 (0.04)

2699	1.14 ± 0.02 (0.02)	1.16 ± 0.05 (0.02)	1.12 ± 0.12 (0.1)

Table 3-6: Dose recovery ratios

The mean ratios of sensitisation-independent stored to prompt normalised signals, after 10^6 s storage (after Sanderson, 1988a) for IRSL 50°C from SUTL2698 and 2699 are 0.89 ± 0.04 and 0.97 ± 0.04, respectively, and for post-IR IRSL 225°C are 1.02 ± 0.14 and 1.14 ± 0.14, respectively (mean values, 0.93 ± 0.06 and 1.08 ± 0.08, IRSL and post-IR IRSL, respectively). The fading rates determined from each samples during the short tests conducted are shown in Table 3-7.

SUTL no.	Stimulation	Delay prior to IRSL readout		Fading ratio
		Prompt / s	Delay / s	
2698	50°C IRSL	8.6×10^4	6.7×10^6	0.89 ± 0.04 (0.01)
	post-IRSL 225°C IRSL	8.6×10^4	6.7×10^6	1.02 ± 0.14 (0.01)
	post-IRSL 290°C IRSL	8.6×10^4	6.7×10^6	0.88 ± 0.41 (0.01)
2699	50°C IRSL	1.7×10^5	6.8×10^6	0.97 ± 0.04 (0.01)
	post-IRSL 225°C IRSL	1.7×10^5	6.8×10^6	1.14 ± 0.14 (0.01)
	post-IRSL 290°C IRSL	1.7×10^5	6.8×10^6	-*

Table 3-7: Fading test parameters, normalised IRSL value, and sensitisation-independent stored to prompt normalised signals for SUTL2698 and 2699
*the post-IR IRSL signal at 290°C lacked sufficient luminescence sensitivity to register the 50 Gy dose in either the prompt or delay cycle.

On the basis of these results, the expectations for the procedure, and the other IRSL SAR quality selection criteria, preference was given to the post-IR IRSL 225°C signals in equivalent dose and subsequent age determinations.

The distribution in equivalent dose values was examined using radial plotting methods (Appendix D). All samples revealed some heterogeneity in their equivalent dose distributions, reflecting variable bleaching at deposition and indicating that each sample enclosed mixed-age materials. Fortuitously, the laboratory profiles provide some measure of control, indicating that the population of lowest equivalent doses represents the better bleached component. For age determinations, the weighted mean of the equivalent dose distribution was used, as for these samples, this encloses the low dose component.

3.3.4. Age determinations

The total dose rate is determined from the sum of the equivalent beta and gamma dose rates, and the cosmic dose rate. Age estimates are determined by dividing the equivalent stored dose by the dose rate. Uncertainty on the age estimates is given by combination of the uncertainty on the dose rates and stored doses, with an additional 5% external error. Table 4-1 lists the total dose rate, stored dose and corresponding age of the sample. The values stated in bold are those used in age determinations. Note that the total effective dose rates listed include the contribution from the external gamma dose rate (appendix C).

4. Conclusions

The post-IR elevated temperature IRSL approach applied to the Koupia terrace aeolianites, coupled to careful dose rate measurement, has succeeded in dating these challenging materials. The reconciliation of HRGS data, converted to infinite matrix dose rates, with measured beta and gamma dose rates, counted over extended periods, enabled total environmental dose rates to be estimated with less than 5% uncertainties.

SUTL No.	Context; equivalent profiling no.	Dose Rate (mGy a^{-1})	Stimulation	Comments on Equivalent Dose Distribution/age distributions	Stored Dose / Gy*		Years BP*
					linear mean	weighted mean	
2698	Alagadi Beach, Koupia, KY14-01(a); Profile OSL12-04, section 2a	1.47±0.06	IRSL 50°C	broad equivalent dose distribution; 9 aliquots within 2σ of linear and weighted means; 3 aliquots tail to a lower apparent dose (~70 Gy); 4 aliquots to a higher apparent dose (~120 Gy)	89 ± 1.9 (7.1)	98.8 ± 1.4 (5.6)	76.1 ± 3.5 (9.1)
			pIR IRSL 225°C	broad equivalent dose distribution; 5 aliquots within 2σ of linear and weighted mean; several high dose outliers (~170 Gy)	109 ± 2.5 (9.4)	**112 ± 2.6(12.5)**	
2699	Mersinlik, Koupia, KY14-02(a); Profile OSL12-20, section 5b	1.61±0.06	IRSL 50°C	broad equivalent dose distribution; 5 aliquots within 2σ of linear and weighted mean; several aliquots tail to a higher apparent dose (~100 Gy)	109 ± 2.5 (9.4)	64.1 ± 0.8 (3.4)	58.7 ± 2.6 (4.1)
			pIR IRSL 225°C	tighter dose distribution; 9 aliquots within 2σ of linear and weighted mean; remaining aliquots within error of means	86.9 ± 1.7 (6.7)	**94.7 ± 2.1 (5.4)**	
			pIR IRSL 290°C	all aliquots within 2σ of linear and weighted means	-	-	

Table 4-1: OSL age determinations for samples SUTL2698 and 2699
*as stated standard errors; in parentheses weighted deviation

5. References

Aitken, M.J., 1983, Dose rate data in SI units: PACT, v. 9, p. 69–76.

Alexander, S.A., 2007, The stability of the remnant luminescence emissions of alkali feldspar [unpublished PhD thesis thesis]: Glasgow, University of Glasgow.

Bagnall, P.S., 1960, The Geology and Mineral Resources of the Pano Lefkara-Larnaca Area. : Geological Survey Department of Cyprus, Memoir, v. 5.

Bailey, R.M., 1998, The form of the optically stimulated luminescence signal of quartz: implications for dating., Unpublished Ph.D. Thesis, University of London.

Baroz, F., 1979, Étude géologique dans le Pentadaktylos et la Mesaoria (Chypre Septentrionale): Nancy, Université de Nancy.

Blair, M.W., Yukihara, E.G., and McKeever, S.W.S., 2005, Experiences with single-aliquot OSL procedures using coarse-grain feldspars: Radiation Measurements, v. 39, p. 361-374.

—, 2006, Progress towards a polymineral single-aliquot OSL dating procedure: Radiation Protection Dosimetry, v. 119, p. 450-453.

Bøtter-Jensen, L., Bulur, E., Duller, G.A.T., and Murray, A.S., 2000, Advances in luminescence instrument systems: Radiation Measurements, v. 32, p. 523-528.

Buylaert, J.P., Murray, A.S., Thomsen, K.J., and Jain, M., 2009, Testing the potential of an elevated temperature IRSL signal from K-feldspar: Radiation Measurements, v. 44, p. 560-565.

Ducloz, C., 1963, Geological map of the Central Kyrenia Range, Geological Survey Department of Cyprus.

—, 1964, Revision of the pliocene and Quaternary stratigraphy of the central Mesaoria. : Nicosia, Cyprus, The Cosmos Press Ltd.

—, 1972, The geology of the bellapais-kyrthrea area of the central Kyrenia range, Bulletin of the Geological Survey Department of Cyprus, Volume 6: Nicosia, Cyprus.

Harrison, R.W., Newell, W.L., Batihanlı, H., Panayides, I., McGeehin, J.P., Mahan, S.A., Ozhur, A., Tsiolakis, E., and Necdet, M., 2004, Tectonic framework and Late Cenozoic tectonic history of the northern part of Cyprus: implications for earthquake hazards and regional tectonics: Journal of Asian Earth Sciences, v. 23, p. 191-210.

Harrison, R.W., Tsiolakis, E., Stone, B.D., Lord, A., Mcgeehin, J.P., Mahan, S.A., and Chirico, P., 2012, Late Pleistocene and Holocene uplift history of Cyprus: implications for active tectonics along the southern margin of the Anatolian microplate: Geological Society, London, Special Publications, v. 372.

Huntley, D.J., Baril, M.R., and Haidar, S., 2007, Tunnelling in plagioclase feldspars: Journal of Physics D: Applied Physics, v. 40, p. 900.

Huntley, D.J., Godfrey-Smith, D.I., and Thewalt, M.L.W., 1985, Optical dating of sediments: Nature, v. 313, p. 105-107.

Huntley, D.J., and Lamothe, M., 2001, Ubiquity of anomalous fading in K-feldspars and the measurement and correction for it in optical dating: Canadian Journal of Earth Sciences, v. 38, p. 1093-1106.

Huntley, D.J., and Lian, O.B., 2006, Some observations on tunnelling of trapped electrons in feldspars and their implications for optical dating: Quaternary Science Reviews, v. 25, p. 2503-2512.

Kinnaird, T., and Robertson, A., 2013, Tectonic and sedimentary response to subduction and incipient continental collision in southern Cyprus, easternmost

Mediterranean region: Geological Society, London, Special Publications, v. 372.
Kinnaird, T.C., Robertson, A.H.F., and Morris, A., 2011, Timing of uplift of the Troodos Massif (Cyprus) constrained by sedimentary and magnetic polarity evidence: Journal of the Geological Society of London, v. 168, p. 457-470.
Knupp, C., 1964, Geological map of the Central Kyrenia Range: Nicosia, Cyprus, Geological Survey Department of Cyprus.
Krbetschek, M.R., Götze, J., Dietrich, A., and Trautmann, T., 1997, Spectral information from minerals relevant for luminescence dating: Radiation Measurements, v. 27, p. 695-748.
Krbetschek, M.R., and Rieser, U., 1995, Luminescence spectra of alkalifeldspars and plagioclases: Radiation Measurements, v. 24, p. 473-477.
Mejdahl, V., 1979, Thermoluminescence daing: Beta-dose attenuation in quartz grains Archaeometry, v. 21, p. 61-72.
Murray, A.S., Buylaert, J.P., Thomsen, K.J., and Jain, M., 2009, The effect of preheating on the IRSL signal from feldspar: Radiation Measurements, v. 44, p. 554-559.
Murray, A.S., and Wintle, A.G., 2000, Luminescence dating of quartz using an improved single-aliquot regenerative-dose protocol: Radiation Measurements, v. 32, p. 57-73.
NEA, 2000, The JEF-2.2 Nuclear Data Library: Nuclear Energy Agency, Organisation for economic Co-operation and Development. JEFF Report, v. 17.
Palamakumbura, R., Robertson, A.F., Kinnaird, T., and Sanderson, D.W., 2015, Sedimentary development and correlation of Late Quaternary terraces in the Kyrenia Range, northern Cyprus, using a combination of sedimentology and optical luminescence data: International Journal of Earth Sciences, p. 1-24.
Poole, A.J., and Robertson, A.H.F., 1991, Quaternary uplift and sea-level change at an active plate boundary, Cyprus: Journal of the Geological Society of London, v. 148, p. 909-921.
—, 1998, Pleistocene fanglomerates deposition related to uplift of the Troodos Ophiolite, Cyprus, *in* Robertson, A.H.F., Emeis, K.-C., Richter, C., and Camerlenghi, A., eds., Proceedings ODP Scientific Results, Volume 160, p. 544-558.
—, 2000, Quaternary marine terraces and aeolinites in coastal south and west Cyprus: implications for regional uplift and sea-level change, *in* Panayides, I., Xenophontos, C., and Malpas, J., eds., Proceedings of the Third Internal Conference on the geology of the Eastern Mediterranean, Volume 160, Cyprus Geological Survey Department, p. 544-568.
Poole, A.J., Shimmield, G.B., and Robertson, A.H.F., 1990, Late Quaternary uplift of the Troodos Ophiolite, Cyprus; uranium-series dating of Pleistocene coral: Geology, v. 18, p. 894-897.
Prescott, J.R., and Hutton, J.T., 1994, Cosmic ray contributions to dose rates for luminescence and ESR dating: Large depths and long-term time variations: Radiation Measurements, v. 23, p. 497-500.
Robertson, A.H.F., Taslı, K., and İnan, N., 2012, Evidence from the Kyrenia Range, Cyprus, of the northerly active margin of the Southern Neotethys during Late Cretaceous–Early Cenozoic time: Geological Magazine, v. 149, p. 264-290.

Robertson, A.H.F., and Woodcock, N.H., 1986, The Role of the Kyrenia Range Lineament, Cyprus, in the Geological Evolution of the Eastern Mediterranean Area, 141-177 p.
Sanderson, D.C.W., 1987, Thermoluminescence dating of vitrified Scottish Forts: Paisley, Paisley college.
—, 1988a, Fading of thermoluminescence in feldspars: Characteristics and corrections: International Journal of Radiation Applications and Instrumentation. Part D. Nuclear Tracks and Radiation Measurements, v. 14, p. 155-161.
—, 1988b, Thick source beta counting (TSBC): A rapid method for measuring beta dose-rates: International Journal of Radiation Applications and Instrumentation. Part D. Nuclear Tracks and Radiation Measurements, v. 14, p. 203-207.
Spooner, N.A., 1992, Optical dating: Preliminary results on the anomalous fading of luminescence from feldspars: Quaternary Science Reviews, v. 11, p. 139-145.
—, 1994, The anomalous fading of infrared-stimulated luminescence from feldspars: Radiation Measurements, v. 23, p. 625-632.
Thiel, C., 2011, On the applicability of post-IR IRSL dating to different environments.
Thomsen, K.J., Murray, A.S., Jain, M., and Bøtter-Jensen, L., 2008, Laboratory fading rates of various luminescence signals from feldspar-rich sediment extracts: Radiation Measurements, v. 43, p. 1474-1486.
Visocekas, R., Spooner, N.A., Zink, A., and Blanc, P., 1994, Tunnel afterglow, fading and infrared emission in thermoluminescence of feldspars: Radiation Measurements, v. 23, p. 377-385.
Visocekas, R., Tale, V., Zink, A., and Tale, I., 1998, Trap spectroscopy and tunnelling luminescence in feldspars: Radiation Measurements, v. 29, p. 427-434.
Wallinga, J., Murray, A., and Wintle, A., 2000, The single-aliquot regenerative-dose (SAR) protocol applied to coarse-grain feldspar: Radiation Measurements, v. 32, p. 529-533.
Weber, J., Schirmer, W., Heller, F., and Bachtadse, V., 2011, Magnetostratigraphy of the Apalós Formation (early Pleistocene): Evidence for pulsed uplift of Cyprus: Geochemistry, Geophysics, Geosystems, v. 12, p. Q01Z22.
Wintle, A.G., 1973, Anomalous Fading of Thermo-luminescence in Mineral Samples: Nature, v. 245, p. 143-144.
Zink, A., Visocekas, R., and Bos, A.J.J., 1995, Comparison of 'blue' and 'infrared' emission bands in thermoluminescence of alkali feldspars: Radiation Measurements, v. 24, p. 513-518.

Appendix A: Luminescence screening measurements

Table A-1: Luminescence screening results obtained using a portable SUERC OSL reader on bulk material. Field profiling measurements were made using a SUERC portable OSL reader, equipped with UG11/GG420/RG780 detection filters, blue LEDs emitting around 470 nm and infrared LEDs emitting 880 nm. Samples were presented as bulk sediment in 50mm plastic petri dishes, and the natural luminescence signals were measured following an interleaved sequence of system dark count (background), infra-red stimulated luminescence and optically stimulated luminescence, similar to that described by Sanderson and Murphy (2010). The readout sequence consisted of a 15 s dark count, 2 × 30 s IRSL stimulations, a 15 s dark count, 2 × 30 s OSL stimulations, and a final dark count. The summary files were extracted from the acquisition software, and interrogated in Excel, to calculate dark count rates, IRSL and OSL integrated signal intensities, depletion rates (parameterized here as a depletion index comprising the ratio of the gross intensity in the first half of the stimulation period to that from the second half) and IRSL/OSL ratios.

Field no.	Lab no.	Height / cm	IRSL signal intensities	IRSL depletion ratio	OSL signal intensities	OSL depletion ratio	IRSL : OSL
Profile OSL12-04, section 2a							
OSL12-04a	2633A	0	119104 ± 360	1.27 ± 0.01	301546 ± 558	1.17 ± 0.01	0.395 ± 0.001
OSL12-04b	2633B	42.1	100387 ± 332	1.26 ± 0.01	389017 ± 631	1.20 ± 0.01	0.258 ± 0.001
OSL12-04c	2633C	60.2	164232 ± 418	1.26 ± 0.01	545472 ± 746	1.17 ± 0.01	0.301 ± 0.001
OSL12-04d	2633D	79.3	75540 ± 292	1.27 ± 0.01	210654 ± 470	1.15 ± 0.01	0.359 ± 0.002
OSL12-04e	2633E	93.8	414537 ± 652	1.26 ± 0.01	1215820 ± 1107	1.13 ± 0.01	0.341 ± 0.001
OSL12-04f	2633F	124.2	306639 ± 563	1.25 ± 0.01	858179 ± 932	1.13 ± 0.01	0.357 ± 0.001
OSL12-04g	2633G	147	571434 ± 763	1.28 ± 0.01	1576657 ± 1260	1.16 ± 0.01	0.362 ± 0.001
OSL12-04h	2633H	192.9	195403 ± 453	1.28 ± 0.01	443644 ± 673	1.13 ± 0.01	0.440 ± 0.001
OSL12-04i	2633I	223.7	244420 ± 504	1.27 ± 0.01	548902 ± 748	1.12 ± 0.01	0.445 ± 0.001
OSL12-04j	2633J	263.3	265151 ± 525	1.27 ± 0.01	631718 ± 801	1.12 ± 0.01	0.420 ± 0.001
OSL12-04k	2633K	296.4	93419 ± 321	1.25 ± 0.01	265347 ± 525	1.11 ± 0.01	0.352 ± 0.001
OSL12-04l	2633L	331.1	260111 ± 520	1.25 ± 0.01	903712 ± 957	1.15 ± 0.01	0.288 ± 0.001
OSL12-04m	2633m	371	119104 ± 360	1.27 ± 0.01	301546 ± 558	1.17 ± 0.01	0.395 ± 0.001
OSL12-04n	2633N	386.5	100387 ± 332	1.26 ± 0.01	389017 ± 631	1.20 ± 0.01	0.258 ± 0.001
Profile OSL12-20, section 5b							
OSL12-20a	2579A	54	148668 ± 387	1.29 ± 0.01	381496 ± 619	1.14 ± 0	0.39 ± 0.001
OSL12-20b	2579B	67	113826 ± 339	1.27 ± 0.01	371789 ± 611	1.15 ± 0	0.306 ± 0.001
OSL12-20c	2579C	90	103119 ± 322	1.27 ± 0.01	391614 ± 627	1.21 ± 0	0.263 ± 0.001

OSL12-20d	2579D	107	133994 ± 368	1.26 ± 0.01	439466 ± 664	1.18 ± 0	0.305 ± 0.001
OSL12-20e	2579E	122	86498 ± 296	1.43 ± 0.01	233570 ± 485	1.18 ± 0	0.37 ± 0.001
OSL12-20f	2579F	144	49702 ± 226	1.28 ± 0.01	140142 ± 376	1.14 ± 0.01	0.355 ± 0.002
OSL12-20g	2579G	164	70849 ± 268	1.24 ± 0.01	246359 ± 498	1.18 ± 0	0.288 ± 0.001
OSL12-20h	2579H	219	61082 ± 249	1.26 ± 0.01	157597 ± 399	1.15 ± 0.01	0.388 ± 0.002
OSL12-20i	2579I	338	163614 ± 406	1.3 ± 0.01	423453 ± 652	1.16 ± 0	0.386 ± 0.001
OSL12-20j	2579J	423	109640 ± 333	1.29 ± 0.01	295214 ± 544	1.15 ± 0	0.371 ± 0.001
OSL12-20k	2579K	551	43750 ± 212	1.28 ± 0.01	154710 ± 395	1.17 ± 0.01	0.283 ± 0.002
OSL12-20l	2579L	625.3	66895 ± 261	1.25 ± 0.01	203815 ± 453	1.15 ± 0.01	0.328 ± 0.001
OSL12-20m	2579m	718.5	64410 ± 256	1.3 ± 0.01	184636 ± 431	1.2 ± 0.01	0.349 ± 0.002
OSL12-20n	2579N	753.4	113757 ± 339	1.29 ± 0.01	341088 ± 585	1.19 ± 0	0.334 ± 0.001
OSL12-20o	2579O	798.2	36957 ± 196	1.3 ± 0.01	128795 ± 360	1.22 ± 0.01	0.287 ± 0.002

Table A-2: Calibrated luminescence screening results, in the form of sensitivity and stored dose estimates, obtained using a simplified two-step SAR procedure on paired aliquots of 15%HF-etched polymineral and 40%HF-etched quartz. Standard mineral preparation procedures as previously utilised in the SUERC luminescence dating laboratories were used to extract polymineral and 40% HF-etched 'quartz' fractions from all samples. Each profiling sample was wet sieved to extract the 90-250 μm fractions, which were then treated with 1M HCl for 10 minutes, etched in 15% HF for 15 minutes and treated with a further 1M HCl for 10 minutes. The 90-250 μm, acid-treated samples were split into two further sub-fractions, one for polymineral analysis and one for quartz analysis. The quartz subsample was treated with 40% HF for 40 minutes, to dissolve the less chemically resistant minerals and to etch the outer part of the grains. The HF etched material was then treated with 1 M HCl for 10 minutes to dissolve any precipitated fluorides. The grains were presented for measurement on 10 mm in diameter stainless steel discs.

Luminescence sensitivities (Photon Counts per Gy) and stored doses (Gy) were evaluated from paired aliquots of the HF-etched quartz and polymineral fractions, using Risø DA-15 automatic readers (following procedures established in Burbidge et al., 2007; Sanderson et al., 2001; Sanderson et al., 2003). The readout cycles comprised a natural readout, followed by readout cycles for a nominal 1Gy test dose, a 5Gy regenerative dose, and a further 1Gy test dose. For the quartz samples, a 240°C preheat held for 30s was used with 60s OSL measurements using the blue LEDs. For the polymineral samples, a 260°C preheat held for 30s was followed by 60s OSL measurements using the IR LEDs at 50°C, the IR LEDs at 225°C (the post-IR IRSL signal), the blue LEDs at 125°C, and a TL measurement to 500°C. Test doses were preheated at the same temperature has the preceding measurement, and held for the same duration.

SUTL no.	Height /cm	polymineral IRSL		quartz IRSL	
Profile OSL12-04, section 2a					
2633A	42.1	132 ± 46	1803 ± 1694	430 ± 56	544 ± 222
2633B	60.2	56 ± 2	1908 ± 1629	682 ± 248	479 ± 169
2633C	80.1	99 ± 26	1899 ± 222	470 ± 387	875 ± 562
2633D	94.6	72 ± 31	3981 ± 1077	369 ± 55	596 ± 60
2633E	125	153 ± 34	4179 ± 3185	1735 ± 713	2775 ± 335
2633F	147.8	148 ± 13	4496 ± 83	541 ± 156	1671 ± 406
2633G	193.7	165 ± 10	3969 ± 270	410 ± 38	372 ± 4
2633H	224.5	174 ± 22	3343 ± 1812	288 ± 254	491 ± 431
2633I	264.1	177 ± 18	6713 ± 2499	560 ± 3	711 ± 15
2633J	297.2	173 ± 24	9540 ± 101	540 ± 19	971 ± 201
2633K	331.9	102 ± 38	9429 ± 5669	308 ± 27	563 ± 197
2633L	371.8	172 ± 71	2689 ± 1011	528 ± 73	1028 ± 158
2633m	387.3	134 ± 23	8911 ± 6155	256 ± 38	1005 ± 729
Profile OSL12-20, section 5b					

2579A	54	99 ± 26	3379 ± 2264	50 ± 13	1365 ± 1354
2579B	67	141 ± 10	2303 ± 820	21 ± 9	972 ± 6
2579C	90	79 ± 4	4113 ± 2634	31 ± 10	516 ± 252
2579D	107	138 ± 15	429 ± 16	43 ± 13	416 ± 157
2579E	122	90 ± 12	745 ± 314	27 ± 3	657 ± 332
2579F	144	89 ± 32	11647 ± 5557	20 ± 2	188 ± 20
2579G	164	55 ± 5	9639 ± 742	8 ± 8	679 ± 653
2579H	219	96 ± 12	9612 ± 3878	21 ± 8	224 ± 19
2579I	338	99 ± 15	10411 ± 1568	16 ± 1	662 ± 87
2579J	423	108 ± 24	6186 ± 1842	65 ± 37	1219 ± 664
2579K	551	57 ± 13	3358 ± 1543	28 ± 5	89 ± 36
2579L	625.3	59 ± 13	7072 ± 136	56 ± 7	2305 ± 669
2579m	718.5	61 ± 5	7692 ± 758	45 ± 14	951 ± 284
2579N	753.4	89 ± 34	5726 ± 3062	56 ± 35	5461 ± 5299
2579O	798.2	63 ± 1	1808 ± 813	13 ± 10	223 ± 23

Appendix B: Dose Response Curves

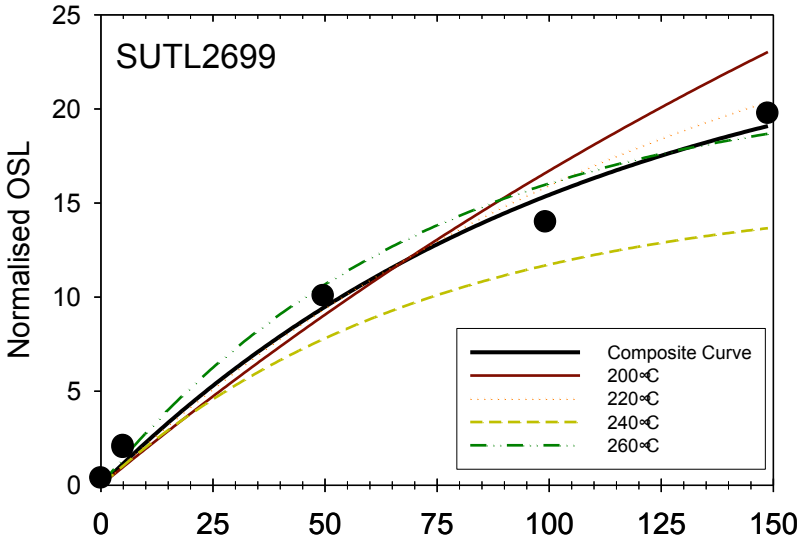

Figure B-1: Dose response curves for SUTL2699 quartz
Key as follows: Composite dose response curve, black; Dose response curve following a 200°C preheat (red); a 220°C preheat (orange); a 240°C preheat (yellow); a 260°C preheat (Green)

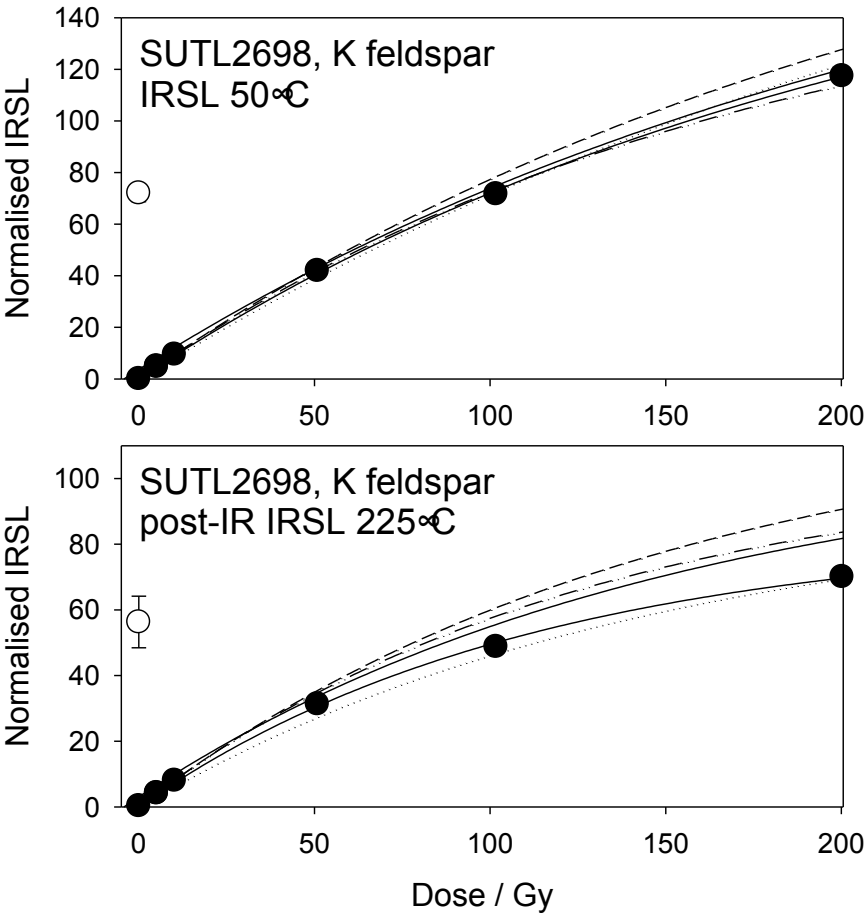

Figure B-2: Composite dose response curves for SUTL2698 K feldspar, following IRSL at 50°C (top plot) and post-IR IRSL at 225°C (bottom plot)

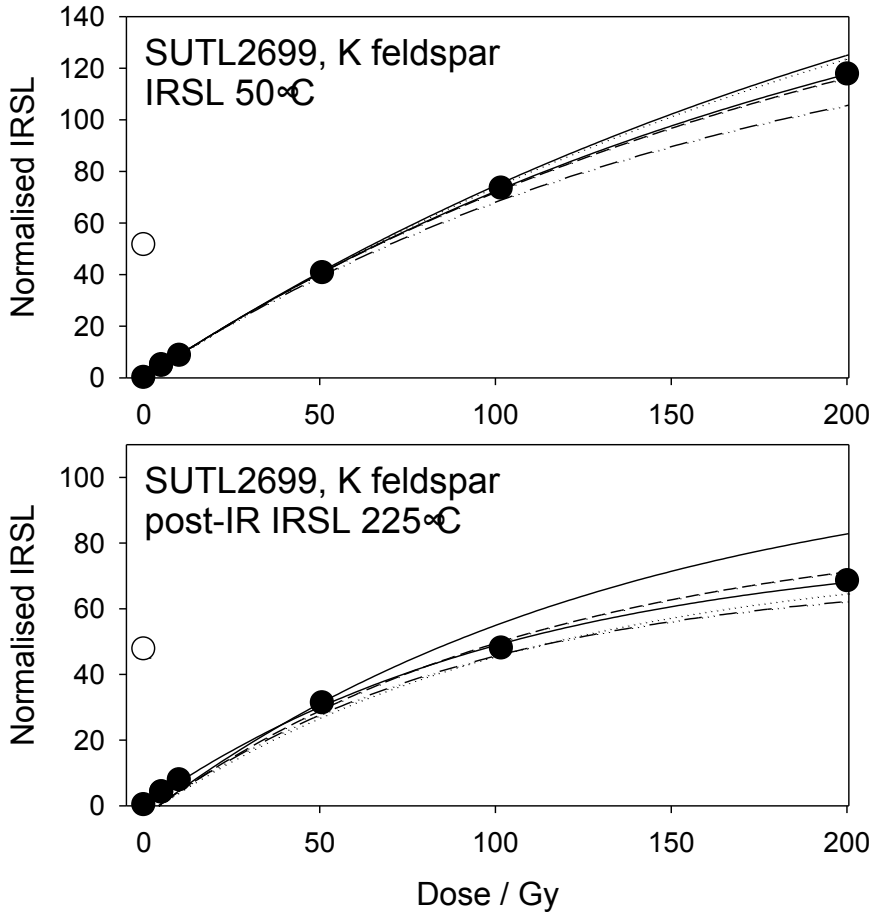

Figure B-3: Composite dose response curves for SUTL2699 K feldspar, following IRSL at 50°C (top plot) and post-IR IRSL at 225°C (bottom plot)

Appendix C: Dose rate determinations for SUTL2698 and 2699

TableC-1: Activity and equivalent concentrations of K, U and Th determined by HRGS

[a]Shap granite reference, working values determined by David Sanderson in 1986, based on HRGS relative to CANMET and NBL standards.

[b]Activity and equivalent concentrations for U, Th and K determined by HRGS (Conversion factors based on NEA (2000) decay constants): 40K: 309.3 Bq kg^{-1} $\%K^{-1}$, 238U: 12.35 Bq kg^{-1} $ppmU^{-1}$, 232Th: 4.057 Bq kg^{-1} ppm Th^{-1}

SUTL no.	Depth / cm	Activity Concentration (Bq kg^{-1})[a]			Equivalent Concentration[b]		
		^{40}K	U	Th	K (%)	U (ppm)	Th (ppm)
2698A		316 ± 6	7.7 ± 0.2	5.8 ± 0.1	1.02 ± 0.02	0.62 ± 0.01	1.43 ± 0.02
2699A		341 ± 10	19.5±0.7	12.4±0.5	1.1 ± 0.03	1.58 ± 0.06	3.06 ± 0.12
2698B		395 ± 7	8.4 ± 0.2	8.6 ± 0.2	1.28 ± 0.02	0.68 ± 0.02	2.11 ± 0.04
2698C		461 ± 6	5.4 ± 0.1	11.3±0.1	1.49 ± 0.02	0.44 ± 0.01	2.80 ± 0.01
2698D		446 ± 6	4.5 ± 0.1	12.4±0.1	1.44 ± 0.02	0.36 ± 0.01	3.05 ± 0.01
2698E		444 ± 6	2.8 ± 0.1	10.7 ± 0	1.44 ± 0.02	0.23 ± 0.01	2.64 ± 0.01
2699B		267 ± 8	16.4±2.1	7.5 ± 0.4	0.86 ± 0.03	1.33 ± 0.17	1.85 ± 0.10
2699C		119 ± 5	63.9±1.8	6.9 ± 0.2	0.39 ± 0.02	5.18 ± 0.14	1.71 ± 0.04
2699E		187 ± 8	8.9 ± 0.4	6.3 ± 0.3	0.6 ± 0.02	0.72 ± 0.03	1.55 ± 0.08

Table C-2: Infinite matrix dose rates determined by HRGS and TSBC.

[a]based on dose rate conversion factors in Aikten (1983) and Sanderson (1987)

SUTL no.	Depth / cm	HRGS, dry (mGy a^{-1})[a]		
		Alpha	Beta	Gamma
2698A		2.79 ± 0.04	0.98 ± 0.02 (1.7%)	0.39 ± 0.01 (1.3%)
2699A		6.64 ± 0.18	1.23 ± 0.03 (2.4%)	0.60 ± 0.01 (2.0%)
2698B		3.46 ± 0.06	1.22 ± 0.02 (1.6%)	0.49 ± 0.01 (1.3%)
2698C		3.28 ± 0.02	1.38 ± 0.02 (1.2%)	0.55 ± 0.01 (0.9%)
2698D		3.27 ± 0.02	1.34 ± 0.02 (1.2%)	0.55 ± 0.01 (0.9%)
2698E		2.58 ± 0.01	1.30 ± 0.02 (1.3%)	0.51 ± 0.01 (1.0%)
2699B		5.06 ± 0.47	0.96 ± 0.03 (3.4%)	0.46 ± 0.02 (4.6%)
2699C		15.65 ± 0.4	1.13 ± 0.03 (2.2%)	0.78 ± 0.02 (2.2%)
2699E		3.14 ± 0.10	0.65 ± 0.02 (3.2%)	0.31 ± 0.01 (2.6%)

Table C-3: Scaling factors, weighted gamma dose rate estimates, and the calculated gamma dose rates received at each of the sampling positions (in bold)

SUTL no.	depth / cm	distance from dating sample / r	weighting factor / $e^{-\mu r}$	gamma dose rate / mGy a^{-1}	gamma dose rate at sampling position/ mGy a^{-1}
2698A		**0**	**1.0**	**0.39 ± 0.06**	
2698C		5	0.607	0.46 ± 0.07	
2698B		30	0.050	0.44 ± 0.06	**0.43 ± 0.02**
2698D		5	0.607	0.46 ± 0.06	
2698E		30	0.050	0.44 ± 0.06	
2699A		**0**	**1.000**	**0.49 ± 0.07**	
2699C		5	0.607	0.70 ± 0.04	**0.54 ± 0.02**
2699B		30	0.050	0.42 ± 0.06	
2699D		-	-	-	

2699E		30	0.050	0.28 ± 0.02	

Table C-4: Water contents, and effective beta and gamma dose rates following water correction.

[a] Effective beta dose rate combining water content corrections with inverse grain size attenuation factors obtained by weighting the 200 μm attenuation factors of Mejdahl (1979) for K, U, and Th by the relative beta dose contributions for each source determined by Gamma Spectrometry.
[b] the sum of the gamma dose components obtained from stratigraphic layers in proximity to the dating sample, weighted relative to distance from the sample position
[c] Total dose rate from beta, gamma and cosmic components

SUTL No.	Water Content (%)			Effective Dose Rate (mGy a^{-1})		
	Fractional	Saturated	Assumed	Beta[a]	Gamma[b]	Total[c]
2698	2	15	10 ± 5	0.85 ± 0.06	**0.43 ± 0.02**	**1.47 ± 0.06**
2699				0.89 ± 0.06	**0.54 ± 0.02**	**1.61 ± 0.06**

Appendix D: Radial plots

Figure D-1: Radial plot for SUTL2698;
circles = IRSL 50°C De's; triangles = post-IR IRSL 225°C De's
weighted mean, post-IR IRSL 225°C De = 112 ± 2.6 (12.5)

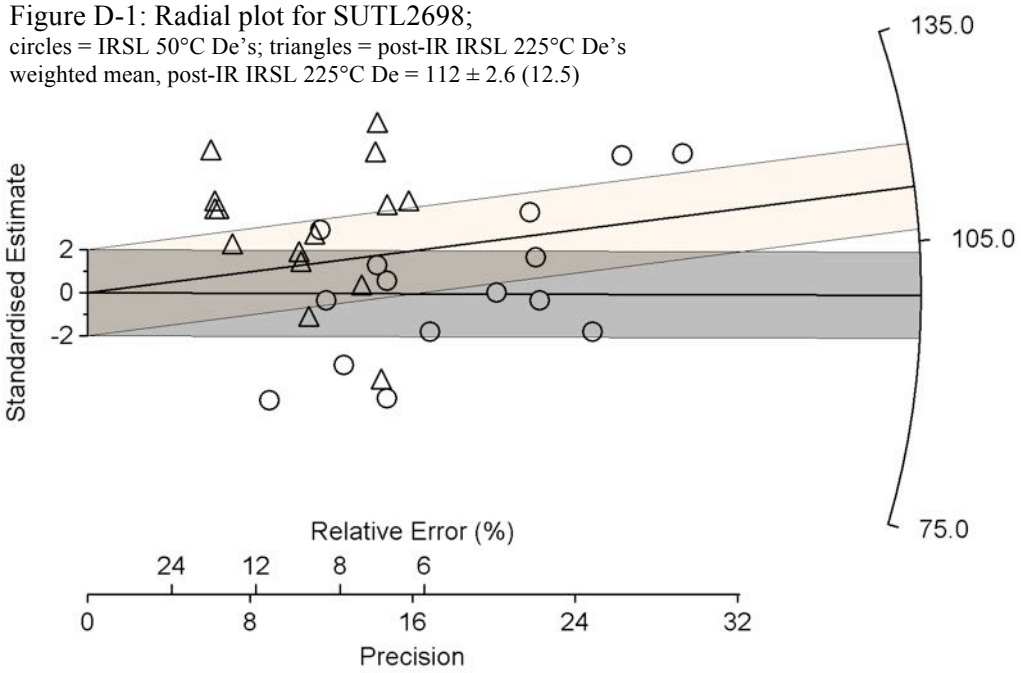

Figure D-2: Radial plot for SUTL2699;
circles = IRSL 50°C De's; triangles = post-IR IRSL 225°C De's
weighted mean, post-IR IRSL 225°C De = 94.7 ± 2.1 (5.4)